INTERACTION BETWEEN TWO MARINE RISERS

by

Wusheng WU

A thesis submitted in fulfilment of the
requirements for the degree of

Doctor of Philosophy

University of Glasgow

Faculty of Engineering

Department of Naval Architecture and Marine Engineering

To the memory of mother

University of Glasgow

Faculty of Engineering

Department of Naval Architecture & Marine Engineering

Abstract

INTERACTION BETWEEN TWO MARINE RISERS

by

Wusheng WU

This thesis takes top tensioned vertical riser interaction as its main study object. It has its focus on the understanding of the mechanism about potential instability of the risers caused by the interaction and the prediction of potential collision. Started from two-dimensional cylinder interaction cases, and later extended into the three-dimensional riser scenarios, the problem is investigated comprehensively. The study covers fluid force prediction, stability analysis, continuation investigation and dynamics simulation. The study disclosed the mechanism of the potential collision when the flow velocity reaches a certain critical value, and provides a robust tool to predict the threshold for the riser collision. Additionally, the investigation shows the difference between marine riser interaction and the similar interaction occurs in other engineering disciplines, such as power transmission lines, heat exchangers etc. Also provided in this thesis are valuable information regarding the riser dynamics should collision occurs. The research will be beneficial to the marine riser designers and operators.

The research described in this thesis is believed to be original unless otherwise explicitly referenced.

SUMMARY

As oil and gas exploration and production moves towards deep and ultra deep water areas these days, the offshore industry is facing challenges, amongst which riser interaction is newly emerging. Essentially this interaction is caused by the wake flow. It can play a detrimental role in carbohydrate extraction and it will be particularly important in ultra deep water development. This thesis takes the top tensioned vertical riser system, such as is used in conjunction with TLPs and Spars, as a main object. It endeavours to deal with the mechanism of the interaction between two marine risers and to predict the potential collision between the two risers.

Deep water risers are so long that flow along the riser length does not change significantly. Therefore, the risers can be simplified into two-dimensional cylinder cases. Such an approach provides a simplified way to understand the issue. On the other hand, in order to understand this subject in real scenarios and predict the phenomena quantitatively, the study is also carried out in the three-dimensional space. The thesis is comprised of seven independent while interrelated parts, viz:

1. Two-dimensional Time-Averaged force estimation

   Utilising the free-streamline model, based on empirical data for flow separation, a numerical procedure is used to seek the time-averaged forces exerted on the downstream cylinders. Such force data constitute the fluid interaction data source for the subsequent cylinder/riser stability and dynamics analyses.

2. Two-dimensional cylinder stability analysis

By adopting the traditional Routh-Hurwitz stability algorithm, combined with the direct numerical eigenvalue seeking technique, the stability of the downstream cylinder at designated positions is thoroughly investigated. Different bifurcation types and different stability areas are comprehensively investigated and identified. The characteristics of the marine riser interaction are identified as well.

3. Two-dimensional continuation investigation

Based on the characteristics of marine riser interaction, a systematic investigation of the continuation and stability is conducted. Such an investigation is a cross examination of the traditional stability analysis. Meanwhile, the possible multiple equilibrium positions of the dynamics system are identified. Such an analysis contributes to a concrete explanation of the cause of two cylinders collision.

4. Two-dimensional dynamics simulation

Based on the foregoing stability investigation, a thorough dynamics simulation is implemented. The investigation is mainly focused on the behaviour after loss of stability of the downstream cylinder. The cylinder motion speed and movement amplitude, together with the time intervals between successive collisions are identified.

5. Three-dimensional statics

The statics of a solitary marine riser has been a well understood topic. However, the statics for wake interaction has never been explained before. In this section, a comprehensive parametric investigation is conducted, non-dimensional parameters are discussed and the effect of different factors is fully addressed.

6. Three-dimensional continuation

Three-dimensional continuation investigation is a direct extension of the two-dimensional continuation study. The riser interaction system is first cast into the modal co-ordinate system which makes the dynamic system into a system with a finite dimension. Pseudo arc length continuation strategy is used, and the two-dimensional like conclusion has been drawn. By using non-dimensional parameters, a useful critical flow condition for general deepwater risers is obtained.

7. Three-dimensional dynamics simulation

Utilising the mode superposition method, the dynamics system of two risers under the action of an ocean current is investigated. The dynamic behaviour of the risers, particularly in a strong ocean current is identified. Such an investigation can be used to explain the observed dynamic behaviour of the risers and it can also serve as a reference for the identification of the possible damage, which may result from collision between two risers.

Among many results yielded in this research, two important ones are listed as follows:

1. Explanation of the cause of collision between two cylinders/risers. It is concluded in this research that the occurrence of collision is caused by loss of stability and disappearance of equilibrium, rather than by the progressive and continuous approach to each other between two cylinders/risers until contact happens.

2. The prediction of critical flow velocity before collision between the two risers starts to occur. The Figure 0.1 shows the relation between critical flow tension factor ($H_w = \rho V_0 \sqrt{l/T_{e0}}$) for different design spacing and top tension factors of deepwater risers. For example, for a pair of 1000 meters long and 8" diameter gas riser, with

weight in water of 275 N/m, top tension factor of 3.0 and design spacing of 30 diameters. Based on the figure, when current flow velocity exceeds 0.45 m/s, the collision between the two risers will occur. Reflected in this figure, the critical flow velocity will be below 1.0 m/s for risers with length over 1000 meters. Additionally, increase top tension or increase the design spacing between the two risers can substantially defer the riser collision to a higher current velocity.

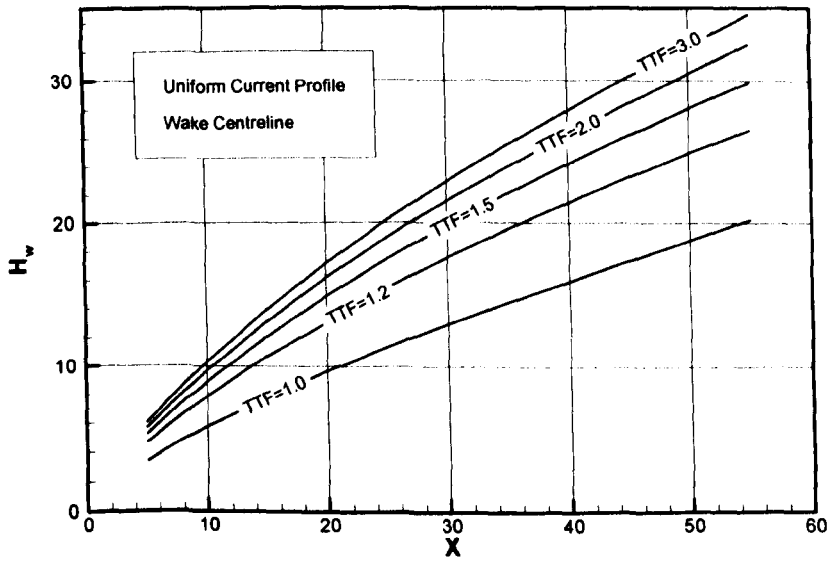

Figure 0.1 Critical H_w for different riser design spacing and top tension factor. $H_w = \rho V_0 \sqrt{l/T_{e0}}$

ACKNOWLEDGEMENT

First I would like to thank my supervisor Dr. Shan Huang who has assisted me tremendously in completing such an elaborate and demanding project. I could not imagine that this could be finished without his constant encouragement and stimulating advice. It made every discussion and advice a most inspiring and memorable one. I would also like to thank Prof. Nigel Barltrop, for his most valuable guidance and help by his tremendous engineering experience, which warrants a most beneficial one to this work for every discussion.

Special thank goes to Dr. Nina Baker, for her careful proofreading and language help during writing up of this thesis. Thanks also go to Mrs. Thelma Will, for her most considerate help in every aspect, which makes my life in Glasgow a most memorable one.

My eternal gratitude to my parents, my sisters, Rujin WU and Ruyin WU, for their endless love and support, I would not have made it this far without their constant encouragement and support.

I also wish to acknowledge the scholarship awarded by the Faculty of Engineering, University of Glasgow for this study, and the Stanley Gray Fellowship awarded by the Institute of Marine Engineering, Science and Technology (Previously known as Institute of Marine Engineering) for this work.

Finally, my deepest thanks to my wife Liping BIAN and my daughter Yue WU, for their love, patience and understanding during these years. Thanks for their unconditional support and love during this study. Particularly for my daughter, her sweet smiles always lighten me up when I was in low.

TABLE OF CONTENTS

LIST OF FIGURES

LIST OF TABLES

Chapter I

INTRODUCTION

1.1 General Remarks

1.1.1 Offshore Oil & Gas Development

Ocean, which covers almost three quarters of the earth, is always so appealing to human beings. It is a virtual cornucopia, with abundant resources as we now know, such as oil, natural gas, minerals, and other possible energy sources, such as wave, tidal, and ocean thermal energy. In 1947 the first offshore platform for oil was installed off the coast of Louisiana in just 6 meters of water. Today there are already over 7,000 offshore platforms around the world in water depths approaching to 3,000 meters.

The offshore oil & gas industry is moving towards deep and ultra deep waters. This development has been so fast that the concept of the deepwater and ultra deepwater has constantly changed. Until 10 years ago, from a European perspective, the start of deepwater was simple: 200 metres and deeper, essentially the edge of the continental shelf. When viewed globally the answer is not so simple. The Gulf of Mexico, Brazil and West Africa have seen deepwater records tumble as discoveries and production have come from depths greater than 1,000 metres. Therefore, 200 metres is simply not considered to be deepwater anymore especially as various organisations have their own definitions, ranging

up to 500 metres and even beyond. To take this into account, the general definition of deepwater, which this thesis will use, starts from 300 metres.

The growth of deep and ultra deep development has been particularly tremendous over the recent three decades. It has been much spurred by the major price increases during the 1970's (Garside, et al, 2001). During this period, significant transformation has taken place in the industry. For example, shown in Figure 1.1, the deepwater production in the Gulf of Mexico has increased tenfold since 1985 for oil and sixfold for gas production. At this

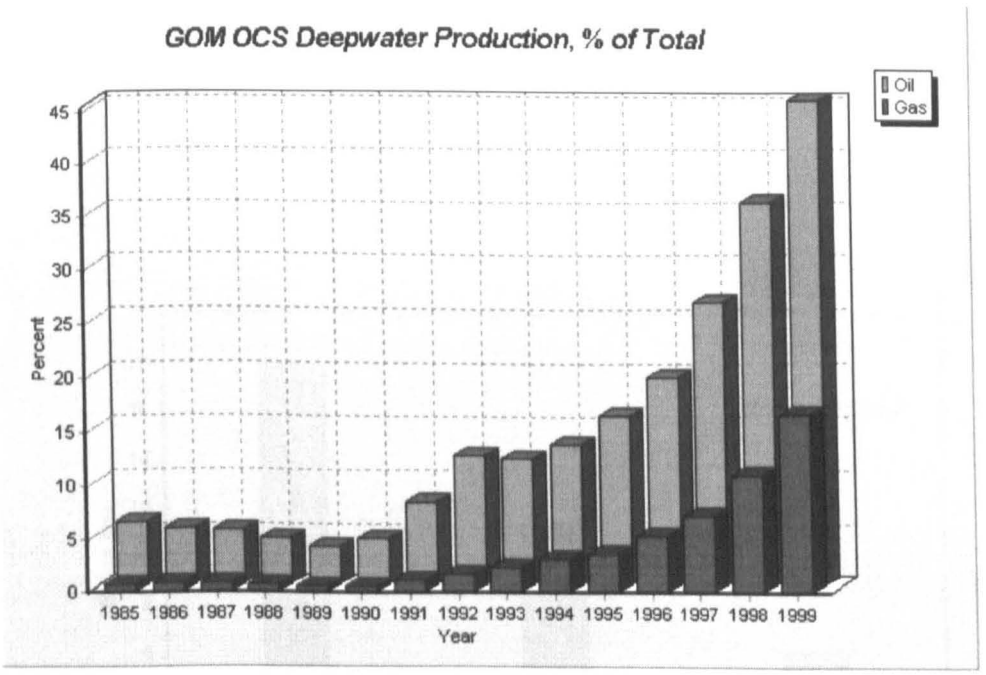

Figure 1.1 Deepwater production, from MMS (MMS, Mineral Management Service, defines deepwater as 1,000 feet of water or greater).

moment, global exploration continues to push into more remote areas and deeper water to target opportunities that are just too exciting to be denied. Over 35 billion barrels oil equivalent in deepwater have been found (Figure 1.2). The main active deepwater development areas around the world are: West Africa, Brazil, Gulf of Mexico, Caspian Sea, and North Atlantic (comprising Norway, W of Shetlands, Ireland, Greenland).

Nevertheless, only 20 percent of resources have been developed and are producing. Industry continues to advance into deeper and more complex settings. In recent time, the number of wells being drilled in the so-called ultradeep water — those in 5,000 feet of water or greater — continues to grow significantly. Currently there are more than eight wells being drilled in water depths of 5,000 feet or greater, four in excess of 7,500 feet. The eight wells and the company operating the well and the water depth are listed in the table 1.1. Such a data is constantly changing with the time. Some pioneering projects have been launched in recent years to challenge the ultra deepwater development, such as DEMO 2000 (Wiencke, 2000), the Norwegian Deepwater Programme in Norway, and Deepstart in Gulf of Mexico. All these show that ultra deep water will be the main arena for offshore development in the years to come.

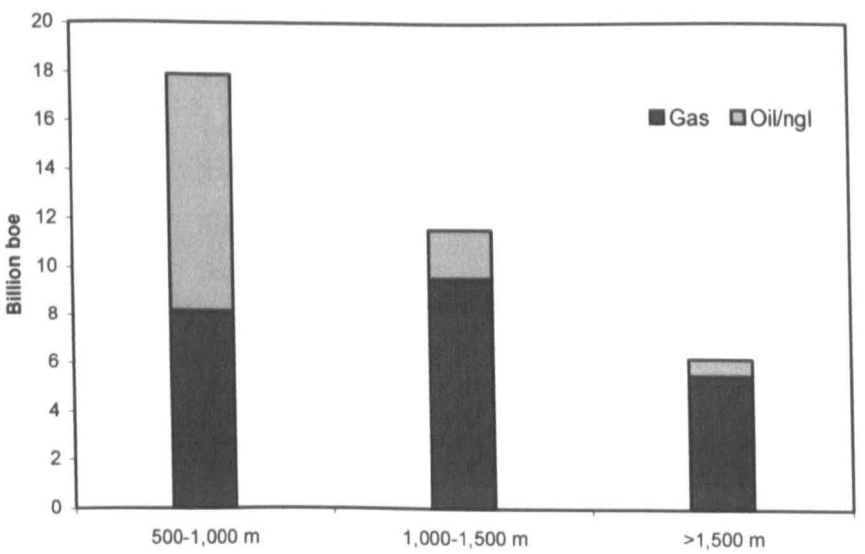

Figure 1.2 Worldwide deepwater discoveries total more than 35 billion boe, about two thirds of that are oil. Source: Shell (Cook, 1999).

Table 1.1 List of present ultra deep water drilling

Operator	Water Depth
Transocean Sedco Forex	9687 feet
BHP Petroleum	8,835 feet
Elf Exploration	7,790 feet
Shell	7,760 feet
Unocal	7,044 feet
BP/Amoco	6,627 feet
BP/Amoco	6,386 feet
BP/Amoco	5,180 feet

1.1.2 Platform and Riser System

Table 1. 2 Category of offshore platform according to connections on seabed

Type of Platform	Connection to Seabed	Example
Fixed-bottom	Piles	Steel jacket
	Gravity	Concrete Gravity Structure (CGS)
Floating	Tethers	Tension Leg Platform (TLP)
	Catenary mooring lines	Semi-submersible, Spar
	Single Point Mooring (SPM)	Ship-shaped vessel (FPSO)

Nearly all the offshore production requires platform and riser systems. Generally, offshore platforms can be categorised according to whether they are rigid structures that extend all the way from above the water surface to the seabed (fixed-bottom platforms), or whether they float near the water surface. They can be further categorised according to the way they are connected to the seabed. Table 1.2 shows a general categorisation of offshore platforms. Due to the spiral rising of cost for fixed-bottom platforms, such as jacket type, a floating production system would be the main option for deepwater and ultra deepwater

developments. By and large, deepwater developments by definition are: floating systems, subsea wells, or a combination of floaters and subsea wells. A key component of the floating production system is the riser system. It has a large influence on the decision made about hull type.

In essence, risers are conduits that connect the wellhead on the ocean floor with the top vessel or platform on the sea surface. They may perform the following specific functions:

1. Convey fluids between the wells and the FPS (i.e. production, injection or circulated fluids).

2. Import, export, or circulate fluids between the FPS and remote equipment or pipeline systems.

3. Guide drilling or workover tools and tubulars to and into the wells.

4. Support auxiliary lines.

5. Serve as, or be incorporated in a mooring element.

6. Other specialized functions such as well bore annulus access for monitoring or fluids injection.

Figure 1.3 shows a functional diagram of the riser system. It is composed of four parts (API, 1998), i.e. Conduit, Top interface, Bottom interface and System integrity.

Associated with different types of floating production systems listed in table 1.2, generally there are three kinds of risers (Barltrop, 1998),

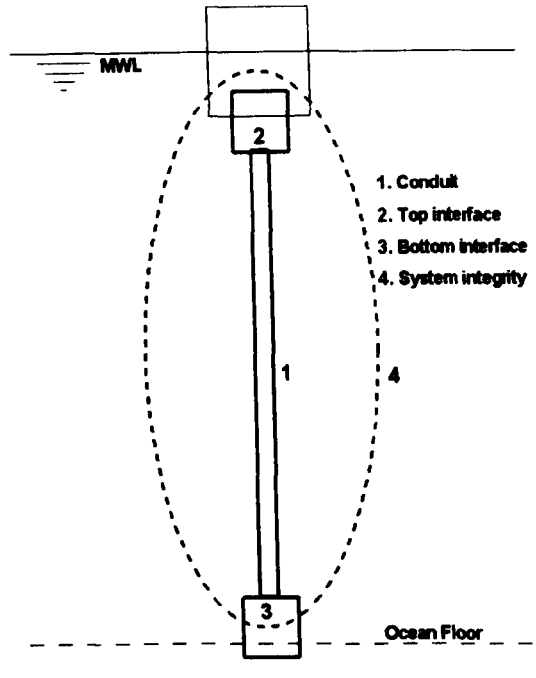

Figure 1.3 Essential functional elements of a riser system.

1. Rigid Riser. Usually these are top tensioned vertical steel pipes. They can be manufactured in a large range of diameters. It is the most versatile for production, as it can handle aggressive fluids and high internal or external pressures. Drilling and work-over operations also generally require a vertical rigid riser. The limitation for this kind of riser is that the movement of the platform has to be small. In deepwater developments, they are often used with TLP and Spars systems, which can meet the small movement requirement with the help of the tethered station keeping.

2. Flexible Riser. Usually steel-polymer composite pipes hung in a simple or S shaped catenary. They are mostly used in conjunction with FPSO or Semi-submersibles due to the fact that they can accommodate the platform's large movement. However, when the operation is in ultra deepwater, the very high static pressure constitutes a big challenge to this kind of riser.

3. Metal Catenary Risers (SCR). Catenary riser made of steel or titanium. It has the benefit of the catenary riser whilst offsetting the inadequacy of the traditional flexible riser in ultra deepwater under high static pressure.

Among these different kinds of risers, the top-tensioned vertical rigid riser is the main object to be studied in this thesis. Some further introduction of such a riser system is presented below.

1.1.3 Top tensioned vertical riser

Figure 1.4 is a schematic of a top tensioned production riser. The main part of the riser is the conduit, which is for fluid transport, control or monitoring system umbilicals, and load paths for structural support must be provided and their continuous operation contained. Most of the time, the conduit are segmented. This is due to the limitations on the maximum continuous length of metal pipe that can be reasonably manufactured, transported, handled, installed, retrieved and replaced. These segments can be joined onsite by mechanical connectors such as threading or by flange, or by welding. The lowest segment may contain a tapered stress joint section or a flex joint in order to transfer structural loads into the riser end termination.

The apparatus on top, corresponding to the top interface in functional diagram Figure 1.3, allows the riser to hang at the surface and attach it to surface valves and piping. It forms the main support of the risers. This apparatus is often composed of tensioner and slip joint. Figure 1.5 shows one schematic about the riser top interface. Seen in the figure, the tensioner forces are transmitted through the slip joint to the upper joint in the riser string. The variation of the tension force is adjusted via the hydropneumatic mechanical system. The slip joint is a mechanical device that attempts to compensate for vessel motion and thereby minimize the effects of such motion on the riser string. It is composed of inner barrel and outer barrel. The inner barrel is attached to the vessel by means of a ball joint on

the bottom of the diverter. The outer barrel, which is attached to the riser string by means of a ball joint (termed the upper ball joint), is supported at the tensioner ring by means of the tensioner cables. The outer barrel is free to translate and rotate relative to the inner barrel (Kozik & Noerager, 1976). In general, the riser tensioner design specifications identify the required nominal tension and the allowable variations in tension. For example, for production riser, 20 percent of tension riser is allowed. The specification also required that the allowable tension variation shall include the effects of all of the negatively contributing factors such as friction losses, gas pressure variation due to riser motion, and the failure of any single component (MacPhaiden & Abbot, 1985).

The seabed portion, the stress or taper joint in the Figure 1.4, also known as the bottom interface in the functional diagram Figure 1.3, contains an apparatus that connects the riser to a wellhead or receptacle. Included are also methods/equipment to space out the riser and to account for bending loads at the bottom and/or top of the system. This portion must also be designed to accommodate riser loads and maintain fluid conduit and pressure integrity.

For the riser system integrity, which includes not only fluid and pressure containment, but structural and global stability as well. The riser may also have bumpers, vortex-suppression devices and other attachments such as buoyancy modules. They are appendages or accessories to alleviate the dynamic problems caused by environment loads etc.

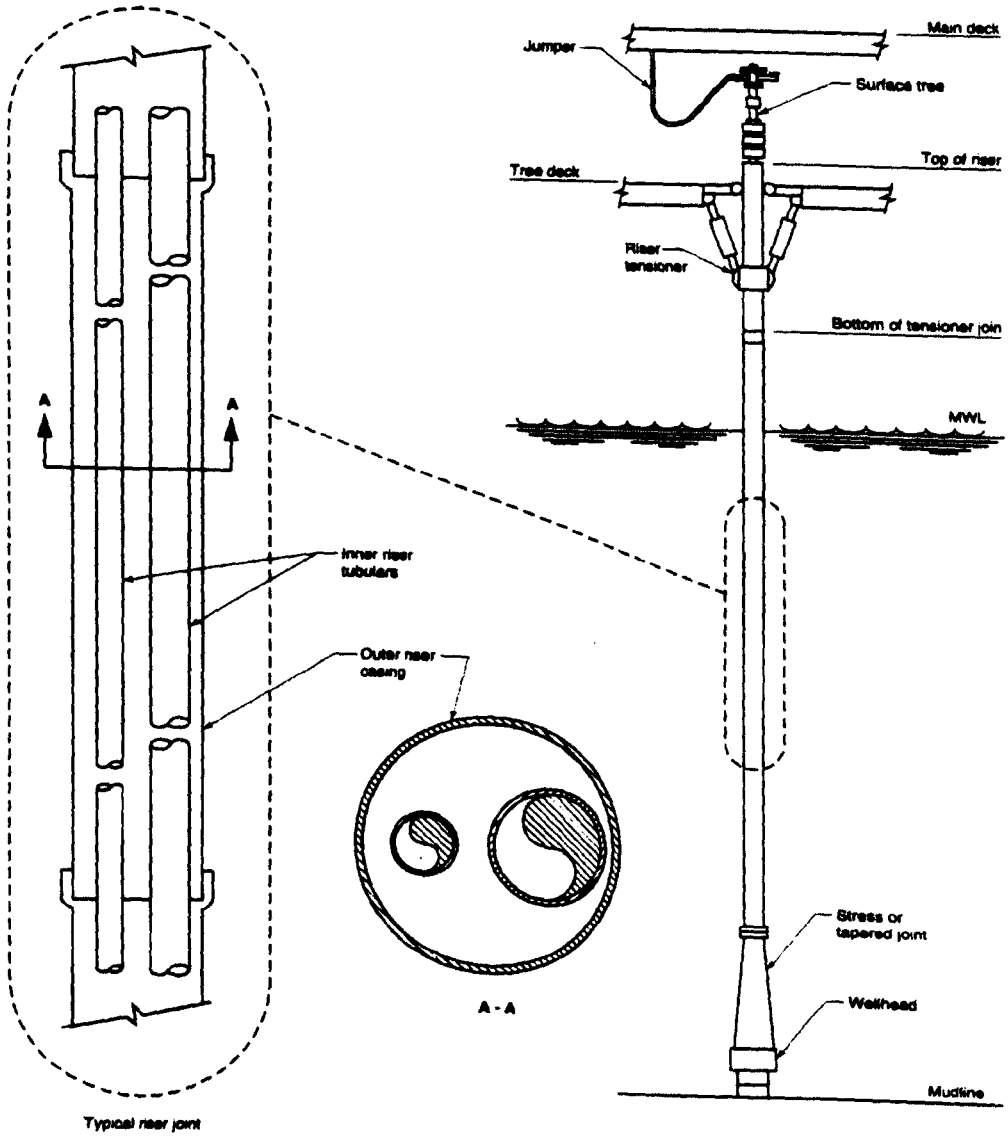

Figure 1.4 Top-tensioned production riser (From API, 1998).

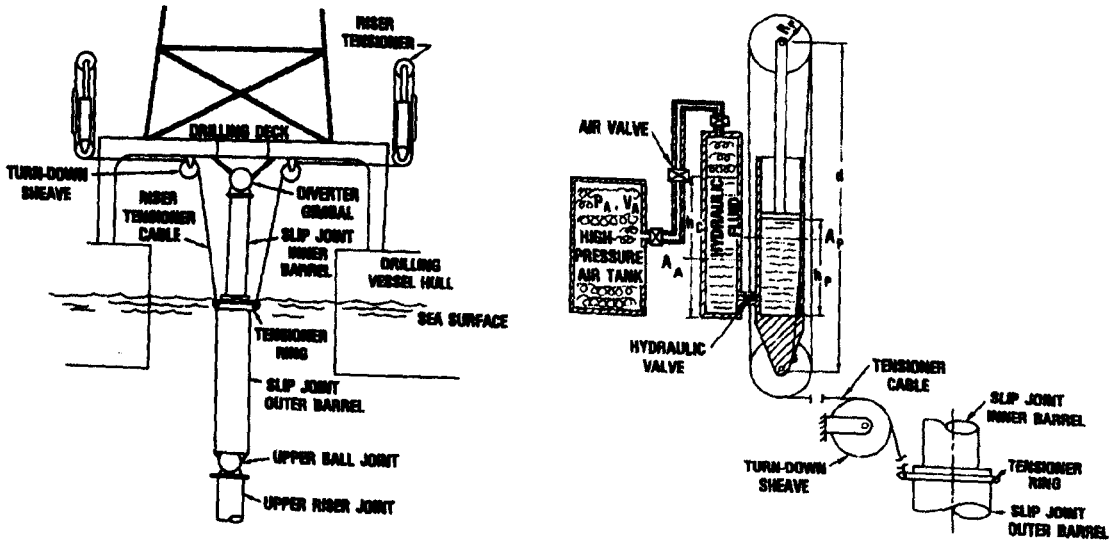

Figure 1.5 Top tensioner mechanism, from Kozik and Noerager (1976).

1.1.4 Challenges to Top Tensioned Vertical Rigid Risers in Deepwater

Top tensioned rigid risers used in conjunction with TLP or Spars are likely to be applied in an array, with typically larger than 10 diameters of clearance. For this kind of riser, fatigue life and potential collision are the two main issues for the riser design.

1. The fatigue life is closely related to the vortex-induced vibration, which has been a problem for risers for decades. In deepwater development, the spacing dependent current, such as shear current or non-unidirectional current, together with possible multiple modes "lock in" can further complicate the phenomena.

2. Potential collision caused by wave and current. The harsh environment can excite individual risers to move around with the platform. If the excitation of the fluid loading is so strong that the envelope of the excursion of individual risers starts to overlap with each other, consequently, the risers can collide with each other. Such collision can also occur between riser and tendons. (Rajabi, 1989)

3. Another problem that can result in risers colliding with each other is the interaction between risers through the wake effect. The fluid loadings experienced by individual risers are not the same due to the fact that some risers are located in the wake of others. In deepwater, the deflection of the risers tends to be large, this kind of fluid interaction can trigger two risers to collide with each other under certain flow conditions, and ultimately can lead some risers to move around. The collision between risers will be harmful to the oil and gas production and possibly destructive to the riser structure, therefore such an interaction is an important issue that warrants a through investigation.

Other challenges for such rigid risers in deep and ultra deep water include:

- Method of deployment,

- Extremely high tensions for top tensioned risers in water depths greater than 2000 meters,

- Accurate prediction of the dynamics etc.

With the offshore industry's determination to move production into ultra deep water, this thesis studies the challenge imposed by interaction caused riser collisions, i.e. the third one of the above challenge list. In order to clarify the mechanism of the interaction, the study will take its focus on the interaction between two risers and started in two-dimensional space.

1.2 Present Investigation

This thesis takes the TLP/Spar rigid riser as its investigation background, focusing on the mechanism of the interaction between two risers, particularly the effect of the upstream wake on the downstream riser. The research covers the estimation of the fluid forces exerted on the downstream riser due to the interaction effect, the stability investigation of the riser pair, and the identification of potential multiple equilibrium states. Based on such a systematic investigation, a simulation of dynamics is then carried out to account for the dynamic behaviour the riser pair can possibly exhibit, and to explain the phenomena observed by some of the researchers in the experiment. The investigation is first unfolded in two-dimensional space with its focus on the explanation of the mechanism of interaction, and then extended in three-dimensional space to address the quantitative relationship about the critical states and corresponding dynamic behaviour.

1.3 The Background of Chosen Topic

The grounds to choose the topic for this thesis investigation are as follows,

1. TLP/Spar are attractive options for future deep and ultra deep water developments, with relatively mature technology available (Snell and Banon,; 2000);

2. Geometrically, among the major components involved in a field development, it is the riser system together with the mooring system that really depends on the water depth. Neither the floating units, nor the subsea equipment depend on water depth to the same extent. On the other hand, the risers are one of the most delicate components of a Floating Production System and need particular attention to their design and deployment from a FPS (Rajabi, 1989). Therefore, among the deepwater challenges, riser has its unique importance.

3. As identified herein, the riser interaction can potentially bring them to collide with each other. To date, the philosophy has been to space the risers further apart in order to avoid riser collisions (ABS, 2001). Such a philosophy needs an effective tool to identify the necessary riser clearance and to address its practicability. Moreover, the mechanism which brings two risers to collide need to be comprehended.

4. Spacing the risers largely to avoid collision in ultra deepwater will result in a significant cost penalty and may even jeopardize the feasibility of the entire system. Therefore, should collision between risers be unavoidable, the damage that the impact can cause will be vital information to marine riser designers.

Based on above rationale, the present thesis conducted a comprehensive investigation into the interaction between two risers. A brief introduction about the theoretical background and literature review on this topic is presented next.

1.4 Theoretical Background and Literature Review

The mechanics of marine riser can be simplified into a problem about cylinders, which has been a subject extensively studied in the past. The exercise of cylinders in engineering is ubiquitous. For example, the application of multiple cylinders can be found in the offshore engineering, such as risers, tendons, or in power generation industry such as tube banks for heat exchangers, twin-bundled and multiple line bundled lines for power transmission. Application can also be found in civil engineering, such as groups of tower buildings, chimneys and power stacks. Though the problem faced by marine risers has its unique characteristics, which will be addressed in this thesis (Chapter 3), the theoretical mechanism has by and large similarities from one to the other. This thesis by no means tries to discuss all the issues related to cylinder applications. However, in order to present a full picture about the background of the problem, a comprehensive introduction and review about the flow over solitary and two/multiple cylinders is presented below.

1.4.1 Solitary Cylinder

1.4.1.1 Fixed cylinder

Perhaps the flow around a solitary cylinder is a most well researched subject in fluid mechanics due to its simplicity in geometry. It has been long recognised that the flow over a smooth circular cylinder is essentially dependent on the Reynolds number. Figure 1.6 presents an overall flow picture at different Reynolds number.

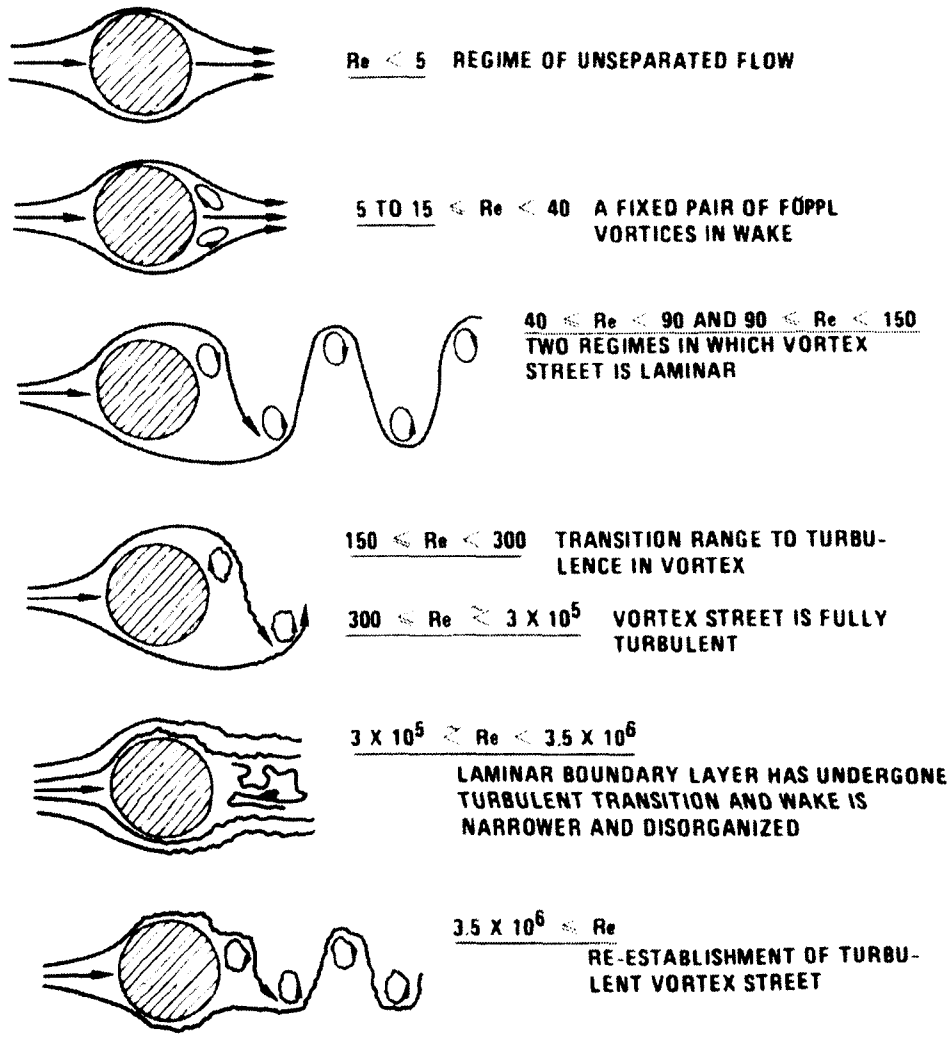

Figure 1.6 Regimes of fluid flow across smooth circular cylinder. Source: Blevins (1990).

It was observed that the flow over a smooth circular cylinder can be categorised into following regimes (Blevins, 1990),

- Re<5, the fluid flow follows the cylinder contours.

- 5 to 15≤Re<40, the flow separates from the back of the cylinder and a symmetric pair of vortices is formed in the near wake.

- 40≤Re<90 and 90≤Re<150, the wake become unstable and one of the vortices breaks away. A laminar periodic wake of staggered vortices of opposite sign is formed.

- $150 \leq Re < 300$, the vortices breaking away from the cylinder become turbulent, although the boundary layer on the cylinder remains laminar.

- $300 \leq Re < 3 \times 10^5$, it is called subcritical Reynolds number. The laminar boundary layers separate at about 80 degrees aft of the nose of the cylinder and the vortex shedding is strong and periodic.

- $1.5 \times 10^5 \leq Re < 3.5 \times 10^6$, transitional Reynolds number. The cylinder boundary layer becomes turbulent, the separation points move aft to 140 degrees, and the cylinder drag coefficient drops to about 0.3.

- $Re > 3.5 \times 10^6$, supercritical Reynolds number. Regular vortex shedding is re-established with a turbulent cylinder boundary layer.

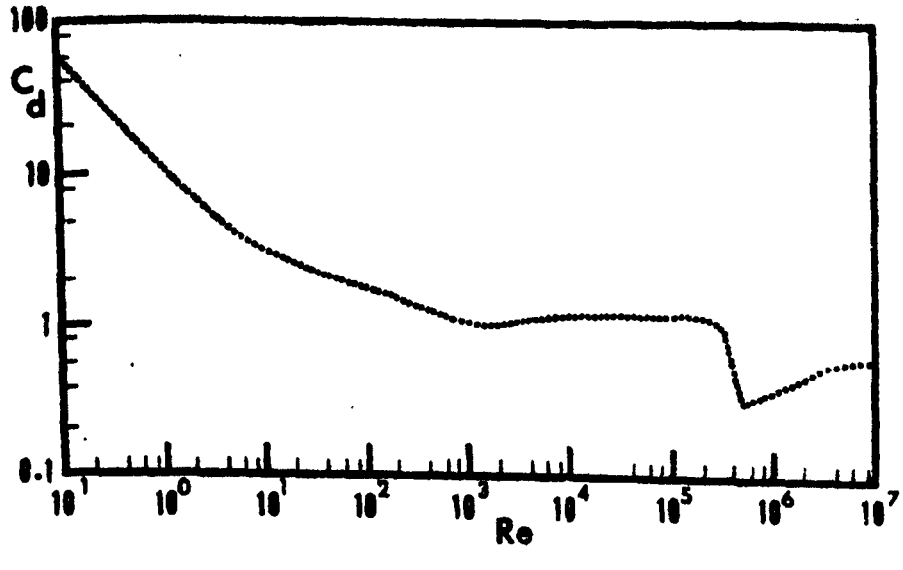

Figure 1.7 Drag coefficient for circular cylinders as a function of Reynolds number (Schlichting, 1968).

Corresponding to the flow variation over the Reynolds number, the fluid forces and the vortex shedding frequencies on the fixed cylinder changes accordingly. Figures 1.7 to 1.9

show the variation of mean drag force coefficient (time averaged), Strouhal number and oscillating lift force vary over Reynolds number respectively.

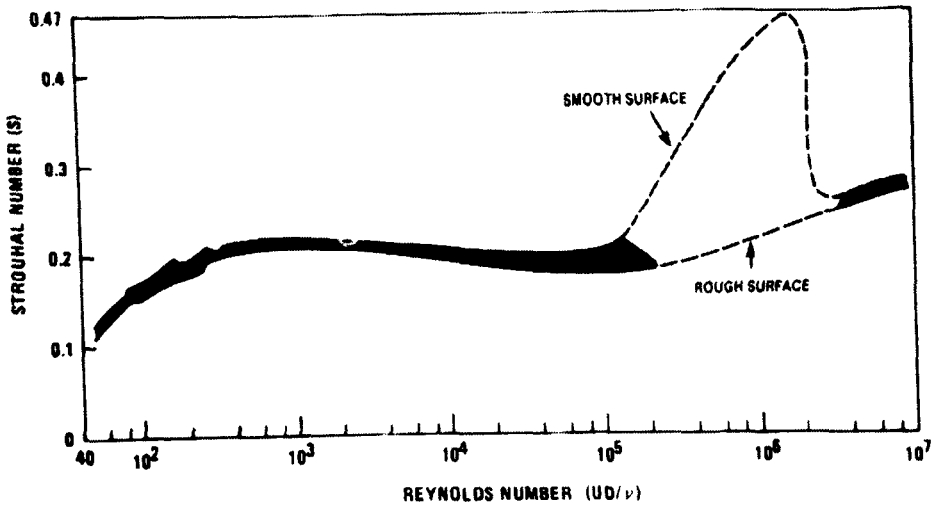

Figure 1.8 Relation between Strouhal number and Reynolds number for circular cylinders. Source: Blevins (1990).

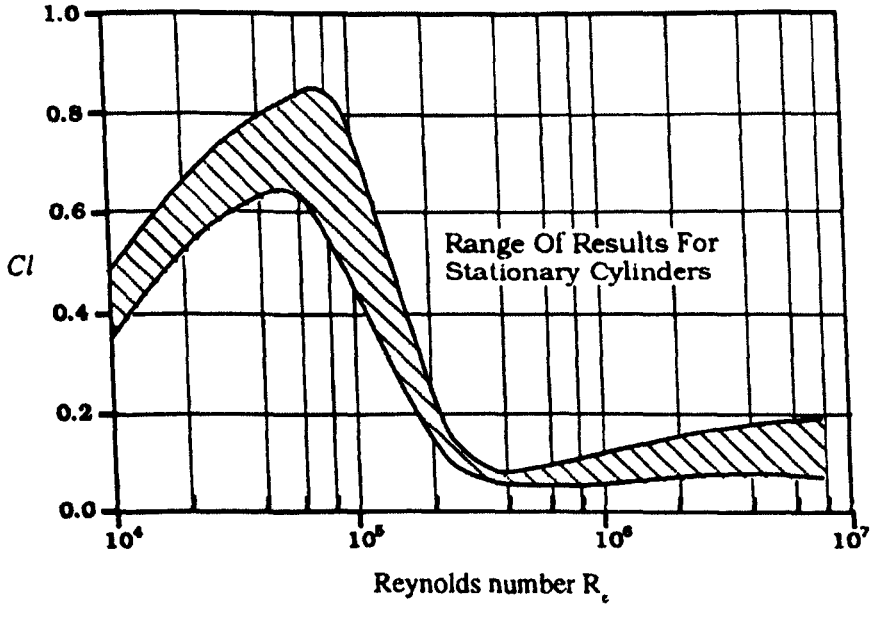

Figure 1.9 Fluctuating lift force coefficient versus Reynolds number for a smooth circular cylinder (Robinson & Hamilton, 1992).

It is interesting to see that in the subcritical Reynolds number regime, the drag force appears to be insensitive to the variation of the Reynolds number and it has a constant value about 1.2. The corresponding Strouhal number in this Reynolds number regime for

vortex shedding is about 0.2. On the other hand, the oscillating lift force coefficient from measurements generally show 0.4 for Reynolds number smaller than 5×10^3. Then, it increases to its maximum rms value of 0.6-0.7 at Reynolds number about 4×10^4, where it remains constant up to Reynolds number 10^5. Then, it decreases to below 0.2 (Reynolds number about 3×10^5), and remains approximately constant at higher Reynolds number (Pantazopoulos, 1994).

In offshore engineering, a typical 12 inches marine riser will have a Reynolds number range from 3×10^3 to 3×10^5 when the current varies from 0.1 m/s to 1 m/s. Therefore, the flow is mostly within the subcritical Reynolds number regime, in which the flow separates from the laminar boundary layer on the cylinder surface and strong vortex shedding is formed in the cylinder's wake.

1.4.1.2 Vortex induced vibration

When the circular cylinder is flexibly mounted, it will undergo vibration under the excitation of vortex shedding induced forces. However, the fluid flow will be complicated when the cylinder is in motion. The fluid flow and motion of the cylinder will interact with each other, which is a classical subject of fluid-structure interaction subject. The most significant feature of such motion is the phenomena of "lock in", or sometimes called "lock on", "synchronisation", or "resonant". It is a situation when the vortex shedding frequency is locked on to the cylinder's vibration. In which the Strouhal relation, that vortex-shedding frequency varies proportionally to the flow velocity, is violated. This phenomenon will persist within a range of flow velocities, for example, when the cylinder is in air, the lock in will exist within the reduced flow velocity (defined as flow velocity divided by system natural frequency and cylinder diameter) 4.75 to 8 and maximum amplitude occurs in the range of 5.5 to 6.5. In water, the phenomena occur in the range of 4.5 to 10 with maximum amplitude falling within the range of 6.5 to 8 (Sarpkaya &

Isaacson, 1981). Experimental observation discovered that there is vortex shedding mode changes in this particular "lock in" flow range (Williams, 1996), which explained the hysteresis effect on the response of the cylinder (Hartlen & Currie, 1970) observed. Excellent reviews about this dynamic phenomena can refer to Pantozoupolous (1994), Sarpkaya (1979), King (1976) and Blevins (1990) etc.

1.4.2 Two Cylinder Interaction

1.4.2.1 Fixed Cylinder Flow Interaction

It was a common practice to assume the two cylinders should behave in a flow in a similar or even identical manner to a solitary cylinder (Ohya, 1989). This assumption is justified only when the two cylinders are sufficiently apart. In most cases, however, the flow over the solitary cylinder will change after a neighbouring cylinder is present. Such a flow will not only depend on the Reynolds number, but also and much more significantly, will depend on the arrangement of the two cylinders. The following introductions are mainly for the subcritical Reynolds number cases as it has been shown that the risers are typically working under subcritical Reynolds number conditions. According to the relative location between the two cylinders, the interaction between the two can be classified into following kinds of interactions Zdravkovich(1977):

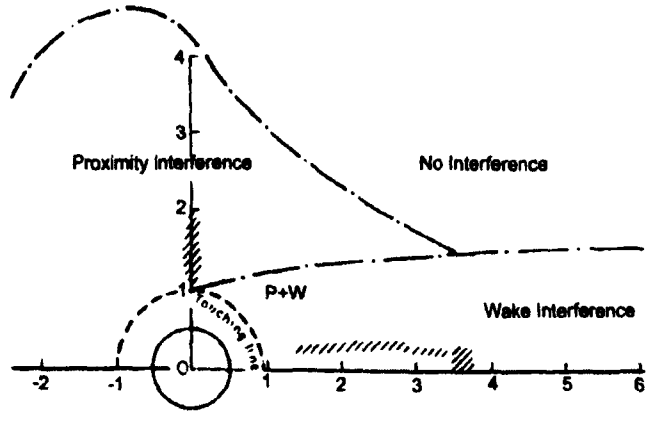

Figure 1.10 Definition of regions of flow interaction for two cylinders interaction, after Zdravkovich (1987). Proximity and wake interaction regions can be further divided. The corresponding subdivisions of these two interaction regions and other details are explained in Zdravkovich (1987).

- Proximity interaction, which takes place when the cylinders are close to each other. But none of them is submerged in the wake of another. There are two kinds of arrangement for such interaction.

  - *Side-by-Side Arrangement*

When the two cylinders are arranged in side-by-side, the flow changes with the variation of the transverse spacing of the two cylinders, i.e. when the two cylinders are within 1.1 to 1.2 diameters distance, the two tend to behave as an integrated one, such as reflected in Figure 1.11. When the spacing is between 1.2 and 2, bistable wake is observed, the wake between two cylinders is different, one is wide and the other is narrow. There is a gap/jet flow between two cylinders. It flows towards the small wake. Also the gap flow can switch direction between the narrow and wide wakes at irregular intervals. When the spacing is further increased to 4 or 5 diameters, the two wakes formed from the two cylinders are coupled and symmetrical with regard to the gap axis. When the spacing is further increased, the interaction will diminish gradually. Generally, interaction is considered to exist within 5 diameters Blevins (1990).

  - *Staggered Arrangement*

When the two cylinders are in staggered arrangement, gap flow existed well over the streamwise direction spacing of 0.15. However, when the spacing is within 0.15 diameters, the flow is bistable, the direction of the gap/jet flow can switch direction intermittently. When the streamwise direction is over 0.15, the narrow upstream cylinder's wake and wide downstream wake prevail the whole region. Meanwhile, the lift and drag force on the downstream cylinder tend to be smaller.

- Combined Proximity and Wake Interaction, which takes place when downstream cylinder is located in the wake of the upstream one and the spacing between the two is relative small. Within such a region, the upstream cylinder is influenced by the presence of the downstream cylinder. For the downstream cylinder, two different arrangements reveal different characteristics:

    - Tandem arrangement

When the spacing between the two cylinders is within 1 to 1.2~1.8 diameters, depending on Reynolds number, the flow separated from the upstream cylinder does not re-attach to the downstream cylinder and alternative vortex shedding is formed behind the downstream cylinder. However, they are originated from the upstream cylinder. The oscillating force on the upstream cylinder is negligible. The schematic about the flow are shown in the Figure 1.11.

When the spacing is increased from 1.8 to 3.4~3.8 diameters depending on Reynolds number, the free shear layers separated from upstream cylinder reattach on the upstream side of the downstream cylinder, a vortex street is formed only behind the downstream cylinder, under such condition, the oscillating forces on the upstream cylinder is still negligible.

    - Staggered arrangement

Two kinds of flow exist for the staggered arrangement. When the transverse spacing is small, such as around 0.2 diameters, and the streamwise spacing is within 1.1 to 3.5 diameters, strong gap flow occurs, which can entail strong wake central pointing lift forces. However, such a gap flow disappears when the transverse spacing is reduced. Outside this special gap flow area towards the wake boundary, the lift force reaches a maximum value

near the edge of the wake boundary when transverse spacing is larger than 0.4 diameters, and diminishes gradually towards zero when the tandem arrangement is reached.

- Wake interaction, which takes place when the downstream cylinder is located within the wake of the upstream one and the spacing between the two is relative large. There is no clear definition about the region of this kind of interaction in literatures so far as no clear boundary between wake interaction and the combined proximity and wake interaction (P+W) can be identified. Here, we define this to be the area when the downstream cylinder is located at the spacing larger than 4 diameters, and there is no significant interaction effect on the upstream cylinder. In such a region, no matter the two cylinders are arranged in tandem or staggered, the upstream cylinder will shed vortex as if otherwise it stands alone in the flow. The downstream cylinder is submerged in the vortex street of the upstream cylinder. The vortex shedding and fluid forces on the downstream cylinder are subject to the characteristics of the upstream wake flow. Such a region extends well over a spacing of hundreds of diameters. The characteristics of the fluid forces on the downstream cylinder will be discussed further in the next section.

- Outside the above defined interaction regions, the interaction on both cylinders are negligible, the two cylinders behave as otherwise a solitary cylinder case.

This thesis mainly deals with the case of wake interaction, in which the spacing between the two cylinders is often more than 10 diameters when at rest. Sometimes, the relative location can trespass the regime of combined interaction of proximity and wake though. The following introduction will have its focus on the wake interaction, and often with a reference to the combined proximity and wake interaction.

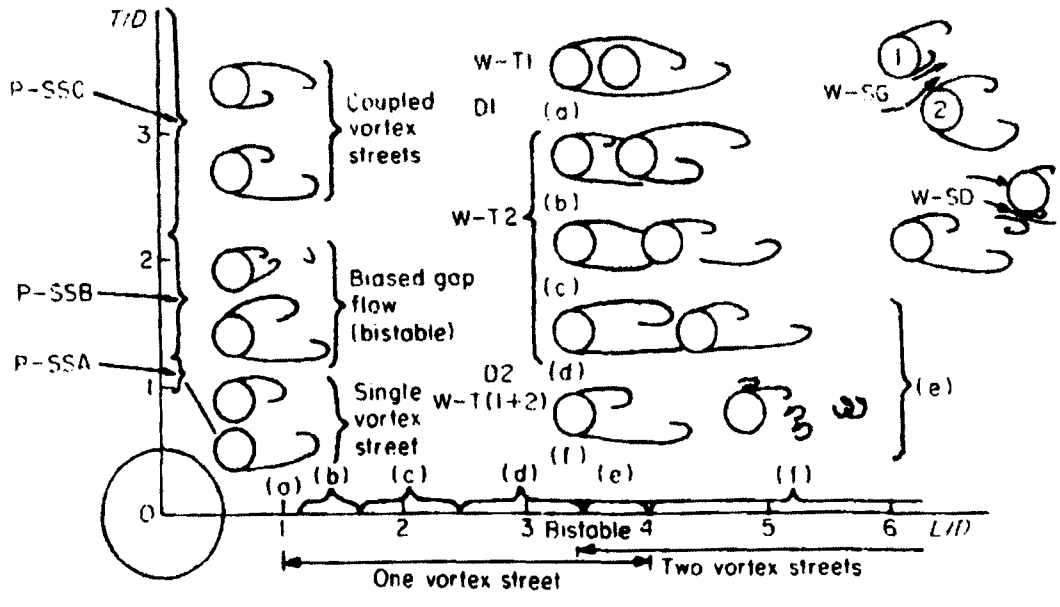

Figure 1.11 Wake flow under different arrangements. The detailed explanation about the symbols, such as P-SSA represents the Proximity interaction for the side-by-side arrangement is given in the Zdravkovich (1987).

1.4.2.2 Fluid forces on downstream cylinder in wake interaction

For the wake interaction, fluid forces on the downstream cylinder is a collective result of the vortex shedding on itself, the incoming turbulent flow from the upstream cylinder and the vortex street of the upstream cylinder. According to the characteristics of the forces in frequency domain, they can be subjectively classified into three categories:

- Vortex induced forces

Due to the alternative vortex shedding behind the downstream cylinder, the forces on the downstream cylinder present a significant periodical signature, which often is affected by the existence of the upstream cylinder. The experimental observation shows that the frequency of vortex shedding on the downstream cylinder tends to be influenced by frequency of upstream cylinder's wake when the two cylinders are at moderate spacing, i.e. around 4 to 5 diameters. However, such a vortex shedding interaction will diminish with

the further increase of the spacing. Eventually, the downstream cylinder will behave as a solitary cylinder.

Compared to the solitary cylinder, the vortex-shedding induced forces generally tend to be larger. Arie et al (1983) investigated the oscillating lift and drag forces on the upstream and downstream cylinders. It is found that,

- The rms (root mean square) of lift and drag on the downstream cylinder is much larger than upstream cylinder for spacing up to 7 diameters. When the spacing between the two is larger than 10 diameters, the difference to the solitary cylinder is by a small amount.

- For the upstream cylinder, the rms of lift was extremely small for the spacing less than critical whereas it was approximately equal to that for a single cylinder beyond the critical spacing.

- For the downstream cylinder, the rms lift was strongly dependent on the spacing and amounted to as high as 2.8 times the value found for a solitary cylinder at the spacing of 4 diameters.

- The rms drag for both cylinders was only weakly dependent on the spacing.

Figure 1.12 shows a comparison of rms of lift and drag on the upstream and downstream cylinders. Similar conclusions can be found for the staggered arrangement (Moriya & Sakamoto, 1985).

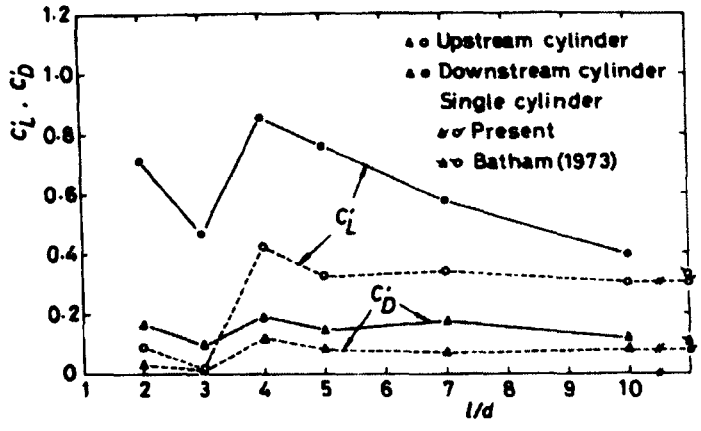

Figure 1.12 Rms lift and drag coefficients plotted against non-dimensional spacing *l/d* for tandem arrangement. Lines for visual aid only, from Arie et al (1983).

- Buffeting force

The inflow to the downstream cylinder is composed of the vortices, which are shed from the upstream one, and embedded within high turbulence. Such a flow produces a temporally random force on the cylinder. In frequency domain, the force spectrum exhibits a broadband nature. Most of the time, the response of the cylinder to such an excitation is relatively small due to the excitation energy is distributed across a broad band of frequency rather than concentrated. The significance of such motion is mainly to contribute towards noise radiation, which is not a concern in offshore engineering. Therefore, research on this subject is not of much interest to the offshore engineering.

- Time averaged force

The third kind of force, which is the focus of present study, is named as time-averaged force. Such a force definition is rather subjective. In practice, all the vortex induced forces, the buffeting force and time averaged force are mixed together to give a total force signal on the cylinder. The time-averaged force can be treated as an average effect of the flow. It is the mean component of the total force signal. In the case of solitary cylinder, it has a

zero component in the cross-flow direction and the mean drag force in the streamwise direction. However, when the downstream cylinder is located within the wake, there is not only the drag force component, but also a nonzero cross-flow component, namely the lift force. The interaction effect on the downstream cylinder's force is significant even when the spacing extends over hundreds of diameters. Figure 1.13 shows the measured drag forces on the upstream and downstream cylinders respectively. This is the first measurement result about two cylinders interaction forces. It was represented by the difference between the drag force measured when there is interaction and the force measured on the solitary cylinder. Figure 1.14 shows the vector of the lift forces and the drag force difference between interaction drag and solitary cylinder drag. Evidently, within the wake interaction, the drag force on the downstream cylinder tends to be reduced. The lift force on the downstream cylinder tends to attract the downstream cylinder towards the wake centreline. Also there is a very small region in the vicinity of the upstream cylinder, in which the drag force increases, beyond which there is no interaction. The figure also indicates the different regions of wake interaction and combined proximity and wake interaction. A further investigation will be carried out in Chapter II.

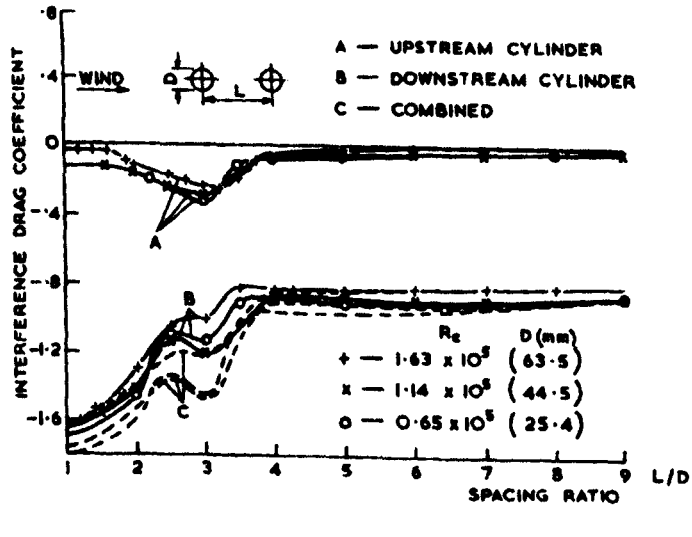

Figure 1.13 Interference drag coefficient for tandem cylinders (Biermann and Herrnstein, 1933).

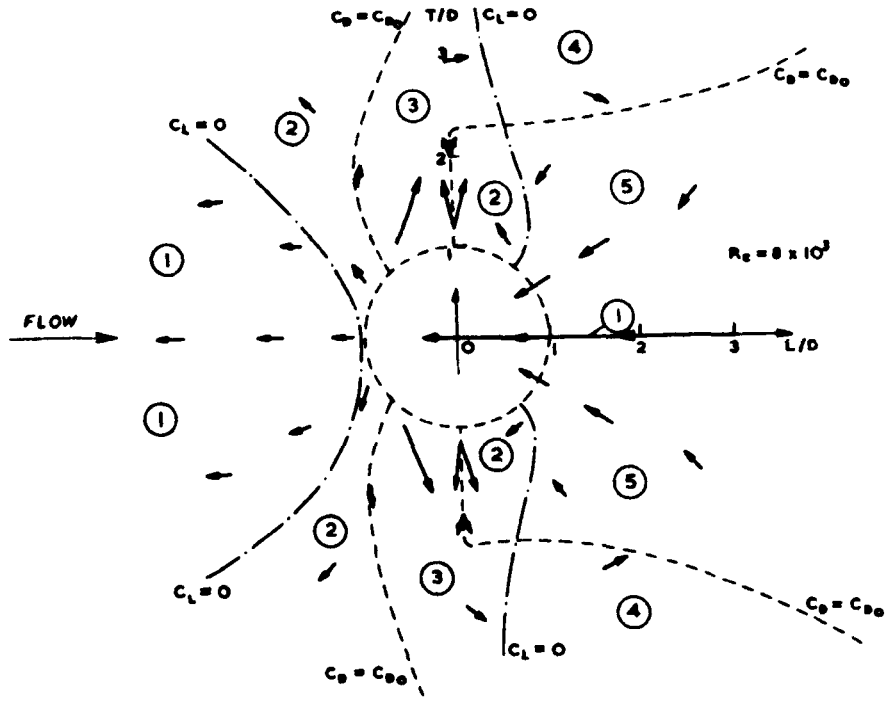

Figure 1.14 Interference force coefficient for all arrangements, from Hori (1959).

Reynolds number effect

The effects of Reynolds number are important for solitary circular cylinder cases. On the other hand, Price and Paidoussis (1983) measured the drag and lift force on the downstream cylinder in the staggered arrangement. Their results at Re=5.3×10^4 were almost in agreement with those of Zdravkovich and Pridden (1977). The effect of Reynolds number in the range of (1.7~8.6) $\times10^4$ was investigated for a number of wake positions and found to be negligible, suggesting that in this subcritical range, Reynolds number does not have a significant effect on the force coefficients.

Nevertheless, from the experience on the solitary cylinders, it is well known that the wake differs significantly when the flow changes from subcritical into postcritical region. Generally the wake is narrowed considerably. Therefore, the forces on the downstream cylinder can change significantly when the flow is in the postcritical Reynolds number. As

stated at the beginning of this thesis, this study takes marine risers as the background. Reynolds number effect is not a concern in the thesis.

1.4.2.3 Flexibly Supported Two Cylinders

When either one or both cylinders are elastic and vibrate, the flow field becomes significantly more complicated because of the interaction of the fluid flow and the cylinder's motion. To engineers, unfortunately this is more likely the case in reality.

Compared to the fixed cylinder interaction, the study on the dynamics of the interaction is relatively fragmented, this may largely be attributed to a much more complicated system presented to the researchers. The factors which may govern the dynamics of the system include:

- The inflow to the cylinder pair, such as the uniformity of the flow, flow turbulence intensity, etc.

- Reynolds number, which determines the viscous effect of the flow.

- Mechanical system characteristics of the two cylinders. Either one of the cylinders is flexible or both of them are flexible. If both cylinders are flexible, the characteristics of the mechanical system of the two can either be identical or different.

- The arrangement of the two cylinders, i.e. the streamwise and transverse spacing between each other.

- The coupling of the fluid and structural dynamic system, i.e. the relation between the fluid vortex shedding excited frequency and the natural frequency of the mechanical system. Also the weight between the fluid force and mechanical force.

Associated with all these factors, the downstream cylinder may exhibit different dynamic behaviours, the most significant ones known so far include,

- Vortex induced vibration
- Wake induced fluidelastic instability (galloping, flutter)

They are elaborated in the following sections respectively.

1.4.3 Vortex-Induced-Vibration

Amongst the two kinds of dynamic behaviour, vortex-induced-vibration is a relatively well-researched subject. Compared to the solitary cylinder, the excitation to the downstream cylinder is affected by the upstream cylinder's vortex shedding and the turbulence formed in its wake, as evidenced by the oscillating forces on the downstream cylinder (Figure 1.12).

A detailed investigation of two tandem arranged cylinders with spacing between 1.2 to 5 (King & Johns, 1976) show that complex mutual interactions can arise between the flow, vortex shedding and the motion of the cylinders in such spacing. The dynamic response of the cylinders is a function of spacing, reduced flow velocity, mass ratio, and damping value. The response is particularly dependent on the spacing. Their observations can be summarised as follows:

- When spacing is smaller than 2.75, symmetric vortices are shed from both cylinders in the range of 1.25 to 2.5 of the reduced flow velocity, and both cylinders will oscillate in the in-line direction provided the mass-damping ratio is less than 2.4.
- When spacing is larger than 2.75, for reduced flow velocity within 1.25 to 2.5, the upstream cylinder is oscillating in-line and shedding symmetric vortices but the downstream cylinder do not oscillate and a wide turbulent wake is found.

- When reduced flow velocity is within 2.7 to 3.8, for all the spacing within 1.5 to 7, the alternative vortex shedding from the upstream cylinder tend to reinforce the shedding process on the downstream cylinder and the amplitude of the downstream cylinder is larger than the upstream cylinder.

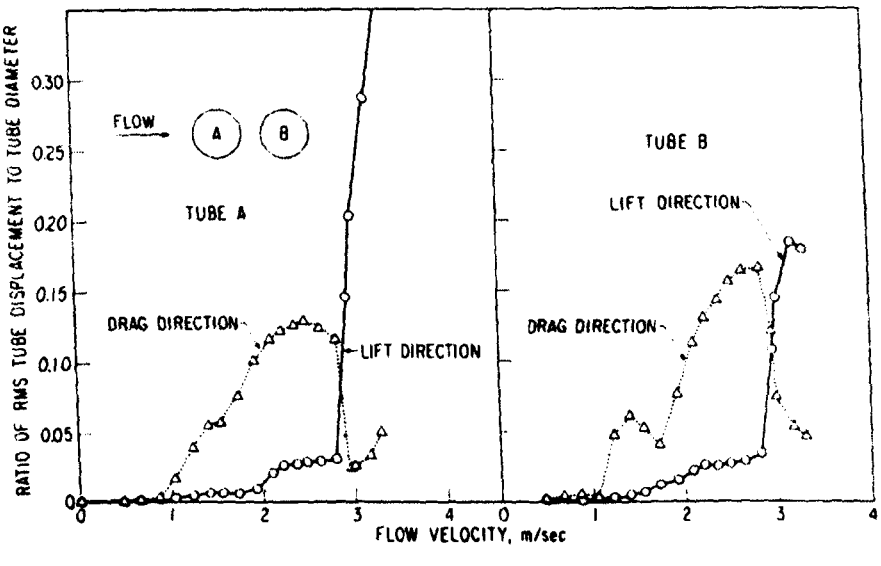

Figure 1.15 Response of two cylinders in tandem as a function of flow velocity, the drag and lift force direction refers to streamwise and cross-flow direction respectively. From Jendrzejczyk *et al* (1979).

The above results were later confirmed by Jendrzejczyk *et al* (1979). Though the later experiment found the response of the downstream cylinder was not always larger than the upstream cylinder. Figure 1.15 shows the response of the two cylinders at the spacing of 1.75. Figure 1.16 shows the orbital paths of two cylinders at several flow velocities equal to 1.7 and 3.0, respectively. It is seen that cylinder motion changes from motion predominantly in the drag direction to lift direction with the flow velocity increases. The two cylinders vibrate out of phase when they execute large oscillations. The orbital paths bend in the downstream direction.

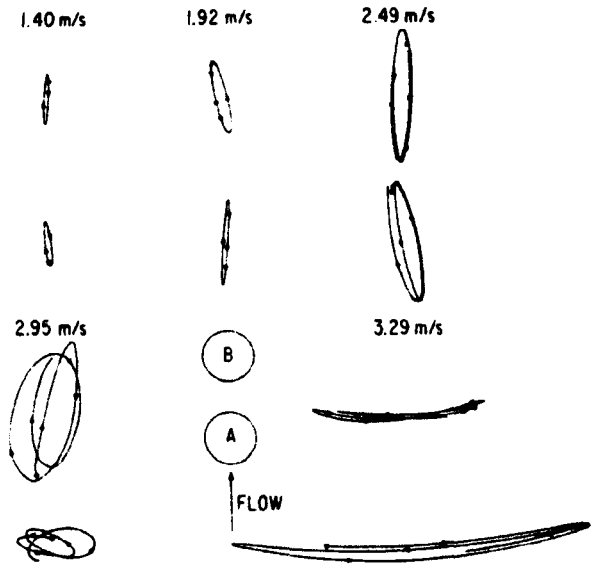

Figure 1.16 Cylinder displacement as a function of flow velocity. From Jendrzejczyk *et al* (1979).

1.4.4 Wake Induced Fluidelastic Instability (Flutter, Galloping)

Wake induced fluidelastic instability refers to such a state that when the downstream cylinder is sitting in the wake of the upstream one, any small disturbance to the system can lead the downstream cylinder to an unstable state, i.e. the small disturbance either be amplified to a large extent until a new balanced state is achieved, or the system breaks or collide with each other ultimately. According to the mathematical characteristics of the system lose its stability, traditionally, the instability is called wake induced galloping and wake induced flutter.

1.4.4.1 Wake induced galloping

Galloping is a behaviour first understood in civil engineering from the phenomena of a solitary bluff body, such as square or D shaped cylinder. The system only has a single degree of freedom. When the fluid force, particularly the lift force, produces fluid damping and cause the system start to have an overall negative damping, the system lost its stability. The dynamic motion associated with such a system is called galloping. The most significant feature of the galloping is its response amplitude increase almost linearly with the flow

velocity and does not disappear at large flow velocity. Therefore, it potentially will cause catastrophic result. Examples of the galloping study can be found from Cheers (1950) and Hunt and Richards (1969) for ice-coated power lines, Parkinson (1971) and Simiu and Scanlan (1986) for bridge decks. There is no galloping phenomenon for a solitary circular cylinder due to its net lift force is zero and its drag force is always positive which guarantees the damping of the system is always positive.

When the downstream cylinder is sitting in the wake, the fluid forces can produces negative system damping. There are mainly three kinds of causes to induce the downstream cylinder to galloping, i.e. gap flow, discontinuity of the flow and negative drag forces. All these occur in the near wake.

The gap flow caused galloping refers to the cases when the two cylinder is within the proximity interaction, due to the switch of the gap flow directions, there is a hysteria effect between the fluid forces and the displacement of the downstream cylinder, such a force displacement relation can trigger the instability of the system. The classical theory about this can refer to that of Robert (1966). Similar explanations are applicable to the region where the flow is considered to be discontinuous.

The negative drag induced galloping. The fluid force on the downstream cylinder is treated to be continuous with the relative displacement when the two cylinders are in the vicinity. Bokaian and Geoola (1984) measured the time-averaged forces on the downstream cylinder systematically. By fix the upstream cylinder, the downstream cylinder is restricted in the streamwise direction and free to move in the cross-flow direction, galloping is observed on the downstream cylinder. Such a dynamic behaviour is justified by the quasi-steady flow theory with the consideration of the negative drag force induced overall negative system damping. The typical feature of such galloping is that the motion

amplitude of the downstream cylinder increase monotonically with the flow speed once a critical state is reached. Therefore, unlike the vortex-induced vibration, the end result of such motion can be immediate destructive. One additional and significant finding in their experiment demonstrated that the vortex induced vibration and galloping can either coexist or they can occur one after the other, which implies that under the circumstances considered, the flow velocity for the occurrence of the galloping is well close to the condition for the lock in phenomena. Figure 1.17 shows the possible dynamic behaviour when two cylinders are arranged in the combined wake and proximity interaction regime or wake interaction regime in the water.

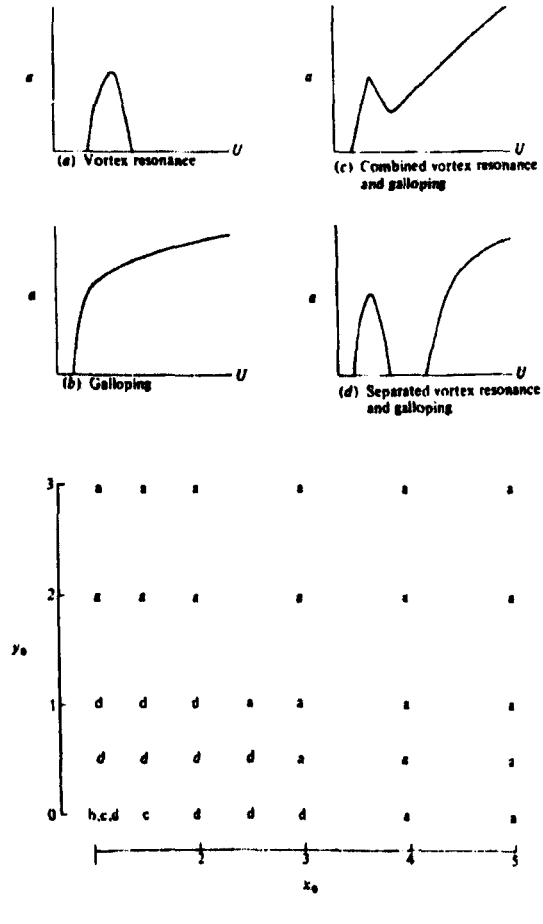

Figure 1.17 Response of a cylinder behind a fixed cylinder oscillating in the cross-flow direction only. From Bokaian and Geoola (1984).

1.4.4.2 Wake induced flutter

Flutter was originated from the aerospace terminology for coupled torsion-plunge instability of airfoil structures. In such cases, the lost of system stability is mainly attributed to the coupling of the structure stiffness and the fluid forces. Theories on the occurrence of flutter can be found in the excellent reviews by Bisplinghoff *et al* (1955), Gordon (1978) etc. The phrase "wake induced flutter" was first introduced to the cylinder interaction by Simpson(1971). It refers the situation of the wake located cylinder lost its stability under the joint action of the fluid force induced stiffness and mechanical stiffness. Therefore, sometimes, it is also called as fluid stiffness controlled fluidelastic instability (Chen, 1986). The wake induced flutter is likely to occur when the two cylinders are separated with a moderate spacing, typically around 10 diameters and the downstream cylinder is located towards the boundary of the wake such as twin power transmission lines. The phenomena has been investigated by many researchers since its discovery, examples are Price (1975), Tsui (1977, 1986), Hardy and Dyke (1995) and Hemon(1999). In general, it was found that the fluid stiffness combined with structural stiffness lead to the unstable system when the flow velocity is high enough and the coupling of the mechanical springs met specific conditions (Simpson, 1979). When the cylinders lost its stability in such a way, it will undergo a large amplitude elliptic trajectory movement in the wake. Figure 1.18 shows an example of such trajectories. When the downstream cylinder is located in the lower half of the wake, due to the drag forces in the inner wake is smaller than in the outer wake, encouraged by the cross-flow direction lift forces, to absorb energy from the flow, the trajectory will be in counter-clockwise direction (Blevins, 1990). Figure 1.19 shows a full-scale field observation of power transmission lines' motion. The instability index of the ordinate in the figure is defined as,

$$I = \frac{1}{60}\sum_i \left(\frac{A_i f_i}{80}\right)^2$$

Here l is the subspan length, A_i is the r.m.s value of the i-th component of the displacement oscillation spectrum at mid-subspan, and f_i is the associated frequency. Therefore, the instability index reflects the motion amplitude and energy. The figure illustrated the amplitude increase with the flow velocity, which explains the significant difference to the vortex-induced vibration.

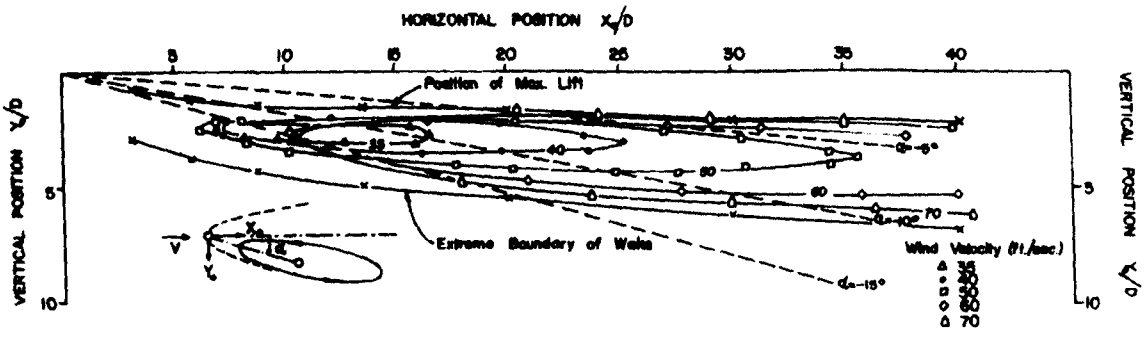

Figure 1.18 Wake induced flutter stability boundary and orbits (Cooper, 1973).

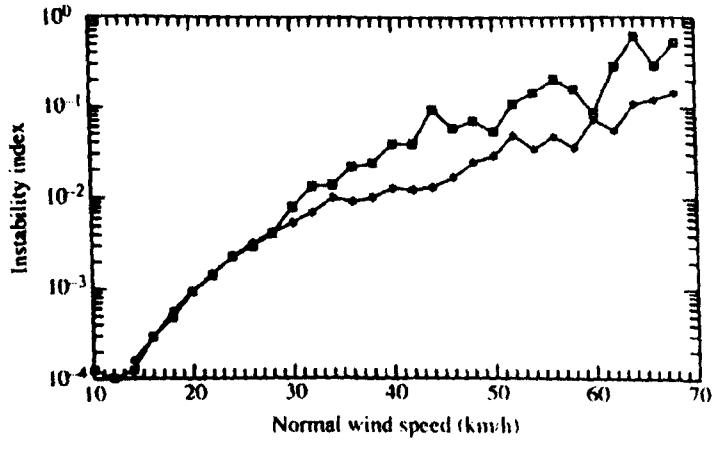

Figure 1.19 Oscillation severity as a spacing to diameter ratio: -*-, spacing a=450 *mm*, diameter d=35.05 *mm*, a/d=13.0; -+-, spacing a=450 *mm*, diameter d=24.3 *mm*, a/d=18.6. From Hardy and Dyke (1995).

Before closing the review on the galloping and flutter here, it should be noted that in the open literature, the definition of wake induced galloping and wake induced flutter is not always clearly distinguishable. For example, the wake induced flutter has been frequently

referred as wake induced galloping, such as in Parkinson (1989), Chen(1986), Brika and Laneville(1999), Jendrzejczyk *et al* (1979).

1.4.5 Researches on riser dynamics and interaction

Marine risers can be considered to be three-dimensional cylinders. Therefore, theories of flow over cylinders and the cylinders' interactions are riser's special cases in two-dimensional space. To understand the three-dimensional effect on the top tensioned vertical risers, studies have been carried out over the years on statics and dynamics of risers, most of them have its focus on the single riser circumstances.

The key features of marine riser design was first defined by Fischer & Ludwig(1966). With statics analysis, they demonstrated the importance of tensioning the riser to prevent buckling and to control deflection and stress. With the enhancement of the computing capability, and probably largely spurred by the progressive deepwater production, the dynamics of marine risers become an indispensable analysis during riser design in 1970s. As the environment in which risers located is never static, such as top vessel movement, persistent wave, variable strength current always accompany with the risers, the risers are always in motion state. Sometimes, the stress caused by the dynamics can be very significant. The tasks for such riser analysis include two parts, i.e. the dynamic response of the risers under the loading condition and to predict environmental loads on the risers. Though practically these two parts are coupled with each other and they should be treated within an integrated system. The common practice of the environmental load prediction is via Morison's equation (Morison, et al, 1950), which is essentially a quasi-steady theory. The fluid forces are dependent only on the instantaneous state of the fluid flow and risers, and it is independent of the history of riser's motion and the flow. The riser structural response analysis can generally be classified into frequency domain analysis and time domain analysis, depending on the discretisation of the response equation (Bernitsas,

1982). Analysis can be further sub-classified, for example, environmental loads include the vortex induced forces, which often has an empirical model or is a statistical model. The above mentioned Morison's equation is mostly applied to wave induced loading only, etc. At the moment, software is available for the analysis of the riser's dynamics, such as Shear 7, VIVA for the analysis of vortex induced vibration etc.

On the other hand, it was until the beginning of 1990s that marine riser interaction started to catch the attention of researchers and engineers. This is mainly due to the fact that the riser interaction is exacerbated by the deepwater condition, stated early here as a new challenge. The first designated project on this kind of riser interaction is contracted by Minerals Management Service (US department of interior), entitled "Interference/Clearance Problems of Risers in Floating Production System" (Rajabi, 1989). However, the first notable publication should probably be attributed to Huse (1993), in which he used the wake shield effect model to account for the drag force on the downstream cylinder and, subsequently, he predicted the critical flow velocity before the collision between two risers occurs. All of such attempts were designed to meet the challenge of deepwater offshore development. Nevertheless, the need for detailed force information about the downstream riser in the wake field and its complexity makes a comprehensive investigation difficult. Without a stability analysis, Huse's explanation about the mechanism for two risers collision is based on conjecture rather than on rigorous analysis. In fact, as will be discussed in the later chapters, it is rather unclear.

Little direct work has been done on the wake induced riser clashing elsewhere, except that in the last couple of years other researchers have joined in the fray (Sagatun, 1999; Li and Morrison, 2000). These recent research contributions focus upon developing simple structural models to quantify impact loading on, and possible damages to, the risers. They attempted to simplify the downstream riser as an equivalent mass that contributes to the

riser collision impact force. The possible damage can then be assessed. If the damage is considered to be tolerable, increasing riser initial spacing may not be required. At the same time as this research was being undertaken, the author realised that a lot of industry research was being done, namely Demo 2000, NDP programme and Deepstart etc., but the critical results and information remain proprietary and are not in the public domain. Up to date, to author's best knowledge, a systematic investigation on the interaction between two marine risers has not yet been seen elsewhere.

1.5 Objectives of the thesis

The main objectives of the thesis are as follows,

1) To identify the mechanism of the riser losing stability

2) To predict the critical condition under which inception of this loss of stability takes place

3) To identify the possible dynamic behaviour should the dynamic phenomena occur

4) To provide guidance to riser designers regarding how to avoid riser collision

5) To compare the phenomena and mechanism against multiple cylinder application in other engineering disciplines

6) To provide information about dynamic state before impact for the estimation of the damage that can occur should collision be unavoidable

1.6 The Structure of the Thesis

This thesis consists of ten independent but interrelated chapters. The main frame of this thesis is composed of two parts. The first part deals with cylinder interaction in two-dimensional space, with a focus on the investigation of the stability of downstream

cylinder, and the identification of the mechanism that bring the two cylinders to collide with each other. The second part deals with the three-dimensional riser interaction, with the aim of predicting quantitatively, the critical state before collision and the dynamic behaviour after occurrence of collision.

Starting with force prediction, Chapter II provides an estimation of the interaction force exerted on the downstream cylinder by using a free streamline model. The data obtained in this chapter forms the basis of the subsequent analysis.

Chapter III deals with the stability analysis, particularly by utilising the traditional Routh-Hurwitz stability algorithm, by which a significant difference between marine riser interaction and cylinder interaction application such as power lines is identified. Subsequently, stable and unstable regions under specified flow conditions are identified for the whole wake field, which clearly shows the possible bifurcation type of the downstream cylinder can occur for a pair of cylinders in water.

Chapter IV explores the potential multiple equilibrium by use of the continuation method. As the two cylinders interaction system is non-linear in nature, the identification of multiple equilibrium states is the first step towards the exploration of the non-linear characteristics of the system. This chapter shows that there can be up to four equilibrium states for a specified cylinder pair. Meanwhile, as this chapter is a sister chapter of Chapter III, the stability at each individual equilibrium state was analysed through a direct, numerical eigenvalues seeking method.

Chapter V investigated the dynamic behaviour of the two cylinders interaction, particularly after losing equilibrium. It depicts the trajectory and dynamic states when wake induced oscillation occurs.

Chapter VI describes the three-dimensional case, with statics analysis. Although substantial analysis has been made in the past regarding marine riser statics, the statics regarding the two risers interaction has not be properly addressed before. In this chapter, a detailed discussion about the statics concerned interaction effect has been presented.

Chapter VII identified the potential multiple equilibrium for a specified marine riser pair. This is an extension of Chapter IV. However, due to the three dimensional effect, the quantitative relation is different to a two-dimensional case. A non-dimensional parameter is attempted to provide some guideline data for riser designers.

Chapter VIII studied the dynamic behaviour of the riser pair, particularly when the riser pair is located in an ocean current, which is stronger than the critical condition. The trajectory and dynamic state, such as velocity before collision, the motion amplitude, and time interval between successive collisions are investigated.

Chapter IX and X provided conclusions of this thesis, and also some recommendations on the future work regarding the further investigation on this subject.

Chapter II

THE ESTIMATION OF LIFT AND DRAG FORCE ON THE DOWNSTREAM CYLINDER OF A PAIR

2.1 General Remarks

A pre-requisite for studying the dynamics of the cylinder interaction is to understand the fluid forces on the cylinders. The time-averaged forces are considered to be most responsible for the cases of fluidelastic instabilities. This chapter endeavors to find an empirical method to provide such necessary fluid force data for the subsequent analysis.

The necessity for the study of such forces began in 1970's when twin-bundled overhead transmission conductors began to be put into use, and the large movement of leeward lines caught a lot of attentions from scientists. A knowledge of the time-averaged force is a pre-requisite for the study of dynamics of leeward cylinders. Explanations for the mechanism and characteristics of such forces were diversified. The first problem for the study of such forces is the direction of the lift. Savkar(1970) used the potential theory to find the force by representing the wake of the windward conductor by a shear layer, and found the lift force is directed away from the centre of the wake, while the experiment of Price(1975) and others found the lift force is directing towards the centre of the wake. Around the nature of the lift force, there are different arguments trying to explain the cause of this force, such as the buoyancy explanation by Maekawa(1964). He suggested that the static pressure on the

centre of the wake is minimum. However, the integration of the static pressure around the cylinder in the wake shows that at most only 30 percent of the force can be attributed to this reason (Best and Cook, 1967). The resolved force of drag, suggested by Mair and Maull(1971), suggested that due to the entrainment of fluid into the wake, the flow velocity is towards the centre of the wake, so that the lift force experienced by the leeward cylinder would be a resolved component of the drag force. It was shown by Price(1976) that this amount is still far from sufficient to account for the lift force. Rawlins(1974) ascribed the lift force to the circulation. He states that, owing to the variation of turbulence and velocity across the wake of the windward cylinder, the two boundary layers from the leeward cylinder feed different amounts of vorticity into their associated shear layers. Applying Kelvin's circulation theorem to this state, Rawlins concludes that a circulation around the cylinder is built up until the rates at which vorticity is discharged from the two boundary layers are equal. He got a lift coefficient which is proportional to the transverse gradient of the drag coefficient. Price(1976) shows that such a result is 30 percent lower than the measured result, and the position of the maximum lift is outward from the measured situation. Detailed discussion on these issues may refer to Price(1976). One currently accepted idea about the nature of this kind of lift force is that there is a collective contribution from the resolved drag, wake entrainment and additional circulation along the inner side of the downstream cylinder. Their relative weight is dependent on parameters like L/D (spacing diameter ratio) and R_e (Ting et al, 1998) etc.

Up to now, to account for the time-averaged forces appropriately by using the full N-S equation solver is still impractical, either due to the limitation by high Reynolds number or the huge amount of computation time, especially when dealing with very widely spaced cylinders such as 10 diameters or more apart. Therefore, nearly all past researches were

conducted using experimental data of force to explain the dynamic behaviour of such interactions. The pioneer and typical work is Simpson (1971).

In this chapter, we consider the lift force due to the different flow separation position on the outer and inner side of the downstream cylinder. The separation position is dependent on the flow velocity around the downstream cylinder. Using the free stream line theory, the lift and drag force are estimated reasonably well, both in magnitude and distribution. It is considered that this is a useful tool for the analysis of the dynamic behaviour of the downstream cylinder, particularly when lacking the necessary large volume of experimental data.

2.2 The Estimation of Lift and Drag Force On the Downstream Cylinder

2.2.1 Concept of the Nature of the Force

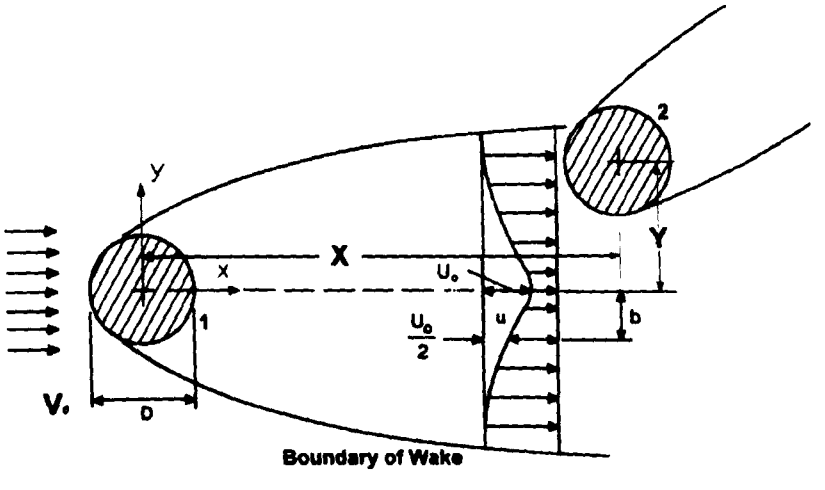

Figure 2.1 Schematic figure of the downstream cylinder located in the wake of upstream one.

Figure 2.1 is a sketch of the flow separation when one cylinder is located in the wake of another (the upstream cylinder and downstream cylinder are referred to as cylinder 1 and cylinder 2 respectively hereafter and in the results presented). Experiments show that the separation point on the inner side of the downstream cylinder is more rearward than that on the outer side. When cylinder 2 is located in the upper half of the wake of cylinder 1, inner side and outer side means the lower, upper part of cylinder 2 respectively as shown in Figure 2.1. From the knowledge of flow separation around a cylinder in uniform low turbulence free stream, it is known that the pressure after separation is nearly equal, especially at the sub-critical Reynolds number region (wake zone, the pressure in this area is called base pressure). The lowest pressure is usually lower when the separation point is located more rearward for the same base pressure. Considering the situation in Figure 2.1, this mechanism makes the pressure on the upper half of the downstream cylinder higher

than that of the lower half. It is believed in this investigation that the above mechanism is the source of the lift force which is directed towards the centre of the wake.

Considering the magnitude of the lift and drag, according to the above suggestion, the asymmetric separation and the base pressure are vital important factors. The base pressure affects the drag force and the asymmetrical separation dictates the lift force. This will also be discussed in the later numerical test about the sensitivity of parameters of base pressure and separation position to the drag force.

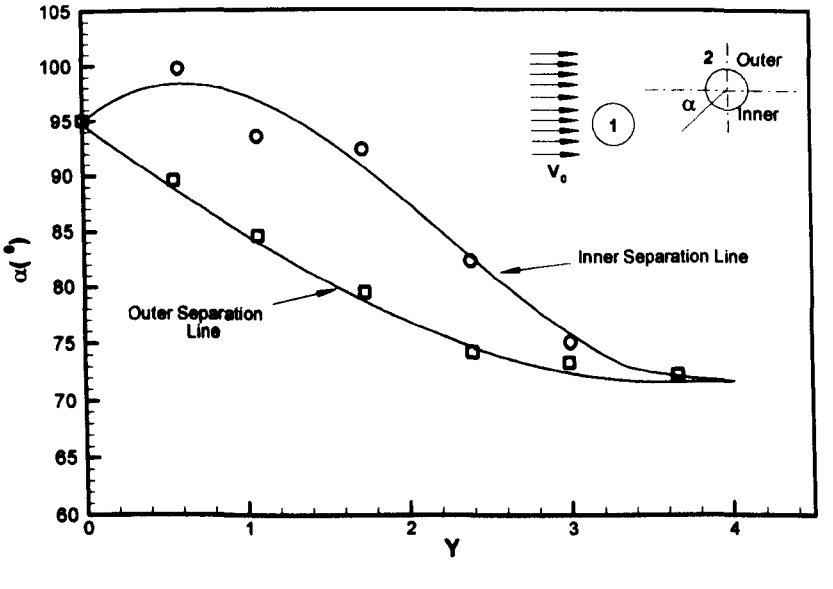

Figure 2.2 Separation position for the leeward conductor, X=6.0, reproduced from Price(1976).

The above hypothesis suggests that it is necessary to find the separation position and base pressure before proceeding to calculate the lift and drag force on the downstream cylinder. Figure 2.2 is a reproduction of an experiment result found by Price (1976). The Figure shows the variation of separation position with different transverse locations at longitudinal spacing X=6. It is clear to see that when Y=0, the separation position is same for the outer side and inner side due to the symmetric characteristics of the wake. The separation angle on the outer side decreases with the increase of Y. Meanwhile, the separation angle on the

inner side increases when the cylinder is moved outward near the wake centre. When the downstream cylinder is located around Y=0.5, the separation position on the inner side is in the most rearwards position. This corresponds to the location when the inner side is located on the centre line of the wake of the upstream one. When the cylinder moves outwards further, the separation position shifts forwards with the increase of Y. Moreover, we can see a very interesting phenomenon, that is that regardless of whether it is the inner side or outer side, when they are at the same transverse location, the separation position is similar.

To identify such a relation of the flow separation with corresponding flow is never an easy matter. Generally, it is incontestable that the flow separation position is related to Reynolds number, turbulence intensity of upstream cylinder's wake flow which impinged on the downstream cylinder, the downstream cylinder surface roughness, the pressure gradient across the upstream cylinder's wake etc. However, as the surface roughness is fixed for a specific situation, it can not be the reason of the variation of lift force across the wake. Although upstream cylinder wake turbulence intensity can be important, a direct relation between separation position and turbulence intensity is hardly persuasive. On the other hand, Reynolds number and pressure gradient are parameters closely related to flow velocity, and moreover, the wake turbulence characteristics are more or less related to wake velocity in some way. It is suggested in this thesis that the flow velocity around the downstream cylinder dictates the flow separation. The quantified relationship between flow separation and flow velocity will be presented in the subsequent sections.

2.2.2 Free Stream Line Model for the Prediction of Forces

The use of free stream theory can be dated back to Kirchhof's attempt to resolve the D'Alembert paradox(1869). The basic hypothesis is that the wake zone is an equal pressure area. In 1970s, free stream line theory was used to study the wake geometric shape of flow

over bluff bodies(Parkinson and Jandali, 1970) and also to correct the blockage effect of wind tunnel walls (Bearman, 1975). Generally, mapping transformations were used, or very few sources (two or four) were distributed to represent the effect of the wake for symmetrical problems. A brief introduction to the numerical model used in this thesis is presented here, which is considered to be more powerful in dealing with the asymmetrical problems.

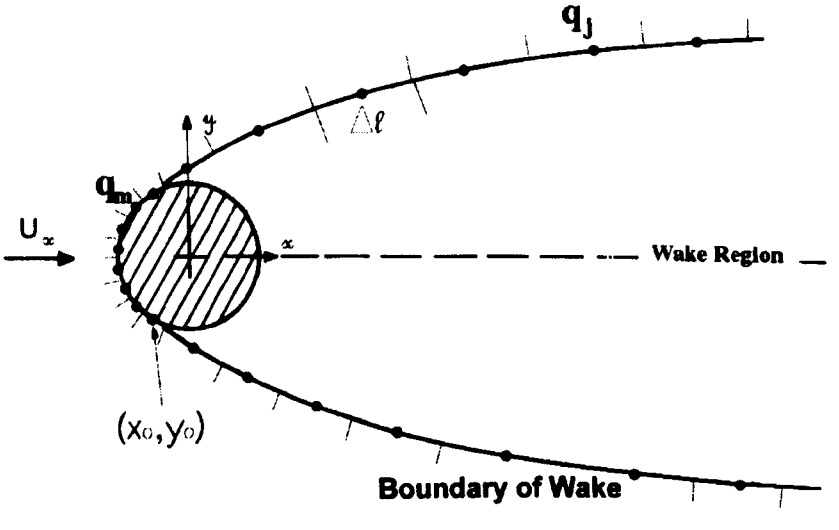

Figure 2.3 Schematic figure for Free Stream Line Model.

As shown in Figure 2.3, the flow outside the wake and body are considered as ideal flow, the wake region is considered to be an equal pressure area. The surface where singularities are distributed includes the wake boundary (free stream line) and the wetted surface of the body, i.e. the region where the flow has not separated. N vortex elements are distributed on the wetted surface of the cylinder, their strengths are unknown $\Gamma(q_n)$, $(n = 1,2,...N)$. M vortex elements are distributed along the free stream line, their strengths are equal to the inflow velocity (including two vortex elements whose lengths are infinite long at both ends of the above boundary to ensure that no flow will leak into the wake). The actual location of the free stream line is unknown. There are N control points on the wetted surface of the

body at which the impeachable condition must be satisfied. Thus, by supposing a location of free stream line, we can get the strength of the vortex on the wetted surface by solving the N equations with N unknown. The control equation can be written as (Lewis, 1991):

$$-\frac{1}{2}\Gamma(q_m)+\sum_{\substack{n=1\\ n\neq m}}^{N}\vec{n}\times[\Gamma(q_n)\vec{K}(q_m,q_n)\times\vec{n}]+\sum_{j=1}^{M}\vec{n}\times\left[U_\infty\vec{K}(q_m,q_j)\times\vec{n}\right]+\vec{n}\times\left(U_\infty\vec{i}\times\vec{n}\right)=0 \quad (2.1)$$

Here, $\vec{R}(q_m,q_n)$ is the vector from q_n to q_m. $\vec{K}(q_m,q_n)$ is the induced velocity at q_m by vortex located at the position q_n of unit strength,

$$K(q_m,q_n)=\frac{\vec{k}\times\vec{R}(q_m,q_n)}{2\pi\left|\vec{R}(q_m,q_n)\right|^2} \quad (2.2)$$

$\Gamma(q_n)$ is the unknown vortex strength at position q_n, U_∞ is the free inflow velocity, $\vec{K}(q_m,q_j)$ is the induced velocity at q_m by the unit strength vortex located on the wake boundary q_j, $\vec{n}$ is the local unit normal vector at q_m, $\vec{i}$ is the unit vector in the direction of axis x, $\vec{k}$ is a unit vector which is along the axis of the cylinder and point towards readers.

Apparently, the requirement that the pressure on the free streamline is equal everywhere can not be guaranteed by this solution immediately. Adjustment of the location of the free streamline has to be made. The correction is made as follows:

Assuming the free streamline behaves like a rope or chain, the position at separation point is fixed. After each time, the induced velocity at free stream line is calculated. The free streamline is realigned according to the local velocity direction in such a way that the flow

in the vicinity of the free stream line is parallel to the free stream. The co-ordinates of the free stream line are corrected by following equations:

$$\begin{cases} \Delta x_j = \dfrac{u_j \cdot \Delta l}{\sqrt{u_j^{\,2} + v_j^{\,2}}} \\ \Delta y_j = \dfrac{v_j \cdot \Delta l}{\sqrt{u_j^{\,2} + v_j^{\,2}}} \end{cases}$$

$$\begin{cases} x_i = x_o + \sum_{j=1}^{i} \Delta x_j \\ y_i = y_o + \sum_{j=1}^{i} \Delta y_j \end{cases} \tag{2.3}$$

Here, u_j, v_j are x, y direction components of the local velocity at j-th element on free stream line respectively. Δl, which is the length of the vortex element on the free stream line, is set equal for every element in the present calculation. x_o, y_o are the co-ordinates of the separation point. x_i, y_i are co-ordinates of the i-th element on the free stream line. In the present calculation, the velocity at the separation point is related to the base pressure, and the flow velocity at the separation point is set to be tangential to the cylinder surface at that position. After getting the new position of the wake boundary, repeating above procedures until the free stream line can reach a position, where the equal pressure can be ensured. The solution at such a state is the final solution for the specified flow separation problem.

2.2.3 Wake Flow Velocity of a Solitary Cylinder

For the interaction between two cylinders, the inflow of the downstream cylinder is the wake of upstream cylinder as shown in Figure 2.1. In order to specify the inflow of the downstream cylinder, it is necessary to explain the wake flow field characteristics of a solitary cylinder in the first place. By applying the momentum theorem to a control surface which encloses the cylinder to be studied, based on Prandtl's mixing length hypothesis, the

first expression for cylinder wake flow velocity was obtained by Schlichting (1968). The expression can be one of the following two forms:

$$\begin{cases} u(x,y) = U_o(x)e^{-0.693\left[\frac{y}{b(x)}\right]^2} \\ b(x) = 0.25 \cdot \sqrt{C_{D1} \cdot D_1 \cdot x} \\ U_o(x) = V_o \cdot \sqrt{\frac{C_{D1}D_1}{x}} \end{cases} \tag{2.4}$$

Referring to Figure 2.1, here

u is the wake velocity deficit at the position x, y;

U_o is the maximum wake velocity deficit on wake centerline at $(x,0)$;

C_{D1}, D_1 are the drag coefficient and diameter, respectively, of the cylinder located in free stream. When interactions between two cylinders are being investigated, they refer to the upstream cylinder;

b is the half width of the wake which is defined as: When $y = b$, $u \approx 0.5U_o$.

Thus the wake flow velocity U can be expressed as:

$$\frac{U(x,y)}{V_0} = 1 - \sqrt{\frac{C_{D1}D_1}{x}} e^{-0.693\left[\frac{y}{b(x)}\right]^2} \tag{2.5}$$

Alternatively, the expression can also be written as:

$$\begin{aligned} b_w &= k_b\sqrt{xC_{D1}D_1} \\ \frac{u}{V_0} &= k_u\left(\frac{x}{C_{D1}D_1}\right)^{-\frac{1}{2}}\left\{1-\left(\frac{y}{b_w}\right)^{\frac{3}{2}}\right\}^2 \end{aligned} \tag{2.6}$$

Here, b_w is the width of the wake, i.e. distance from the wake centreline to the wake boundary. k_b, k_u are constants which can be derived from theoretical analysis or obtained from experimental results. It is approximately that $k_b \approx 0.569$, $k_u \approx 0.976$. Essentially the two expressions above are same. In this chapter and subsequent analysis, the first form is utilised.

Above results are valid only for the far wake field, for example, $x/D_1 > 10$. When the distance x is small, the wake velocity deficit tends to be over predicted and the width of the wake tends to be under predicted. Modifications need to be introduced. One example was made by Huse (1993). He supposed the wake originated at somewhere in front of the location of the cylinder. It is named as a virtual source. Thus the distance x from the cylinder location in (2.4) is replaced by modified distance x_m which is measured from the virtual source, as shown in Figure 2.4.

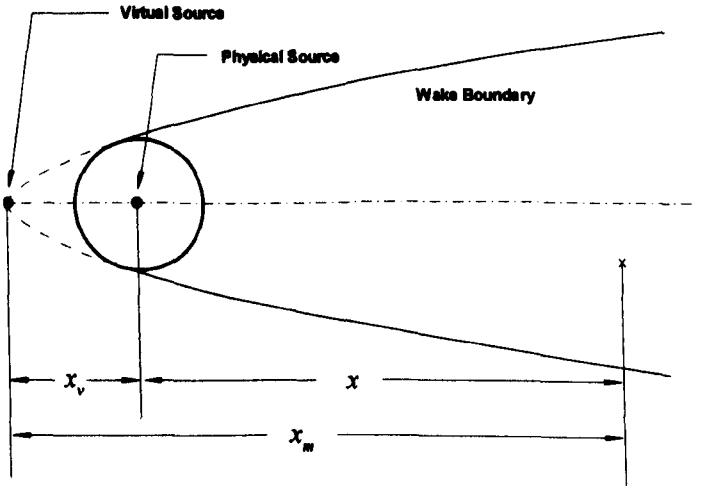

Figure 2.4 Schematic figure about longitudinal distance modification.

$$x_m = x + x_v$$

x_v is the distance from virtual source to the cylinder location. It is suggested as (Huse, 1993):

$$x_v = 4D_1/C_{D1}$$

The modified wake flow velocity expression are as follows[1]:

$$u(x,y) = U_o(x)e^{-0.693\cdot\left[\frac{y}{b(x)}\right]^2}$$

$$U_o(x) = V_o \cdot \sqrt{C_{D1} \cdot D_1 / x_m} \tag{2.5}$$

$$b(x) = 0.25 \cdot \sqrt{C_{D1} \cdot D_1 \cdot x_m}$$

Apparently the effect of above x_v will diminish with the increase of distance x, which is in accordance with the distance modification requirement.

2.2.4 Determination of Separation Angle and Base Pressure

As discussed above, the separation position and base pressure play vital roles in determining the lift force and drag force acting on the downstream cylinder. For a specific cylinder (with a defined Reynolds number, surface roughness etc), it is assumed that the separation is mainly dependent on the flow velocity. The reasoning and evidence of this has been discussed in section 2.2.1. The downstream cylinder functions like a blunt airfoil. Figure 2.5 shows the sketch of the flow separation position with the flow velocity. As shown in the figure,

$$\begin{aligned} \alpha_1 &= (\alpha_o + \alpha_i)/2 \\ \alpha_2 &= (\alpha_o - \alpha_i)/2 \end{aligned} \tag{2.6}$$

[1] In original paper, the coefficient –0.693 was misprinted as –0.639

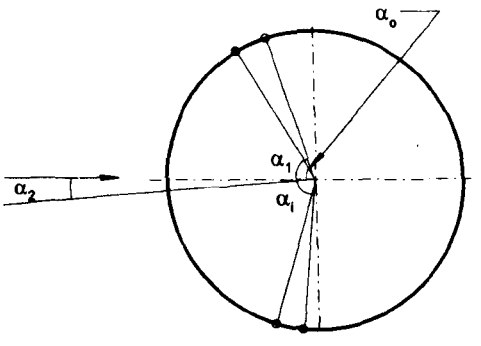

Figure 2.5 Schematic of flow separation angle.

Here α_1 represents the average separation angle. It is considered that the average separation angle of the downstream cylinder is dependent on the inflow velocity at the centre of downstream cylinder. α_2 is the difference of the separation angle between outer and inner position. α_0, α_i are separation angles on the upper and lower part of the cylinder respectively. The difference of the separation position was considered to be dependent on the gradient of the velocity at the location of the downstream cylinder. The investigation made in this thesis is mainly focused on the sub-critical Reynolds number region, and the following relation is suggested.

$$\alpha_{o,i} = \alpha_f\big|_{\mathrm{Re}} + c_1\left(\frac{u}{V_0}\right)^{c_2} \pm\left[c_3\left(\frac{D}{U}\frac{\partial u}{\partial y}\right)+c_4\left(\frac{D^3}{U}\frac{\partial^3 u}{\partial y^3}\right)\right] \tag{2.7}$$

Here $\alpha_f\big|_{\mathrm{Re}}$ represents the flow separation position when a solitary cylinder is sitting in the free stream at Reynolds number of Re. By regressing Price's experimental results at the longitudinal position of X=6, the coefficients are obtained as follows:

$$\begin{cases} c_1 = 30.0158 \\ c_2 = 0.2054 \\ c_3 = -32.01 \\ c_4 = -4.98 \end{cases} \tag{2.8}$$

The regression curve is plotted in Figure 2.2.

The base pressure is another complex variable. Williamson (1996) shows that the base pressure is sensitive to the process of vortex formation in the near wake, which itself is affected strongly by the evolution of various two-dimensional and three-dimensional wake instabilities, as Reynolds number are varied. However, the experiments show that when Reynolds number is within the region of about 10^4 to 10^5, the base pressure does not change much. When the cylinder is located in the wake of another one, there is pressure head loss in the wake. The static pressure of the oncoming flow in the upstream cylinder wake differs considerably to the free stream. It is not practical to relate the downstream cylinder wake pressure to the free stream parameter. Therefore, the downstream cylinder is treated as a single cylinder located in a high turbulence flow. Based on the successful experience of using the wake shield effect to explain the multiple cylinder drag force (Huse, 1993), and also, some experiments that show that turbulence intensity has very little effect on the base pressure (Bearman, 1989), in the present investigation, the base pressure is set to be equal to that of a single cylinder located in free stream. Similarly, this reflects that the variation of the drag force coefficient acting on the downstream cylinder is mainly due to the variation of the wake flow velocity.

2.3 Prediction for a Solitary Cylinder Using Free Stream Line Model

A single cylinder in a uniform flow is considered here and two scenarios are calculated. One is for flow separated at 80^0 with base pressure coefficient -0.96. The other is for flow separated at 117.5^0 with a base pressure of -0.38. These two scenarios may represent laminar flow separation and turbulent flow separation respectively. The calculation used 50

vortex elements on the wetted surface and 50 on the wake boundary. Figure 2.6 is a comparison of the calculated result with the experiment conducted by Roshko (1954) and Bearmean (1968) respectively. From Figure 2.6, we can see that the prediction of the pressure distribution agrees very well with the experiment result. For completeness, two wake boundary shapes are also presented here (Figure 2.7). We can see that the wake in the two scenarios differs significantly in size. This is also in agreement with the experimental result.

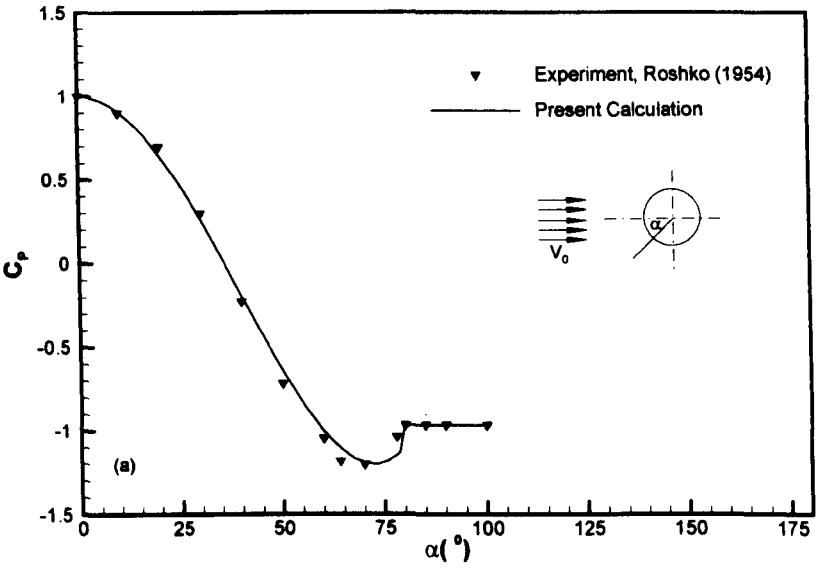

Figure 2.6 (a) Pressure distribution on the wetted surface, Separation at 80^0, C_{pb}=-0.96.

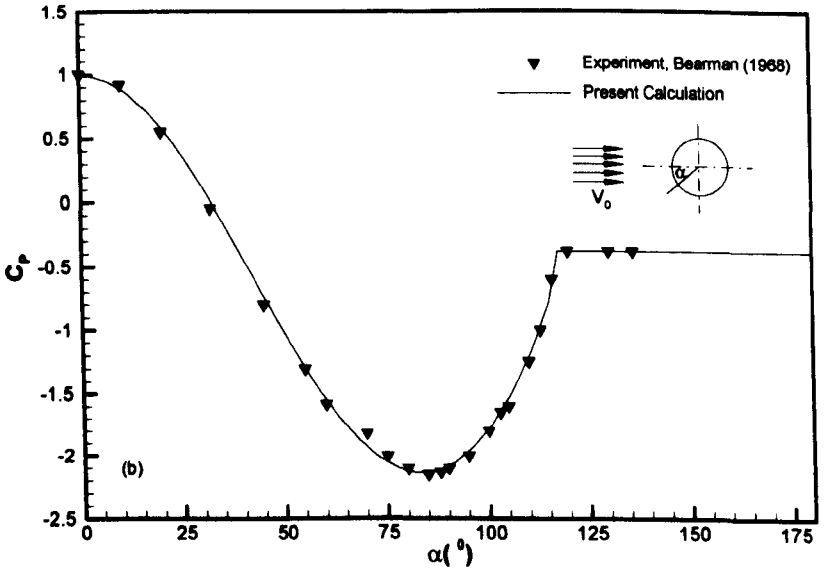

Figure 2.6(b) Pressure distribution on the wetted surface, Separation at 117.5^0, C_{pb}=-0.38.

2.3.1 Sensitivity of Base Pressure and Separation Position to Drag Force

In order to examine the role which base pressure and separation position play in lift and drag force calculations, some numerical tests have been carried out on the sensitivity of

such parameters to the force. For a single cylinder in uniform flow, the separation is symmetric.

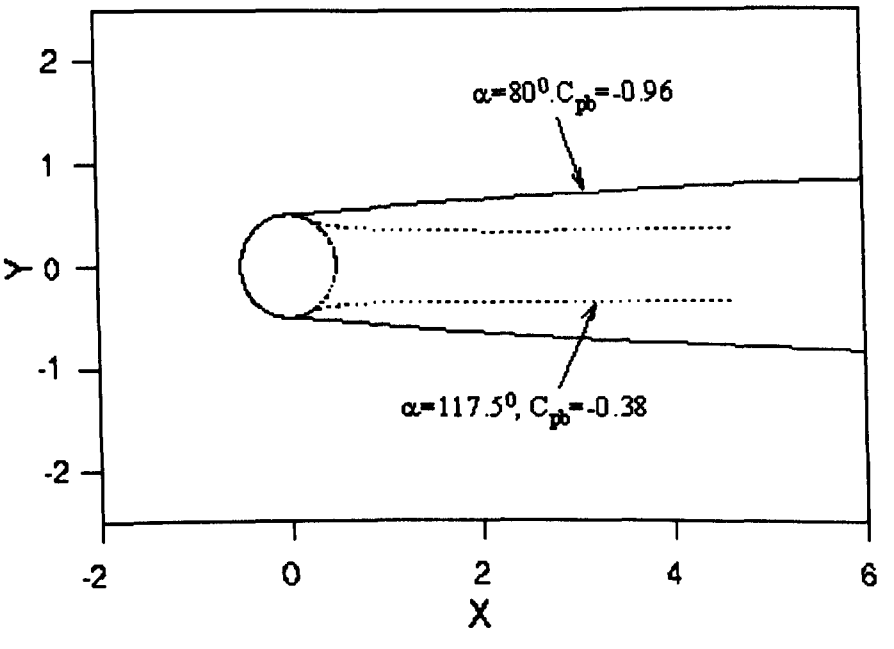

Figure 2.7 Wake geometrical shape for two different separation scenarios.

If the base pressure is set as constant, and the separation angle varied from 81^0 to 110^0, then Table 2.1 is the calculated result. It should be noted that as this is a numerical test, the separation angle is set subjectively. Nevertheless, in reality, the base pressure and separation position are related in certain ways, so they should not be set arbitrarily. We can see that when the separation position is changed from 81^0 to 110^0, while keeping the base pressure constant (this is a very significant change in the separation position), the change of the drag coefficient only amounts to 4%. If, on the other hand, the separation position is kept fixed, and the base pressure is change from -1.12 to -0.8, about 29% increase of the base pressure, the drag coefficient is reduced from 1.188 to 0.883, about 26% of the decrease.

These results show that the drag coefficient is sensitive to the value of the base pressure, whilst very insensitive to the separation position. It is easy to infer, from the discussion

about the nature of the lift force, that the lift force is sensitive to the separation position. In section 2.3 it was mentioned that the base pressure for a cylinder in wake is chosen as equal to that when it is located in the free stream. One reason is that, because Huse(1993) predicted the drag force for multiple cylinders successfully by supposing the drag coefficient in the wake to be equal to that in free stream, the result of this hypothesis is consistent with Huse's methodology, according to the numerical test conducted here about the relation between the base pressure and drag coefficient.

Table 2.1 Numerical test about sensitivity of base pressure and separation position on drag force.

NO.	C_{pb}	Separation angle α^0	C_D
1	-1.12	81^0	1.188
2	-1.12	95^0	1.167
3	-1.12	110^0	1.138
4	-1.0	81^0	1.074
5	-0.9	81^0	0.979
6	-0.8	81^0	0.883

2.4 Prediction of Lift and Drag Force of the Downstream Cylinder

When one cylinder is located in the wake of another, the incoming flow velocity for the downstream cylinder differs from the free stream velocity, as expressed in section 2.2.3. Apparently the velocity where the downstream cylinder covers is not uniform. The same method as Huse(1993) used is applied here to account for the average incoming velocity for the downstream cylinder, i.e. first taking rms (root mean square) value of u which covers the area of the downstream cylinder. The incoming velocity is then obtained by

subtracting it from the free stream velocity: $U = V_o - rms(u)$. Such a value is used in the following calculation of lift and drag force of the downstream cylinder.

2.4.1 Two Cylinders with Same Diameter(D_1:D_2=1:1)

The prediction of the lift and drag force on the downstream cylinder is based on the same method as for a single cylinder, provided that the separation position and base pressure are known. The result for C_D, C_L is scaled to free stream velocity by the consideration of the wake velocity as stated in section 2.2.3. According to the philosophy discussed in Section 2.3, the separation angle is first sought, then the calculated sample is referred to the Reynolds number around the order of 10^4, where the drag coefficient of a solitary cylinder in a free stream is about 1.2. This sets the base pressure at around -1.12. The calculated separation angles at X=12 and X=18 are shown in Figure 2.8. Under the above condition,

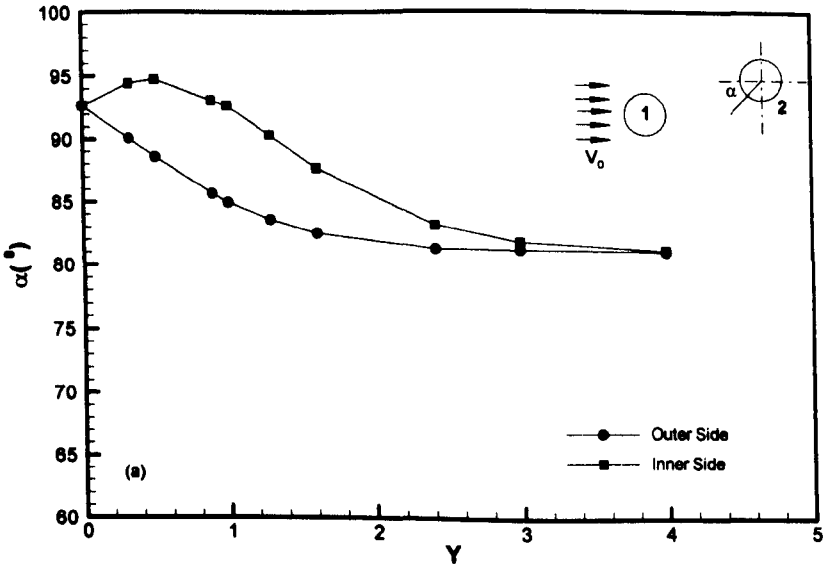

Figure 2.8(a) Separation angle profile at X=12.

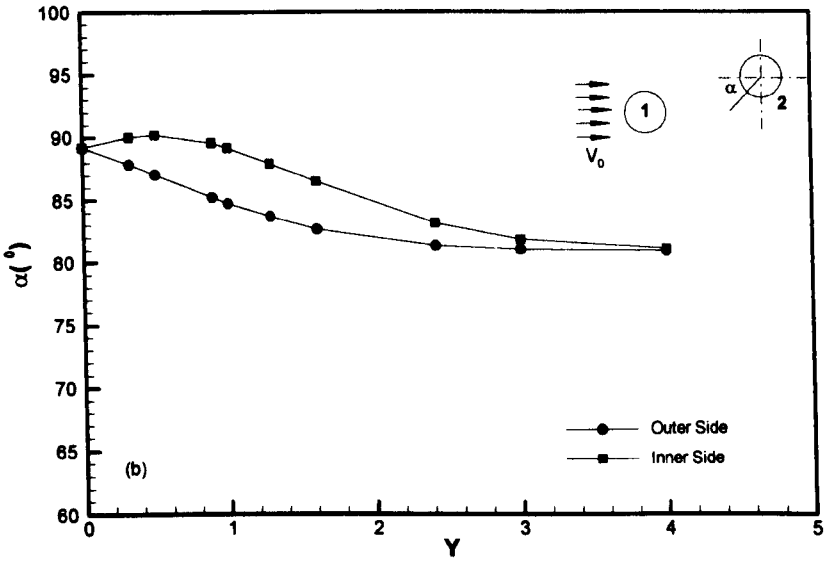

Figure 2.8(b) Separation angle profile at X=18.

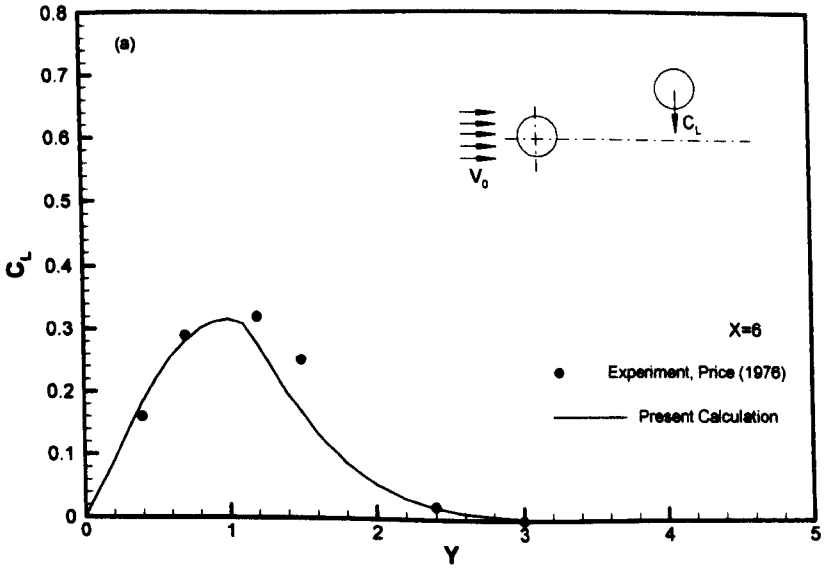

Figure 2.9(a) Variation of time-averaged force on the downstream cylinder across the wake, lift.

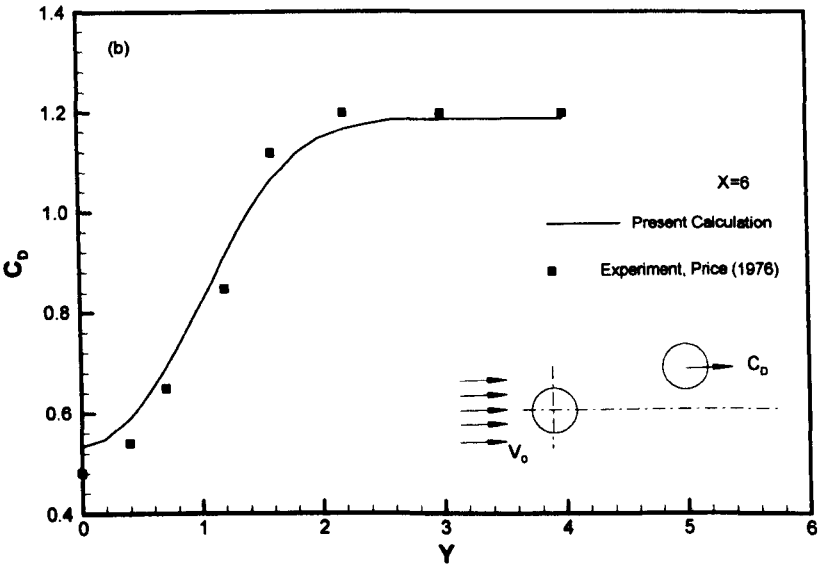

Figure 2.9(b) Variation of time-averaged force on the downstream cylinder across the wake, drag.

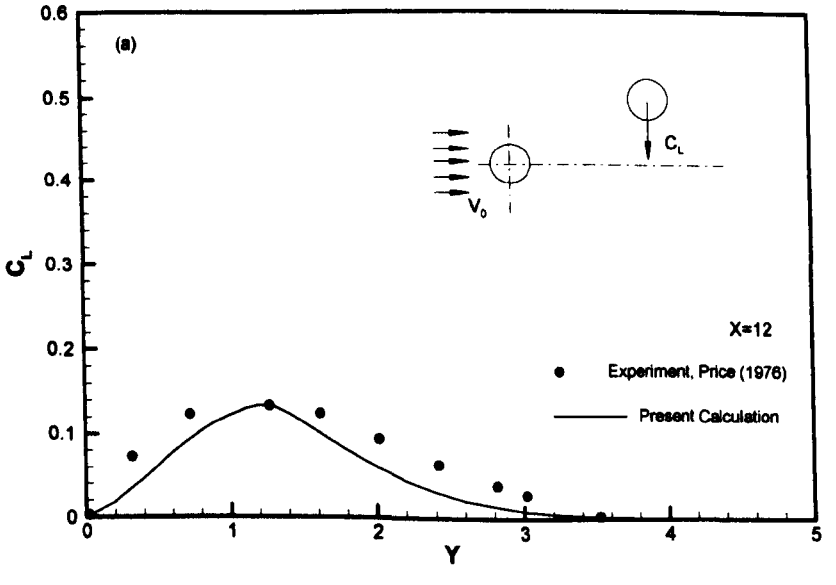

Figure 2.10(a) Variation of time-averaged force on the downstream cylinder across the wake, lift.

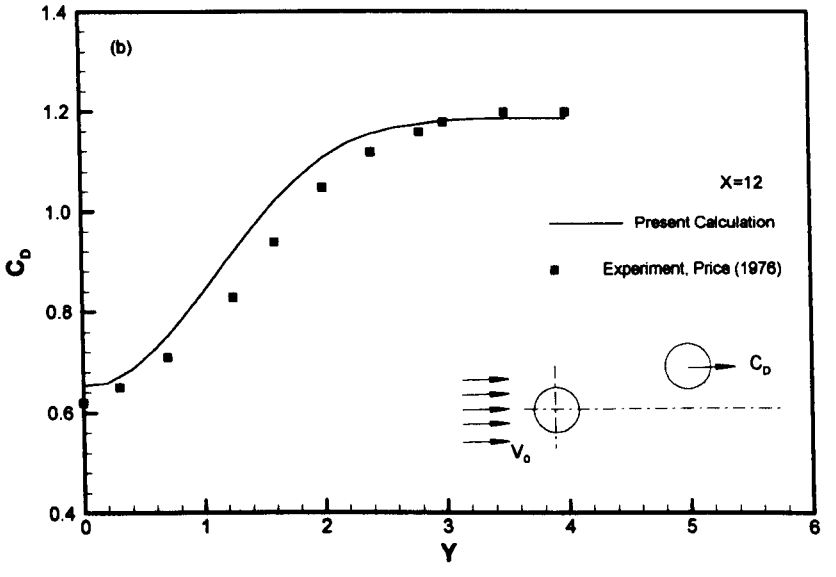

Figure 2.10(b) Variation of time-averaged force on the downstream cylinder across the wake, drag.

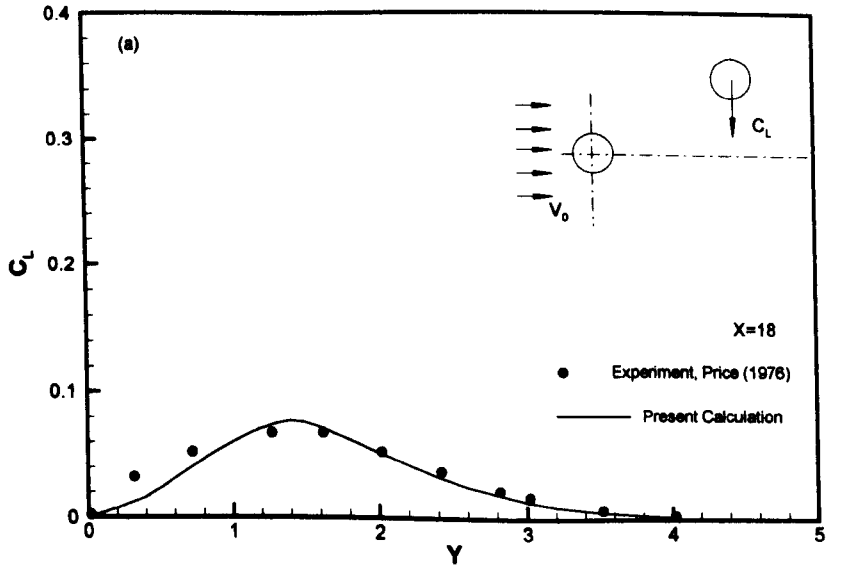

Figure 2.11(a) Variation of time-averaged force on the downstream cylinder across the wake, lift.

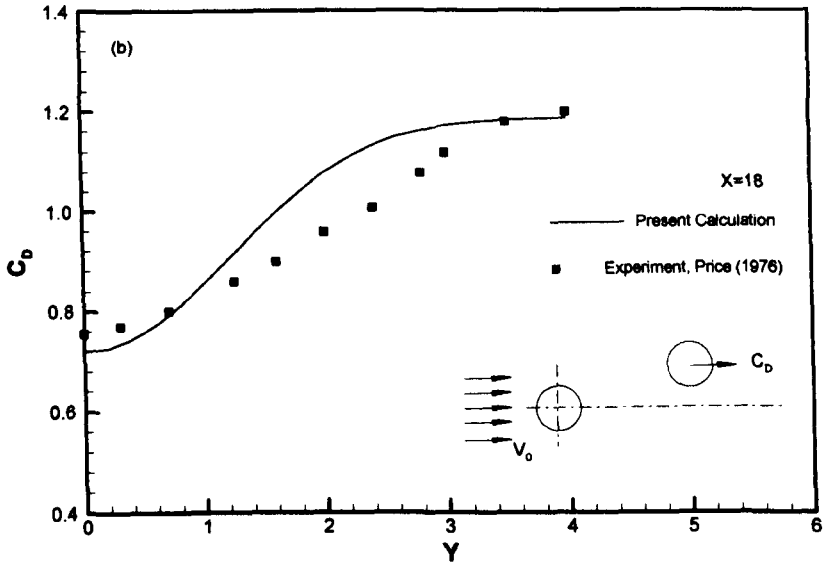

Figure 2.11(b) Variation of time-averaged force on the downstream cylinder across the wake, drag.

the lift and drag force coefficients are calculated and presented in Figure 2.9 to Figure 2.11.

From Figure 2.9 to Figure 2.11, it can be seen that the result agrees well with the experiment, both in its magnitude and its variation with the longitudinal and transverse distance. Such a result will enable this thesis to predict the dynamic behaviour of the downstream cylinder. Comparing Figure 2.9 and 2.10, 2.11, it can be seen that with the increase of the streamwise distance, the maximum lift force magnitude decreases, and the position of maximum lift is shifted outward. This is well reflected in the Figures, and compared to the experiment of Price(1976), the agreement of magnitude relation between at X=6.0, 12.0 and 18.0 is also satisfactory. For the drag coefficient, it is very clear that the shield effect diminishes with the increase of the streamwise distance x, at the same time, wake boundary widens with the increase of the distance x. These effects are all presented in Figure 2.9(b) to 2.11(b). The main difference from the experiment is that the width where lift force is large is not as wide as the experiment at a small distance. At a large distance, the wake width is a little underestimated in this calculation. However, bearing in

mind that such a prediction is to serve the purpose of dynamic analysis, these discrepancies are well acceptable.

2.4.1.1 Comparison of Pressure Distribution

The fluid force coefficients presented here are all calculated by the integration of pressure over the cylinder surface. It is worthwhile to compare pressure distributions between calculation and experiments. However, as stated in the base pressure discussion, the calculation of pressure coefficients is made solely dependent on the ambient flow of the downstream cylinder, i.e. the wake of the upstream cylinder. A transformation is needed for the purpose of comparison.

Let

$$C_p = \frac{p - p_\infty}{\frac{1}{2}\rho V_0^2}$$

be the definition of pressure coefficients and used in the experiments, and

$$C_{pc} = \frac{p - p_w}{\frac{1}{2}\rho U^2}$$

be the definition of pressure coefficients of the calculation.

Let C_{p02} be the measured pressure coefficient at the stagnation point on the downstream cylinder, The following transformation is obtained:

$$C_p = C_{p02} - \left(1 - C_{pc}\right)\left(\frac{U}{V_0}\right)^2$$

By such a transformation, the calculated pressure coefficients can then be presented in the same way as the experimental data. The comparison of the calculated results and experimental results is shown in Figure 2.12. It is seen from the Figure that the drop from maximum pressure to minimum pressure agrees very well between present prediction and experimental result. In addition, the shift of the position at which the maximum pressure occurs agrees well between prediction and experimental result. The fairly good agreement for the base pressure gives support for the hypothesis set for the base pressure in section 2.2.4. Therefore, the agreement is satisfactory.

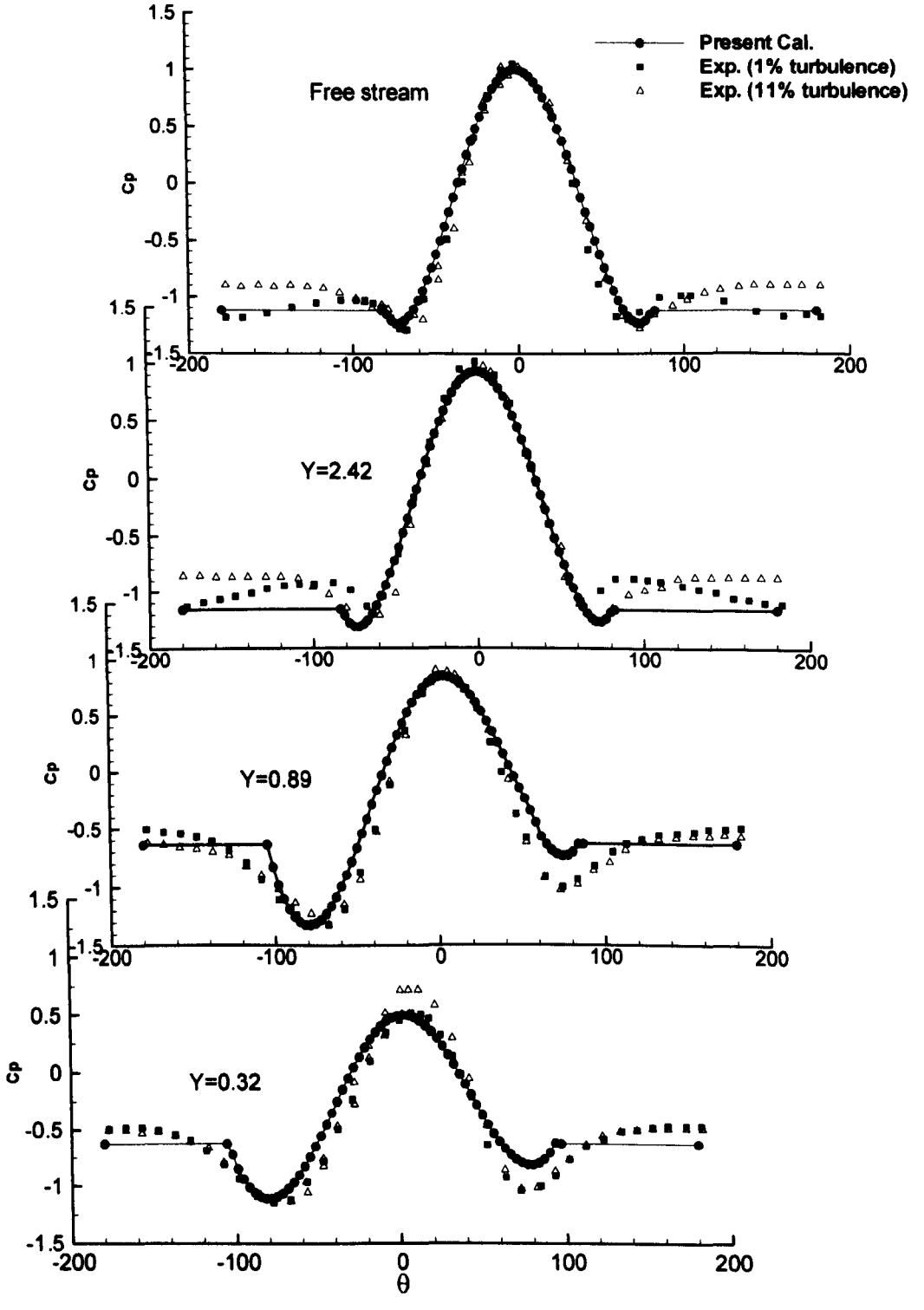

Figure 2.12 Comparison of pressure distribution between calculation and experiments.

2.4.2 *Downstream Cylinder is Smaller Than Upstream Cylinder(D_1:D_2=2:1,4:1)*

Sometimes, two cylinders may have different diameters. Experiments show that reducing the diameter ratio of leeward to windward cylinder to 1:2 will decrease the maximum lift by 40 per cent, and a further reduction in diameter ratio to 1:4 will decrease the maximum lift coefficient by 91 per cent. On the other hand, such a difference in cylinder diameter ratio has no significant effect on drag coefficient. Most of the arguments described in the literature review can not explain these phenomena. It is easy to understand that if people, in explaining the lift, fully rely on the drag coefficient, no big change of lift coefficient can be expected due to the insensitive nature of drag coefficient to the diameter ratio which was shown by the experiments. However, according to the hypothesis presented in this thesis, it is not difficult to understand that this kind of effect will happen if the cylinder diameters are different between the upstream cylinder and downstream cylinder.

Asymmetrical separation flow around a cylinder is like the flow over an airfoil with an angle of attack. When the cylinder in the wake is smaller, attack angle depends on the difference of the separation positions between the outer side and inner side, due to the area it covers being smaller, the difference in the separation position will be smaller. This is similar to the reduced attack angle which leads to the lower lift force. Figure 2.13 to Figure 2.15 give the prediction results which show the difference when the diameter ratios of two cylinders are different. It can be seen that the result in Figure 2.13 is very similar to the experimental finding. The maximum lift, when the downstream cylinder is half size of the upstream one, is 63% of that when the two cylinders have the same diameters (experiments show 60%). According to Figure 2.14, when X=12.0, the maximum lift of downstream small cylinder is 59% of that for same size cylinder. The experiments show that it is around 50%. While the location of the maximum lift is shifted inwards when the downstream cylinder is small, the drag coefficient shows there is no big difference between different diameter ratios.

According to the comparison, when the diameter ratio is 2:1, the predicted result in this thesis is in good agreement with the experiments.

Figure 2.15 shows the situation when the diameter of the downstream cylinder is only one-fourth of the upstream one. The maximum lift on the downstream cylinder is 35% of that for diameter ratio of 1:1. This result is quite a bit higher than in the experiment, which shows only 9%. However, experiments found that the lift force will change direction near the wake outer boundary. This phenomenon has not been reflected in the calculation. It is considered that, if the diameter difference is significantly large, other factors may also affect the flow around the downstream cylinder considerably. On the other hand, the drag coefficient for such a situation is still in good agreement with the experiments. This is because drag force is insensitive to the flow separation position.

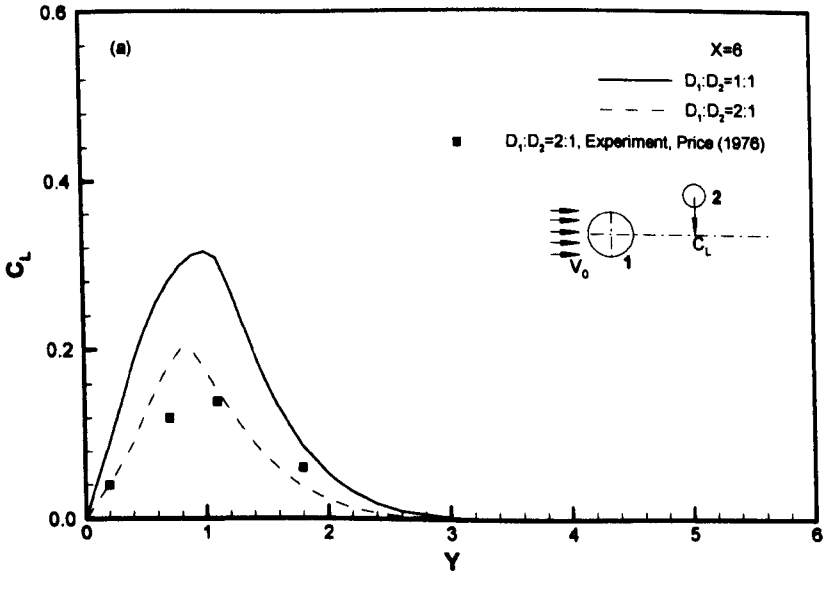

Figure 2.13(a) Comparison of lift force for different diameter ratios. The downstream cylinder is smaller than the upstream one, at X=6.

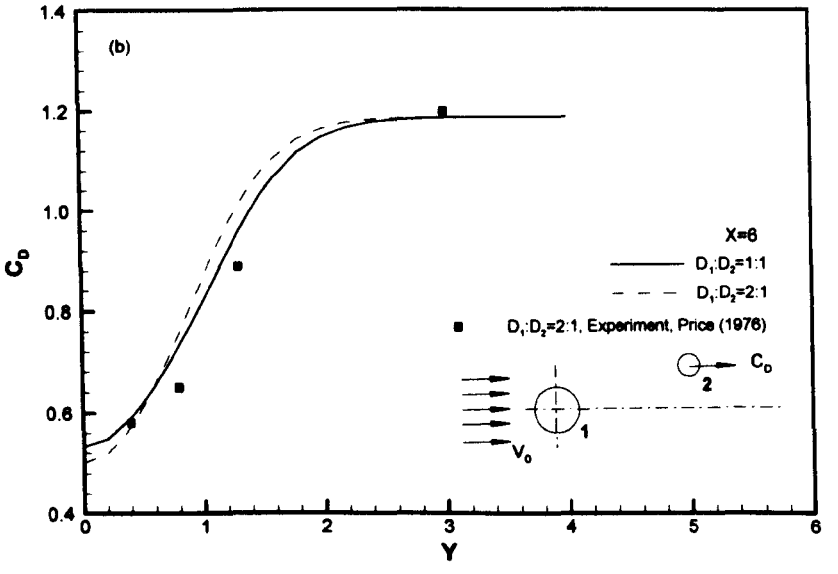

Figure 2.13(b) Comparison of drag force for different diameter ratios. The downstream cylinder is smaller than the upstream one, at X=6.

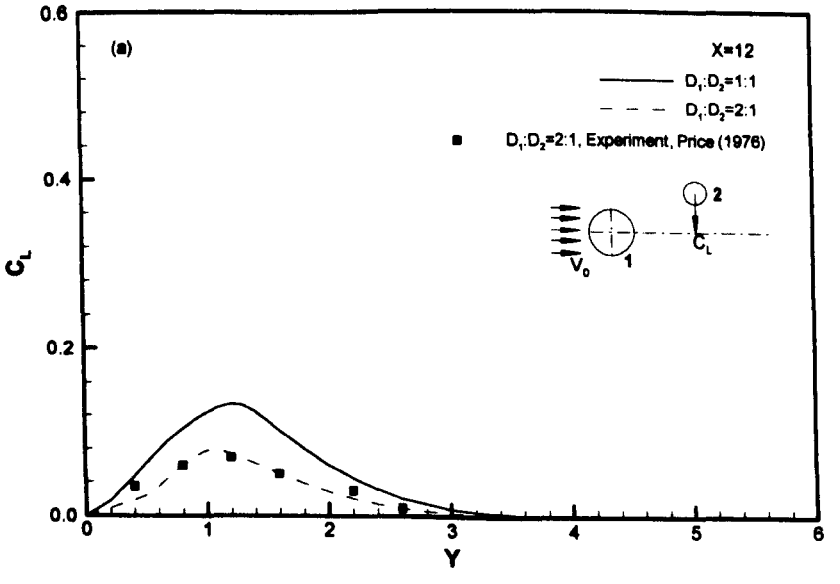

Figure 2.14(a) Comparison of lift force for different diameter ratios. The downstream cylinder is smaller than the upstream one, at X=12.

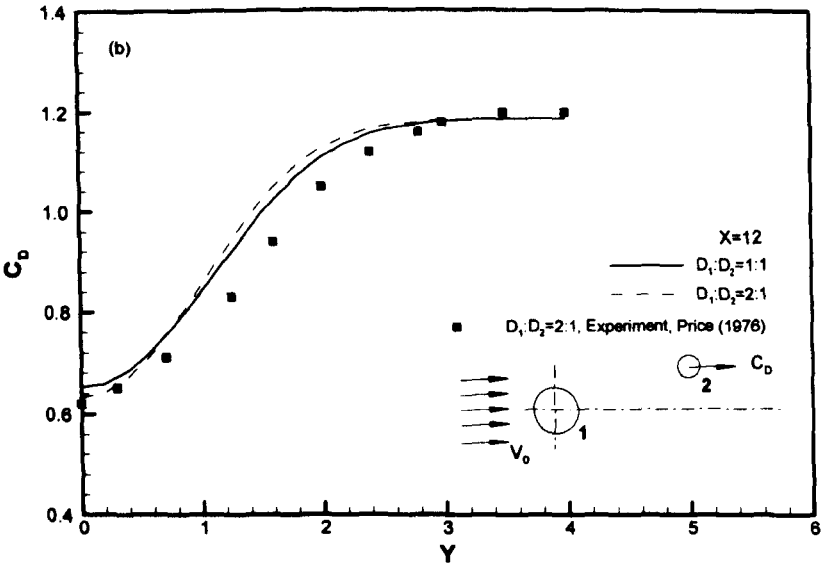

Figure 2.14(b) Comparison of drag force for different diameter ratios. The downstream cylinder is smaller than the upstream one, at X=12.

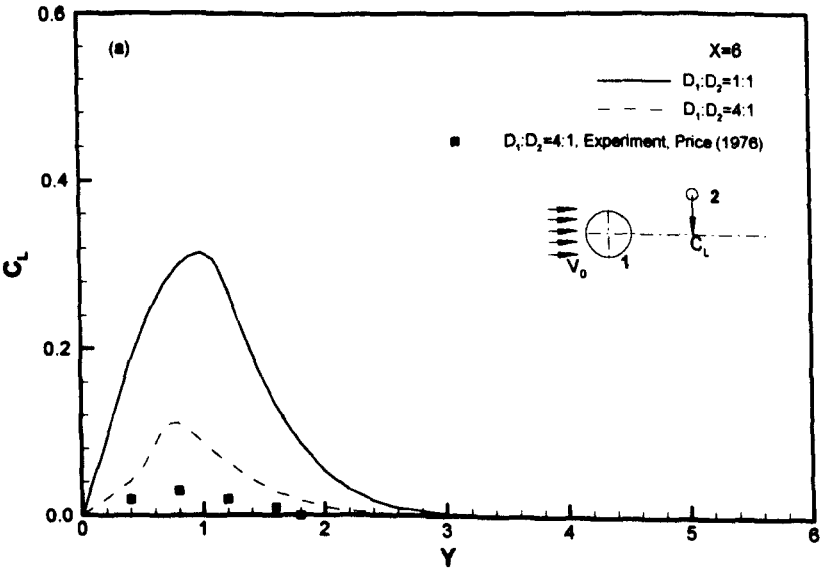

Figure 2.15(a) Comparison of lift force for different diameter ratios. The downstream cylinder is smaller than the upstream one, at X=6.

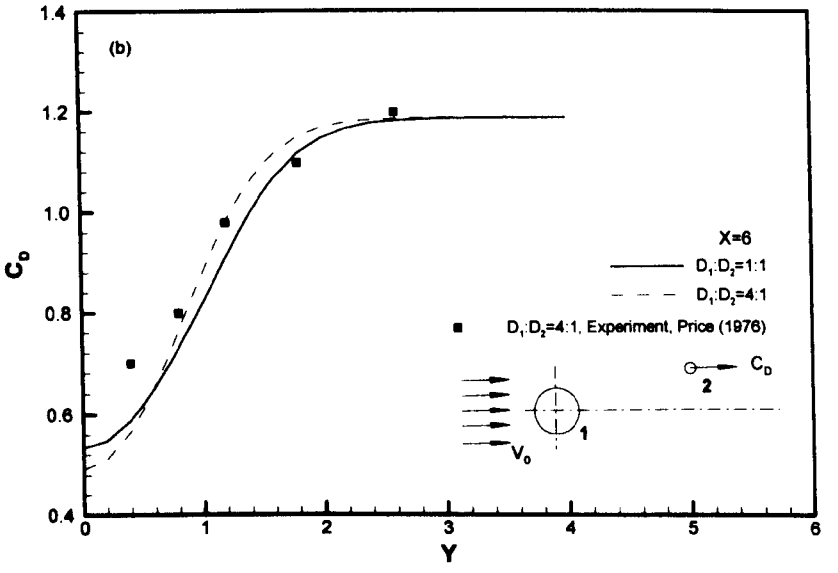

Figure 2.15(b) Comparison of drag force for different diameter ratios. The downstream cylinder is smaller than the upstream one, at X=6.

2.4.3 Downstream Cylinder is Larger Than Upstream Cylinder(D_1:D_2=1:2)

It is not expected that the method explained here can account for the fluid force on the downstream cylinder very well, for the situation when the downstream cylinder is larger than the upstream one. Because in that situation, the wake will be thought to be altered significantly due to the existence of the large downstream cylinder. Nevertheless, an attempt is made here for the diameter ratio(D_1:D_2) equal to 1:2, with the result shown in Figure 2.16. The trends of the variation of lift and drag agree well with the experiment. The maximum lift now is increased by 27% compared to the same cylinder size situation, while the experiment result is 63%, and the drag coefficient near the wake centre is detectably larger than in the situation for same cylinder size in small range of Y. There is no such difference in the experiments. However, when the downstream cylinder moves outwards, the result is in good agreement with the experiments.

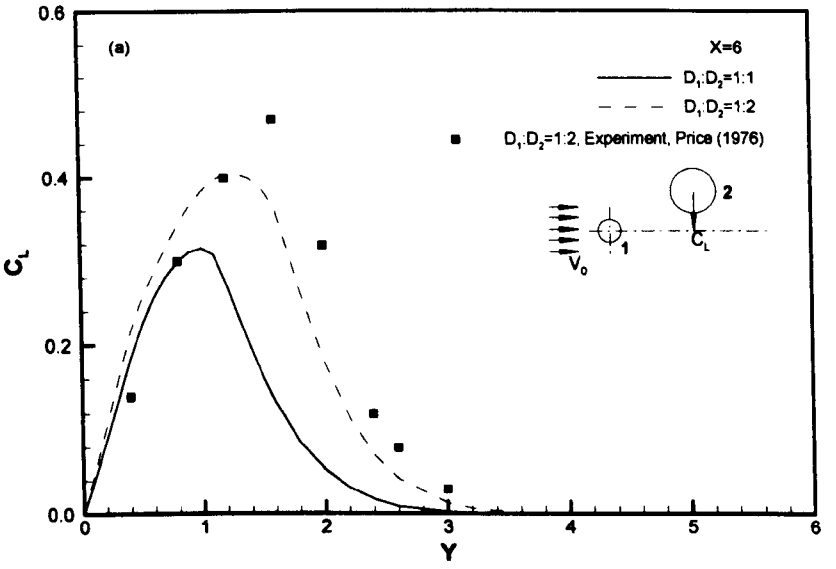

Figure 2.16(a) Comparison of lift force for different diameter ratios. The downstream cylinder is larger than the upstream one, at X=6.

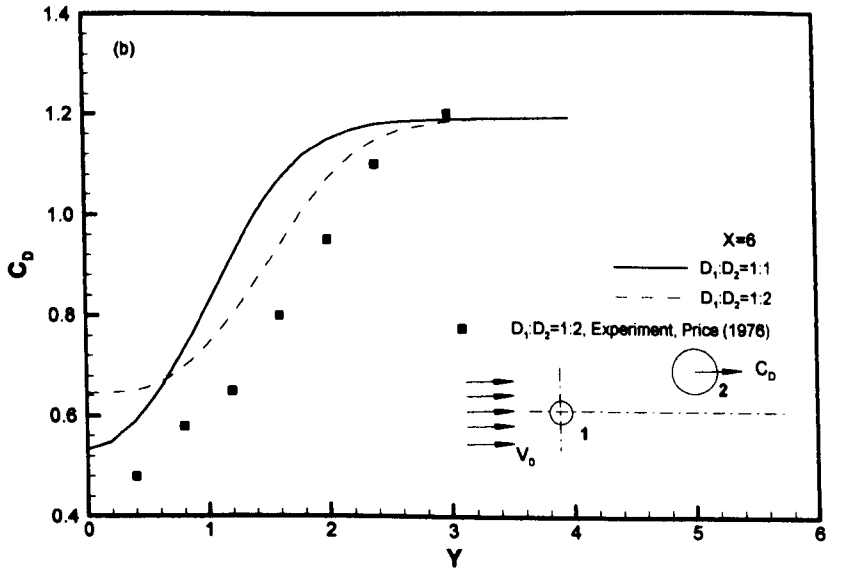

Figure 2.16(b) Comparison of drag force for different diameter ratios. The downstream cylinder is larger than the upstream one, at X=6.

2.5 Summaries

Concluding the investigation conducted in this chapter, a practical method has been developed with a new philosophy which is able to account for the time-averaged force exerted on the downstream cylinder. The method is based on the experimental data to specify the separation situation for the downstream cylinder, which may bring some difficulties. However, by the use of existing experimental data, the calculation shows encouraging agreement with the experiment. Also, the method predicts well the situation when the downstream cylinder is half the diameter of the upstream one. Even for the special cases of a very small downstream cylinder or large downstream cylinder, the present method shows good correlation of the lift force and drag force variation. The method is considered to be a useful tool for the dynamic analysis of the interaction between two cylinders. Further, it may provide a new view on the nature of lift and drag force on the downstream cylinder. Finally, it should be noted that the method introduced in this thesis is mostly applicable to sub-critical Reynolds number region.

Chapter III

STABILITY OF THE DOWNSTREAM CYLINDER IN TWO-DIMENSIONAL SPACE

3.1 General Remarks

Collision between two cylinders/risers when located in water at high flow speed has been observed in experiments (Bryndum & Anderson, 1999; Huse, 1993). The essential physics of the interaction between two cylinders/risers is the problem of two cylinders interaction in fluid. It occurs in many other engineering applications, such as interactions between two power transmission lines in the power industry, interaction between tubes in heat exchangers (including steam generators, boilers and condensers) and nuclear reactors, interference of chimneys or building groups in civil engineering, also interaction among bundle risers. Since 1960s, substantial amounts of theoretical and experimental research have been carried out to investigate the different fluidelastic phenomena. Table 3.1 tries to outline the main characteristics for each of the different cylinder applications.

Each of the investigations made so far focused on its own engineering background, as enumerated in the above table. The general approaches adopted are based on quasi-steady flow theory, which essentially suppose that flow responds to the movement of the cylinder instantly. Often, by utilising experimental data of the fluid forces, the stability of each dynamic system was then analysed (e.g. Simpson 1971; Price and others 1993 etc). However, there appears to be no published paper which

Table 3.1 Comparison between different applications for cylinder interaction

Problem	Characteristics				Phenomena	Representative Work
	s/D[1]	a	L/D	U_R		
Power Line	10 ~20	~ 2×10^{-4}	~2000	~30	Flutter	(Simpson 1971; Price 1975; Tsui 1977,1986)
Tube Bank	1.2~3.0	10^{-4} ~ 10^{-1}	40 ~400	~20	Fluidelastic Instability(damping or stiffness controlled)	(Blevins, 1979 Lever and Weaver, 1986)
Chimneys Groups	~1.5	$\sim10^{-3}$	<10	~2	VIV only	(Wong 1985, Sockel,H. and Kronke, I., 1987)
Bundle Riser	<5	~0.2	> 500	~2	VIV, Galloping or Combined	(Overvik and others 1983; Price and others 1993)
TLP/SPAR Riser	10 ~30	~0.2	2000+	~30	To be answered	(Huse 1996; Huse 1993)

has tried to correlate these fragmented investigations into a systematic study of a whole wake field and to explore the characteristics of marine riser interaction. No paper has been published to account for the marine riser interaction like collision by using the stability theory.

A full review of the different theoretical methods employed to investigate the fluid-elastic behaviour is beyond the scope of this thesis, but reference can be made to Price (1995).

This thesis, takes marine riser interaction as its main background, and a through investigation covering both near and far wake fields is made to illustrate the mathematical characteristics of the two cylinder interaction. The analysis is based on varied forms of Morison's equation. A full Routh-Hurwitz stability algorithm is utilised together with direct numerical eigenvalue seeking technique to investigate the stability of the two cylinder interaction. The effects of control parameters such as stiffness ratio, spring coupling and particularly the mass parameter, are addressed. The author does not intend to pretend such an analysis method is original, however, due to the characteristics of marine risers, new results are obtained. The investigation conducted here is the most comprehensive one, covering a wide range of cylinder spacings and mass parameters. It was found

[1] S : cylinder centre to centre distance, D: cylinder diameter, $a = \rho D^2/2m$, L: cylinder length, $U_R = V_n/\omega D$

that there is a restriction imposed by mass parameter for the Hopf bifurcation to occur. Stationary bifurcation is more likely to occur in riser interaction, particularly when the two risers are separated by a fair amount of spacing. A clarified explanation of the stability and stable/unstable region evolution with control parameter is also presented.

3.2 Mathematical Formulation

3.2.1 Fluid Forces

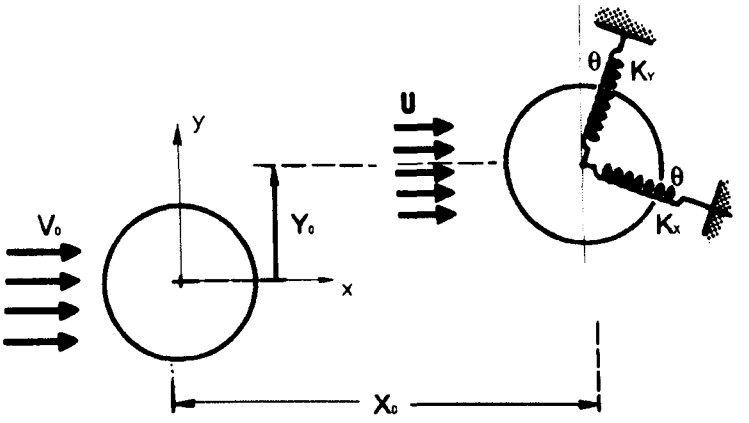

Figure 3.1 A schematic diagram of arrangement of two cylinders, the upstream cylinder is also supported by springs.

Figure 3.1 shows a cylinder located in the wake of another one. Both the downstream and upstream cylinders are elastically mounted. Supposing the interaction from the downstream cylinder to the upstream cylinder can be neglected, then the stability of the downstream cylinder is the main concern of this chapter, which is strongly dependent on the relative position of the downstream cylinder behind the balanced upstream one. The co-ordinate system has its origin at the centre of the upstream cylinder equilibrium position. The two springs for the downstream cylinder are perpendicular to each other, with an angle of θ between the x axis and the K_x spring as shown in Figure 3.1. It is assumed that the lengths of the two springs are much larger than the small displacements of the downstream cylinder away from its equilibrium. Therefore, the angle is assumed to be constant in present analysis. Such a co-ordinate system is mainly for the purpose of stability analysis for the downstream cylinder. Because the displacement caused by the fluid forces

can be significant for marine risers, an absolute co-ordinate system fixed to the earth will be utilised in the next chapter.

Figure 3.2 is a schematic diagram which shows the velocity triangle and the resultant fluid force acting on the downstream cylinder. Supposing the flow responds to the movement of cylinder

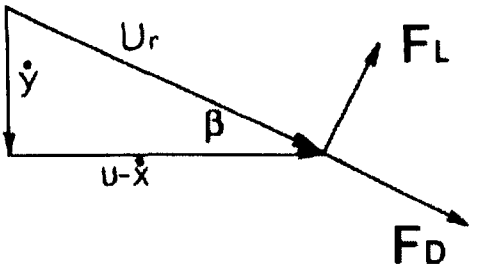

Figure 3.2 A schematic diagram of velocity, and fluid forces for quasi-steady flow model.

instantly, then fluid forces are given by:

$$\begin{cases} F_x = F_D\cos\beta - F_L\sin\beta - c_m\dfrac{\rho\pi D^2}{4}\ddot{x} = \dfrac{1}{2}\rho U_r^2 D\left(\overline{C}_D\cos\beta - \overline{C}_L\sin\beta\right) - c_m\dfrac{\rho\pi D^2}{4}\ddot{x} \\ F_y = F_D\sin\beta + F_L\cos\beta - c_m\dfrac{\rho\pi D^2}{4}\ddot{y} = \dfrac{1}{2}\rho U_r^2 D\left(\overline{C}_D\sin\beta + \overline{C}_L\cos\beta\right) - c_m\dfrac{\rho\pi D^2}{4}\ddot{y} \end{cases} \quad (3.1)$$

Where F_x, F_y are fluid forces in the x, y directions, respectively;

$U_r\left(=\sqrt{(U-\dot{x})^2+\dot{y}^2}\right)$ is the relative velocity to the downstream cylinder;

ρ is fluid density,

D is diameter of the cylinder,

β is the angle of the relative velocity to the x axis;

c_m is fluid added mass coefficient due to the acceleration of the cylinder (which can be determined by potential flow theory).

$\overline{C}_{D,L} = \dfrac{F_{D,L}}{\rho U^2 D/2}$ with F_D, F_L being the drag and lift forces respectively.

It is shown in Figure 3.2 that

$$\begin{cases} \cos\beta = \dfrac{U - \dot{x}}{U_r} \\ \sin\beta = -\dfrac{\dot{y}}{U_r} \\ U_r = \sqrt{(U-\dot{x})^2 + \dot{y}^2} \end{cases} \tag{3.2}$$

Substituting Equation (3.2) into Equation (3.1), we have

$$\begin{cases} F_x = \dfrac{1}{2}\rho U_r D\left[\overline{C}_D(U-\dot{x}) + \overline{C}_L\dot{y}\right] - c_m\dfrac{\rho D^2}{4}\ddot{x} \\ F_y = \dfrac{1}{2}\rho U_r D\left[-\overline{C}_D\dot{y} + \overline{C}_L(U-\dot{x})\right] - c_m\dfrac{\rho D^2}{4}\ddot{y} \end{cases} \tag{3.3}$$

Essentially, this is a varied form of Morison type equation for fluid forces acting on a moving cylinder with the consideration of transverse forces.

In order to utilise the force coefficients obtained by Free Stream Line method, let $b = U/V_0$. The reference velocity for the force coefficients can then be transformed from the local wake velocity U to the free stream velocity V_0 by the following relations:

$$\overline{C}_{D,L} = C_{D,L}/b^2$$

Where $C_{D,L} = \dfrac{F_{D,L}}{\rho V_0^2 D/2}$; (3.4)

For small motions around an equilibrium position, i.e. $\dot{x}/U, \dot{y}/U \sim o(1)$, the forces can be linearised and given as

$$\begin{bmatrix} F_x \\ F_y \end{bmatrix} = \frac{1}{2}\rho V_o^2 D \begin{bmatrix} C_D \\ C_L \end{bmatrix} + \frac{1}{2}\rho V_o^2 D \begin{bmatrix} -2C_D & C_L \\ -2C_L & -C_D \end{bmatrix} \times \begin{bmatrix} \dot{x}/U \\ \dot{y}/U \end{bmatrix} - c_m \frac{\rho\pi D^2}{4} \begin{bmatrix} \ddot{x} \\ \ddot{y} \end{bmatrix} \tag{3.5}$$

Further as C_D, C_L are position dependent, these force coefficients can also be expanded around the equilibrium position (x_0, y_0):

$$\begin{bmatrix} C_D \\ C_L \end{bmatrix} = \begin{bmatrix} C_D \\ C_L \end{bmatrix}_{\substack{x=x_o \\ y=y_o}} + \begin{bmatrix} C_{DX} & C_{DY} \\ C_{LX} & C_{LY} \end{bmatrix}_{\substack{x=x_o \\ y=y_o}} \times \begin{bmatrix} X - X_0 \\ Y - Y_0 \end{bmatrix} \tag{3.6}$$

where $X = x/D$, $Y = y/D$,

$$C_{DX} = \frac{\partial C_D}{\partial X}, C_{DY} = \frac{\partial C_D}{\partial Y}, C_{LX} = \frac{\partial C_L}{\partial X}, C_{LY} = \frac{\partial C_L}{\partial Y}$$

Substituting Equation (3.6) into Equation (3.5), we have:

$$\begin{aligned} \begin{bmatrix} F_x \\ F_y \end{bmatrix} = {} & \frac{1}{2}\rho V_o^2 D \begin{bmatrix} C_{D0} \\ C_{L0} \end{bmatrix} + \frac{1}{2}\rho V_0^2 D \begin{bmatrix} C_{DX} & C_{DY} \\ C_{LX} & C_{LY} \end{bmatrix} \begin{bmatrix} X - X_0 \\ Y - Y_0 \end{bmatrix} \\ & + \frac{1}{2}\rho V_0^2 D \begin{bmatrix} -2C_{D0} & C_{L0} \\ -2C_{L0} & -C_{D0} \end{bmatrix} \begin{bmatrix} \dot{X}D/U \\ \dot{Y}D/U \end{bmatrix} - c_m \frac{\rho\pi D^3}{4} \begin{bmatrix} \ddot{X} \\ \ddot{Y} \end{bmatrix} \end{aligned} \tag{3.7}$$

Equation (3.7) is the linearised form of the fluid force acting on the downstream cylinder when the downstream cylinder is located at the equilibrium position (x_0, y_0). Because the matrix

$$\frac{\rho V_0^2 D}{2}\begin{bmatrix} C_{DX} & C_{DY} \\ C_{LX} & C_{LY} \end{bmatrix} \tag{3.8}$$

functions like a spring stiffness matrix, which accounts for the fluid recovery force when cylinder is deviated from equilibrium position, it is called the *fluid stiffness* matrix, whilst

$$\frac{\rho V_0^2 D^2}{2U}\begin{bmatrix} -2C_{D0} & C_{L0} \\ -2C_{L0} & -C_{D0} \end{bmatrix} \tag{3.9}$$

behaves like coefficient matrix for a damping system, which explain the consumed energy when a cylinder moves about, it is called the *fluid damping* matrix in this thesis.

3.2.2 Equations of Motion

The motion of the downstream cylinder is governed by

$$\begin{aligned} m\underline{I}\begin{bmatrix} \ddot{x} \\ \ddot{y} \end{bmatrix} + \begin{bmatrix} c_x\cos^2\theta + c_y\sin^2\theta & (c_x - c_y)\sin\theta\cos\theta \\ (c_x - c_y)\sin\theta\cos\theta & c_x\sin^2\theta + c_y\cos^2\theta \end{bmatrix}\begin{bmatrix} \dot{x} \\ \dot{y} \end{bmatrix} \\ + \begin{bmatrix} K_x\cos^2\theta + K_y\sin^2\theta & (K_x - K_y)\sin\theta\cos\theta \\ (K_x - K_y)\sin\theta\cos\theta & K_x\sin^2\theta + K_y\cos^2\theta \end{bmatrix}\begin{bmatrix} x - x_s \\ y - y_s \end{bmatrix} = \begin{bmatrix} F_x \\ F_y \end{bmatrix} \end{aligned} \tag{3.10}$$

where m is the structural mass per unit length of cylinder. K_x, K_y are the spring stiffnesses in x, y directions, respectively. (x_s, y_s) is the initial position of the downstream cylinder when no current is present. The right hand side of the equation includes the fluid forces in (x, y) directions, as presented in Equation (3.7). Substituting Equation (3.7) into Equation (3.10), non-dimensionalising x, y with the cylinder diameter and introducing $\tau = \omega_x t$ with $\omega_x = \sqrt{K_x / (m + c_m \rho \pi D^2/4)}$, the equation of motion around the equilibrium position can be re-written as:

$$\begin{bmatrix} \ddot{\tilde{X}} \\ \ddot{\tilde{Y}} \end{bmatrix} + \begin{bmatrix} 2\xi_x\left(R_k R_\xi \sin^2\theta + \cos^2\theta\right) + \dfrac{2a}{b} U_R C_{D0} & 2\xi_x\left(\left(R_k R_\xi - 1\right)\sin\theta\cos\theta\right) - \dfrac{a}{b} U_R C_{L0} \\ 2\xi_x\left(\left(R_k R_\xi - 1\right)\sin\theta\cos\theta\right) + \dfrac{2a}{b} U_R C_{L0} & 2\xi_x\left(R_k R_\xi \cos^2\theta + \sin^2\theta\right) + \dfrac{a}{b} U_R C_{D0} \end{bmatrix} \times \begin{bmatrix} \dot{\tilde{X}} \\ \dot{\tilde{Y}} \end{bmatrix}$$

$$+ \begin{bmatrix} R_k^2 \sin^2\theta + \cos^2\theta - aU_R^2 C_{DX} & (R_k^2 - 1)\sin\theta\cos\theta - aU_R^2 C_{DY} \\ (R_k^2 - 1)\sin\theta\cos\theta - aU_R^2 C_{LX} & R_k^2 \cos^2\theta + \sin^2\theta - aU_R^2 C_{LY} \end{bmatrix} \times \begin{bmatrix} \tilde{X} \\ \tilde{Y} \end{bmatrix} = 0 \tag{3.11}$$

with

$$\begin{bmatrix} \tilde{X} \\ \tilde{Y} \end{bmatrix} = \begin{bmatrix} X - X_o \\ Y - Y_o \end{bmatrix}$$

and

$$\begin{bmatrix} R_k^2 \sin^2\theta + \cos^2\theta & (R_k^2 - 1)\sin\theta\cos\theta \\ (R_k^2 - 1)\sin\theta\cos\theta & R_k^2 \cos^2\theta + \sin^2\theta \end{bmatrix} \times \begin{bmatrix} X_0 - X_s \\ Y_0 - Y_s \end{bmatrix} = aU_R^2 \begin{bmatrix} C_{D0} \\ C_{L0} \end{bmatrix} \tag{3.12}$$

Here, $U_R = \dfrac{V_0}{\omega_x D}$ is reduced flow velocity.

$$\xi_x = \frac{c_x}{2\left(m + \dfrac{c_m \rho \pi D^2}{4}\right)\omega_x}$$

$R_k = \left(\dfrac{K_y}{K_x}\right)^{1/2}$ is the stiffness ratio between two orthognal directions.

$a = \dfrac{\rho D^2}{2\left(m + c_m \dfrac{\rho \pi D^2}{4}\right)}$ is often referred as the mass parameter, which, as will be seen, is the vitally important parameter in determing fluid elastic behaviour.

$R_\xi = \frac{c_y}{c_x}$ is the damping ratio between two spring directions. The inclusion of this term is to identify the role of the structural damping.

For notation convenience, the tidle bar is dropped in the following discussion. Equation (3.11) represents a spring physically coupled system with the consideration of structural and fluid dampings. It is the basic equation to determine the stability of the downstream cylinder. Before delving into the stability analysis, some special forms are discussed here to show the relation between different simplified systems.

3.2.2.1 Uncoupled, Undamped System

The simplest form of the dynamics equation (3.11) is the uncoupled and undamped system, which is often mentioned in research into power transmission lines and often called "undamped flutter theory". The system neglects both the structural damping as well as the fluid damping, i.e. $\xi, aU_R C_D, aU_R C_L \Rightarrow 0$ and $\theta = 0^0$.

It should be noted that such a hypothesis is tenable only when the mass parameter is small. The system can then be simplified as,

$$\begin{bmatrix} \ddot{X} \\ \ddot{Y} \end{bmatrix} + \begin{bmatrix} 1 - aU_R^2 C_{DX} & -aU_R^2 C_{DY} \\ -aU_R^2 C_{LX} & R_k^2 - aU_R^2 C_{LY} \end{bmatrix} \times \begin{bmatrix} X \\ Y \end{bmatrix} = 0 \qquad (3.13)$$

3.2.2.2 Uncoupled System With Fluid Damping

The form of (3.13) is simplest when the mass parameter is set as small. However, the cases, such as marine risers in water, do not satisfy these conditions. Therefore, a simple form with the consideration of the fluid damping while keep the spring uncoupled is the basic form for the consideration of riser interaction:

$$\begin{bmatrix}\ddot{X}\\ \ddot{Y}\end{bmatrix}+\frac{a}{b}U_R\begin{bmatrix}2C_{D0} & -C_{L0}\\ 2C_{L0} & C_{D0}\end{bmatrix}\times\begin{bmatrix}\dot{X}\\ \dot{Y}\end{bmatrix}+\begin{bmatrix}1-aU_R^2C_{DX} & -aU_R^2C_{DY}\\ -aU_R^2C_{LX} & R_k^2-aU_R^2C_{LY}\end{bmatrix}\times\begin{bmatrix}X\\ Y\end{bmatrix}=0 \qquad (3.14)$$

3.2.2.3 Coupled System Without Damping

Generally, the two springs for downstream cylinder are coupled as shown in Figure 3.1. A straightforward way to explain the effect of spring coupling is by utilising the case of an undamped coupled system. It is seen that in Equation (3.13), fluid stiffness is coupled while the physical spring is uncoupled. To apply this kind of result to the spring coupled system, a transformation can be made to uncouple the physical spring system. The system can be written as.

$$\begin{bmatrix}\ddot{X}\\ \ddot{Y}\end{bmatrix}+\begin{bmatrix}1 & 0\\ 0 & R_k^2\end{bmatrix}\begin{bmatrix}X\\ Y\end{bmatrix}-aU_R^2$$
$$\times\begin{bmatrix}c_{DX}\cos^2\theta+c_{LY}\sin^2\theta-(c_{LX}+c_{DY})\sin\theta\cos\theta & c_{DY}\cos^2\theta-c_{LX}\sin^2\theta+(c_{DX}-c_{LY})\sin\theta\cos\theta\\ c_{LX}\cos^2\theta-c_{DY}\sin^2\theta+(c_{DX}-c_{LY})\sin\theta\cos\theta & c_{DX}\sin^2\theta+c_{LY}\cos^2\theta+(c_{Lx}+c_{DY})\sin\theta\cos\theta\end{bmatrix}\begin{bmatrix}X\\ Y\end{bmatrix}=0 \qquad (3.15)$$

According to Equation (3.15), the effect of a coupled spring can be understood as the uncoupled system under the action of a transformed fluid force field.

The stability analysis in this thesis is made either via the traditional method of Routh-Hurwitz stability algorithm, or by a direct numerical eigenvalue analysis. Routh-Hurwitz method provides the critical state of the system with analytic solution, however, it does not show the variation of the system stability. On the other hand, the numerical eigenvalue analysis provides detailed information of eigenvalue variation, however, to pick up the critical state can be difficult and time consuming. In order to obtain both the information about the critical state and the variation of the system stability, the two methods have been used jointly. The following section presents the application of

the Routh-Hurwitz stability algorithm. Combined with a direct numerical eigenvalue analysis method, the numerical results will be presented systematically in Section 3.4.

3.3 Stability Analysis

3.3.1 Traditional Method: Routh-Hurwitz Stability Algorithm

By assuming

$$\begin{bmatrix} X \\ Y \end{bmatrix} = \begin{bmatrix} A_x \\ A_y \end{bmatrix} e^{\lambda \tau},$$

The stability of the downstream cylinder (3.11) can then be determined by the eigenvalue λ from the following characteristic equation:

$$\begin{vmatrix} a_{11} & a_{12} \\ a_{21} & a_{22} \end{vmatrix} = 0 \tag{3.16}$$

where

$$a_{11} = \lambda^2 + 2\left[\xi_x\left(R_k R_\xi \sin^2\theta + \cos^2\theta\right) + \frac{a}{b} U_R C_{D0}\right]\lambda + R_k^2 \sin^2\theta + \cos^2\theta - aU_R^2 C_{DX}$$

$$a_{12} = \left[2\xi_x\left(R_k R_\xi - 1\right)\sin\theta\cos\theta - \frac{a}{b} U_R C_{L0}\right]\lambda + \left(R_k^2 - 1\right)\sin\theta\cos\theta - aU_R^2 C_{DY}$$

$$a_{21} = 2\left[\xi_x\left(R_k R_\xi - 1\right)\sin\theta\cos\theta + \frac{a}{b} U_R C_{L0}\right]\lambda + \left(R_k^2 - 1\right)\sin\theta\cos\theta - aU_R^2 C_{LX}$$

$$a_{22} = \lambda^2 + \left[2\xi_x \cdot \left(R_k R_\xi \cos^2\theta + \sin^2\theta\right) + \frac{a}{b} U_R C_{D0}\right]\lambda + R_k^2 \cos^2\theta + \sin^2\theta - aU_R^2 C_{LY}$$

For notation convenience, following symbols are adopted hereafter: $c_{d0} = \frac{C_{D0}}{b}$, $c_{l0} = \frac{C_{L0}}{b}$

Equation (3.16) can be rearranged to give the following fourth-order algebraic equation about eigenvalue λ,

$$\sum_{j=0}^{4} c_j \lambda^j = 0 \tag{3.17}$$

where

$c_4 = 1$

$$c_3 = 3aU_R C_{d0} + 2\xi_x\left(R_K R_\xi + 1\right)$$

$$c_2 = 2a^2U_R^2\left(C_{d0}^2 + C_{l0}^2\right) - aU_R^2\left(C_{DX} + C_{LY}\right) + 4R_k R_\xi \xi_x^2 + R_k^2 + 1$$
$$+2aU_R\xi_x\left[C_{d0}\left(R_k R_\xi\left(1+\cos^2\theta\right)+1+\sin^2\theta\right) - C_{l0}\left(R_k R_\xi - 1\right)\sin\theta\cos\theta\right]$$

$$c_1 = -a^2U_R^3\left[C_{d0}\left(C_{DX} + 2C_{LY}\right) + C_{l0}\left(C_{LX} - 2C_{DY}\right)\right]$$
$$-2aU_R^2\xi_x\left[C_{LY}\left(R_k R_\xi \sin^2\theta + \cos^2\theta\right) + C_{DX}\left(R_k R_\xi \cos^2 + \sin^2\theta\right)\right.$$
$$\left.-C_{DY}\left(R_k R_\xi - 1\right) - C_{LX}\left(R_k R_\xi - 1\right)\sin\theta\cos\theta\right]$$
$$+aU_R\left[C_{d0}\left[R_k^2\left(\cos^2\theta + 1\right) + \sin^2\theta + 1\right] - C_{l0}\left(R_k^2 - 1\right)\sin\theta\cos\theta\right]$$
$$+2\xi_x\left(R_k^2 + R_k R_\xi\right)$$

$$c_0 = a^2U_R^4\left(C_{DX}C_{LY} - C_{LX}C_{DY}\right) + R_k^2 - aU_R\left[C_{DX}\left(R_k^2\cos^2\theta + \sin^2\theta\right)\right.$$
$$\left.+C_{LY}\left(R_k^2\sin^2\theta + \cos^2\theta\right) - \left(C_{DY} + C_{LX}\right)\left(R_k^2 - 1\right)\sin\theta\cos\theta\right]$$

The downstream cylinder will become unstable if the solution of λ has a positive real part. However, seeking the solution of λ directly from Eq (3.17) can be a computationally intensive task and the identification of the critical state can be tedious. The Routh-Hurwitz stability algorithm can release such a burden to find the stability of the system without solving the fourth-order algebraic equation. According to the algorithm, for a stable system, the following inequalities have to be satisfied:

$$\begin{cases} c_3 > 0 \\ c_2c_3 - c_1 > 0 \\ c_1c_2c_3 - c_1^2 - c_3^2c_0 > 0 \\ c_0\left(c_1c_2c_3 - c_1^2 - c_3^2c_0\right) > 0 \end{cases} \tag{3.18}$$

Generally, there are two possible routes for the equilibrium position to lose its stability, namely through either Hopf or stationary bifurcation. The former corresponds, physically, to a flutter or galloping oscillation and, mathematically, is the transverse crossing of the imaginary axis of a pair of eigenvalues, whereas the stationary bifurcation corresponds to an unstable movement away from the equilibrium position and, mathematically, is the crossing of the imaginary axis of an eigenvalue at the real axis. According to this algorithm, when one of the inequalities in (3.18) is not satisfied, the system is then unstable. The state when one of inequalities in (3.18) begins first to be violated corresponds to the critical state of bifurcation. The two scenarios of bifurcation are discussed separately in the following sections, and for clarity, the following analysis is first presented for the case of uncoupled system with the structural damping neglected, the case in the simplest form which is applicable to the marine riser interaction, as discussed in the section of 3.2.2.2.

3.3.1.1 Hopf bifurcation

Experimental measurements for the fluid forces on the downstream cylinder show that drag force does not have to be positive, which means the fluid damping matrix can be either positive definite or not positive definite. However, the mechanism of Hopf bifurcation for these two cases can be different. In following analysis, we discussed these two cases separately.

3.3.1.1.1 Fluid Damping Matrix Positive Definite (FDMPD)

The fluid damping matrix positive definite area encompasses most of the wake area, where drag force is positive. Within such an area, it is clear that c_3 is always positive. It is also found that $c_2c_3 - c_1$ is always positive. According to (3.18), the indicator for critical state of Hopf bifurcation is given by:

$$\begin{cases} c_1 \cdot c_2 \cdot c_3 - c_1^2 - c_3^2 c_0 = 0 \\ c_1 > 0 \end{cases} \tag{3.19}$$

Equation (3.19) can be re-written as

$$\begin{cases} A_1 \cdot U_R^4 + A_2 U_R^2 + A_3 = 0 \\ c_1 > 0 \end{cases} \tag{3.20}$$

where

$$\begin{aligned}
a^{-2}C_{d0}^{-2} \cdot A_3 &= 2\left(R_k^2 - 1\right)^2 \\
a^{-3}C_{d0}^{-2}A_2 &= 3\left[\left(2R_k^2+1\right)\left[2a\left(C_{d0}^2 + C_{l0}^2\right) - \left(C_{DX} + C_{LY}\right)\right] - \left(R_k^2+1\right)\cdot\left[2C_{LY} + C_{DX} - R_f\left(2C_{DY} - C_{LX}\right)\right]\right] \\
&\quad + 9\left(R_k^2 C_{DX} + C_{LY}\right) + 2\left(2R_k^2+1\right)\left[2C_{LY} + C_{DX} - R_f\left(2C_{DY} - C_{LX}\right)\right] \\
a^{-4}C_{d0}^{-2}A_1 &= 3\left[2a\left(C_{d0}^2 + C_{l0}^2\right) - \left(C_{DX} + C_{LY}\right)\right]\left[R_f\left(2C_{DY} - C_{LX}\right) - 2C_{LY} - C_{DX}\right] \\
&\quad - 9\left(C_{DX}C_{LY} - C_{LX}C_{DY}\right) - \left[2C_{LY} + C_{DX} - R_f\left(2C_{DY} - C_{LX}\right)\right]^2 \\
R_f &= C_{L0}/C_{D0}
\end{aligned} \tag{3.21}$$

If a real positive root of U_R for (3.20) exists and the condition $c_1 > 0$ holds, the Hopf bifurcation will occur. This loss of stability (of the downstream cylinder) is commonly referred as fluid stiffness controlled fluidelastic instability or wake induced flutter. The existence of U_R requires that the following condition must be satisfied:

$$\Delta_u = A_2^2 - 4A_1A_3 > 0 \tag{3.22}$$

Equation (3.22) can be re-written as:

$$\begin{aligned}
\Delta_u &= 4\left(2R_k^2+1\right)^2\left(C_{d0}^2 + C_{l0}^2\right)^2 a^2 + \left(1 - R_k^2\right)^2\left[R_f^2\left(2C_{DY} - C_{LX}\right)^2 - 8C_{LX}C_{DY}\right] \\
&\quad + 4\left(1 - R_k^2\right)\left(C_{d0}^2 + C_{l0}^2\right) \times \left[R_f\left(2C_{DY} - C_{LX}\right)\left(2R_k^2 - 1\right) + 4\left(C_{LY} - R_k^2 C_{DX}\right)\right]a \\
&> 0
\end{aligned} \tag{3.23}$$

Equation (3.23) is a necessary condition for Hopf bifurcation to occur, which imposes certain restrictions on the mass parameter and the stiffness ratio R_k. For a particular case of stiffness ratio, a must satisfy the following conditions:

$$0 < a < \frac{R_k^2 - 1}{2\left(2R_k^2 + 1\right)^2\left(C_{d0}^2 + C_{l0}^2\right)}\left[R_f\left(2C_{DY} - C_{LX}\right)\left(2R_k^2 - 1\right) + 4\left(C_{LY} - R_k^2 C_{DX}\right) - 2\,\mathrm{sgn}\left(R_k^2 - 1\right)\left(2\Delta_a\right)^{1/2}\right] \tag{3.24a}$$

When

$$\begin{aligned}\Delta_a = &-R_k^2 R_f^2\left(2C_{DY} - C_{LX}\right)^2 + C_{LX}C_{DY}\left(2R_k^2 + 1\right)^2 \\ &+\left(C_{LY} - R_k^2 C_{DX}\right) \times \left[R_f\left(2R_k^2 - 1\right)\left(2C_{DY} - C_{LX}\right) + 2\left(C_{LY} - R_k^2 C_{DX}\right)\right] \\ &> 0\end{aligned} \tag{3.24b}$$

However, when

$$\Delta_a \le 0 \tag{3.25}$$

The existence of real U_R which makes $c_1c_2c_3 - c_1^2 - c_3^2c_0 = 0$ is automatically guaranteed.

These conditions show the restriction of mass parameter on the system Hopf bifurcation. From condition (3.23) it can be seen that stiffness ratio and mass parameter are two interrelated parameters. It shows that for a similar system with same stiffness ratio, a system with a large mass parameter is more stable to the fluid stiffness controlled Hopf bifurcation.

The reason can be understood in the following way. Fluid damping is proportional to aU_R, while fluid stiffness is proportional to aU_R^2. For a fluid damping matrix positive definite case, fluid damping consumes energy when the cylinder moves. The only way to bring energy into the system, to cause instability, is via the fluid stiffness coupling. Such energy has to counterbalance with the energy consumed by the system damping. Imagining two scenarios, one with a small mass parameter a_1 and the other with a large mass parameter a_2, when $a_1U_{R1}^2 = a_2U_{R2}^2$, the input energy by fluid stiffness is same for two systems. However, due to $a_2 > a_1$, the energy consumed by the fluid damping for the large mass parameter case is $\sqrt{a_2/a_1}$ times more than for the small mass parameter one, which makes the Hopf bifurcation much more difficult to occur, hence the system with a large mass parameter is more stable with regard to Hopf bifurcation.

By solving Equation (3.20), the critical reduced velocity for the system to lose and gain its stability is given by:

$$aU_R^2 = \left\{-\left\{6a\left(2R_k^2+1\right)\left(C_{d0}^2+C_{l0}^2\right)+\left(R_k^2-1\right)\left[R_f\left(2C_{DY}-C_{LX}\right)+4\left(C_{LY}-C_{DX}\right)\right]\right\}\pm 3\Delta_u^{1/2}\right\}$$
$$\div 2\left\{6a\left(C_{d0}^2+C_{l0}^2\right)\left[R_f\left(2C_{DY}-C_{LX}\right)-2C_{LY}-C_{DX}\right]+\left[-4C_{DX}C_{LY}+\left(4R_f^2+9\right)C_{LX}C_{DY}\right.\right.$$
$$\left.\left.+R_f\left(-2C_{DX}C_{DY}+C_{DX}C_{LX}+2C_{LY}C_{DY}-C_{LX}C_{LY}\right)\right]+2\left(C_{DX}^2+C_{LY}^2\right)-R_f^2\left(C_{LX}^2+4C_{DY}^2\right)\right\} \tag{3.26a}$$

together with the condition of

$$aU_R^2\left[C_{DX}+2C_{LY}+R_f\left(C_{LX}-2C_{DY}\right)\right]<1+2R_k^2 \tag{3.26b}$$

Discussion

From above analysis, together with the condition for stiffness ratio (3.24b), in the fluid damping matrix positive definite area, mathematically, there are the following possibilities for Δ_a and Δ_u regarding the Hopf bifurcation, i.e.

(c.1) $4C_{LX}C_{DY}-2R_fC_{DX}\left(2C_{DY}-C_{LX}\right)+2C_{DX}^2<0$, and

$$\Delta_k=\left[-R_f^2\left(2C_{DY}-C_{LX}\right)^2+R_f\left(2C_{DY}-C_{LX}\right)\left(2C_{LY}+C_{DX}\right)+4\left(C_{LX}C_{DY}-C_{DX}C_{LY}\right)\right]^2$$
$$-4\left[4C_{LX}C_{DY}-2R_fC_{DX}\left(2C_{DY}-C_{LX}\right)+2C_{DX}^2\right]\left[C_{LX}C_{DY}-R_fC_{LY}\left(2C_{DY}-C_{LX}\right)+2C_{LY}^2\right]$$
$$<0$$

Which makes $\Delta_a<0$.

If the above conditions are satisfied, Hopf bifurcation is independent of stiffness ratio and mass parameter.

(c.2) $\Delta_k>0$

Mathematically, there exists a value for R_k which makes $\Delta_a < 0$. When there is a physically sensible R_k, Hopf bifurcation is independent of mass parameters under such a condition.

(c.3) $\Delta_a > 0, \Delta_u > 0$

For values of R_k other than (c.1) and (c.2), Δ_a is positive. For such vales of R_k, the mass parameter has to satisfy the restriction condition of (3.24) should any Hopf bifurcation be possible. It is further seen that when, and only when, $U_R^2 > 0$ and (3.26b) are satisfied, the Hopf bifurcation can occur. The traditional wake induced flutter for transmission line falls into this category. If the solution is $U_R^2 > 0$ while $c_1 < 0$, it is only an indicator that the system has lost its stability before flow velocity reaches solution of U_R via stationary bifurcation. Other solutions, of negative U_R^2, only show Hopf bifurcation as not being possible.

(c.4) $\Delta_a > 0$ and $\Delta_u < 0$

Such combination of Δ_a and Δ_u only shows that Hopf bifurcation is not possible.

Undamped Flutter Theory and the Effect of Spring Coupling Angle θ

When the damping (both structural and fluid) is neglected, as shown in (3.23), when

$$C_{LX}C_{DY} < 0 \tag{3.27}$$

then $\Delta_u > 0$, Hopf bifurcation becomes potential. Such an area is usually located at the outer part of the wake. This is the conclusion of classical undamped wake induced flutter theory (Blevins, 1990). However, the spring coupling essentially changes the characteristics of the fluid force, as shown in Equation 3.15, and eventually it can alter the stability characteristics significantly.

Considering the same undamped case, the former condition (3.27) for flutter becomes:

$$\begin{aligned}&\left[C_{LX}\cos^2\theta - C_{DY}\sin^2\theta + (C_{DX} - C_{LY})\sin\theta\cos\theta\right]\\ &\times\left[C_{DY}\cos^2\theta - C_{LX}\sin^2\theta + (C_{DX} - C_{LY})\sin\theta\cos\theta\right] < 0\end{aligned} \tag{3.28}$$

which makes the possibility of Hopf bifurcation increased or decreased, depending on whether the coupling angle is smaller or larger than

$$\frac{1}{2}\tan^{-1}\frac{2(C_{LX} + C_{DY})(C_{DX} - C_{LY})}{(C_{LX} + C_{DY})^2 - (C_{DX} - C_{LY})^2}$$

the involvement of $(C_{DX} - C_{LY})$ makes the stability more position and coupling dependent. The condition (3.28) can be re-written as:

$$\left[(C_{DX} - C_{LY})^2 - (C_{LX} - C_{DY})^2\right]\tan^2(2\theta) + 2(C_{DX} - C_{LY})(C_{DY} + C_{LX})\tan(2\theta) + 4C_{DY}C_{LX} < 0 \tag{3.29}$$

Potentially, most part of the wake can meet the condition of (3.29), as long as coupling angle is appropriate. Nevertheless, it should be emphasized here that the coupling angle has demonstrated a significant role it can play in the system stability. This conclusion is drawn from undamped flutter theory and applies mainly for small mass parameter cases. The condition for a Hopf bifurcation to occur, when mass parameter is large, can be much more strict, which will be seen in the later presented results.

One interesting point here is that, no matter how the coupling angle changes or whatever the mass parameter may be, Hopf bifurcation is unlikely to occur on the wake centreline. As for the case of

$\theta = 0^0$, then $\Delta_u = 0$, and when $\theta \neq 0^0$, it is seen that (3.29) is impossible to satisfy. Therefore, the wake centreline is always a Hopf bifurcation free area for FDMPD.

3.3.1.1.2 Fluid Damping Matrix Not Positive Definite (FDMNPD)

In such a region, the negative fluid damping can self-excite the movement of the downstream cylinder, even for a single-degree-of-freedom system(Bokaian 1989; Bokaian & Geoola 1984), as long as the energy brought in by the fluid damping can counter-balance the energy consumed by the system. If structural damping is neglected, the results show that as long as the fluid drag force is negative, the system is unstable. When structural damping is considered, by utilising condition (3.18), it is seen that Hopf bifurcation occurs when $c_3 = 0$. This kind of instability is often referred as wake induced galloping. The critical flow velocity for Hopf bifurcation is:

$$aU_R = -4\xi / 3C_{d0} \text{ for } R_k = R_\xi = 1 \tag{3.27}$$

3.3.1.2 Stationary bifurcation

Another possible scenario for losing stability is through the stationary bifurcation. It can be seen from Equation (3.17) that when $c_0 = 0$, then one of the eigenvalues is zero. If all other conditions of (3.18) are satisfied, it is a critical state for a stationary bifurcation and the corresponding reduced velocity is the critical reduced velocity. When the reduced velocity is larger than this critical value, one of eigenvalues can become a positive real number. Therefore, the critical state of the stationary bifurcation is given by:

$$c_0 = 0 \tag{3.28}$$

The physical interpretation of this condition can be drawn from Equation (3.11). It is clear that the fluid stiffness is proportional to the aU_R^2. As the reduced velocity increases, it is possible that the fluid stiffness will become larger than the spring stiffness, resulting in an effective negative stiffness

along certain directions. This would be dependent on the particlar spring coupling. Under this circumstance the system will lose its stability as any disturbance will grow with time.

By solving Equation (3.28), the solution of the critical reduced velocity is given by:

$$aU_R^2 = \frac{\left(R_k^2 C_{DX} + C_{LY}\right) - \sqrt{\left(R_k^2 C_{DX} - C_{LY}\right)^2 + 4R_k^2 C_{LX} C_{DY}}}{2\left(C_{DX} C_{LY} - C_{LX} C_{DY}\right)} \tag{3.29a}$$

together with condition

$$\begin{cases} c_3 > 0 \\ c_1 > 0 \\ c_2 c_3 - c_1 > 0 \end{cases} \tag{3.29b}$$

(3.29a) also shows that when

$\left(R_k^2 C_{DX} - C_{LY}\right)^2 + 4R_k^2 C_{LX} C_{DY} < 0$

or

$C_{DX} C_{LY} - C_{DY} C_{LX} > 0$ and $R_k^2 C_{DX} + C_{LY} < 0$,

there are no stationary bifurcations.

3.3.2 Direct Numerical Eigenvalue Seeking

The stability of system (3.11) can be analysed directly by seeking numerical eigenvalues. Because the matrix is of 4×4 size, the calculation is straightforward. By predefining the sets of control parameters, such as stiffness ratio, mass parameter, coupling angle, structural damping coefficient, and relative location and by varying the parameter of flow velocity, the stability can be analysed systematically. The advantage of the method is its straightforwardness, irrespective of physical parameter conditions. Meanwhile, the variation of eigenvalues can shed light on the understanding of the process of losing or gaining stability. The shortcomings are: the extra work needed to pick out the critical state if it is of interest to the investigation, the effect of individual control parameter isn't straightforward and if the system is in high order, the computation can be time consuming.

The systematic analysis made in this thesis is a combination of traditional Routh-Hurwitz stability algorithm and direct numerical eigenvalue seeking.

3.4 Numerical Results

The drag and lift coefficients on the downstream cylinder are the prerequisites for the stability analysis. These coefficients are dependent upon the position of the downstream cylinder relative to the upstream one. The results of calculations made in previous chapter, together with collated experimental data for small spacings between two cylinders (Bokaian & Geoola, 1984; Zdravkovich, 1977 etc.) are used. The calculation of wake flow velocity U is made by the method introduced in Chapter II.

The stability analysis is carried out by assuming that the downstream cylinder is situated at an arbitrary equilibrium position. This is followed by finding the critical value of the reduced velocity, beyond which the cylinder will become unstable. The values of the mass parameter, stiffness ratio, and coupling angle are allowed to vary within certain ranges.

The calculations show that, typically, the whole wake can be classified into four scenarios based upon the uncoupled case:

(a) FDMPD at the wake centreline and inner part of the wake with medium or large spacings,

(b) FDMPD at outer part of the wake with medium or large spacings,

(c) FDMPD with $\Delta_a < 0$,

(d) and the FDMNPD.

The results are presented according to different regions separately.

3.4.1 Outer Wake at Medium or Large Spacing (FDMPD)

Figures 3.3 and 3.4 are stability boundary diagrams for mass parameters of *0.2* and 2×10^{-4}, at a given equilibrium position of X_0 = *5* and Y_0 = *2*. The mass parameter of *0.2* represents the case for marine risers. The small mass parameter shown here is to give a comparison to account for the effect of the mass parameter. The position is located at the outer part of the wake, with medium spacing, which holds the most fluid force characteristics at large spacing, the spring coupling angle θ is 0^0.

It is seen that for the case of marine risers, i.e. large mass parameter, the most likely type of bifurcation that will be encountered is stationary bifurcation. Mathematically, if the abscissa R_k reaches a high ratio, say *1.75* here, it is possible that the system can become unstable via Hopf bifurcation. Nevertheless, for the practical case of marine risers, the spring stiffness ratio represents the ratio of stiffness in the out-of-plane and in-plane motions, which is close to and often smaller than *1*. For this reason, the stationary bifurcation is more likely to be the case under these conditions. On the other hand, when the mass parameter is small (ref. Figure 3.4), as with the case of transmission lines in air, the route for the system to become unstable is more likely via the Hopf bifurcation. Although stationary bifurcation is theoretically possible, the critical speed is unrealistically high. Calculations also show that, at position X_0=*5*, Y_0=*2*, when $R_k > 1.75$, then $\Delta_a < 0$ (ref. Figure 3.5). This is the scenario for Hopf bifurcation being independent of mass parameter. This is the case for (c.2), as discussed in section 3.3.1.1.1. Under such conditions, the downstream cylinder tends to Hopf bifurcation as long as flow velocity reaches the critical state, no matter large or small the mass parameter may be. However, according to Figure 3.5, $R_k < 1.75$, $\Delta_a > 0$, Hopf bifurcation is dependent on mass parameter and stiffness ratio, and the limitation on mass parameter (3.24) applies. Hopf bifurcation is possible only when mass parameter is below the critical line shown in the Figure 3.6. This explains the difference shown in Figure 3.3 and 3.4. These

results are typical for the downstream cylinder located at the outer part of the wake, with medium or large spacing.

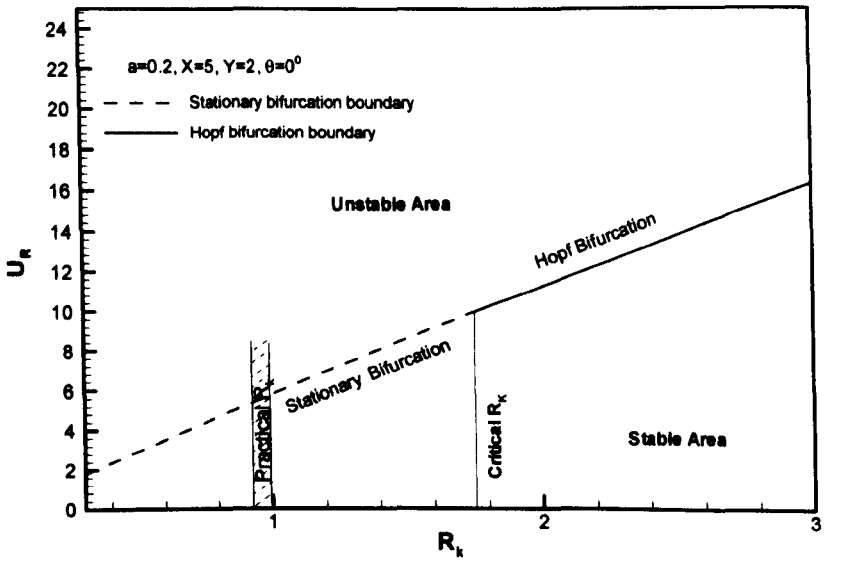

Figure 3.3 Stability boundary at spacing of $X_0=5$, $Y_0=2$ with $a=0.2$, $\theta=0^0$, typical for marine riser cases.

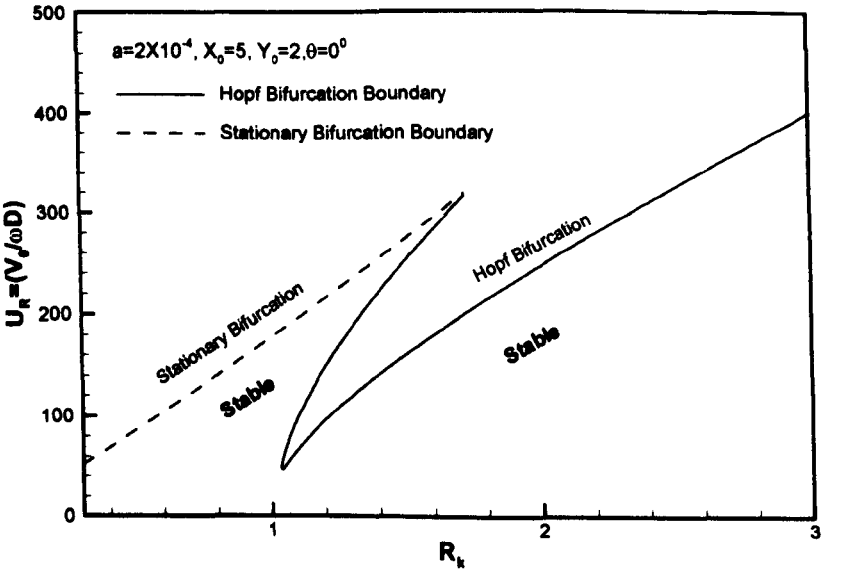

Figure 3. 4 Stability boundary at spacing of $X_0=5$, $Y_0=2$ with $a=2\ 10^{-4}$, $\theta=0^0$, typical for transmission lines case.

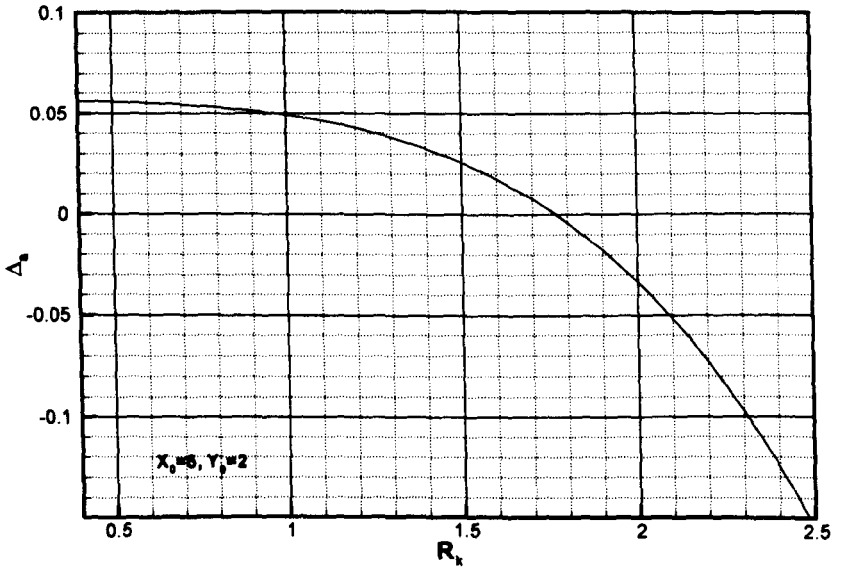

Figure 3. 5 Variation of Δ_a with stiffness ratio at position X_0=5, Y_0=2.

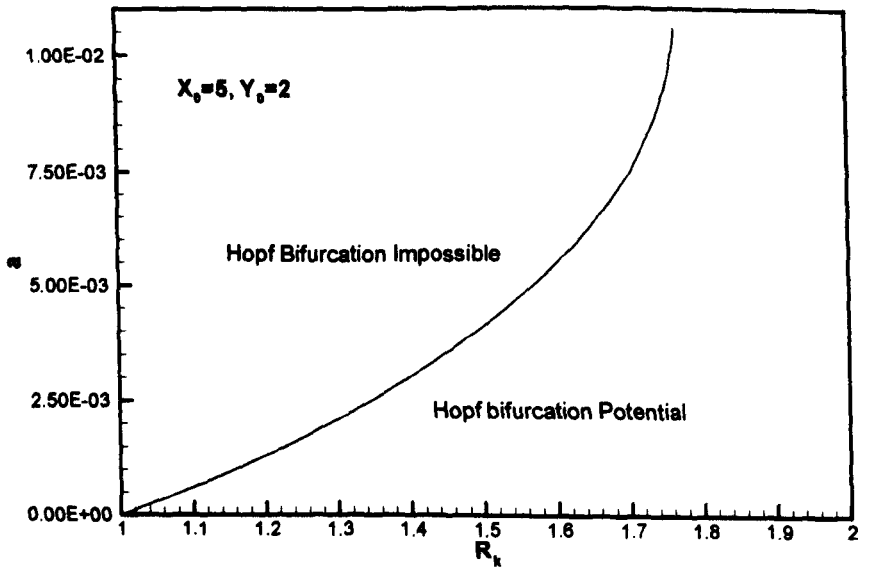

Figure 3. 6 Hopf bifurcation restriction on mass parameter for position X_0=5, Y_0=2.

Figures 3.7 to 3.10 show the cases for position of $X_0=8$, $Y_0=2.5$ and $X_0=10$, $Y_0=2.5$ respectively. It is seen that all these positions share the same characteristics of the stability boundary with the case of $X_0=5$, $Y_0=2$.

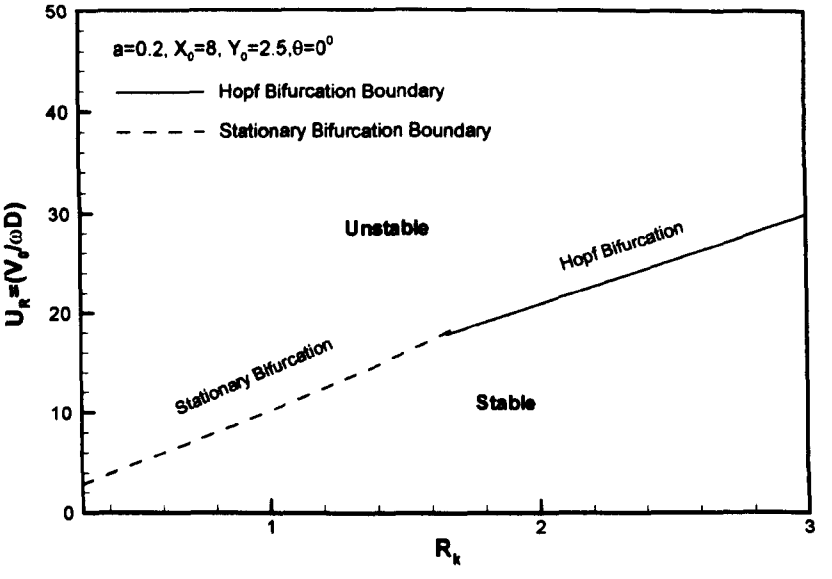

Figure 3.7 Stability boundary for position $X_0=8$, $Y_0=2.5$, $a=0.2$.

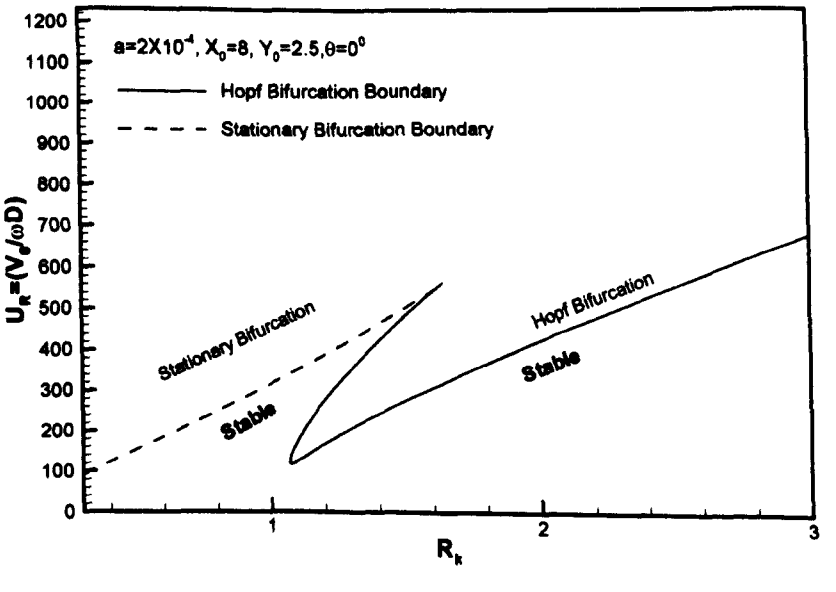

Figure 3.8 Stability boundary for position $X_0=8$, $Y_0=2.5$, $a=2\times10^{-4}$

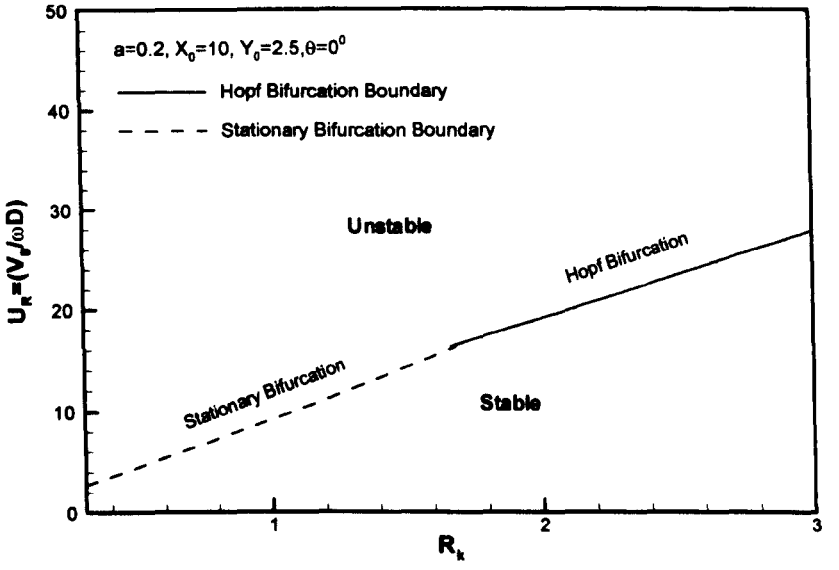

Figure 3.9 Stability boundary at position $X_0=10$, $Y_0=2.5$, $a=0.2$.

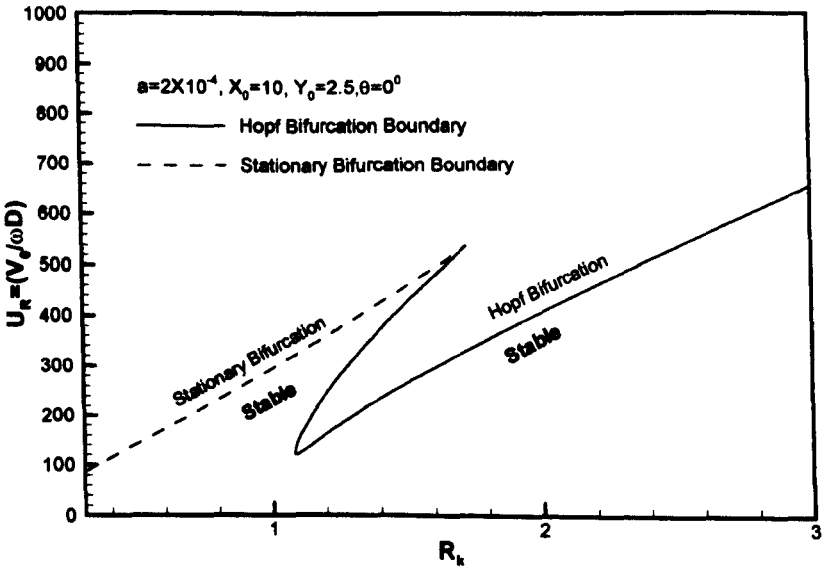

Figure 3.10 Stability boundary at position $X_0=10$, $Y_0=2.5$, $a=2\times10^{-4}$.

3.4.1.1 The Effect of Mass Parameter, Structural Damping, Spring Coupling

Figure 3.11 is an alternative view of the relationship between stiffness ratio and mass parameter. It shows the variation of the stability boundary with mass parameter at the location $X_0=5$, $Y_0=2$. The stiffness ratio is set as *1.1* and there is no spring coupling. It is seen that for the specified stiffness ratio, when mass parameter is small, with the increasing of flow velocity, the cylinder will lose stability via Hopf bifurcation and gain stability when flow velocity is further increased to another critical state. Finally, the cylinder will lose its stability via stationary bifurcation. However, when mass parameter is large, under the specified stiffness ratio, the cylinder will lose its stability only via stationary bifurcation. Figures 3.12 and 3.13 show the variation of eigenvalue with flow velocity for the case of $a=0.2$ and $a=2\times10^{-4}$ with $R_k=1.1$ at $X_0=5$, $Y_0=2$ respectively. It is seen that for the case of $a=0.2$, before the flow velocity reaches critical state, the eigenvalue pair first arrive at the real axis. At critical state, i.e. point S labelled in the Figure 3.12, one of the eigenvalue pair gets to the origin of the complex plane of eigenvalues. When flow velocity is further increased, one eigenvalue will pass the imaginary axis onto the real axis and stay in the right half of the eigenvalue plane. On the other hand, for the case of $a=2\times10^{-4}$, the eigenvalue first transverse the imaginary axis at critical state of Hopf bifurcation, i.e. H_1 as labelled in the Figure 3.13, and the eigenvalue pair will stay in the right half plane for certain ranges of flow velocity. When flow velocity reaches another critical state H_2, where the system gains its stability, the eigenvalue pair transverses across the imaginary axis and back to the left half plane. Finally, when flow velocity is further increased, the eigenvalue will reach the real axis and pass to the right half plane through origin at S in the figure, exhibiting stationary bifurcation.

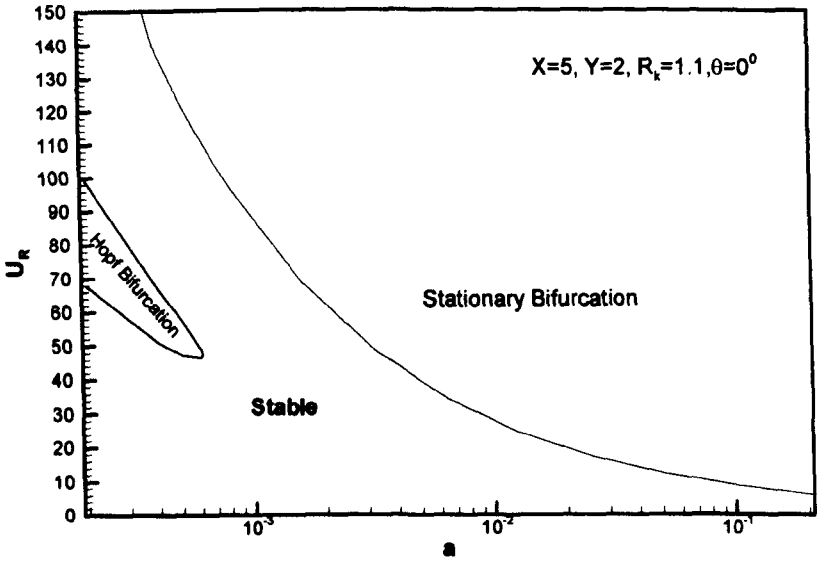

Figure 3.11 Effect of mass parameter on stability boundary.

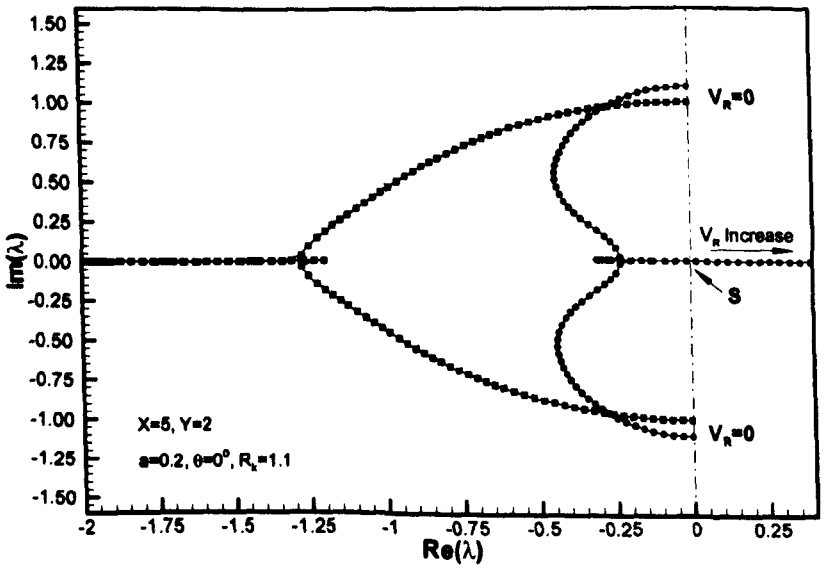

Figure 3.12 Variation of eigenvalues with flow velocity.

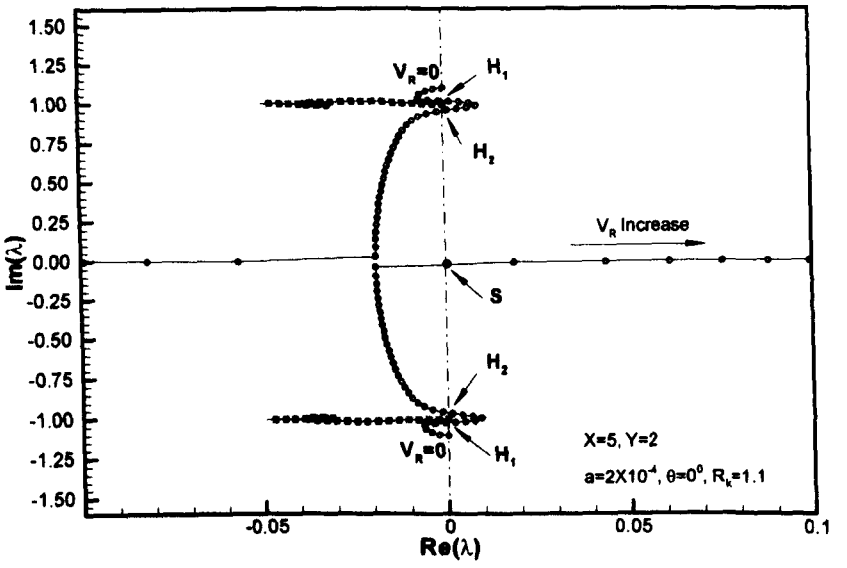

Figure 3.13 Variation of eigenvalues with flow velocity.

Figures 3.14 and 3.15 show the effect of spring coupling. The relative spacing and stiffness ratio are taken as having the same value as above. It is seen that for a large mass parameter, no matter how the spring coupling angle changes, there is only stationary bifurcation, whilst for small mass parameter the coupling angle can make the Hopf bifurcation disappear or vice versa. Essentially, it can be viewed as the result of a changed fluid force field. This is in agreement with the discussion about the effect of θ which is based on the case of the undamped condition. The result shows that the effect of spring coupling to large mass parameter is lessened. Figure 3.16 shows the effect of structural damping on the Hopf bifurcation boundary. As it is obvious that damping has no effect on stationary bifurcation, however, the figure shows that Hopf bifurcation (stiffness controlled fluidelastic stability) is insensitive to the structural damping even for small mass parameter. Only when the structural damping is large enough, can the Hopf bifurcation be suppressed.

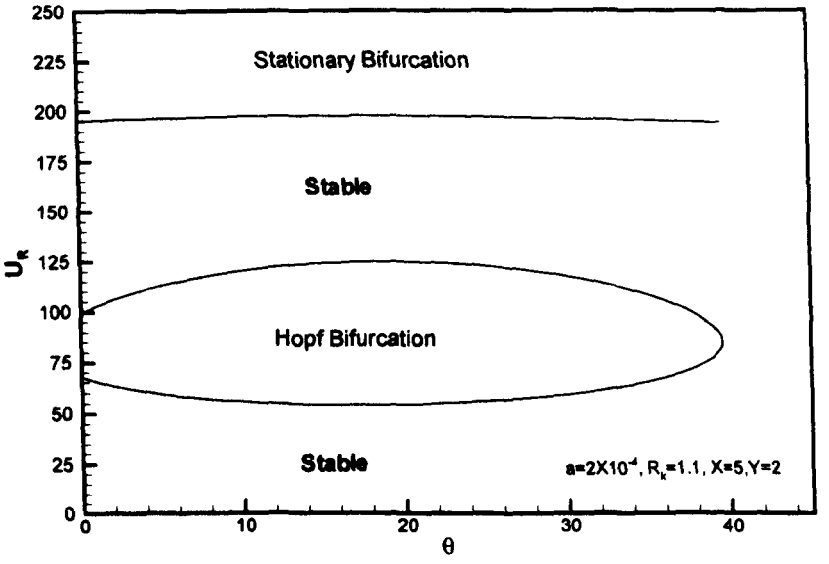

Figure 3.14 Effect of spring coupling angle on stability boundary.

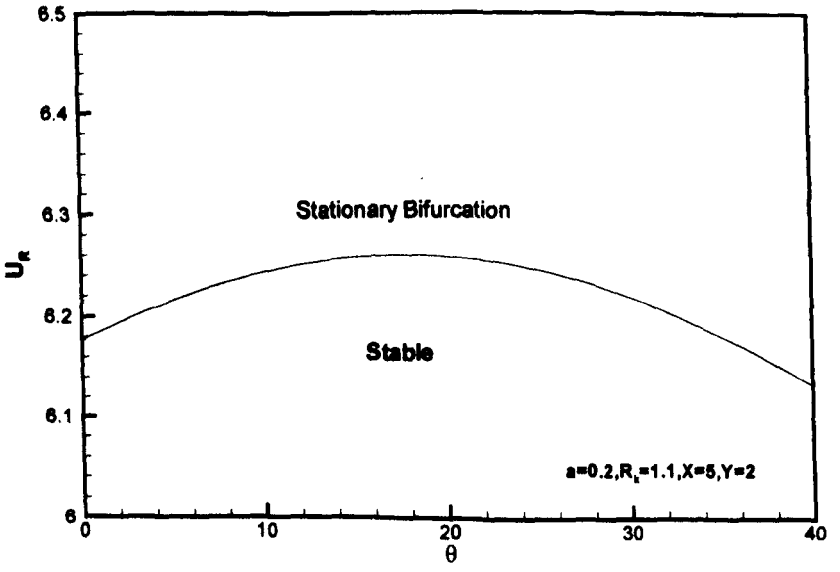

Figure 3.15 Effect of spring coupling angle on stability boundary.

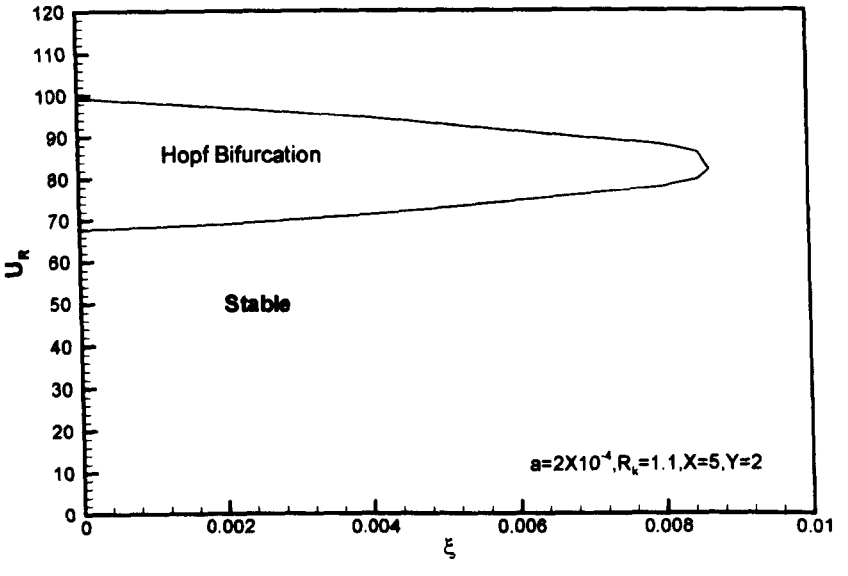

Figure 3.16 Effect of structural damping on stability boundary.

3.4.2 Inner Wake and Centreline With Medium or Large Separation (FDMPD)

Figures 3.17 and 3.18 are representative cases for the downstream cylinder located near or on the wake centreline at large spacing. It is unlikely to be Hopf bifurcation, no matter whether the mass parameters are small or large. The variation of the stability boundary with the stiffness ratio or coupling angle is only due to the variation of stiffness in Y direction or the coupling effect. Such a bifurcation boundary is independent of structural damping and insensitive to the spring coupling angle and stiffness ratio. This is a Hopf bifurcation free area. It also can be seen that the critical speed is proportional to the root square of mass parameter as has been shown in equation 3.29. If mass parameter is very small, the critical speed can be so unrealistically high that practically it will not occur. However, such bifurcation is likely to happen for a large mass parameter such as marine risers.

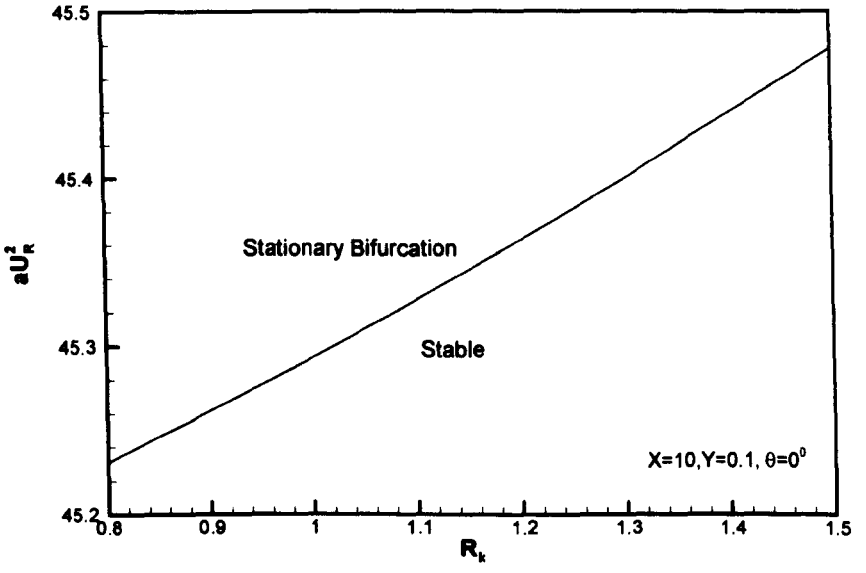

Figure 3.17 Stability boundary at $X_0=10, Y_0=0.1$.

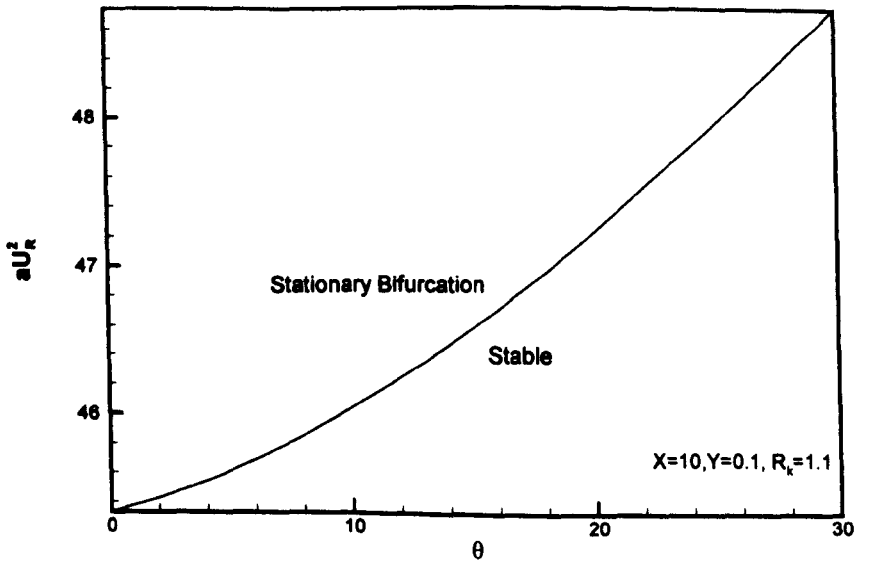

Figure 3.18 Stability boundary at $X_0=10, Y_0=0.1$.

3.4.3 Small or Medium Spacing With $\Delta_a < 0$ (FDMPD)

When the cylinder spacing approaches the medium to small range, although the drag force is positive, the variation of the fluid force coefficient becomes significant in such a way that potentially it can cause the downstream cylinder to lose its stability either via Hopf bifurcation or stationary bifurcation. Figures 3.19 and 3.20 are the cases for the location of X_0=*2*, Y_0=*0.5* and X_0=*2*, Y_0=*1* with $\theta = 0^0$ and stiffness ration of *1.01*. It is seen that Hopf bifurcation is likely to happen no matter how small or large the mass parameter is. The abscissa in these two figures are structural damping coefficients, which shows that the Hopf bifurcation can be replaced by stationary bifurcation when the damping coefficient is large enough for a small mass parameter. However, it is hard to suppress a Hopf bifurcation for large mass parameters such as marine risers. Such a region is located in the vicinity of upstream cylinder and the fluid drag force is positive. Calculation shows such a region is insensitive to mass parameter and stiffness ratio and often with $\Delta_a < 0$ as shown in Figure 3.21, such a scenario is the case of c.2 in the discussion of section 3.3.1.1.1.

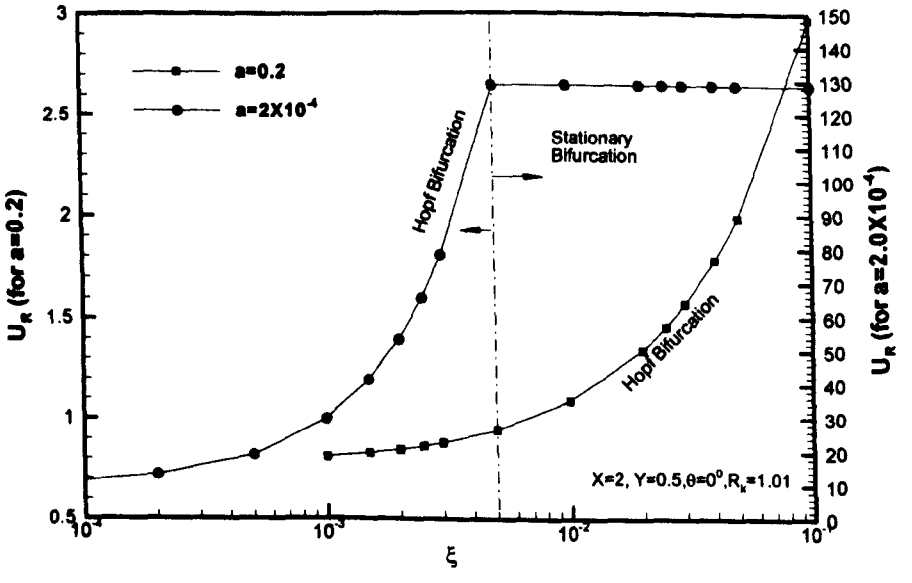

Figure 3.19 Stability boundary for small spacing with R_k=*1.01*.

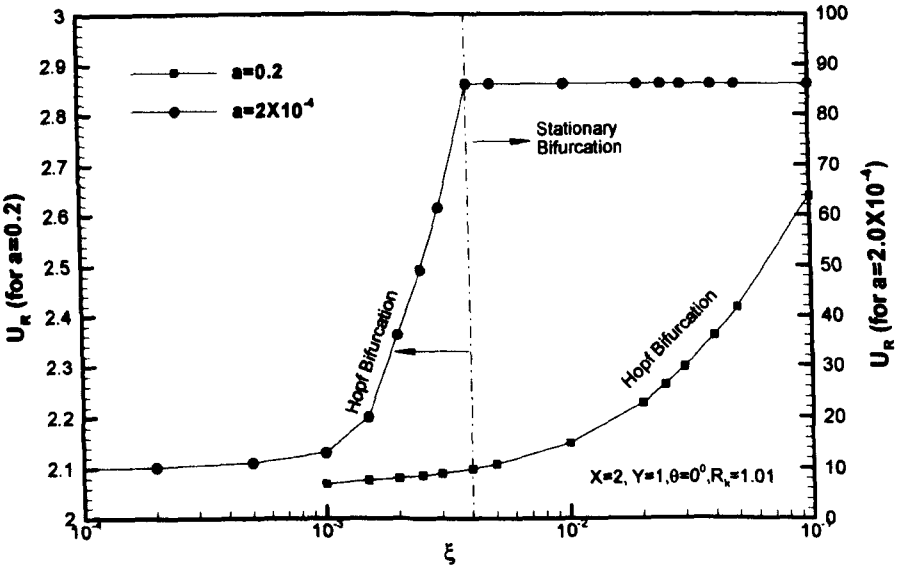

Figure 3.20 Stability boundary for small spacing with $R_k=1.01$.

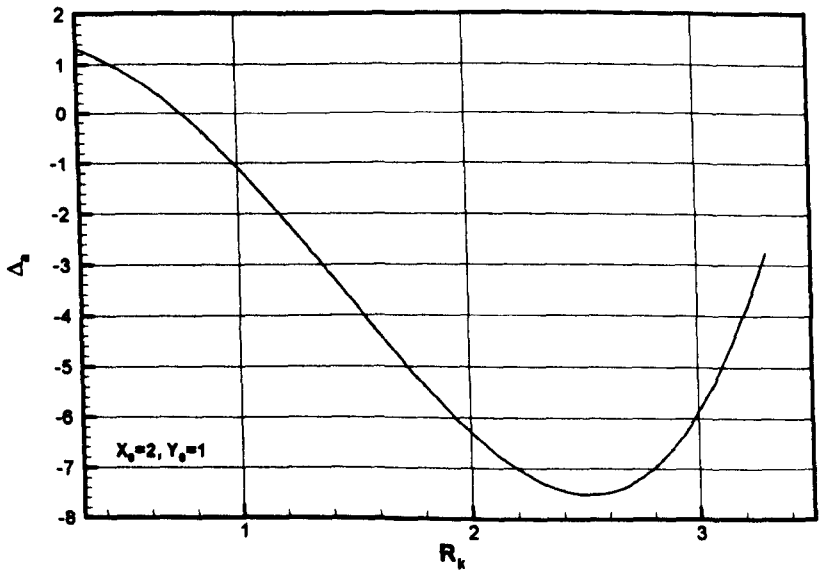

Figure 3.21 Variation of Δ_a with stiffness ratio at $X_0=2$, $Y_0=1$.

3.4.4 Small Spacing (FDMNPD)

Figures 3.22 and 3.23 show the stability boundary when the downstream cylinder is balanced at position of $X_0=2$, $Y_0=0$ and $Y_0=0.1$ respectively. The abscissa is structural damping. Such positions are within the region of negative fluid drag force. It is seen that, no matter whether the mass parameter is large or small, the downstream cylinder is prone to the Hopf bifurcation. The incipient velocity for the Hopf bifurcation is sensitive to the structural damping when the mass parameter is small, which explains why Hopf bifurcation can be supressed by the large structural damping. When the structural damping is large enough, the Hopf bifurcation can be transformed into the stationary bifurcation. On the other hand, the incipient velocity is less sensitive to the structral damping when the mass parameter is large, as in the case of marine riser interaction, which implies that the Hopf bifurcation is hard to supress. The difference related to the mass parameter is essentially caused by the interrelation of the structural and fluid damping. As can be perceived, such a region is damping controlled, and the stability is insensitive to the spring coupling or the stiffness ratio.

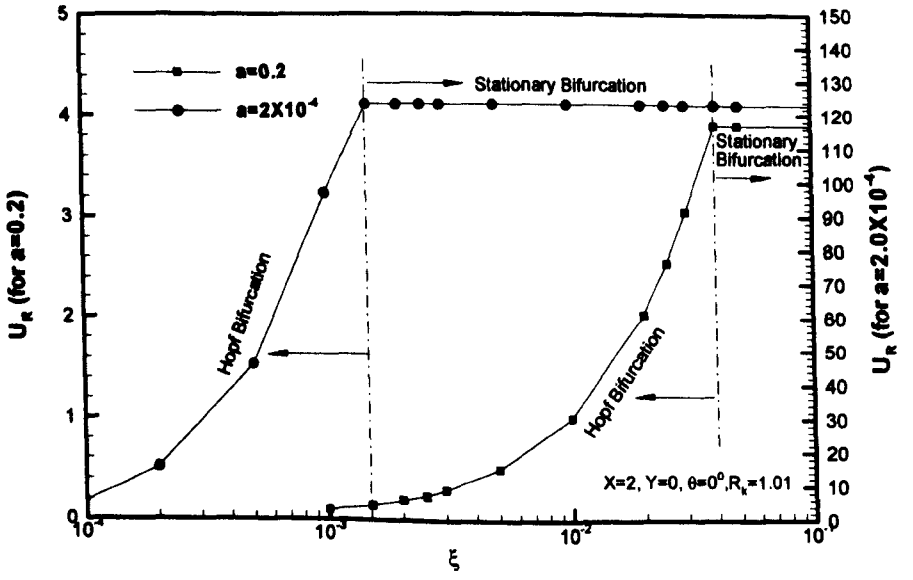

Figure 3.22 Stability boundary for position $X_0=2$, $Y_0=0$, with $R_k=1.01$.

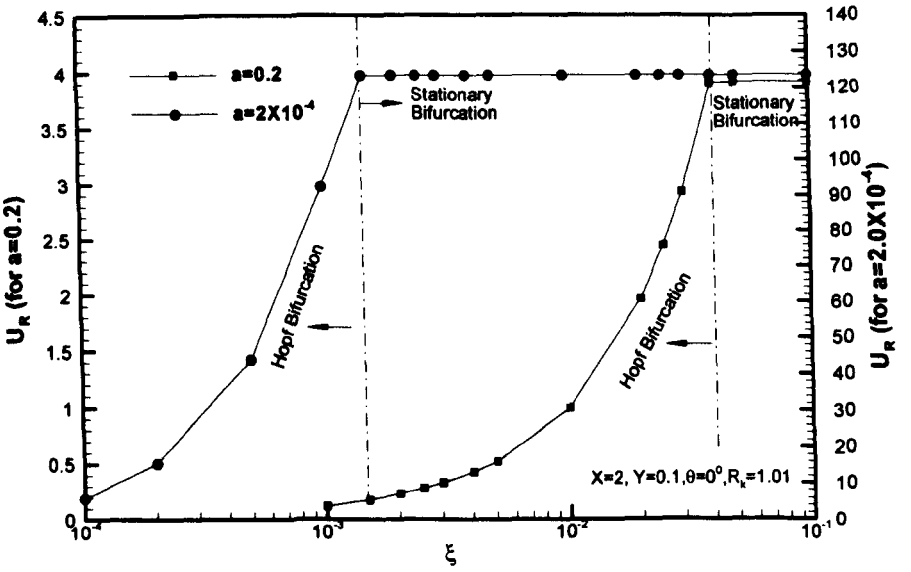

Figure 3.23 Stability boundary for position $X_0=2$, $Y_0=0.1$ with $R_k=1.01$.

3.5 Stable/Unstable Region Maps

Figures 3.24 to 3.41 are maps which show the stability of downstream cylinder at different locations, under specified mass parameters, stiffness ratios and spring coupling angles. Table 3.2 is the summary of the parameters adopted in these calculations.

Table 3. 2 Parameters for the maps.

Parameter	Value			
a	0.2	0.02	0.0002	
R_k	0.95, 1.0		1.05	1.1
U_R	2, 3, 4, 5, 8, 10, 12, 15		10, 20, 30, 40, 50, 60, 80, 100	
θ	0^0, 5^0, 10^0			

The shaded circle symbol represents an unstable location caused by Hopf bifurcation. The shaded square is an unstable location caused by stationary bifurcation. While hollow square represent stable area, the shaded circle sign with a plus sign inside also represents an unstable position caused by

Hopf bifurcation. The difference to the shaded circle without plus sign is that at such locations, there is a higher flow velocity, which can make the system regain its stability. In general, it is seen that in the vicinity of the upstream cylinder where the drag force is negative or its nearby area with $\Delta_a < 0$, Hopf bifurcation is likely to occur irrespective of the mass parameter and less sensitive to coupling angle. The unstable area spreads with the increase of flow velocity. On the other hand, in the area of medium or large spacing, stationary bifurcation is more likely to be the cause for the downstream cylinder to be unstable. Generally, stationary bifurcation starts from small spacing at outer wake region and spreads towards downstream and inner wake. Particularly shown in the figures, the spring coupling angle has no significant effect for the mass parameter of 0.02 and 0.2. However, it is a very important factor when mass parameter is 2×10^{-4}, for example, comparing Figure 3.36 and 3.38, 3.40, the large θ has led to a significantly enlarged unstable area.

Also implied in these figures is that, at the vicinity of the upstream cylinder and when the mass parameter is large such as with risers, there is a high chance that the fluidelastic behaviour can interact with the vortex induced vibration. Such an implication is consistent with the experimental observations (Bokaian, 1984).

3.6 Summaries

Based upon the work presented in this chapter, the following conclusions can be drawn:

1. In general the downstream cylinder can lose its stability and become unstable through two different types of bifurcation, i.e. Hopf bifurcation and stationary bifurcation.

2. Unlike power transmission lines, where the mass parameter is generally very small, in marine applications stationary bifurcation is the more likely scenario, particularly when two cylinders are widely spaced.

3. The value of the reduced velocity at the inception of instability is strongly influenced by the mass parameter. For stationary bifurcation, the critical reduced velocity is inversely proportional to the root square of mass parameter.

4. Stiffness ratio can be very important in the form of system bifurcation, however, a practical system often has a stiffness ratio close to 1.0. Spring coupling angle can significantly alter the stability characteristics when the mass parameter is small. However, when mass parameter is large, the role of spring coupling is insignificant.

5. To answer the question in table 3.1, the loss of stability is either in the way of fluid stiffness controlled, particularly when spacing between two cylinders is large, or fluid damping controlled, when the two cylinders are near to each other.

6. The systematic map of stable and unstable locations under specified flow condition and cylinder arrangements serves as a guide to judge stability when the equilibrium of two cylinders has been identified, additionally it quantitatively explains the effect of parameters, such as mass parameter, spring coupling angle, stiffness ratio, reduced flow velocity and equilibrium location on the stability and bifurcation type.

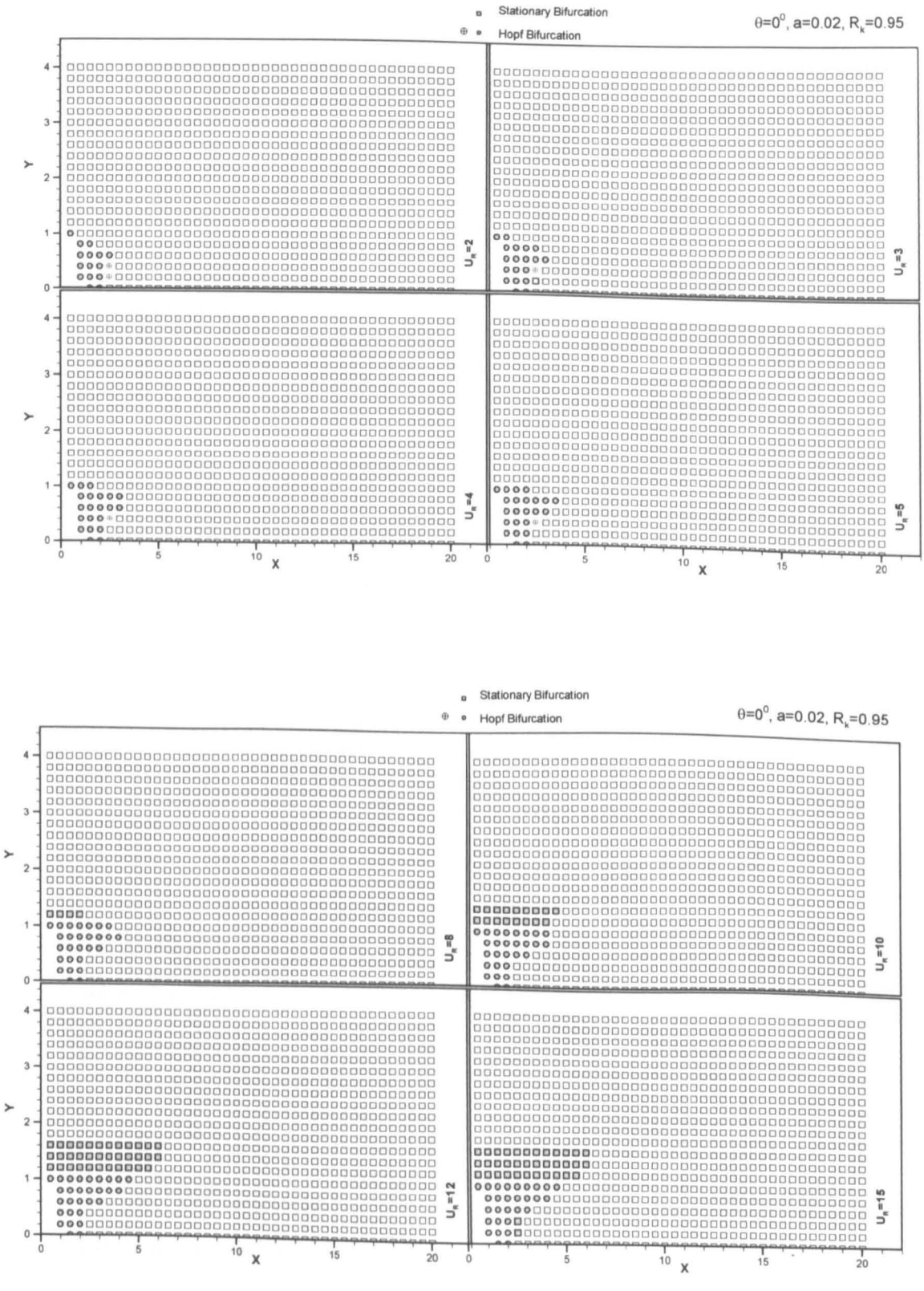

Figure 3.24 Stable/unstable equilibrium locations for the downstream cylinder under specified mass parameter a=0.02, spring coupling angle θ=0⁰, stiffness ratio R_k=0.95 and flow velocity.

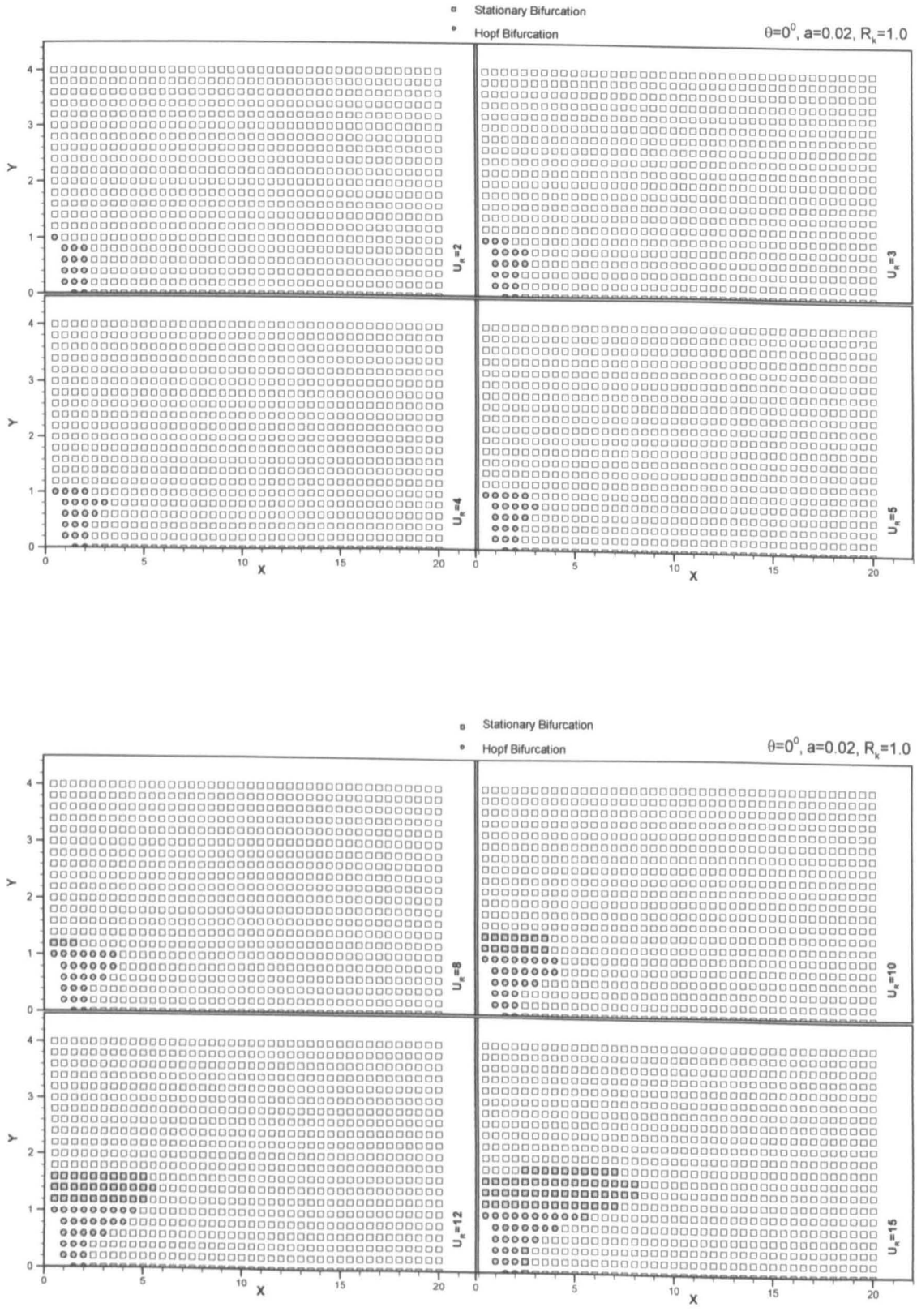

Figure 3.25 Stable/unstable equilibrium locations for the downstream cylinder under specified mass parameter a=0.02, spring coupling angle θ=0^0, stiffness ratio R_k=1.0 and flow velocity.

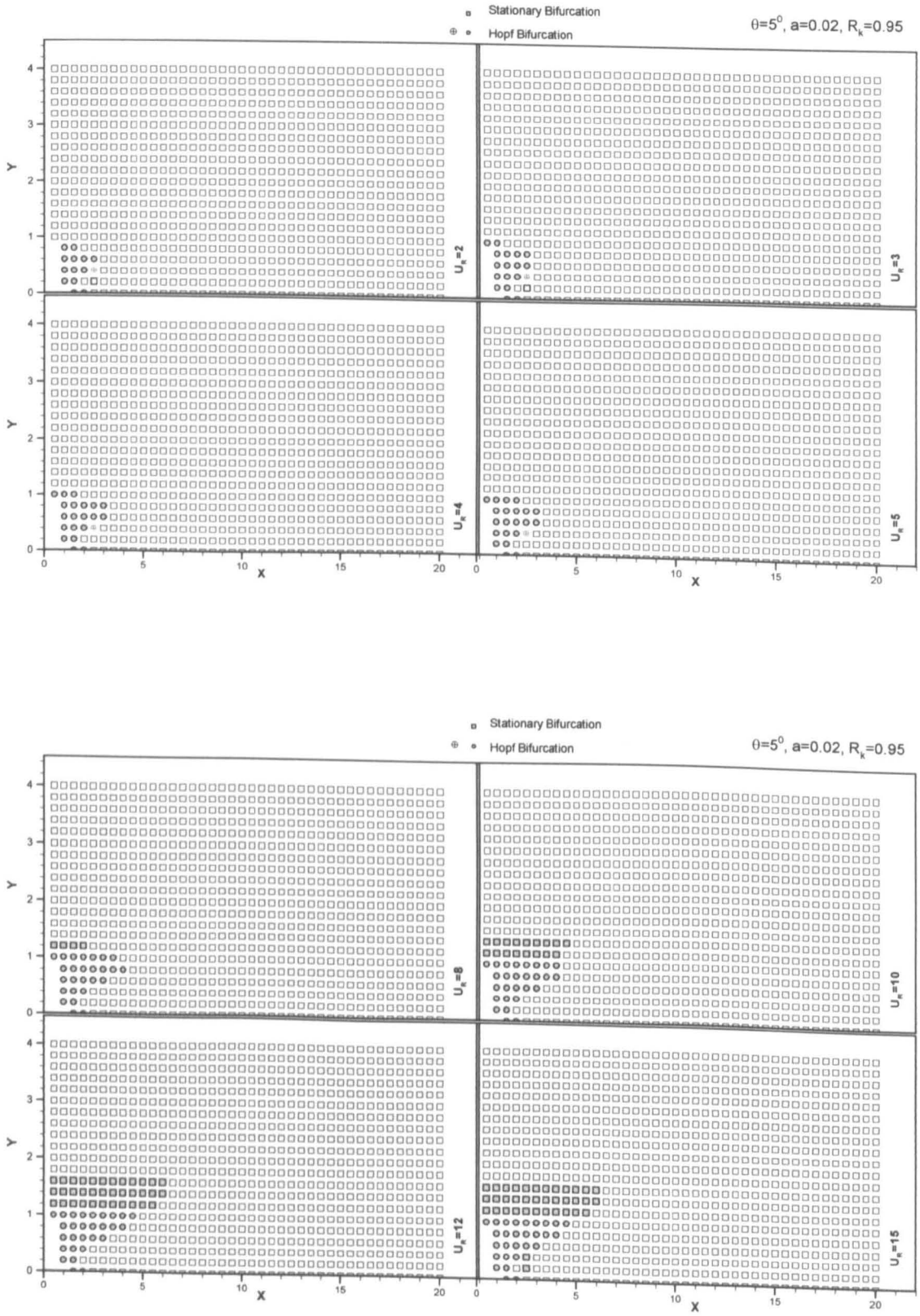

Figure 3.26 Stable/unstable equilibrium locations for the downstream cylinder under specified mass parameter a=0.02, spring coupling angle θ=5^0, stiffness ratio R_k=0.95 and flow velocity.

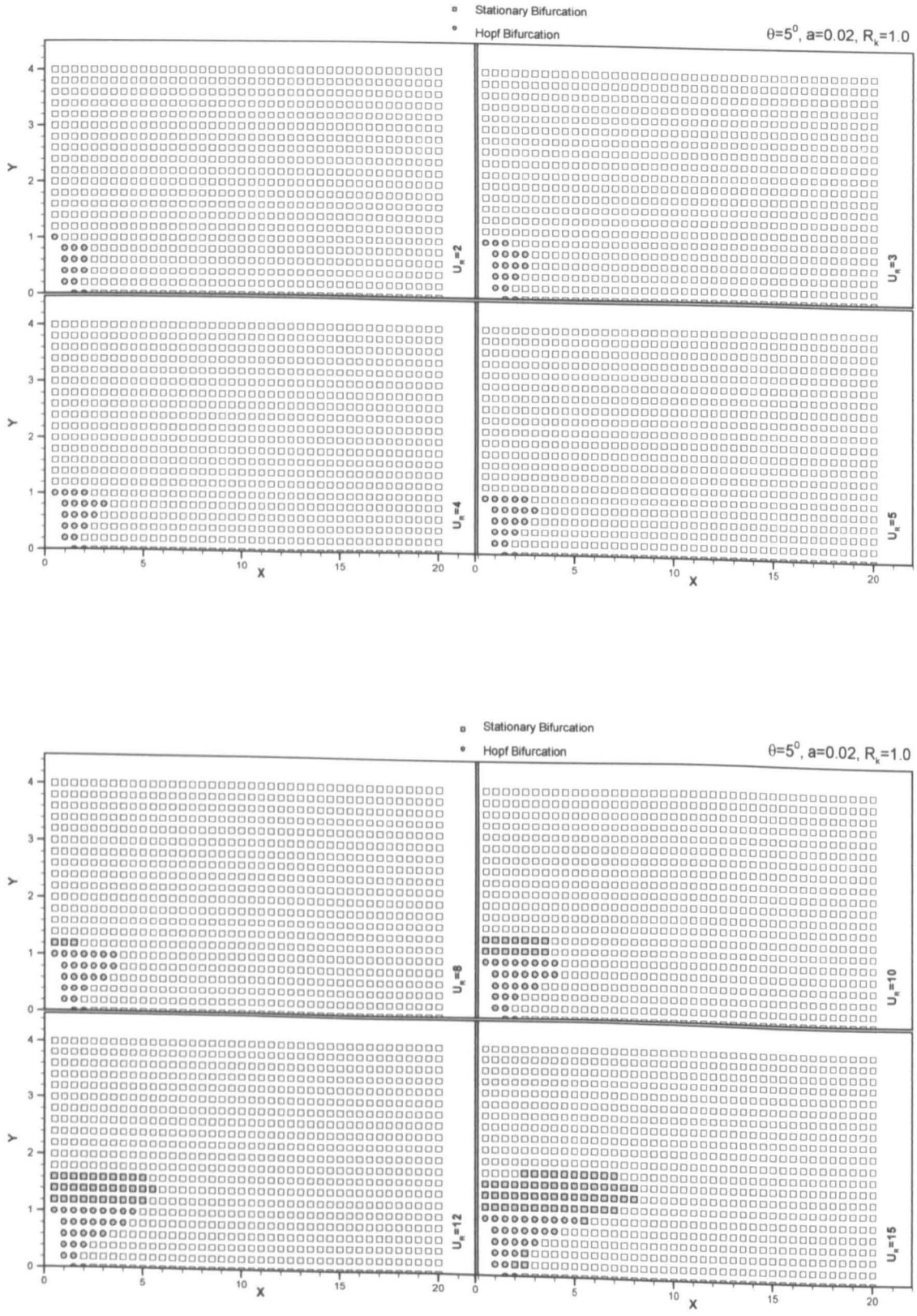

Figure 3.27 Stable/unstable equilibrium locations for the downstream cylinder under specified mass parameter a=0.02, spring coupling angle θ=5⁰, stiffness ratio R_k=1.0 and flow velocity.

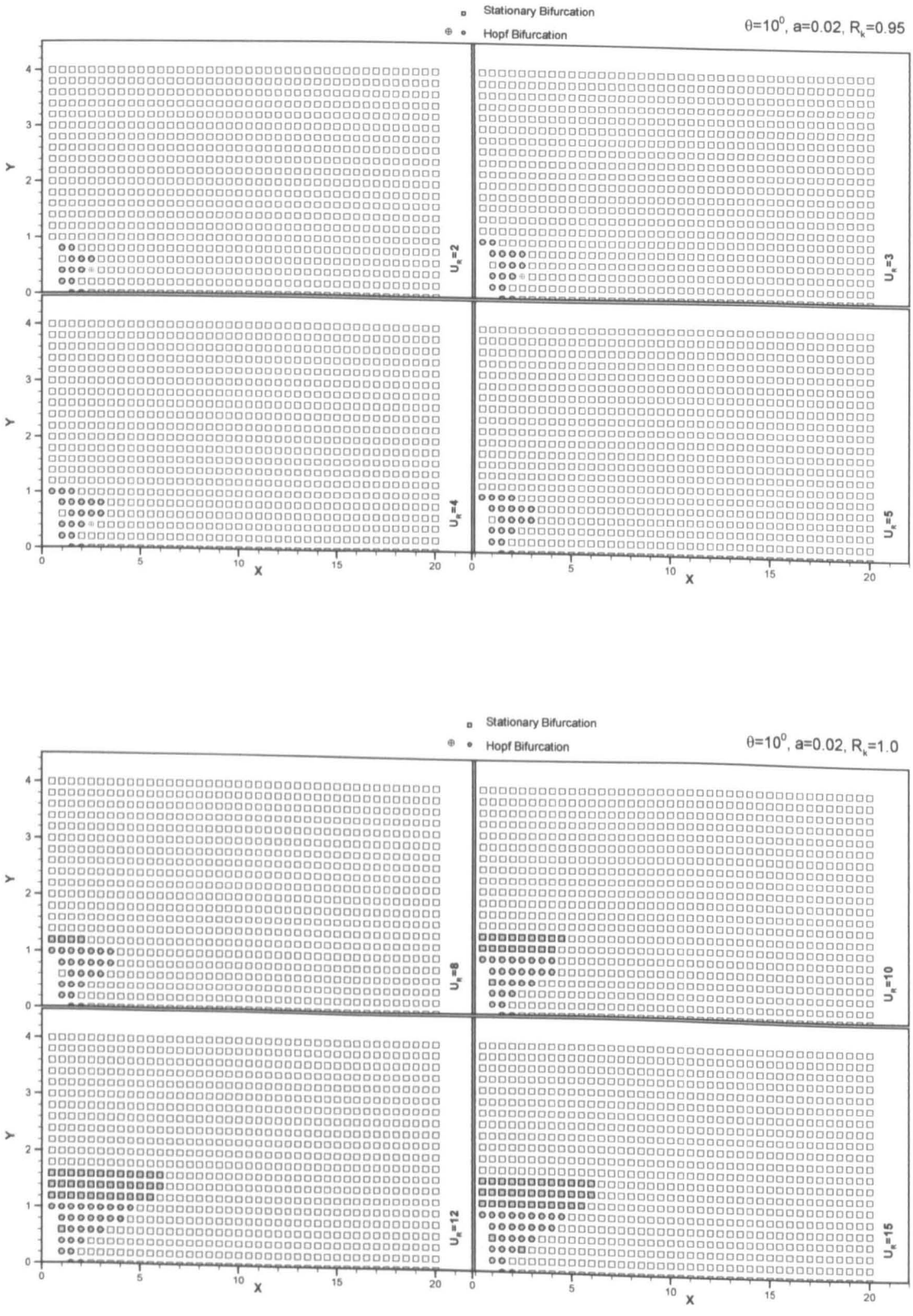

Figure 3.28 Stable/unstable equilibrium locations for the downstream cylinder under specified mass parameter a=0.02, spring coupling angle θ=10^0, stiffness ratio R_k=0.95 and flow velocity.

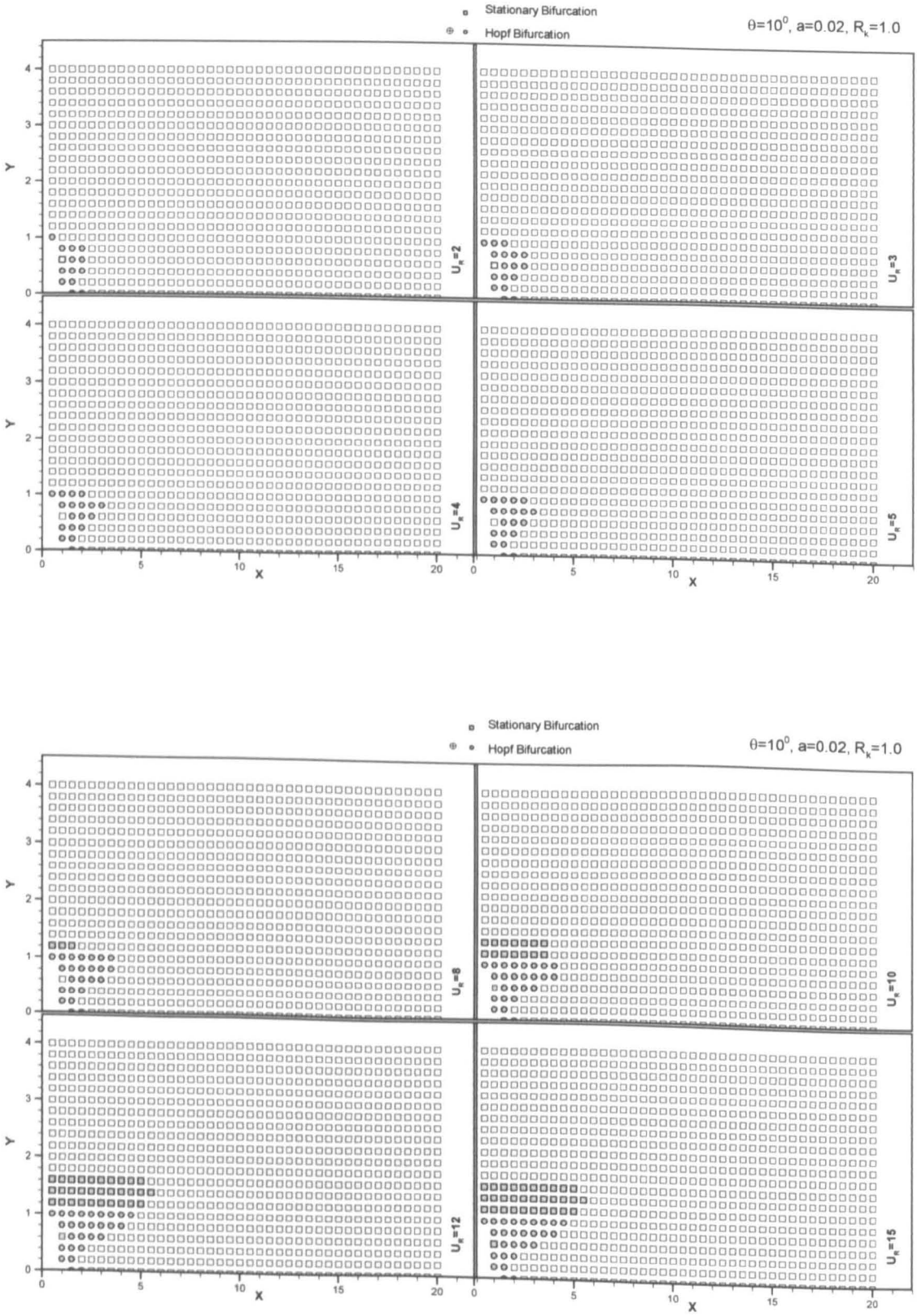

Figure 3.29 Stable/unstable equilibrium locations for the downstream cylinder under specified mass parameter a=0.02, spring coupling angle θ=10^0, stiffness ratio R_k=1.0 and flow velocity.

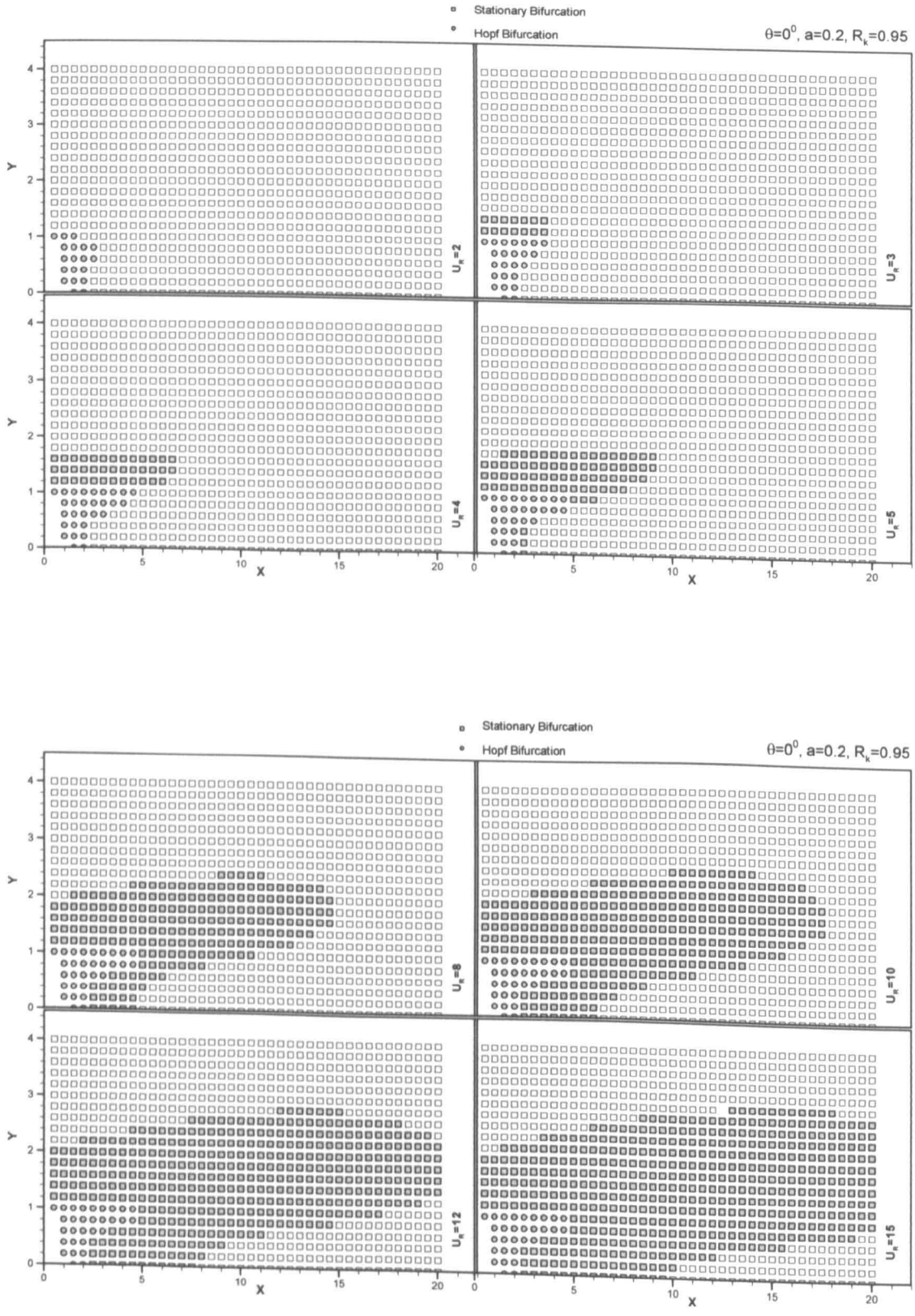

Figure 3.30 Stable/unstable equilibrium locations for the downstream cylinder under specified mass parameter a=0.2, spring coupling angle θ=0^0, stiffness ratio R_k=0.95 and flow velocity.

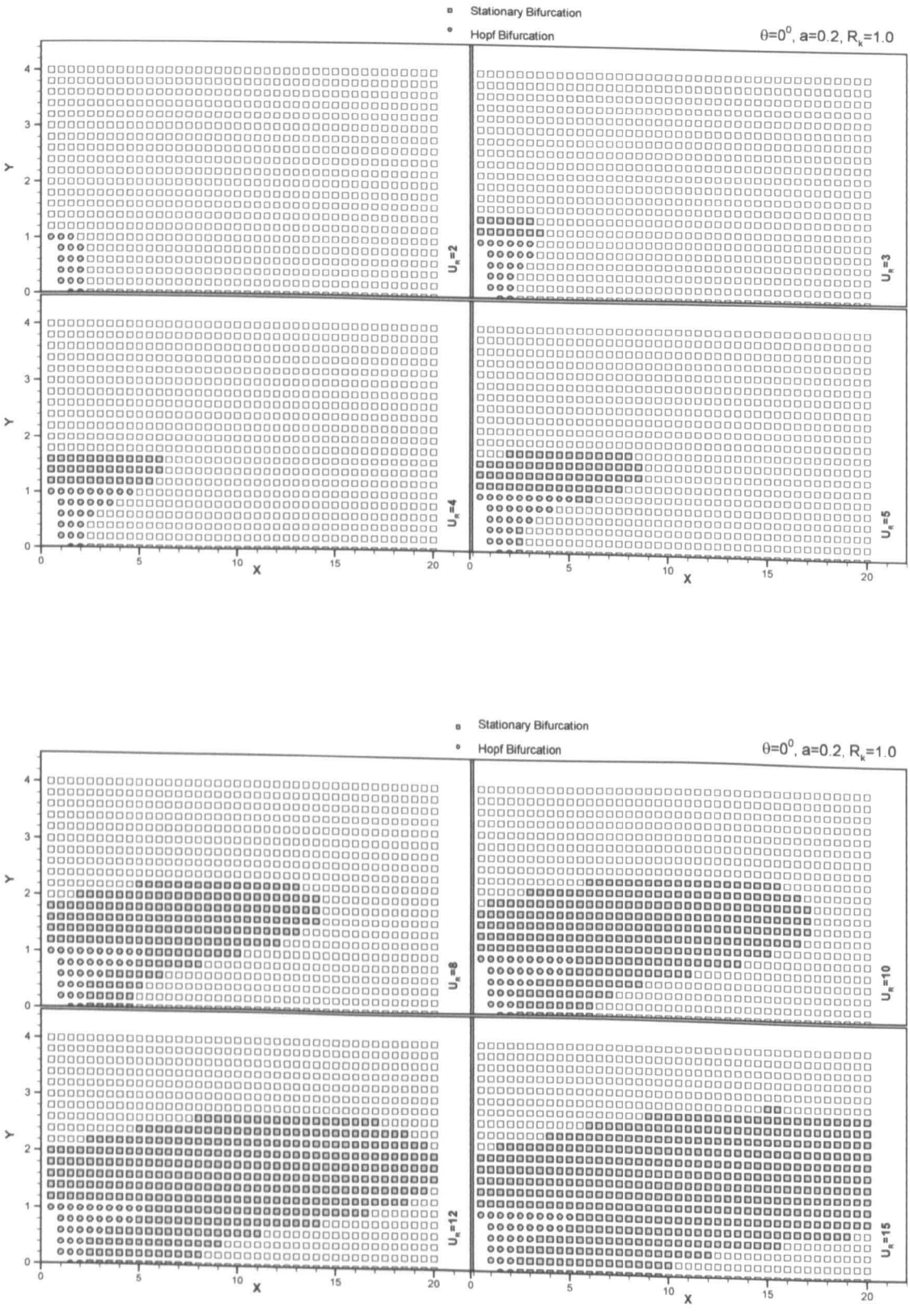

Figure 3.31 Stable/unstable equilibrium locations for the downstream cylinder under specified mass parameter a=0.2, spring coupling angle θ=0^0, stiffness ratio R_k=1.0 and flow velocity.

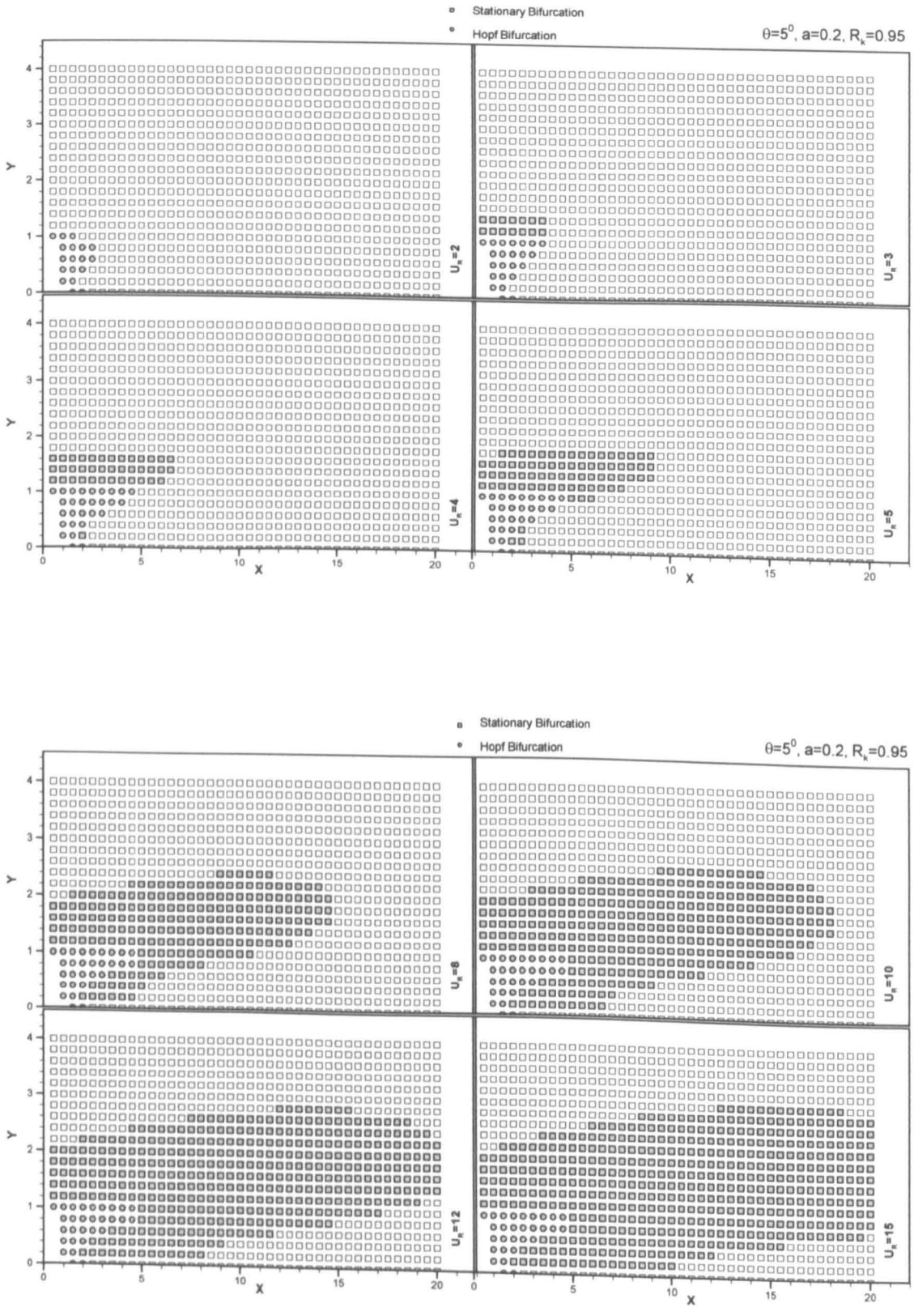

Figure 3.32 Stable/unstable equilibrium locations for the downstream cylinder under specified mass parameter a=0.2, spring coupling angle θ=5⁰, stiffness ratio R_k=0.95 and flow velocity.

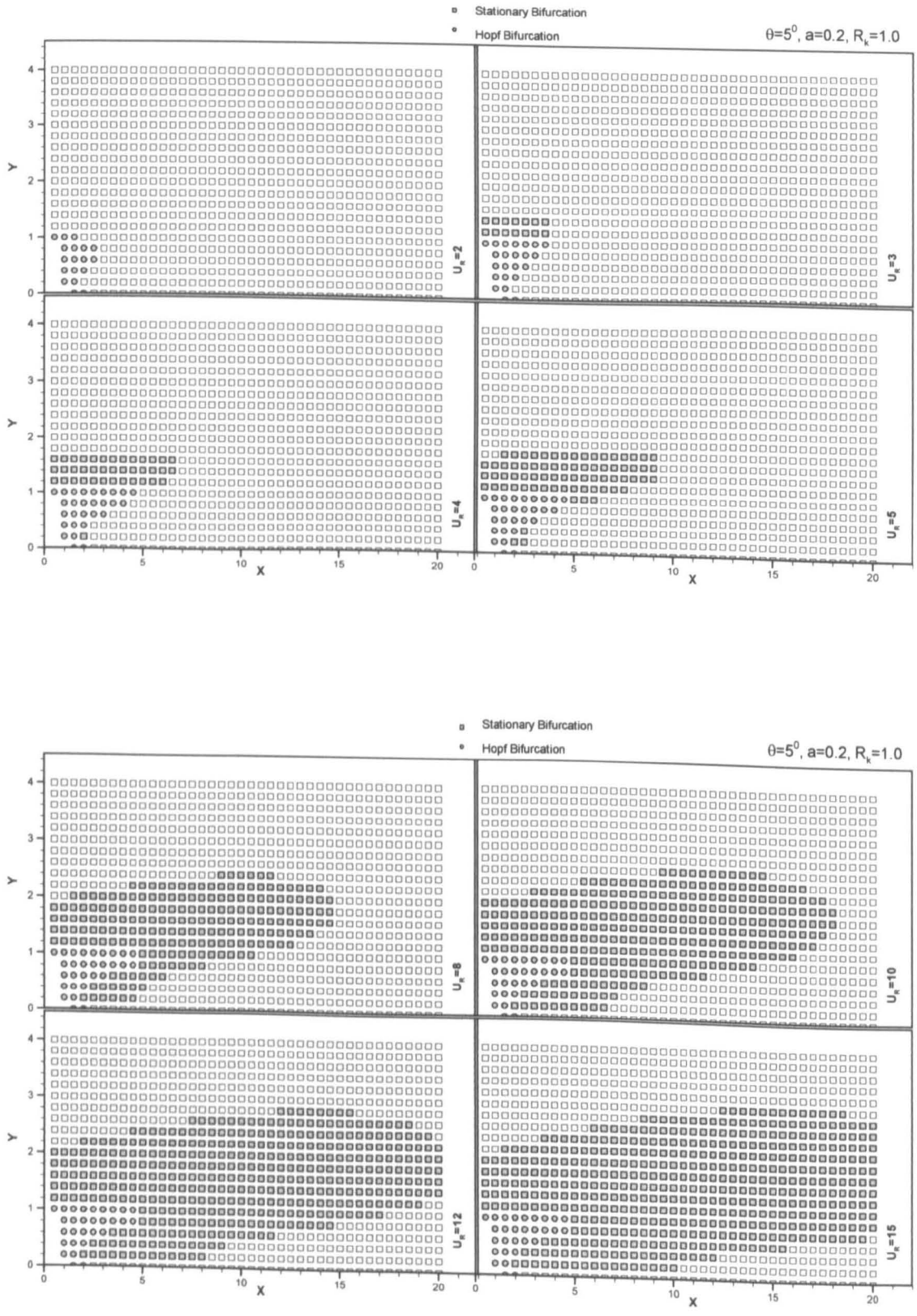

Figure 3.33 Stable/unstable equilibrium locations for the downstream cylinder under specified mass parameter a=0.2, spring coupling angle θ=5⁰, stiffness ratio R_k=1.0 and flow velocity.

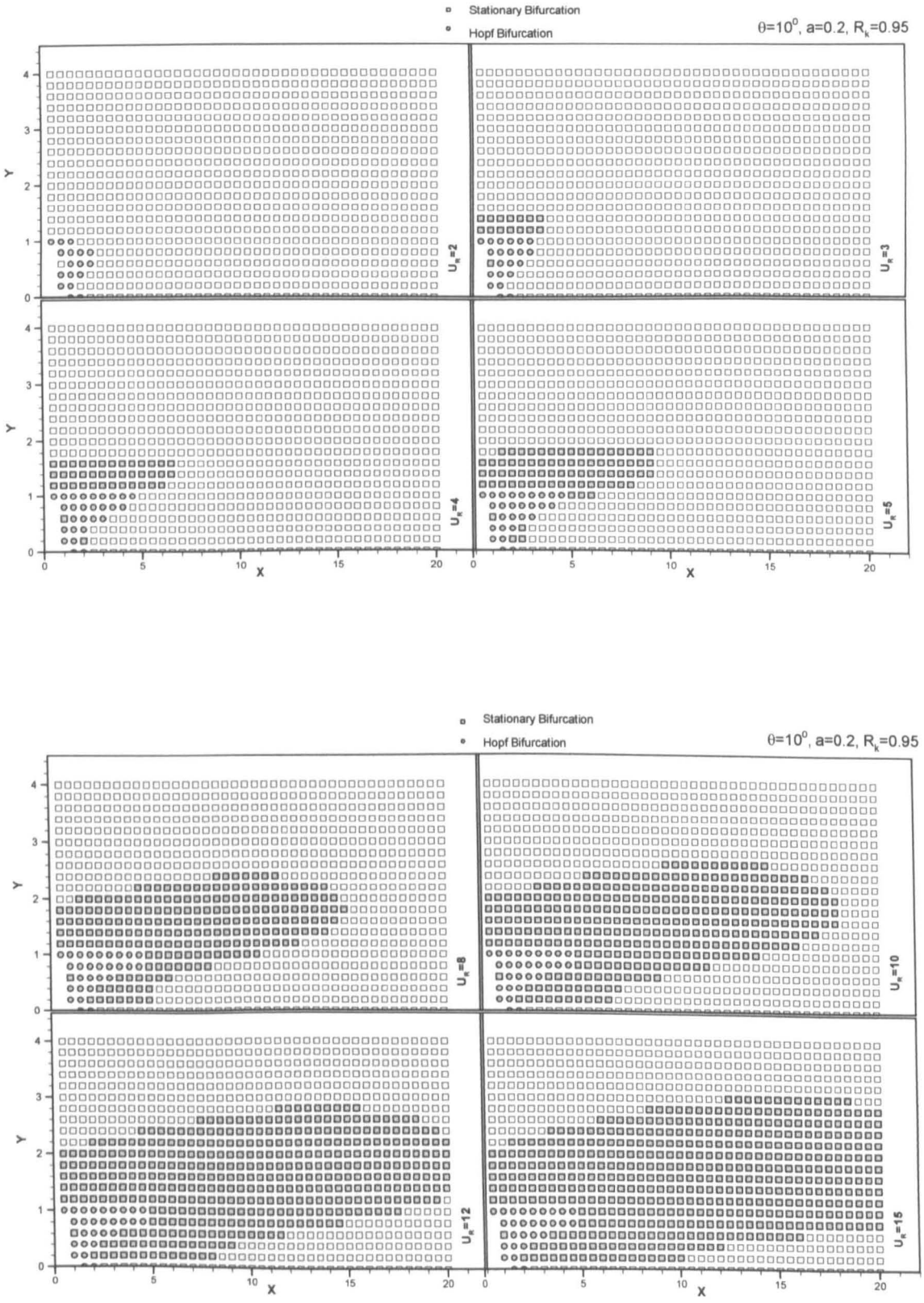

Figure 3.34 Stable/unstable equilibrium locations for the downstream cylinder under specified mass parameter a=0.2, spring coupling angle θ=10^0, stiffness ratio R_k=0.95 and flow velocity.

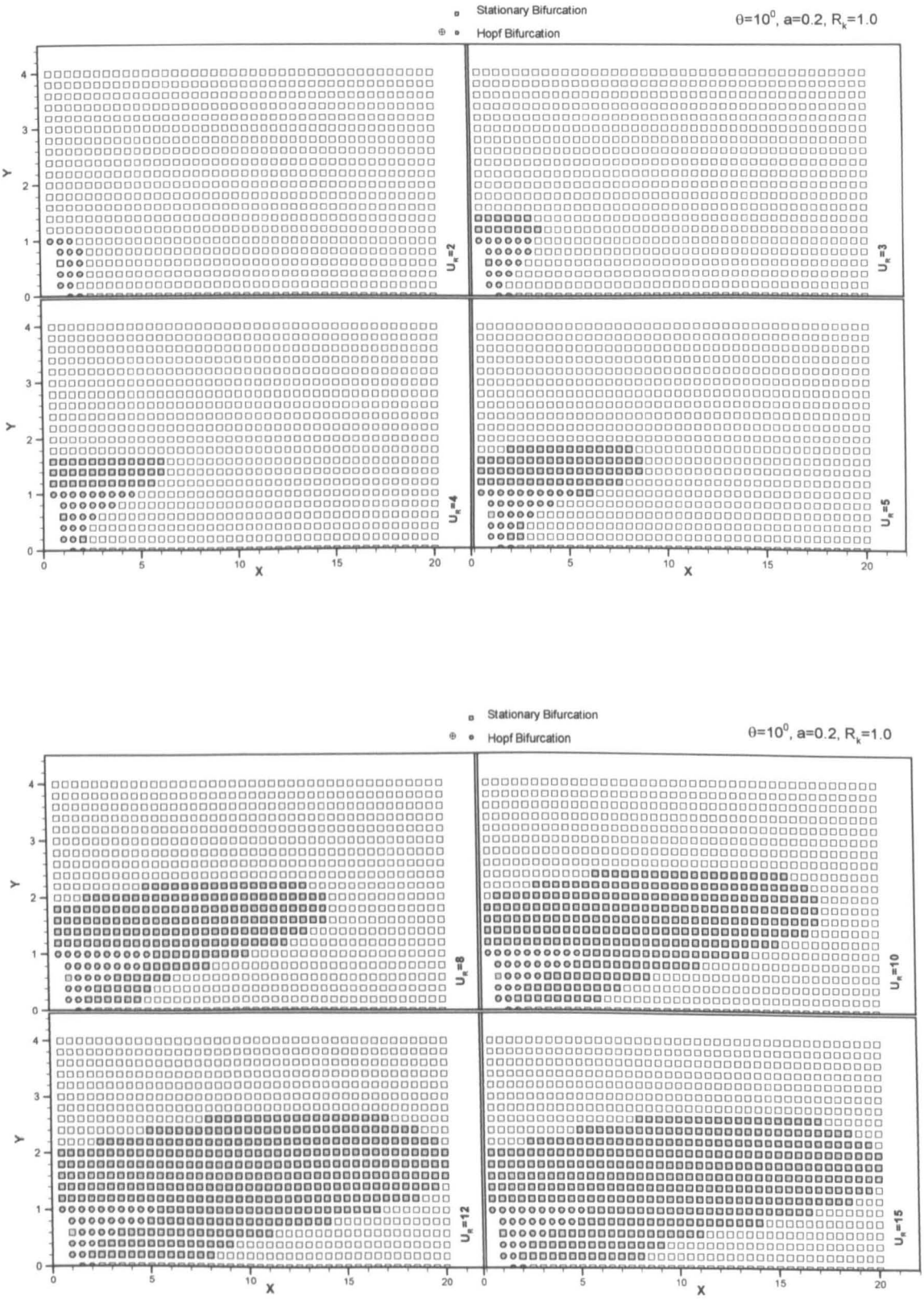

Figure 3.35 Stable/unstable equilibrium locations for the downstream cylinder under specified mass parameter a=0.2, spring coupling angle θ=10^0, stiffness ratio R_k=1.0 and flow velocity.

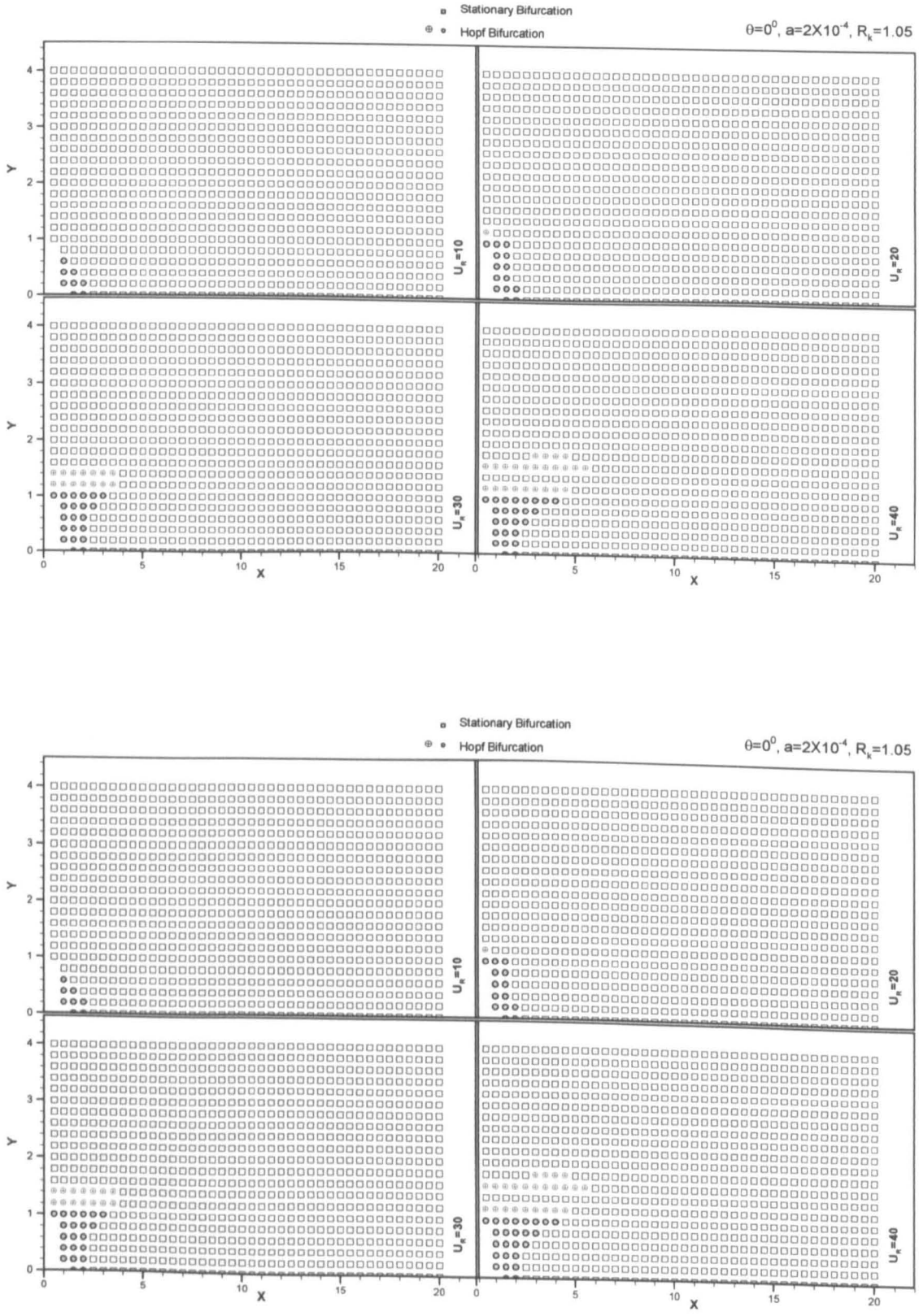

Figure 3.36 Stable/unstable equilibrium locations for the downstream cylinder under specified mass parameter a=2.0×10^{-4}, spring coupling angle θ=0^0, stiffness ratio R_k=1.05and flow velocity.

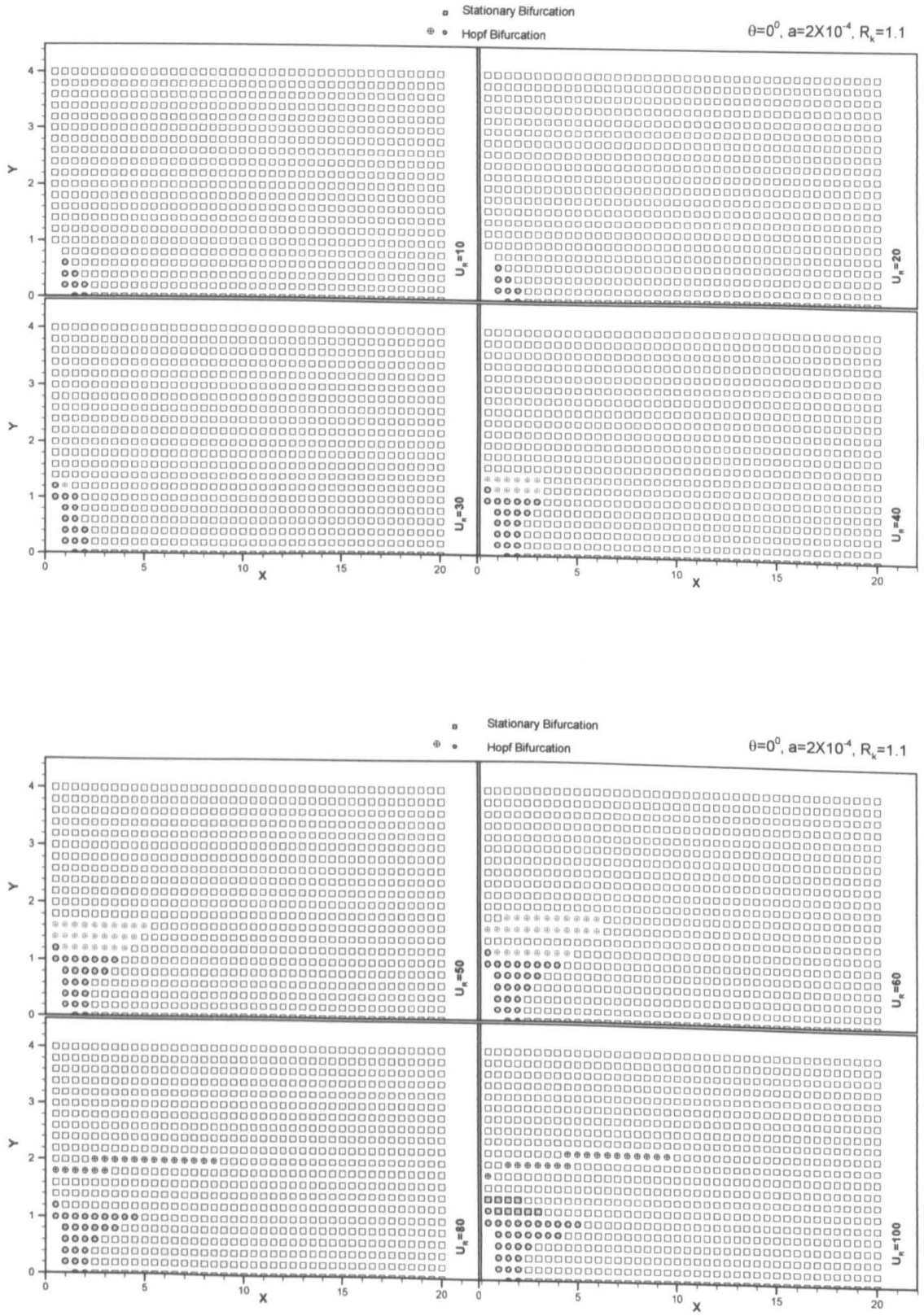

Figure 3.37 Stable/unstable equilibrium locations for the downstream cylinder under specified mass parameter a=2.0×10^{-4}, spring coupling angle θ=0^0, stiffness ratio R_k=1.1 and flow velocity.

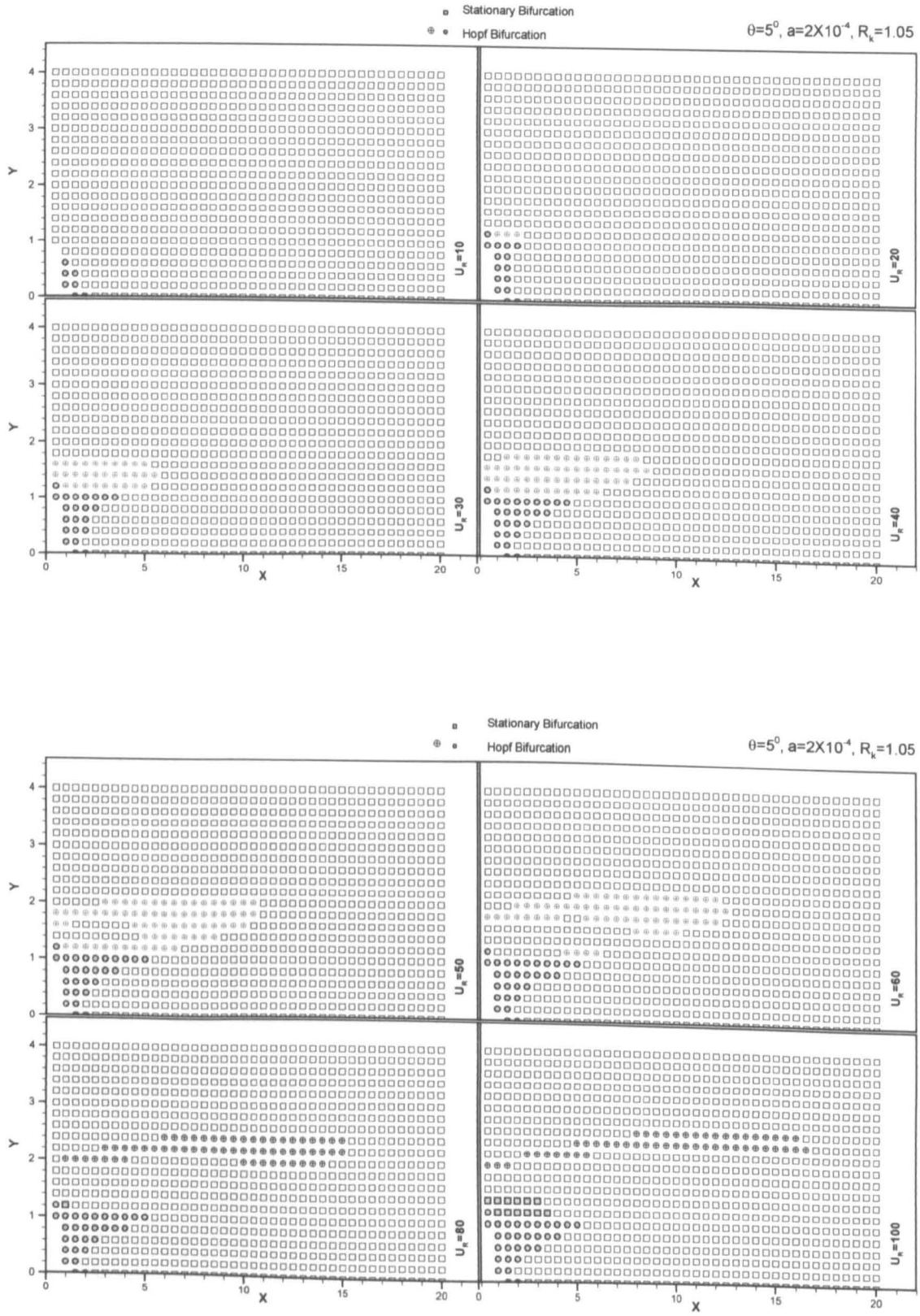

Figure 3.38 Stable/unstable equilibrium locations for the downstream cylinder under specified mass parameter a=2.0×10^{-4}, spring coupling angle θ=5^0, stiffness ratio R_k=1.05 and flow velocity.

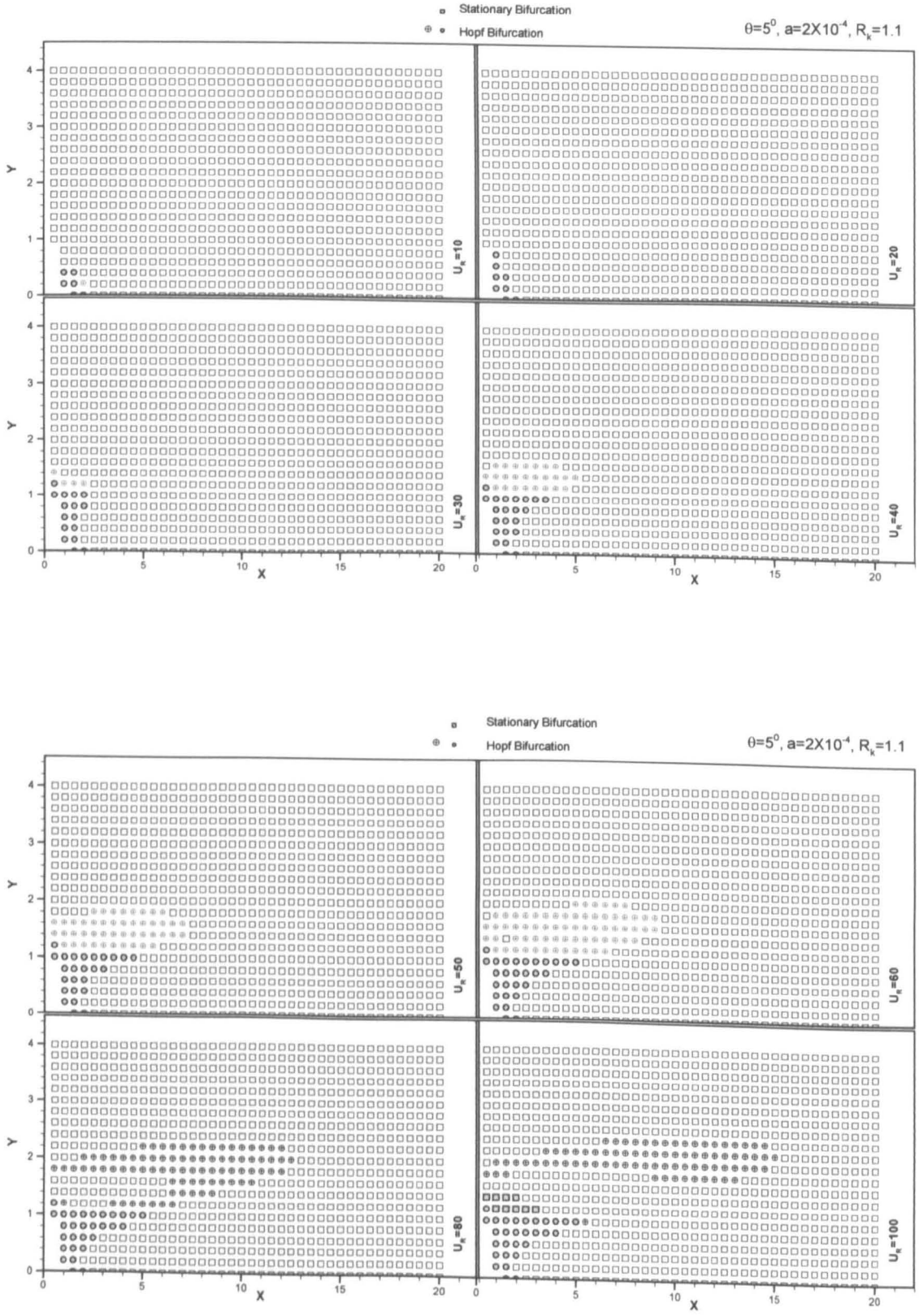

Figure 3.39 Stable/unstable equilibrium locations for the downstream cylinder under specified mass parameter a=2.0×10^{-4}, spring coupling angle θ=5^{0}, stiffness ratio R_k=1.1 and flow velocity.

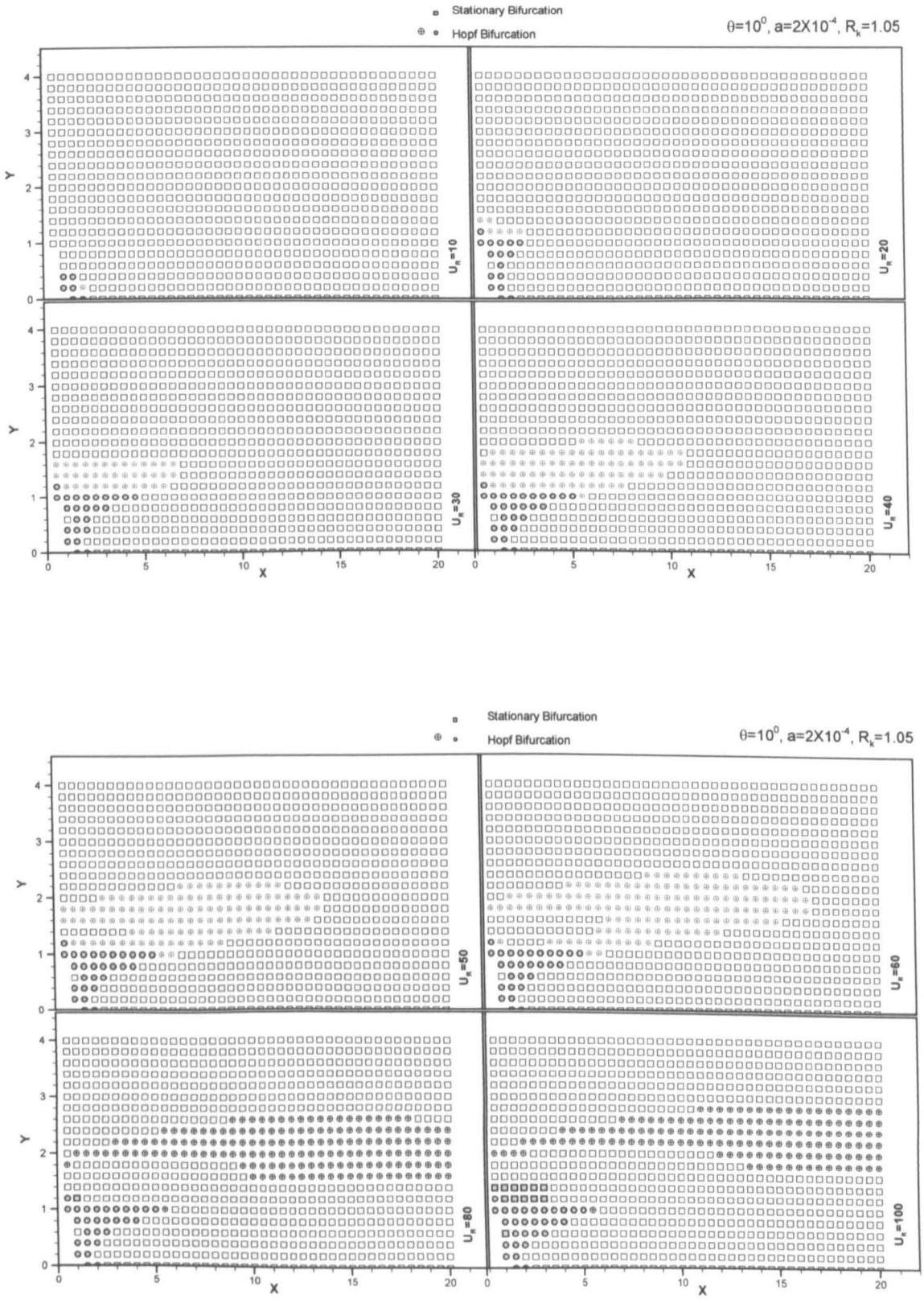

Figure 3.40 Stable/unstable equilibrium locations for the downstream cylinder under specified mass parameter a=2.0×10^{-4}, spring coupling angle θ=10^0, stiffness ratio R_k=1.05 and flow velocity.

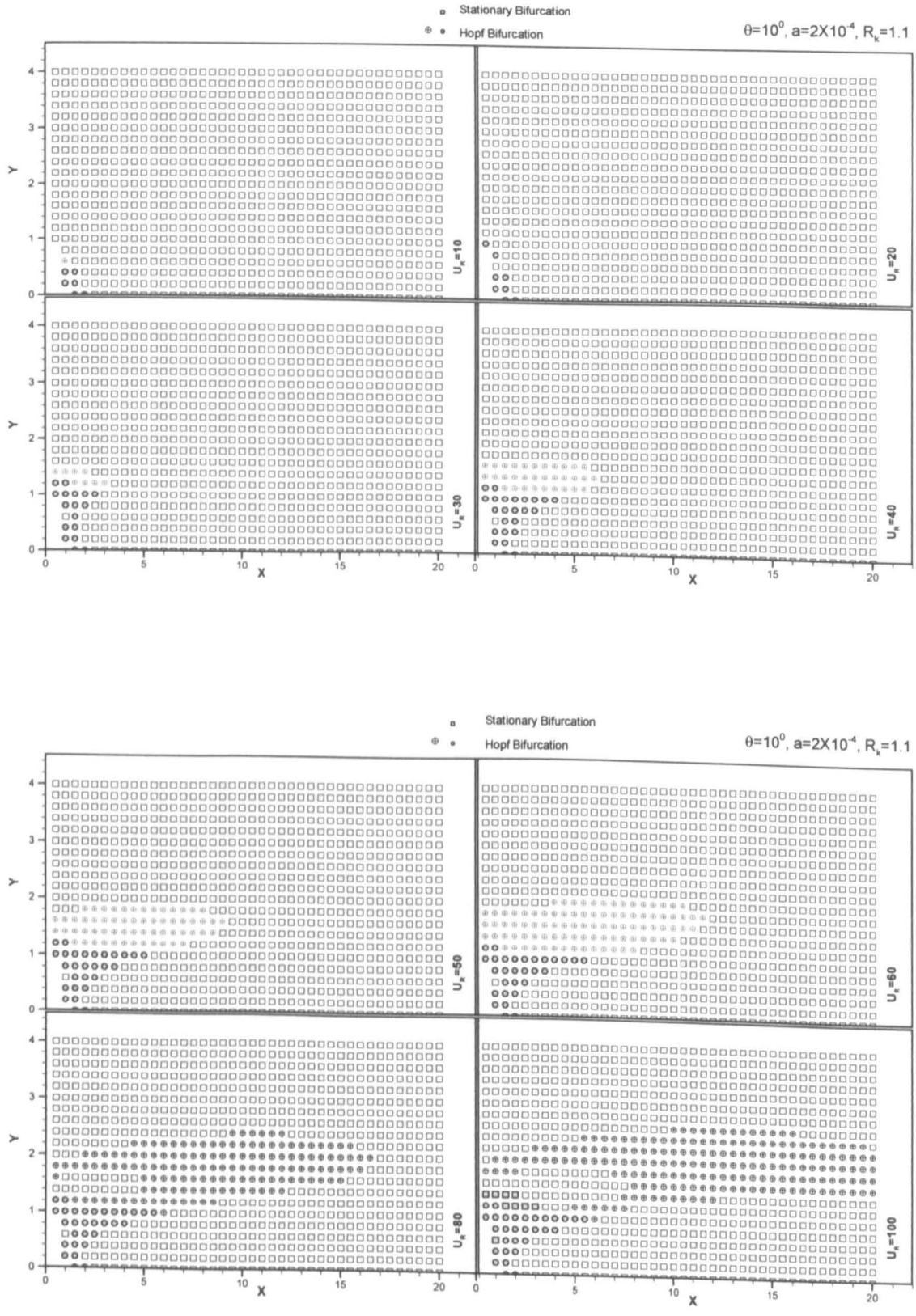

Figure 3.41 Stable/unstable equilibrium locations for the downstream cylinder under specified mass parameter a=2.0×10^{-4}, spring coupling angle θ=10^{0}, stiffness ratio R_k=1.1 and flow velocity.

Chapter IV

CONTINUATION INVESTIGATION INTO INTERACTION OF TWO CYLINDERS

4.1 General Remarks

In chapter III, traditional tools were used to analyse the stability of the downstream cylinder, i.e. the utilisation of Routh-Hurwitz stability algorithm. The Routh-Hurwitz stability criteria can identify the critical state of the stability. However, the critical state does not show detailed information about the variation of the stability and it can not answer a question like "In what kind of arrangement, for a specified spacing, are the two cylinders more likely to lose stability?". Also, the method is often limited to very small number of degrees of freedom. In order to learn detailed information about the effect of control parameters, such as flow velocity, cylinder arrangement etc. on the stability of the cylinder, a numerical investigation concerning continuation has to be made.

Looking back at the investigation into cylinder interaction, particularly on the issue of the stability of the cylinders, most researchers have focused solely on the stability itself. More specifically, most attention has been given to the identification of possibility of instability and the seeking of critical states(Simpson 1971; Price 1975, Price and Others 1993; Tsui 1986; Tsui 1977). Some investigations provided parameter effect such as structural damping, cylinder arrangement (Price 1975; Price and others 1993) etc. However, not a

single article has given consideration to the possible multiple equilibrium states and the structure of bifurcation for such a non-linear system. This is partly because most of the investigations have concentrated on the problems of power transmission lines only, which is a particular case for very small mass parameter. Nevertheless, when the interaction between marine risers is considered, the variation of equilibrium position with flow velocity can be significant. As shown in Chapter III, the stability of a downstream cylinder depends on both the relative position and flow velocity. The information about the equilibrium position can therefore be vitally important.

To find equilibrium positions for a given system, numerical tools are probably the most useful, in particular when:

1) The non-linear system itself does not have analytical specification itself. For example, in the problem experienced here, the fluid force coefficients themselves do not provide accurate analytical expressions concerning the different arrangement of cylinders.

2) The problem can be extremely difficult to solve analytically.

The challenge faced by the numerical tool is the requirement to find all the possible equilibrium states for the specified nonlinear system. It is easy to understand that the stable state is much easier to trace, For example, by specifying an initial position for two cylinders with a stable equilibrium position, solving the dynamic system in time domain, then the cylinder is likely to rest on those positions. To exhaust the equilibrium positions, however, continuation and branching techniques have to be used.

The essence of continuation is based on the hypothesis that the equilibrium positions are continuous functions of the control parameter. Supposing one equilibrium position is known at the beginning then, by a small variation of control parameter, the corresponding

equilibrium position for the varied control parameter should stay close to the first known equilibrium position and can be obtained by solving the non-linear dynamic system. By repeating this procedure up to the required control parameter, all the equilibrium positions related to the first known equilibrium can then be traced. The technique to find such chain positions is called "*continuation*". The chain of the solutions is called the "*branch*". However, the solutions explored in this way often comprise a continuous relation between equilibrium position and control parameter, and discontinuity can occur at times. The existence of multiple equilibrium positions implies that multiple branches can exist. The continuation technique only sorts out the branch corresponding to the particular first position. However, most of the time, these branches will intersect with each other. By identifying these intersection points, a switch of branch can be made to change the path of continuation and to trace other branches. Such a technique to identify intersections and switch the branch is often called "*branching*". The seeking of chained solutions by continuation is usually irrespective of stability. To realise the stability analysis of the solution, the technique of stability analysis will then be required. The systematic description of the treatment method for the non-linear dynamic system can be found from references (Seydel 1994; Kubicek and Marek 1983).

In this chapter, a full continuation investigation is launched, to try to identify the multiple equilibrium states of the downstream cylinder. The corresponding stability for each equilibrium position is analysed by a direct numerical eigenvalues seeking method regarding its Jacobian matrix. It is seen that for a specified arrangement, there can be up to four equilibrium positions for certain flow velocities. However, when flow velocity exceeds a certain value, there can be no physical equilibrium positions. Critical state is defined in this chapter to identify the flow velocity before the downstream cylinder loses its ultimate equilibrium state.

4.2 Theoretical Formulation

4.2.1 Formulation

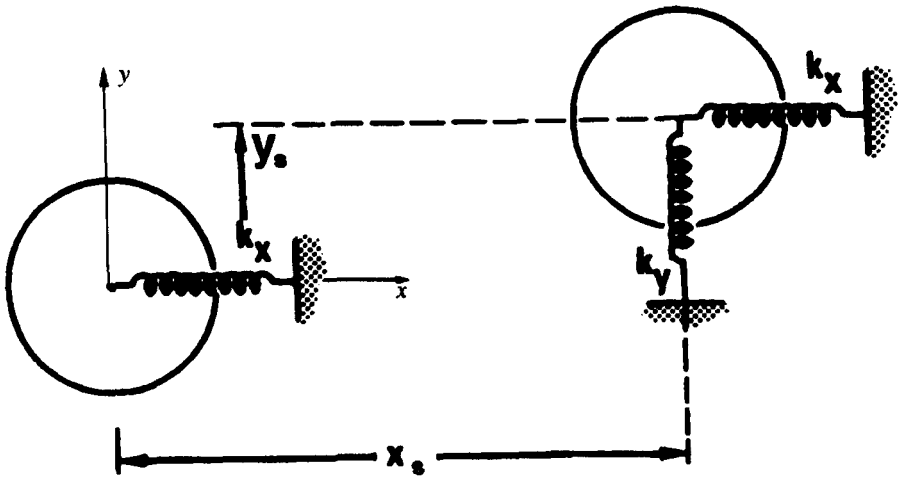

Figure 4.1 Schematic diagram for the system to be investigated.

Figure 4.1 is a schematic diagram of the two cylinders system investigated in this chapter. The upstream cylinder is supported by a streamwise direction spring only, while the downstream cylinder is supported by both a streamwise and cross flow direction spring. The co-ordinate system has its origin at the centre of the upstream cylinder's location when the fluid is stationary, with its *x axis* parallel to the flow direction and pointing towards downstream. The initial position of the downstream cylinder is (X_S, Y_S). The reason why the spring coupling is neglected in this chapter has been described in Chapter III. Furthermore, it is assumed here that the springs are ideal, i.e. the direction of the two springs supporting the downstream cylinder will not change with the displacement of the downstream cylinder. For such a system, the dynamics equations concerning the equilibrium position of both upstream and downstream cylinder are expressed as a system of six first-order differential equations:

$$\dot{\tilde{x}} = \tilde{f}(\tilde{x})$$

with

$$\tilde{f}(\tilde{x}) = \begin{Bmatrix} x_2 \\ aU_R^2 C_{D1} - 2\xi_x x_2 - x_1 \\ x_4 \\ aU_R^2 \sqrt{\left(1-\frac{x_4}{bU_R}\right)^2 + \left(\frac{x_6}{bU_R}\right)^2}\left[C_{D2}\left(1-\frac{x_4}{bU_R}\right) + C_{L2}\frac{x_6}{bU_R}\right] - 2\xi_x x_4 - x_3 \\ x_6 \\ aU_R^2 \sqrt{\left(1-\frac{x_4}{bU_R}\right)^2 + \left(\frac{x_6}{bU_R}\right)^2}\left[C_{L2}\left(1-\frac{x_4}{bU_R}\right) - C_{D2}\frac{x_6}{bU_R}\right] - 2R_k\xi_y x_6 - R_k^2 x_5 \end{Bmatrix} \tag{4.1}$$

$$\tilde{x} = \begin{Bmatrix} x_1 \\ x_2 \\ x_3 \\ x_4 \\ x_5 \\ x_6 \end{Bmatrix} \tag{4.2}$$

The form of x_1, x_3, x_5 are expressed as:

$$\begin{cases} x_1 = X_1 \\ x_3 = X_2 - X_s \\ x_5 = Y_2 - Y_s \end{cases} \tag{4.3}$$

X_1 is the position of upstream cylinder at reduced flow velocity of U_R. x_1, x_3, x_5 represent the non-dimensional streamwise displacement of upstream cylinder, streamwise and transverse displacement of the downstream cylinder from the initial positions, respectively. x_2, x_4, x_6 are their corresponding velocities in non-dimensional form. C_{D1} is the drag coefficient for upstream cylinder. The stability analysis for corresponding

equilibrium positions is made by direct numerical eigenvalue seeking for the Jacobian matrix of system (4.1) with

$$J_{i,j} = \frac{\partial \tilde{f}_i}{\partial x_j} \tag{4.4}$$

This serves as a parallel comparison with the analysis made in Chapter III, an alternative statement of the investigation is presented in the Appendix A.

Equation (4.1) is a sixth-order standard autonomous system. The control parameters in the equations include reduced flow velocity U_R, stiffness ratio R_k, mass parameter a and different initial positions of (X_S, Y_S). The main issue in this chapter will be the reduced flow velocity.

4.2.2 Continuation Procedures

As shown in the previous chapter, stationary bifurcation is most likely to be the bifurcation type which the system will experience when it lose its stability. In order to avoid the problem which might arise with the turning points, an arc length method (Seydel 1994) was utilised in the analysis. The following equation serves as a complementary equation to system (4.1).

$$p(y,\lambda,s) = \sum_{i=1}^{4}(x-x_i)^2 + \left[\lambda - \lambda(s_j)\right]^2 - \left(s-s_j\right)^2 = 0 \tag{4.5}$$

Here s is the arc length along the continuation solution curve. λ is the control parameter. In the present study, the control parameter U_R is mainly investigated. Equation (4.5) together with (4.1) constitute self-contained non-linear equations, among which the continuation step length $\left(s-s_j\right)$ is prescribed beforehand. Such a system is solvable by predictor and corrector two steps method.

4.2.2.1 Predictor Step:

Predictor is a procedure to provide an initial guess for equilibrium based on the already known equilibrium. The procedure starts from a known solution (x^j, λ_j), which can be sought at a small reduced flow velocity for system (4.1). In fact, the specified position of (X_s, Y_s)itself is an equilibrium at zero flow velocity. By taking prescribed arc length $\Delta s = s - s_j$, in present investigation, the predictor is implemented by way of AKIMA extrapolation. The AKIMA interpolation is based on a piecewise function composed of a set of polynomials, each of degree three, at most, and applicable to successive intervals of the given points. In this method, the slope of the curve is determined at each given point locally, and each polynomial representing a portion of the curve between a pair of given points is determined by the coordinates of and the slopes at the points. The formulations of the interpolation are as follows.

Generally, the curve slope at each given point is determined by points in addition to itself. For example, assuming there are 5 successive points as 1,2,3,4 and 5. Their corresponding slopes are denoted by m_1, m_2, m_3 and m_4 for each segment, i.e. 12, 23, 34, and 45. The curve slope at point 3 is then determined by the following formulation:

$$t = \frac{|m_4 - m_3| m_2 + |m_2 - m_1| m_3}{|m_4 - m_3| + |m_2 - m_1|} \tag{4.6}$$

Subsequently, the interpolation scheme for a point x which lies in the interval $[x_1, x_2]$ is expressed as:

$$y = p_0 + p_1(x - x_1) + p_2(x - x_1)^2 + p_3(x - x_1)^3$$

Where

$$p_0 = y_1$$

$$p_1 = t_1$$

$$p_2 = \frac{3\frac{y_2 - y_1}{x_2 - x_1} - 2t_1 - t_2}{x_2 - x_1}$$

$$p_3 = \frac{t_1 + t_2 - 2\frac{y_2 - y_1}{x_2 - x_1}}{(x_2 - x_1)^2}$$

(x_i, y_i) is the coordinate of point *i*. Detailed introduction of the method can refer to (Akima 1970, 1978).

4.2.2.2 Corrector Step

The objective of corrector step is to find the exact equilibrium based on the guess provided by predictor step. In this chapter, it is made via the modified version of M.J.D. Powell's hybrid algorithm contained in the package of IMSL library (IMSL user manual), which is a variation of Newton's method. The classical Newton-Raphson iteration for solving non-linear equations requires a good estimation at the start otherwise the solution may fails to converge. A common strategy to resolve this trouble is to retain the iteration direction, but to restrict the length of successive corrections. Different schemes have been produced based on such a philosophy. The Powell's hybrid algorithm is one of them. The Algorithm uses a finite-difference approximation to the Jacobian and takes precautions to avoid large step sizes or increasing residuals. For further description, (see More and others 1980). Since a Finite Difference Method is used to estimate the Jacobian, the byproduct of the Jacobian matrix can be used for the stability analysis in present investigation.

4.2.2.3 Branching:

The detecting of the branching is made via the test function of the real part of the eigenvalue. When near the position where the real part of the eigenvalue sign changes, the switch of the continuation is then made by the direct method.

4.3 Numerical Results and Discussion

As the focus of this thesis is on marine riser interactions, additionally, the displacement caused by flow for small mass parameter is relatively small. The present chapter sets the control parameters as $a=0.2$, $R_k=1.0$, $\xi_x=\xi_y=0$, there is no spring coupling, and initial spacing X_S varies from *5* to *30* and Y_S varies from *0* to *3*. Three representative areas are investigated, i.e. the wake centreline, inner wake and outer wake respectively. For each area, systematic calculation results about continuation and corresponding stability analysis are presented. The control parameter in these cases is concentrated on reduced flow speed.

4.3.1 Wake Centreline

It is apparent that the cylinder on wake centreline will stay on the centreline because of the symmetry property of the wake. There is no lift force on the wake centreline. The lift force is directing towards it when the downstream cylinder is deviated from wake centreline. Figure 4.2 to Figure 4.7 are continuation results for position $X_S=5, 8, 10, 15, 20, 30$ *with* $Y_S=0$ respectively. It is seen that as the flow velocity increases, both the upstream cylinder and downstream cylinder are pushed back as shown in the figures. Nevertheless, due to the wake shielding effect, the displacement of downstream cylinder is not as large as that of the upstream one. When the reduced velocity increases to certain level, two equilibrium positions of the downstream cylinder emerge with one close to the upstream cylinder and another further downstream. With further increase of the reduced flow velocity a state is then reached where the two equilibrium positions converge into a single equilibrium position and above this reduced velocity no equilibrium positions exist. Such a state *when flow velocity exceeds this state there will be no equilibrium* is defined as critical state in this investigation, the corresponding reduced flow velocity is defined as critical flow velocity and the state is labelled as M. In the presented six different spacing cases, all the variation

of the equilibrium have the same characteristics except the critical flow velocity are different.

The accompanying eigenvalue figures show the variation of eigenvalues with the reduced velocity. The label S in these figures represents the position at which stationary bifurcation occurs. D is the state at which the downstream cylinder moves far most downstream in position. It can be seen that before the downstream cylinder moves to D, as labelled as Range I in the Figure 4.2(b), the cylinder is always stable. In the course from D to M, labelled as Range II in the figure, when initial spacing is smaller than or equal to δ, the cylinder is possible to exhibit Hopf bifurcation, H is the Hopf bifurcation point. Such a result is a little unexpected. As we know in most cases, the turning point is a transition point which change the branch stability from stable to unstable or vice-versa. In reality, such scenario of turning point which connects between unstable branches does exist, such as examples given by Seydel (1994). In the meantime, when $X_S > \delta$, the Hopf bifurcation disappears. The state from M to the upstream branch of the equilibrium (the one close to upstream cylinder), called range III here, is unstable as can be seen from the eigenvalues, typically with one pair of eigenvalues be real number, and one of the pair is positive. Comparing all the critical state on Figures 4.2(a) to 4.7(a), it is seen that the spacing between the two cylinders at these critical states increases with the initial spacing. When the initial spacing is smaller than 8 diameters, examining the stability under the different flow velocity by the use of the results of Figure 3.31 produced in Chapter III, before the flow velocity reaches its critical value, the spacing between the two has decreased to such a state that Hopf bifurcation becomes possible, both equilibrium are unstable if there are two equilibrium under one flow velocity. On the other hand, when the initial spacing is larger than 8 diameters, there will always be an equilibrium which has a relative large spacing at

which Hopf bifurcation not possible. At the critical state, the losing stability occurs by the stationary bifurcation.

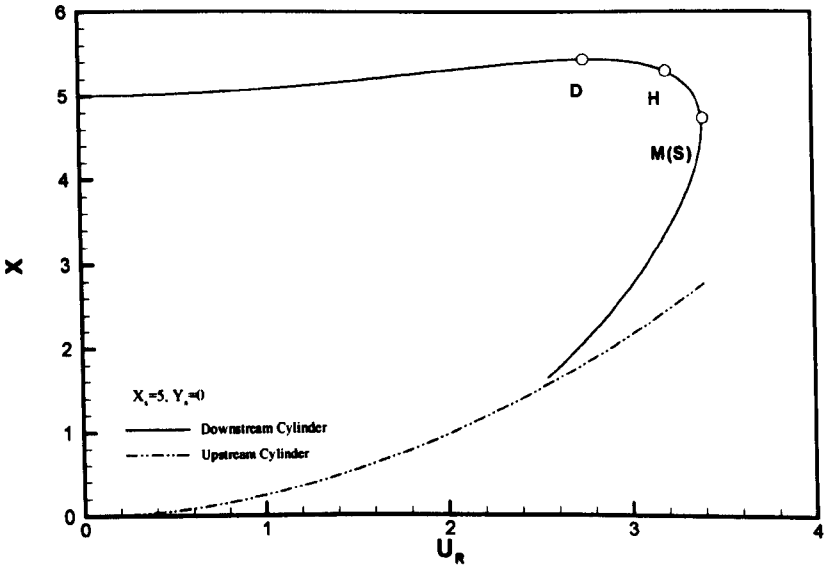

Figure 4.2(a) Continuation for X_s=5, Y_s=0 *with* a=0.2.

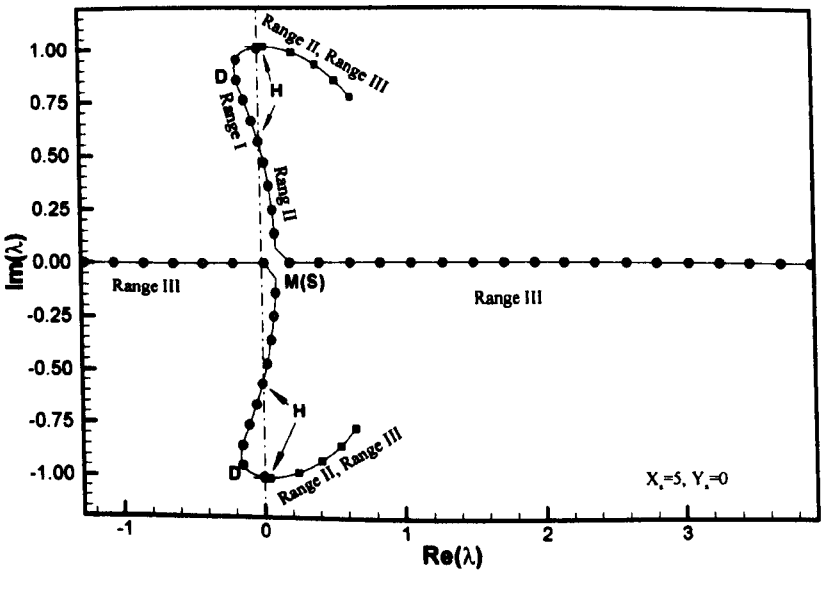

Figure 4.2(b) Variation of eigenvalues for X_s=5, Y_s=0, a=0.2.

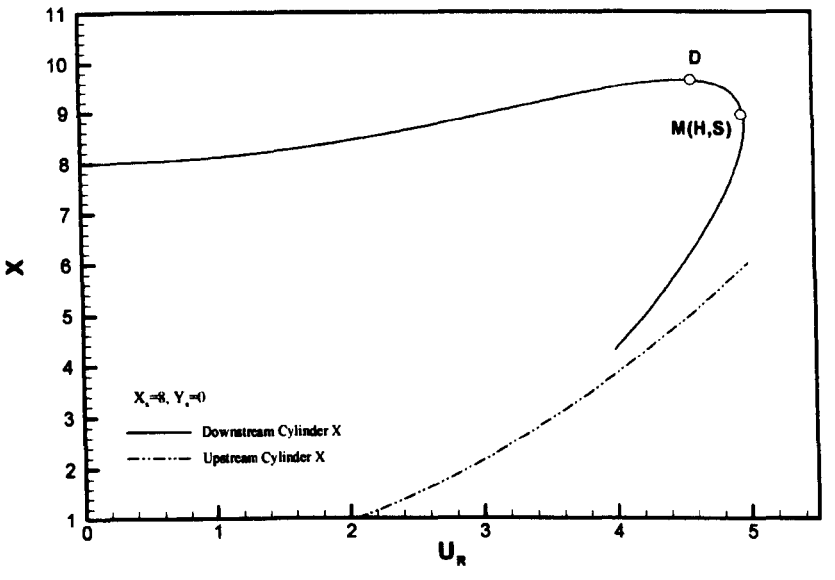

Figure 4.3(a) Continuation for X_s=8, Y_s=0 *with a=0.2.*

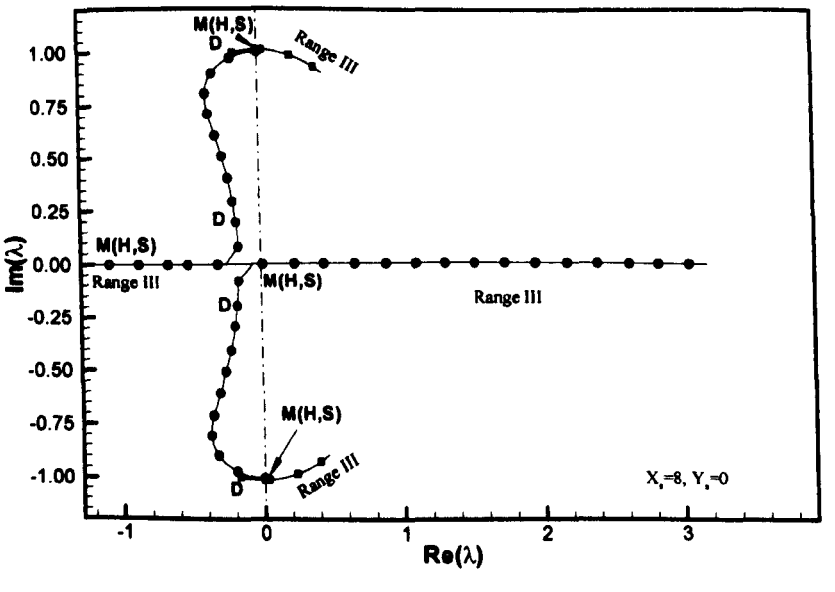

Figure 4.3(b) Variation of eigenvalues for X_s=8, Y_s=0.

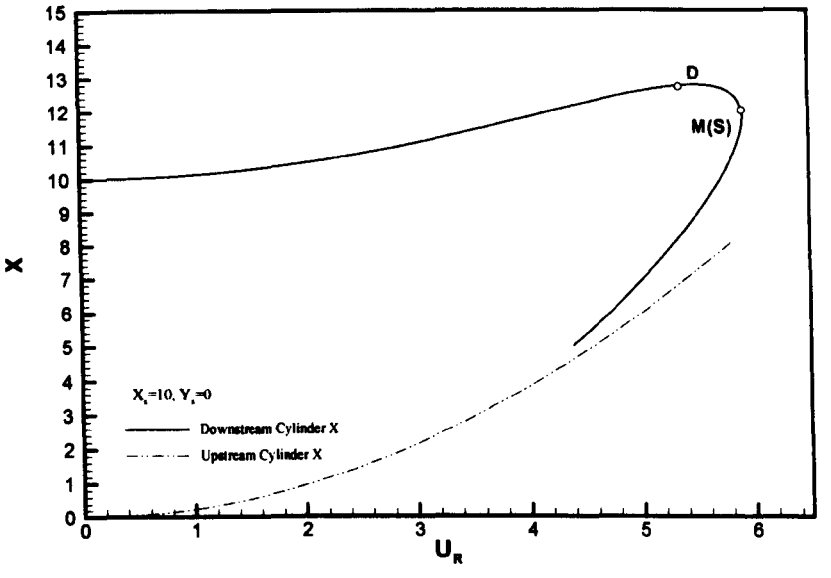

Figure 4.4(a) Continuation for X_S=*10*, Y_S=*0 with a=0.2.*

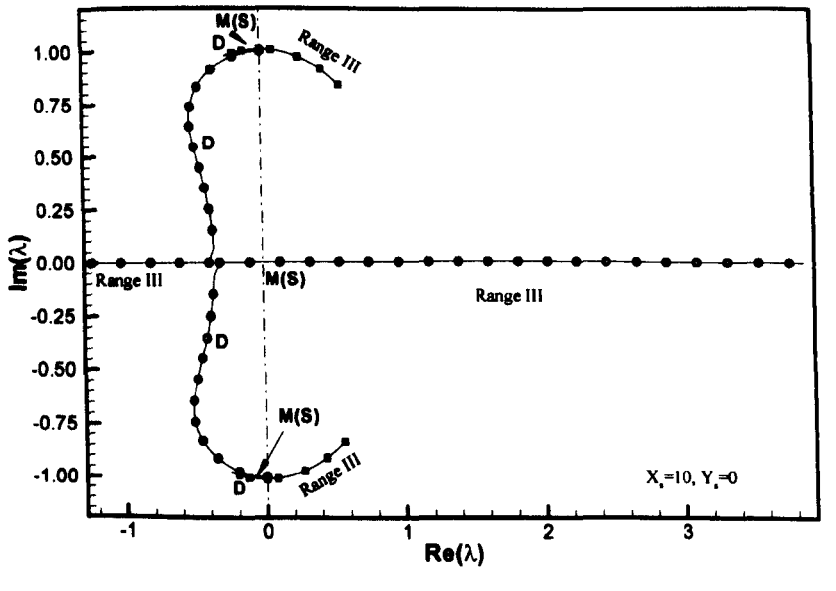

Figure 4.4(b) Variation of eigenvalues for X_S=*10*, Y_S=*0.*

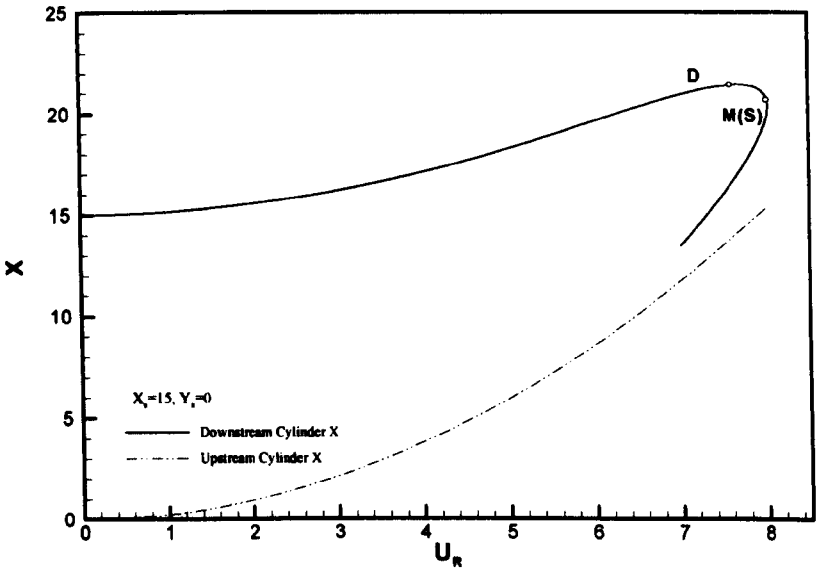

Figure 4.5(a) Continuation for X_s=*15*, Y_s=*0 with a=0.2.*

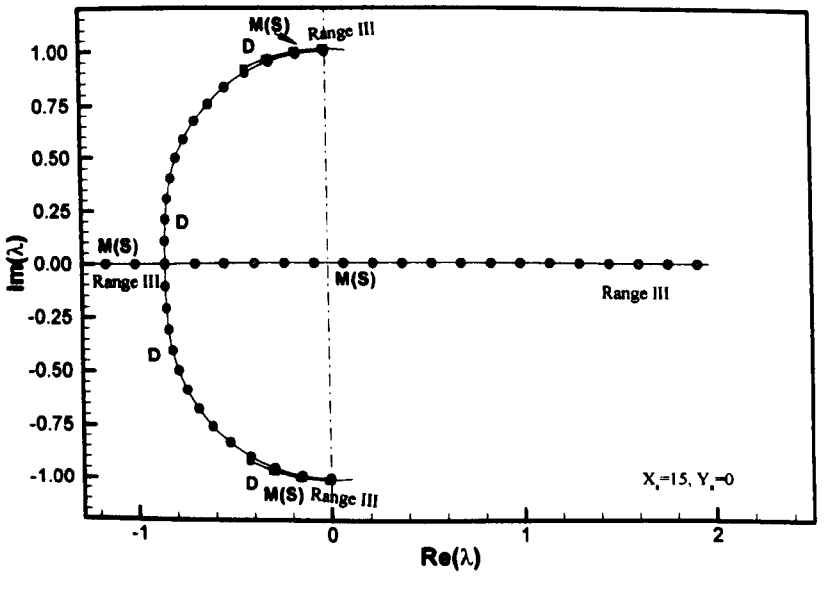

Figure 4.5(b) Variation of eigenvalues for X_s=*15*, Y_s=*0*.

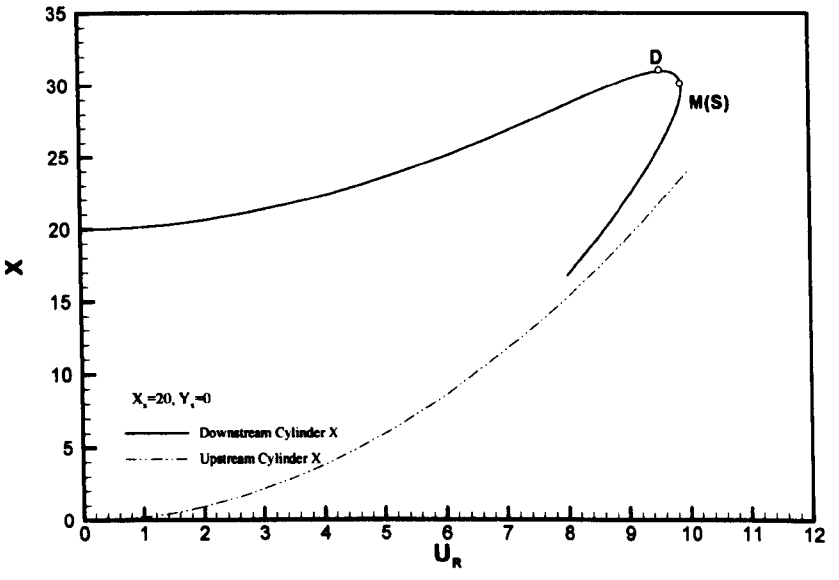

Figure 4.6(a) Continuation for X_S=*20*, Y_S=*0 with a=0.2.*

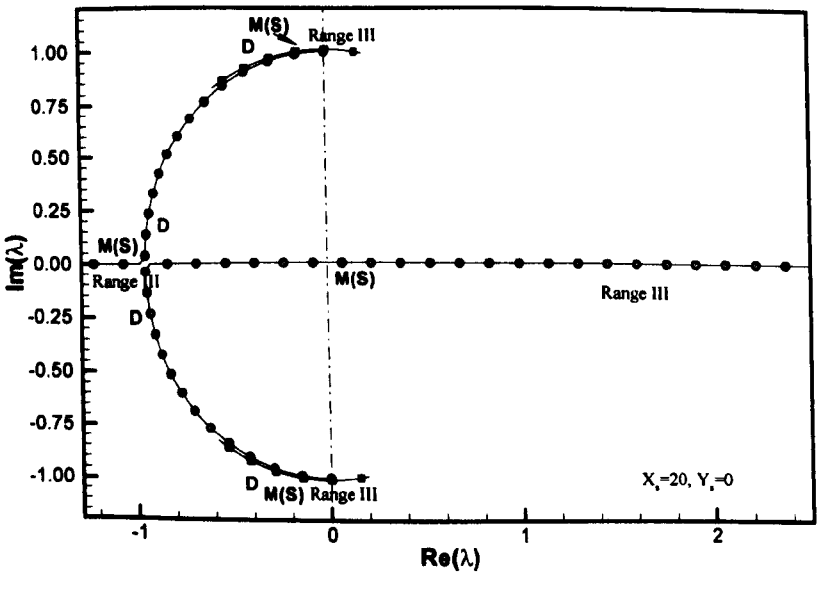

Figure 4.6(b) Variation of eigenvalues for X_S=*20*, Y_S=*0.*

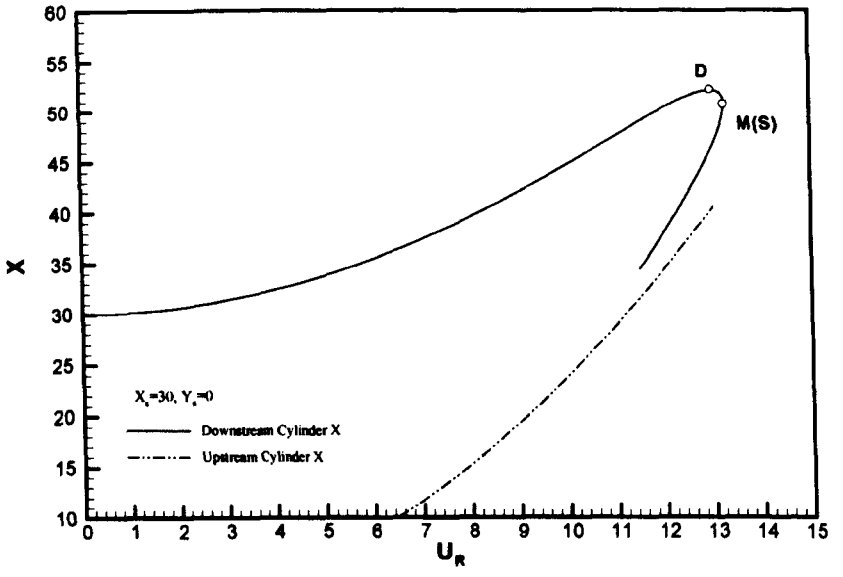

Figure 4.7(a) Continuation for $X_s=30$, $Y_s=0$ *with* $a=0.2$.

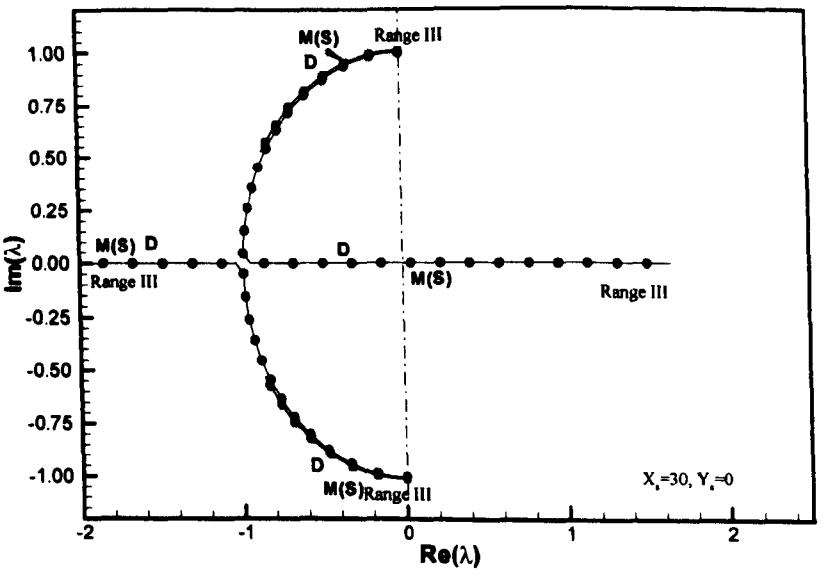

Figure 4.7(b) Variation of eigenvalues for $X_s=30$, $Y_s=0$.

4.3.2 Inner wake position

Figures 4.8 to 4.11 are the continuation results for positions (5,1), (8,1), (10, 1) and (15,1) and corresponding variations of eigenvalues with flow velocity respectively. These locations are close to the wake centreline and are generally called inner wake positions here. It is seen that the results are very similar to the cases when the two cylinders are arranged in tandem. Both cylinders are pushed towards downstream with the increase of flow velocity. Meanwhile, the downstream cylinder is moving towards inner part of the wake due to the lift force. When the flow velocity reaches a certain value, which is dependent on initial spacing, there will be two equilibrium positions, One will be located very near to the upstream one while the other is located somewhere downstream. A critical flow velocity exists above which there will be no equilibrium positions. Examining the accompanying eigenvalues variation with flow velocity, it can be seen that the general trend is same as the case on the wake centreline. When the two cylinders are initially arranged with a relative small spacing, say less than 8 diameters, and when the flow velocity is high enough, before reaching the critical state, the downstream cylinder can lose its stability via Hopf bifurcation. At critical state, stationary bifurcation occurs. For such a critical state, which is a turning point in the continuation diagram, the stability before and after the turning point are both unstable. Typically, before the turning point, the state corresponds to a pair of conjugate complex eigenvalues with positive real parts whilst after the turning point, the corresponding eigenvalues will have a pair of real number with at least one being positive. However, when the initial spacing exceeds a certain level, typically larger than 8 diameters (exact data depends on mass parameter), only stationary bifurcation will occur. It can be seen from the accompanying eigenvalues, that the turning point is the critical state and also of the stationary bifurcation.

Such an inner wake characteristic spreads with the streamwise distance. At large streamwise distance, at the transverse location of $Y_S=2$ or even larger, the continuation results will have the same characteristics.

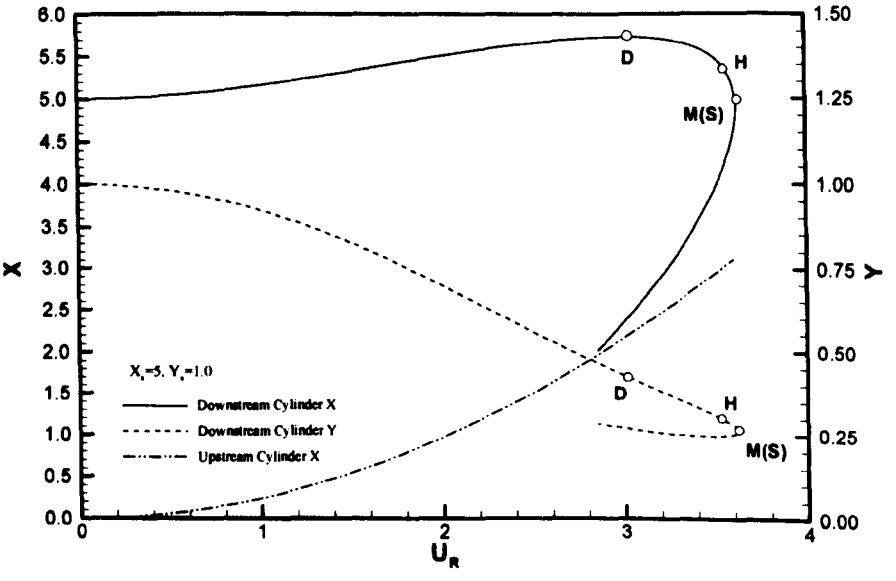

Figure 4.8(a) Continuation for $X_S=5$, $Y_S=1$.

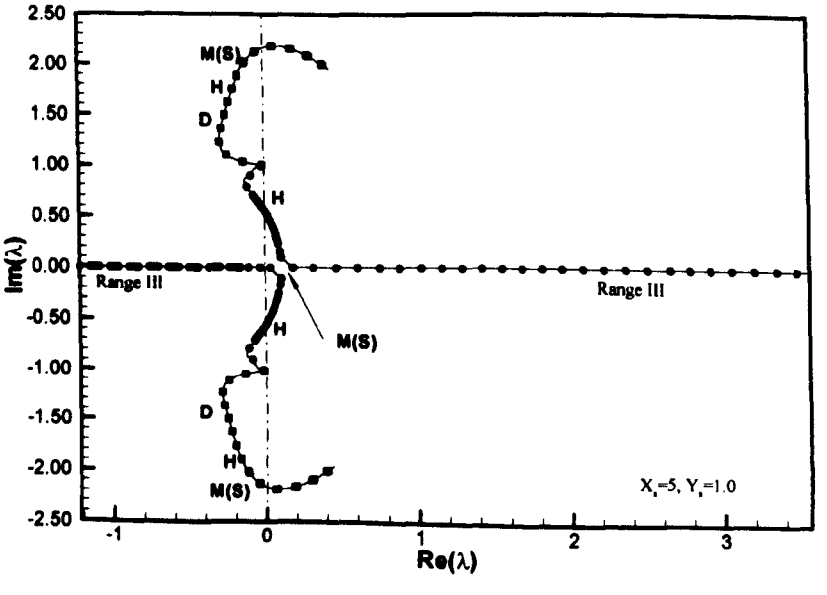

Figure 4.8(b) Continuation for $X_S=5$, $Y_S=1$.

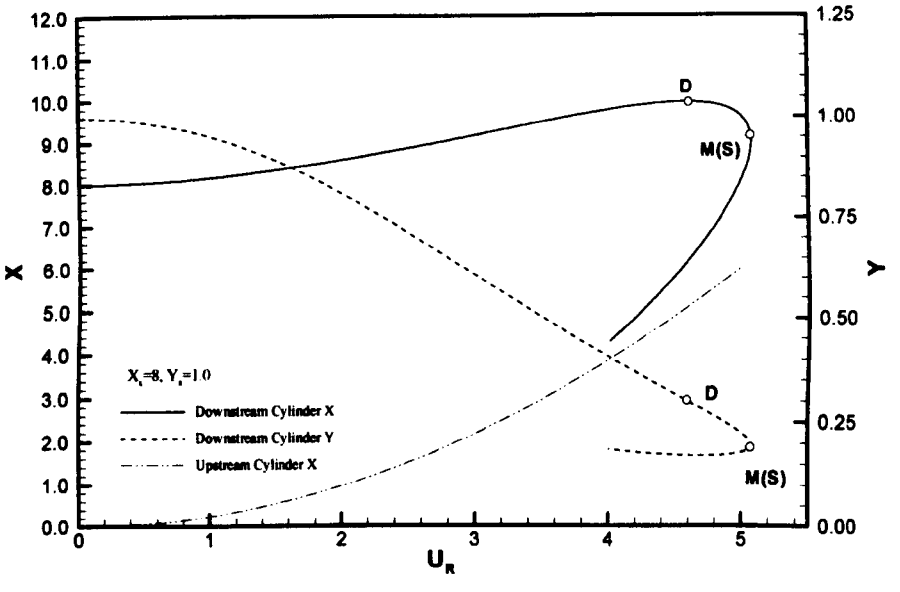

Figure 4.9(a) Continuation for X_S=*8*, Y_S=*1*.

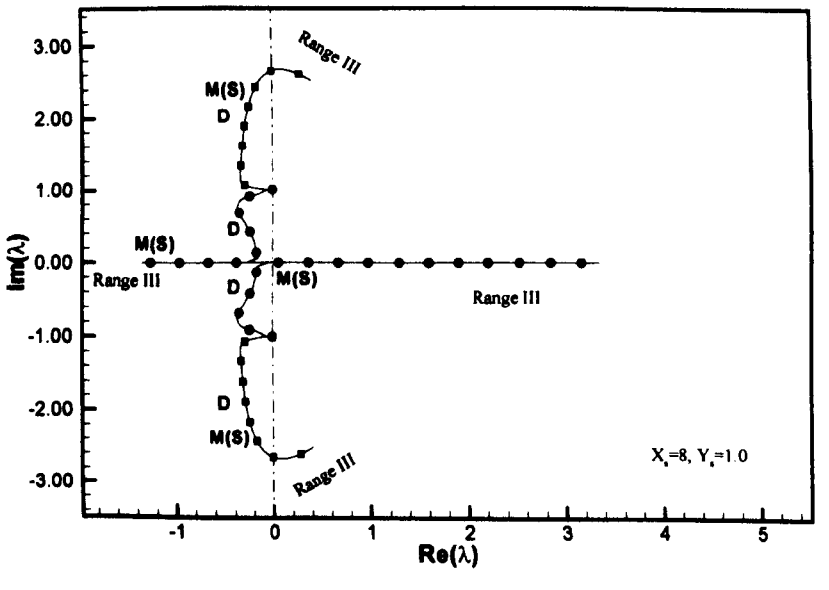

Figure 4.9(b) Continuation for X_S=*8*, Y_S=*1*.

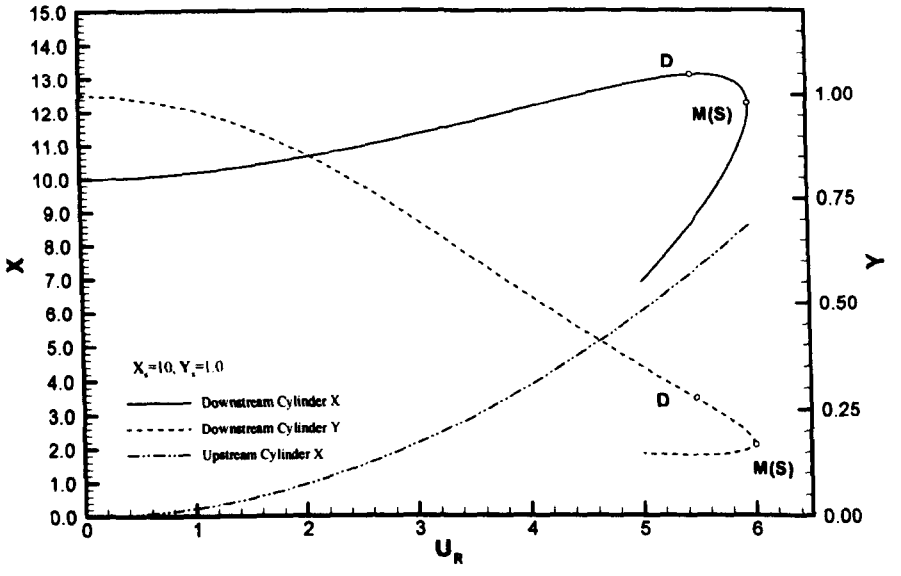

Figure 4.10(a) Continuation for X_S=*10*, Y_S=*1*.

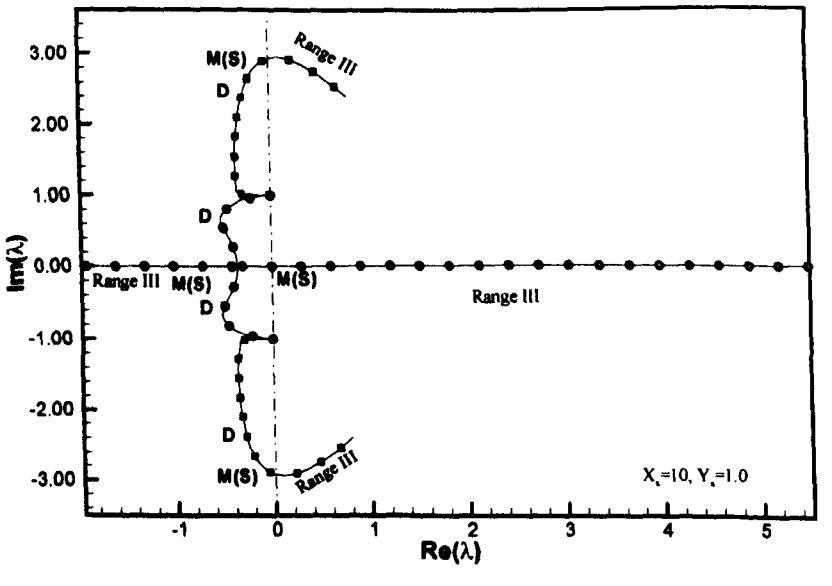

Figure 4.10(b) Continuation for X_S=*10*, Y_S=*1*.

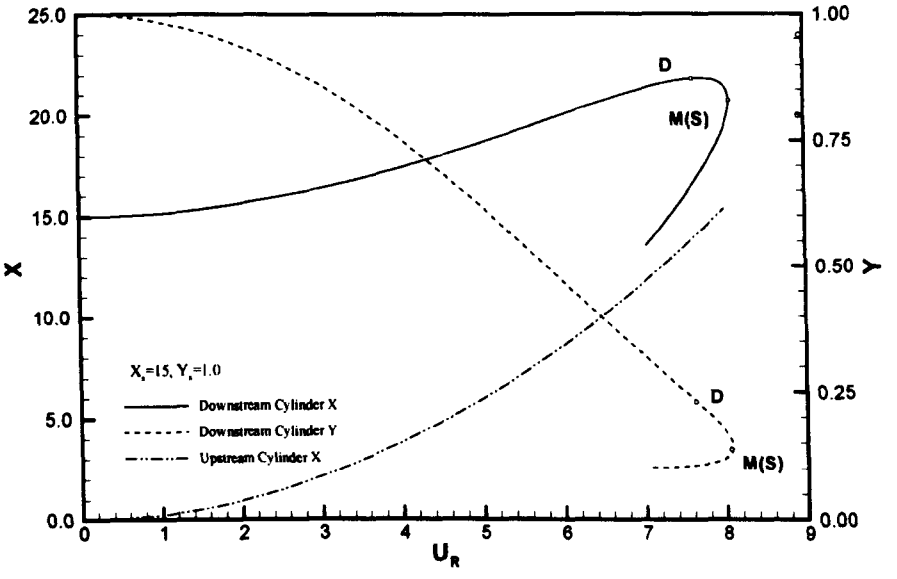

Figure 4.11(a) Continuation for X_S=*15*, Y_S=*1*.

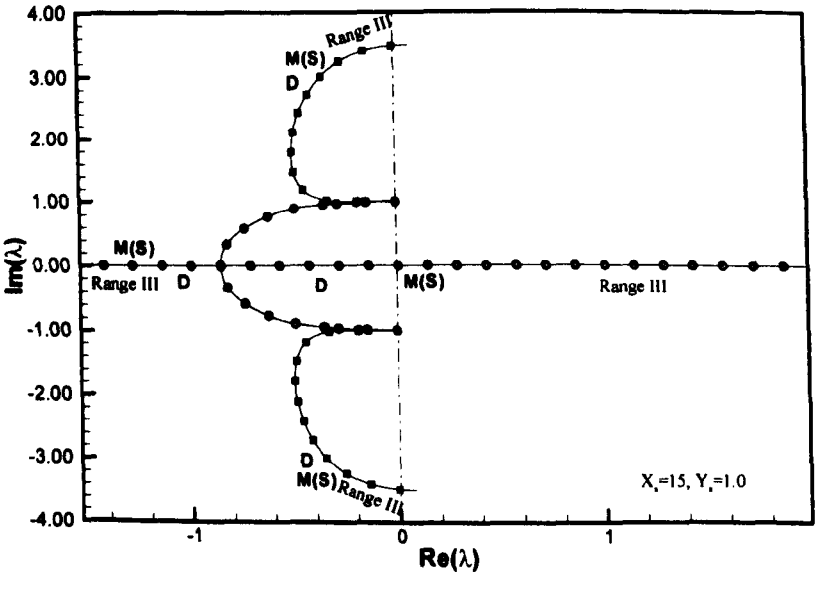

Figure 4.11(b) Continuation for X_S=*15*, Y_S=*1*.

4.3.3 Outer wake position

Figures 4.12 to 4.22 show the scenario when the downstream cylinder is initially positioned at the outer part of the wake, with the following arrangement:

Table 4. 1 Arrangement of the cylinder pair for the calculation.

Streamwise spacing X_S	Transverse spacing Y_S
5, 8, 10, 15, 30	2, 2.5, 3

The continuation results show that, in general, with the increase of flow velocity, the downstream cylinder is slowly pulled towards the centre of the wake and the rate of change in the transverse location is increased with the move inwards of the downstream cylinder. With the further increase of flow velocity, firstly one additional equilibrium point will appear which is close to the upstream cylinder, after which a state Q, at which three equilibrium points coexist occurs. The third equilibrium point is located between the previous two equilibrium points. When the flow velocity increases further, the middle equilibrium state is split into two equilibrium points. One is close to the downstream equilibrium point, which constitutes a downstream pair, and the other is close to the upstream one and forms the upstream pair. When the flow velocity is increased further, depending on the initial transverse location, one of the two equilibrium pairs will first converge and then disappear. The remaining pair will converge at a higher flow velocity. The maximum streamwise position that the downstream cylinder can reach is the downstream pair convergence point. The state of the last convergence is defined as the critical state, and after such a state, no equilibrium will exist.

The accompanying eigenvalue analysis shows that the downstream cylinder is always stable on the path from its initial position to the downstream pair convergence position D, which is also a stationary bifurcation point (S). From D to Q the equilibrium is unstable, which

corresponds to the stationary bifurcation with a pair of real eigenvalues, one being positive. From Q to another position of stationary bifurcation M, there are three possibilities:

1) It is stable in the whole path from Q to M, with both pairs of eigenvalues located within the left half of the eigenvalue plane, such as shown in Figures 4.15 to 4.22 for X_S=*8, 10, 15, 20, 30.* It is clear that when X_S>8, the equilibrium position located on Q to M is always stable.

2) As shown in Figures 4.12, and 4.14, for initial position X_S=*5*,Y_S=*2*, X_S=*6*, Y_S=*2.1*, within the path from Q to M, there is a critical state labelled as H, and from Q to H is stable. However, H is a critical state of Hopf bifurcation, and from H up to M, the path is unstable. Figure 4.14(c) is an enlarged figure which shows the variation of eigenvalues around the Hopf bifurcation, and it also clearly shows that Hopf bifurcation exists in the course from Q to M.

3) As can be perceived from Figure 4.12 for X_S=5, Y_S=2.0, the whole path from Q to M can be unstable when initial spacing is further reduced.

From the upstream pair convergence point to the upstream branch (the equilibrium close to the upstream cylinder), all the equilibrium states are unstable, often with a pair of real eigenvalues, and one of the pair being positive.

Comparing to the cases when the two cylinders are arranged in tandem, all these results show that there are two possibilities of stability change at the turning point, i.e. either a change of stability or both branches before and after turning point are unstable. The later scenario only occurs when the initial spacing between the two cylinders is relative small.

Figure 4.22 shows the variation of the equilibrium structure at streamwise location of 5 diameters, and with different transverse locations. It shows the emergence of multiple

equilibrium states when the transverse distance is large enough. Such a variation is a continuous process with changing transverse distance.

In order to identify the most vulnerable arrangement for specified two cylinder spacing, Figure 4.23 shows the variation of critical flow velocity with the coming flow angles. It is seen that the minimum critical flow velocity occurs on the wake centreline for the two cylinders arranged by same distance. In this comparison calculation, the variable is the flow direction. The figure also shows that the critical flow velocity does not change much when the flow direction is close to the case of 0 degree angle. The explanation for this can be deduced directly from the continuation diagram, as in most of the cases, the critical state occurs near the wake centreline. Such a result is very useful to riser designers. Should the collision between two risers has to be avoided, the tandem arrangement is the most important case to examine.

Figure 4.24 shows the variation in critical flow velocity with the initial arrangement and corresponding spacing under the critical state. It is seen that critical flow velocity increases significantly with initial spacing as well as its corresponding spacing at the critical state. This means that an appropriate increase in cylinder spacing can effectively delay the loss of stability of the downstream cylinder. The figure also shows that when the downstream cylinder is initially located at the outer part of the wake, the critical flow velocity is significantly higher than the case when it is placed at inner wake. This is caused by the fact that when there are multiple equilibria, the ultimate loss of stability occurs by the convergence of the downstream equilibrium pair when the downstream cylinder is located towards the wake boundary.

4.4 Summaries

For a cylinder located in the wake of an upstream cylinder, there can exist multiple stable/unstable equilibrium positions due to the complicated force field in the wake. On the wake centreline and innermost wake positions, the number of equilibrium positions is two, whereas in the outer wake region there can be as many as four equilibrium positions.

Further, there exists a critical reduced velocity, which is defined in this chapter as

$$U_R = V_0/\omega_x D$$

Above this critical velocity, there will be no equilibrium positions. This indicates a likely clashing between two cylinders once the critical velocity is exceeded. The numerical computation shows that the most vulnerable arrangement for a specified spacing is when the two are arranged in tandem form. The eigenvalue analysis shows that most of the time, stationary bifurcation is how the downstream cylinder loses stability, particularly when initial spacing is larger than 8 diameters. Such a quantitative conclusion is subject to the mass parameter be close to 0.2, otherwise the exact spacing giving rise to Hopf bifurcation may be slightly changed. This is consistent with the previous analysis. Finally, it is worth noting that the analysis results presented in this chapter show that the critical flow velocity is well within the range of many deepwater riser system operating conditions, which implies that the collision between risers is an important issue for design of risers.

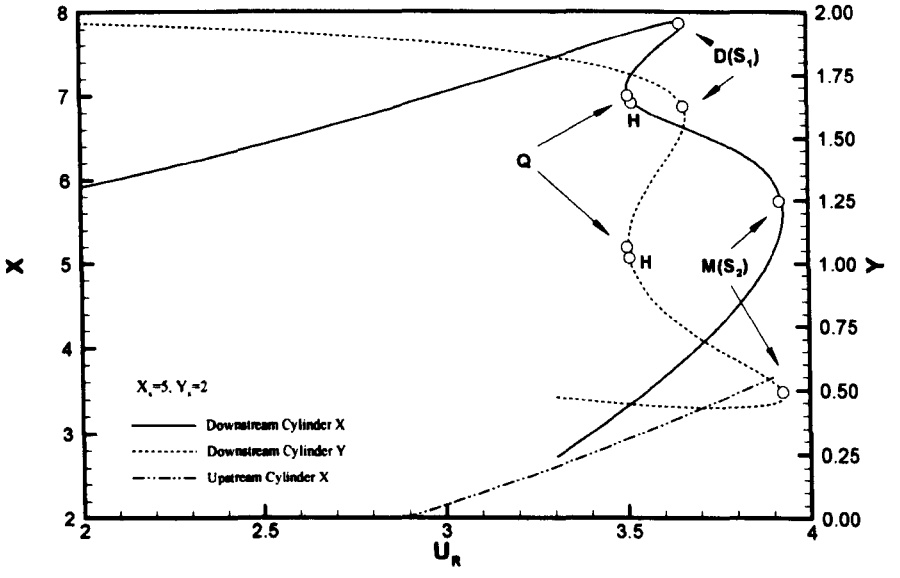

Figure 4.12(a) Continuation diagram for X_5=5, Y_5=2, *a*=0.2.

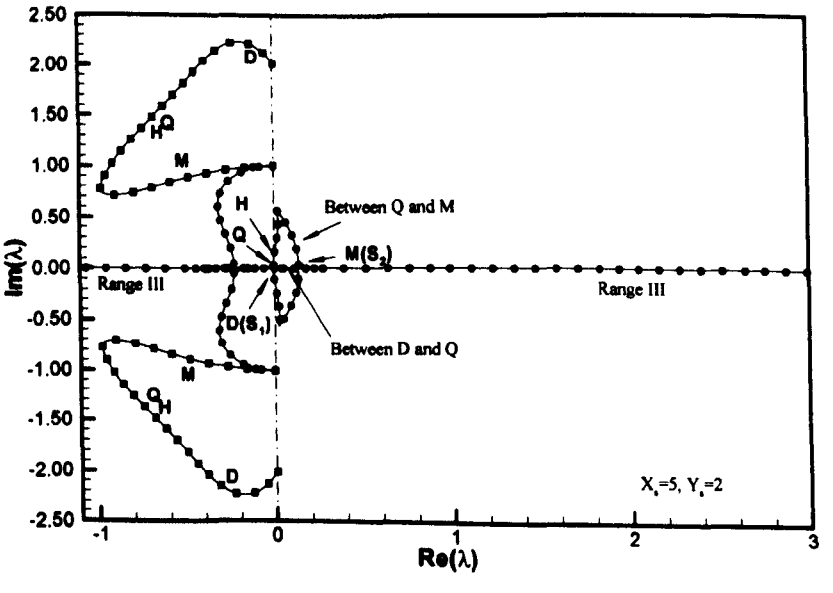

Figure 4.12(b) Variation of eigenvalues with flow velocity for X_5=5, Y_5=2, *a*=0.2.

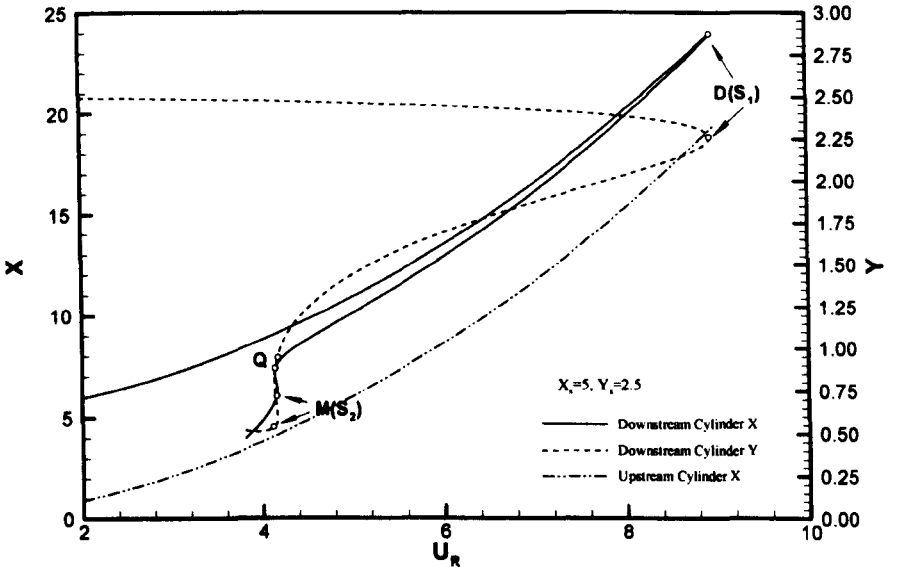

Figure 4.13(a) Continuation diagram for X_s=5, Y_s=2.5, a=0.2.

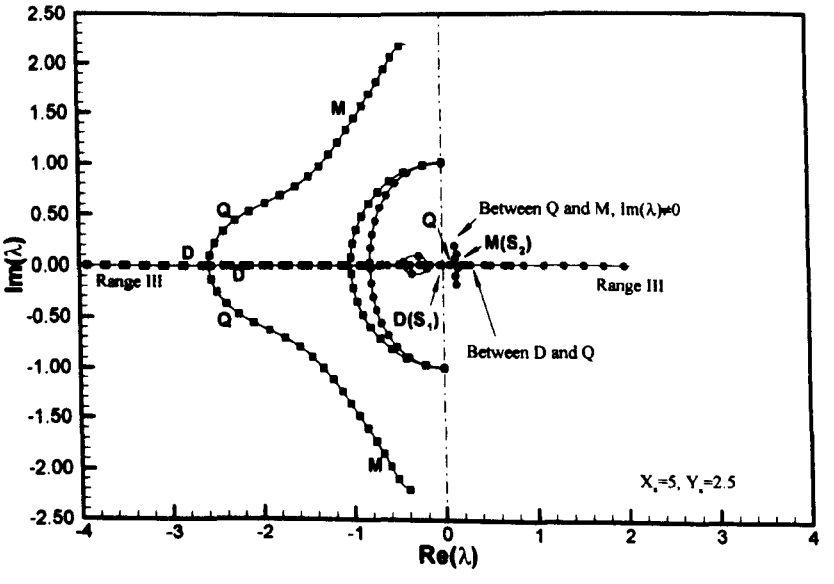

Figure 4.13(b) Variation of eigenvalues with flow velocity for X_s=5, Y_s=2, a=0.2.

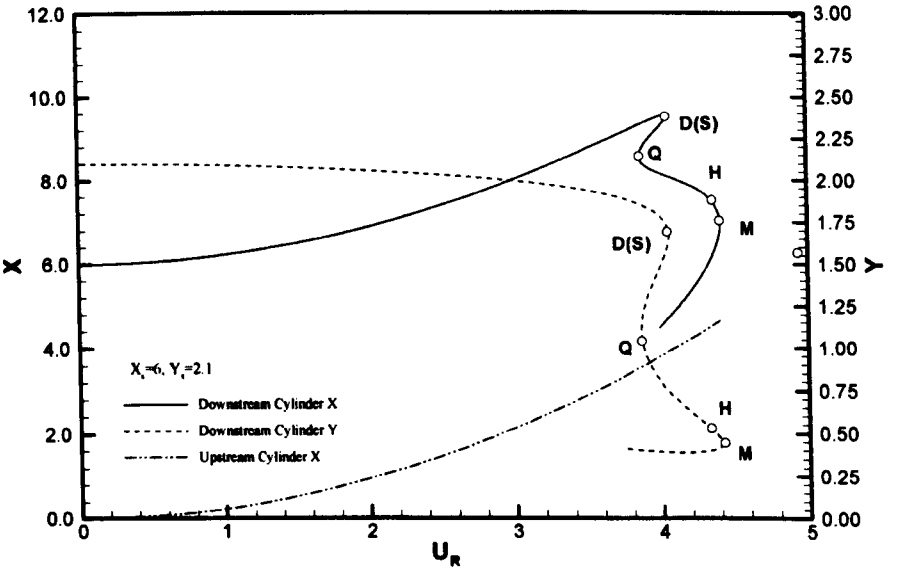

Figure 4.14(a) Continuation diagram for X_s=6, Y_s=2.1, a=0.2.

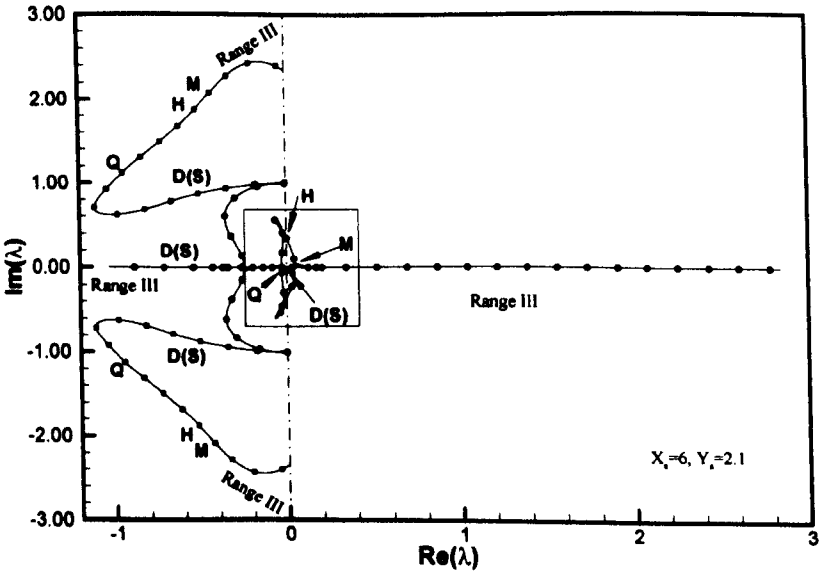

Figure 4.14(b) Variation of eigenvalues with flow velocity for X_s=6, Y_s=2.1, a=0.2.

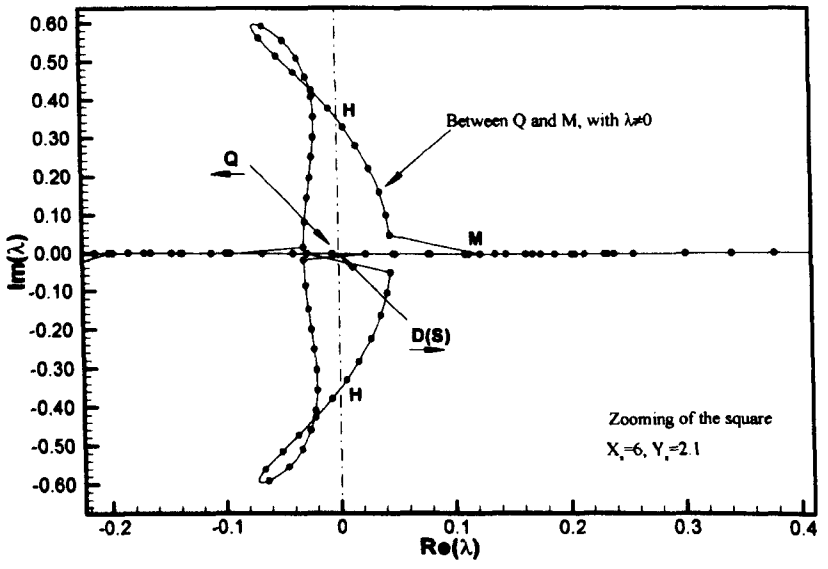

Figure 4.14(c) Variation of eigenvalues with flow velocity for X_S=*6*, Y_S=*2.1*, *a=0.2*, zoom of square window in Figure 4.14(b).

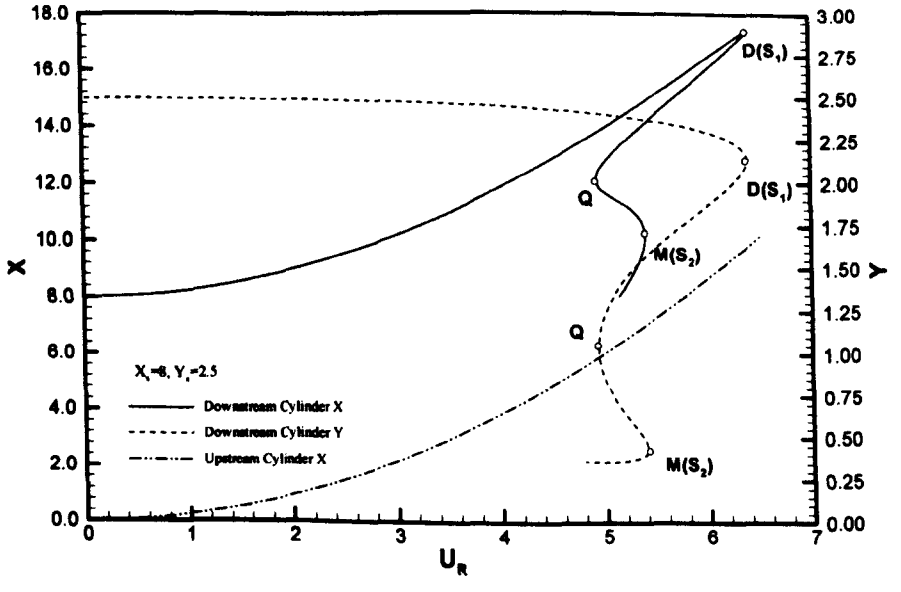

Figure 4.15(a) Continuation diagram for X_S=*8*, Y_S=*2.5*, *a=0.2*.

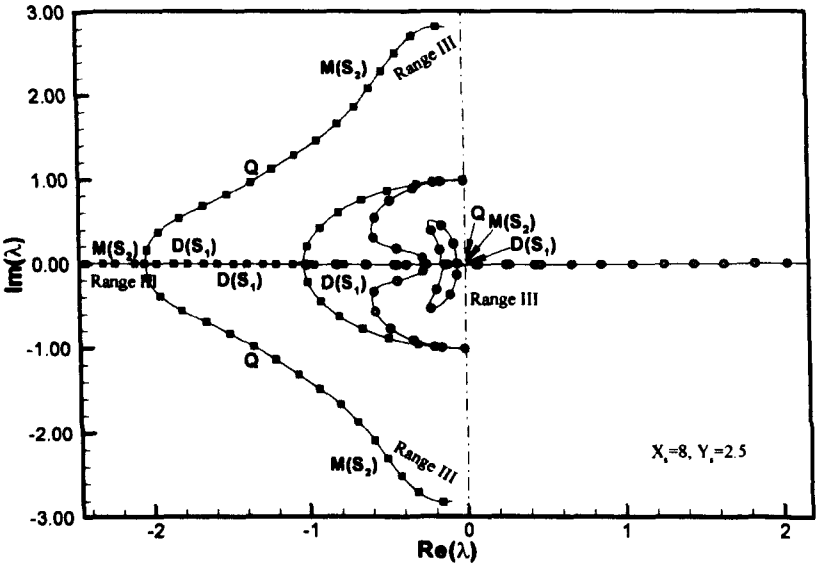

Figure 4.15(b) Variation of eigenvalues with flow velocity for X_S=*8*, Y_S=*2.5*, *a*=*0.2*.

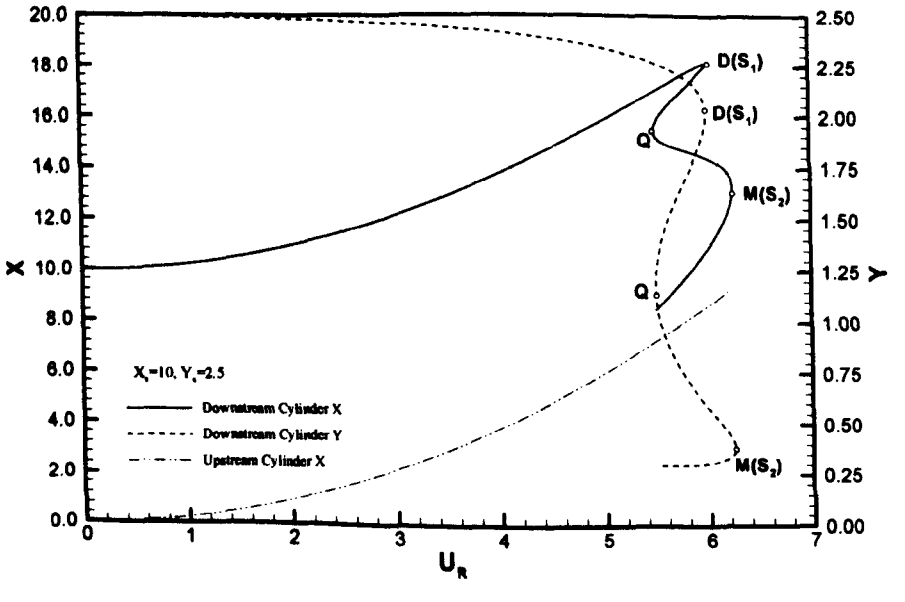

Figure 4.16(a) Continuation diagram for X_S=*10*, Y_S=*2.5*, *a*=*0.2*.

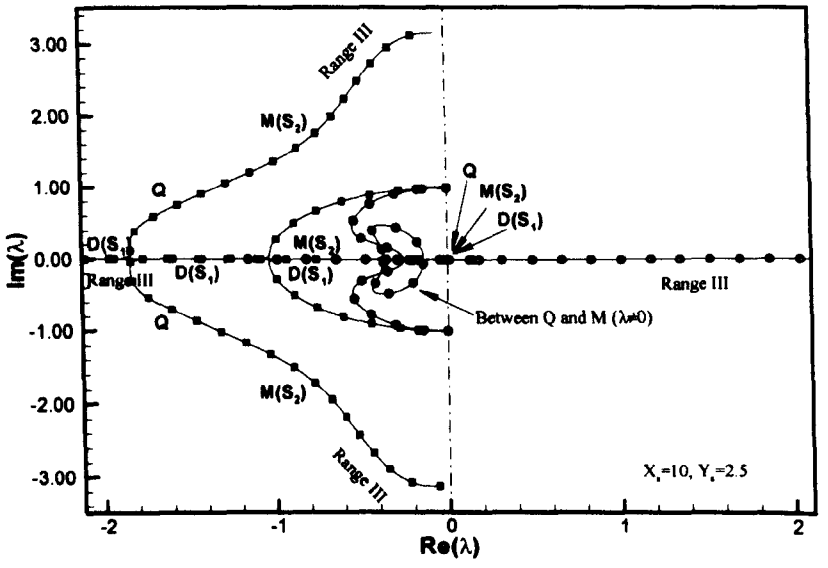

Figure 4.16(b) Variation of eigenvalues with flow velocity for X_S=*10*, Y_S=*2.5*, *a=0.2.*

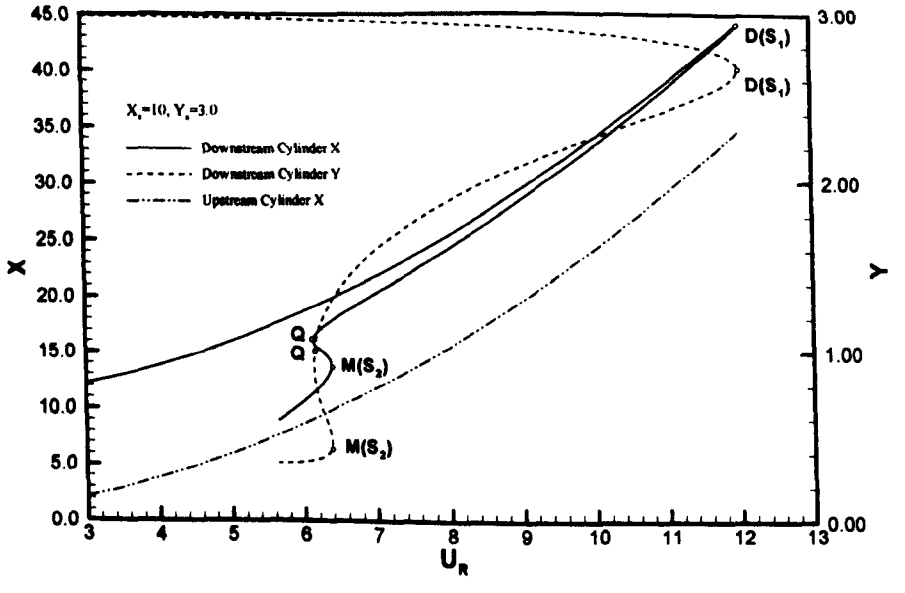

Figure 4.17(a) Continuation diagram for X_S=*10*, Y_S=*3.0*, *a=0.2.*

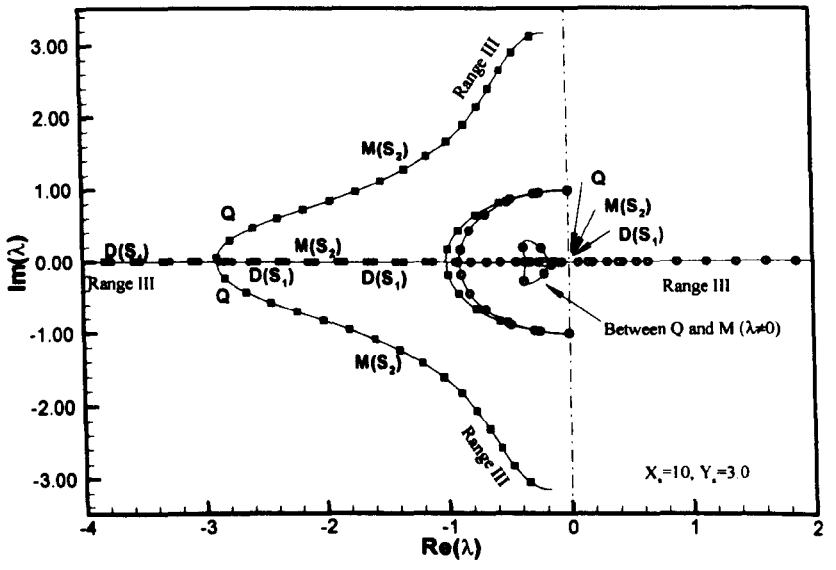

Figure 4.17(b) Variation of eigenvalues with flow velocity for X_S=*10*, Y_S=*3.0*, *a*=*0.2*.

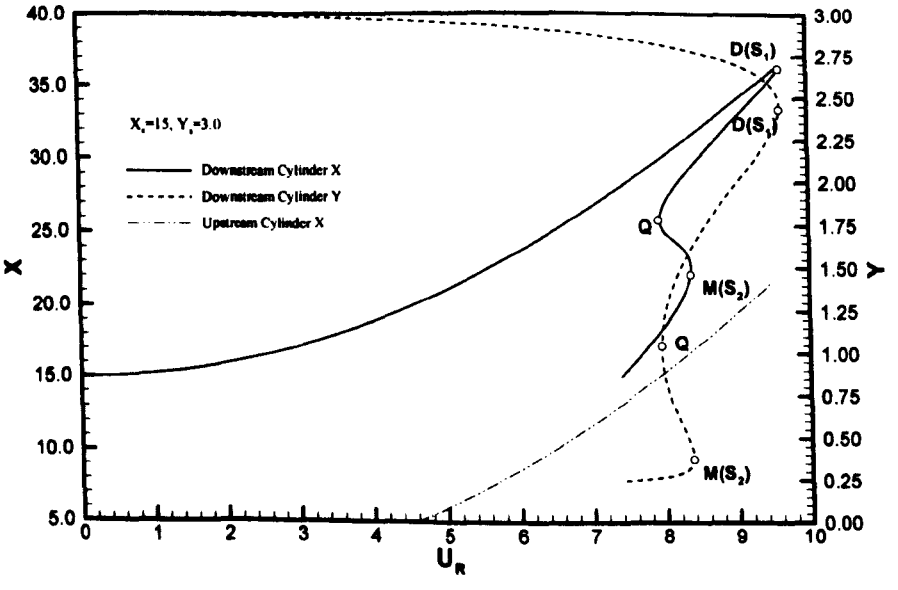

Figure 4.18(a) Continuation diagram for X_S=*15*, Y_S=*3.0*, *a*=*0.2*.

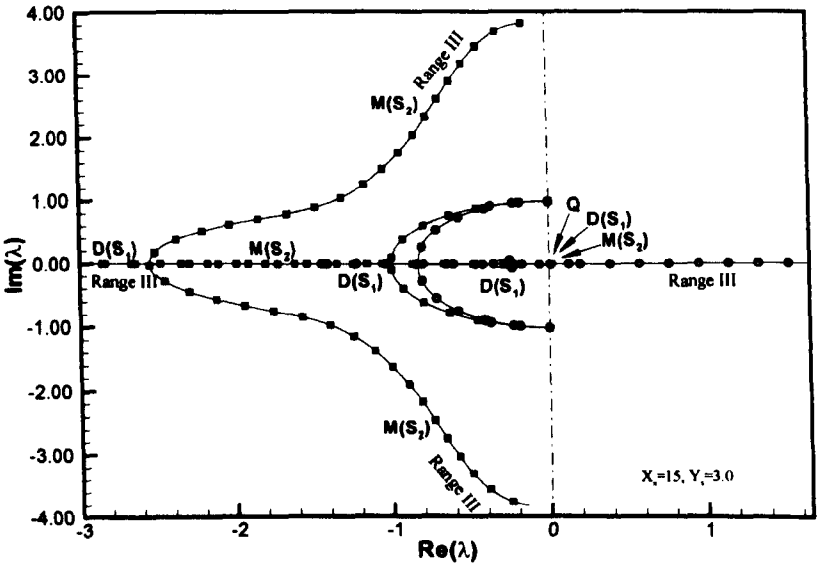

Figure 4.18(b) Variation of eigenvalues with flow velocity for X_S=*15*, Y_S=*3.0*, *a*=*0.2*.

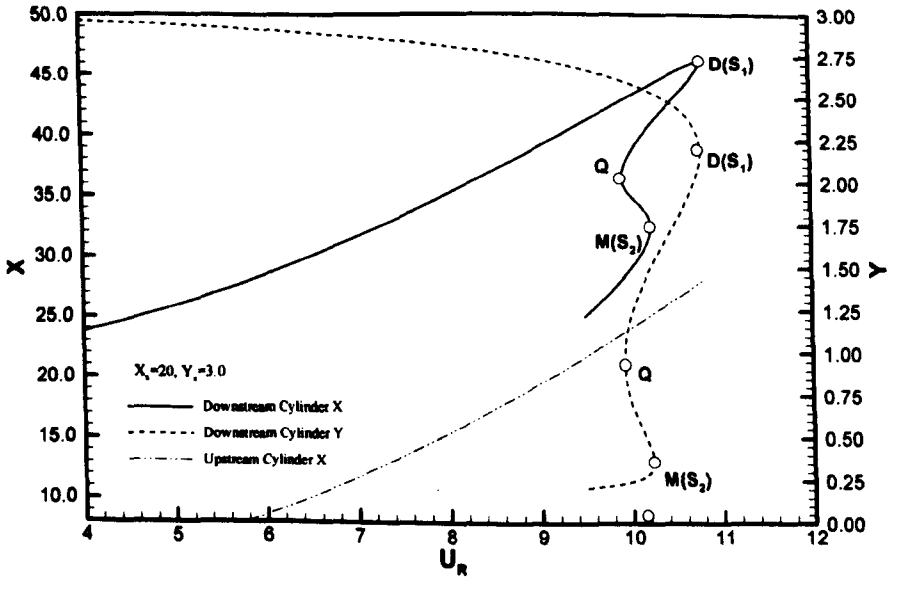

Figure 4.19(a) Continuation diagram for X_S=*20*, Y_S=*3.0*, *a*=*0.2*.

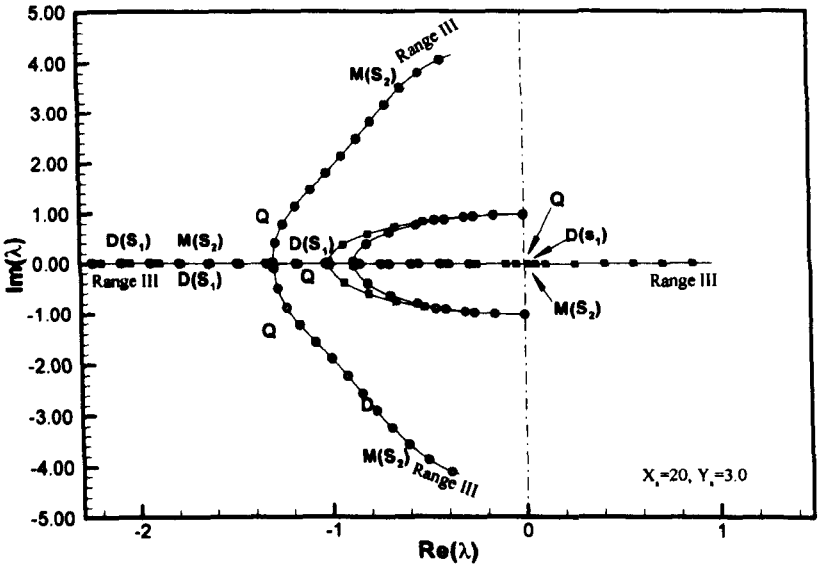

Figure 4.19(b) Variation of eigenvalues with flow velocity for X_1=*20*, Y_1=*3.0*, *a*=*0.2*.

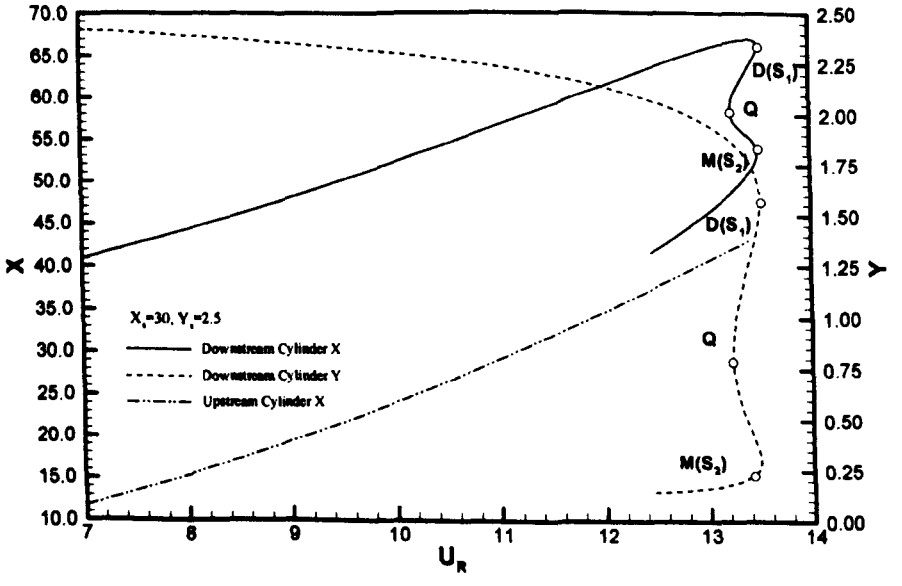

Figure 4.20(a) Continuation diagram for X_1=*30*, Y_1=*2.5*, *a*=*0.2*.

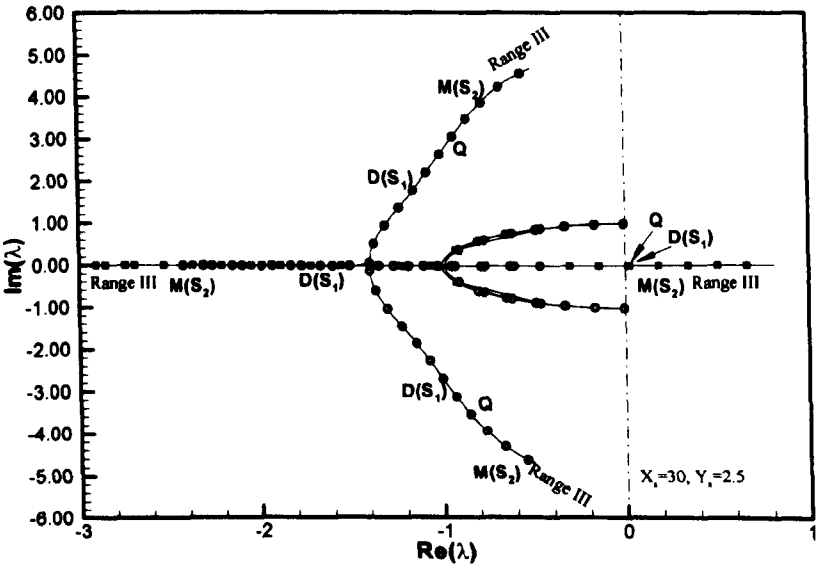

Figure 4.20(b) Variation of eigenvalues with flow velocity for X_S=*30*, Y_S=*2.5*, *a=0.2*.

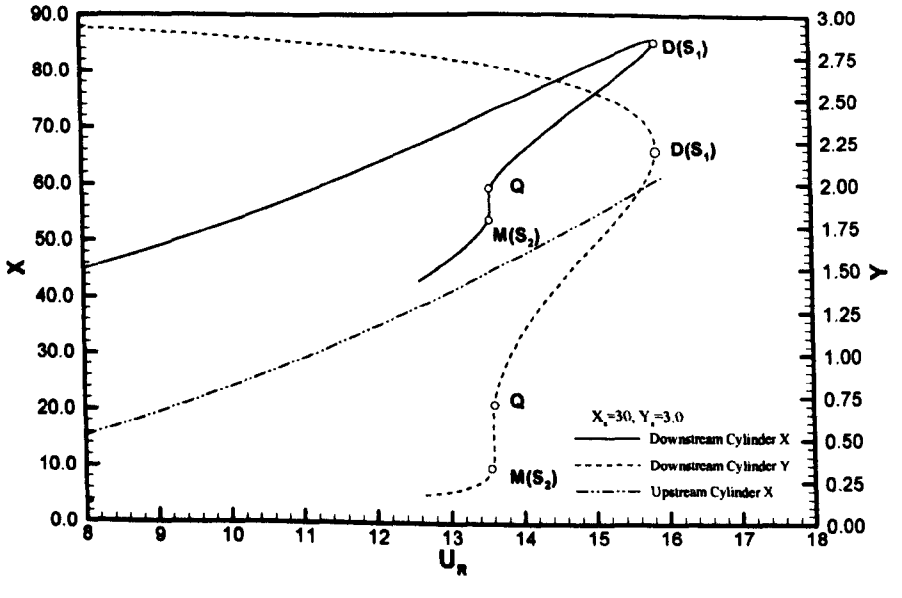

Figure 4.21(a) Continuation diagram for X_S=*30*, Y_S=*3.0*, *a=0.2*.

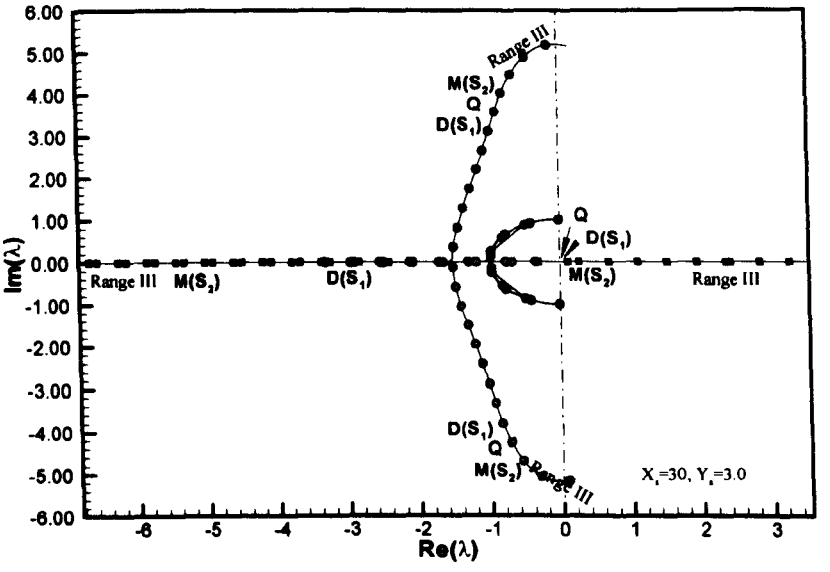

Figure 4.21(b) Variation of eigenvalues with flow velocity for X_S=*30*, Y_S=*3.0*, *a=0.2.*

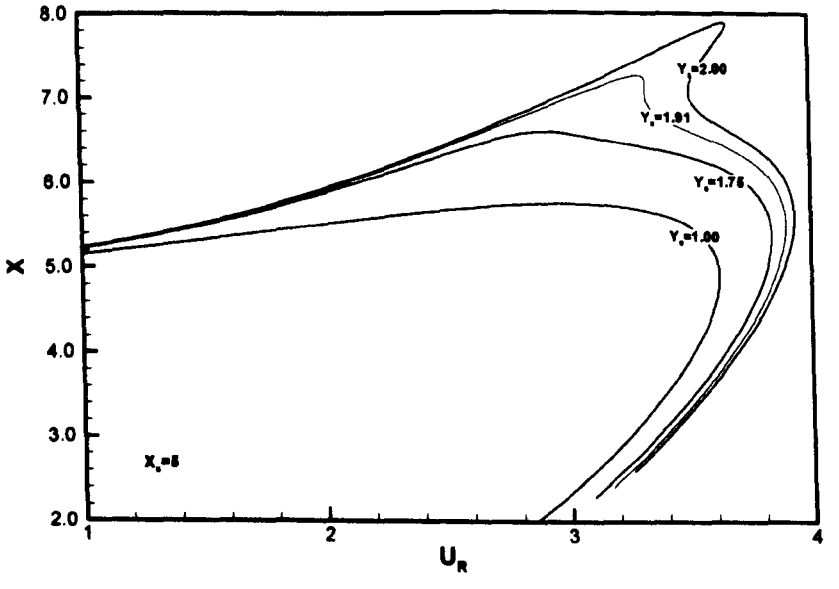

Figure 4.22(a) Streamwise direction displacement for different continuation diagram at the same streamwise direction spacing of 10 diameters, with *a=0.2.*

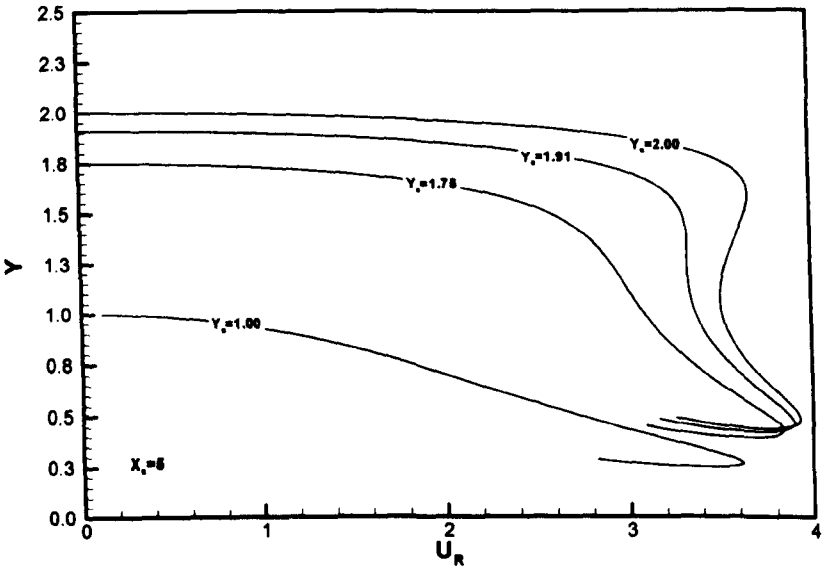

Figure 4.22(b) Transverse direction displacement for different continuation diagram at the same streamwise direction spacing of 10 diameters, with *a=0.2.*

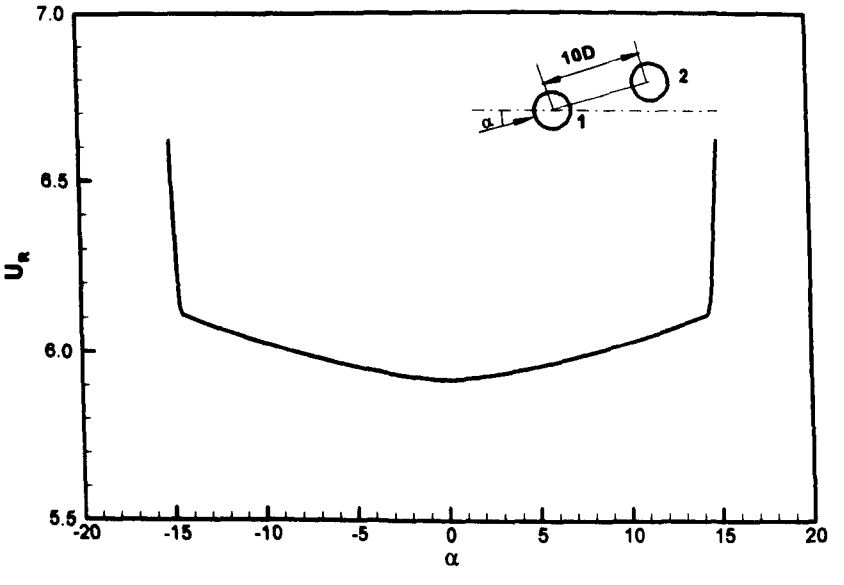

Figure 4.23 Variation of critical flow velocity with coming flow direction for the same distance arrangement, S/D=10.

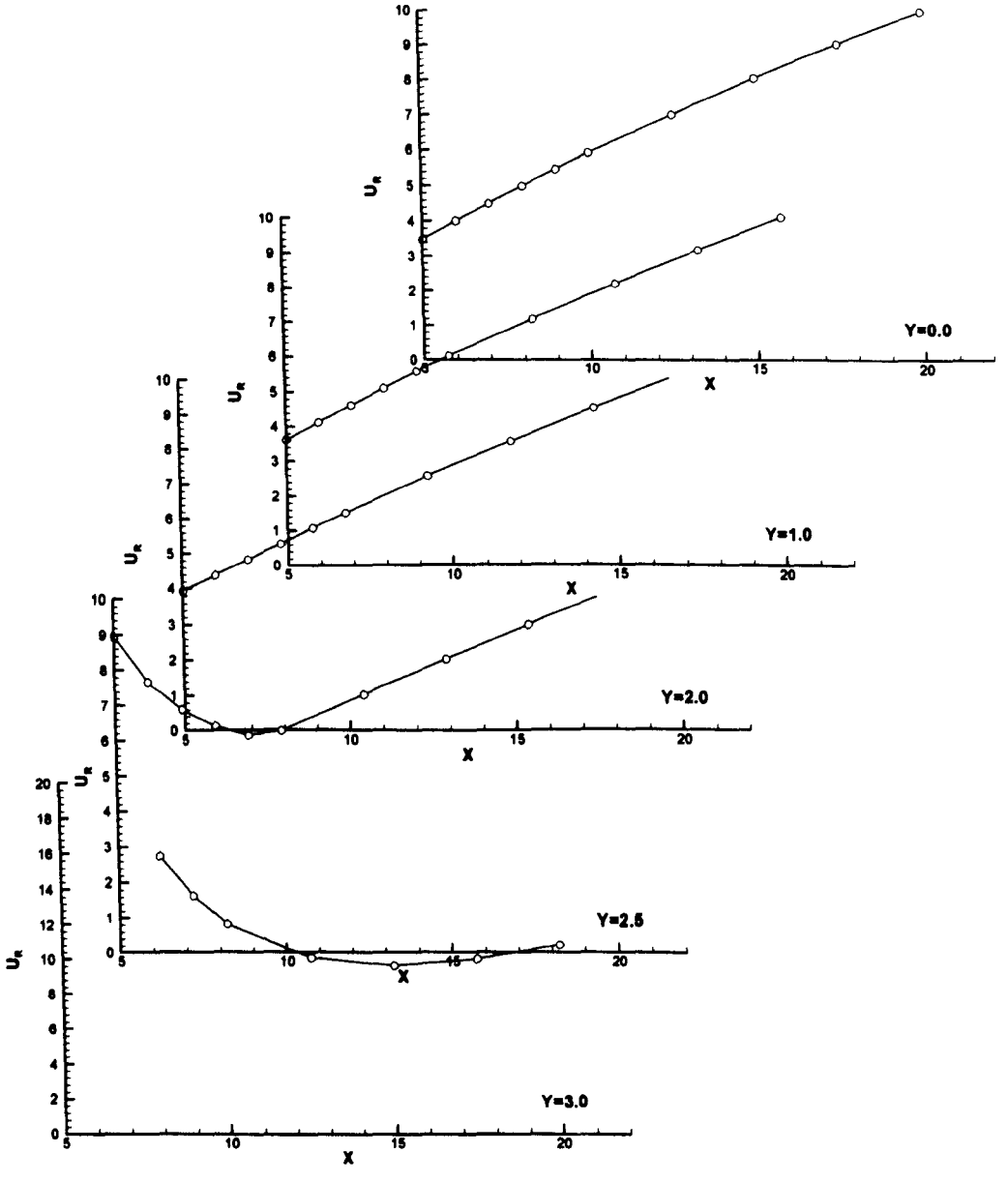

Figure 4.24(a) Critical flow velocity at different locations for $a=0.2$.

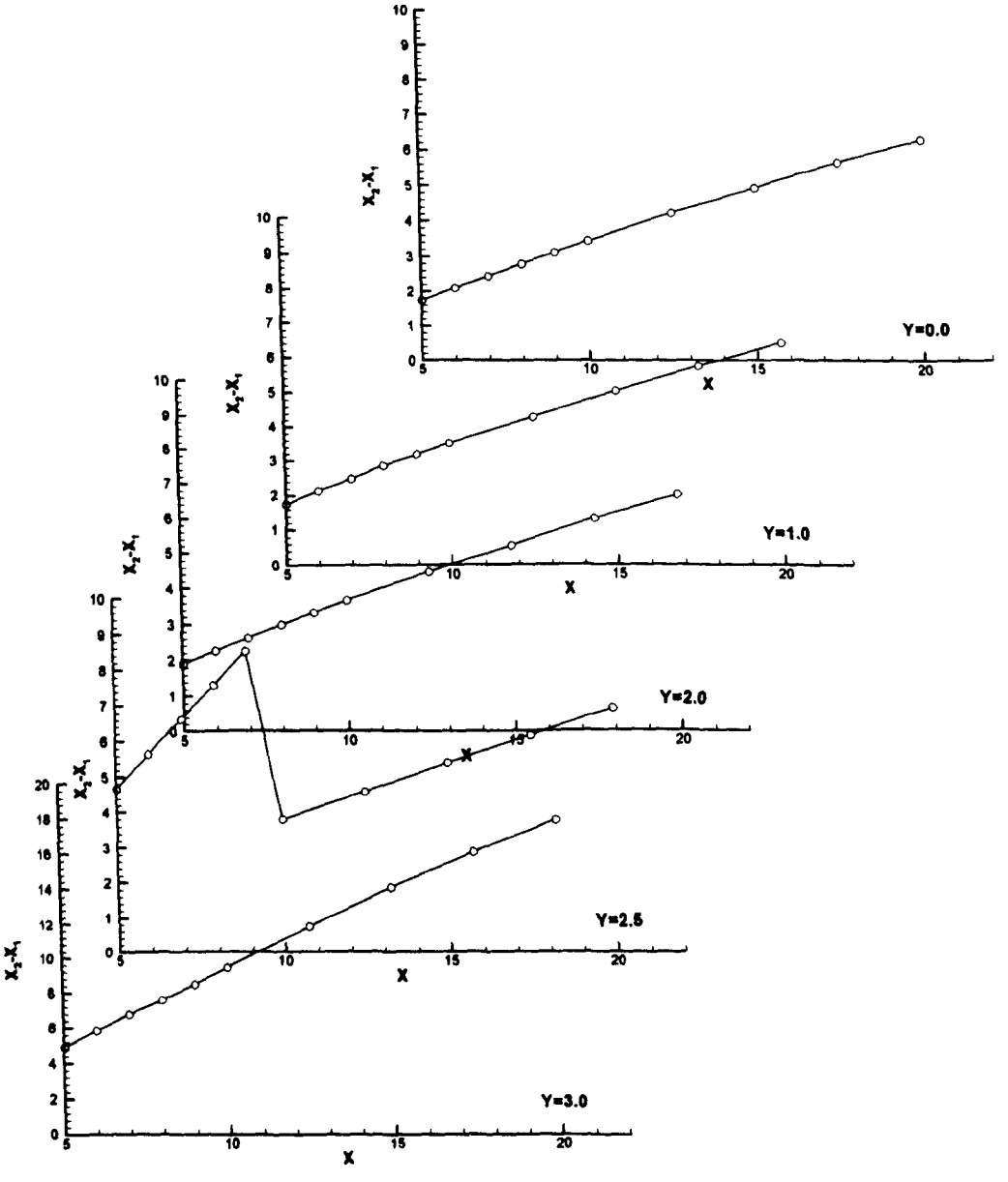

Figure 4.24 (b) Critical spacing at different location at critical velocity for $a=0.2$.

Chapter V

DYNAMICS SIMULATION OF INTERACTION OF TWO CYLINDERS IN TWO-DIMENSIONAL SPACE

5.1 General Remarks

For power transmission lines, when the flow velocity exceeds the critical flow state, periodical large amplitude movement with an elliptical trajectory will occur. Its motion will be in a clockwise direction when the downstream cylinder is located in the upper half of the wake and counter-clockwise when the downstream cylinder is located in the lower half of the wake. Such movements usually have amplitudes of several diameters, and grow with the increase of flow velocity (Blevins, 1990, Price, 1990, Hardy & Dyke, 1995). The continuation and stability investigation conducted in Chapter III and IV (also cf. Wu et al, 2000, 2001a, 2001b) has shown, in general, the interaction between two cylinders in water loses its stability through stationary bifurcation, typically when the spacing between two cylinders is larger than 8 diameters. When the flow velocity exceeds the critical flow velocity, any disturbance on the downstream cylinder is likely to be amplified. The dynamic motion under such conditions is of interest to the marine riser designers and operators, in particular its motion trajectory and the momentum of the cylinder immediately before the collision should it occur.

In this chapter, a comprehensive simulation is conducted to account for the dynamics after the downstream loses its stability. Both large spaced and relatively small spaced cylinder pairs are considered, and the scenarios before the flow velocity reaches the critical velocity are also discussed. A collision model is attempted, in order to account for the course of

collision when it does take place. The investigation endeavours to show the possible motion trajectory of the downstream cylinder and its dynamic behaviour.

5.2 Theoretical Formulation

As shown in the schematic diagram Figure 5.1, both the upstream cylinder and downstream cylinder are supported by two orthogonal springs. The origin of the co-ordinate system is set at the centre of the upstream cylinder when the fluid is stationary, the x axis is pointing towards downstream in the inflow direction, and y is in the cross-flow direction. Consideration of the cylinders in water is the main interest of this chapter. The x direction spring is assumed to be aligned in the direction of flow, and the springs are assumed to be ideal, so that the motion of the cylinder does not alter the arrangement of the two springs. The stiffness of the four springs is assumed to be the same. For such a system, the equation of motion can be written as:

$$m\underline{I}\begin{bmatrix}\ddot{x}_i\\ \ddot{y}_i\end{bmatrix}+c\underline{I}\begin{bmatrix}\dot{x}_i\\ \dot{y}_i\end{bmatrix}+k\underline{I}\begin{bmatrix}x_i\\ y_i\end{bmatrix}=\begin{bmatrix}F_{xi}\\ F_{yi}\end{bmatrix} \qquad (i=1,2) \tag{5.1}$$

Here $i=1,2$ represents the upstream and downstream cylinders respectively. m is the mass of the cylinder per unit length, c is structure damping coefficient, k is the stiffness of the spring, (x_i, y_i) is the displacement by which they have deviated from their corresponding layout positions (x_{si}, y_{si})[1]. F_{xi}, F_{yi} are the fluid forces applied on the two cylinders. $\underline{I}$ is the unit matrix.

[1] The layout position corresponds to the arrangement when flow is stationary, with $x_{s1}=y_{s1}=0, x_{s2}=x_s, y_{s2}=y_s$

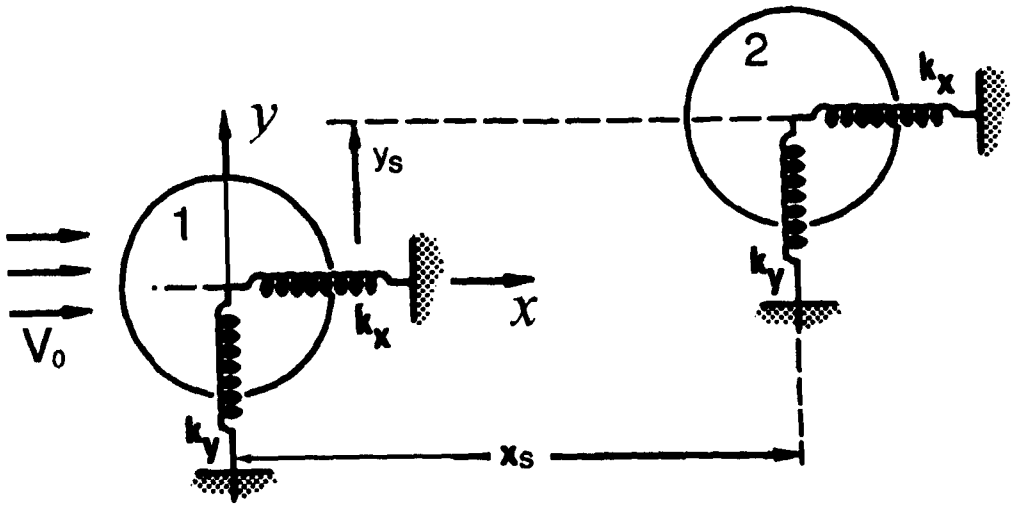

Figure 5.1 Schematic diagram of co-ordinate system.

According to quasi-steady flow theory, the fluid forces can be expressed as:

$$\begin{cases} F_{xi} = \frac{1}{2}\rho U_{ri} D\left[\bar{C}_{Di}\left(U_i - \dot{x}_i\right) + \bar{C}_{Li}\dot{y}_i\right] - c_m \frac{\rho\pi D^2}{4}\ddot{x}_i \\ F_{yi} = \frac{1}{2}\rho U_{ri} D\left[-\bar{C}_{Di}\dot{y}_i + \bar{C}_{Li}\left(U_i - \dot{x}_i\right)\right] - c_m \frac{\rho\pi D^2}{4}\ddot{y}_i \end{cases} \qquad (i = 1, 2) \qquad (5.2)$$

In equation (5.2), $U_i = V_0$ for the upstream cylinder, c_m is the fluid added mass coefficient, the definitions of other parameters are the same as those in Chapter III.

Such a dynamic system can be written in the standard form of the first order differential equations:

$$\dot{\tilde{x}} = \tilde{f}(\tilde{x}) \qquad (5.3)$$

where

$$\tilde{f}(\tilde{x}) = \begin{Bmatrix} x_2 \\ aU_R^2 C_{D1} - 2\xi x_2 - x_1 \\ x_4 \\ aU_R^2 \sqrt{\left(1-\frac{V_0 x_4}{UU_R}\right)^2 + \left(\frac{V_0 x_6}{UU_R}\right)^2}\left[C_{D2}\left(1-\frac{V_0 x_4}{UU_R}\right) + C_{L2}\frac{V_0 x_6}{UU_R}\right] - 2\xi x_4 - x_3 \\ x_6 \\ aU_R^2 \sqrt{\left(1-\frac{V_0 x_4}{UU_R}\right)^2 + \left(\frac{V_0 x_6}{UU_R}\right)^2}\left[C_{L2}\left(1-\frac{V_0 x_4}{UU_R}\right) - C_{D2}\frac{V_0 x_6}{UU_R}\right] - 2\xi x_6 - x_5 \end{Bmatrix}$$

$$\tilde{x} = \{x_1, x_2, x_3, x_4, x_5, x_6\}^T$$

Here, x_1, x_3, x_5 represent the non-dimensional displacements deviated from the layout position in streamwise and cross-flow directions respectively, and x_2, x_4, x_6 are their corresponding velocity terms.

5.2.1 The Applicability of the System

The dynamic system (5.3) is suitable when the two cylinders are separated with a fair amount of distance and with a large reduced flow velocity. The latter condition is easy to meet in the present applications. When the two cylinders move close to each other, the mechanism of the interaction will become more complicated, particularly with regard to the interaction forces applied on the downstream cylinder. In this investigation, it is considered that the interaction comprises two parts. One is the viscous flow effect, which determines the time-averaged force, and the other is the potential flow effect.

When the two cylinders are far apart form each other, the potential flow part of the interaction force is negligible. This is reflected in the fluid added mass term, which is assumed to be equivalent to the case of a solitary cylinder located in a still flow. When the two cylinders move closer, the potential flow effect can be significantly altered. Such kind of effect is assumed to be able to be reflected in the interaction force term and the fluid added mass.

Numerical computation has been carried out in the appendix B to account for this effect through the interaction force term. As shown in the Appendix B, this kind of effect only is significant when the two cylinders are very close to each other, such as less than 2 diameters. On the other hand, within such a small range, the collision effect can be very important because the variation of the cylinder speed is very significant and the time interval during which the two cylinders stay within such a small distance is very short. Therefore, in the presentation of the numerical results, the proximity interaction is not considered.

5.2.2 Consideration of Collision (Impact Model)

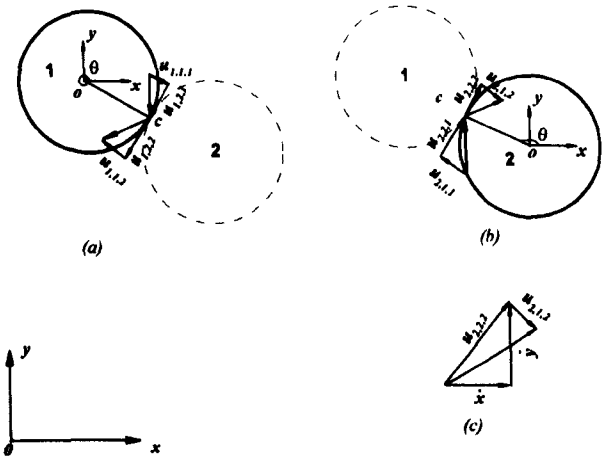

Figure 5.1 Schematic diagram showing the course of impact, (*a*) for upstream cylinder, (*b*) for downstream cylinder (*c*) co-ordinates transformation

The characteristics of the fluid force on the downstream cylinder and its stability implies that a collision between downstream cylinder and upstream cylinder can occur during the movement of the downstream cylinder. However, the course of the collision can be complicated, as it depends on different factors such as the material of the cylinder, the detailed information on the cylinder surface etc. In this thesis, the collision is accounted for by:

1). Momentum conservation for the radial and tangential motion respectively and

2). energy losses for the radial and tangential motions

Although such collision models are basic, the detailed information about the impact is not the theme of this thesis, and the sophisticated impact model can be easily incorporated into present investigation if it is required.

Figure 5.2 is a schematic diagram showing the planar motion of two cylinders and their impact. The contact position between two cylinders is at C and the normal and transverse velocities for upstream and downstream cylinder are represented by $u_{i,j,k}$. Here, $i=1, 2$ denotes upstream and downstream cylinder respectively, $j=1, 2$ represents normal and tangential velocities, $k=1, 2$ indicates before and after collision. According to the hypothesis outlined above,

1). Conservation of momentum in radial motion

$$u_{1,1,1} + u_{2,1,1} = u_{1,1,2} + u_{2,1,2} \tag{5.4}$$

Here, the masses of the two cylinders are assumed to be equal. Therefore, they have been left out in the equation.

2). Conservation of momentum in tangential motion

$$u_{1,2,1} + u_{2,2,1} = u_{1,2,2} + u_{2,2,2} \tag{5.5}$$

3). Supposing energy has the following relations

$$\begin{aligned} u_{1,1,2}^2 + u_{2,1,2}^2 &= k_r \left(u_{1,1,1}^2 + u_{2,1,1}^2 \right) \\ u_{1,2,2}^2 + u_{2,2,2}^2 &= k_t \left(u_{1,2,1}^2 + u_{2,2,1}^2 \right) \end{aligned} \tag{5.6}$$

The coefficients k_r and k_t show the energy losses during the collision in radial and tangential directions respectively. The solving of above equations leads to the motion of the cylinders immediately after the collision. For simplicity, k_r and k_t are both taken as unity in the subsequent computation cases.

The velocity diagram in Figure 5.2(c) relates the polar co-ordinate velocities derived above to their Cartesian counterparts. The transformation equations before impact, for instance, are

$$\begin{aligned} \dot{x} &= u_{1,1,2}\cos\theta + u_{1,1,2}\sin\theta \\ \dot{y} &= u_{1,1,2}\sin\theta + u_{1,1,2}\cos\theta \end{aligned} \tag{5.7}$$

5.3 Numerical Procedures

The fifth-order Runge-Kutta-Verner integration method (Hull, et al 1976) is applied in this investigation to seek the trajectory of the cylinder pair. The initial condition is specified beforehand, and the integration in time domain is made step by step until a specified time instant is reached. The collision model is embedded in the numerical integration. A detector is constantly monitoring the spacing between the two cylinders, and when the collision between the two cylinders is detected, collision model is then applied.

5.4 Dynamics Simulation Results

Following the procedures outlined above, numerical simulation explores the dynamic behaviour of a pair of cylinders under the predefined condition of flow velocity. All the calculations have set the mass parameter of 0.2 except where otherwise specifically stated. The typical calculation results are presented as follows.

5.4.1 Wake Centreline & Inner Wake

Figures 5.2 to 5.9 show the scenarios when the pair of cylinder is arranged in such a way that the downstream cylinder is near or on the wake centreline of the upstream cylinder. It is seen that when the flow velocity is below the critical velocity and before any bifurcation occurs, the downstream cylinder quickly approaches the equilibrium position irrespective of the initial positions. Figure 5.2 shows the case for X_S=5, Y_S=0 under flow velocity U_R=3.0. Initially the two cylinders are located at the position of (0,0) and (5,0) respectively. It is seen that the two cylinders are both pushed downstream simultaneously by the flow. The upstream cylinder reaches its equilibrium almost directly, whereas the downstream cylinder rests at its equilibrium after one cycle of oscillation. This difference is due to the relatively smaller fluid damping on the downstream cylinder attributed to the reduced fluid drag force.

When the spacing of two cylinders is relatively small, say less than 8, it can be seen from Figure 5.3 that, when the flow velocity is just smaller than critical flow velocity, the quasi-periodical movement will occur, and possibly with slight intermittent collisions. The phase diagram shows the stable quasi-periodic nature of the motion. The velocity data (Figures 5.3(e) and 5.3(f)) show that the motions in cross-flow and flow directions are comparable, but the motion period is slight larger than the natural period of the system. Referring to the stability analysis, this kind of movement is initiated by the loss of stability, because the spacing between two cylinders is so small that the amplitude of the motion is large enough already to bring two cylinders to contact with each other. Figure 5.4 shows the case when the flow velocity has exceeded the critical flow velocity. It is seen that the cylinder moves around, with collisions occurring from time to time. Although the motion of the downstream cylinder is not periodical, the time interval between successive collisions is very regular, and it has the same order of magnitude as the system's natural period. The main acceleration of the downstream cylinder occurs immediately before collision, i.e. in the

short time interval before the collision. The downstream cylinder is sucked towards the upstream cylinder, and the velocity is significantly larger than the vortex induced vibration motion can possibly show. In the above cases, the final dynamic movement of the downstream cylinder depends solely on the flow velocity. The initial positions of the two cylinders only contribute to the early transition movement of the cylinder.

Figure 5.5 shows the case for the same arrangement of X_S=5, Y_S=0. However, the mass parameter is set as *0.02*. The flow velocity shown in the figure is 12.65, which is correlated with case *a=0.2* by the similarity of aU_R^2, and exceeds the critical flow velocity. Comparing with Figure 5.4, it is seen that although the fluid force acting on the two cylinders are the same for the two cases, the amplitude of the downstream cylinder movement is larger than the case of a=0.2. Such a difference can be attributed to the reduced fluid damping. In spite of this, the time interval between two successive collisions is close to the natural period of the system. The general trajectory is similar: both exhibit irregular paths.

Figure 5.6 shows the case with X_S=*10*, Y_S=*0* and U_R=*5.9*. Although the flow velocity is very close to the corresponding critical flow velocity, however, as there is no Hopf bifurcation when the initial spacing between two cylinders is larger than 8 diameters, the downstream cylinder approaches to its equilibrium directly.

Figures 5.7 to 5.9 show the cases when the flow velocity has exceeded the critical flow velocity and the initial streamwise direction spacings between the two cylinders are 10 and 20 diameters, with transverse distance of 0 or 1 diameter. It is seen in all the cases presented that large amplitude movement of the downstream cylinder was observed, with occasional collision between two cylinders from time to time. The main motion occurs in the direction of flow, and the amplitude of the motion is well correlated to their initial spacing.

This amplitude can be understood in the following way: for the case of $a=0.2$, which shows the significant large fluid damping, the most upstream position the downstream cylinder can reach is limited by the presence of the upstream cylinder, and the most downstream position it can possibly reach is when it is not affected by the upstream cylinder. These two extreme locations are the bounds for the movement of the downstream cylinder, and equals the initial spacing between two cylinders. Examining the velocity of the downstream cylinder immediately before collision, it is seen that, most of the time, it can be as high as 5, which is a significantly high velocity when compared to 1 for the maximum lock in amplitude for the two dimensional case.

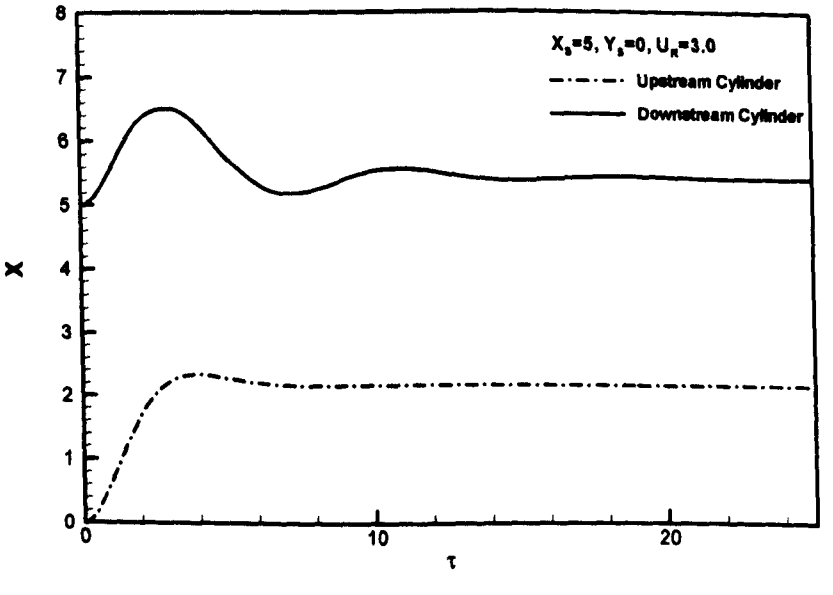

Figure 5.2(a) Streamwise direction displacement.

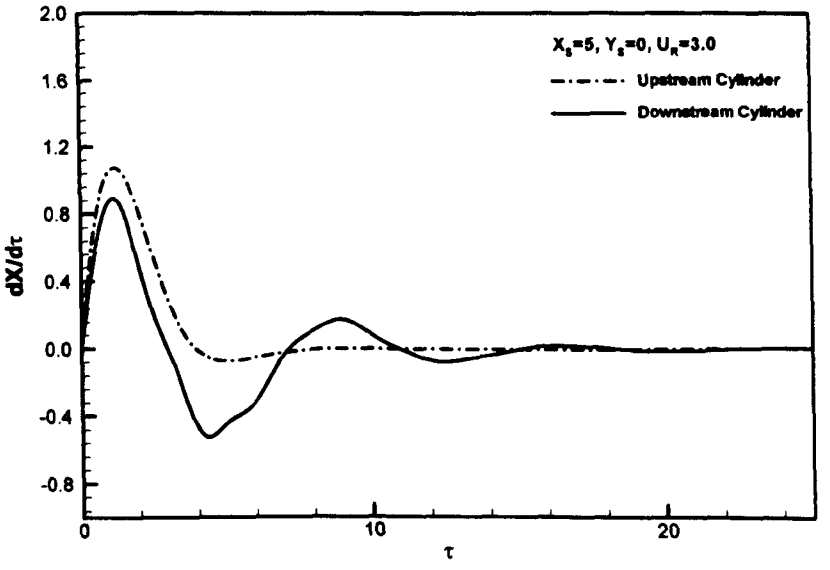

Figure 5.2(b) Streamwise direction velocity.

Figure 5.2 The transition from initial arrangement to equilibrium, a=0.2, U_R=3.0. Initially, the upstream cylinder is located at (0,0) and the downstream cylinder at (5,0). The corresponding critical flow velocity for this layout is U_R=3.48.

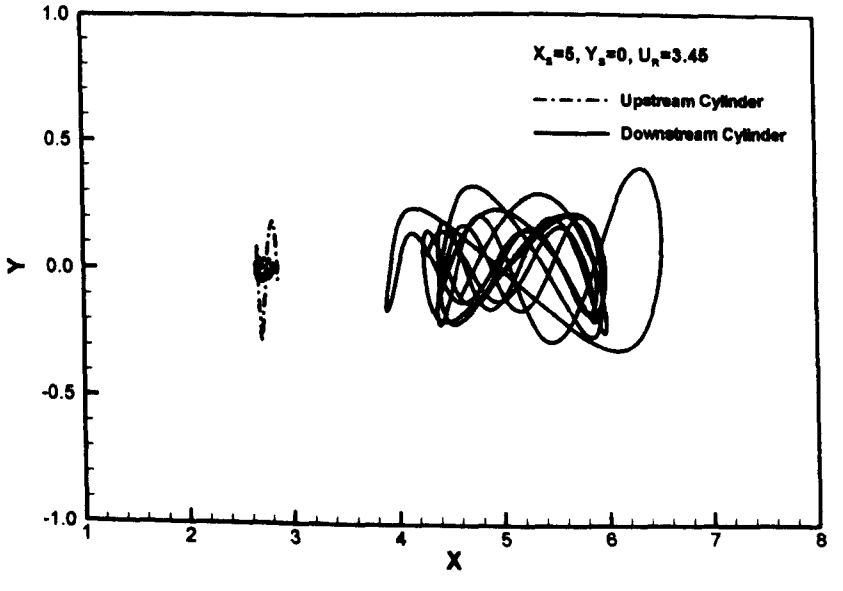

Figure 5.3(a) Trajectory.

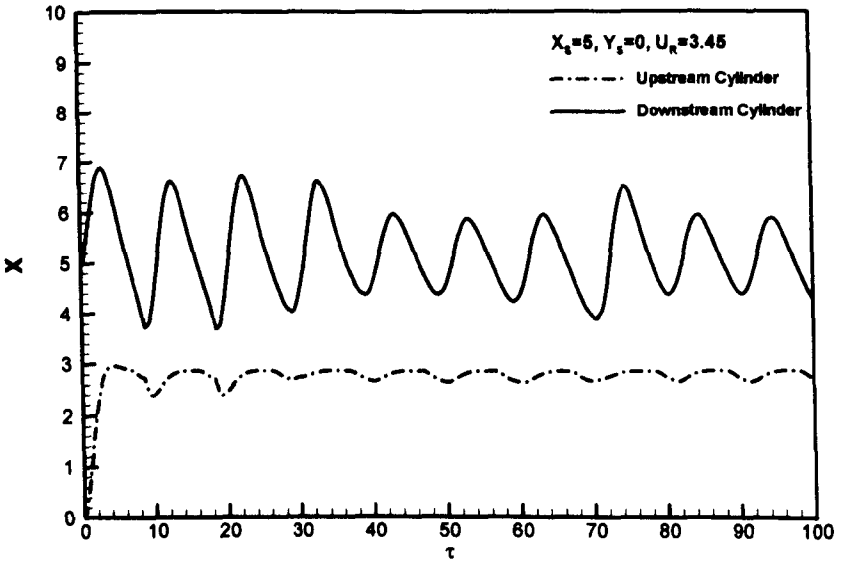

Figure 5.3(b) Streamwise direction displacement.

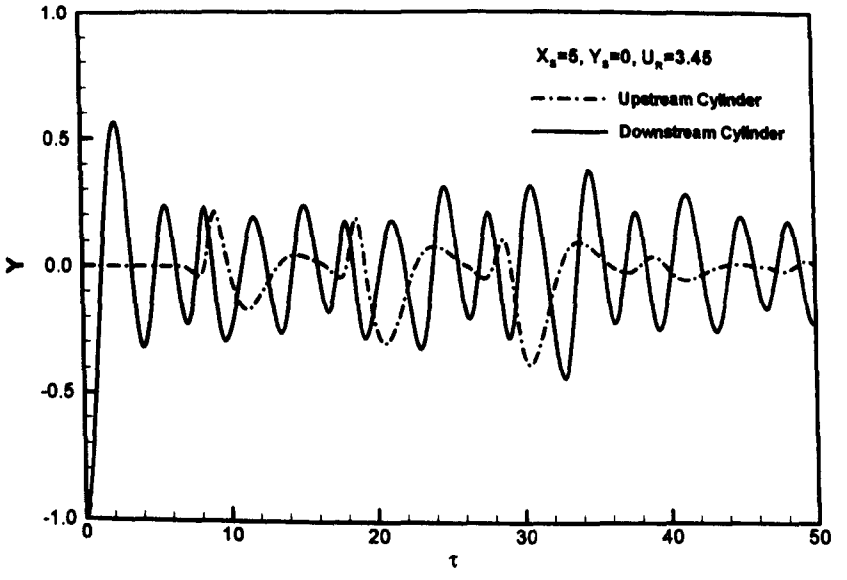

Figure 5.3(c) Cross-flow direction displacement

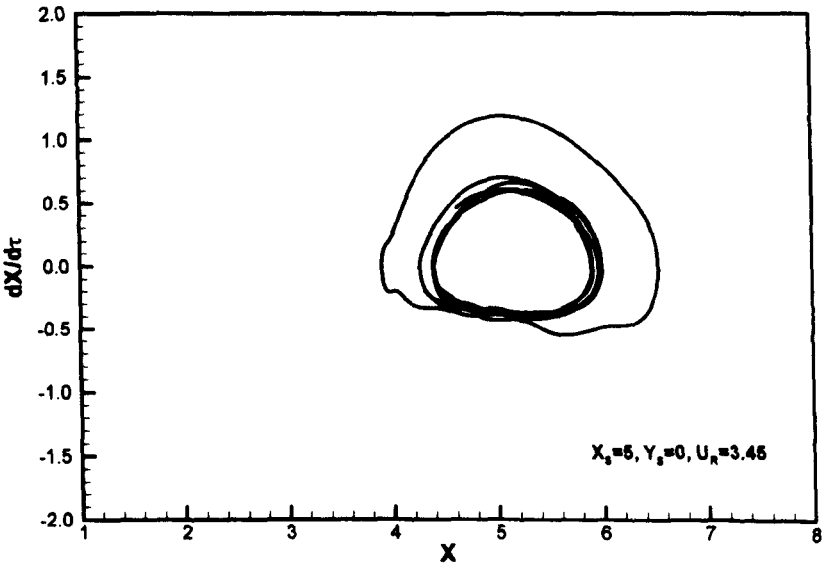

Figure 5.3(d) Phase diagram for streamwise direction motion

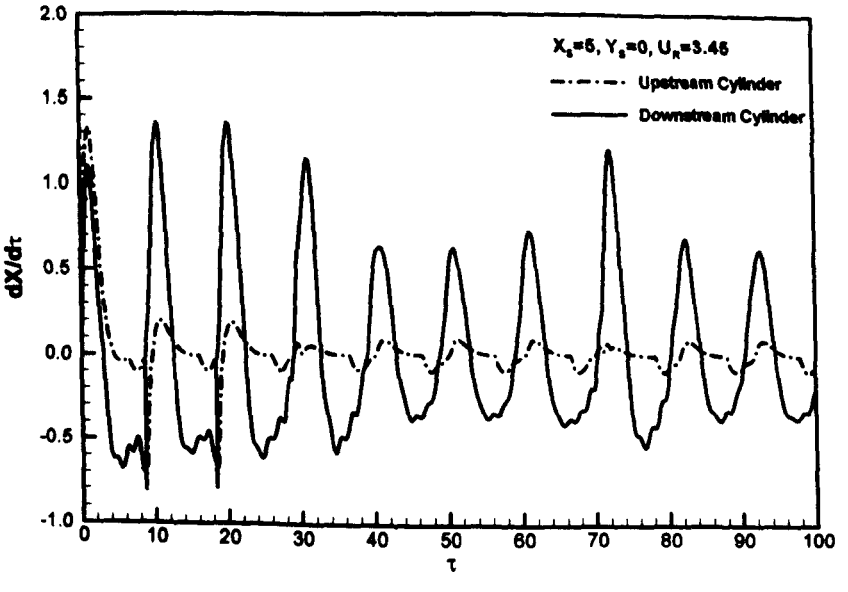

Figure 5.3(e) Streamwise direction velocity.

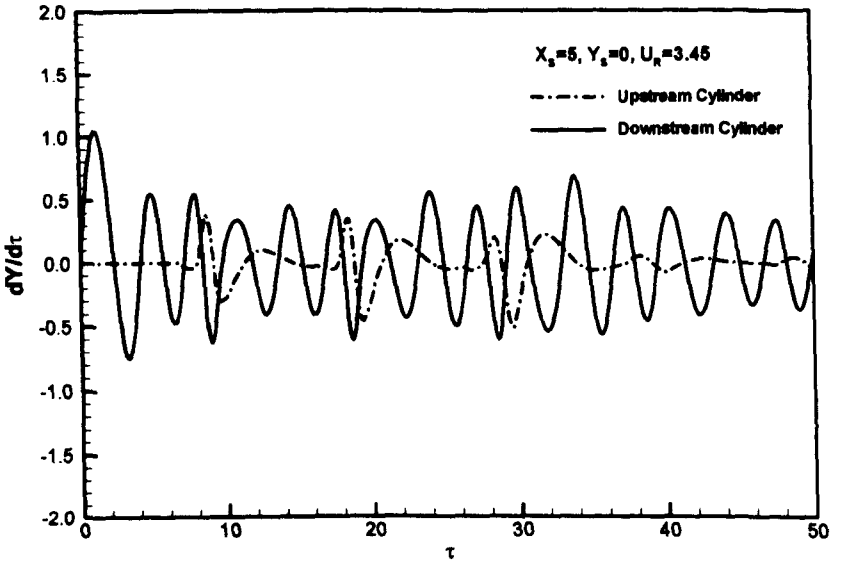

Figure 5.3(f) Cross-flow direction velocity.

Figure 5.3 The motion of downstream cylinder after Hopf bifurcation and, the flow velocity is below the critical flow velocity, a=0.2, U_R=3.45 .

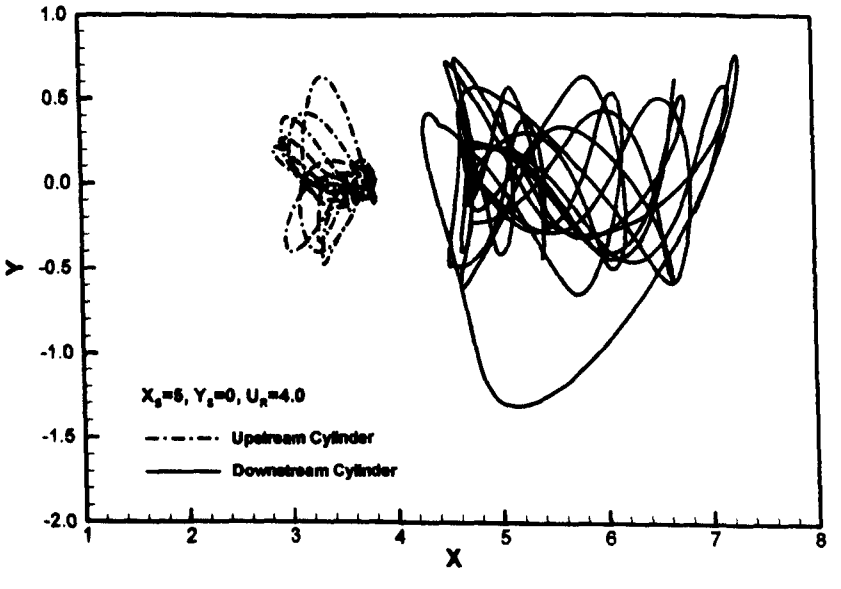

Figure 5.4(a) Trajectory.

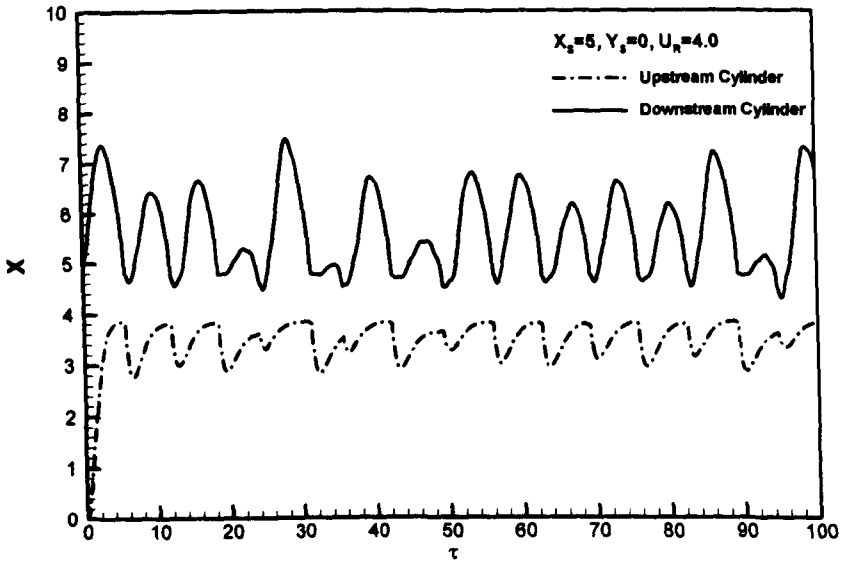

Figure 5.4(b) Streamwise direction displacement.

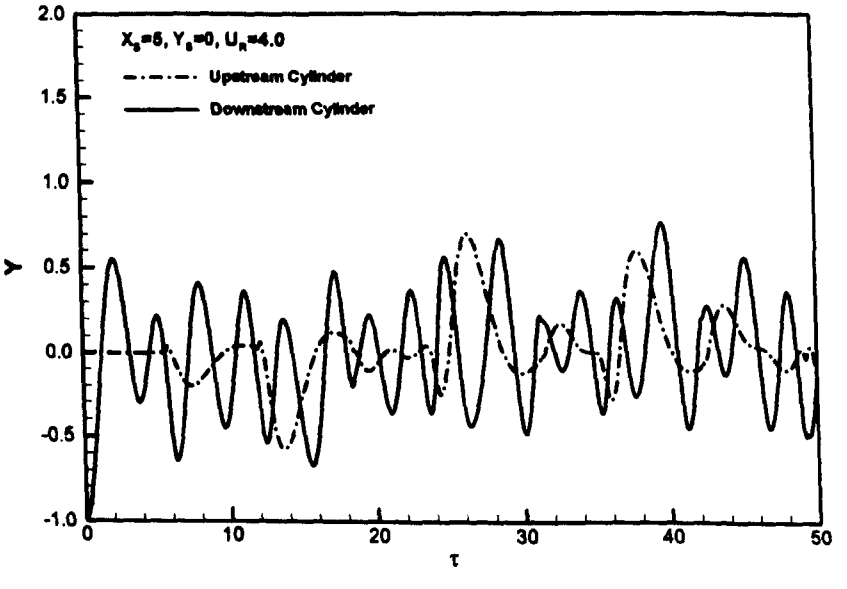

Figure 5.4(c) Cross-flow direction displacement

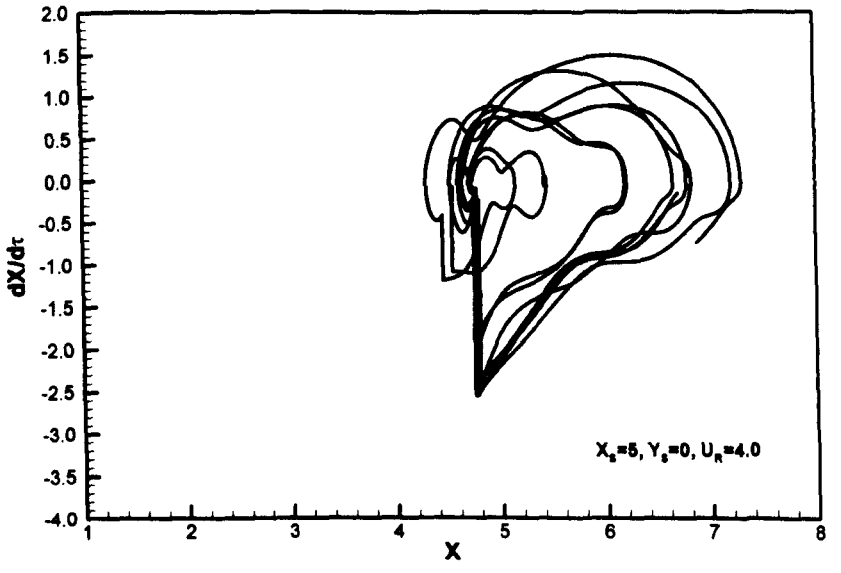

Figure 5.4(d) Streamwise direction motion phase diagram

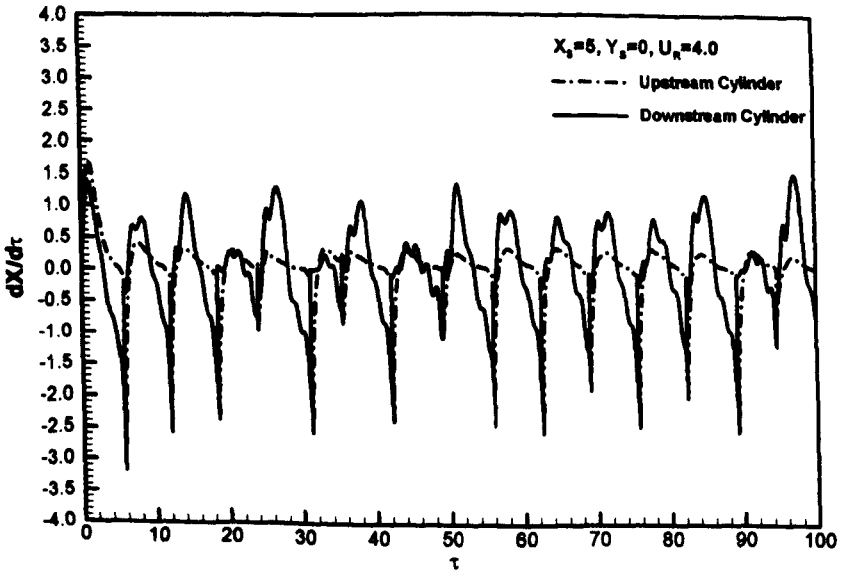

Figure 5.4(e) Streamwise direction motion velocity.

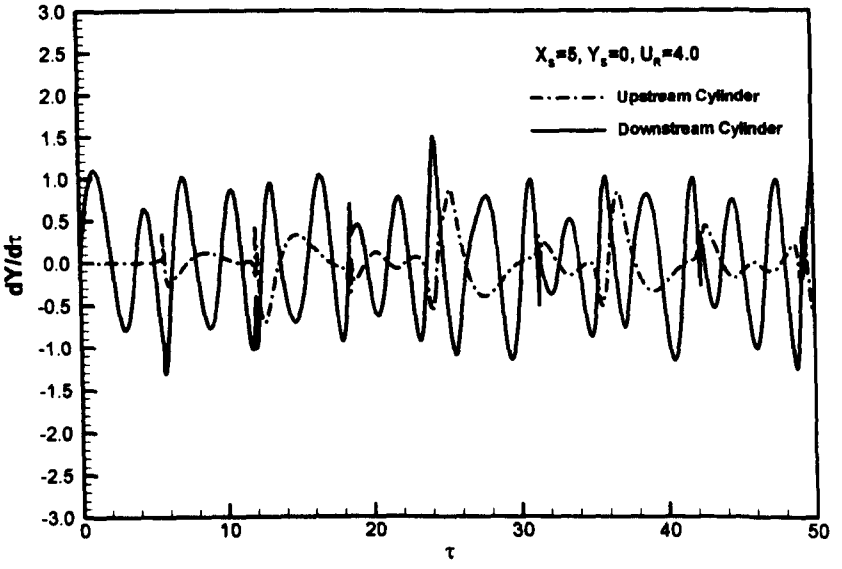

Figure 5.4(f) Cross-flow direction velocity.

Figure 5.4 A case for a=0.2, U_R=4.0 which has exceeded the critical flow velocity.

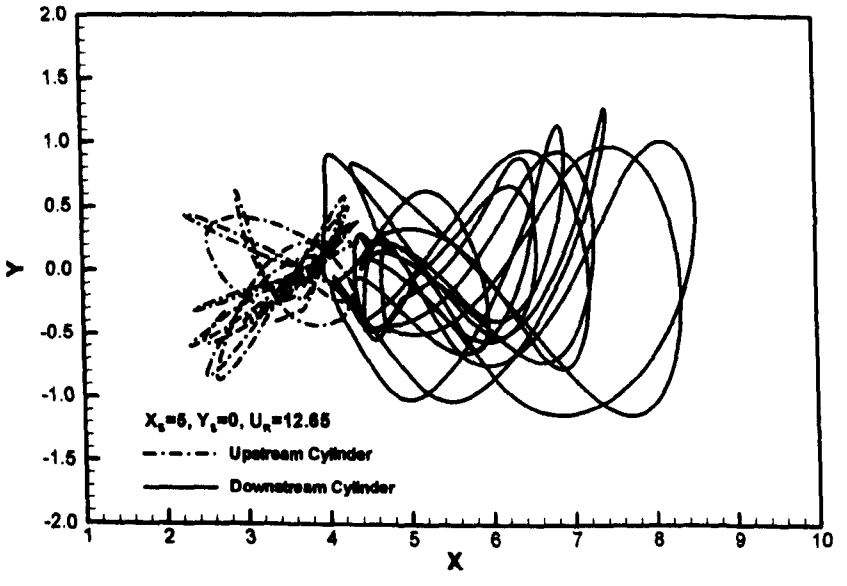

Figure 5.5(a) Trajectory.

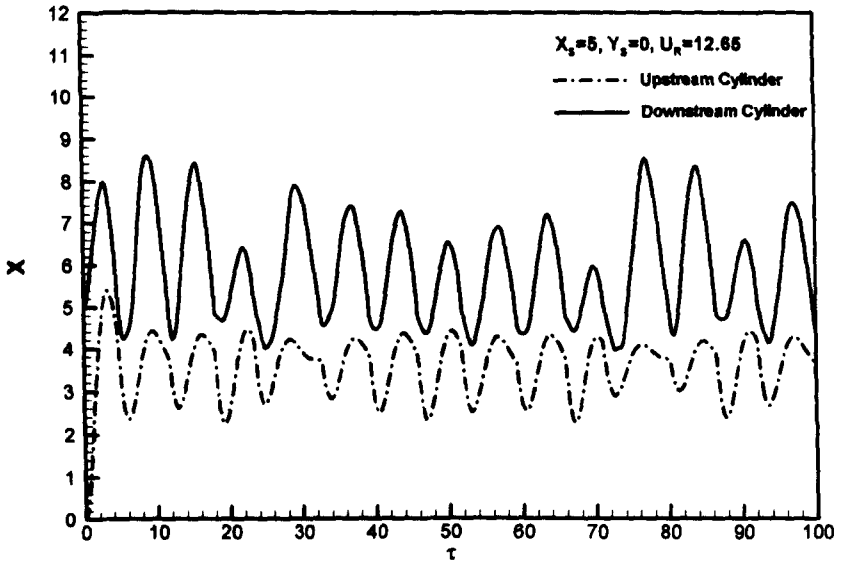

Figure 5.5(b) Streamwise direction displacement.

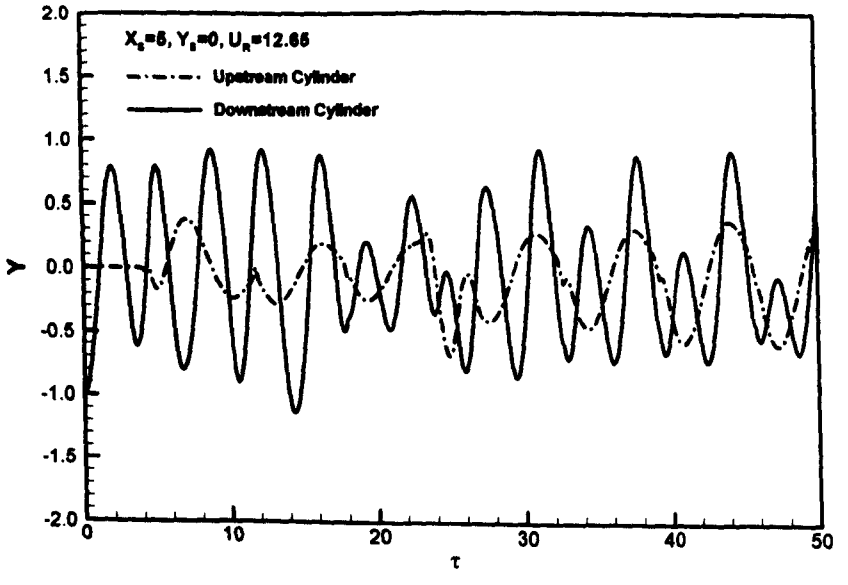

Figure 5.5(c) Cross-flow direction displacement

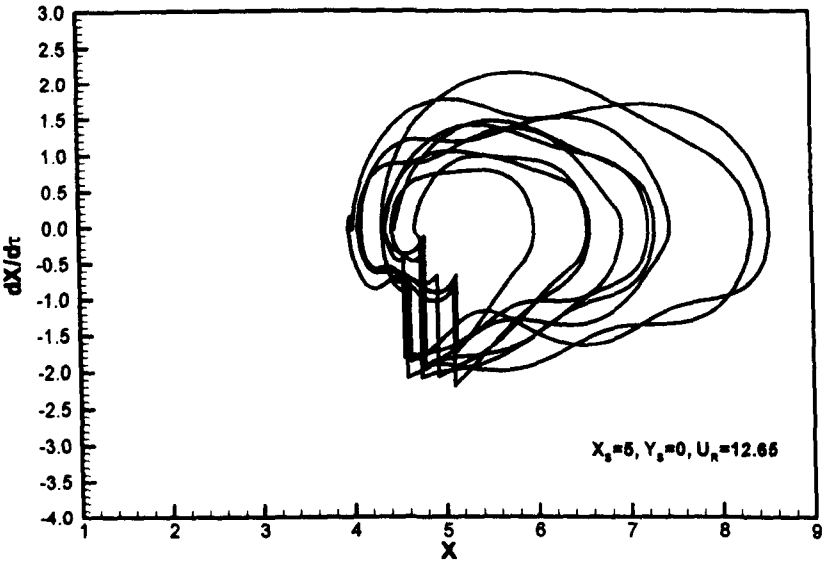

Figure 5.5(d) Streamwise direction motion phase diagram

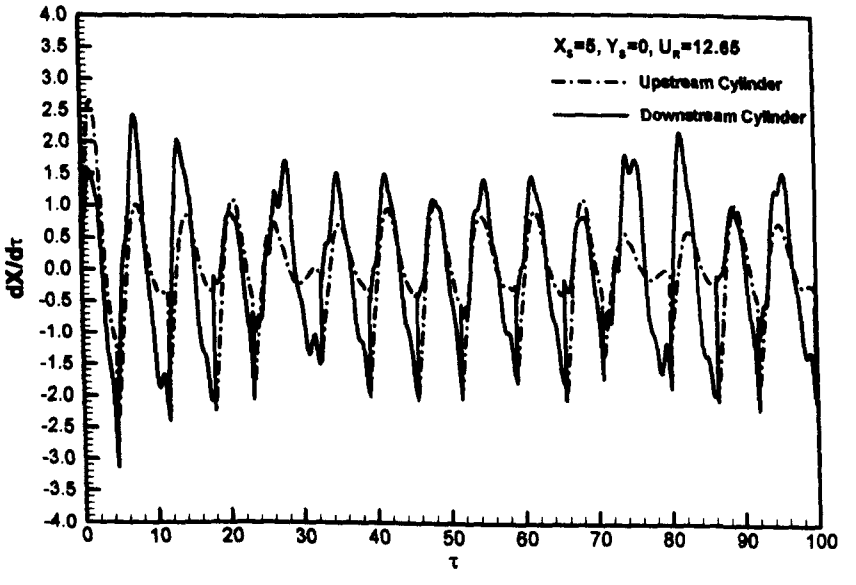

Figure 5.5(e) Streamwise direction velocity.

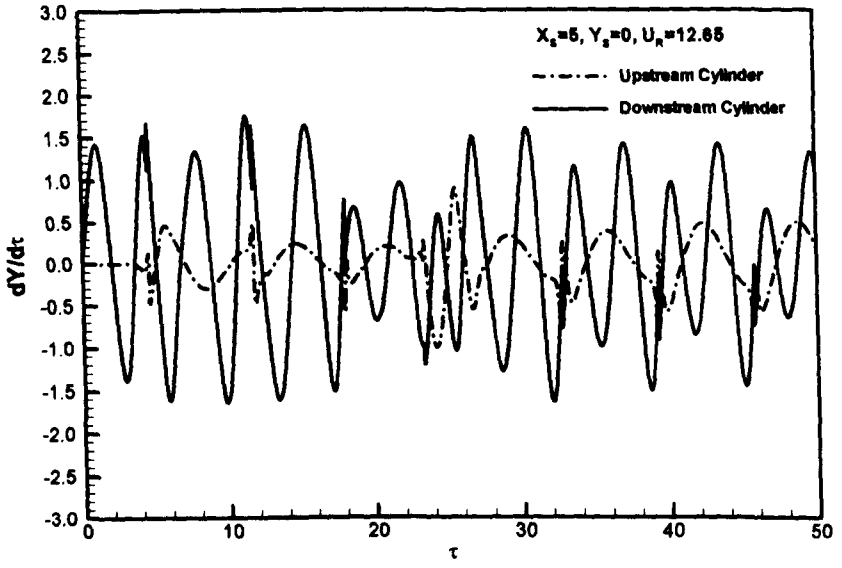

Figure 5.5(f) Cross-flow direction velocity.

Figure 5.5 A case for a=0.02, U_R=12.65, the flow velocity has exceeded the critical flow velocity.

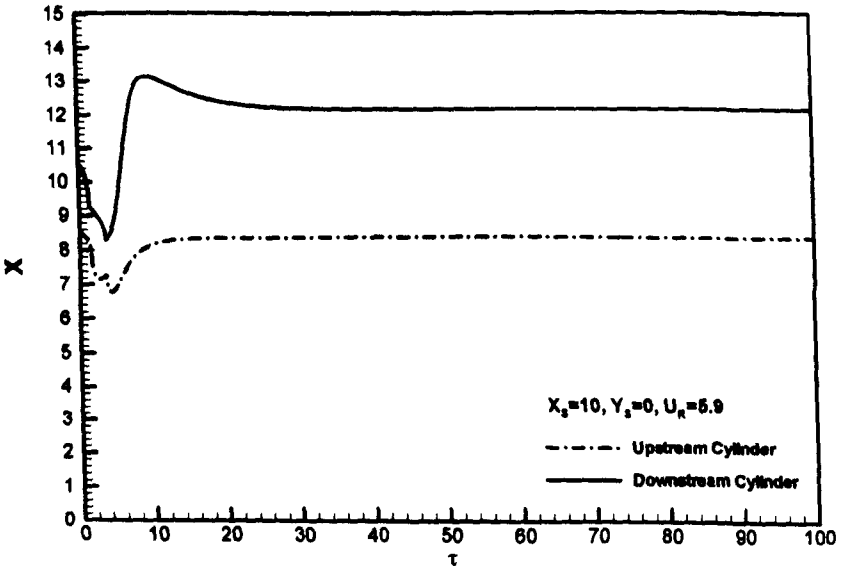

Figure 5.6 Transition from equilibrium immediately before critical flow velocity, with initial arrangement of (8.5,0), (10.5,0).

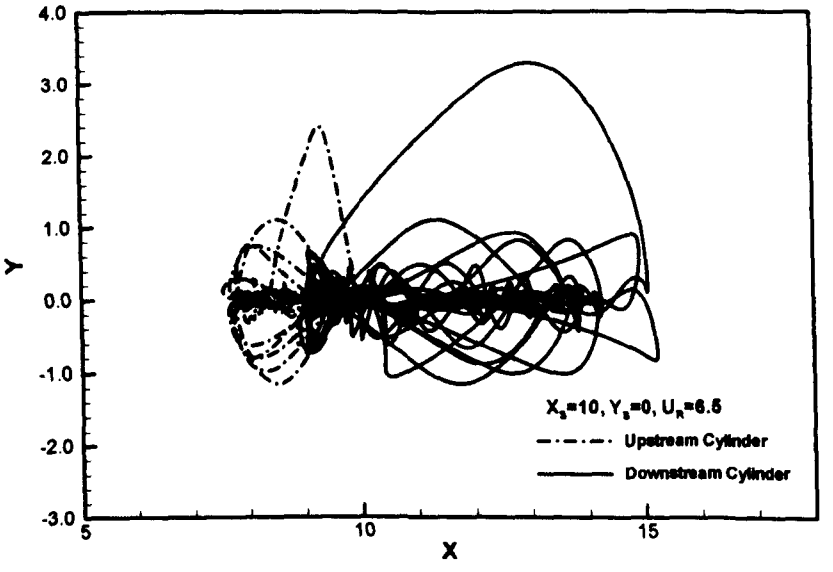

Figure 5.7(a) Trajectory for (10,0).

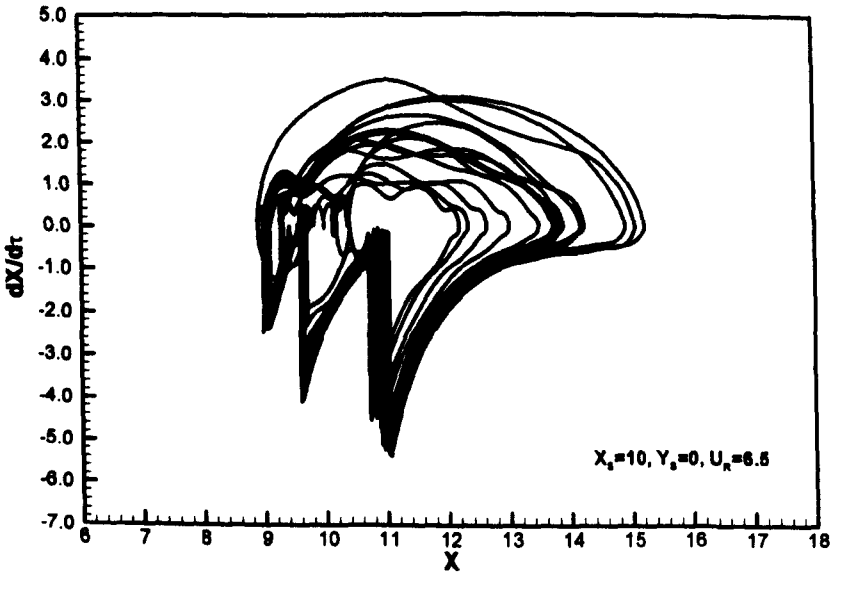

Figure 5.7(b) Streamwise direction motion phase diagram.

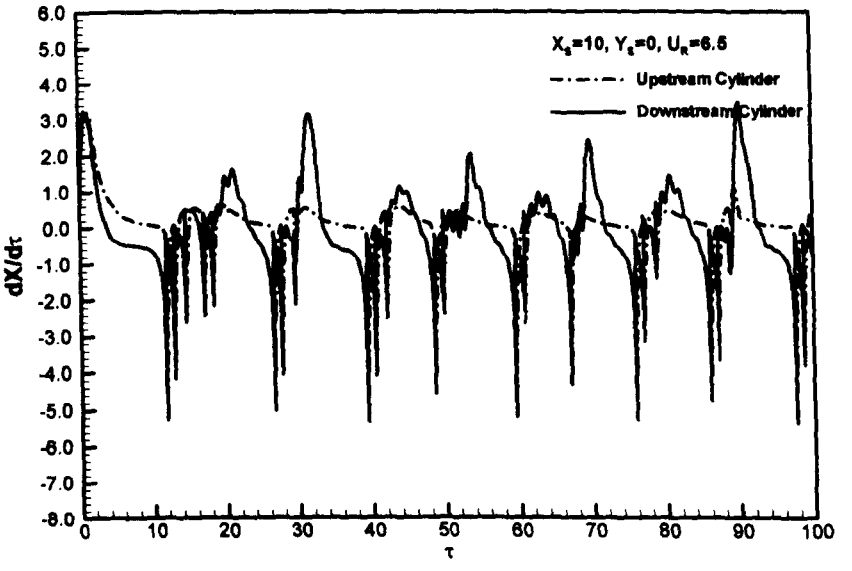

Figure 5.7(c) Streamwise direction velocity.

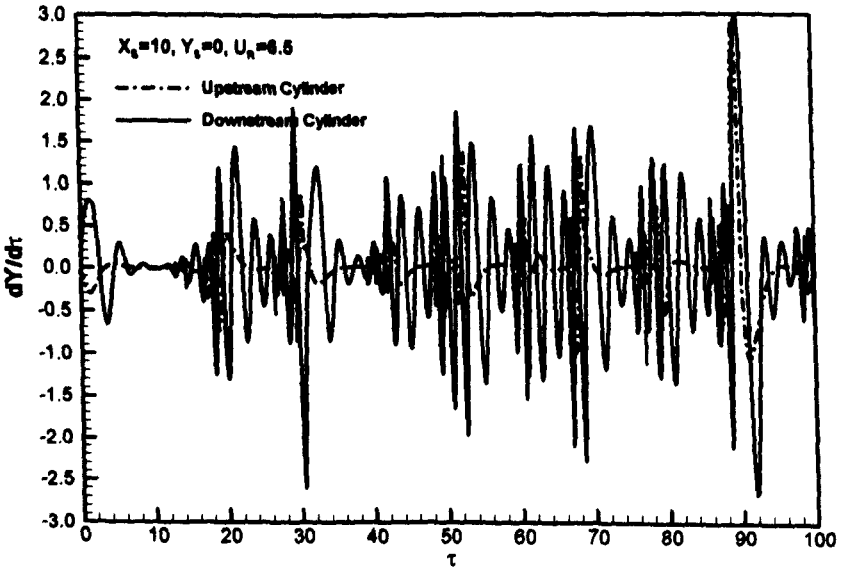

Figure 5.7(d) Motion trajectory.

Figure 5.7 A case after flow velocity exceeds the critical flow velocity, a=0.2, U_R=6.5, the corresponding critical flow velocity is 5.9.

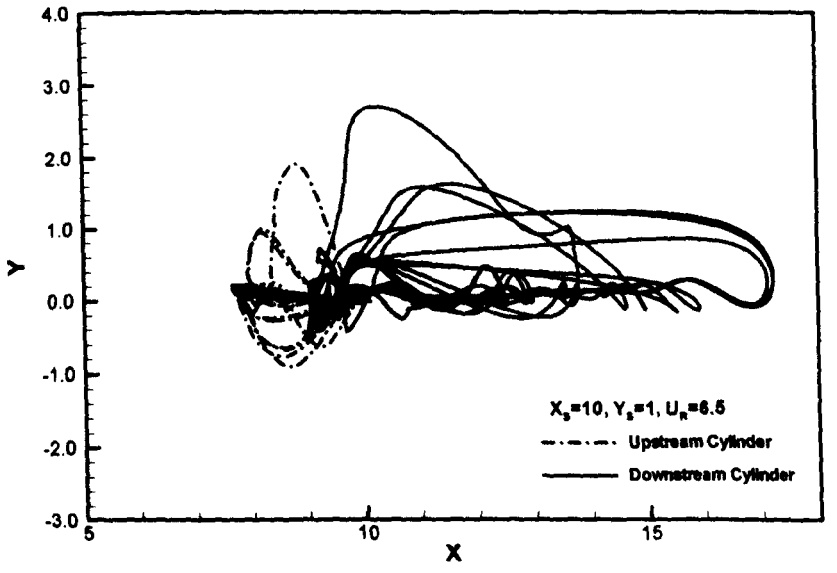

Figure 5.8(a) Trajectory.

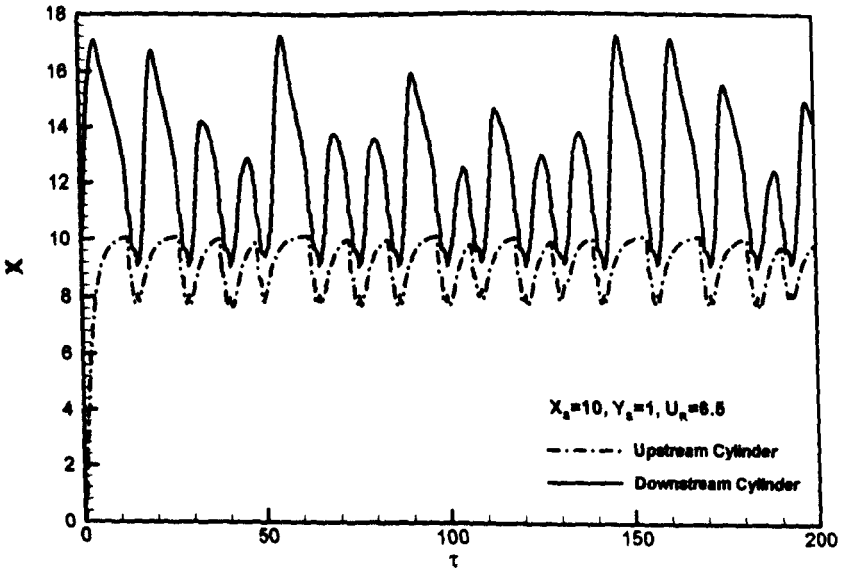

Figure 5.8(b) Streamwise direction displacement.

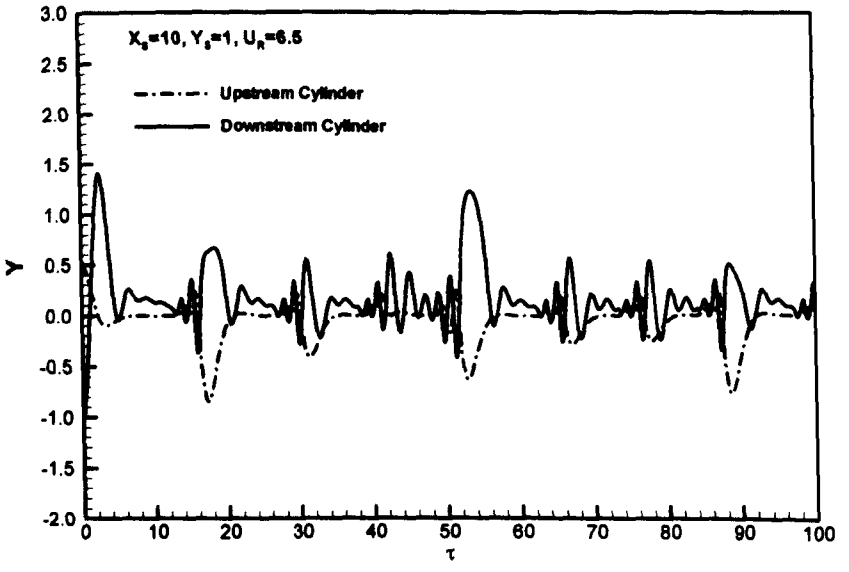

Figure 5.8(c) Cross-flow direction displacement.

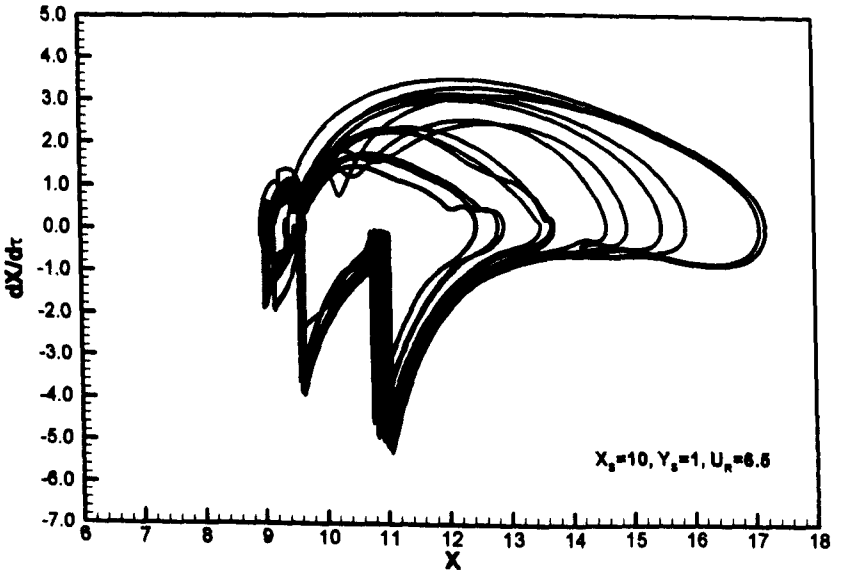

Figure 5.8(d) Streamwise direction motion phase diagram.

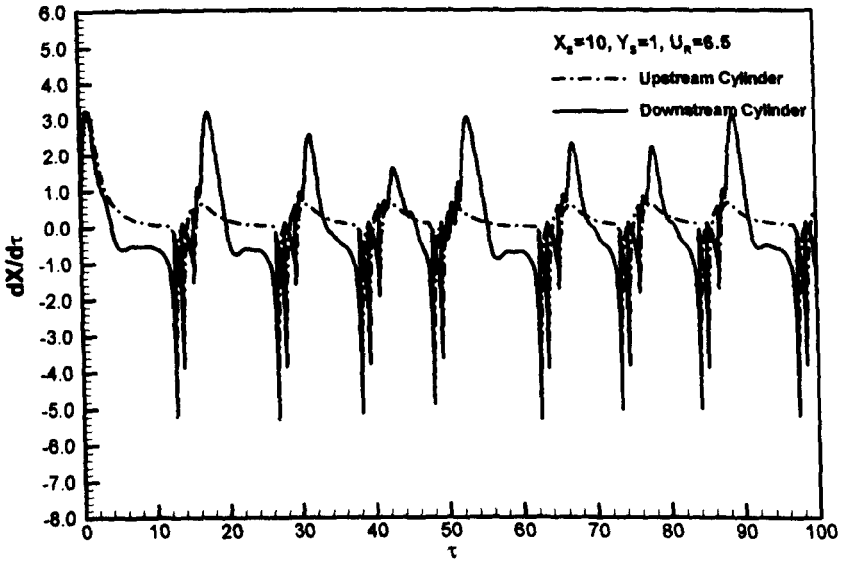

Figure 5.8(e) Streamwise direction velocity.

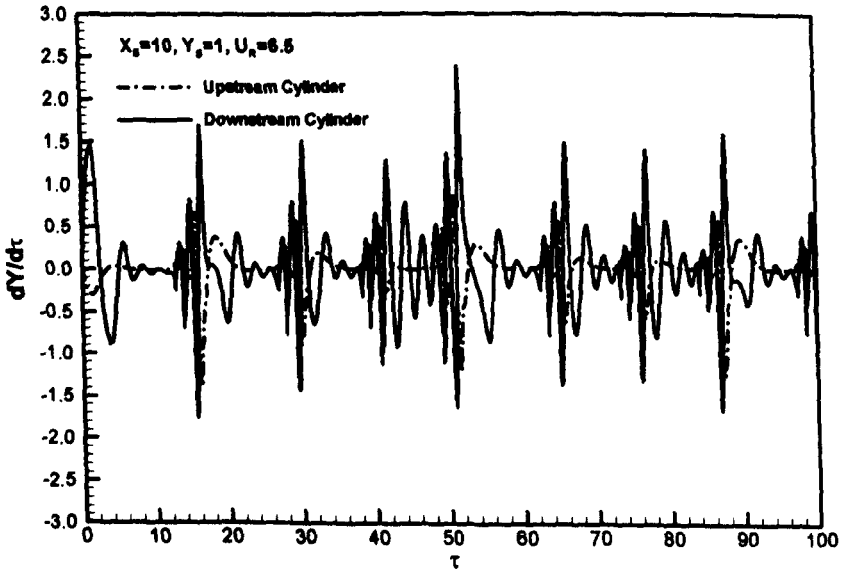

Figure 5.8(f) Cross-flow direction velocity.

Figure 5.8 A case at off-wake centreline, after the critical flow velocity.

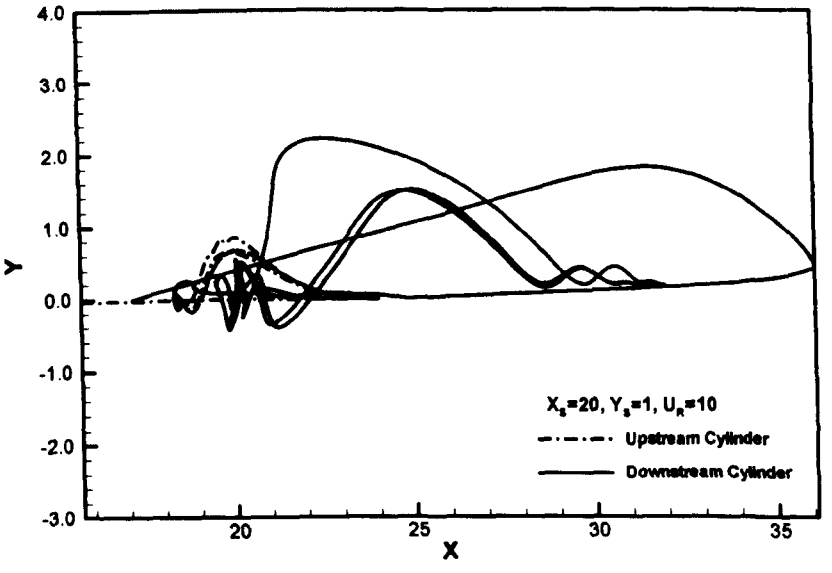

Figure 5.9 Trajectory; a case at off wake centreline and after the critical flow velocity.

5.4.2 *Outer Wake*

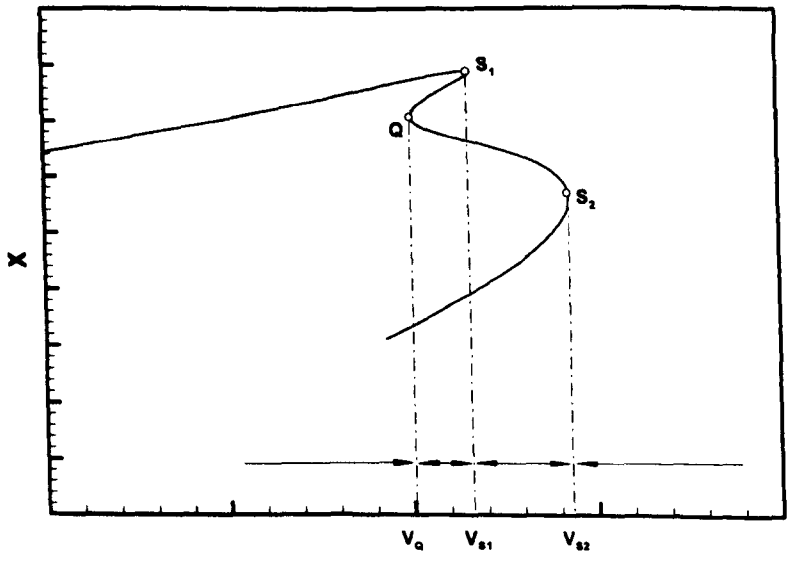

Figure 5.10 Schematic diagram about equilibrium states.

When the downstream cylinder is initially arranged at the outer wake, there can be up to four equilibrium states under certain flow velocities. Figure 5.10 is a schematic diagram of

the possible equilibrium states at different flow velocities. Labels S_1 and S_2 represent the first and second convergence points of the equilibrium pairs. Not shown in the figure is that, as well as S_1 being the converging point of the downstream pair, it can also be the convergence point of the upstream pair as well. S_2 is the critical point of the system. Discussion of the dynamics for such an arrangement according to different flow velocity ranges follows.

5.4.2.1 Low Flow Velocity ($V_0<V_Q$)

When the flow velocity is smaller than V_Q, the downstream cylinder will approach its only stable equilibrium state, irrespective of the initial relative positions of the two cylinders. Although there are two equilibrium states when the flow velocity is close to V_Q, the other equilibrium, which is located near the upstream cylinder, is unstable. When the initial position of the downstream cylinder is located near the unstable equilibrium point, it only exhibits temporary movement around the equilibrium and will transit to the stable equilibrium eventually. The final state will rest at the stable downstream equilibrium position. This process is identical to the transition for two cylinders arranged in tandem or the case when the downstream cylinder is located at the inner wake position. Figure 5.11 is a case for $X_S=5$, $Y_S=2$ at $U_R=3.0$. Initially the two cylinders are placed at their layout position. It is then seen that the two cylinders are pushed at almost the same speed towards their equilibrium. The whole course of transition only lasts one natural period time interval.

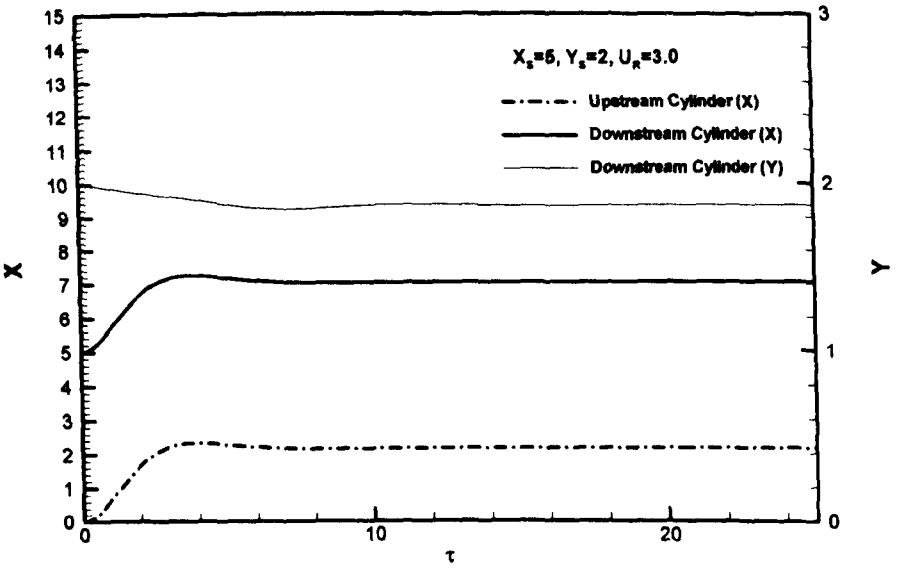

Figure 5.11(a) Displacement.

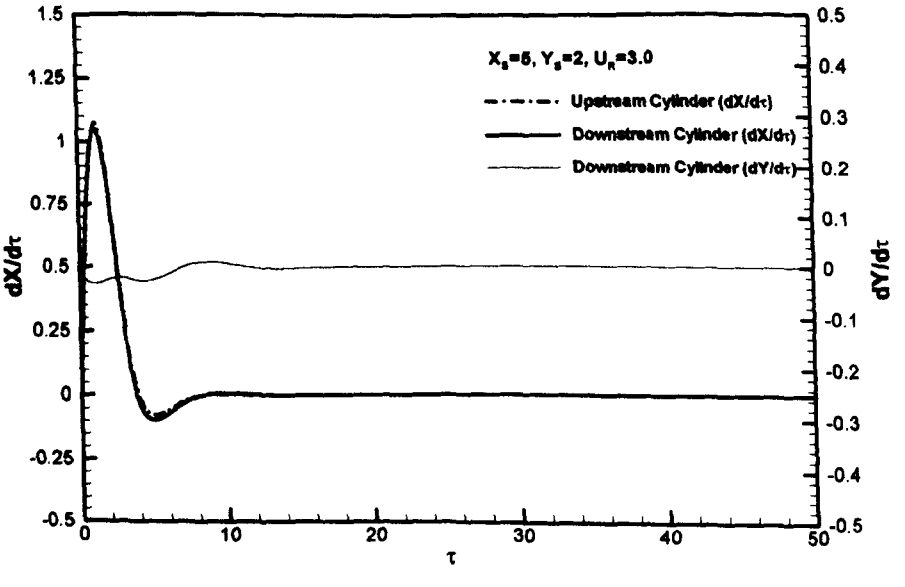

Figure 5.11(b) Transition motion velocity.

Figure 5.11 Transition from initial layout position to its equilibrium at low flow velocity

5.4.2.2 Velocity $V_Q < V_0 < V_{S1}$

When the flow velocity is between the point Q and the first merger point of the equilibrium pair, depending on the initial spacing between two cylinders and the initial disturbance on the two cylinders, the downstream cylinder can exhibit different dynamic behaviour. When the spacing between two cylinders is smaller than 8 diameters, the downstream cylinder can either rest at its stable equilibrium or exhibit periodic movement. Figures 5.12 and 5.13 show the case for the initial arrangement of X_S=5, Y_S=2. It is seen that, depending on the initial locations (initial disturbance), the downstream cylinder can either rest at its stable equilibrium (Figure 5.12), or exhibit stable periodical movement (Figure 5.13). When the initial spacing between two cylinders is large enough, the downstream cylinder will rest at its corresponding equilibrium state, due to the coexistence of two stable equilibrium points. The final balanced position is dependent on its initial location. Figure 5.14 is a map showing the corresponding attraction domains for the different equilibrium points for X_S=10, Y_S=2.5 at U_R=5.8. Initially, the upstream cylinder is located at its corresponding equilibrium. The line shown in the figure demarcates the ultimate position the downstream cylinder will go to. When the downstream cylinder is initially located above the demarcation line, the cylinder will eventually rest at the upper stable equilibrium shown in the figure. Otherwise, the cylinder will rest at the stable lower equilibrium state. The demarcation line represents the attraction for the unstable equilibrium located on that line.

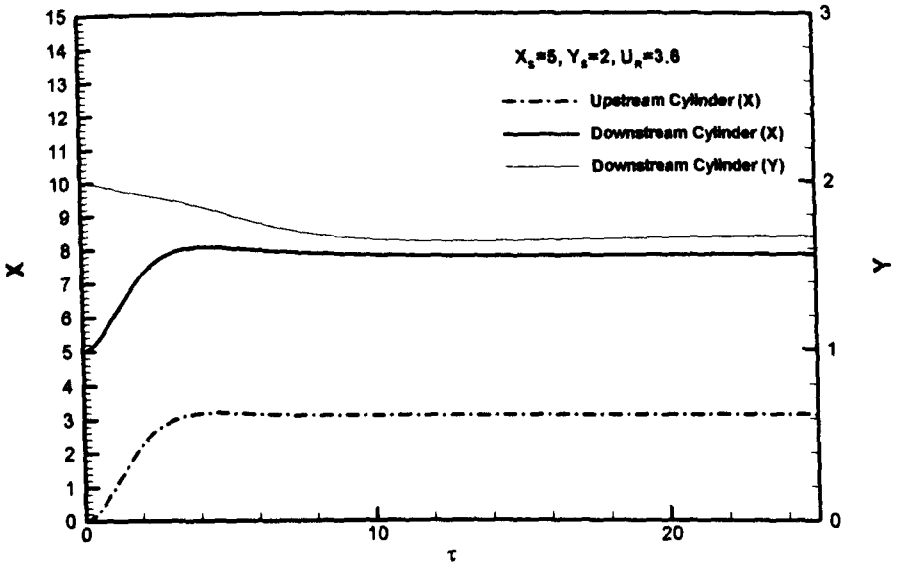

Figure 5.12(a) Displacement.

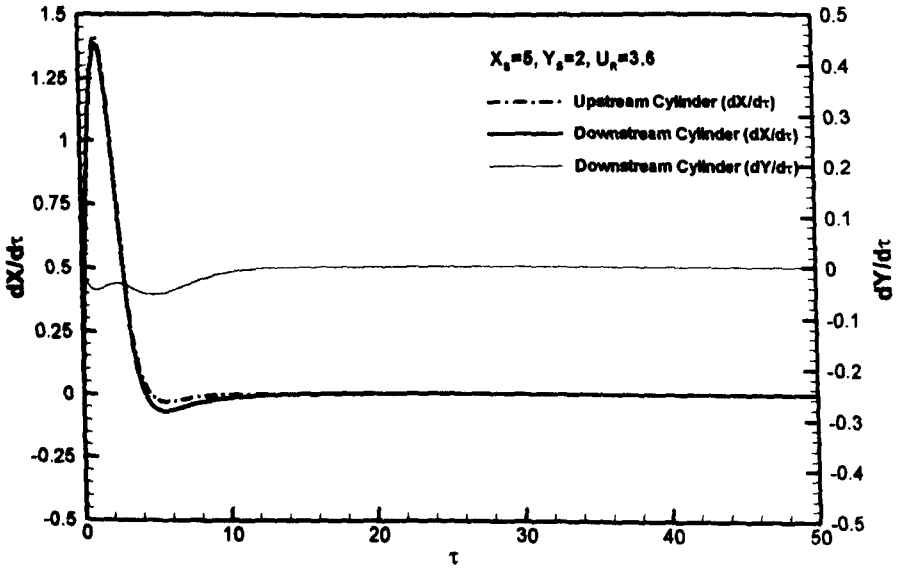

Figure 5.12(b) Velocity; one possible route for the cylinder pair when initially two cylinders are located at (0,0) and (5,2) with flow velocity of U_R=3.6 .

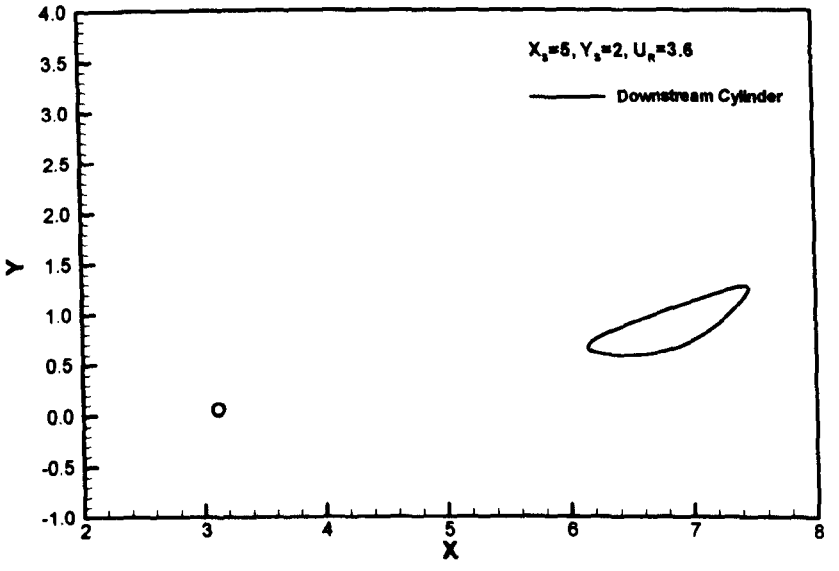

Figure 5.13(a) Trajectory.

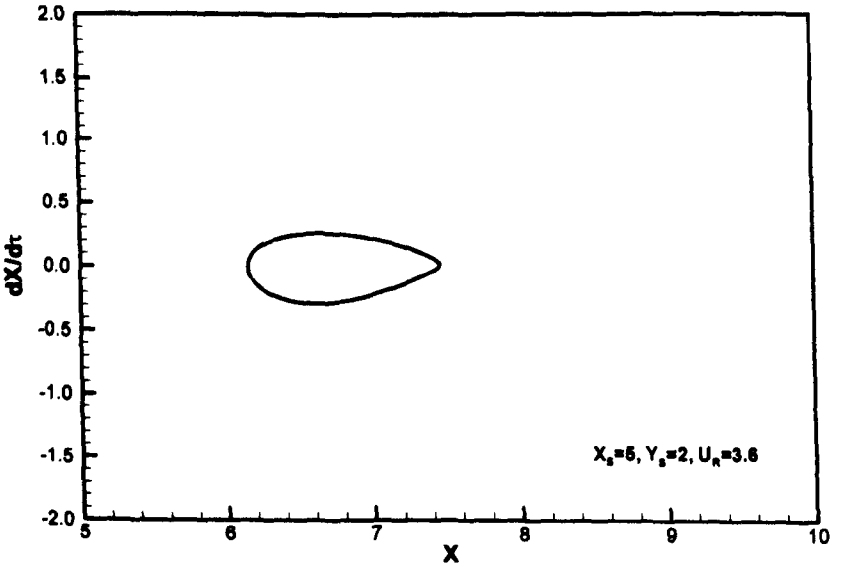

Figure 5.13(b) Streamwise direction movement phase diagram; one possible route for the cylinder pair when initially two cylinders are located at (3,0) and (8,0) with flow velocity of U_R=3.6 .

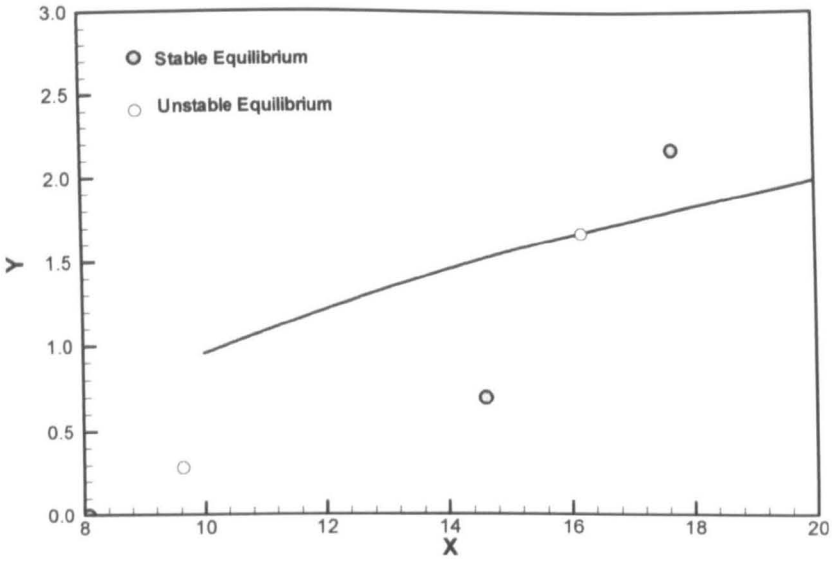

Figure 5.14 Attraction domain between equilibrium sates for initial upstream cylinder located at (8.07,0).

5.4.2.3 $V_{S1}<V_0<V_{S2}$

When the flow velocity is larger than the first merger point and smaller than the critical flow velocity, the downstream cylinder is either to be attracted to its equilibrium position or it starts to move around, depending on the initial spacing between the two cylinders. When the initial spacing between the two cylinders is larger than 8 diameters, the downstream cylinder is likely to transit to its equilibrium, in the same process as the two tandem arranged cylinders. When the initial spacing is smaller than 8 diameters, as shown in Figures 5.15 and 5.16, the downstream cylinder tends to oscillate around its unstable equilibrium. If the velocity is larger enough, as shown in Figure 5.16, such an oscillation can bring two cylinders to collide with each other.

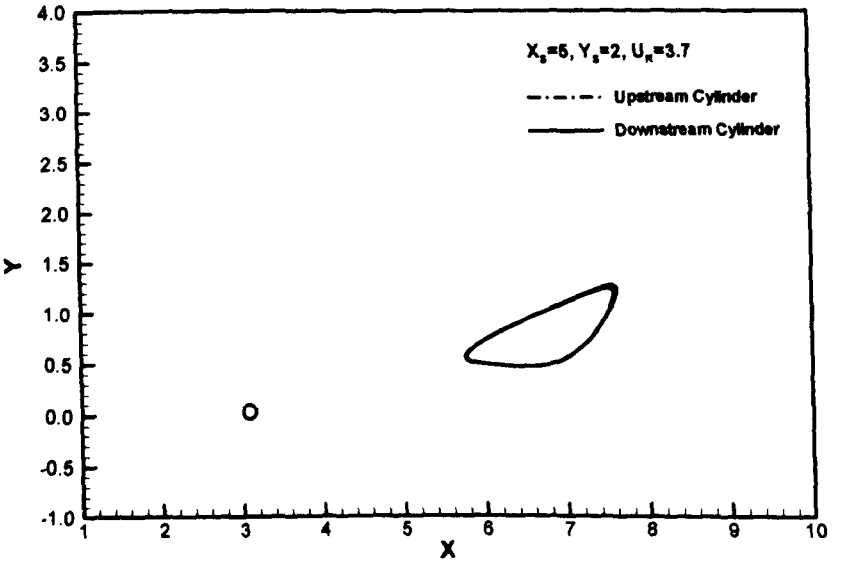

Figure 5.15(a) Trajectory.

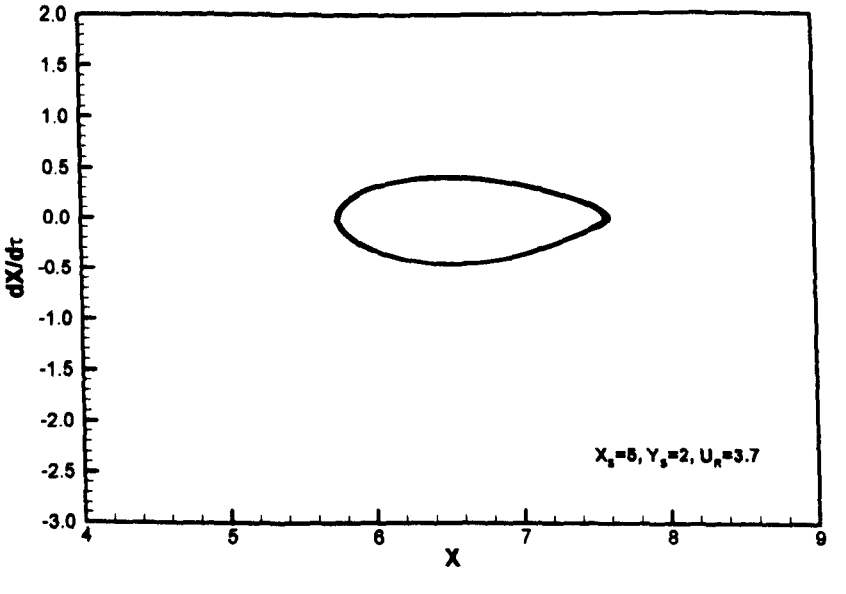

Figure 5.15(b) Streamwise motion phase diagram.

Figure 5.15 A case when the movement of the downstream cylinder is not enough to bring the two cylinders to collide with each other.

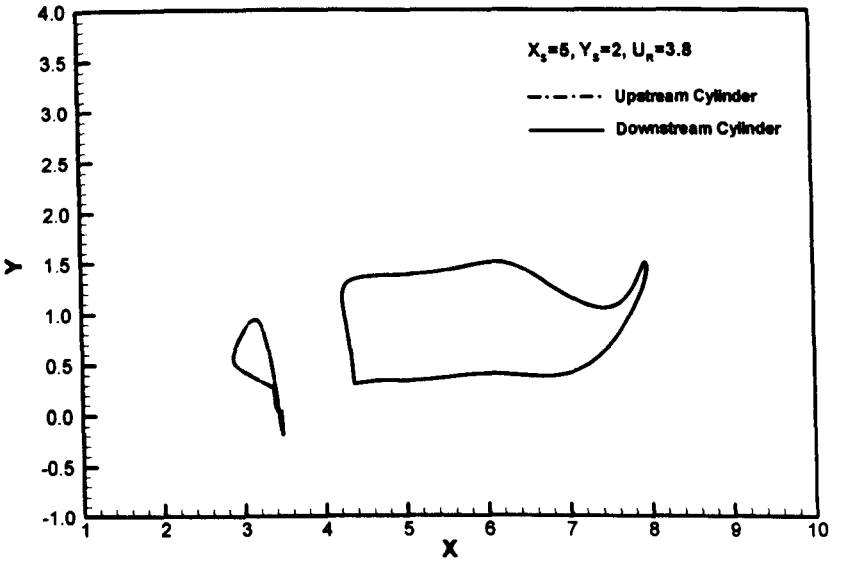

Figure 5.16(a) Trajectory.

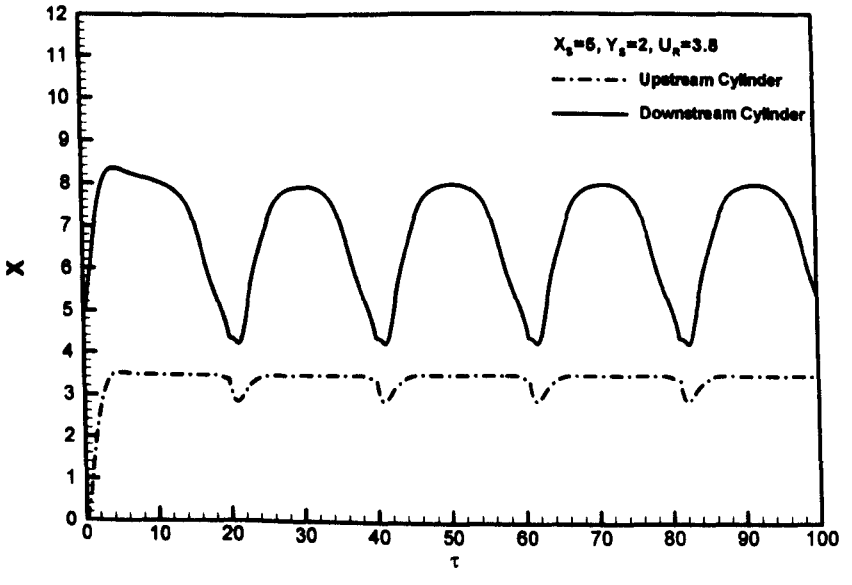

Figure 5.16(b) Streamwise direction displacement.

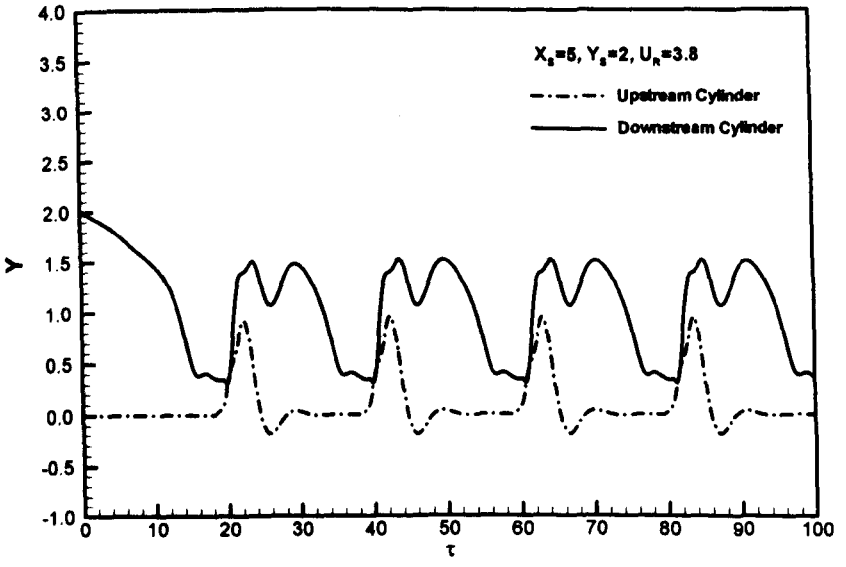

Figure 5.16(c) Cross-flow direction displacement.

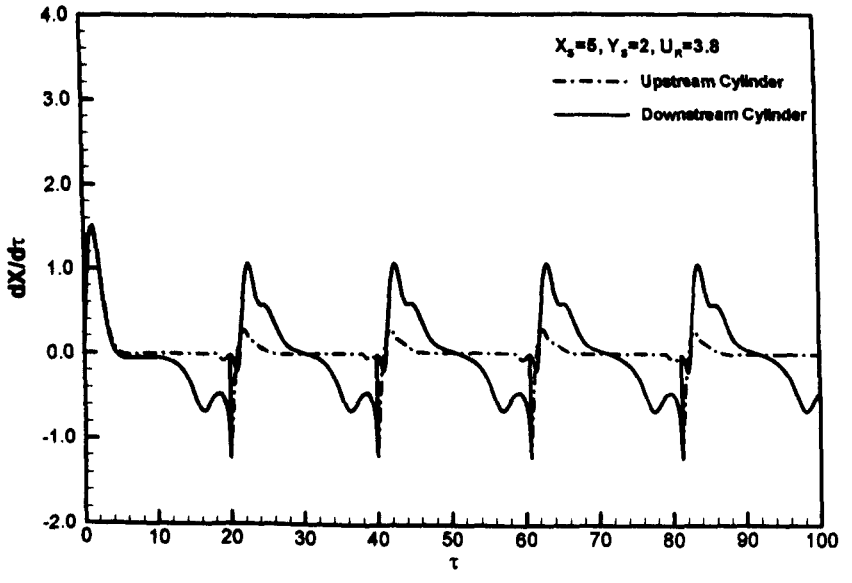

Figure 5.16(d) Streamwise direction velocity.

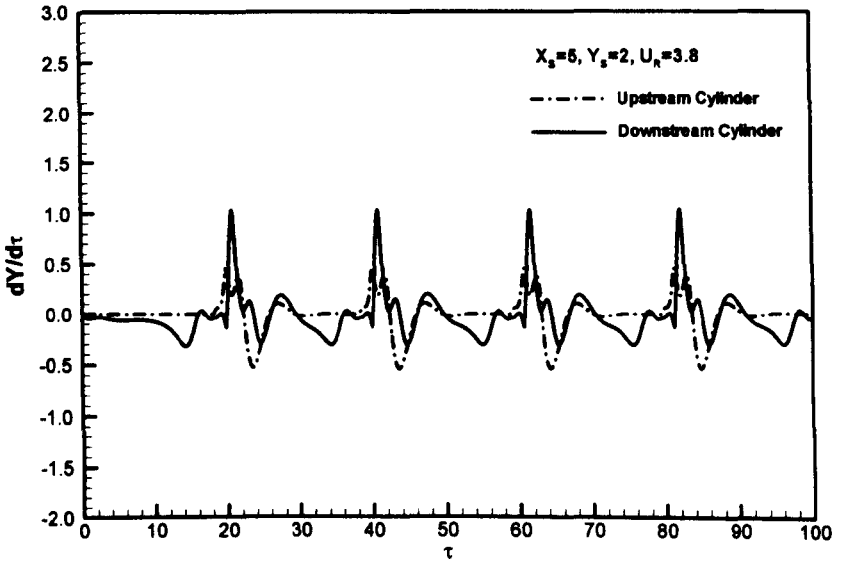

Figure 5.16(e) Cross-flow direction velocity.

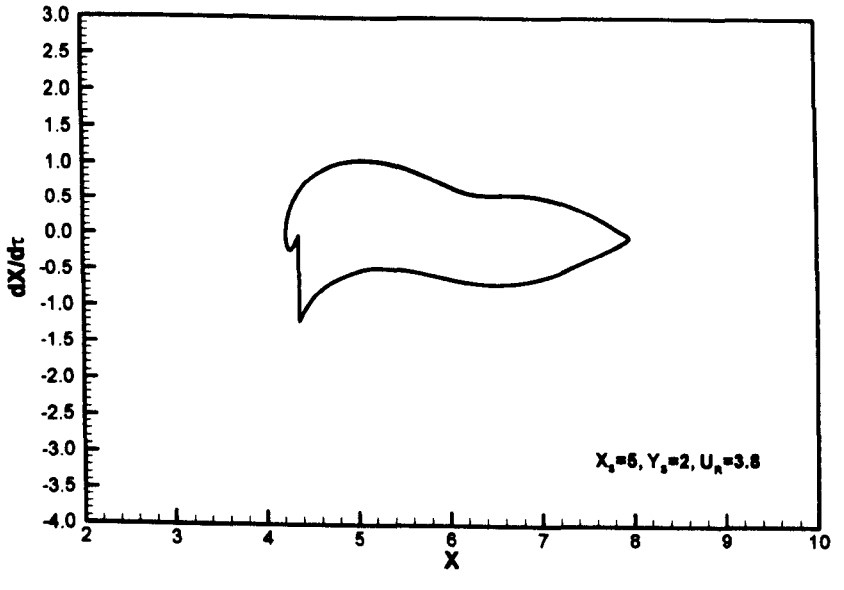

Figure 5.16(f) Streamwise direction motion phase diagram.

Figure 5.16 A case started by losing stability and the amplitude of the motion bring two cylinders to collide with each other.

5.4.2.4 Large Flow Velocity ($V_0 > V_{S2}$)

When the flow velocity exceeds the critical flow velocity, as revealed in the continuation investigation, no physical equilibrium points will exist. The downstream cylinder will wander around, regardless of the initial disturbance between the two cylinders. Figures 5.17 to 5.20 show the case with streamwise spacing varying from 5 diameters to 20 diameters.

As can be seen from these figures, when the flow velocity exceeds the critical velocity, collision between the two cylinders is expected, on an irregular basis. The amplitude of the downstream cylinder does not change significantly with the flow velocity, although the velocity immediately before the collision does significantly change. The amplitude corresponds approximately to its initial design spacing. The time interval between successive collisions is larger than the natural period of the system. Most of the time, the cylinder moves at small velocity, with the main acceleration completing within a short period immediately before the collision. In two-dimensional space, such a velocity can reach 5, which is significantly larger than the vortex induced vibration amplitude. Therefore, in the evaluation of causes of possible damage, wake induced oscillation should be considered appropriately.

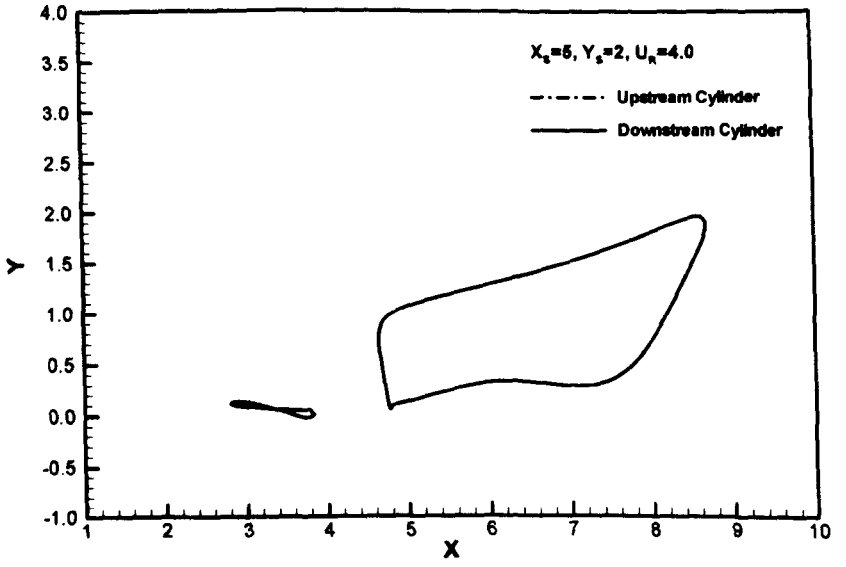

Figure 5.17(a) Trajectory.

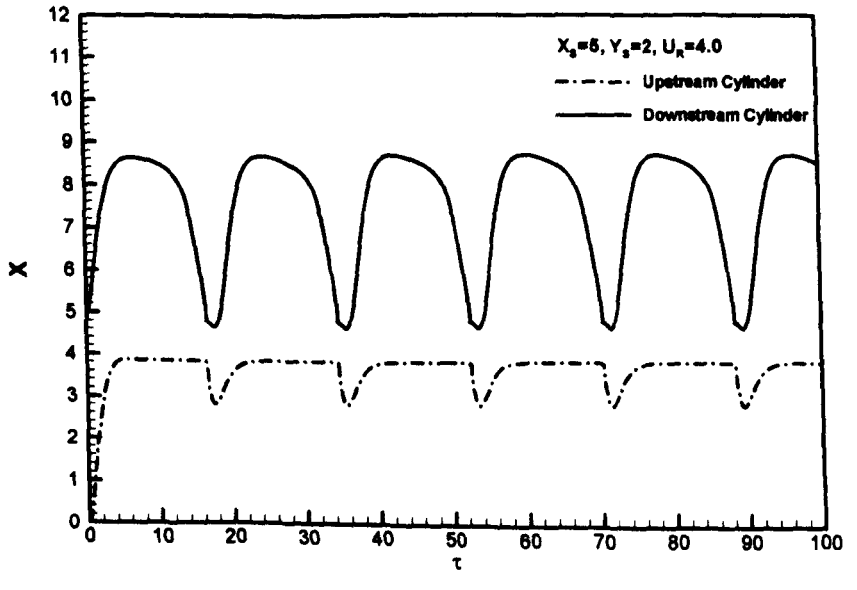

Figure 5.17(b) Streamwise direction displacement.

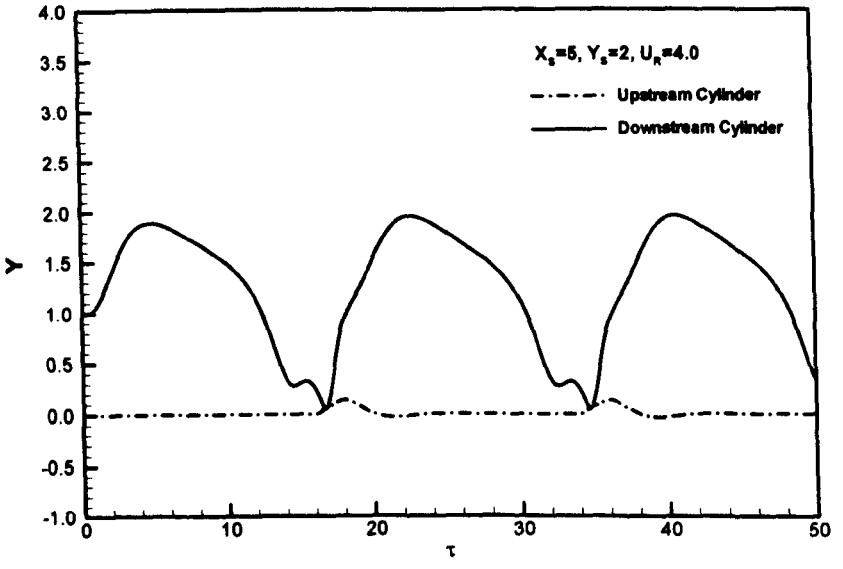

Figure 5.17(c) Cross-flow direction displacement.

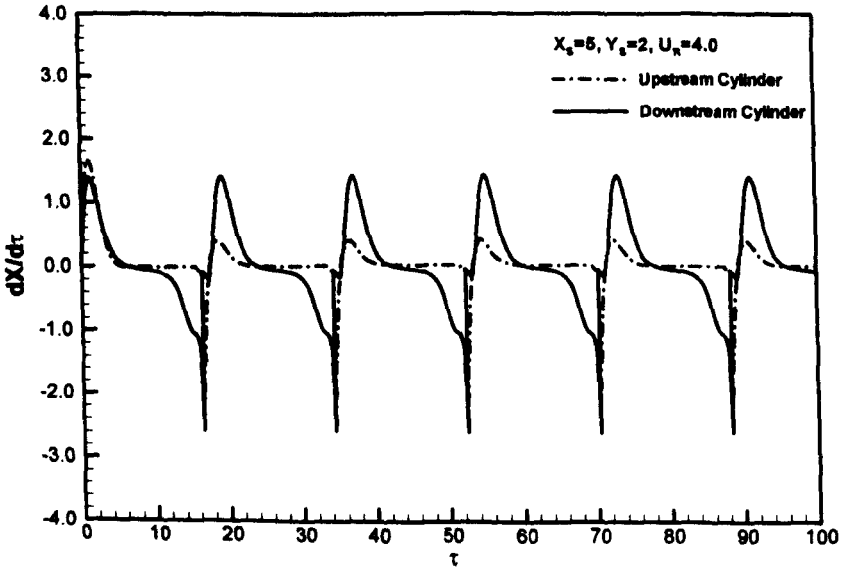

Figure 5.17(d) Streamwise direction velocity.

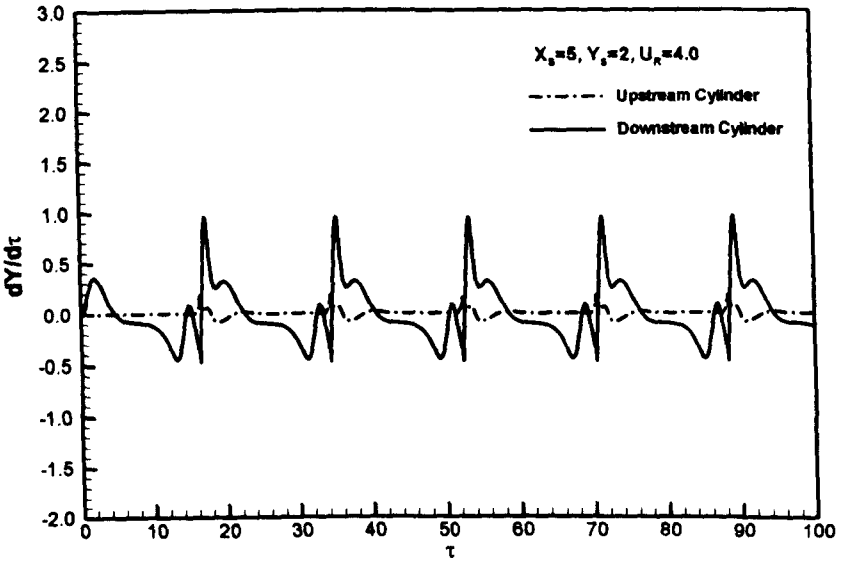

Figure 5.17(e) Cross-flow direction velocity.

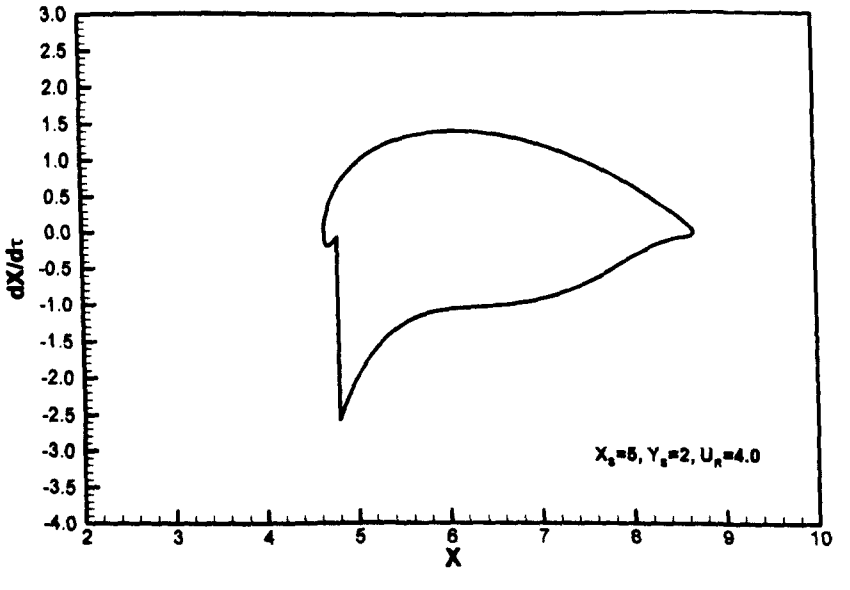

Figure 5.17(f) Streamwise direction motion phase diagram

Figure 5.17 A case for X_S=5, Y_S=2, UR=4.0 which has exceeded the corresponding critical flow velocity.

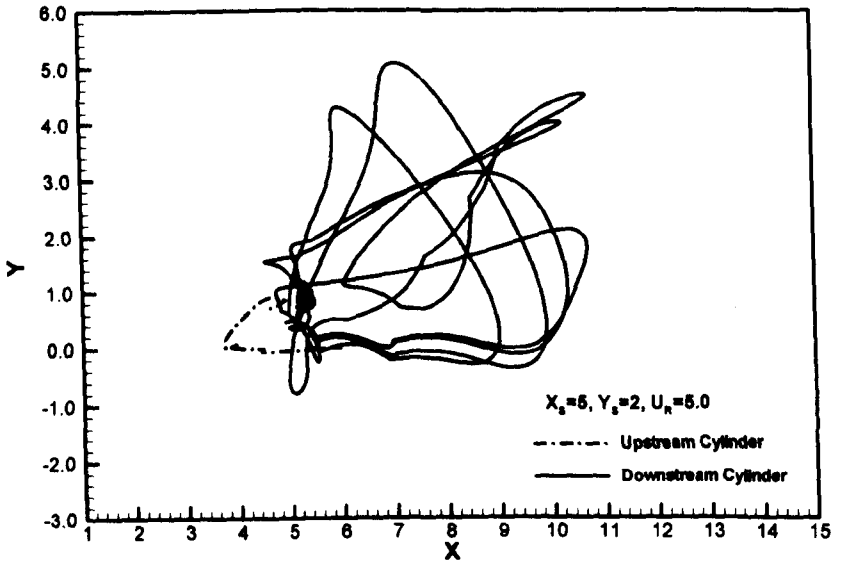

Figure 5.18(a) Trajectory.

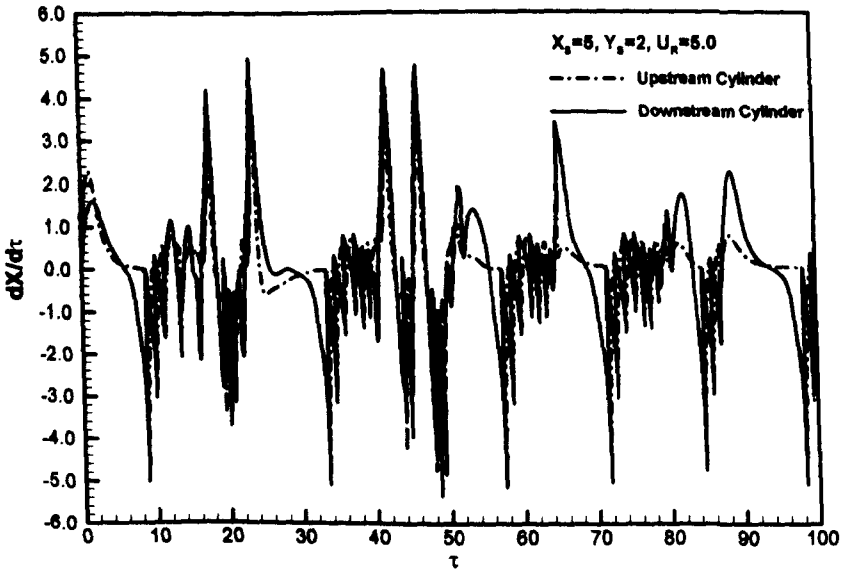

Figure 5.18(b) Streamwise Direction Velocity.

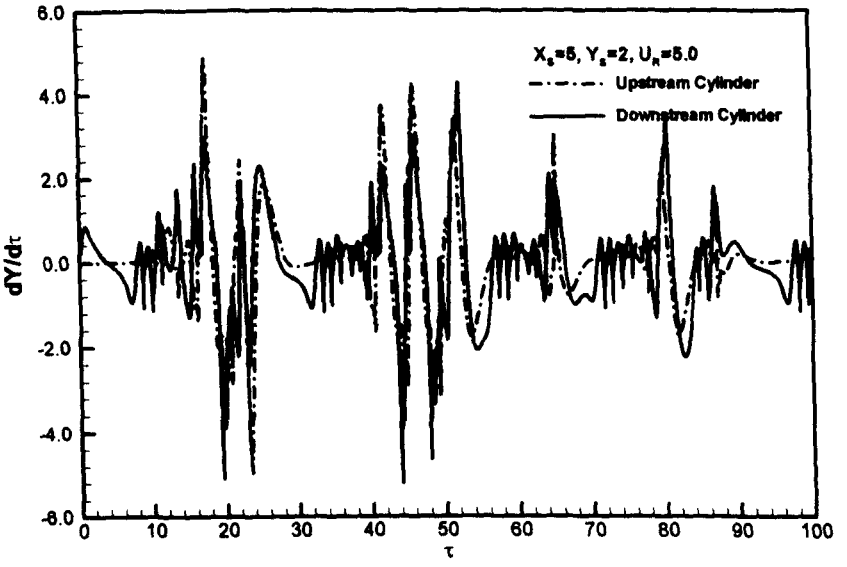

Figure 5.18(c) Cross-Flow Direction Velocity.

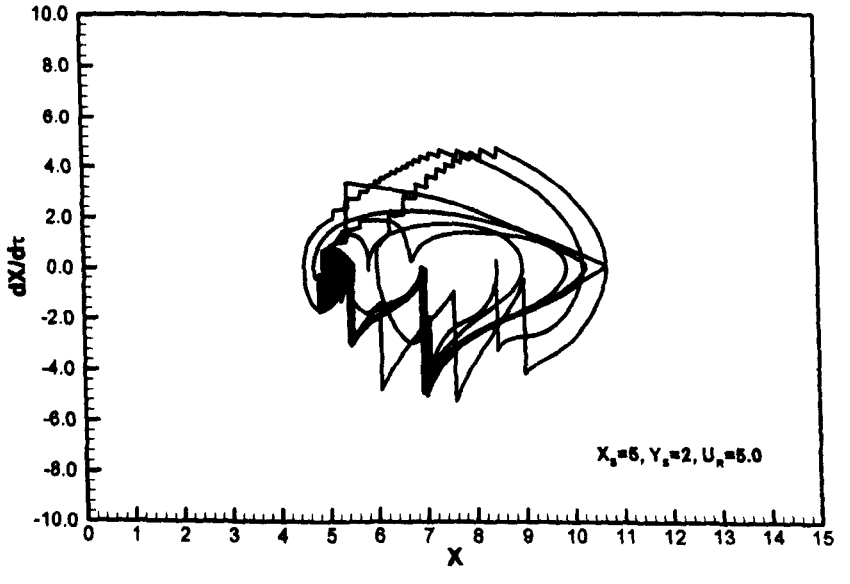

Figure 5.18(d) Streamwise Direction Motion Phase Diagram.

Figure 5.18 A case for Xs=5, Ys=2, UR=5.0.

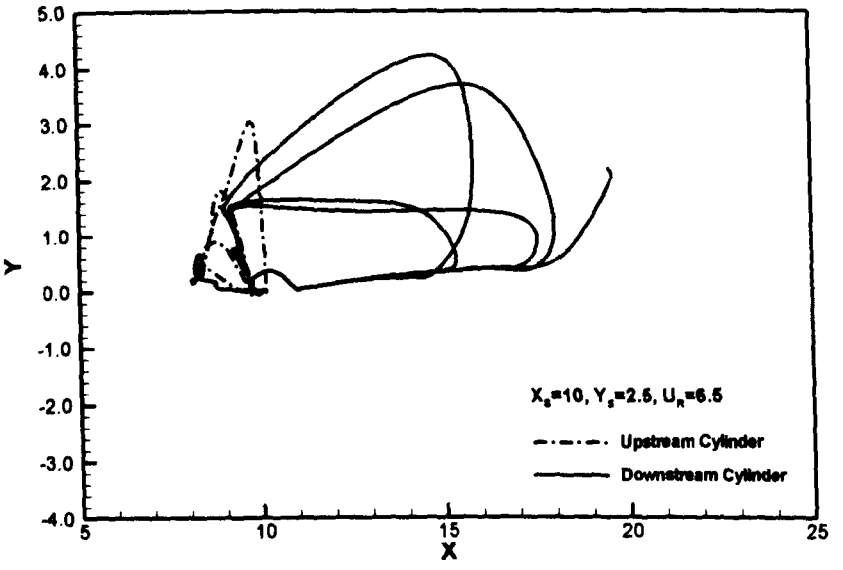

Figure 5.19(a) Trajectory.

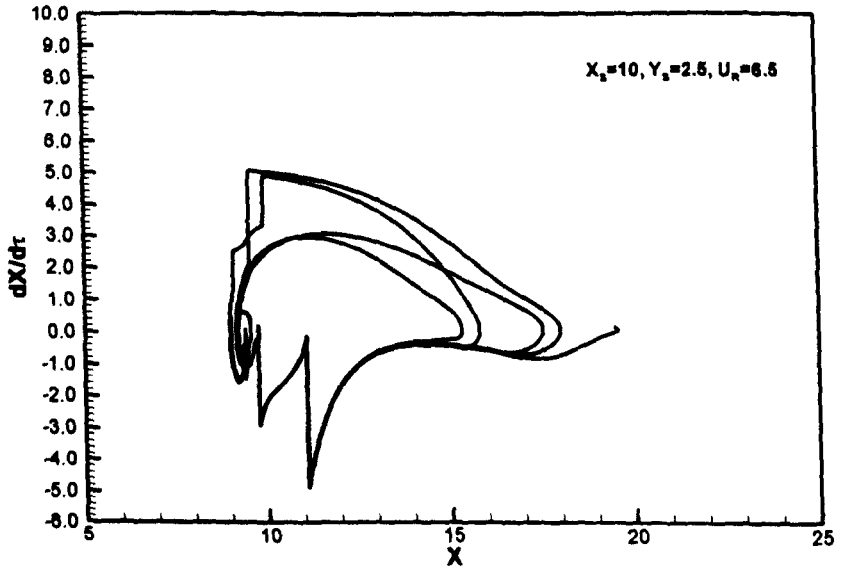

Figure 5.19(b) Streamwise Direction Motion Phase Diagram; X_S=10, Y_S=2.5 .

Figure 5.19 A case for X_S=10, Y_S=2.5, U_R=6.5 which has exceeded its corresponding critical flow velocity.

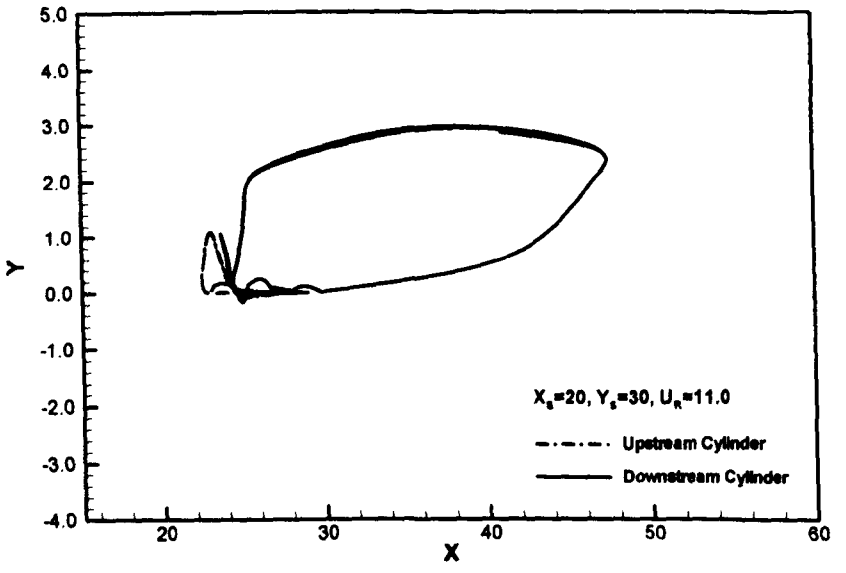

Figure 5.20 Trajectory; X_S=20, Y_S=3.0, U_R=11.0, a case with its flow velocity has exceeded the critical value.

5.5 Summaries

The dynamic simulation conducted in this chapter disclosed the characteristics of the movement of the downstream cylinder under the action of the time-averaged forces, and can be summarised as follows:

1) When flow velocity is small, regardless of whether the two cylinders are in tandem or staggered, and irrespective of the initial distances apart, the downstream cylinder tends to approach its equilibrium swiftly;

2) When the layout of the two cylinders and the flow velocity are such that there are four equilibrium states, the dynamic behaviour of the downstream cylinder is dependent on the initial distance apart of the two cylinders. If the spacing between two cylinders is smaller than 8 diameters, then the downstream cylinder can either exhibit periodic movement or rest at its equilibrium, depending on the initial disturbance of the system. If the initial spacing between two cylinders is larger than 8 diameters, the downstream

cylinder may rest at a different equilibrium point, depending on its initial spacing. This conclusion is based on the mass parameter of 0.2. However, the 8 diameters spacing index varies with mass parameters.

3) When the flow velocity approaches the critical velocity, depending on the initial spacing, if there is no stable equilibrium, then the downstream cylinder will exhibit periodic movement irrespective of its initial disturbance. This movement amplitude will depend on the flow velocity. When the flow velocity is large enough, the amplitude of the movement can bring the two cylinders to collide with each other. If one of the equilibrium points is stable, then the downstream cylinder ultimately approaches its equilibrium.

4) When the flow velocity is higher than the critical flow velocity, regardless of the initial spacing of the two cylinders, the downstream cylinder tends to move around, and collision between the two cylinders is likely to occur. The duration between successive collisions corresponds to its natural period, although the movement can exhibit stochastic behaviour from time to time;

5) The velocity of the cylinder before collision can reach as high as 5 in non-dimensional form, which implies that the wake induced cylinder motion velocity can be much higher than the vortex induced vibration can show. This is important for the evaluation of the damage caused by the collision. Meanwhile, the wake induced downstream cylinder motion mainly occurs in streamwise direction, instead of cross-flow direction which the vortex induced vibration often exhibits.

6) Parameter aU_R^2 shows similarity with the critical state for a stationary bifurcation. However, it is not simple to find the similarity of the downstream cylinder's motion after the flow velocity exceeds the critical flow velocity. In general, the smaller the

mass parameter, the larger the motion velocity can occur. Such a relation is attributed to the effect of the related fluid damping.

7) The maximum amplitude that the movement of the downstream cylinder can possibly display is the layout distance between the two cylinders. This conclusion is consistent with the experimental observations (Huse, 1996).

Although the model of collision utilised in this investigation is straight forward, according to the investigation results presented in this chapter, it has been able to reflect the key feature of the collision. It is worth noting that the results obtained in this chapter agree well with the experimental observation conducted by DHI (Bryndum & Anderson, 1999).

Chapter VI

STATICS OF A PAIR OF MARINE RISERS

6.1 General Remarks

So far, the interaction between two cylinders in two dimensions has been investigated systematically, from the interaction forces to the stability analysis, followed by dynamic analysis. The results show that under certain conditions for the specified pair of cylinders, the downstream cylinder can exhibit different dynamic phenomena. However, most of the time, in practical engineering the interaction between cylinders occurs in three-dimensional space. In order to understand the practical riser interaction, following questions need to be answered: Does the three-dimensional effect affect the riser interaction qualitatively? Can the result in two-dimensional space be directly applied to the three-dimensional scenario, or how can it be applied? In the following chapters, the interactions will be examined comprehensively in three-dimensional space.

6.1.1 Issues Related to Statics In Marine Riser Design

A marine riser is essentially a conductor pipe in oil and gas development, which connects the wellhead at the sea floor with the top vessel on the sea surface. It is used to convey oil or gas or drilling fluid, depending on its functionality and as a guiding tool between wells and top vessel. The key features of marine riser design, regarding statics, were defined by Fischer & Ludwig(1966) who showed, with static analysis, the importance of tensioning the riser to prevent buckling and to control deflection and stress.

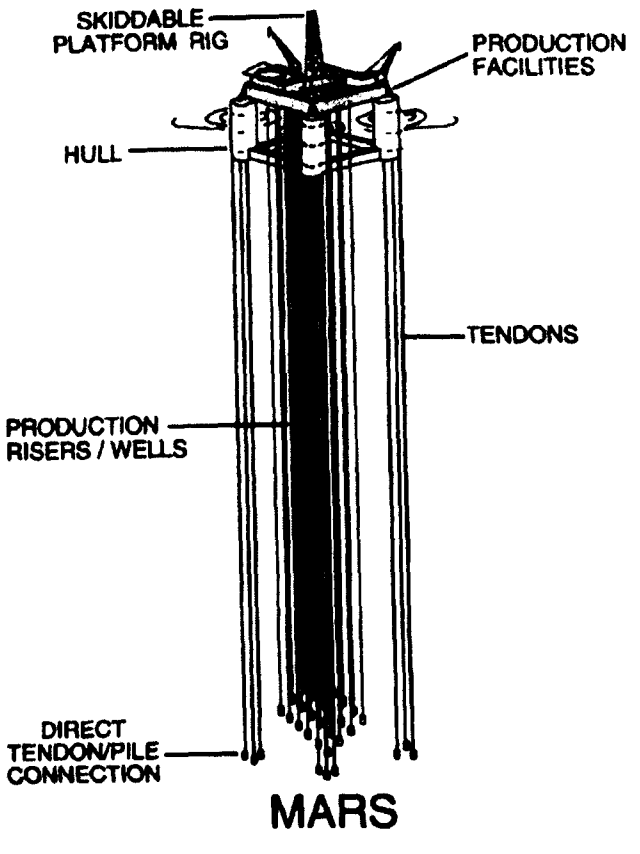

Figure 6.1 Schematic of TLP risers arrangement.

However, quite often, a cluster of risers, rather than a single riser, is used in oil and gas production. For example, the particular type of TLP and Spar risers investigated in this thesis is a cluster of rigid risers. They are linked between wellheads and vessel independently. Shown as an example in Figure 6.1 is a schematic of the 24 well slots riser array on the platform Mars, which is operated in the Gulf of Mexico about 130 miles southeast of New Orleans in water depth of 2,940 feet. For such an arrangement of marine risers, vortex induced vibration, time-averaged force induced riser deflection and potential oscillation are the main issues for the riser design. The vortex induced vibration is a dynamic problem due to the high frequency vibration, which usually determines the fatigue life of risers. These phenomena have been investigated extensively, reference to vortex induced vibration can be found in (Sarpkaya 1979; Pantazopoulos 1994), and recent work on this topic can be found in (Triantafyllou et al 1994; Larsen et al 1996; Vandiver 1998) etc.

On the other hand, the time-averaged force is a static as well as dynamic concern. In the past, investigation into riser statics only considered solitary risers. However, with multiple risers located around, and possible significant differences in deflections due to the interactions between risers, caused by ocean currents, static analysis which investigates the

interference effect as well as buckling effect and deflection control should be taken seriously. The extreme scenario of the interference effect is that two marine risers collide with each other in an ocean current. According to the investigation made into the two-dimensional cylinder interaction, such a phenomenon is caused by the loss of stability of the downstream riser under the action of a time-averaged force. It is not pronounced in shallow water operations, because the deflection of risers caused by current is insignificant. However, it has been recognised that the deflection of risers is proportional to the square of the depth of water (Huse 1993). With oil and gas exploration and development now moving towards ever deeper waters, the deflection of the riser will be increased significantly. Meanwhile, riser collision can play a detrimental role in oil and gas production. All these concerns make the statics related clearance between risers to be another important issue in riser design. In this chapter, the static deflection of risers caused by ocean current, with the consideration of interaction between two risers will be investigated.

6.1.2 Theoretical Approaches Used in the Riser Analysis (Statics)

The key objective for the riser interaction statics analysis is: for a pair of risers with specified physical and geometrical parameters, to find out the geometrical shape (or equilibrium state) and corresponding stress within riser if necessary. Further objectives are to identify the effect of every important control parameter, which could affect the final equilibrium state, such as top tension, riser weight, ocean current etc.

Mathematically, the statics is a system of two fourth-order differential equations with boundary conditions defined. Due to the nonlinear nature of both the structure coupling and fluid interaction, the classical solution to such a problem will be confined within very limited cases, and a numerical technique is an inevitable means to find the solution. There are a variety of ways to solve such a system, such as multi-shooting method, finite

difference method, finite element method, lumped method, and modal superposition method etc. Mathematically, all the methods above are used to discretise the differential equation into a set of simultaneous algebraic equations which are then solvable. The difference lies in the choice of discretisation method, as described below.

- Finite Difference Method

First the physical domain is discretized into many finite intervals. Differential equations are discretized by substituting derivatives with finite differences. Such a method is derived from the definition of derivatives, i.e. when the finite difference used is fine enough, then the approximate expression of the rate of change approaches the exact derivatives. The partial differential equation is thus cast into a system of simultaneous equations with the unknown at discretised positions. The boundary condition is incorporated into such a simultaneous equation and a self-contained system is thus formed and is solvable. This method is widely used in the numerical analysis of N-S equations in fluid dynamics as well as in other engineering applications. Detailed explanation can be found in (Mitchell, 1980).

- Finite Element Method

Finite Element Method discretises the system in such a way that the fluid domain or structure domain is divided into a lot of elements. Within each element, the solution is approximated by shape functions, which ensures that the boundary conditions are perfectly defined. By assembling these element equations, a large system is thus formed and is solvable. Such a method facilitates the detailed simulation of the element which hence is powerful in dealing with complex structures as well as fluid dynamics, reference can be made to Akin (1982).

- Lumped Method

Lumped method is a simplified version of the Finite Element Method, which mainly simplifies the physically continuous elements into concentrated mass elements. Due to the reduced number of degrees-of-freedom, this means a large saving on the computing memory required to solve the equation. Hence the lumped method is advantageous on computing efficiency. Such a method is often applied in the analysis of mooring lines, and cables for complex integrated system analysis, for example (Huang, 1992).

- Modal Superposition Method

Modal superposition method is an implementation of Galerkin's method, where the co-ordinate system is first transformed into the modal co-ordinate system. In such a system, the boundary condition is perfectly defined due to the nature of the modes. Because of the convergence characteristics of the system in the modal co-ordinate system, the modes can be truncated to a finite number. Therefore, the system is converted into a set of finite number of algebraic equations. This method will be applied in the subsequent analysis.

- Shooting Method

Shooting method is a classical method for systems where there is an Ordinary Differential Equation with boundary conditions defined. By supposing boundary value (for example, the curvature of the riser) at one end, and integrating the ordinary differential equation (e.g. by Runge-Kutta method), the corresponding control at the other end of the riser can be obtained. If the resultant control can satisfy the boundary condition there, then the solution is the one which is being sought. Otherwise, a refined initial guess at the first end is made, and the above procedure is repeated until the solution at the other end can satisfy the boundary condition. Such a solution technique is straightforward, for example, (Huse 1993). Mathematically, this method is very similar to the Finite Difference Method in the normal discretization sense. The main difference lies in that the shooting method solves

the equation by iteration, while Finite Difference Method solves the system simultaneously, and also the shooting method can have unfixed discretized intervals.

6.1.3 Method used in the present work

In this chapter, the theoretical model of statics for the interaction between two marine risers is presented, followed by the modal superposition method to tackle the statics problem. The solution procedure is detailed in this chapter. The simulation of practical problem in the laboratory environment is also discussed. Finally, sample calculations are provided, and effects of individual parameters are elaborated. The stability and related dynamic behaviour will be discussed in the succeeding chapters.

6.2 Theoretical Formulation

Figure 6.2 is a schematic diagram of one riser located in the wake of another. The upstream riser can be either rigid or flexible. The origin of the co-ordinate system is chosen to be at the top of the riser (which represents the top connector for marine risers), the x co-ordinate is in the direction of the flow, y is in the cross-flow direction while z is made vertically downwards. The initial stream-wise distance between two risers is X_S, the cross-flow distance between two risers is Y_S. Both of them have been non-dimensionalized by upstream riser diameter, and capital symbols in this Chapter refer to non-dimensional quantity. For simplicity, the two risers have the same diameter in the present investigation, although it is not a restriction of the investigation method used here. The unstrained riser length is l_0. The top end of the riser can be above the water surface. The distance from riser top end to water surface is z_0. The bottom end of the riser is either fully attached to the floor or hanging in the water, as it would be during installation of marine risers or hang-off condition etc. The main focus in this thesis supposes that riser is fully attached to the floor, although the later situation can be considered in a similar way.

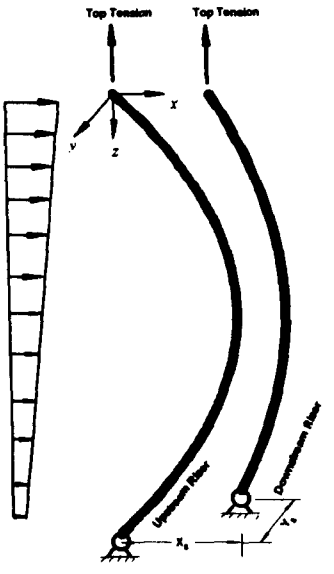

Figure 6.2 Schematic figure of the statics for two riser interaction.

6.2.1 Formulation of Problem

If the case is restricted to small angles, using linear strain analysis, then an initially straight riser can be modelled as a tensioned beam. The static equilibrium equation for lateral displacement of a tensioned beam is (Krolikowski & Gay, 1980, Furnes, 2000):

$$\begin{cases} \dfrac{d^2}{ds^2}\left[EI(s)\dfrac{d^2x}{ds^2}\right]-\dfrac{d}{ds}\left(T_e(s)\dfrac{dx}{ds}\right)=F_x(z) \\ \dfrac{d^2}{ds^2}\left[EI(s)\dfrac{d^2y}{ds^2}\right]-\dfrac{d}{ds}\left(T_e(s)\dfrac{dy}{ds}\right)=F_y(z) \\ \dfrac{d}{ds}\left(T_e\dfrac{dz}{ds}\right)=\begin{cases} -m_s g+\rho_0 gA_0-\rho_i gA_i & \textit{bottom fully contact with floor} \\ -m_s g+\rho_0 gA_0-\rho_i gA_i+P_0A_0H(z-z_B) & \textit{bottom not attached to the floor} \end{cases} \end{cases} \tag{6.1}$$

Where

A_0, A_i : Outer and internal areas of riser cross section;

EI : Bending stiffness of the riser structure;

F_x : Applied fluid loading in the flow direction;

F_y: Applied fluid loading in the cross-flow direction;

g: gravity acceleration;

m_s: Structural mass per unit length;

s: The distance along the riser from the top end;

x: Streamwise displacement;

y: Cross-flow displacement;

z: Vertical distance downwards from top end (from origin of the co-ordinate system)

T_e: Effective tension of the riser, $T_e = T + P_0 A_0 - P_i A_i$

P_0: Flow static pressure around the riser,

$$P_0 = P_a + \rho_h g(z - z_0) H(z - z_0)$$

P_a: Air pressure on water surface

$H(z - z_0)$: Heaviside function

P_i: Pressure inside the riser with its cross-section area of A_i

T: Tension within the riser structure;

ρ_0: The density of the fluid outside of the riser

$$\rho_0 = \begin{cases} \rho_a & (z < z_0) \\ \rho_h & (z \geq z_0) \end{cases}$$

ρ_a, ρ_h, ρ_i : Density of air, water and inner fluid in the riser respectively;

The boundary condition for the downstream riser:

$$\begin{cases} x = 0 \\ y = 0 \\ \dfrac{d^2x}{dz^2} = 0 \text{ at top } z = 0 \\ \dfrac{d^2y}{dz^2} = 0 \\ T = T_0 \end{cases} \tag{6.2}$$

$$\begin{cases} x = 0 \\ y = 0 \\ \dfrac{d^2x}{dz^2} = 0 \\ \dfrac{d^2y}{dz^2} = 0 \end{cases} \text{ at bottom } z = l_H \tag{6.3}$$

Here l_H is the vertical distance between top and bottom end after deflection. Due to the tensile property of the riser, l_H will not be the same as the vertical projection in z direction of original length of the riser l_0, as this length is not known beforehand. The procedure to tackle this will be discussed later in this section.

Due to the fact that the investigation is within the small angle hypothesis, i.e. the profile of the riser is flat,

$$dx/ds, dy/ds << 1 \text{ and } d/ds \approx d/dz$$

The normal requirement for such a simplification needs the ratio of maximum defection to riser length is less than 1:8 (Irvine, 1981).

According to longitudinal balance in equation (6.1), we have

1. Bottom fully attached to floor:

$$T_e = T + P_0 A_0 - P_i A_i \approx T_{e0} - m_e g z$$

2. Bottom hanging in water with the distance of z_B from top to end

$$T_e = T + P_0 A_0 - P_i A_i \approx \begin{cases} T_{0e} - m_e g z & (z < z_B) \\ T_{0e} - m_e g z + (P_0 A_0)_{bottom} & (z = z_B) \end{cases}$$

Here

$$T_{e0} = T_0 + (P_0 A_0)_{top} - (P_i A_i)_{top}, \quad m_e = m - \rho_0 A_0 + \rho_i A_i$$

Although the solving procedure for a riser not attached to floor is similar to the problem of riser bottom attached to the floor, for clarity reason, it will not be detailed hereafter. Let

$$x = X \cdot l_H, y = Y \cdot l_H, z = Z \cdot l_H$$

The bending stiffness is further supposed to be equal everywhere, The control equation can be simplified as:

$$\begin{cases} \dfrac{EI}{l_H^3}\dfrac{d^4X}{dZ^4} - \left(\dfrac{T_{e0}}{l_Z} - m_e g Z\right)\dfrac{d^2X}{dZ^2} + m_e g \dfrac{dX}{dZ} = \dfrac{1}{2}\rho U^2 D C_D(X(Z), Y(Z)) \\ \dfrac{EI}{l_H^3}\dfrac{d^4Y}{dZ^4} - \left(\dfrac{T_{e0}}{l_Z} - m_e g Z\right)\dfrac{d^2Y}{dZ^2} + m_e g \dfrac{dY}{dZ} = \dfrac{1}{2}\rho U^2 D C_L(X(Z), Y(Z)) \end{cases} \tag{6.4}$$

As shown in (6.4), the de-coupling of the structure displacement between X and Y brought by the simplification $d/ds \approx d/dz$ still can not make displacement of X and Y be

independent to each other due to the coupling by the fluid force coefficients on the right hand side of the equation.

However, the problem to be considered for equation (6.4) is relatively uncomplicated. The essential feature of the problem is that the fluid force is in two dimensions and they are functions of positions themselves. This will lead to the deflected riser being in three dimensions, so that the deflected riser will not necessarily be confined within a single plane.

6.2.2 Numerical Method Employed

Modal superposition method is used in the present analysis. By considering the mode of a pinned-pinned beam, the solution of X, Y can be expressed as:

$$\begin{cases} X(Z) = \sum_{r=1}^{\infty} a_r \phi_r \\ Y(Z) = \sum_{r=1}^{\infty} b_r \phi_r \end{cases} \tag{6.5}$$

Here $\phi_r = \sin(r\pi z)$, $(r = 1, 2 \cdots\cdots)$ is the r-th order mode shape,

Due to the orthogonal property of the modes, ϕ_r possesses the following characteristics:

$$\int_0^1 \phi_i \phi_j dZ = \begin{cases} 1/2 \\ 0 \end{cases} \tag{6.6}$$

By substituting (6.5) into (6.4), The control equation in the x direction can be simplified to:

$$\sum_{r=1}^{\infty} \frac{EI}{l_H^3} (r\pi)^4 a_r \phi_r + \sum_{r=1}^{\infty} (r\pi)^2 \frac{T_{e0}}{l_H} a_r \phi_r + \sum_{r=1}^{\infty} m_e g Z a_r \phi_r'' + m_e g \sum_{r=1}^{\infty} a_r \phi_r' = \frac{1}{2} \rho V_0^2 D C_D (X(Z), Y(Z)) \tag{6.7}$$

Expanding term of $Z\phi_r''$ and ϕ_r' with the modal co-ordinates, after mathematical manipulation, equation (6.7) can be written as:

$$\sum_{r=1}^{\infty}\left[\frac{EI}{l_H^3}(r\pi)^4\phi_r+\frac{T_{e0}}{l_H}(r\pi)^2\phi_r-(r\pi)^2 m_e g\sum_{S=1}^{\infty}C_{rs}\phi_S+m_e gr\pi\sum_{s=1}^{\infty}D_{rs}\phi_s\right]a_r = \frac{1}{2}\rho V_0^2 DC_D(X(Z),Y(Z)) \tag{6.8}$$

Here

$$C_{rs}=2\int_0^1 Z\sin(r\pi Z)\sin(s\pi Z)dZ=\begin{cases}\dfrac{1}{2} & r=s\\ \dfrac{4rs}{\pi^2(s^2-r^2)^2}\left[(-1)^{r+s}-1\right] & r\neq s\end{cases}$$

$$D_{rs}=2\int_0^1\sin(s\pi z)\cos(r\pi z)dz=\begin{cases}0 & r=s\\ \dfrac{2s}{\pi}\left[\dfrac{1-(-1)^{r+s}}{s^2-r^2}\right] & r\neq s\end{cases}$$

Although the equation has infinite number of modes, the numerical calculation can truncate the high order terms and it should converge fairly quickly because the deflected risers have some simple and smooth geometrical shapes. By applying the property of orthogonal characteristics between individual modes to equation (6.6), multiplying by ϕ_k on both sides of the equation and integrating about Z from 0 to 1, the equation for modal co-ordinates can be changed into:

$$\left[\frac{EI}{l_H^3}(k\pi)^4+\frac{T_{e0}}{l_H}(k\pi)^2\right]a_k-\sum_{r=1}^{\infty}\left[(r\pi)^2 m_e gC_{rk}-m_e g(r\pi)D_{rk}\right]a_r=\int_0^1\rho V_0^2 DC_D(X(Z),Y(Z))\phi_k dZ \tag{6.10}$$

The same approaches applies to the analysis of the deflection occurring in the y direction, so the equation can be written as:

$$\left[\frac{EI}{l_H^3}(k\pi)^4+\frac{T_{e0}}{l_H}(k\pi)^2\right]b_k-\sum_{r=1}^{\infty}\left[(r\pi)^2 m_e gC_{rk}-m_e g(r\pi)D_{rk}\right]b_r=\int_0^1\rho V_0^2 DC_L(X(Z),Y(Z))\phi_k dZ \tag{6.11}$$

Equations (6.10) and (6.11) constitute a closed form for a_k, b_k provided that l_H is known. The equation can be solved simultaneously or iterated one after another for the non-linear coupling terms of C_D, C_L.

The determination of fluid force coefficients C_D, C_L is directly based on the two-dimensional result by applying strip theory. It is assumed that the fluid force coefficient at a particular location depends on its position relative to its counterpart upstream riser. The validity of such a hypothesis could be argued. Basically, the fluid force possesses a random nature and has a component of periodical force related to the vortex shedding. Such a time variant force has a certain correlation along the riser length. This correlation factor is an important reason for causing experimental data scatter from one researcher to another(Pantazopoulos 1994). However, it is only the time-averaged force which is of interest to the present investigation. The flow velocity investigated here is well outside of the range of lock in phenomena. Even for the vortex induced forces, the correlation along the riser is weak. Therefore, the time-averaged force at different location is assumed to be independent of neighbouring positions.

So far, the condition on the l_H has not been addressed. This is a variable which can not be known beforehand, according to the constraint of the Hooke's law, with which the elastic riser should comply. The vertical length l_H and unstrained length l_0 should obey the following relation:

$$\frac{l_0}{l_H} = \int_0^1 \frac{EA}{EA + T_{e0} - m_e g Z l_H - P_0 A_0 + P_i A_i} \times \sqrt{\left[\sum_{k=1}^{\infty} a_k (k\pi)\cos(k\pi Z)\right]^2 + \left[\sum_{k=1}^{\infty} b_k (k\pi)\cos(k\pi Z)\right]^2 + 1} \cdot dz \tag{6.12}$$

To solve the equations (6.10), (6.11) and (6.12), iterations have to be made. The procedure is as follows:

1. Assume a value of l_H ;

2. Find the solution of deflected riser according to (6.10) and (6.11);

3. Find the corresponding unstrained length by (6.12), which normally will not be exactly the same as the given original length.

4. According to the available assumed l_H and the corresponding unstrained length, modify the value of l_H . Then repeat the above procedure steps 2 to 4, until the solution satisfies the condition that the corresponding unstrained length is equal to the original length. Then the solution of final X,Y is the deflection which was being sought.

6.2.3 Consideration of Similarity

Similarity is an important rule when tests need to be conducted. It is also vitally important for the analysis of the results. Considering the similarity requirement for hydrodynamics and structure statics, it is seen that the deflection of the riser depends mainly on the following parameters:

$$\frac{x,y}{D} = f\left(\frac{D}{l}, R_e, \frac{EI}{T_{e0}l^2}, \frac{T_{e0}}{m_e g l}, \sqrt{\frac{\rho}{T_{e0}}} V_0 l, C_{D,L}\right) \tag{6.13}$$

Among these parameters, D/l simply represents the geometrical similarity,

R_e is Reynolds number, which is the basic requirement for hydrodynamic similarity;

$EI/T_{e0}l^2$ reflects the relative importance of bending stiffness and top tension;

$\frac{T_{e0}}{m_e g l}$ is the top tension factor which is the ratio of effective tension on top to the riser's weight in water;

$\sqrt{\frac{\rho}{T_{e0}}} V_0 l$ is called as flow tension factor in this thesis and is represented by H_w, $H_w^2 \times C_{D,L}$ reflects the relation between transverse loading and the top tension. The application of parameter H_w will be further discussed in the next chapter.

It is easy to show that within these non-dimensional parameters in equation (6.13), contradictions persist which prevent simulation. For example, the third and fourth parameters make a pair of conflicting parameters. Also, trying to meet the requirements of the structure dynamics will violate the requirements of the fluid dynamics similarity, particularly the condition of Reynolds number similarity. Therefore a compromise has to be made and favour has to be given to more important parameters. Table 6.1 gives two possible plan options to choose from, for similarity parameters when experiments are conducted.

It is seen that both plans violate Reynolds number similarity for the fluid dynamics. Additionally, for the scale plan 1, $EI/T_{e0}l^2$ can not be simulated, and for the plan 2, $T_{e0}/m_e gl$ is violated. Theoretically, the plan 1 is better than 2, because for very long risers, $EI/T_{e0}l^2$ is a very small quantity which simply means the bending stiffness is not important when compared to the tension effect in determining the deflection. Furthermore, such a plan can keep the top tension proportional to the net weight of risers in water, which is a practical situation for risers. However, the shortcoming for such a simulation is the difficulty in the control of the flow velocity, which is scaled down to $\sqrt{\lambda}$. If the scale ratio is *30*, for a full

scale case with current velocity of *1.0* m/s, the test current velocity can only be *0.2* m/s, which is too small a quantity to be controlled even in the laboratory. Another shortcoming is the violation of the Reynolds number in plan 1, which is much worse than plan 2. The Reynolds number for the model is only *1/900* of that for full scale if the scale ratio is *30*. Such a Reynolds number in plan 1 is so small that it makes the flow dynamics significantly different from that for full scale. For practical considerations, the scale plan 2 would be a better selection. Although the similarity law of $T_{e0}/m_e gl$ is violated, however, it is a rather less sensitive parameter in controlling the riser deflection. This will be demonstrated in the numerical results.

Table 6. 1 Experimental similarity parameter for static deflection.

PARAMETERS	SCALE PLAN 1	SCALE PLAN 2
Diameter, Length etc. Geometrical Parameters	λ [1]	λ
Flow Velocity V_0	$\sqrt{\lambda}$	1
Tension at the Top T_0	λ^3	λ^2
Bending Stiffness EI	λ^4	λ^4
Fluid outside and inside of the riser	1	1
Violated Parameters	$EI/T_{e0}l^2$, Re	$T_{e0}/m_e gl$, Re

[1] Here $\lambda\left(=l_{model}/l_{full}\right)$ is the model dimension scale ratio.

6.3 Numerical Results

6.3.1 Benchmark Test of the Program

Before any prediction is made about the riser statics, the program is first checked against the results published by the American Petroleum Institute(American Petroleum Institute, 1992). In 1992, 14 organisations participated in a numerical comparison organised by API committee to find out the degree of agreement among their riser analysis computer programs and to present data which could then be used to validate other such programs.

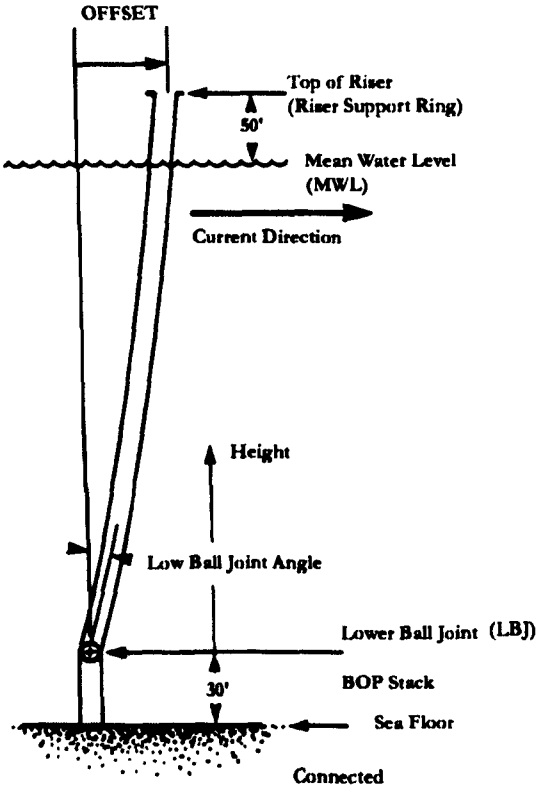

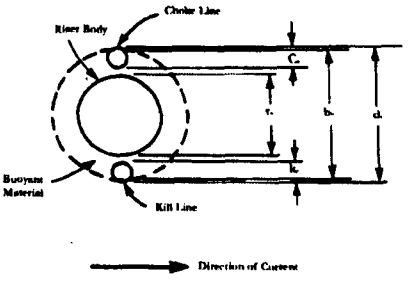

Figure 6.3 A schematic diagram of the drilling Riser used for present investigation.

The model used was a drilling riser with one choke line and one kill line. The drilling line is filled with drilling mud and the choke line and kill line are filled with sea water. Figure 6.3 is a schematic diagram of the model used. The definitions of the parameters used in the calculation are listed in table 6.2.

The comparison of present calculation results against the results published by API is shown in tables 6.3 and 6.4. It is seen that the results agree very well with the results provided by the API, including the deflection angle at top connector and Lower Ball Joint, maximum bending moment and their locations. This gives confidence in the subsequent calculation for the interaction between two risers

Table 6. 2 Sample calculation data (API, 1992).

Vertical Distance		
Mean Water Level to Riser Tensioner Ring, *(Feet)*	50.0	
Sea Floor to Lower Ball Joint*(Feet)*	30.0	
Riser Data		
Diameters, Inches		
Riser Pipe Outside Diameter	21.0	
Riser Pipe Inside Diameter	20.0	
Choke Line and Kill Line Outside Diameter	4.0	
Choke Line and Kill Line Inside Diameter	3.0	
Buoyant Material Outside Diameter	38.0	
Modulus of Elasticity of Riser Pipe, E, (psi×10^6)	30	
Densities, (pounds/cubic foot)		
Seawater	64.0	
Drilling Mud	89.8	
Hydraulic Force Constants		
C_D, Drag Coefficient	0.7	
D_e, Effective Diameter for Current and Wave		
Unbuoyed Riser (inches)	29.0	
Buoyed Riser	38.0	
Weight (pounds), of 50-foot Joint, Complete With All Associated Lines, Couplings, and Buoyant Material, If Any		
	Wa, in air	Wp, in seawater
Unbuoyed, 21-in	8800	7660
Buoyed, 21-in (3000-ft water depth)	14740	2950
Current:		
A.	Linear, ½ knot at mean water level, zero at lower ball joint	
B.	Linear, 2 knot at mean water level, 0.4 knot at lower ball joint	
Riser Length (feet)	1520	3020
Top Tension (Kips)	370	500
	600	650
Static Offset (feet)	45	90

Table 6. 3 Comparison of calculation result with API published data (1500 ft Case).

Tension		Tension 1		Tension 2	
Current		Current A	Current B	Current A	Current B
Max Bending Stress (Kips)	Cal.	3.91	5.81	0.76	1.04
	Literature[2]	3.91	6.04	0.71	1.00
Location of Max Bending Stress (*ft*)	Cal.(ft)	106.4	121.6	91.2	91.2
	Literature	122.45	125.12	118.15	121.35
Angle From Vertical (°)	Cal.(LBJ)	4.53	6.53	2.51	3.12
	Literature	4.57	6.63	2.52	3.12
Angle From Vertical (°)	Cal.(Top)	0.65	0.77	1.15	0.36
	Literature	0.64	0.77	1.14	0.36

Table 6. 4 Comparison of calculation result with API published data (3000 ft Case).

Tension		Tension 1		Tension 2	
Current		Current A	Current B	Current A	Current B
Max Bending Stress (Kips)	Cal.	1.01	1.94	0.45	0.98
	Literature	1.03	2.11	0.44	0.96
Location of Max Bending stress(*ft*)	Cal.(ft)	151.00	151.00	160.06	2838.80
	Literature	150.70	158.41	140.72	2839.91
Angle From Vertical (°)	Cal.(LBJ)	3.33	5.71	2.59	4.01
	Literature	3.45	6.22	2.64	4.14
Angle From Vertical (°)	Cal.(Top)	0.76	1.72	1.09	0.82
	Literature	0.80	1.85	1.06	0.87

The riser data for the following systematic investigation is presented in table 6.4. They are taken from a riser model data. Both risers are filled with fluid from top to bottom end. The top end of the riser is located at the mean water level, and the current has a uniform profile. The results are presented mainly in the form of geometrical shape of the risers.

Table 6.5 Parameters chosen for sample calculation (with model and prototype parameters for the convenience of comparison).

Parameter[3]	Model	Prototype
Diameter of riser D_0	0.01 (m)	0.30 (m)
Thickness of wall t	0.001 (m)	0.03(m)
Unstrained length l_o	44.4 (m)	1332.0 (m)
Material	Stainless Steel	
Mass(Include Added Mass)		317.87 (Kg/m)
Young's module E	2.1×10^{11}(N/m^2)	2.1×10^{11}(N/m^2)
Bending stiffness EI	60.86 (N•m^2)	4.93×10^{7}(N•m^2)
Top Tension T_0	4.12 (KN) 8.24 (KN)	2.709×10^{6}(N) 3.708×10^{6}(N) 7.416×10^{6}(N)
Weight of riser W in water	1.88 (N/m)	1.695 (KN/m)
Flow velocity V_0	0.5 ~ 1.5 (m/s)	0.5~1.5 (m/s)

6.3.2 *Comparison Between a Free-Stand Riser and One Stand on the Wake Centreline of a Rigid Riser*

Figure 6.4 is a geometrical shape comparison between a free-stand riser and one stand in the wake of a rigid riser. The riser in the wake is located on the wake central line with initial streamwise separation of *10* diameters.

[2] API data presented here is the mean result of the data provided by the different parties.

[3] The parameters selected here are chosen from a cluster of riser models (Huse 1996).

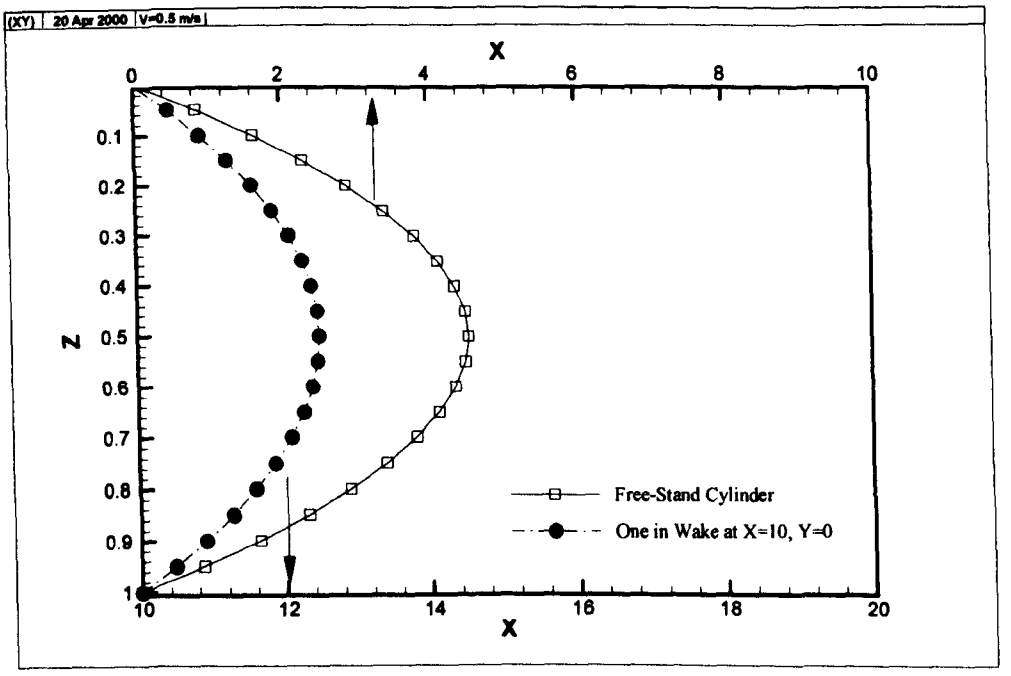

Figure 6.5(a)

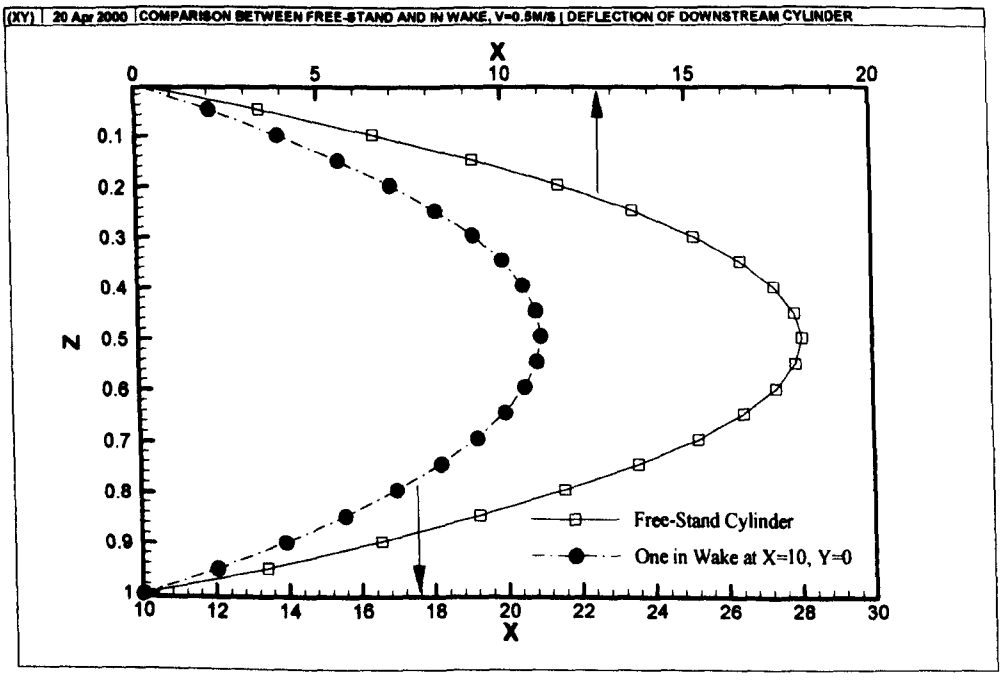

Figure 6.5(b)

Figure 6.4 Comparison between free-stand riser and one sitting in wake,with l_0=1332 (m), T_0=7.416×10^6 (N); (a) V_0=0.5 m/s, (b) V_0=1.0 m/s.

The figure shows that the streamwise deflection in the wake differs significantly from the free-stand riser. The difference amounts to *45* and *38* percent for the calculated scenario for flow velocities of *0.5* and *1.0 (m/s)* respectively. The deflection of the free stand riser here can be regarded as the scenario of an upstream riser as well. On the other hand, although the streamwise deflection reaches more than 10 diameters, the variation in vertical length is very small and can be neglected should the displacement of the top end be considered. The elongation of the riser only amounts to *0.03* percent of the original length for this particular case. This implies that the top end can be simplified as fixed when the dynamics of the riser are to be considered, especially when the displacements related to dynamic terms are much smaller than those related to the static terms. Also shown in figure 6.4 is the effect of the flow velocity. It is seen that the difference between a free-stand riser and riser in the wake is more significant for the low flow velocity. Such an effect is a reflection of the nonlinear nature of the problem. When flow velocity is lower, the wake shield effect is more pronounced because the spacing is relatively small, compared to the large flow velocity situation in present calculated scenarios.

6.3.3 Effect of Un-Strained Length of Riser On the Deflection

Table 6.6 shows the effect of different un-strained riser lengths on the deflection of the riser. The comparison of the effect of the un-strained riser length can be difficult due to the similarity issues. Here, in all these comparison calculations, the pretension is kept as same ratio of the total weight of risers in water. All other parameters are chosen according to full scale parameters shown in table 6.2, with flow velocity of 1.0 m/s and top tension factor 3.28. In order to facilitate the calculation, the comparison is made for the free-stand riser only.

It is seen that, when the length is large enough, the maximum deflection is increased linearly with the un-strained length. When the length is significantly small, the effect of

bending stiffness on the deflection is significant, and the above linear relation is not complied with. For the case presented, when the riser length reaches over 100 meters, i.e. $EI/T_{e0}l_0^2$ is smaller than 10^{-3}, the role of tension begins to take over, and the deflection becomes solely dictated by tension. This is the case for deepwater risers. In fact, under such conditions, the very long riser can be simplified as a string case. It should be noted here that in all these comparisons, the tension of the riser is kept linearly varied with riser length in order to ensure the constant top tension factor. If the tension is kept as constant, which is possible by utilising buoyancy attaching to marine risers, then the deflection varies proportionally to the square of the riser length (Huse 1996).

Table 6. 6 Maximum deflection for different unstrained length.

unstrained length (m)	deflection (x/D)
25	0.05
50	0.45
100	1.46
500	8.01
1000	16.00
1500	24.04

The above result implies that when the length is relatively small, for a steel riser, the deflection in the streamwise direction is negligible due to the rigidity of the riser. With the increase in length, the deflection becomes more and more noticeable and important. This is the driving force causing interaction between risers that should be considered in today's deepwater offshore oil and gas developments.

6.3.4 Comparison When the Upstream Riser is Rigid and Flexible.

The difference between the free-stand riser and the riser sitting in wake is significant. In fluidelastic experiments, when a two risers interaction is studied, sometimes the upstream riser is simplified by using a rigid riser. Questions are raised here about the effect of an upstream riser when it is flexible. By adopting the foregoing parameters for the both risers, a comparison is made for the downstream riser located on the wake centreline. The upstream riser is either rigid or flexible. The current velocity is 0.5 m/s and 0.6 m/s respectively. As shown in Figure 6.5, the difference is reduced with the decrease of flow velocity. Figure 6.5 also shows that when the upstream riser is flexible, the deflection of the downstream riser is smaller than that when the upstream riser is rigid. This contradicts the intuitive feeling that when the upstream riser is pushed downstream by the flow, the downstream riser might be pushed further by the flow to keep up the spacing between two risers. The reason is that when the upstream riser

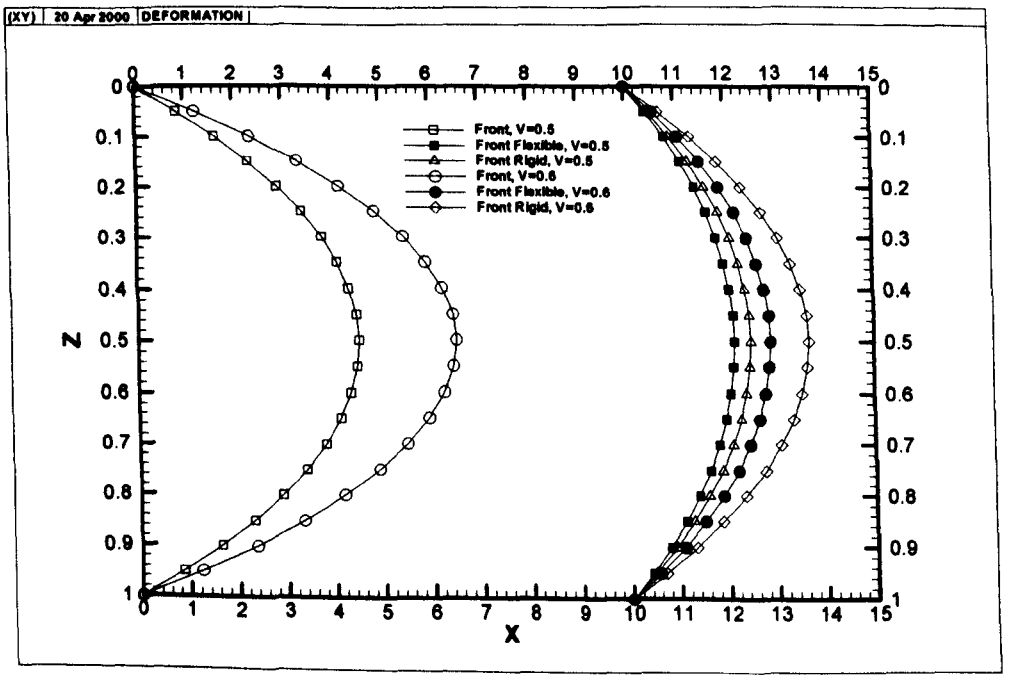

Figure 6.5 Effect of rigid and flexible upstream riser, l_0=1332m, T_0=7.436×10^6 (N).

moves downstream, the drag forces acting on the downstream riser are reduced. Therefore the deflections become smaller, and this is the factor which causes the two risers potentially to clash with each other. Such an effect becomes more significant with the increase of flow velocity, which moves the upstream riser towards downstream and increases the interaction.

In order to make a comparison with the two-dimensional theory, the state of the flow is checked to estimate the reduced flow velocity. Neglecting the bending stiffness, the first mode frequency of *1332 meter* riser with top tension factor of *1.5* is about $0.023Hz$. Therefore, even for the flow velocity of $0.5(m/s)$, the reduced velocity reaches *12*, which is a significantly high value and more than enough to bring two risers into interaction and to lose stability under certain arrangements.

6.3.5 Three-Dimensional Geometrical Shape of the Riser in Wake

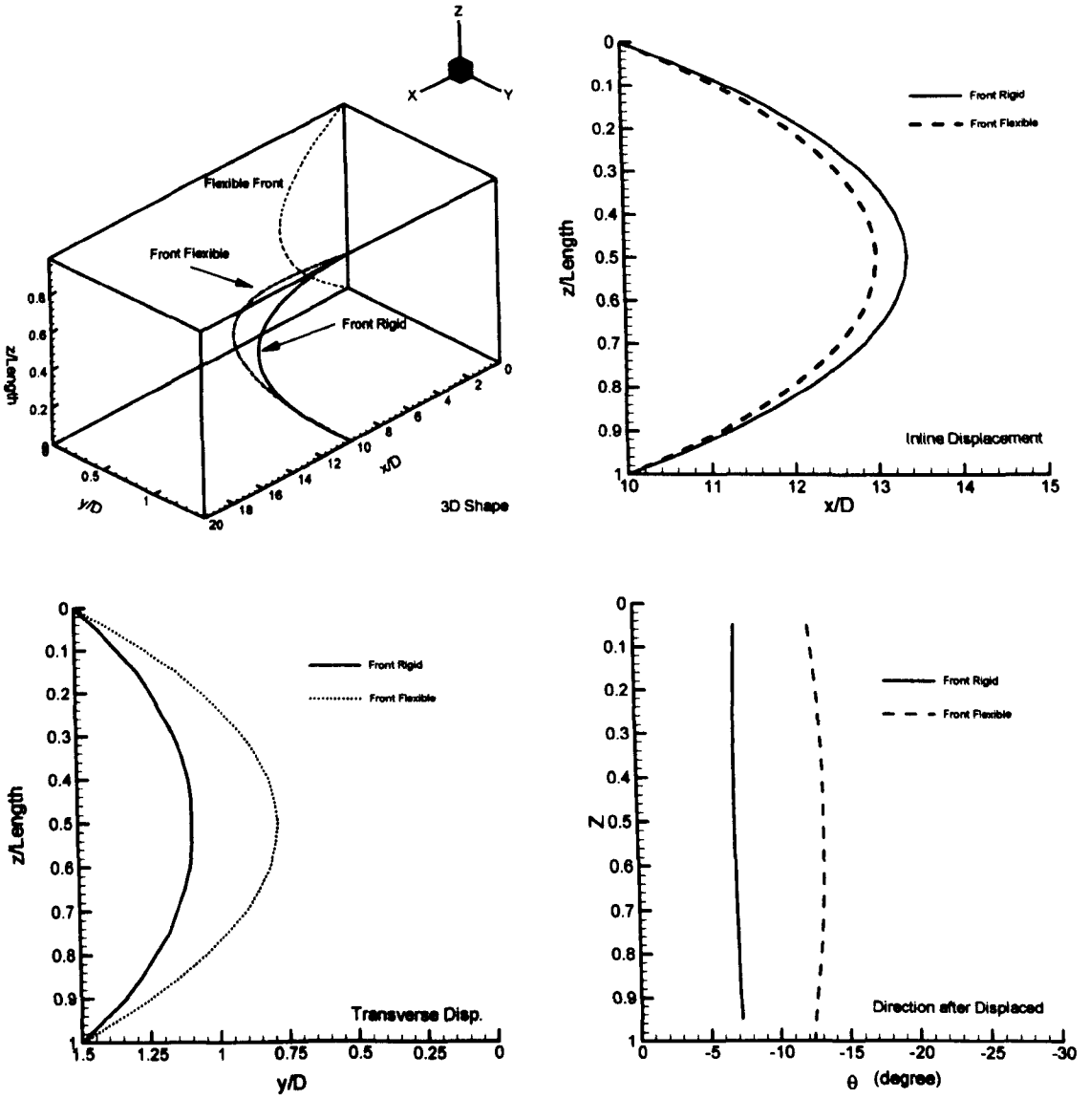

Figure 6.6 Three dimensional shape of a pair of risers. The upstream riser is either rigid or flexible.

Figure 6.6 shows the three-dimensional geometrical shape of a riser located in the wake. The comparison is also made with an upstream riser that is either rigid or flexible. The physical parameters adopted here are as follows:

D=0.30 (meter)

l_0*=1332 (meter)*

TTF=3.28

V_0*=0.5 (m/s)*

The downstream riser is chosen at the transverse location of *1.5* diameters when at rest. The figure demonstrates that when the upstream riser is flexible, the transverse deflection of the downstream riser is much larger than that for the rigid scenario. This is because if the upstream riser is flexible, the downstream riser at equilibrium position has a small spacing with the upstream riser, which makes the lift force much larger than that for the rigid riser and leads to a large deflection in the transverse direction. Probably the most interesting feature of this figure is that no matter whether the upstream riser is rigid or flexible, the deflection angle is nearly a constant along the riser. The deflection angle is defined as the angle between the line which connects the displaced position and original position and the x axis of the co-ordinate system. The results show that the deflected riser is nearly within a plane. This supports the two-dimensional simplified model (using two orthogonal springs to simulate the in-plane and out-of-plane stiffness). However, evidently, the angle varies depending upon whether the upstream riser is rigid and flexible. Care must be taken to address the problem related to the inclined spring arrangement angle when the problem is sensitive to the angle arrangement.

6.3.6 Comparison of Risers Sitting at Different Transverse Locations in the Wake

Comparison is made to illustrate the effects of staggered arrangement, by varying the transverse location. In the presented example, the streamwise spacing is chosen at 10 diameters. Three different cross-flow distances are selected, i.e. 1, 1.2 and 2 times of diameters respectively. Figures 6.7 and 6.8 show the transverse displacement at different cross-flow locations, and Figures 6.9 and Figure 6.10 give the comparison for the streamwise direction displacement. Figures 6.11 and 6.12 show the comparison of the deflection angle at different locations.

The comparison of the deflection angle (Figure 6.11 for rigid upstream riser and Figure 6.12 for flexible upstream riser) shows that, although for a given initial separation and flow

velocity the deflection is strongly dependent on these conditions, the deflected riser is generally within a plane and the fluid force always acts in three-dimensions. Also it is clear that the deflection corresponds well to the lift force magnitude. The deflection is largest when the riser is located at the transverse location of about *2* diameters. It should be noted that the deflection angle can be significantly different for different arrangements, which again implies that the spring coupling angle varies significantly should the two-dimensional model be applied.

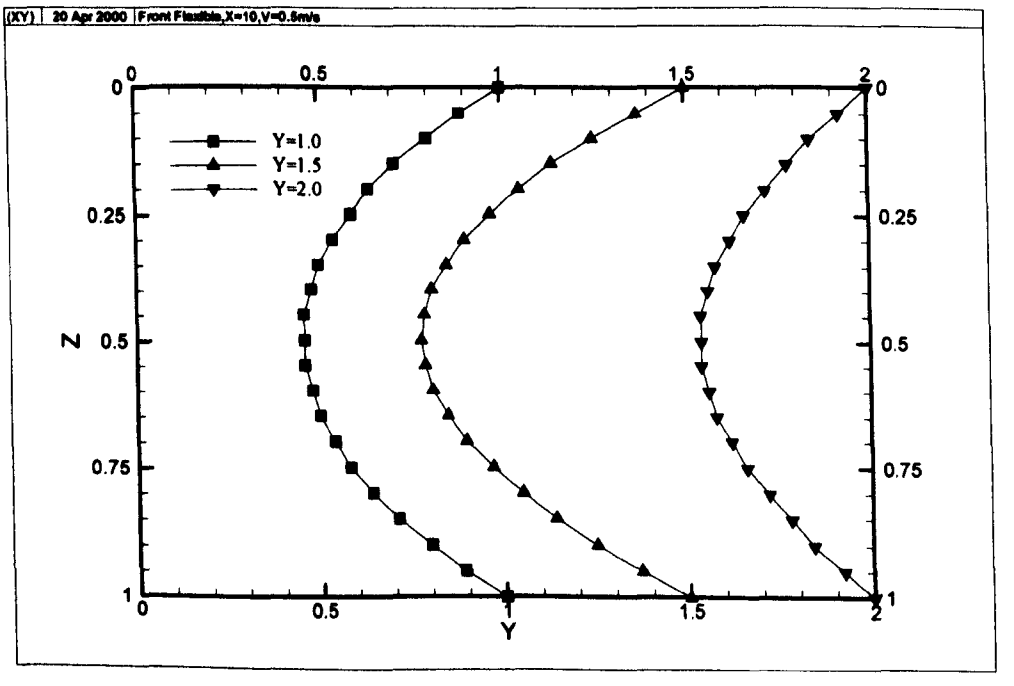

Figure 6.7 Transverse deflection comparison for different transverse initial locations, upstream riser is flexible, the design streamwise spacing is 10 diameters.

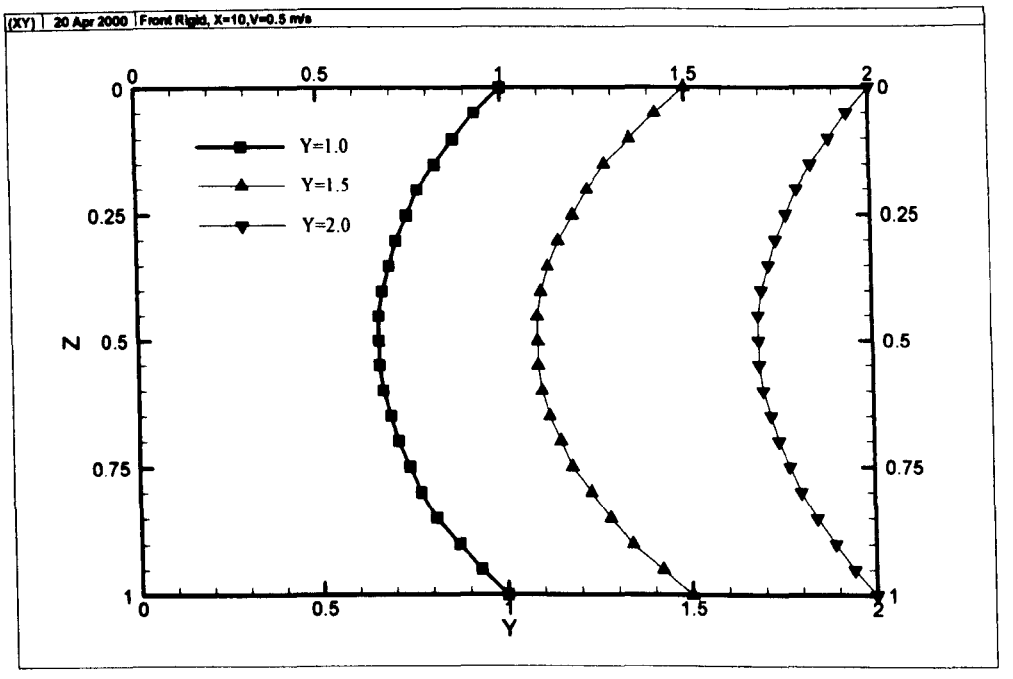

Figure 6.8 Transverse deflection comparison for different transverse initial locations, upstream riser is rigid, the design streamwise spacing is 10 diameters.

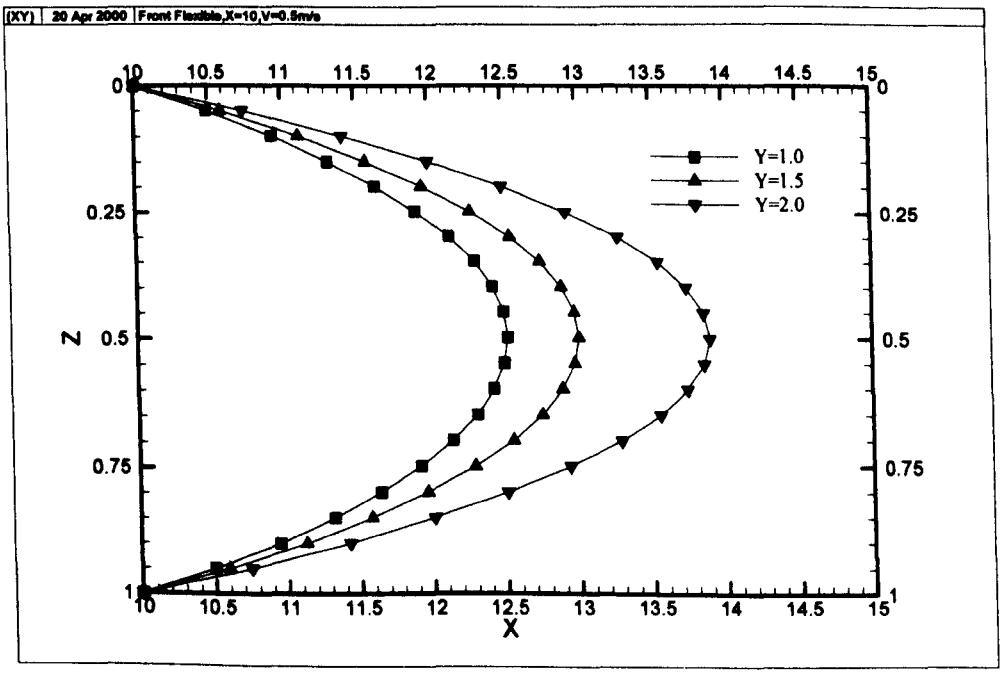

Figure 6.9 Streamwise deflection comparison for different transverse initial locations, upstream riser is flexible, the design streamwise spacing is 10 diameters.

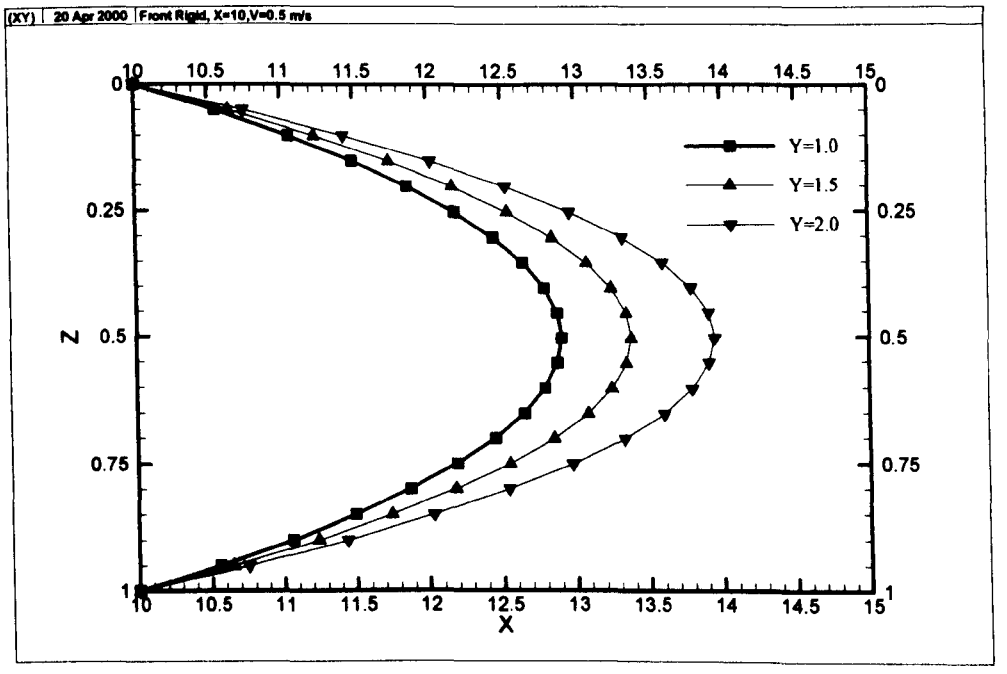

Figure 6.10 Streamwise deflection comparison for different transverse initial locations, upstream riser is rigid, the design streamwise spacing is 10 diameters.

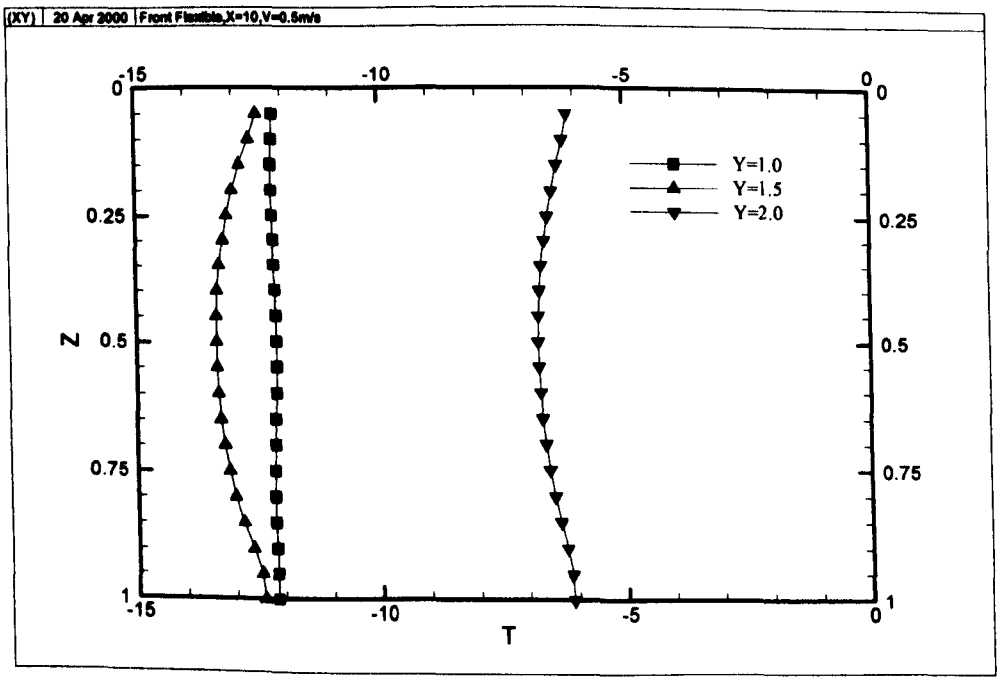

Figure 6.11 Comparison of deflection angle for different transverse locations when upstream riser is flexible, the design streamwise spacing is 10 diameters.

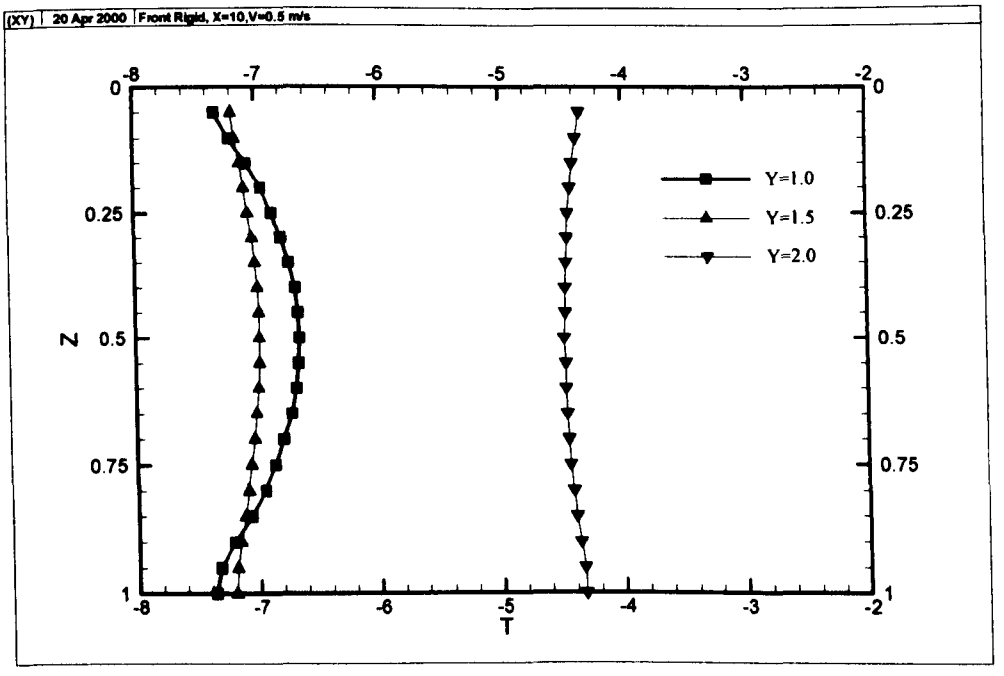

Figure 6.12 Comparison of deflection angle for different transverse locations downstream of a rigid riser, design streamwise spacing is 10 diameters.

6.3.7 *Effect of Top Tension* $\left(EI/T_{e0}l^2, m_e gl/T_{e0}, H_w\right)$

Top tension is a key factor in the design of marine risers. It determines the deflection of the riser and the bottom joint angle. Too high top tension will sacrifice effective payload on the floating production vessel. Sometimes, therefore, the buoyancy module is used to reduce the tension. On the other hand, too low tension can lead to buckling of the riser. According to the non-dimensional parameter listed in equation (6.13), the top tension is reflected in three parameters, among which top tension factor is an important parameter in riser design practice. As has been indicated here before, $EI/T_{e0}l^2$ shows the relation between bending stiffness and tension, when $EI/T_{e0}l^2 << 1$, the bending stiffness can be negligible and top tension will takes dominant role in determining the deflection of the riser. On the other hand, parameter H_w reflects the amplitude of the flow forces, which determines the amplitude of the deflection. In order to examine the role of the TTF (Top

Tension Factor), a sample calculation for the constant parameter of $EI/T_{e0}l^2 (<< 1)$ and H_w is made. Figure 6.13 shows that when tension is much larger than weight, the deflection distribution along the riser is nearly symmetrical, corresponding to a taut string. When the top tension factor is lower, the location at which the maximum deflection occurs moves towards to the lower part of the riser, due to the effect of weight, and the lower ball joint angle is significantly increased. The TTF determines the geometrical shape of the deflected riser.

Figure 6.14 shows the riser pair with constant weight. The only varying parameter is the top tension, i.e. all the three non-dimensional parameters related to top tension are varying. It is seen that the effect of the top tension is very significant, and the small tension not only gives a larger deflection, its maximum deflection location has also moved downwards due to its lowered TTF. Therefore, top tension plays a most significant role in the deflection of risers. High top tension can reduce the deflection and the deflection angle at lower ball joint angle.

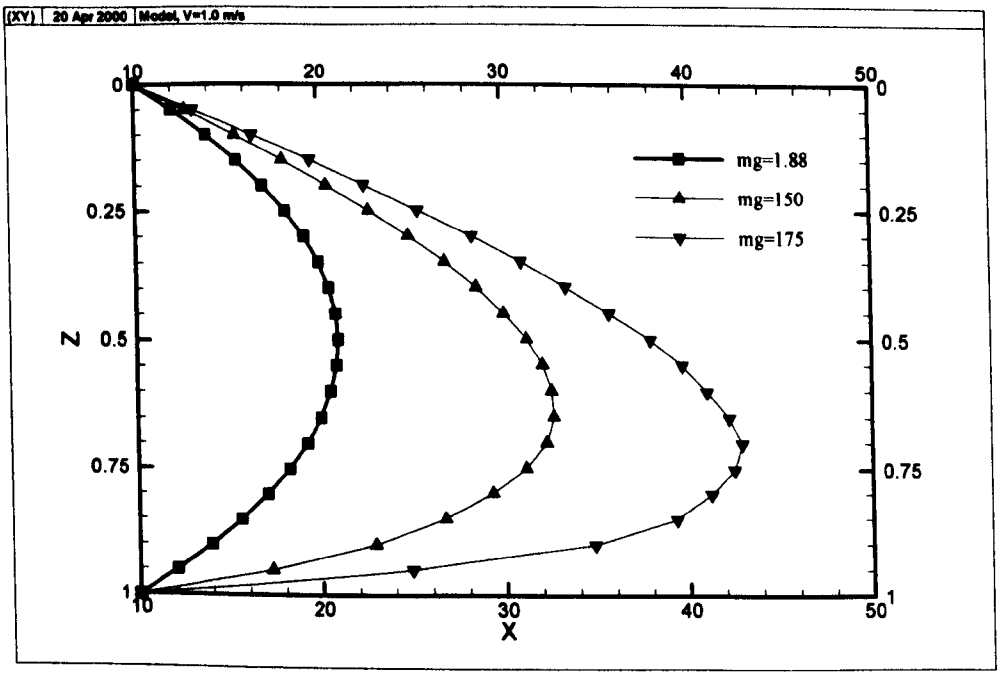

Figure 6.13 Effect of top tension factor on deflection of the riser downstream of a rigid riser.

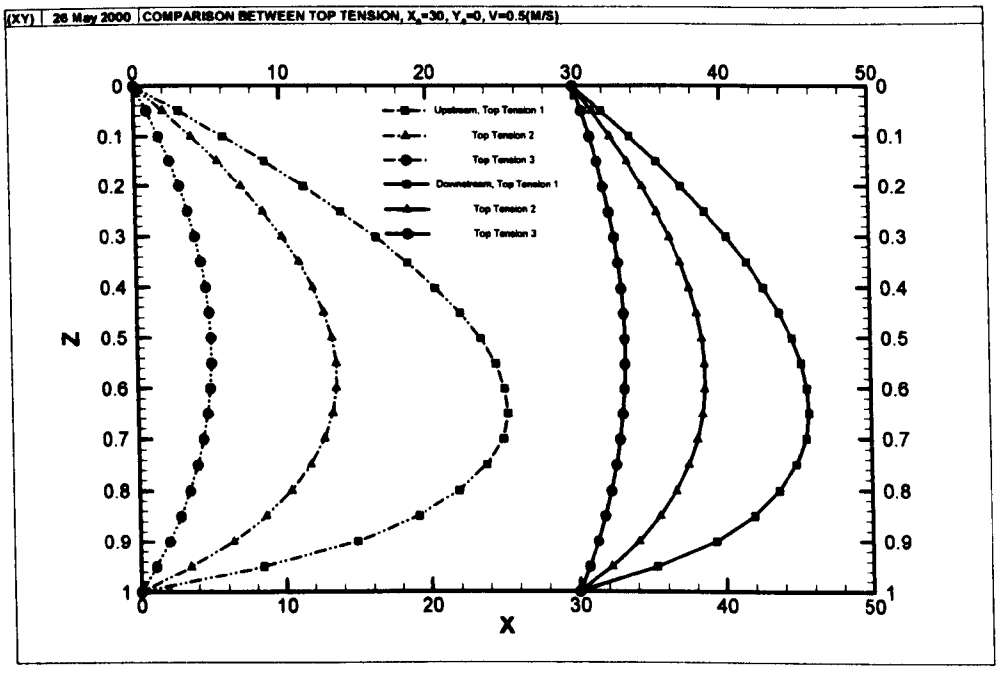

Figure 6.14 Effect of top tension on the deflection of risers, X_S=30, Y_S=0, V_0=0.5 (m/s). The three top tension factor refers to data in Table 6.5.

6.3.8 *Effect of Initial Spacing*

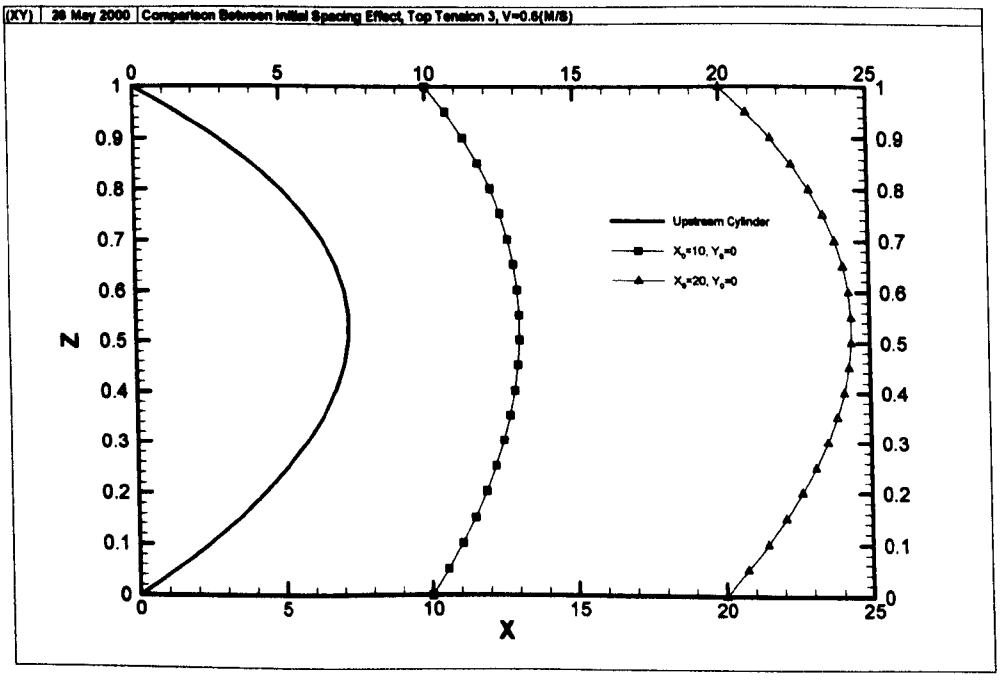

Figure 6.15 Effect of initial spacing between upstream and downstream riser.

Nearly all the sample investigations presented here so far are for a streamwise spacing of *10* diameters. Obviously, the interaction varies with the initial spacing. The closer the

spacing, the stronger the interaction. Figure 6.15 shows the scenario at flow velocity of *0.6 m/s*. With both risers sitting on the wake centreline downstream of a flexible riser. One is at spacing of *10* diameters and the other is at *20* diameters. It is clearly to be seen that the deflection of the far downstream riser is very much similar to the upstream riser, which means a weaker interaction than the smaller spaced riser. This spacing difference will lead to mainly quantitative differences for the interaction. The detailed quantitative effect will be identified in the following chapter.

6.3.9 Effect of Transverse Force

Transverse force is a factor easily overlooked during the design of marine risers and study of riser interactions. This is partly because the relative small amplitude of the transverse displacement and also the difficulty in the identification of transverse force magnitude. However it will give worries to engineers, especially when interaction between risers is an important concern. In the power transmission industry, it is a major factor, together with the drag forces that produce the phenomena of wake induced flutter. The analysis in the two-dimensional case also shows that stationary bifurcation is usually a combination of the contributions of both lift and drag force. A comparison is made here to clarify the role of the lift forces. Figures 6.16 and 6.17 show the difference between taking lift into consideration under flow velocity of *0.5m/s*. The comparison is made at X_s=*10*, Y_s=*1* and *2* respectively.

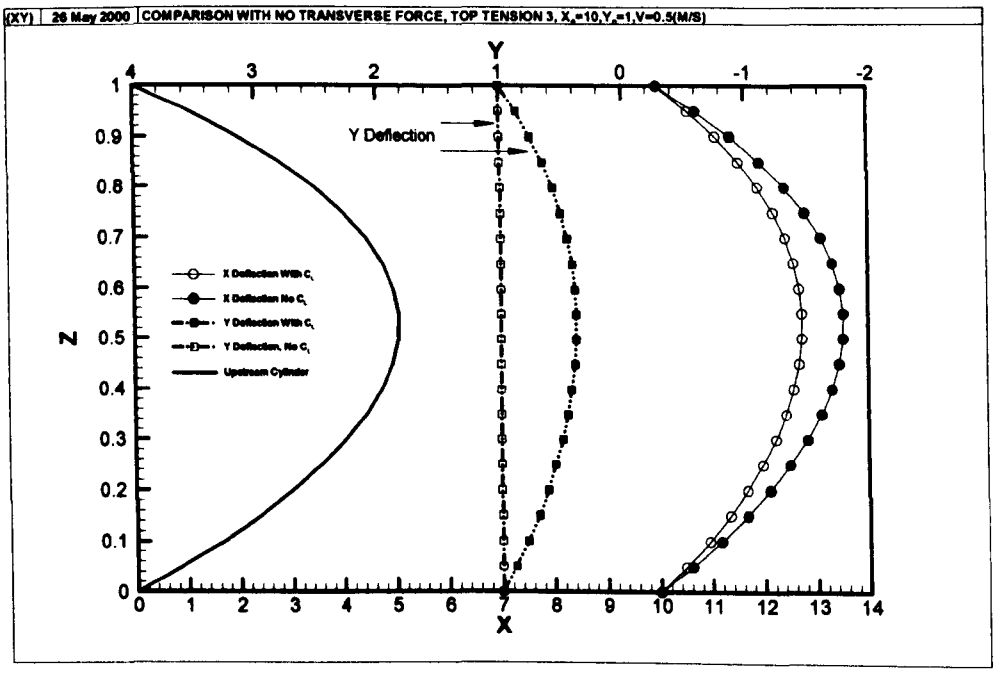

Figure 6.16 Comparison of deflection with and without transverse force taken into account, design spacing X_S=10, Y_S=1, at V_0=0.5 (m/s) with l_0=1332 (m), T_0=7.416×10^6 (N).

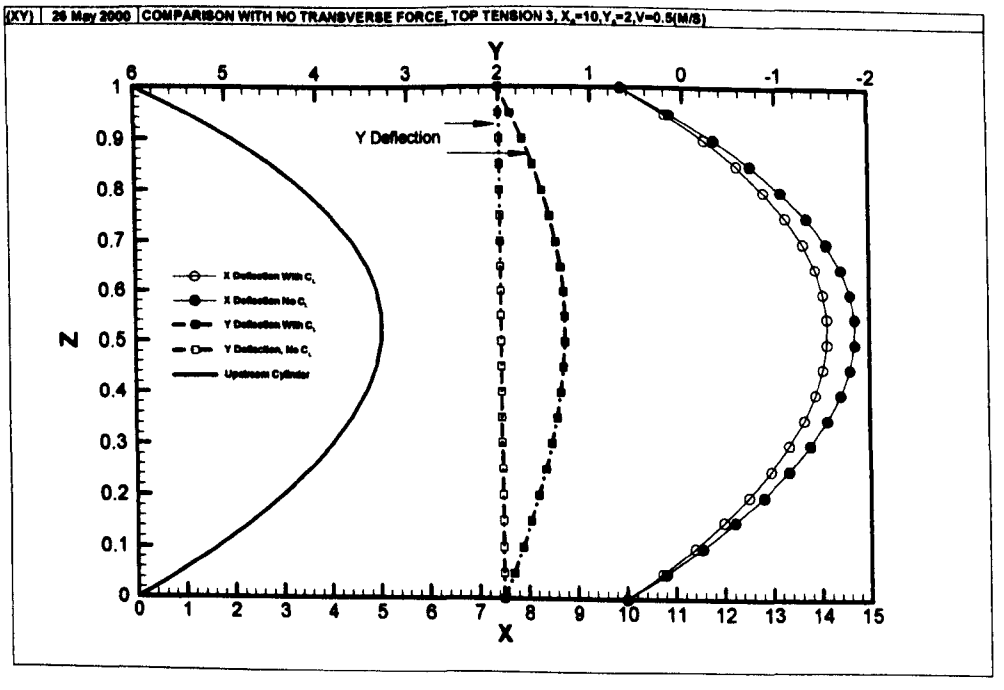

Figure 6.17 Comparison of deflection with and without transverse force taken into account, design spacing X_S=10, Y_S=2, at V=0.5 (m/s) with l_0=1332 (m), T_0=7.416×10^6 (N).

Clearly, the deflection in the y direction is different, as there is no y direction displacement if no lift force is considered. On the other hand, if the lift force is considered, then the y direction displacement is of the order of *1* diameter. For a flow velocity of around *0.5 m/s*, there is a noticeable difference in the deflection in x direction. For the velocity considered here, the difference is again of the order of *1* diameter, and the difference will be enlarged with the increase of flow velocity. The case which did not take the lift force into consideration, has a larger x direction displacement. This is because the effect of lift force pulls the riser towards wake centreline and the corresponding drag force is smaller. Inherently, this is a nonlinear behaviour related to the nature of the fluid force. As with the importance of the transverse location in the determination of the critical state, so also the consideration of the transverse force plays an important role in the investigation of riser interaction.

6.3.10 Discussion of Test Similarity

The discussion of the laboratory simulation of the statics of very large scale models has shown that plan 2 (as shown in table 6.2) is more feasible than the theoretically better plan 1. Inevitably, the violation of top tension factor will bring a deviation effect on the simulated statics of long riser interaction. Numerical comparison is carried out here to show the quantitative difference brought by such an un-simulated parameter. The hydrodynamic situation is also simulated. Figures 6.18 and 6.19 show the difference between the model result and full scale result for a riser sitting in the wake of a rigid riser and a flexible riser at velocity of V_0=*1.0 (m/s)* respectively.

From the figure it is seen that the difference between model and full scale behind the rigid riser is about *10* percent. However, when the upstream riser is flexible, the difference for the downstream riser is much smaller. It should be noted that when the interactions

between two risers are the main interest of the experiment, the relative spacing between two risers can be a primary interest. As shown in Figure 6.19, for the presented case, the difference is less than 10 percent. Such a deviation is acceptable for the experimental requirement. The model scale of present comparison is made based on *1:30* as listed on table 6.2, which is a significant large ratio.

Before closing the parametric study, it should be noted that throughout the present investigation, the small sag length ratio hypothesis has been constantly checked. It has been shown that the ratio of maximum deflection to the length of riser is well within the range of 1/8, in fact it is of the order of 10^{-3}. Therefore the simplification is fully justified within the present investigation.

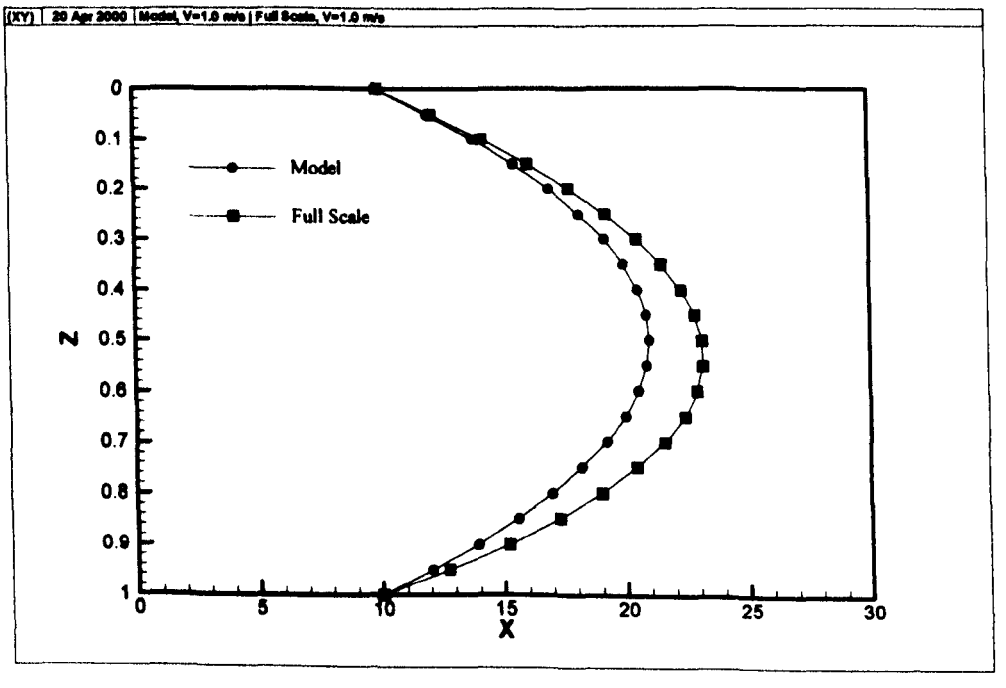

Figure 6.18 Comparison between model and full scale for both in rigid riser wake, V_0=1.0 (m/s), scale ratio λ=1:30, model: l_0=44.4 (*m*), T_0=8.24 (KN), full scale: l_0=1332 (*m*), T_0=7.416X10^6 (N).

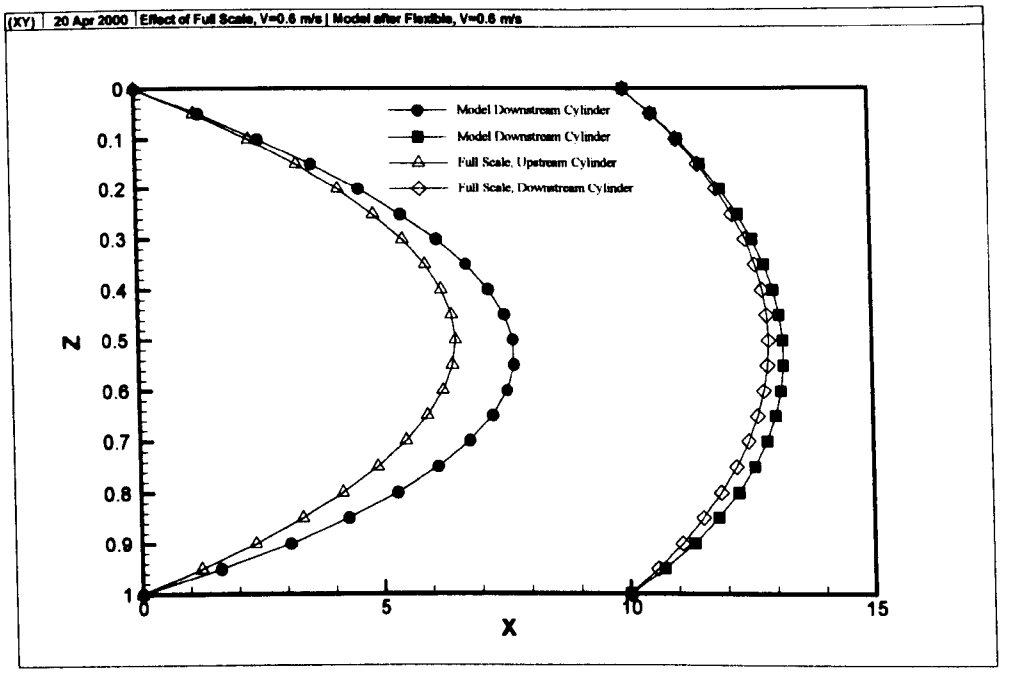

Figure 6.19 Comparison between model and full Scale for both in flexible riser wake (V_0=0.6 m/s). model: l_0=44.4 (m), T_0=8.24 (KN), full scale: l_0=1332 (m), T_0=7.416×10^6 (N).

6.4 Summaries

Numerical computation for two marine risers under time-averaged force action has been carried out by the modal superposition method. The program produced here was validated against the published API data. Based upon parametric study about two marine risers, conclusions are drawn as follows:

1. Effect of wake is important in determining the deflection of the downstream risers, particularly when the risers are getting longer as oil and gas development is moving into deeper waters. The amplitude of riser deflection is comparable with the normal design clearance between risers.

2. To appropriately account for the effect of an upstream riser is very important when the downstream riser is under static analysis. Where the upstream riser is rigid, the deflection of downstream riser differs significantly from when there is a flexible

upstream riser. Care must be taken in conducting riser interaction experiments if simplifying the upstream riser as rigid.

3. Even when the streamwise displacement reaches more than 10 diameters for a riser of 2000 diameters long, the variation in the vertical distance between top and bottom is small and negligible.

4. Even though the fluid forces are three-dimensional, the deflected riser is nearly within a plane. The angle of the deflection is strongly dependent on the location of the riser in the wake.

5. The effect of the top tension factor is a very important factor in determining the amplitude and shape of the deflection. Bending stiffness is negligible in identifying the amplitude of deflection for deepwater risers.

6. Parameter H_w reflects the relation between hydrodynamic transverse loading and the axial tension, it is an important similarity parameter in determine the riser displacement.

7. The model experiment to simulate the interaction of two very long risers is difficult. The similarity plan to use full scale flow velocity while neglecting the top tension factor (Plan 2 as listed in table 6.1) could be a better option.

Chapter VII

CONTINUATION AND STABILITY ANALYSIS FOR A PAIR OF MARINE RISERS

7.1 Introduction

7.1.1 General Remarks

The interaction between two cylinders in two-dimensional spaces shows that under certain flow conditions for specified two cylinders arrangements, there can be more than one equilibrium point for the downstream cylinder. Following on from the previous chapter, the following questions need to be answered for the investigation of interaction between two marine risers:

- How many equilibrium states are there for a specified arrangement of two risers and flow conditions?
- Are all the equilibrium states stable?
- When and how can two risers collide with each other if it is possible?
- What is the effect of top tension factor, initial spacing, flow velocity etc. on the equilibrium state?

To answer these questions, continuation and stability analysis is required. As shown in Chapter IV, the continuation can identify the multiple equilibrium states. However, because the analysis has moved from two-dimensional space to three-dimensional space, ordinary differential equations have been replaced by partial differential equations to describe the dynamics of the system. Necessary numerical procedures need to be taken to change the partial differential equations into a multiple finite degree of freedom system, so that the continuation can be implemented.

No previous investigations into the interaction between two marine risers have systematically adopted the approach of continuation, although possible collisions between marine risers have been recognised (Huse 1993). It is the view of this thesis that, to explain the mechanism of possible collision between two risers and to accurately identify critical states, such a specialised analysis is needed. This chapter deals with the identification of multiple equilibrium states and the critical state before collision.

7.1.2 Method Used in This Work

Continuing with the modal superposition method, the dynamic system for a riser located in the wake of another is investigated by the continuation method together with stability analysis. The continuation is based on the control parameter of pseudo arc length, and stability is analysed using the discretised system in a modal co-ordinate system through eigenvalue evaluation at individual equilibrium states. Because of the implication of the engineering applications, stability analysis was focused on the first and second mode eigenvalues.

7.2 Theoretical Formulation

7.2.1 Problem specification

Compared to Chapter VI, the objective here is to seek all the equilibrium states of the specified system, and to analyse the stability of the corresponding dynamic system.

Therefore, the system for the equilibrium states is the same as the one used in Chapter VI. Additionally, a linearised dynamic system around the above equilibrium states is supplemented for the stability analysis.

Based on the assumption of small lateral displacement both in streamwise direction and cross-flow direction compared to the riser length, the linearised dynamic system for a three-dimensional riser sitting in the wake of another at equilibrium $X = X_0(Z)$, $Y = Y_0(Z)$ is written as (Krolikowski & Gay, 1980, Furnes, 2000):

$$\begin{cases} \dfrac{\partial^2 u}{\partial t^2} + \dfrac{c}{m}\dfrac{\partial u}{\partial t} + \dfrac{EI}{ml_H^4}\dfrac{\partial^4 u}{\partial Z^4} - \dfrac{1}{ml_H^2}\dfrac{\partial}{\partial Z}\left[(T_{e0} - m_e g l_H Z)\dfrac{\partial u}{\partial Z}\right] \\ -\dfrac{EA}{ml_H^2}\left(\dfrac{d^2X}{dZ^2}\dfrac{dX}{dZ}\dfrac{\partial u}{\partial Z} + \dfrac{d^2X}{dZ^2}\dfrac{dY}{dZ}\dfrac{\partial v}{\partial Z}\right) \\ = \dfrac{\rho UD}{2m}\left[-2C_D\dfrac{\partial u}{\partial t} + C_L\dfrac{\partial v}{\partial t} + U\left(C_{DX}u + C_{DY}v\right)\right] \\ \\ \dfrac{\partial^2 v}{\partial t^2} + \dfrac{c}{m}\dfrac{\partial v}{\partial t} + \dfrac{EI}{ml_H^4}\dfrac{\partial^4 v}{\partial Z^4} - \dfrac{1}{ml_H^2}\dfrac{\partial}{\partial Z}\left[(T_{e0} - m_e g l_H Z)\dfrac{\partial v}{\partial Z}\right] \\ -\dfrac{EA}{ml_H^2}\left(\dfrac{d^2Y}{dZ^2}\dfrac{dX}{dZ}\dfrac{\partial u}{\partial Z} + \dfrac{d^2Y}{dZ^2}\dfrac{dY}{dZ}\dfrac{\partial v}{\partial Z}\right) \\ = \dfrac{\rho UD}{2m}\left[-2C_L\dfrac{\partial u}{\partial t} - C_D\dfrac{\partial v}{\partial t} + U\left(C_{DX}u + C_{DY}v\right)\right] \end{cases} \tag{7.1}$$

Here,

u, v: Inline and cross-flow displacement deviated from the equilibrium position respectively, which has been non-dimensionalised by the riser length

$m = m_s + m_a$: Mass per unit length, including m_s, the mass of structure and the fluid inside the riser and m_a, the fluid added mass

c: Structural damping

t : Time

The definitions of other parameters are the same as in previous Chapter.

At the equilibrium state, $X = X_0(Z)$, $Y = Y_0(Z)$, the following conditions hold,

$$\begin{cases} \dfrac{EI}{l_H^2}\dfrac{d^4X}{dZ^4} - \dfrac{d}{dZ}\left[(T_{e0} - m_e g Z l_H)\dfrac{dX}{dZ}\right] = F_{x0}\cdot l_H \\ \dfrac{EI}{l_H^2}\dfrac{d^4Y}{dZ^4} - \dfrac{d}{dZ}\left[(T_{e0} - m_e g Z l_H)\dfrac{dY}{dZ}\right] = F_{y0}\cdot l_H \end{cases} \tag{7.2}$$

Here, F_{x0}, F_{y0} : Fluid loading in x and y directions when the riser is located at its equilibrium of (X_0, Y_0).

The boundary conditions of the system are defined as both ends of the riser being supported in a pinned-pinned way, i.e.

$$\begin{cases} X = Y = u = v = 0 \\ \dfrac{\partial^2 X}{\partial Z^2} = \dfrac{\partial^2 Y}{\partial Z^2} = \dfrac{\partial^2 u}{\partial Z^2} = \dfrac{\partial^2 v}{\partial Z^2} = 0 \end{cases} \tag{7.3}$$

(at Z=*0 and* Z=1)

7.2.2 Solution Procedures

The modal superposition method is used in this chapter to carry out the continuation and stability analysis, by introducing the modal shape function,

$$\begin{cases} X(Z) = \sum_{r=1}^{\infty} a_r\phi_r & UC_D = \sum_{r=1}^{\infty} f_{Dr}\phi_r & UC_L = \sum_{r=1}^{\infty} f_{Lr}\phi_r \\ Y(Z) = \sum_{r=1}^{\infty} b_r\phi_r & U^2C_{DX} = \sum_{r=1}^{\infty} f_{DX,r}\phi_r & U^2C_{LX} = \sum_{r=1}^{\infty} f_{LX,r}\phi_r \\ \tilde{u} = \sum_{r=1}^{\infty} c_r\phi_r & U^2C_{DY} = \sum_{r=1}^{\infty} f_{DY,r}\phi_r & U^2C_{LY} = \sum_{r=1}^{\infty} f_{LY,r}\phi_r \\ \tilde{v} = \sum_{r=1}^{\infty} d_r\phi_r & \phi_r = \sin(r\pi Z) & \end{cases} \tag{7.4}$$

Substituting (7.4) into (7.1), multiplying ϕ_s on both sides of the equation, and integrating (7.1) both sides for Z from 0 to 1, after some mathematical manipulation, the dynamic system can be written as:

$$
\begin{cases}
\dot{c}_s = X_s \\
\dot{X}_s = -\dfrac{c}{m}X_s - \dfrac{\rho D}{m}\sum\limits_{r=1}^{N}\sum\limits_{k=1}^{N} X_r f_{Dk} w_{r,k,s} + \dfrac{\rho D}{2m}\sum\limits_{r=1}^{N}\sum\limits_{k=1}^{N} Y_r f_{Lk} w_{r,k,s} \\
\quad + \dfrac{\rho D}{2m}\left(\sum\limits_{r=1}^{N}\sum\limits_{k=1}^{N} c_r f_{DX,k} w_{r,k,s} + d_r f_{DY,k} w_{r,k,s}\right) \\
\quad + \dfrac{m_e}{m}\sum\limits_{k=1}^{N}\left(\dfrac{g}{l_H}(s\pi)^2 C_{sk} c_k - \dfrac{g}{l_H}(s\pi) D_{sk} c_k\right) - \dfrac{(s\pi)^2}{ml_H^2}\left[\dfrac{EI(s\pi)^2}{l_H^2} + T_{e0}\right] c_s \\
\quad + \dfrac{EA}{ml_Z^2}\sum\limits_{k=1}^{N}(g_{sk} c_k + h_{sk} d_k) \\
\dot{d}_s = Y_s \\
\dot{Y}_s = -\dfrac{c}{m}Y_s - \dfrac{\rho D}{m}\sum\limits_{r=1}^{N}\sum\limits_{k=1}^{N} X_r f_{Lk} w_{r,k,s} - \dfrac{\rho D}{2m}\sum\limits_{r=1}^{N}\sum\limits_{k=1}^{N} Y_r f_{Dk} w_{r,k,s} \\
\quad + \dfrac{\rho D}{2m}\left(\sum\limits_{r=1}^{N}\sum\limits_{k=1}^{N} c_r f_{LX,k} w_{r,k,s} + d_r f_{LY,k} w_{r,k,s}\right) \\
\quad + \dfrac{m_e}{m}\sum\limits_{k=1}^{N}\left(\dfrac{g}{l_H}(s\pi)^2 C_{sk} d_k - \dfrac{g}{l_H}(s\pi) D_{sk} d_k\right) - \dfrac{(s\pi)^2}{ml_H^2}\left[\dfrac{EI(s\pi)^2}{l_H^2} + T_{e0}\right] d_s \\
\quad + \dfrac{EA}{ml_Z^2}\sum\limits_{k=1}^{N}(p_{sk} c_k + q_{sk} d_k)
\end{cases}
\tag{7.5}
$$

Here:

$$
C_{sk} = 2\int_0^1 Z\sin(k\pi Z)\sin(s\pi Z)dZ = \begin{cases} \dfrac{1}{2} & k = s \\ \dfrac{4ks}{\pi^2\left(s^2 - k^2\right)^2}\left[(-1)^{k+s} - 1\right] & k \neq s \end{cases}
$$

$$D_{sk} = 2\int_0^1 \sin(s\pi z)\cos(k\pi z)dz = \begin{cases} 0 & k = s \\ \dfrac{2s}{\pi}\left[\dfrac{1-(-1)^{k+s}}{s^2-k^2}\right] & k \neq s \end{cases}$$

$$w_{r,k,s} = \begin{cases} 0 & (k+r+s) \text{ is even number} \\ -\dfrac{1}{\pi}\left(\dfrac{1}{k+r+s} + \dfrac{1}{k-r-s} - \dfrac{1}{k+r-s} - \dfrac{1}{k-r+s}\right) & (k+r+s) \text{ is odd number} \end{cases}$$

$$g_{sk} = \frac{\pi^4}{4} kc_k \sum_{m=1}^{N} m^2 a_m \left(\sum_{\substack{r=-m+k-s \\ r\geq 1}}^{N} ra_r + \sum_{\substack{r=m+k+s \\ r\geq 1}}^{N} ra_r + \sum_{\substack{r=m-k+s \\ r\geq 1}}^{N} ra_r - \sum_{\substack{r=-m+k+s \\ r\geq 1}}^{N} ra_r - \sum_{\substack{r=-m-k+s \\ r\geq 1}}^{N} ra_r - \sum_{\substack{r=m-k-s \\ r\geq 1}}^{N} ra_r - \sum_{\substack{r=m+k-s \\ r\geq 1}}^{N} ra_r \right)$$

$$h_{sk} = \frac{\pi^4}{4} kc_k \sum_{m=1}^{N} m^2 a_m \left(\sum_{\substack{r=-m+k-s \\ r\geq 1}}^{N} rb_r + \sum_{\substack{r=m+k+s \\ r\geq 1}}^{N} rb_r + \sum_{\substack{r=m-k+s \\ r\geq 1}}^{N} rb_r - \sum_{\substack{r=-m+k+s \\ r\geq 1}}^{N} rb_r - \sum_{\substack{r=-m-k+s \\ r\geq 1}}^{N} rb_r - \sum_{\substack{r=m-k-s \\ r\geq 1}}^{N} rb_r - \sum_{\substack{r=m+k-s \\ r\geq 1}}^{N} rb_r \right)$$

$$p_{sk} = \frac{\pi^4}{4} kc_k \sum_{m=1}^{N} m^2 b_m \left(\sum_{\substack{r=-m+k-s \\ r\geq 1}}^{N} ra_r + \sum_{\substack{r=m+k+s \\ r\geq 1}}^{N} ra_r + \sum_{\substack{r=m-k+s \\ r\geq 1}}^{N} ra_r - \sum_{\substack{r=-m+k+s \\ r\geq 1}}^{N} ra_r - \sum_{\substack{r=-m-k+s \\ r\geq 1}}^{N} ra_r - \sum_{\substack{r=m-k-s \\ r\geq 1}}^{N} ra_r - \sum_{\substack{r=m+k-s \\ r\geq 1}}^{N} ra_r \right)$$

$$q_{sk} = \frac{\pi^4}{4} kc_k \sum_{m=1}^{N} m^2 b_m \left(\sum_{\substack{r=-m+k-s \\ r\geq 1}}^{N} rb_r + \sum_{\substack{r=m+k+s \\ r\geq 1}}^{N} rb_r + \sum_{\substack{r=m-k+s \\ r\geq 1}}^{N} rb_r - \sum_{\substack{r=-m+k+s \\ r\geq 1}}^{N} rb_r - \sum_{\substack{r=-m-k+s \\ r\geq 1}}^{N} rb_r - \sum_{\substack{r=m-k-s \\ r\geq 1}}^{N} rb_r - \sum_{\substack{r=m+k-s \\ r\geq 1}}^{N} rb_r \right)$$

Equation (7.5) is the dynamic system for the downstream riser in the modal co-ordinate system. Although the modal co-ordinates are in infinite numbers, based on the quick convergence characteristics of the system, normally only the lower order mode co-ordinates are important and need to be analysed. So is the eigenvalue of the dynamic system. In practical calculation, the summation over the modes can be truncated at N-th order, which makes the system into 4N-dimensional first-order ordinary differential equations. Experience in previous chapter show that N takes 6 is enough for statics. However, N needs to take 15 to 20 when stability analysis is conducted.

7.2.3 Continuation

The existence of multiple equilibrium states is the basic characteristic of nonlinear dynamic systems. According to the results found in Chapter IV, in two-dimensional space there can be more than one equilibrium state for a given condition of initial arrangement and flow velocity. In order to seek the multiple equilibrium states, the continuation technique has been applied. The given system is a 4N non-linear equations where N is the total mode number in the calculation. The parametric strategy will heavily rely on the method of arc length, because turning points are likely to occur. A weighted pseudo arc length strategy is used in this numerical analysis. The pseudo arc length is represented by the displacement of the mid-point of the riser and the flow velocity, expressed as follows:

$$ds = \sqrt{\beta\left[dx^2 + dy^2\right] + (1-\beta)dV^2} \tag{7.6}$$

Here β is the weight coefficient, which takes the value from 0 to 1.

In the expression in modal co-ordinate system, the arc length is expressed as:

$$ds = \sqrt{\beta\left[\left(\sum_{k=1}^{N}(a_k - a_k^{i-1})\phi_k\right)^2 + \left(\sum_{k=1}^{N}(b_k - b_k^{i-1})\phi_k\right)^2\right] + (1-\beta)dV^2} \tag{7.7}$$

Such an expression is physically intuitive, which gives the result for the position of the downstream riser at the middle point.

The selection of parameters β is the key to the success of the continuation process. The value of β reflects the relative importance of the flow velocity parameter or the displacement of the middle point of the riser. The experience of continuation in two-dimensional space shows that when the equilibrium point is near its maximum streamwise displacement, it is very sensitive to the streamwise deflection. At such states, more weight

should be given to the flow velocity, and β should take a small value. When the equilibrium is near its critical state, on the other hand, β should adopt a large value to avoid the sensitive relation to flow velocity that can cause the failure of the continuation. The numerical analysis in a three-dimensional space shows that extra care should be taken to realise a successful continuation.

In this investigation, again, the continuation is implemented by the predictor and correction two steps method. The difference from the two-dimensional investigation is that the present continuation is conducted in a higher dimensional space. A detailed description may found in Seydel (1994). The Akima interpolation has been applied in the predictor step, which provides a 3rd order spline curve along the control parameter of the arc length. The carrying out of such a method is straightforward, and the estimation provided by such a predictor is good enough for the corrector step to converge with the equilibrium point. The modified Powell hybrid algorithm and a finite-difference approximation to the Jacobian are used to solve the nonlinear system (More and others 1980).

7.2.4 Stability Analysis

For the differential equation(7.5), there are two ways to determine the stability of the equilibrium state.

One is the method of stability testing, literally to simulate the dynamic behaviour of the system, starting from a predefined state, which is near the equilibrium state, and to observe the behaviour over a long period of time. If the state is close enough to, or reaches, the equilibrium state, then the state is called stable. Such a method is always time consuming.

Another method is to cast the system into a discretised system, i.e. transform a continuous system into a multiple degrees-of-freedom system, such as from (7.1) to (7.5) derived

above. Such a system is an ordinary differential equation system. This makes it possible to use the concept of an eigenvalue system to investigate the stability of the system. This is the method applied in this investigation. The corresponding Jacobian matrix for the dynamic system (7.5) is shown in equation (7.9).

7.2.5 Continuation Procedure and Identification of Critical State

The continuation can be started from the statics analysis under a specified low flow velocity. Experience shows that the corresponding equilibrium state is often stable. Increasing the flow velocity along the arc by a prescribed arc length, the next equilibrium state is first estimated by the interpolation technique. For the very first step of the continuation, the first equilibrium is used directly as the estimated equilibrium in the predictor. The corrector is then used to seek the exact equilibrium. Step by step, the full chain of the equilibrium can be realised. At certain steps, adjustment of arc length weight factor is utilised if necessary. When the critical state (turning point) is met during the continuation, it is identified by solving an additional equation. The supplementary equation for the critical state is given by:

$$\frac{dX}{dV_0} = 0 \tag{7.8}$$

Here X directly takes the streamwise co-ordinate difference between the downstream riser and upstream riser, V_0 is the free stream velocity.

$$
\begin{Bmatrix}
\begin{bmatrix} \dot{c}_1 \\ \dot{c}_2 \\ \vdots \\ \dot{c}_N \end{bmatrix} \\
\begin{bmatrix} \dot{X}_1 \\ \dot{X}_2 \\ \vdots \\ \dot{X}_N \end{bmatrix} \\
\begin{bmatrix} \dot{d}_1 \\ \dot{d}_2 \\ \vdots \\ \dot{d}_N \end{bmatrix} \\
\begin{bmatrix} \dot{Y}_1 \\ \dot{Y}_2 \\ \vdots \\ \dot{Y}_N \end{bmatrix}
\end{Bmatrix} =
\begin{Bmatrix}
\begin{bmatrix} 0 & \cdots & 0 \\ \vdots & \ddots & \vdots \\ 0 & \cdots & 0 \end{bmatrix} & \begin{bmatrix} 1 & \cdots & 0 \\ \vdots & \ddots & \vdots \\ 0 & \cdots & 1 \end{bmatrix} & \begin{bmatrix} 0 & \cdots & 0 \\ \vdots & \ddots & \vdots \\ 0 & \cdots & 0 \end{bmatrix} & \begin{bmatrix} 0 & \cdots & 0 \\ \vdots & \ddots & \vdots \\ 0 & \cdots & 0 \end{bmatrix} \\
\begin{bmatrix} \dfrac{\rho D}{2m}\sum_{k=1}^{N} f_{DX,k} w_{r,k,s} + \dfrac{EA}{ml_H^2} g_{sr} \\ + \dfrac{m_e}{m}\dfrac{g}{l_H}\left[(s\pi)^2 C_{sr} - (s\pi) D_{sr}\right] \\ - \dfrac{(s\pi)^2}{ml_H^2}\left[\dfrac{EI(s\pi)^2}{l_H^2} + T_{e0}\right]\delta_{sr} \end{bmatrix}_{s,r} & \left[-\dfrac{c}{m}\delta_{sr} - \dfrac{\rho D}{m}\sum_{k=1}^{N} f_{Dk} w_{r,k,s}\right]_{s,r} & \begin{bmatrix} \dfrac{\rho D}{2m}\sum_{k=1}^{N} f_{DY,k} w_{r,k,s} \\ + \dfrac{EA}{ml_H^2} h_{sr} \end{bmatrix}_{s,r} & \left[\dfrac{\rho D}{2m}\sum_{k=1}^{N} f_{Lk} w_{r,k,s}\right]_{s,r} \\
\begin{bmatrix} 0 & \cdots & 0 \\ \vdots & \ddots & \vdots \\ 0 & \cdots & 0 \end{bmatrix} & \begin{bmatrix} 0 & \cdots & 0 \\ \vdots & \ddots & \vdots \\ 0 & \cdots & 0 \end{bmatrix} & \begin{bmatrix} 0 & \cdots & 0 \\ \vdots & \ddots & \vdots \\ 0 & \cdots & 0 \end{bmatrix} & \begin{bmatrix} 1 & \cdots & 0 \\ \vdots & \ddots & \vdots \\ 0 & \cdots & 1 \end{bmatrix} \\
\begin{bmatrix} \dfrac{\rho D}{2m}\sum_{k=1}^{N} f_{LX,k} w_{r,k,s} \\ + \dfrac{EA}{ml_H^2} p_{sr} \end{bmatrix}_{s,r} & \left[-\dfrac{\rho D}{m}\sum_{k=1}^{N} f_{Lk} w_{r,k,s}\right]_{s,r} & \begin{bmatrix} \dfrac{\rho D}{2m}\sum_{k=1}^{N} f_{LY,k} w_{r,k,s} + \dfrac{EA}{ml_H^2} q_{sr} \\ + \dfrac{m_e}{m}\dfrac{g}{l_H}\left[(s\pi)^2 C_{sr} - (s\pi) D_{sr}\right] \\ - \dfrac{(s\pi)^2}{ml_H^2}\left[\dfrac{EI(s\pi)^2}{l_H^2} + T_{e0}\right]\delta_{sr} \end{bmatrix}_{s,r} & \left[-\dfrac{c}{m}\delta_{sr} - \dfrac{\rho D}{2m}\sum_{k=1}^{N} f_{Dk} w_{r,k,s}\right]_{s,r}
\end{Bmatrix} \times
\begin{Bmatrix}
\begin{bmatrix} c_1 \\ c_2 \\ \vdots \\ c_N \end{bmatrix} \\
\begin{bmatrix} X_1 \\ X_2 \\ \vdots \\ X_N \end{bmatrix} \\
\begin{bmatrix} d_1 \\ d_2 \\ \vdots \\ d_N \end{bmatrix} \\
\begin{bmatrix} Y_1 \\ Y_2 \\ \vdots \\ Y_N \end{bmatrix}
\end{Bmatrix}
\tag{7.9}
$$

7.3 Numerical Results

The marine riser data taken for the investigation carried out in this chapter is mainly adopted from table 6.2, The 12" riser pair have length of 1332 meters and a top tension of 7.416×10^6 N (with top tension factor 3.28) unless otherwise explicitly stated. The analysis is carried out for the downstream riser located both on wake centreline and off-wake centreline.

7.3.1 Wake Centreline

Figures 7.1 to 7.3 show the continuation and stability analysis results for the two marine risers separated with X_s=8, 10 and 15 diameters respectively. Among these, Figures 7.1(a), 7.2(a) and 7.3(a) show the positions of middle point of the two risers, i.e. the displacement at Z=0.5. Figures 7.1(b, c), 7.2(b, c) and 7.3(b, c) are the results of the eigenvalues showing the stability at the corresponding equilibrium states, and the rest show the geometrical shape of the two risers under corresponding flow velocity. It is seen that both upstream riser and downstream riser move towards downstream with the increase of the flow speed, because of their increased drag force in the direction of flow. However, the variation of movement of the upstream riser, which is almost proportional to the square of the flow speed, is larger than the downstream one. Such a difference in the variation of deflection with flow velocity brings the two risers closer. When the flow speed reaches a certain level, depending on the top tension and initial spacing of the two risers, two equilibrium states start to exist. One is located downstream and the other is very close to the upstream riser. The latter is usually unstable. When flow velocity is increased further, the downstream riser first reaches a maximum downstream position D, after which the downstream riser begins to move towards upstream if the flow speed is further increased. Eventually, the two equilibrium states merge at an increased flow velocity. Such a position, M, is unique at

which only one equilibrium exists, and is defined as the critical state for the riser pair interaction. There will be no equilibrium if the flow velocity is further increased.

Examining the variation of eigenvalues with the flow speed, Figure 7.1(b) gives the first mode eigenvalues while Figure 7.1(c) shows the second mode eigenvalues. It is seen that when the flow velocity is zero, the pair of the eigenvalues has no real parts when the damping of the system is neglected. When velocity is increased until it reaches the state H, the first mode starts to turn into an unstable state, via a Hopf bifurcation. Such a characteristic depends on the initial spacing and the riser's top tension. Although the details of the variation of eigenvalues differ from situation to situation, the qualitative trends for every case discussed here are same. The existence of a Hopf bifurcation point H only occurs when spacing between two risers is relatively small, and it disappears when spacing becomes large. On the other hand, under this situation, for 10 diameters spacing, even here there is a Hopf bifurcation. The state is very close to the critical state, which implies that the Hopf bifurcation is not important practically. The variation of second mode eigenvalues shows that, often, the eigenvalue pair transverse the imaginary axis through the Hopf bifurcation at point H_2, Nevertheless, H_2 always occurs at a higher flow velocity than the corresponding flow velocity for the point at which the first mode loses its stability. Such a result shows that the first mode of the riser is the most vulnerable to the wake induced instability. This is consistent with the experimental observation that the wake-induced oscillation is a low frequency motion. Also, the results shown here are consistent with the two-dimensional results. Figures 7.2(d) and 7.3(d) are the deflected geometrical shape of risers at flow velocity close to the critical speed. It can be seen that the two coexisting equilibrium states can both bend towards downstream. Figures 7.1(d), 7.2(e) and 7.3(e) show the geometrical shape of the two risers when flow velocity is just above the state where the additional equilibrium states start to appear. Often the two equilibrium

states have two different deflection directions, one towards downstream which is stable. The other one has its middle part bent towards the upstream riser because of the negative drag force, and the latter one is unstable.

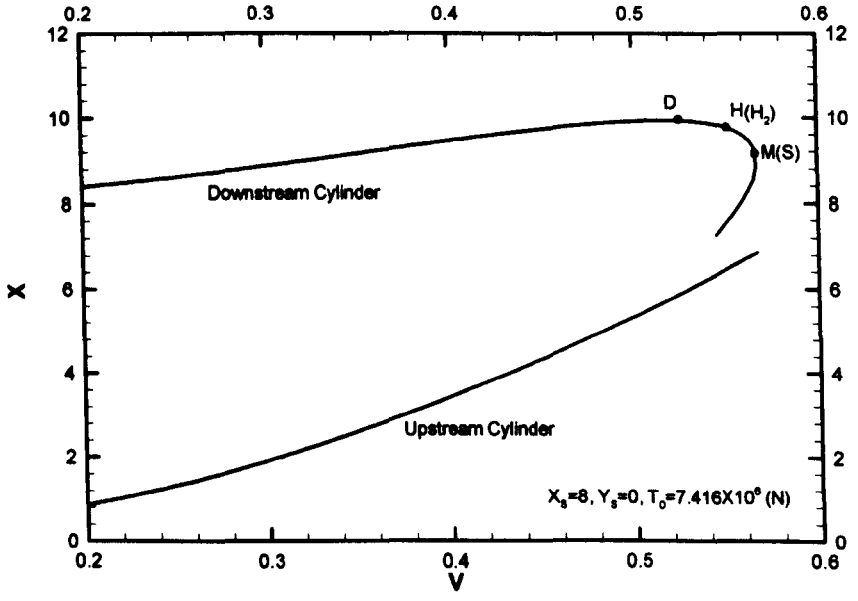

Figure 7.1(a) Displacement of the middle point of the riser.

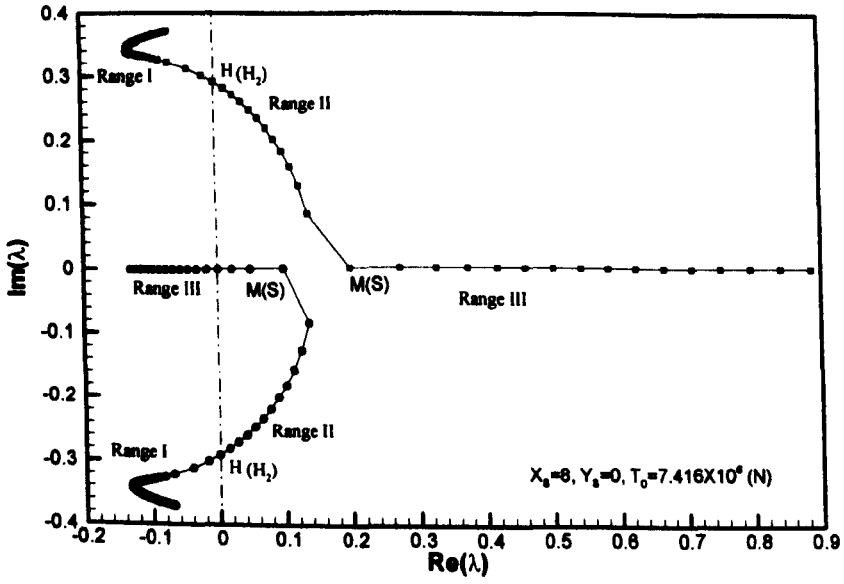

Figure 7.1(b) Variation of first mode eigenvalue with the flow velocity.

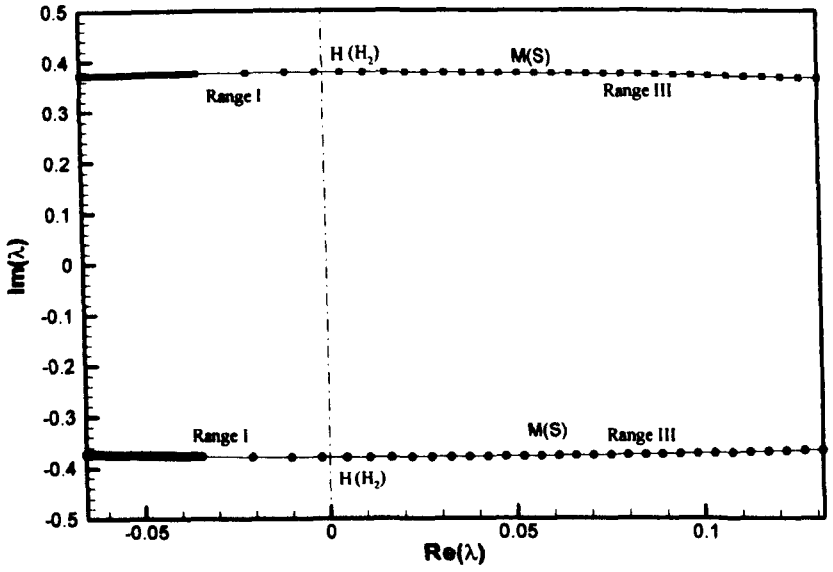

Figure 7.1(c) Variation of second mode eigenvalue with flow velocity.

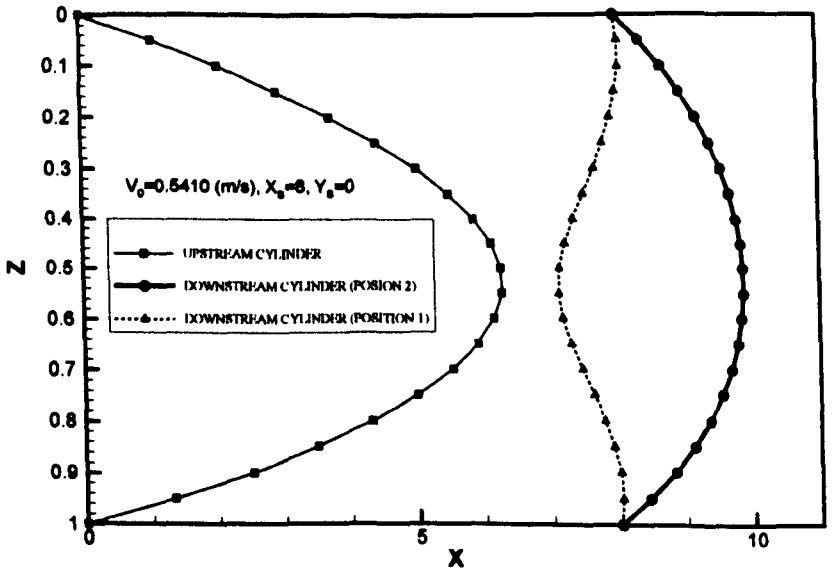

Figure 7.1 (d) Geometrical shape under the current of V_0=0.5410 (m/s).

Figure 7.1 Continuation for the riser pair with design spacing of X_S=8, Y_S=0, T_0=7.416X10^6 (N)

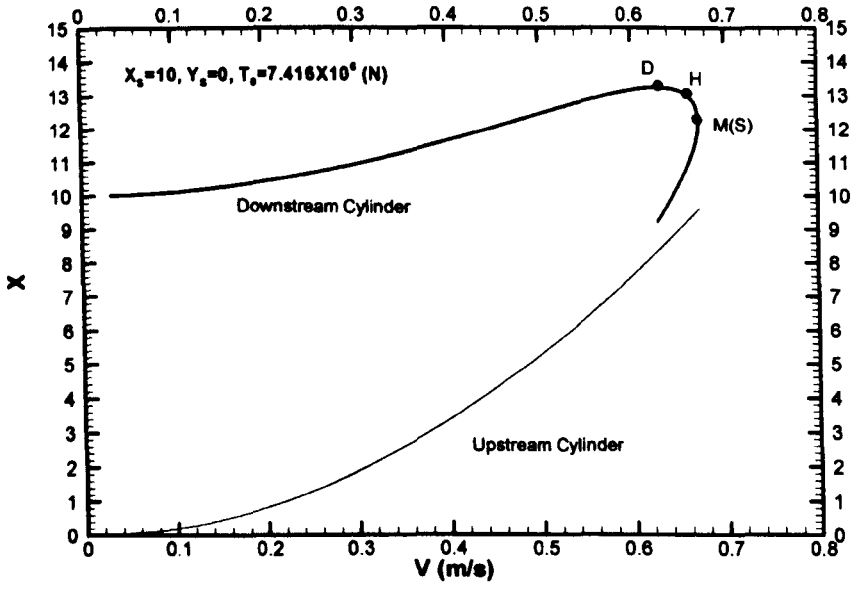

Figure 7.2(a) Displacement of the middle point of the riser.

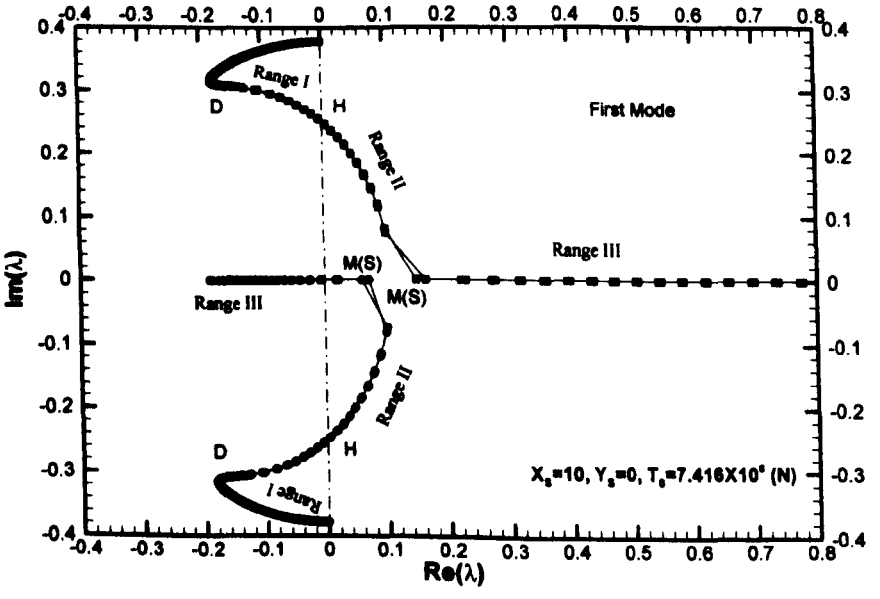

Figure 7.2(b) Variation of first mode eigenvalue with the flow velocity.

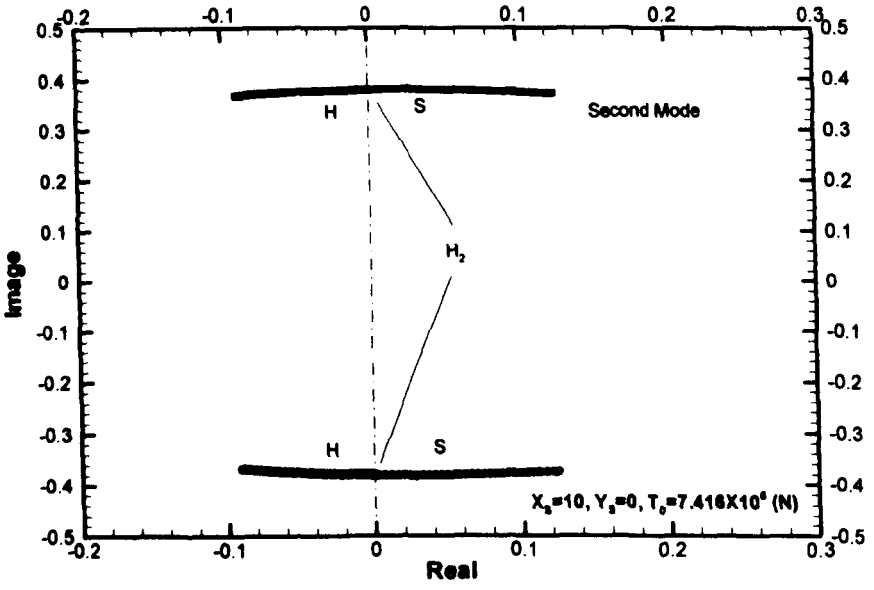

Figure 7.2(c) Variation of second mode eigenvalue with flow velocity.

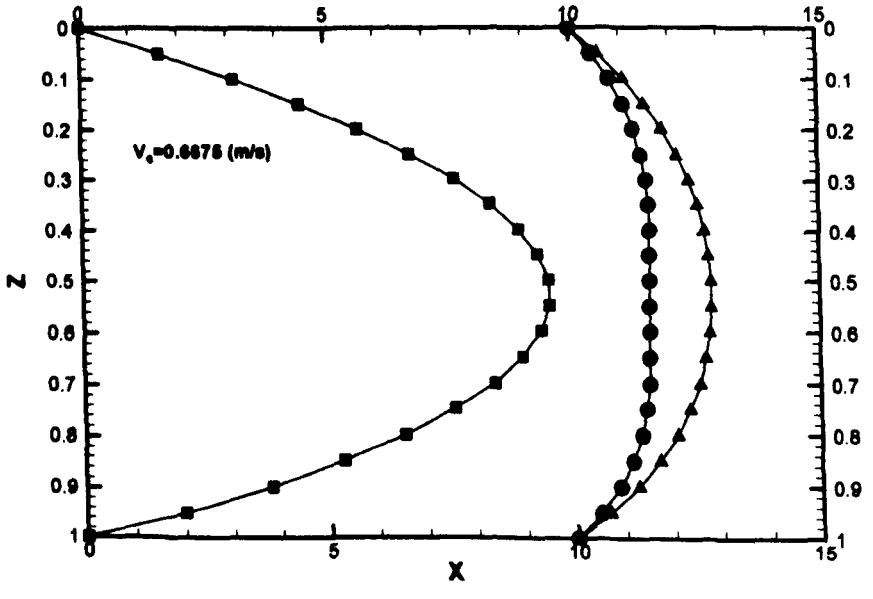

Figure 7.2(d) Geometrical shape of the two risers under the current of V_0=0.6675 (m/s).

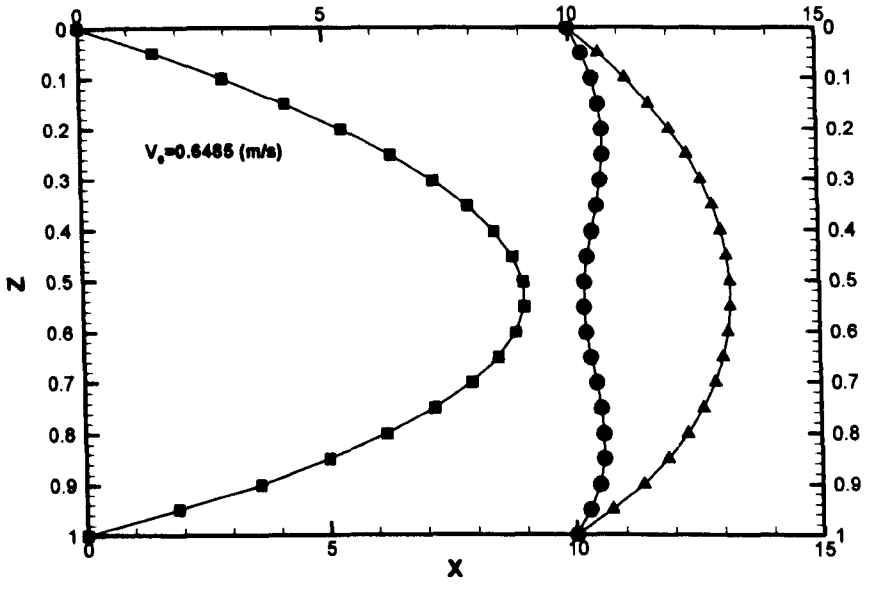

Figure 7.2(e) Geometrical shape under the current of V_0=0.6485 (m/s).

Figure 7.2 Continuation for the riser pair with design spacing of X_S=10, Y_S=0, T_0=7.416×10^6 (N)

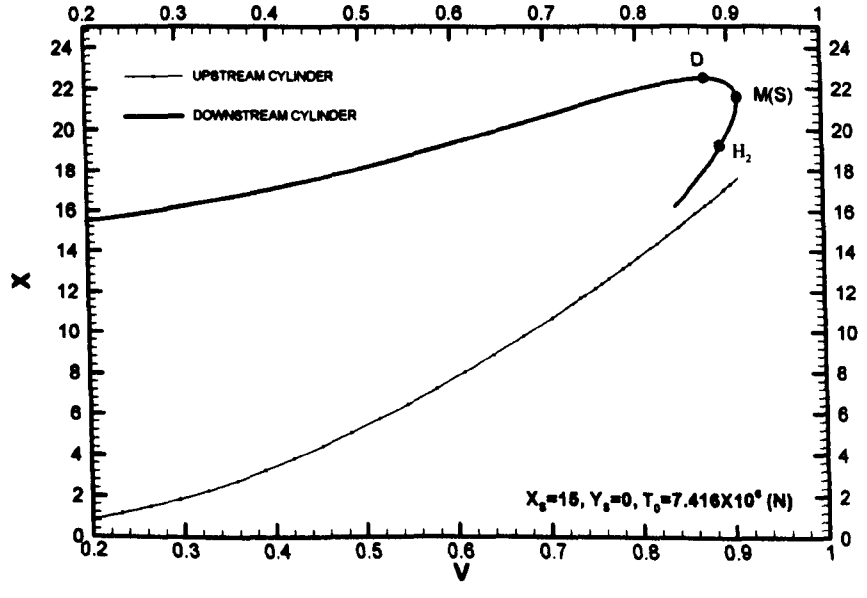

Figure 7.3(a) Displacement of the middle point of the risers.

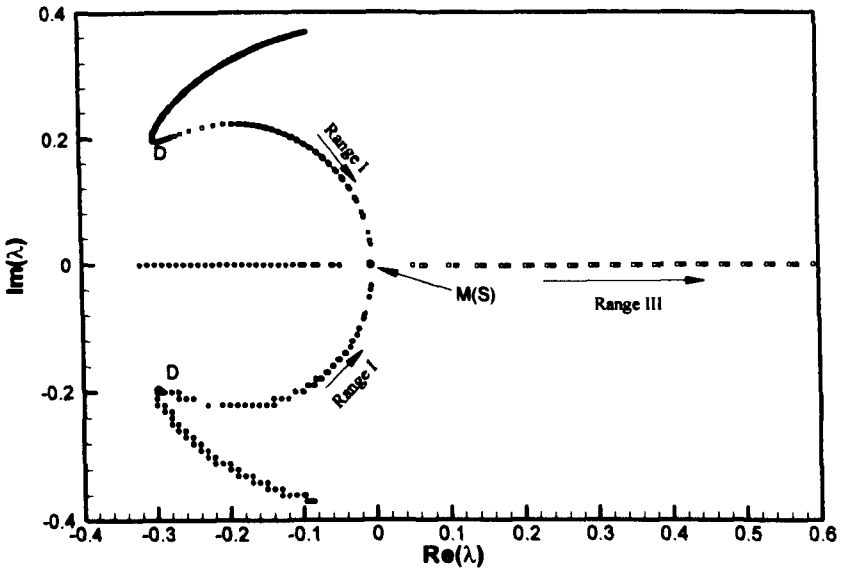

Figure 7.3(b) Variation of first mode eigenvalue with the flow velocity.

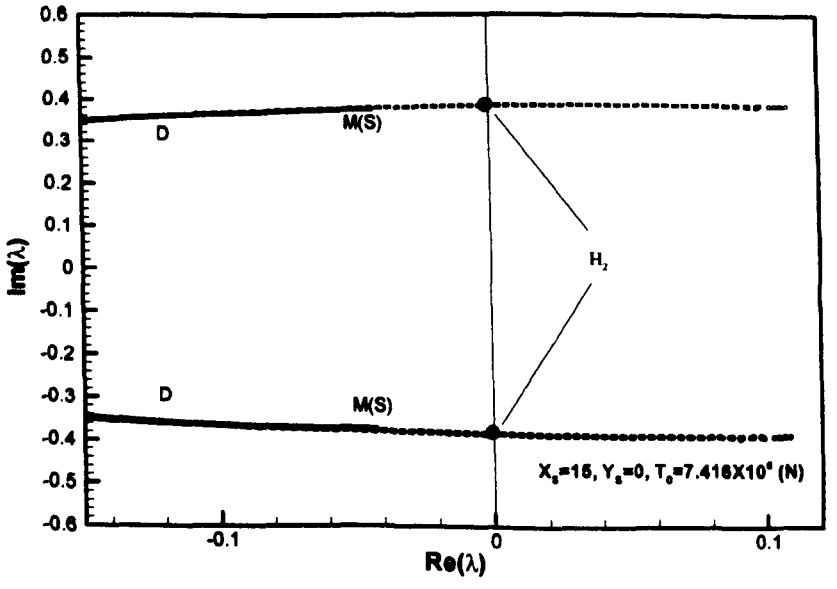

Figure 7.3(c) Variation of second mode eigenvalue with flow velocity.

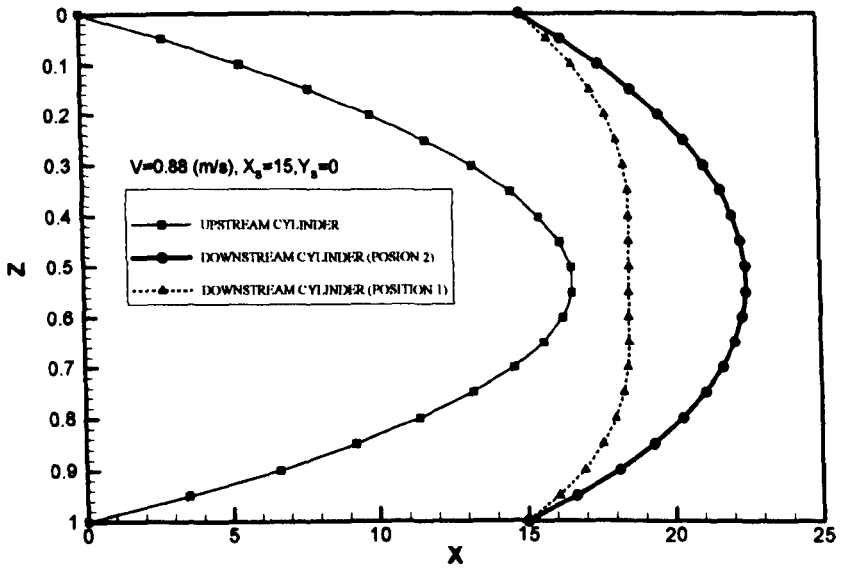

Figure 7.3(d) Geometrical shape under the current of V_0=0.8800 (m/s).

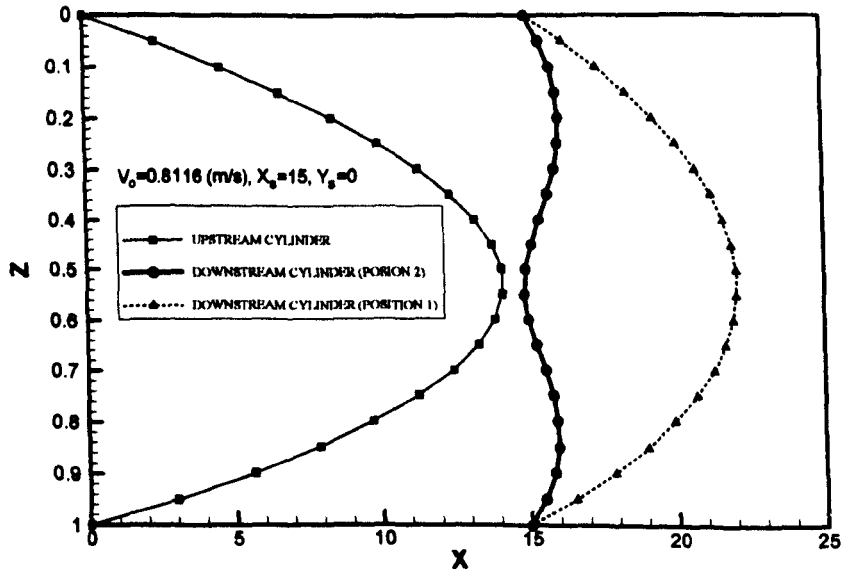

Figure 7.3(c) Geometrical shape under the current of V_0=0.8116 (m/s)

Figure 7.3 Continuation for the riser pair with design spacing of X_S=15, Y_S=0, T_0=7.416X10^6 (N).

7.3.1.1 Explanation of Double Equilibrium States

The continuation analysis for two tandem arranged risers shows that there is a critical state. When flow velocity is larger than the critical state, there will be no equilibrium, which implies that two risers are likely to collide with each other when flow velocity is high enough. The understanding of the critical point M can be made via the two-dimensional case by the following sketches 7.4.

Figure 7.4(a) shows that, when the flow velocity is low, there is only one equilibrium state, which is stable. The linear relation between displacement and mechanical force represents the recovery force of the riser and the slope of the line represents the stiffness of the spring in two dimensions. Such a slope will not change, as long as the non-linearity of spring stiffness is not introduced into the present analysis. Figure 7.4(b) shows that with the increase of flow velocity, two equilibrium states begin to emerge, with one stable and the other unstable. When the flow velocity is increased further, a critical state with only one equilibrium state emerges which highlights the M point in the three-dimensional case. At this point, not only the mechanical spring force balances the fluid force, but the stiffness of the spring is equal to the equivalent fluid force spring stiffness. When the flow velocity is larger than this critical flow velocity, there may not be any physical equilibrium states, which simply means that the downstream riser can not find balanced positions. It is envisaged that after this flow velocity, the collision between the downstream riser and upstream riser will be inevitable. From these figures and the interpretation from the two-dimensional case, when flow velocity exceeds the one corresponding to the critical position M, collision between the two risers is likely to occur. Further referring to figure 7.4, the slope of the linear spring recovery force reflects the relationship of the tension within riser and the riser displacement in three-dimensional case. A change in the tension will alter the slope and hence the critical point of the intersection between the linear line and the drag force curve. Also because the magnitude of the fluid force changes with the flow velocity,

the initial spacing difference will eventually change the critical points as well. Thus the critical state is closely related to the tension of the riser as well as the initial spacing. The quantitative relationship will be explored in a later section.

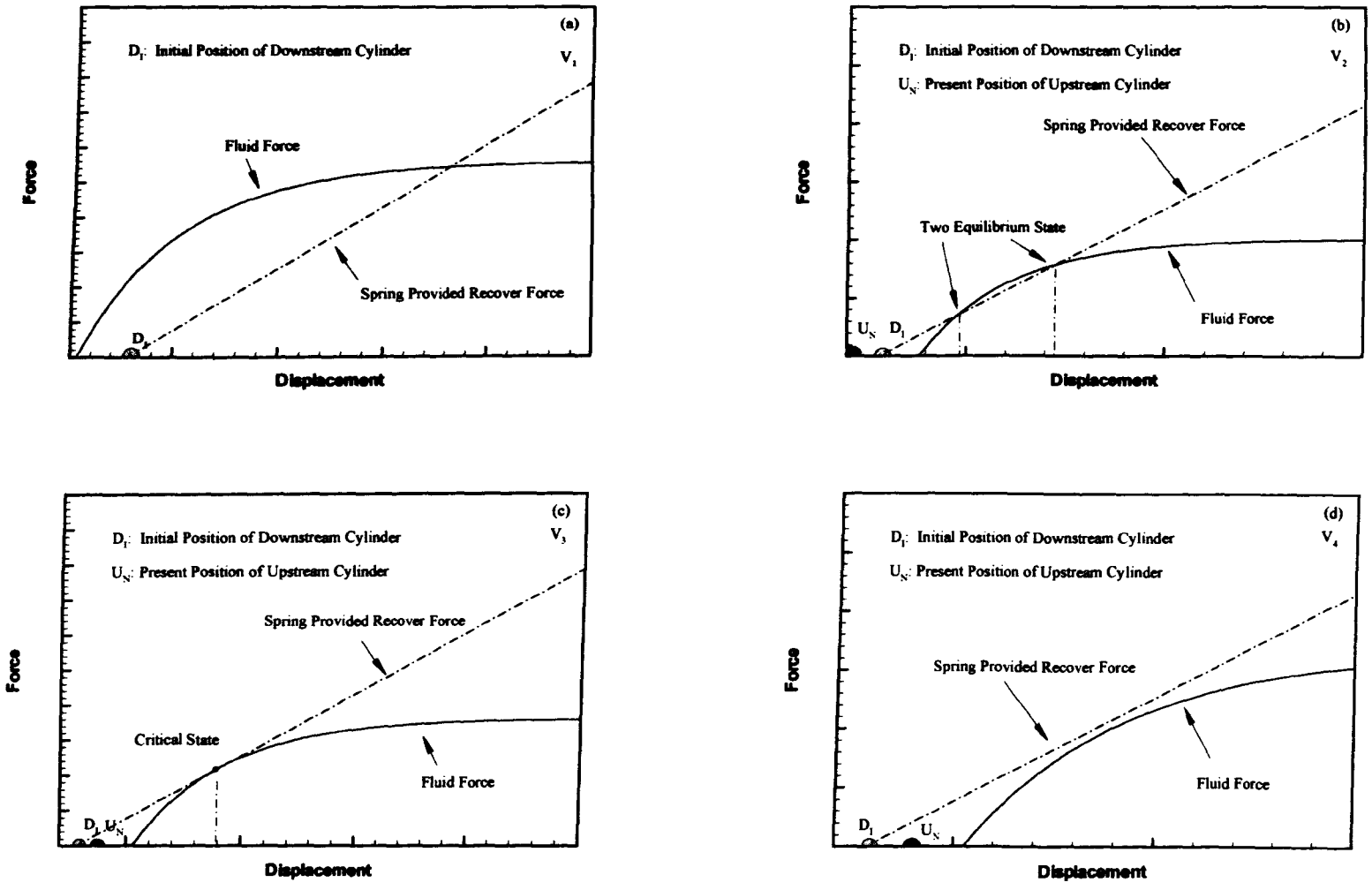

Figure 7.4 A schematic figure of the critical state and double equilibrium states.

7.3.1.2 Discussion of API Recommendation and Huse's Work

The most recognised criteria to date regarding the onset of two risers to collide were proposed by Huse (1993) as recommended by API (1998). Compared to the method utilized in present study, Huse only account for the streamwise drag force while take no account of the cross flow forces. In the meantime, Huse only studied the situation when two risers are arranged in tandem. According to Huse's explanation of riser collision criteria, collision starts when the spacing between two risers is equal to the riser diameter. In other words, the two risers already contact with each other at critical state. Figure 7.5 is a redrawing of the sketch of the collision between two risers (Huse, 1993). According to the present analysis, the recommendation is only a special case when the spacing corresponding to the critical state is equal to one diameter. According to the present study, the critical state is directly related to the stability change and reflected by a turning point on the continuation diagram. Therefore, the conclusion of the API recommendation is inaccurate. The drawback of such a recommendation lies in the following:

1. The inaccuracy of the identification of critical state. The recommended critical state corresponds to the state when an additional equilibrium state starts to appear. The new emerged equilibrium state is in fact unstable. The real critical state occurs at a significantly higher flow velocity. For example, in Figure 7.3(a), the critical flow velocity identified by Huse's method would be 0.84 m/s rather than present 0.91 m/s. The difference is about 10 percent for this case. Such a difference can be even larger depending on the top tension factor and design spacing between the two risers.

2. It is misleading on the understanding of the dynamics at the post-critical state. According to the recommendation, it is easily speculated that if collision occurs,

the intermittent collision is caused by vortex-induced vibration, such as in the recent research conducted by (Halse, 2000; Kaasen et al, 2000; Magne et al, 2001). All of these assumed the vortex-induced vibration is the main contribution to the riser collision. They do not account for the real impact effect when two risers collide, neither do they explain the large amplitude low frequency movement of the downstream riser as observed in the experiment.

Therefore, their recommendations have not shed any light on the real possible effects after the critical states. From the present analysis it is seen that after collision starts, further contact is unavoidable. Rather than vortex induced vibration, the non-stop intermittent collision is essentially caused by the disappearance of equilibrium states. For these reasons, the present analysis presents a much clearer picture of the mechanism between two risers' collision, and can identify more accurately the critical state just before the collision occurs.

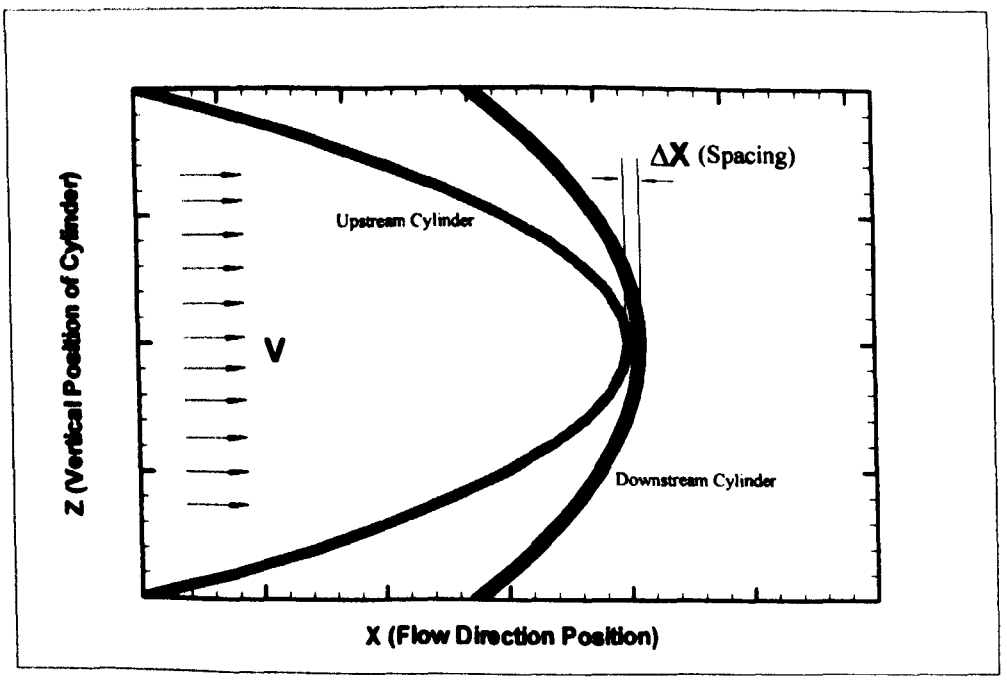

Figure 7.5 Schematic of the mechanism of riser collision (Sketch redrawn from Huse, 1993), when ΔX=D, riser collision occurs.

7.3.2 Off Wake Centreline Scenarios

7.3.2.1 Inner Wake Position

Figures 7.6 to 7.7 are results for the downstream riser, initially located off the wake centreline. The results presented here are for a typical streamwise spacing of *10* diameters, with the transverse location of *0.5* to *2.0* diameters respectively. The top tension factor is taken as *3.28*. It is seen that due to the effect of the transverse force, with the increase of flow velocity, the downstream riser is pulled towards the wake centreline while it moves towards downstream. When the flow velocity reaches a certain level, similar to the situation on the wake centreline, the downstream riser will have two equilibrium states, with one located downstream and the other close to the upstream riser. Further increase in the flow velocity means that the downstream riser will reach a maximum deflection state D, after which the downstream riser's deflection will be decreased if flow velocity is further increased. A critical state exists under which two equilibrium states merge. This is a turning point on the continuation curve of deflection with regard to the control parameter of flow velocity. When the flow velocity is larger than the critical flow velocity, there will be no physical equilibrium.

Figures 7.6(a), 7.7(a) show the details of such variation. The stability analysis shows that the variation of eigenvalue is similar to that when the downstream riser is located on the wake centreline. Also, for the case of streamwise spacing of 10 diameters, there is a Hopf bifurcation point H, immediately before the critical state M. However, the two states H and M are so close to each other that the existence of Hopf bifurcation is hardly distinguishable.

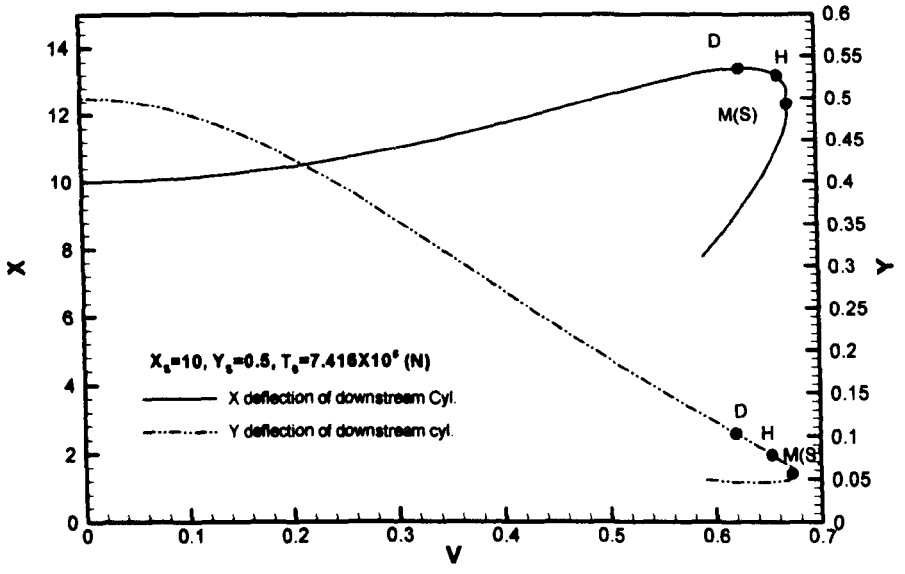

Figure 7.6(a) Displacement of the middle point of the upstream and downstream risers.

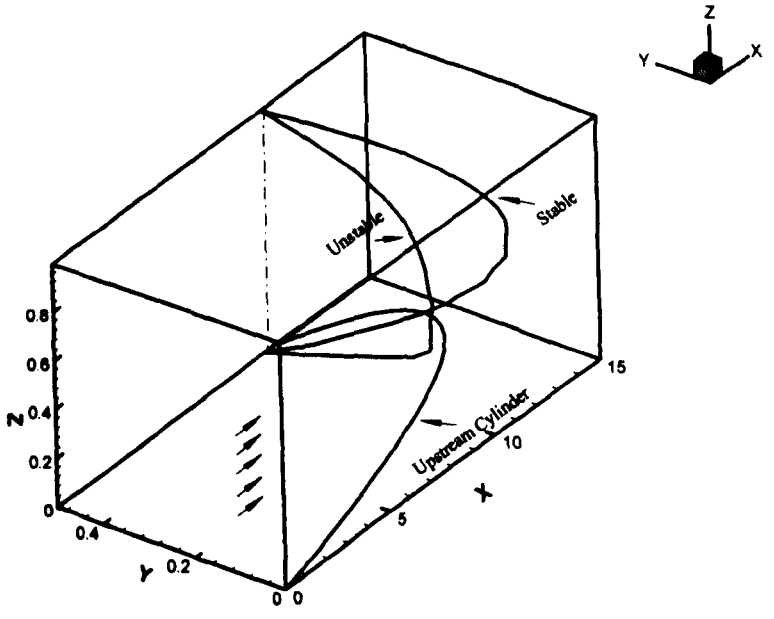

Figure 7.6(b) Geometrical shape of two risers at flow velocity of V_0=0.6 (m/s).

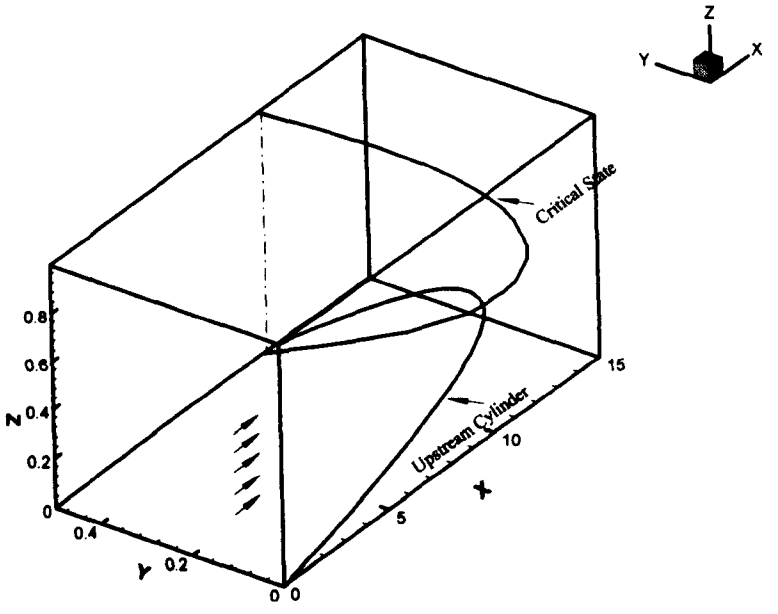

Figure 7.6(c) Geometrical shape of 12" riser pair at critical state (Only one equilibrium state).

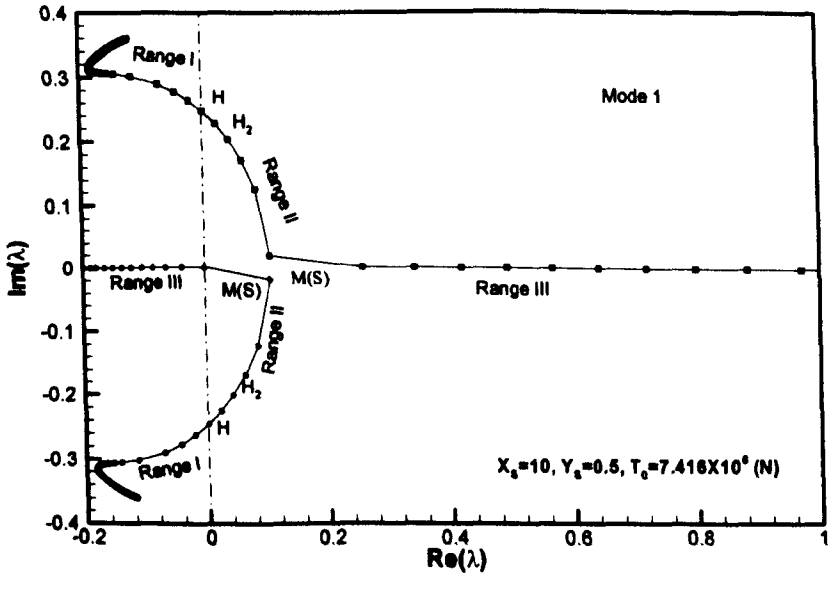

Figure 7.6(d) Variation of first mode eigenvalue with the flow velocity.

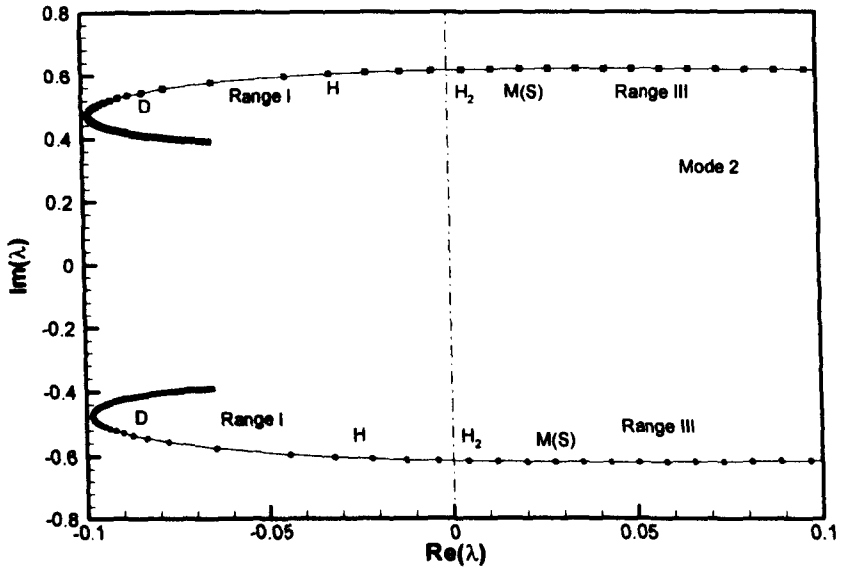

Figure 7.6(e) Variation of second mode eigenvalue with flow velocity.

Figure 7.6 continuation analysis for the riser pair with X_S=10, Y_S=0.5, TTF=3.28 .

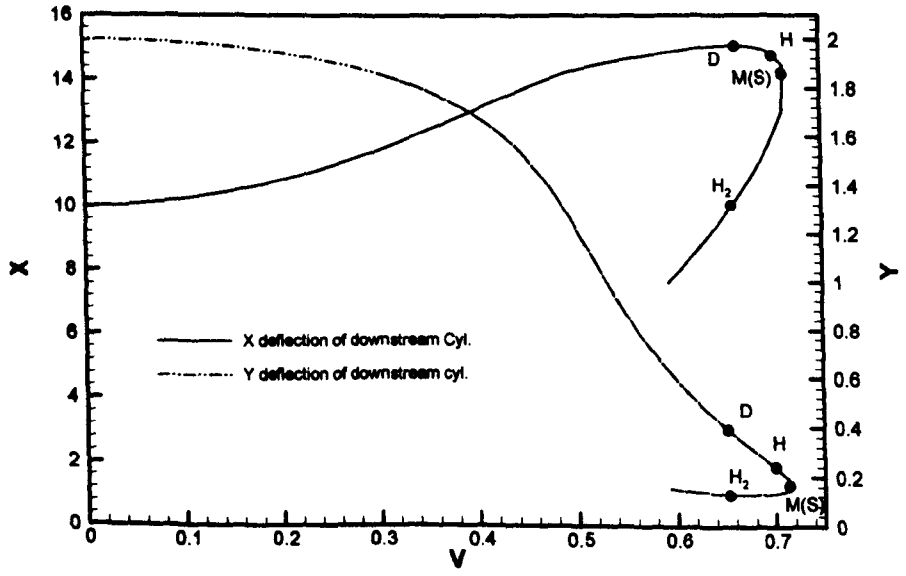

Figure 7.7(a) Displacement of the middle point of the upstream and downstream risers.

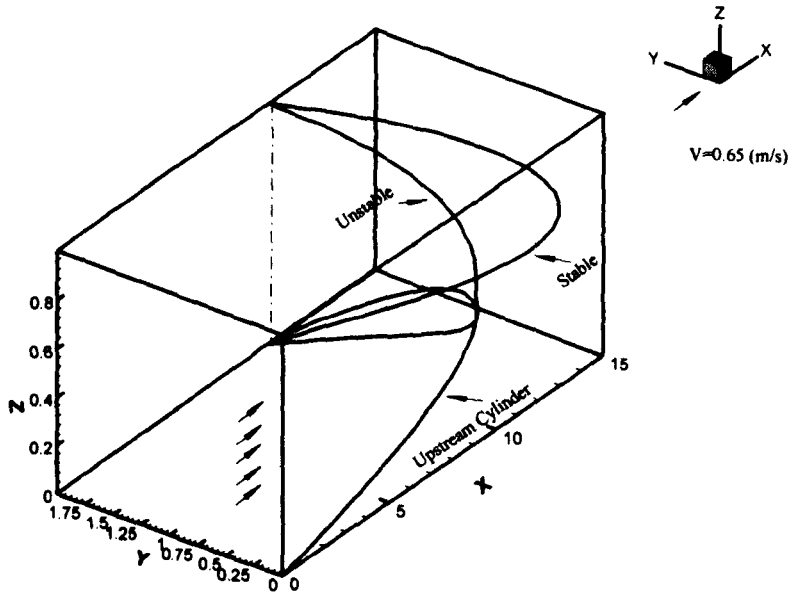

Figure 7.7(b) Geometrical shape of two risers at flow velocity of V_0=0.650 (m/s).

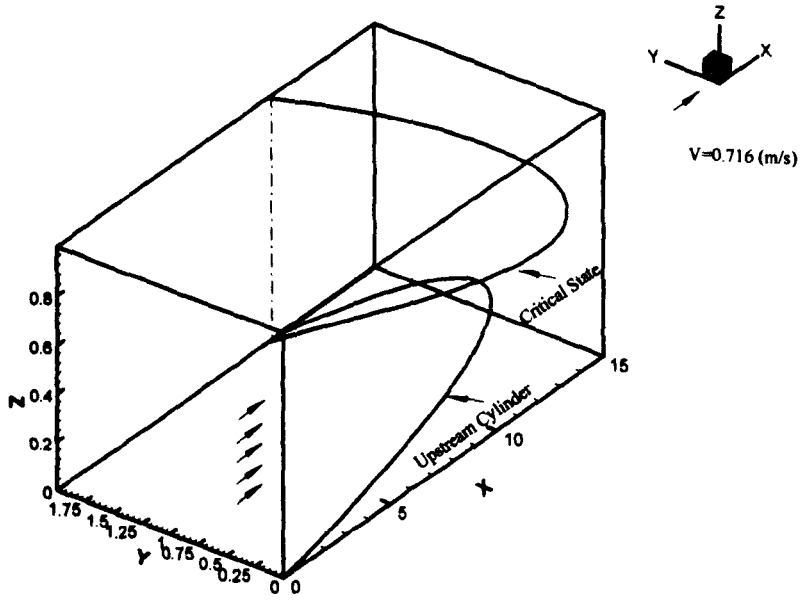

Figure 7.7(c) Geometrical shape of two risers at flow velocity of V_0=0.716 (*m/s*), critical state.

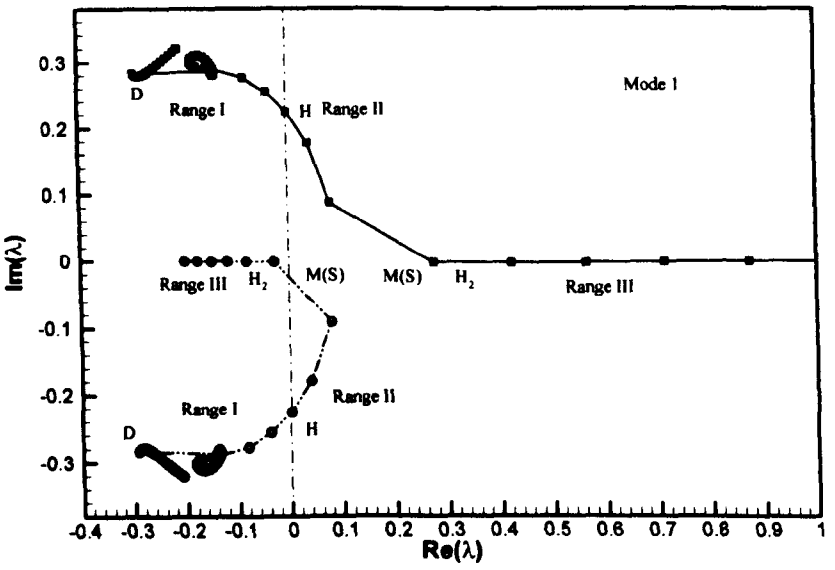

Figure 7.7(d)) Variation of first mode eigenvalue with the flow velocity.

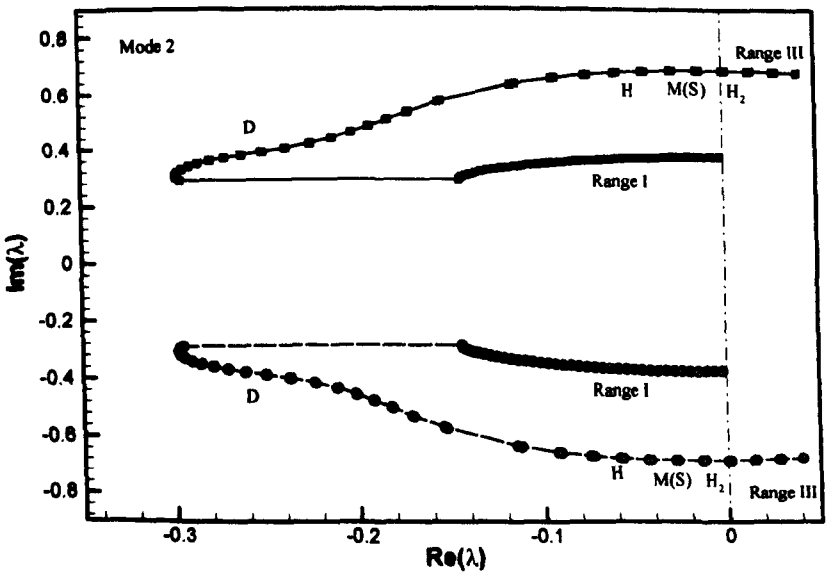

Figure 7.7(e) Variation of second mode eigenvalue with flow velocity.

Figure 7.7 continuation analysis for the riser pair with X_S=10, Y_S=2, TTF=3.28 .

7.3.2.2 Outer Wake Position

Figures 7.8 Figure 7.9 are results for streamwise location of 10 diameters, with transverse location of *2.5* and *3.0* diameters, which are the locations for the wake induced flutter that can often occur in power transmission lines. In all these cases, the top tension factor is kept as 3.28. It is seen from figure 7.8(a, b) and 7.9(a, b) that, with the increase of flow velocity, the downstream riser is pulled towards the wake centreline while it moves towards downstream. However, when the flow velocity reaches a certain value, depending on the top tension and initial arrangement, the downstream riser will have two, three and four equilibrium states respectively, depending on the flow velocity. Nevertheless, there will be no equilibrium at all ultimately when the flow velocity is high enough. In the course of the variation from four equilibrium states to none, the process of equilibrium pair merger is the same as occurred in two-dimensional space, i.e. the downstream pair and upstream pair converged one after another, the order depending on the initial arrangement. Figures 7.8(c, d) also show the variation of different mode coordinates with flow velocity, the definition of modal co-ordinates is shown in equation (7.4). It shows that all the individual mode coordinates have the same variation course as the riser middle point displacement. All of them have monotonic variation with regard to flow velocity. Figure 7.8(e) shows the geometry of each individual equilibrium state when the flow velocity is 0.685 m/s. Under such a flow velocity, there are four equilibrium states altogether for the downstream riser, only two of which are stable, i.e. the most downstream one and the second to the most upstream one shown in Figure 7.8(e). Figure 7.9 shows a case when the downstream riser is located near the wake boundary initially. As in the case shown in Figure 7.8, there is a maximum of four equilibrium states. The critical state is located at the merger point of the downstream equilibrium pair, which is significantly larger in flow velocity than the merger point of upstream equilibrium pair. Figure 7.10 shows the variation of the equilibrium for different initial arrangements. It is seen that for the same streamwise spacing of 10 diameters, with the increase of initial transverse distance, the maximum number of equilibrium states is increased from two to four. All the variations are continuous with regard to flow velocity and transverse distance. Figure

7.10(c) shows the variation of critical velocity with the transverse distance. It shows that the critical flow velocity is smallest on wake centreline for the same streamwise design spacing, and that the variation of critical flow velocity with transverse spacing is insensitive when the downstream riser is placed near the wake centerline. Rapid increase of the critical velocity occurs when the downstream riser is located near wake boundary, a location where multiple equilibrium states exist for certain flow velocity.

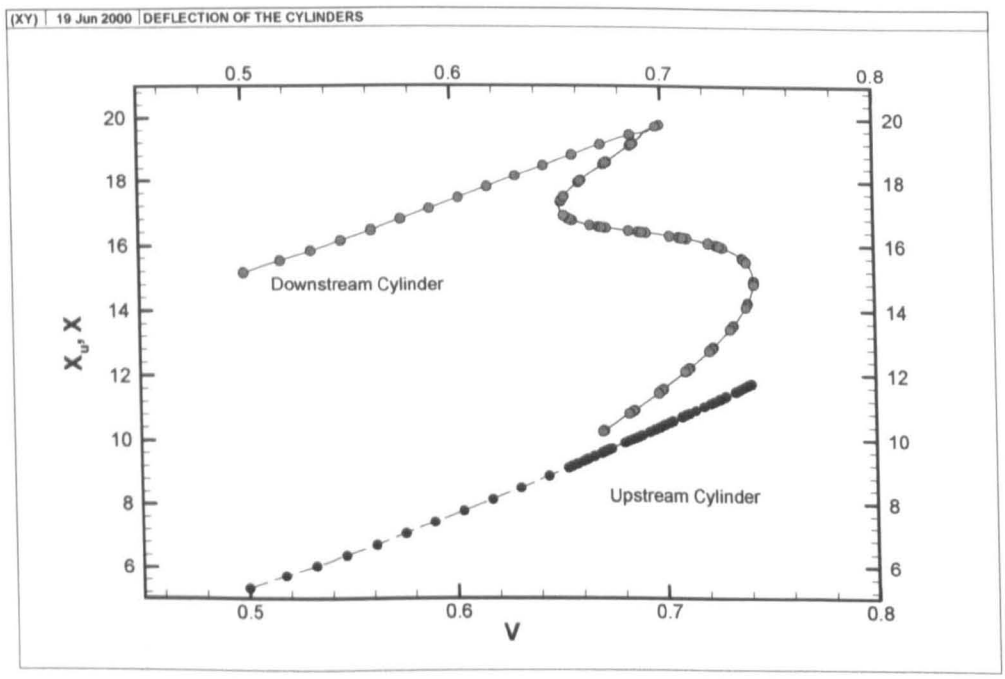

Figure 7.8(a) Streamwise displacement of riser middle point with flow velocity for a pair of 12" Riser Pair, X_S=10, Y_S=2.5, TTF=3.28 .

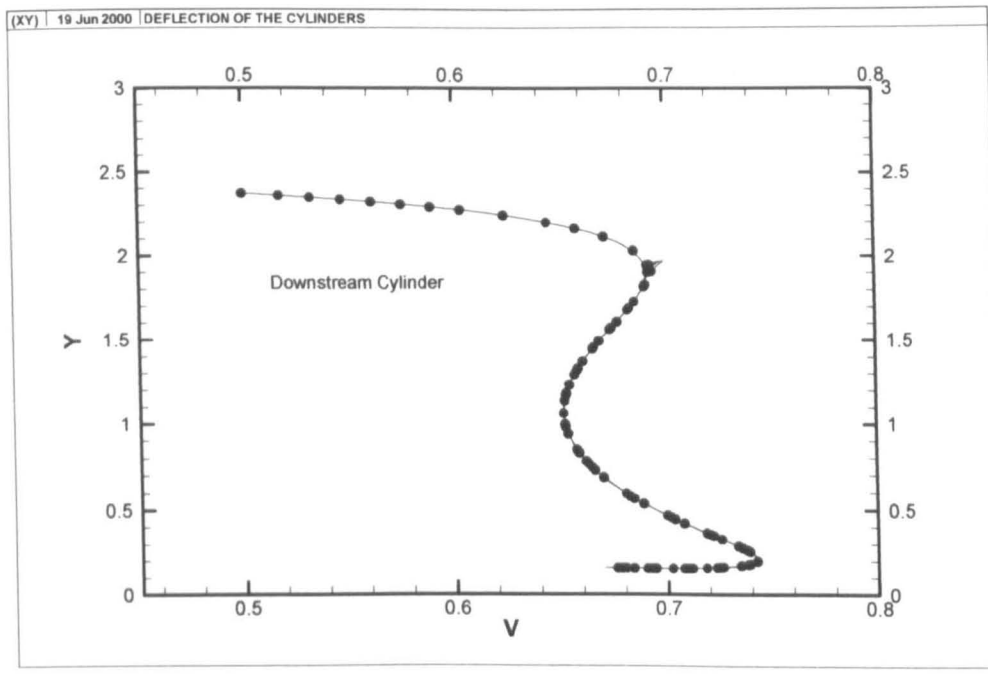

Figure 7.8(b) Transverse displacement of riser middle point with flow velocity for a pair of 12" Riser Pair, X_S=10, Y_S=2.5, TTF=3.28 .

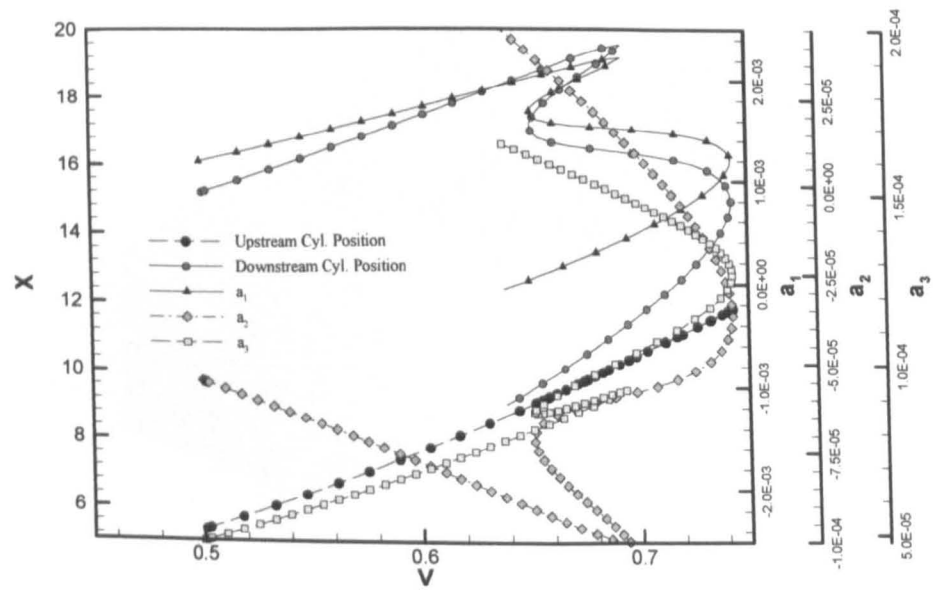

Figure 7.8(c) Variation of modal co-ordinates with flow velocity for the 12" riser pair.

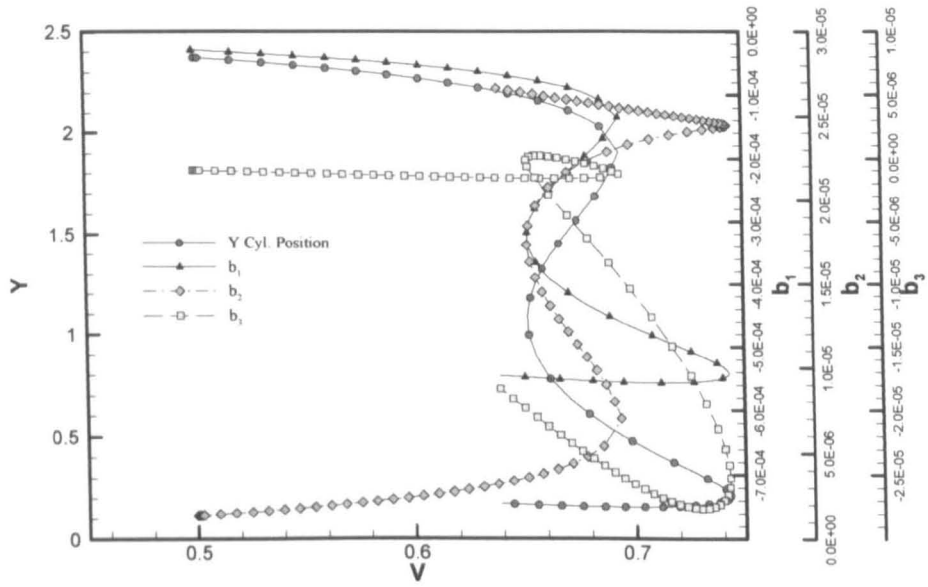

Figure 7.8(d) Variation of modal co-ordinates with flow velocity for the 12" riser pair.

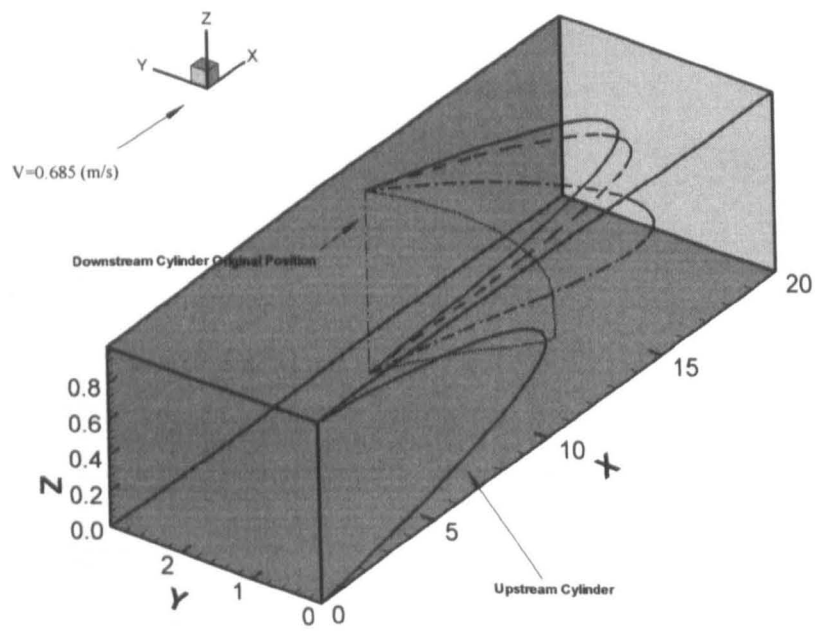

Figure 7.8(e) Geometrical shape of each individual equilibrium states for the riser pair at flow velocity of V_0=0.685 (m/s).

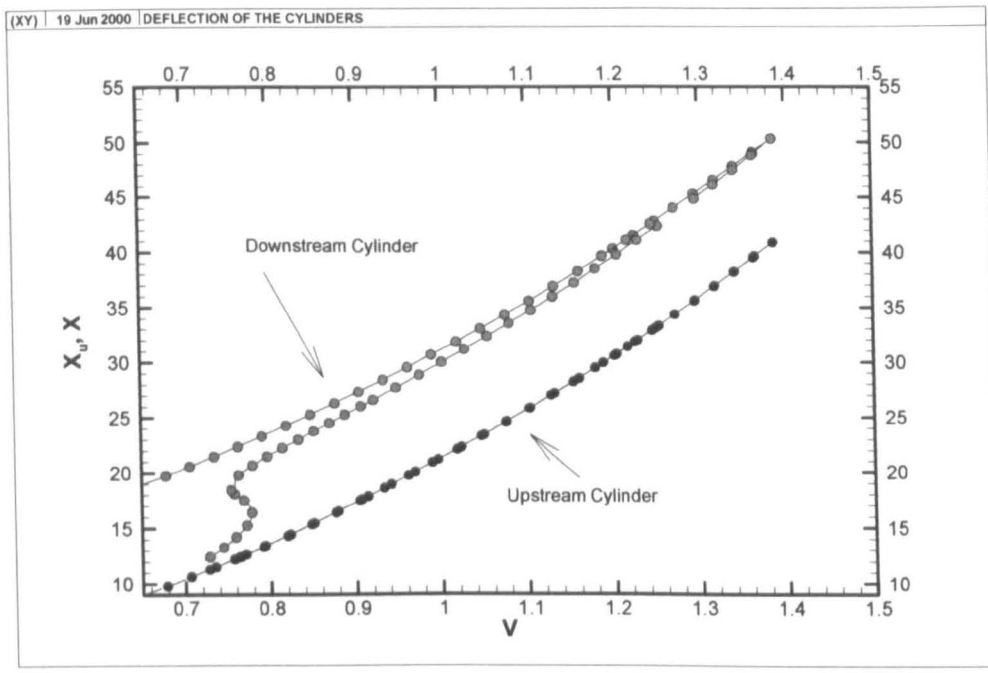

Figure 7.9(a) Streamwise displacement of riser middle point with flow velocity for a pair of 12" riser pair, X_S=10, Y_S=3.0, TTF=3.28 .

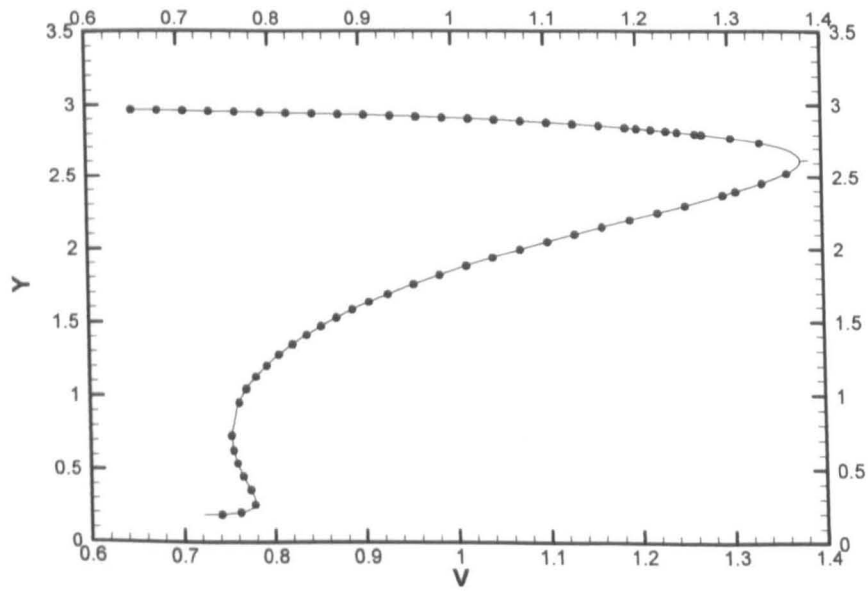

Figure 7.9(b) transverse displacement of riser middle point with flow velocity for a pair of 12" riser pair, X_S=10, Y_S=3.0, TTF=3.28 .

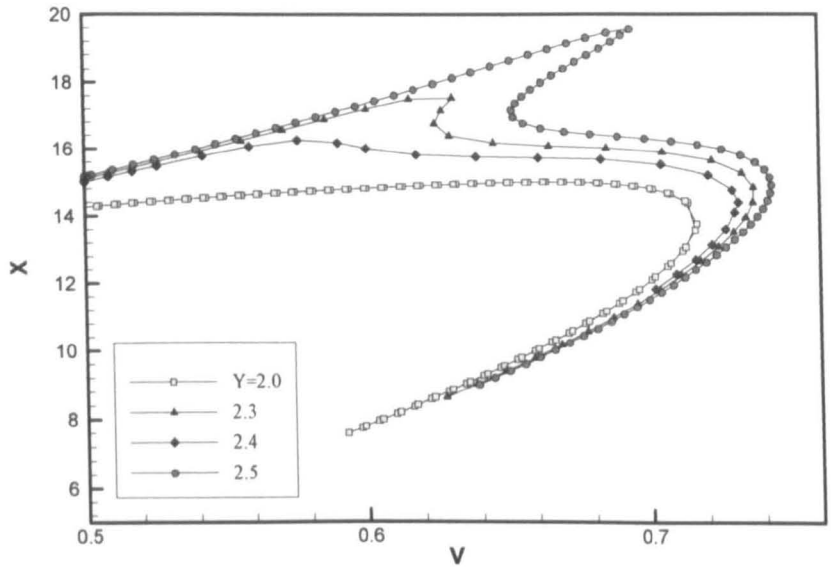

Figure 7.10(a) Transition of equilibrium states from inner wake to outer wake at X_S=10, TTF=3.28, the streamwise displacement.

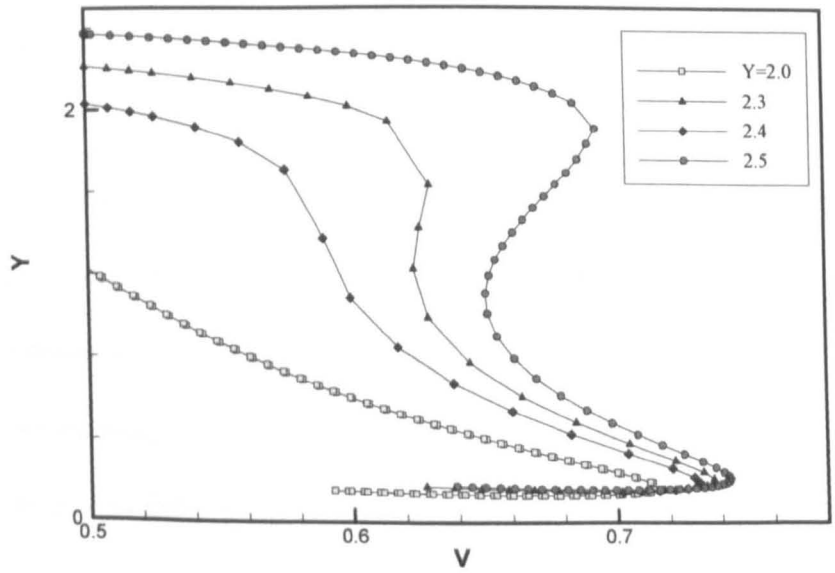

Figure 7.10(b) Transition of equilibrium states from inner wake to outer wake at X_S=10, TTF=3.28, the transverse displacement.

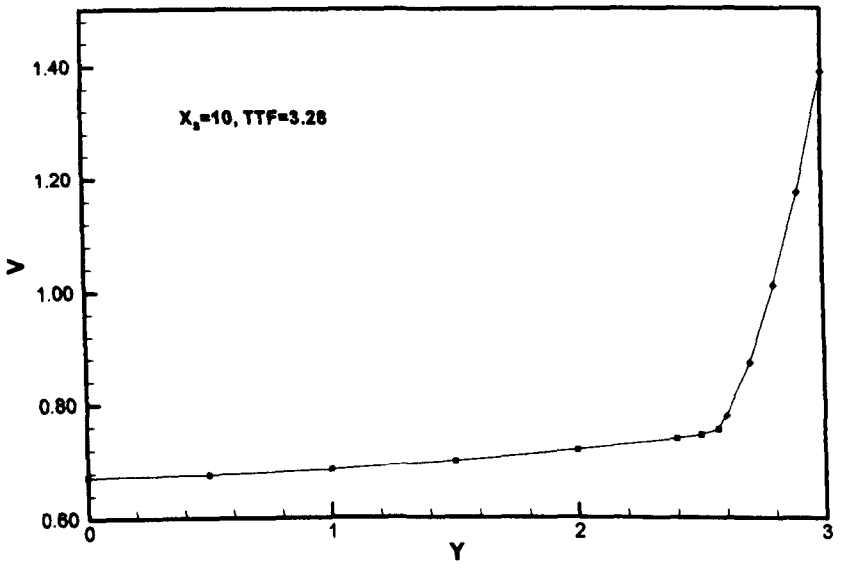

Figure 7.10(c) Critical Flow Velocity for X_S=10, with top tension of 7.416×10^6 (N), i.e. TTF=3.28 .

7.3.3 Critical State Against Design Spacing

For marine riser designers, if collision between risers is to be avoided, they need to know the critical flow velocity above which collision starts to occur for the specified top tension factor and clearance. Alternatively, for a specified ocean current, designers need to know the minimum top tension factor and clearance to keep two risers away from each other. Comparison between tandem and staggered arrangements has indicated that the critical flow velocity is smallest when the two risers are arranged inline. Accordingly, calculations were carried out to examine the critical state when the two risers are arranged inline. Figures 7.11 to 7.13 show the critical flow velocity and the corresponding middle riser position spacing variation with the riser clearance for three different top tension factors. It is seen that critical flow velocity and corresponding spacing increase with the increase of initial spacing, which reflects the increasing of clearance between risers, is a simple way to delay the possibility of riser collision. From the figure, it also can be seen that the effect of initial spacing is significant on the critical spacing. When the design spacing between two risers is larger, the corresponding spacing between two risers at critical state is significantly larger than 1 diameter. In fact, it has reached 8 diameters for the 30 diameters of

design spacing. Such a result shows a significant difference between present calculations and the recommendations provided by API.

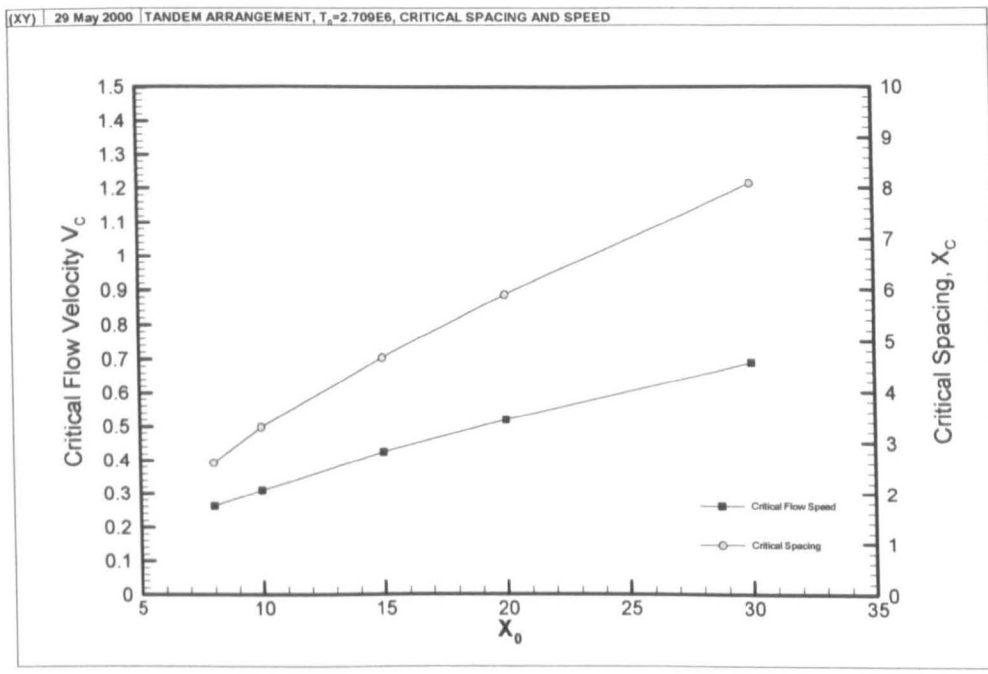

Figure 7.11 TTF=1.2, critical flow velocity and corresponding riser middle position spacing.

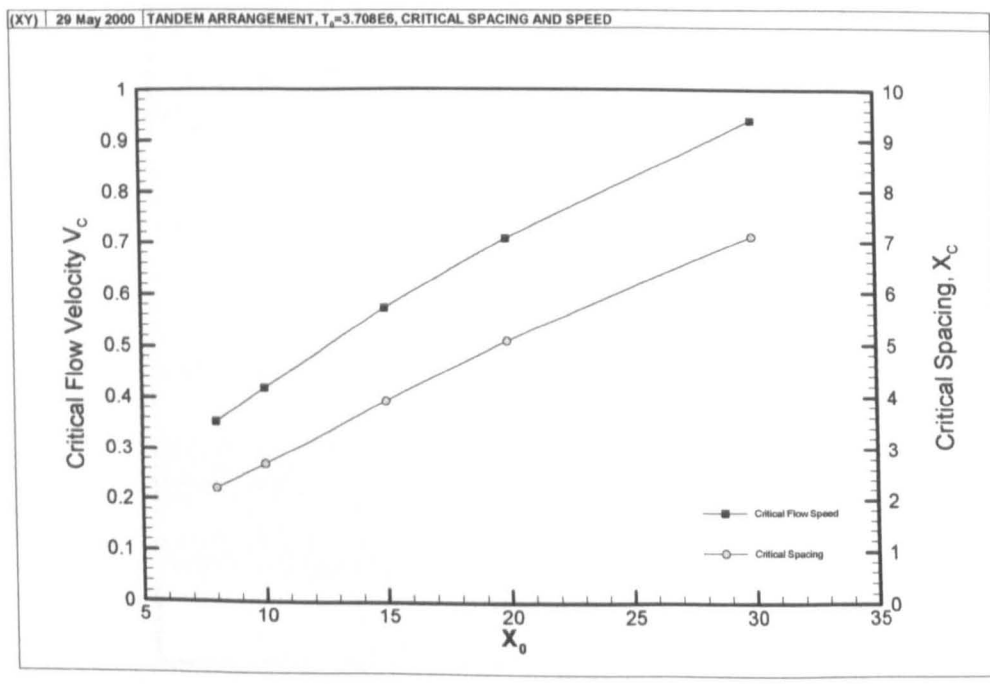

Figure 7.12 TTF=1.64, critical flow velocity and corresponding riser middle position spacing.

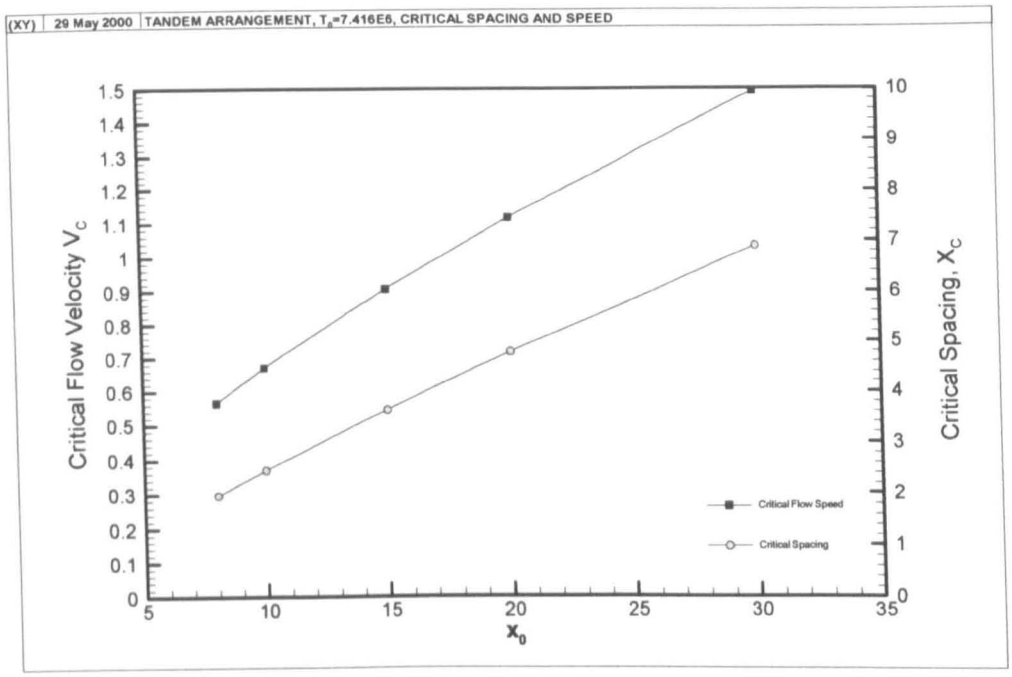

Figure 7.13 TTF=3.28, critical flow velocity and corresponding riser middle position spacing.

Table 7. 1 Parameters for a pair of 8" gas riser

Parameters	Value	Unit
Outer Diameter	0.2032	m
Internal pressure	34487055.0	N/m^2
Wall thickness	0.0130	m
Internal Diameter	0.1772	m
Internal fluid	gas	
Specific gravity	0.0	
length	1332.0	m
mass (steel)	60.88	kg/m
mass internal	0.0	kg/m
mass (added)	33.24	kg/m
mass	94.12	kg/m
mass parameter	0.2248	
weight in water	271.14	N/m
total weight	361157	N
Top Tension Factor	1.5 2.0 2.5	

In order to examine the effect of different kinds of risers, and to provide more comprehensive data regarding the different top tension factor, two additional calculations are made. One is for a pair of 8 inch gas risers which has the parameters shown in Table 7.1.

The other is a pair of 10 inch production risers with one small tube located within the larger outer side one, which has the parameters as listed in Table 7.2.

Figures 7.14 to 7.17 show the variation of critical flow velocity with specified top tension factor and design clearance. It is seen that all the data are consistent with each other regarding the relationship between critical flow velocity and the initial spacing although quantitatively such a relationship is dependent on the top tension and riser types.

7.3.4 Comparison With Two-Dimensional Results

When the two cylinders interact in two-dimensional space, it has been shown that the non-dimensional parameter aU_R^2 reflects the balance between fluid stiffness and the structural stiffness. It is the indicator for the stationary bifurcation. In three-dimensional space, the definition of a similar parameter can be difficult because of the existence of multiple mode frequency. However, as observed in the experiments (Huse, 1996), the wake induced oscillation is a kind of low frequency motion. The deflection of the riser is most significant in its first mode as shown in Figure 7.8. In addition, the first mode is the mode to lose its stability first should any instability occur. Therefore, an attempt is made to define the reduced flow velocity as:

$$U_R = \frac{V_0}{\omega_1 D}$$

Where ω_1 is the first mode frequency when the riser is in still water. By using such a non-dimensional parameter, the effect of the top tension factor is investigated for the 8" riser pair with design spacing as Xs=15, Ys=0. Figure 7.18 shows the variation of aU_R^2 at critical state with the top tension factor. It can be seen that the critical aU_R^2 increases with top tension factor and

approaches a constant when top tension factor is large enough (larger than 2.0 for the presented case). Also depicted in the figure is a reference line for the critical aU_R^2 for two-dimensional case. The discrepancy between two-dimensional and three-dimensional results is attributed to the three dimensional effects. If the risers are assumed to be deflected in a perfect first mode shape, according to the statics control equations (6.11) and (6.12), because when the riser is under the critical state, the spacing along the riser is not constant, and the fluid loading is not constant along riser, which means that it is impossible for parameter aU_R^2 to match the two dimensional case. This explains the similar results observed by Tsui(1986) in power transmission lines. Figure 7.19 shows the calculated critical sate results in non-dimensional form. As can be seen, even though the risers have different geometrical parameters, the critical aU_R^2 mainly depends on top tension factor and the design spacing. When the top tension is very large, the results tend to converge with each other. On the other hand, the larger the design spacing, the larger the discrepancy which exists between 2D results. Such an increased 3D effect is because of the increased variation of fluid force along the riser at the critical state.

7.3.5 Relation of Critical State H_w with TTF and Design Spacing

In Chapter VI, it has been pointed out that the displacement of the riser is a function of Top tension factor TTF, flow tension factor H_w. Therefore, it is possible to relate the critical state by theses non-dimensional parameters. Figure 7.20 shows the relation of the critical H_w for three different riser pairs with the same constant top tension factor of 2.0, the design spacing is set as 10 diameters. It is clearly seen that for deep water risers, the critical H_w is nearly constant for the same top tension factor and design spacing. As a result, graph can be drawn to show the relation between the critical H_w and the top tension factor and design spacing. Such a graph will be applicable to the general deepwater designs. Figure 7.21 can work as a general guide for riser design to predict collisions. From this figure, it can be seen that for deepwater risers over 1000 meters, the critical flow velocity which bring the two risers to collide will be under 1 m/s.

Table 7. 2 Parameters for a pair of production risers

Parameter	Value	Unit
Length	1032	m
Outer Pipe		
Outer Diameter	0.2445	m
Wall Thickness	0.0138	m
Internal Diameter	0.2169	m
Inner piper		
Outer Diameter	0.1143	m
Wall Thickness	0.00688	m
Internal Diameter	0.10054	m
Mass		
Riser	78.5138	kg/m
Tubing	18.2261	kg/m
Annulus	27.3826	kg/m
Internal fluid	7.1451	kg/m
Added mass	48.1251	kg/m
Total mass	179.3927	kg/m
Mass parameter	0.1708	
Riser weight in water	815.6287	N/m
Total weight in water	841728.8	N
Top Tension Factor	1.5	

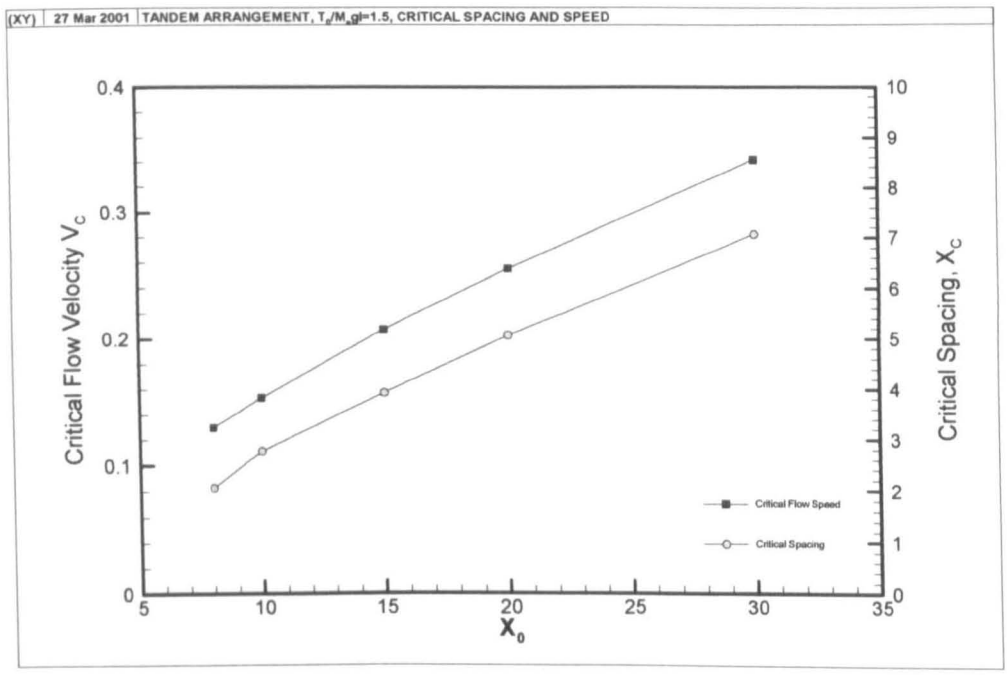

Figure 7.14 TTF=1.5, critical flow speed and corresponding middle riser position spacing.

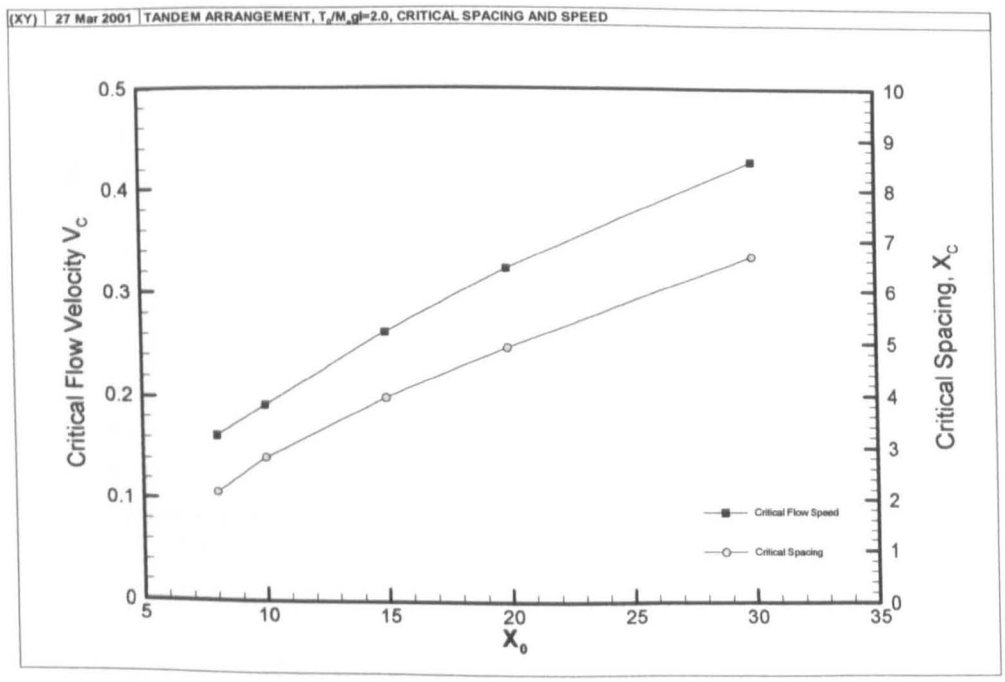

Figure 7.15 TTF=2.0, critical flow speed and corresponding middle riser position spacing.

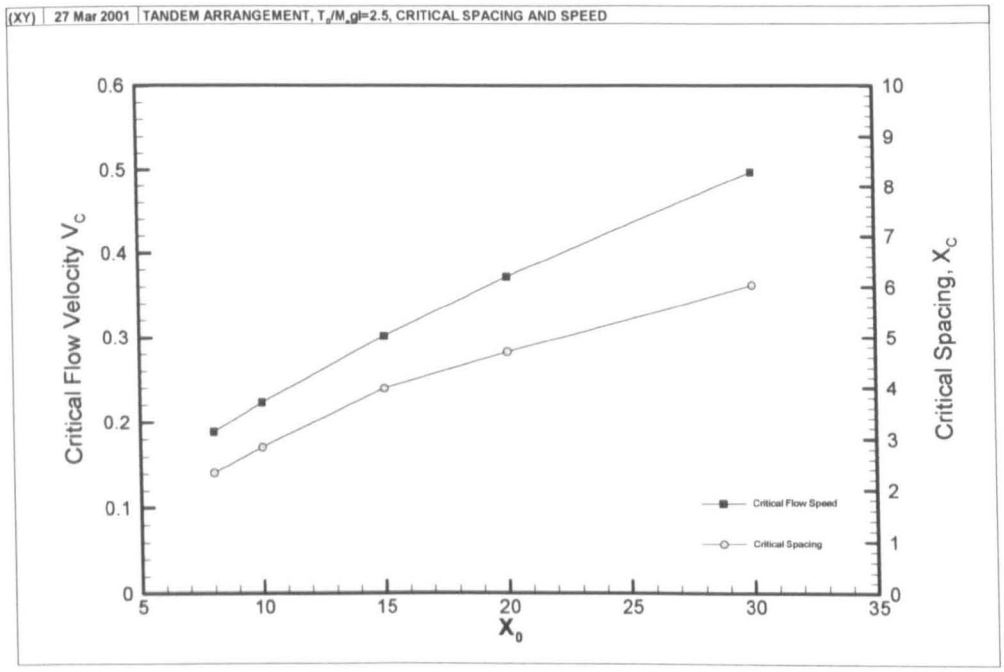

Figure 7.16 TTF=2.5, critical flow speed and corresponding middle riser position spacing.

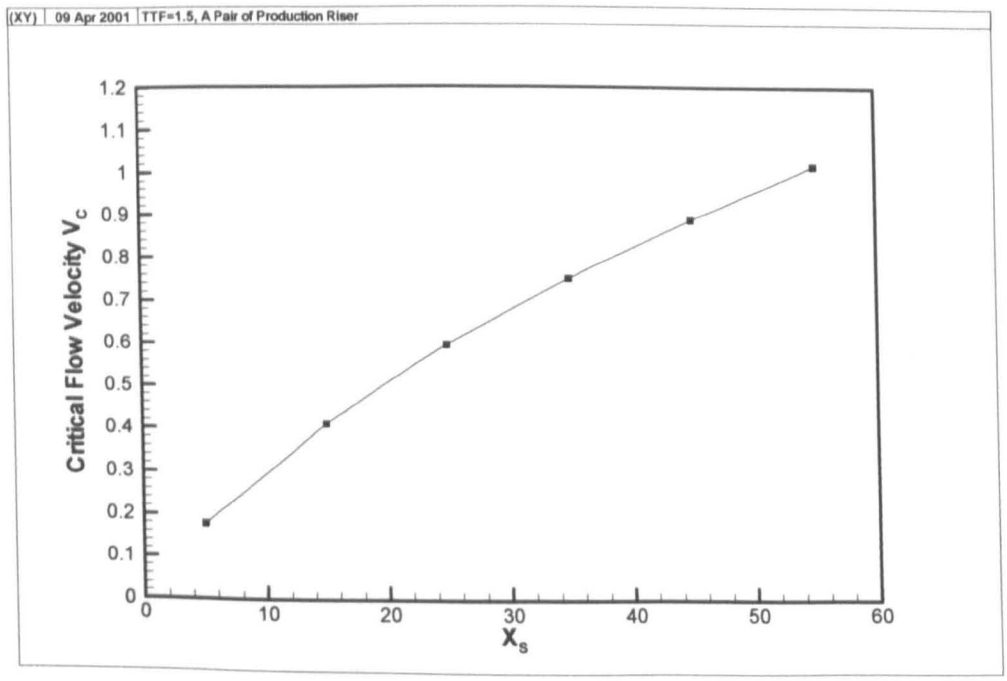

Figure 7.17 TTF=1.5, critical flow speed for different design clearance.

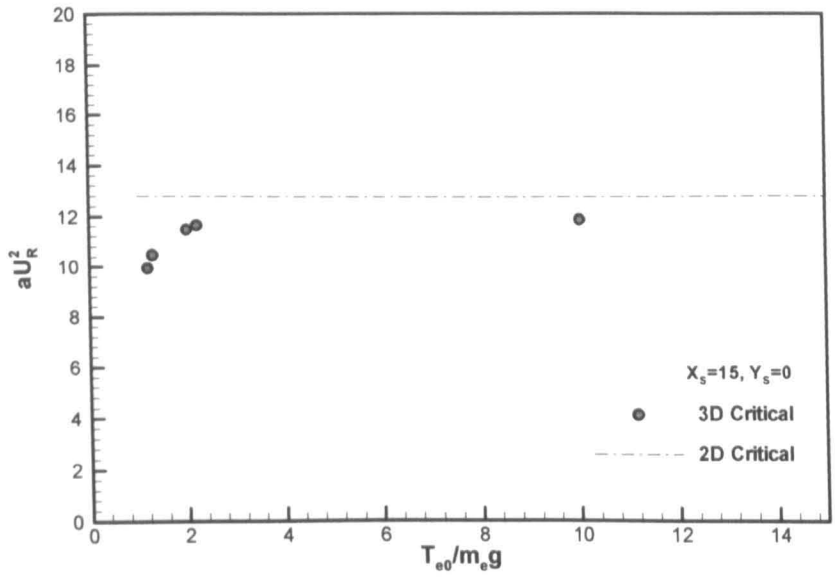

Figure 7.18 Variation of critical value of aU_R^2 for a pair of 8" gas risers against different top tension factors (X_S=15, Y_S=0).

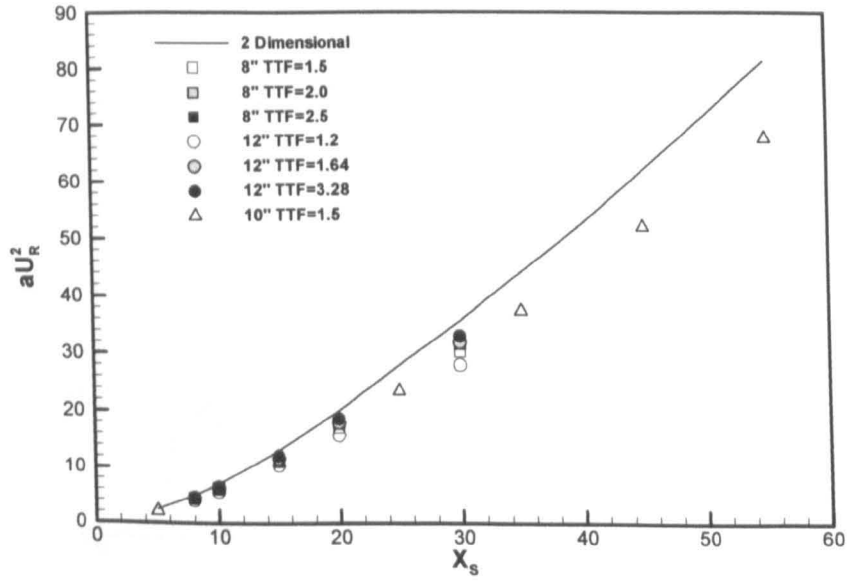

Figure 7.19 Critical parameter of aU_R^2 Vs design spacing.

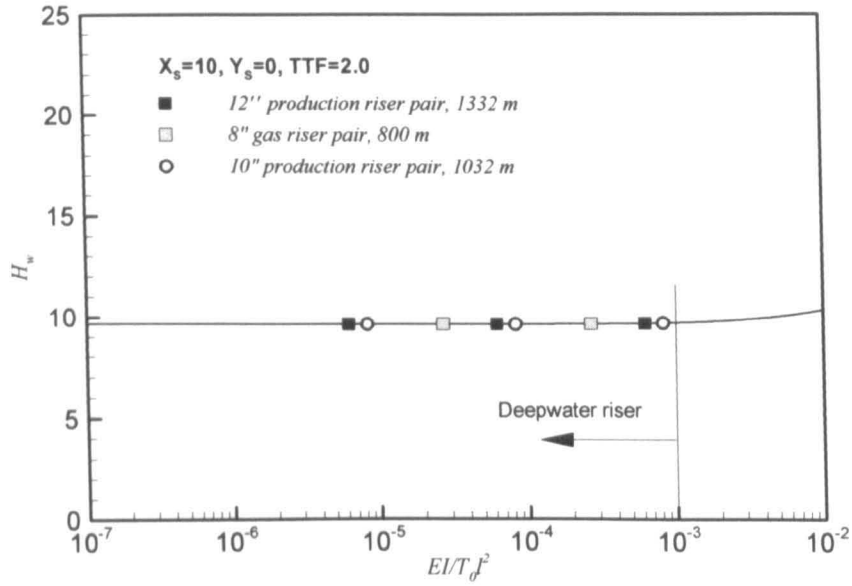

Figure 7.20 Variation of H_w with $EI/T_{e0}l^2$ for constant top tension factor.

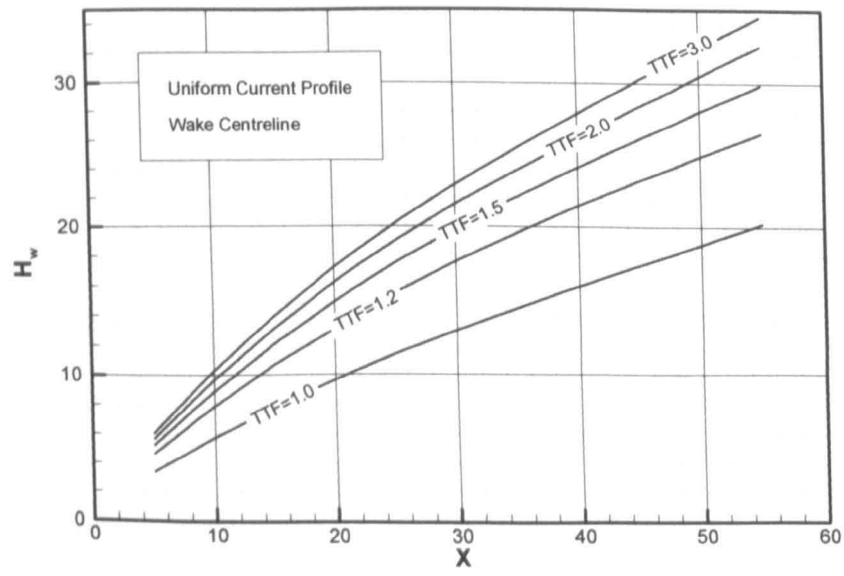

Figure 7.21 Critical H_w for different design spacing and top tension factor.

7.4 Summaries

The continuation in conjunction with stability analysis about interaction between two marine risers is implemented in this chapter. The numerical calculations show that great care should be taken in the implementation of continuation strategy, particularly for the predictor step. An inappropriate chosen continuation strategy can lead to failure. The numerical calculation results show that qualitatively, it agrees with those finds in the two-dimensional study. The following conclusions are drawn from the investigation:

1. When the two risers are arranged in tandem, there can be either: no equilibrium state, one or two equilibrium states, depending on the initial spacing, top tension, and flow velocity etc. The state immediately before the disappearance of the equilibrium state corresponds to the critical state above which collisions between two risers are likely to occur. Also the critical state is corresponds to a stationary bifurcation state and is a turning point on the continuation diagram.

2. When the downstream riser is located in the inner wake position, the continuation results are very similar to the case for two risers arranged in tandem, except that the critical state occurs at a larger flow velocity than in a tandem arrangement.

3. When the downstream riser is located at the outer part of the wake, there may be up to four equilibrium states, with one or two which are stable. Nevertheless, when the flow velocity is large enough, there will be a critical state above which there will be no equilibrium states.

4. The comparison between the three-dimensional investigation and the two-dimensional results shows that the critical parameter aU_R^2, defined by first mode frequency, increases with the increase of top tension factor. When the top tension factor is large enough, it

approaches a constant, which is smaller than the value found in the two dimensional investigation.

5. The critical parameter aU_R^2 depends mainly on the top tension factor and design spacing. For general purpose of riser design, the guide curve can be made for the specified top tension factor, and design spacing, to check its critical parameter of aU_R^2.

6. A general purpose riser design guide graph has been obtained which can be used to predict the critical flow velocity before the riser collision occurs at specified design spacing and top tension factors.

Chapter IIX

DYNAMICS SIMULATION FOR A PAIR OF MARINE RISERS

8.1 Introduction

8.1.1 General Remarks

Marine risers are rarely at rest since their deployment in ocean. Time varying ocean currents, together with harsh waves are often constant companions of the risers. Such an ocean environment can excite the marine riser directly via wave force and vortex shedding induced forces, or indirectly via top vessel motion. Apart from these, as indicated in the foregoing analysis, the time-averaged force caused by riser interaction in ocean current can ultimately also lead risers to move around. The importance of riser dynamics in their design has been long recognised (Fish & Ludvig, 1966, Bernitsas, 1982). One of the direct consequences of such dynamics is the fatigue life of the risers. In the recent four to five decades, concerted efforts have been made to understand the mechanism of vortex-induced vibration and to predict such an effect. The most recent work can be seen from Bokaian, 1994; Vandiver, 1997; Furnes, 1999; Willden et al, 2001; Moe et al, 2001. When the oil and gas development companies started to operate in deepwater, for example, 3000ft to 10,000 ft or even deeper, the response of riser structure became an increasing concern. In such deep water, the TLP like risers behave virtually like string in the ocean current. For vortex-induced vibration, multiple modes can be excited simultaneously, as

indicated by Vandiver (1996) *etc.* Rajabi (1989), Duggal *et al* (1993) investigated pairs of tendons/risers under wave excitation, and demonstrated potential collisions between individual tendons/risers. However, so far, nothing has been published which account for riser dynamics with the consideration of risers interaction caused by ocean current, particularly via the time-averaged forces. The direct, perceptible effect of such dynamics is the intermittently collision between individual riser as observed by (Huse, 1993, 1996; Bryndum and Andersen, 1999). In this chapter, a systematic investigation into time-averaged force induced riser dynamics has been made. As much effort has been made on the predicting of riser dynamics, a brief overview of the existing work is stated at the outset.

8.1.2 Overview of Existing Work on Riser Dynamics

8.1.2.1 Systems Covered

Because different researchers have different research objectives, the riser system has been investigated in different levels of complexity. The earliest investigations were focused on the solitary riser's statics and dynamics (Fisher & Ludvig 1966; Gosse & Barksdale 1969) etc. Now, different integrated systems have been looked into, such as the coupled system of top vessel and riser (or mooring lines), and also consideration of the sea bed effect (O'Brien & McNamara 1989; Heurtier et al, 2001). Multiple riser effect without direct fluid interaction was also included in some of the researches (Ormberg et al 1999). Some studies have focused on the detailed investigation of top joint effect and the dynamics under the condition of riser installation and hang-off (Watters et al 1998; Sattamini & Ferranti 1993; Patrikalakis & Yoon 1990; Teigen et al 1990). The high performance of modern computers has made it possible to consider even more complicated and detailed structure systems. However, study into risers affected by flow is mostly confined within the scope of small spacing between risers, such a study, targeted on the bundle risers, was carried out by Vlahopoulos & Bernitsas 1991. The dynamics of TLP like riser pair or group remains un-

explored, although the significance of riser interaction has been recognized in recent years (Huse, 1996).

8.1.2.2 Numerical Method Employed

It was shown that differences in riser deflection due to non-linearity can be as high as 28 percent in the maximum displacement (Bernitsas & Kokarakis 1988). Because of such a non-linearity in the nature of the problem, both in structural dynamic terms and hydrodynamic forces terms, to obtain a classical solution is not generally possible. Recourse to numerical technique has to be made. In the numerical investigation of riser dynamics, the fluid forces are usually assumed to be known beforehand (the Morison's equation is often employed), which means the interaction of the structural dynamics to flow is not considered. Mathematically, it is required to solve a fourth-order partial differential equation in time and space domain. The boundary conditions are often defined at both ends of the risers, with the bottom end fixed and top end fixed or with a prescribed movement. The problem in time domain is either steady state or transient. For steady-state problems, there is no specific condition need to be defined (such as static problem or steady state vibration concern). Otherwise, the problem needs to specify the initial condition for the riser.

The objective of the numerical technique is to discretise the partial differential equation into solvable simultaneous equations. According to different methods of the discretisation in space domain, the numerical technique is usually classified into:

1) Finite Difference Method, such as (Burke 1973, Morgan 1975, Huagui, 1994),

2) Finite Element Method (for example, Gardner & Kotch 1976),

3) and also Modal Superposition Method (Modi et al 1994, Furnes, 1999) etc.

The clarifications of these methods were provided in Chapter VI.

According to the discretisation method in time domain, the approaches are classified into time history analysis and steady-state frequency domain analysis (Bernitsas, 1989). The time history analysis method starts from the transient state and obtains the solution in time history until a steady state solution is achieved or some specified time instant has been reached. The frequency domain analysis solves the partial differential equation in frequency domain by supposing the solution has steady state form solutions. The frequency domain method has the advantage of high efficiency while it has to linearise the control equation. The time domain solution usually calls for much more computation time and most of such computations have been spent on the transient state when the ultimate state to be sought is steady. The preference between above two methods is largely dependent on the requirement of the investigation.

8.1.3 Present investigation

In this chapter, by using the modal superposition method, a three-dimensional riser interaction code in time domain is implemented. The code is validated against published API data about the riser dynamics. Subsequently, a detailed parametric study on the interaction was carried out. The dynamics of riser interaction has been examined systematically. The results show that wake-induced oscillation is a low frequency, large amplitude movement. The quick motion mainly occurs when two risers are close to each other, i.e. immediately before and after the collision. The motion speed of riser before imminent collision is significant and comparable to the possible maximum amplitude of the high order vortex induced-vibration motion. Such a result suggests that a rethink is needed for the investigation of collisions between two risers in which most investigations have assumed the vortex-induced vibration is the main contributor towards collision effect, such as Halse, 2000; Kaasen et al, 2000; Magne et al, 2001 etc.

8.2 Theoretical Formulation

8.2.1 Mathematical Definition of the Problem

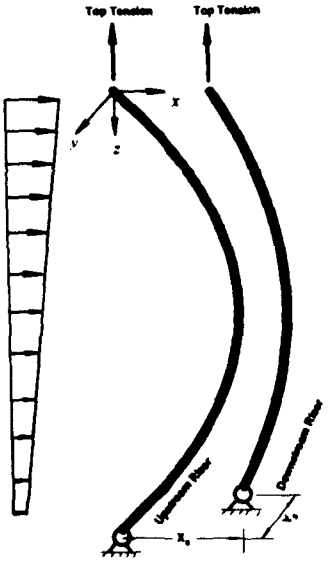

Figure 8.1 Sketch of two flexible riser system.

8.2.1.1 Structural Dynamic System

Compared to the statics and continuation investigation conducted in the previous two chapters, the riser dynamics in this chapter focuses on risers' time domain behaviour particularly under specified high current. Therefore, unlike the dynamic system treated in stability analysis, the structural displacement in this Chapter is treated as a whole, which literally is the sum of the static displacement investigated in Chapter 6 and the dynamic displacement discussed in the Chapter 7, though small displacement hypothesis will be still applicable to such a system because the displacement is small when compared to riser length. Additionally, the top connector of the riser can move with the top vessel as will be reflected in the specification of the boundary conditions.

Figure 8.1 redraws the co-ordinate system used in Chapter 6. For simplicity, let the two risers have the same uniform geometrical property and mechanical performance. The

linearised structural dynamic response of the risers to the fluid excitation are expressed as (Krolikowski & Gay, 1980, API, 1998)

$$\begin{cases} m\dfrac{\partial^2 x_i}{\partial t^2}+c\dfrac{\partial x_i}{\partial t}+\dfrac{\partial^2}{\partial z^2}\left(EI\dfrac{\partial^2 x_i}{\partial z^2}\right)-\dfrac{\partial}{\partial z}\left(T_{ei}\dfrac{\partial x_i}{\partial z}\right)=F_{xi} \\ m\dfrac{\partial^2 y_i}{\partial t^2}+c\dfrac{\partial y_i}{\partial t}+\dfrac{\partial^2}{\partial z^2}\left(EI\dfrac{\partial^2 y_i}{\partial z^2}\right)-\dfrac{\partial}{\partial z}\left(T_{ei}\dfrac{\partial y_i}{\partial z}\right)=F_{yi} \qquad (i=1,2) \end{cases} \tag{8.1}$$

Here, subscript $i=1,2$ denotes the upstream and downstream riser respectively. The movement of upstream riser in the transverse direction is also included in order to generalise the problem, the definitions of other parameters are the same as before. F_{xi}, F_{yi} are fluid forces applied on the riser in x, y direction respectively, which is a function of time as well as depth. The source of this kind of fluid loading can be time-averaged force as well as wave force or vortex-induced force depending on the focus of the research. In this Chapter, the time-averaged force is the main concern, while the wave force has been used to validate the computer code.

8.2.1.2 The definition of boundary condition

Let the bottom of the riser at the lower ball joint be pinned, and the top connector at the riser support ring be simulated by a spring with stiffness of k_T. The boundary condition can be written as

$$\begin{cases} x_i(z=0)=x_v(t);\ \ x_i(z=l_{Hi})=0; \\ \left.\dfrac{\partial^2 x_i}{\partial z^2}\right|_{z=0,l_{Hi}}=0 \\ y_i(z=0)=y_v(t);\ \ y_i(z=l_{Hi})=0 \\ \left.\dfrac{\partial^2 y_i}{\partial z^2}\right|_{z=0,l_{Hi}}=0 \\ \Delta T_i(t)=k_T\Delta l_{Hi}(t) \qquad (i=1,2) \end{cases} \tag{8.2}$$

Here, ΔT_i is the variation of the top tension. l_{Hi} $(i=1,2)$ is the vertical distance between riser support ring and lower ball joint, Δl_{Hi} is the vertical displacement of top riser support ring. x_v, y_v are excursions in x, y directions respectively which are related to the top vessel motion.

8.2.1.3 Non-dimensional form of the system

Let

$$Z_i = \frac{z_i(t)}{l_{Hi}(t)} \tag{8.3}$$

$$\begin{cases} X_i(Z_i,t) = \dfrac{x_i(z_i,t) - \left(1.0 - \dfrac{z_i}{l_{Hi}}\right)x_v(t)}{l_{Hi}(t)} \\ Y_i(Z_i,t) = \dfrac{y_i(z_i,t) - \left(1.0 - \dfrac{z_i}{l_{Hi}}\right)y_v(t)}{l_{Hi}(t)} \end{cases} \qquad (i=1,2) \tag{8.4}$$

As the movement of the riser in vertical direction is assumed to be small when compared to that in transverse and streamwise directions, the non-dimensional form of the structural dynamic system and its corresponding boundary condition are then transformed into the following form:

$$\begin{aligned} &\frac{\partial^2 X_i}{\partial t^2} + \frac{c}{m}\frac{\partial X_i}{\partial t} + \frac{EI}{ml_{Hi}^4}\frac{\partial^4 X_i}{\partial Z_i^4} - \frac{T_{ei}}{ml_{Hi}^2}\frac{\partial^2 X_i}{\partial Z_i^2} - \frac{1}{ml_{Hi}^2}\frac{\partial T_{ei}}{\partial Z_i}\frac{\partial X_i}{\partial Z_i} \\ &+ \frac{X_{Vi}}{ml_{Hi}^2}\frac{\partial T_{ei}}{\partial Z_i} + (1-Z_i)\frac{\partial^2 X_{Vi}}{\partial t^2} + \frac{c}{m}(1-Z_i)\frac{\partial X_{Vi}}{\partial t} = \frac{F_{xi}}{ml_{Hi}} \end{aligned}$$

$$\begin{aligned} &\frac{\partial^2 Y_i}{\partial t^2} + \frac{c}{m}\frac{\partial Y_i}{\partial t} + \frac{EI}{ml_{Hi}^4}\frac{\partial^4 Y_i}{\partial Z_i^4} - \frac{T_{ei}}{ml_{Hi}^2}\frac{\partial^2 Y_i}{\partial Z_i^2} - \frac{1}{ml_{Hi}^2}\frac{\partial T_{ei}}{\partial Z_i}\frac{\partial Y_i}{\partial Z_i} \\ &+ \frac{Y_{Vi}}{ml_{Hi}^2}\frac{\partial T_{ei}}{\partial Z_i} + (1-Z_i)\frac{\partial^2 Y_{Vi}}{\partial t^2} + \frac{c}{m}(1-Z_i)\frac{\partial Y_{Vi}}{\partial t} = \frac{F_{yi}}{ml_{Hi}} \qquad (i=1,2) \end{aligned} \tag{8.5}$$

Here,

$$X_{Vi} = \frac{x_v}{l_{Hi}}, \quad Y_{Vi} = \frac{y_v}{l_{Hi}}$$

$$\begin{cases} X_i = 0; \ \dfrac{\partial^2 X_i}{\partial Z_i^2} = 0 \\ Y_i = 0; \ \dfrac{\partial^2 Y_i}{\partial Z_i^2} = 0 \\ at \ \ Z_i = 0, 1 \qquad\qquad (i = 1, 2) \end{cases} \tag{8.6}$$

$$\Delta T_i(t) = k_T \Delta l_{Hi}(t)$$

The boundary condition in 8.6 is homogeneous. For such a system, the Hooke's law can be expressed as:

$$\frac{l_{0i}}{\sqrt{l_{Hi}^2 + d_x^2 + d_y^2}} = \int_0^1 \frac{EA}{EA + T_{ei} + \sum P_o A_o - \sum P_i A_i} \sqrt{1 + \left(\frac{\partial X_i}{\partial Z_i}\right)^2 + \left(\frac{\partial Y_i}{\partial Z_i}\right)^2} \ dZ_i \tag{8.7}$$

Here l_{0i} is the riser original length, E is Young's modulus, A is the cross section area of the riser, P_0 is the static pressure outside the riser, P_i is the static pressure inside the riser. A_0 and A_i are outer and internal cross section areas respectively, and the summation is made when the riser consists of multiple tubes.

In the above structural dynamic equations, the displacement of x, y, the distance between riser ends l_{Hi} and the top tension are unknowns. Equation 8.5 to 8.7 form a self contained system should the external excitation of fluid force is known. The standard first-order differential equations are expressed in the following form,

$$\dot{\tilde{p}} = f(\tilde{p}, t)$$

with

$$\begin{cases}
\dot{p}_1 = p_2 \\
\dot{p}_2 = -\dfrac{c}{m}p_2 - \dfrac{EI}{ml_{H1}^4}\dfrac{\partial^4 p_1}{\partial Z_1^4} + \dfrac{T_{e1}}{ml_{H1}^2}\dfrac{\partial^2 p_1}{\partial Z_1^2} + \dfrac{1}{ml_{H1}^2}\dfrac{\partial T_{e1}}{\partial Z_1}\dfrac{\partial p_1}{\partial Z_1} \\
\quad -\dfrac{X_{V1}}{ml_{H1}^2}\dfrac{\partial T_{e1}}{\partial Z_1} - (1-Z_1)\dfrac{\partial^2 X_{V1}}{\partial t^2} - \dfrac{c}{m}(1-Z_1)\dfrac{\partial X_{V1}}{\partial t} + \dfrac{F_{x1}}{ml_{H1}} \\
\dot{p}_3 = p_4 \\
\dot{p}_4 = -\dfrac{c}{m}p_4 - \dfrac{EI}{ml_{H1}^4}\dfrac{\partial^4 p_3}{\partial Z_1^4} + \dfrac{T_{e1}}{ml_{H1}^2}\dfrac{\partial^2 p_3}{\partial Z_1^2} + \dfrac{1}{ml_{H1}^2}\dfrac{\partial T_{e1}}{\partial Z_1}\dfrac{\partial p_3}{\partial Z_1} \\
\quad -\dfrac{X_{V1}}{ml_{H1}^2}\dfrac{\partial T_{e1}}{\partial Z_1} - (1-Z_1)\dfrac{\partial^2 X_{V1}}{\partial t^2} - \dfrac{c}{m}(1-Z_1)\dfrac{\partial X_{V1}}{\partial t} + \dfrac{F_{y1}}{ml_{H1}} \\
\dot{p}_5 = p_6 \\
\dot{p}_6 = -\dfrac{c}{m}p_6 - \dfrac{EI}{ml_{H2}^4}\dfrac{\partial^4 p_5}{\partial Z_2^4} + \dfrac{T_{e2}}{ml_{H2}^2}\dfrac{\partial^2 p_5}{\partial Z_2^2} + \dfrac{1}{ml_{H2}^2}\dfrac{\partial T_{e2}}{\partial Z_2}\dfrac{\partial p_5}{\partial Z_2} \\
\quad -\dfrac{X_{V2}}{ml_{H2}^2}\dfrac{\partial T_{e2}}{\partial Z_2} - (1-Z_2)\dfrac{\partial^2 X_{V2}}{\partial t^2} - \dfrac{c}{m}(1-Z_2)\dfrac{\partial X_{V2}}{\partial t} + \dfrac{F_{x2}}{ml_{H2}} \\
\dot{p}_7 = p_8 \\
\dot{p}_8 = -\dfrac{c}{m}p_8 - \dfrac{EI}{ml_{H2}^4}\dfrac{\partial^4 p_7}{\partial Z_2^4} + \dfrac{T_{e2}}{ml_{H2}^2}\dfrac{\partial^2 p_7}{\partial Z_2^2} + \dfrac{1}{ml_{H2}^2}\dfrac{\partial T_{e2}}{\partial Z_2}\dfrac{\partial p_7}{\partial Z_2} \\
\quad -\dfrac{X_{V2}}{ml_{H2}^2}\dfrac{\partial T_{e2}}{\partial Z_2} - (1-Z_2)\dfrac{\partial^2 X_{V2}}{\partial t^2} - \dfrac{c}{m}(1-Z_2)\dfrac{\partial X_{V2}}{\partial t} + \dfrac{F_{y2}}{ml_{H2}}
\end{cases} \tag{8.8}$$

and $\tilde{p} = \{p_1, p_2, p_3, p_4, p_5, p_6, p_7, p_8\}^T$, p_1, p_3, p_5, p_7 stand for the displacement of upstream and downstream riser in x and y direction respectively, p_2, p_4, p_6, p_8 are their corresponding velocity terms.

8.2.2 Hydrodynamic Forces

The hydrodynamic force in equation 8.5 can be both space and time dependent. In the investigation made in this chapter, both wave forces and time-averaged forces are considered, the inclusion of wave force being mainly for the purpose of validating the computing program.

8.2.2.1 Time-averaged Force

The time-averaged force is further applied by the two dimensional approach. By supposing the averaged effects at different depths of the riser are independent of each other, the time-averaged fluid force is only dependent on the relative position between two risers at the specified depth. When the ocean current is non-uniform along the water column, a linear interpolation scheme is applied at the desired riser depth position. For a specified water depth, the time-averaged force is expressed as:

$$\begin{cases} F_{x1_j} = \frac{1}{2}\rho\left|V_{0_j} - \dot{x}_{1_j}\right|\left(V_{0_j} - \dot{x}_{1_j}\right)DC_{D1} \\ F_{y1_j} = 0 \\ F_{x2_j} = \frac{1}{2}\rho U_{r2_j}(Z_j)D\left[\left(U_j - \dot{x}_{2_j}\right)C_{D2} + \dot{y}_{2_j}C_{L2}\right] \\ F_{y2_j} = \frac{1}{2}\rho U_{r2_j}(Z_j)D\left[\left(U_j - \dot{x}_{2_j}\right)C_{L2} - \dot{y}_{2_j}C_{D2}\right] \end{cases} \tag{8.9}$$

The subscript j represents the different riser depth.

8.2.2.1.1 Wave force, inline movement only

In the presence of waves, the fluid forces applied on the risers can be represented by Morison's Equation as follows,

$$
\begin{cases}
F_{x1j} = \dfrac{1}{2}\rho\left(V_{0j} + u_{w1j} - \dot{x}_{1j}\right)\left|V_{0j} + u_{w1j} - \dot{x}_{1j}\right| C_{D1} \\
\qquad + \rho\dfrac{\pi D^2}{4}\left(1 + c_m\right)\left[\dot{u}_{w1j} + \left(V_{0j} + u_{w1j} - \dot{x}_{1j}\right)\dfrac{\partial u_{w1j}}{\partial x}\right] - \rho c_m \ddot{x}_{1j}\dfrac{\pi D^2}{4} \\
F_{y1j} = 0 \\
F_{x2j} = \dfrac{1}{2}\rho\left(U_j + u_{w2j} - \dot{x}_{2j}\right)\left|U_j + u_{w2j} - \dot{x}_{2j}\right| C_{D2}\left(Z_{i,j}, t\right) \\
\qquad + \rho\dfrac{\pi D^2}{4}\left(1 + c_m\right)\left[\dot{u}_{w2j} + \left(U_j + u_{w2j} - \dot{x}_{2j}\right)\dfrac{\partial\left(U_j + u_{w2j}\right)}{\partial x}\right] - \rho c_m \ddot{x}_{2j}\dfrac{\pi D^2}{4} \\
F_{y2j} = 0
\end{cases}
\tag{8.10}
$$

It should be noted that the transverse force caused by vortex shedding is not the content of the investigation in this chapter.

8.2.3 Solution Procedures

Equation 8.3 is solved by the modal superposition method, together with time domain Runge-Kutta integration. The methodology behind is the same as that for statics analysis. The solution procedure is as follows:

1. Specify an initial state of the two risers at given flow condition for specified riser pair. The initial state can be design position[1] or any other specified state;

2. Solving the dynamic system at a given time step by Runge-Kutta integration. Implicitly, double iteration scheme is applied, with one similar to that used in statics analysis to comply with the Hooke's law and the other for the consideration of top tension variation;

3. Utilising the above time step as the initial state, find the next time step state, such a time marching continues until the specified time reached.

[1] Design position represents the state for two risers when the fluid flow is stationary and there are no disturbances.

8.3 Numerical Results

8.3.1 Dynamics of a Solitary Drilling Riser

In order to validate the present numerical programs, a calculation was made to check against the published data by API (API, 1992). The chosen case is for a solitary drilling riser, 10 inches in diameter and 1520 ft in length. The specifications of the riser, with its kill line and choke line are provided in table 6.2, Chapter VI. The operation condition is specified as follows:

Table 8. 1 Flow excitation specification.

Parameter	Value	Unit
Top Tension	*370* *600*	*Kips*
Static Offset at the Top	*90*	*Feet*
Vessel surge amplitude (peak to peak)	*26.7*	*Feet*
Vessel surge phase angle relative to the wave crescent	*-90°*	
Vessel surge period	*12.8*	*Sec.*
H, wave height, peak to trough	*40*	*Feet*
T, wave period	*12.8*	*Sec.*
Current profile	Linear, *2 Knot* at Mean Water Level, *0.4 Knot* at lower ball joint	

Figure 8.2 and Figure 8.3 show the calculated results, compared to the API published data, for the deflection envelope and bending stress for the case of top tension of 370 Kips and 600 Kips respectively. The right hand side envelope is the maximum deflection or bending stress varying with depth, while the left hand side envelope denotes the minimum deflection or bending stress. The API results shown in the figure are composed of two curves for each specific envelope line, which itself shows the variation of the results supplied to the API by different institutions. It is seen that both geometrical shape and bending stress agree very well with the API published results. This gives the confidence in the subsequent calculations for the dynamics of two risers interaction. Additionally, in

order to examine the convergence of the numerical calculation, comparison is made for computation using different mode numbers. Shown in Figure 8.4 is a comparison of deflection and bending stress envelope between mode number of 20 and 40. It is seen that in Figure 8.4, the geometrical figure has converged very satisfactorily when the total mode number participated in the calculation is taken as 20. However, for detailed information such as bending stress, the calculation with mode number of 40 shows a slight difference to the mode number of 20 although, generally speaking, both results have nearly converged with each other. This is due to the relative slow convergence for terms of bending stress. Based on such a comparison, in the subsequent computation, the mode number is generally taken as 20 in order to make the calculation more efficient.

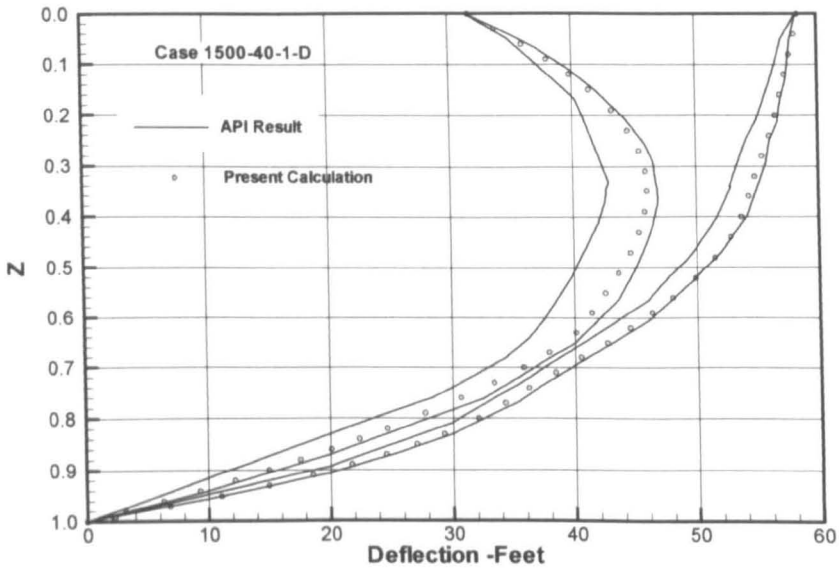

Figure 8.2(a)

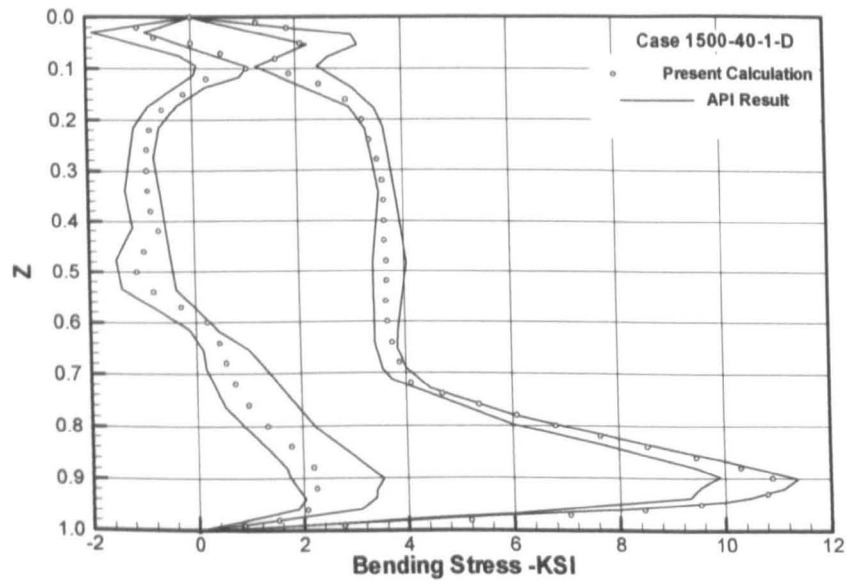

Figure 8.2(b)

Figure 8.2 Comparison of present calculation and API published result for a solitary drilling riser. Top tension 370 Kips. (a) Displacement; (b) Bending stress.

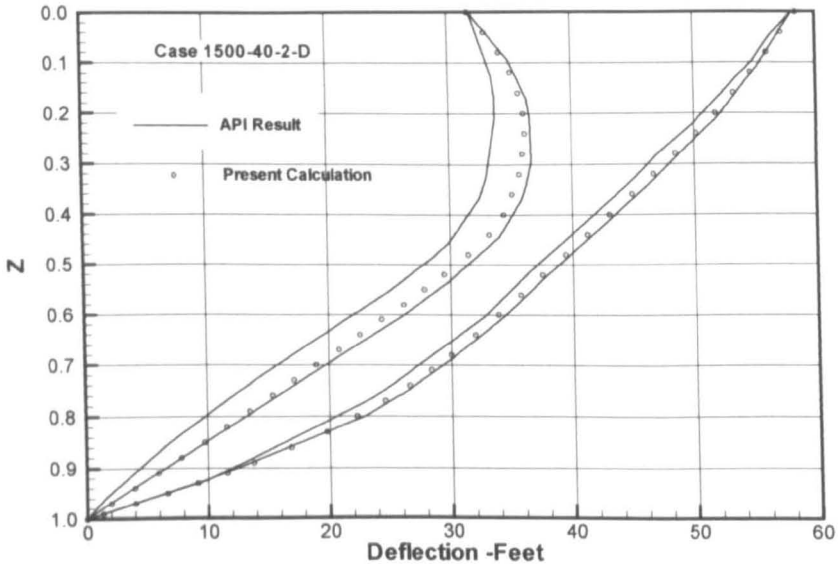

Figure 8.3(a)

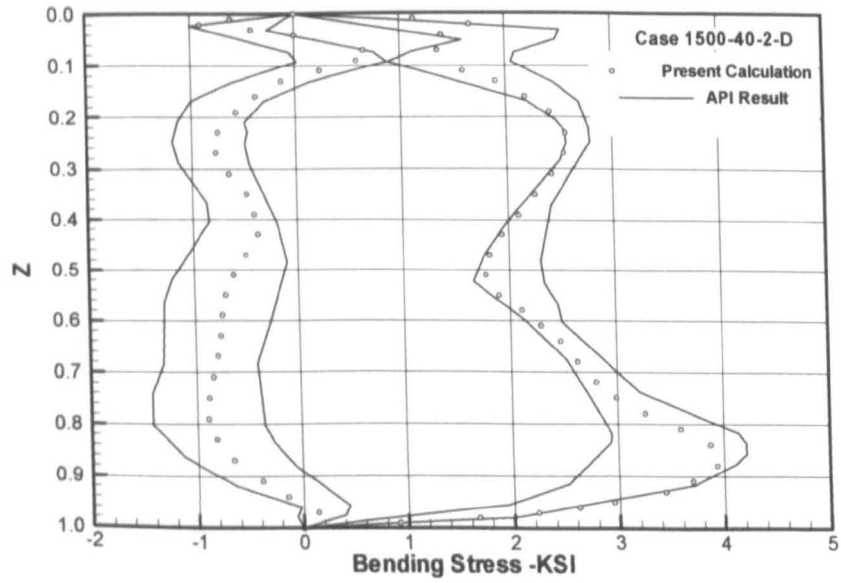

Figure 8.3 (b)

Figure 8.3 Comparison of present calculation and API published result for a solitary drilling riser. Top tension 600 Kips. (a) Displacement; (b) Bending stress.

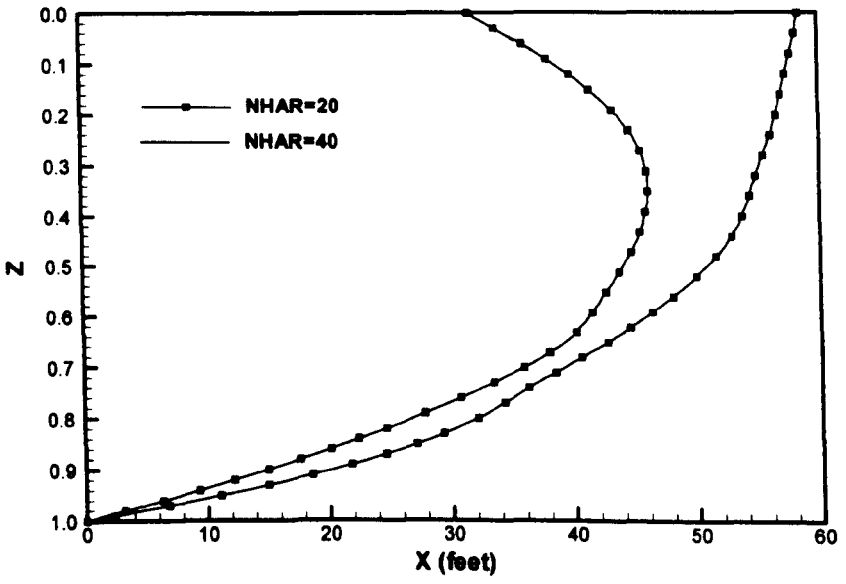

Figure 8.4(a)

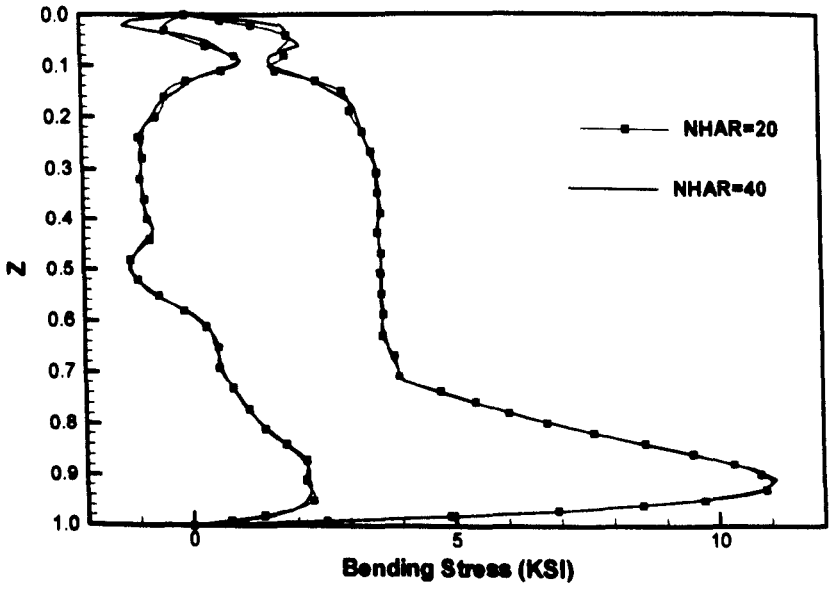

Figure 8.4(b)

Figure 8.4 Comparison of displacement and bending stress by using different mode numbers. Top tension 370 Kips, riser length: 1520 feet, wave height: 40 feet. (a) Displacement, (b) Bending stress.

8.3.2 Transition of A Pair of Risers Under Steady Current Only

In the subsequent systematic analysis of the dynamics of a pair of marine risers, the specification of the riser taken in the analysis is as follows:

Table 8. 2 Specification of the riser pair.

Geometrical Data	**Value**	**Unit**
Outer Diameter (m)	*0.30*	*m*
Internal Diameter (m)	*0.24*	*m*
Riser Length (m)	*1332.0*	*m*
Depth of Mean Water Level (m)	*1332.0*	*m*
Property of Riser		
Young's Modulus E	2.10×10^{11}	N/m^2
Bending Stiffness EI	4.93×10^{7}	$N\cdot m^2$
Mass of Riser		
Weight in Water (KN/m)	*1.695*	*KN/m*
Density of Water (Kg/m^3)	*1025.0*	Kg/m^3
Hydrodynamic Loading		
Current Profile and Velocity (m/s)	*Uniform Profile*	*m/s*
	0.5 ~ 1.5	
Added Mass Coefficient	*1.0*	
Drag Coefficient in Free Stream	*1.2*	
Top Tension (N)	2.709×10^{6}	*N*
	3.708×10^{6}	
	7.416×10^{6}	

8.3.2.1 Tandem Arrangement

Figure 8.5 shows that the riser pair experienced a transition from the design position to, and finally rested at, their corresponding equilibrium states. The pair is initially separated by 10 diameters and in tandem arrangement, located at their corresponding design position, and only the time-averaged forces are considered. Under the sudden increase of the flow velocity, the downstream riser is pushed downstream. Due to the inertial effect, the downstream riser passed its equilibrium in the first place, then recovered immediately to its equilibrium. Shown in Figure 8.5(a) is the deflection at different positions of the riser. It is seen that different parts of the riser move almost in phase with each other. The figure shows that the fluid damping is significant as the riser approaches to its equilibrium state so quickly. Figure 8.5(b) is the final equilibrium geometry of the riser pair. As indicated in Chapter 7, the above 12" pair riser under 0.5 m/s current is stable at their equilibrium state. The results here are consistent with the foregoing analysis.

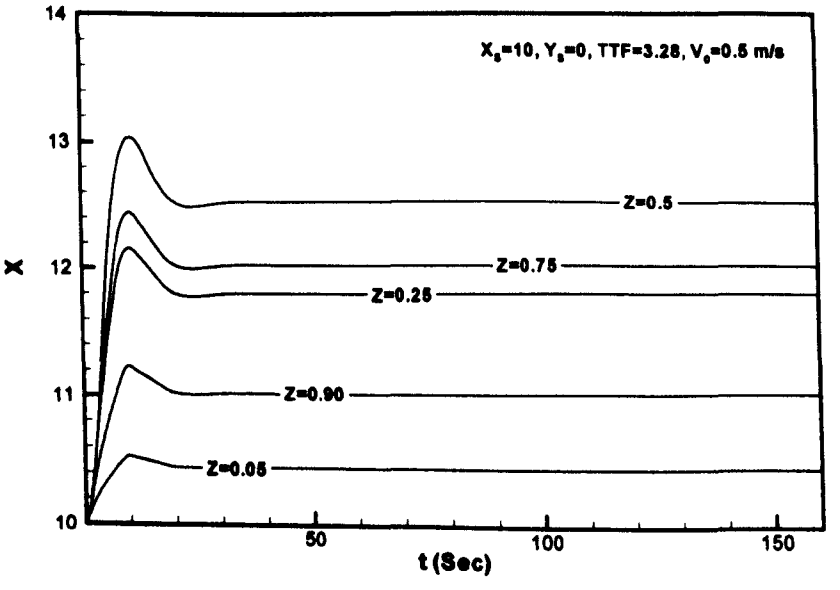

Figure 8.5(a)

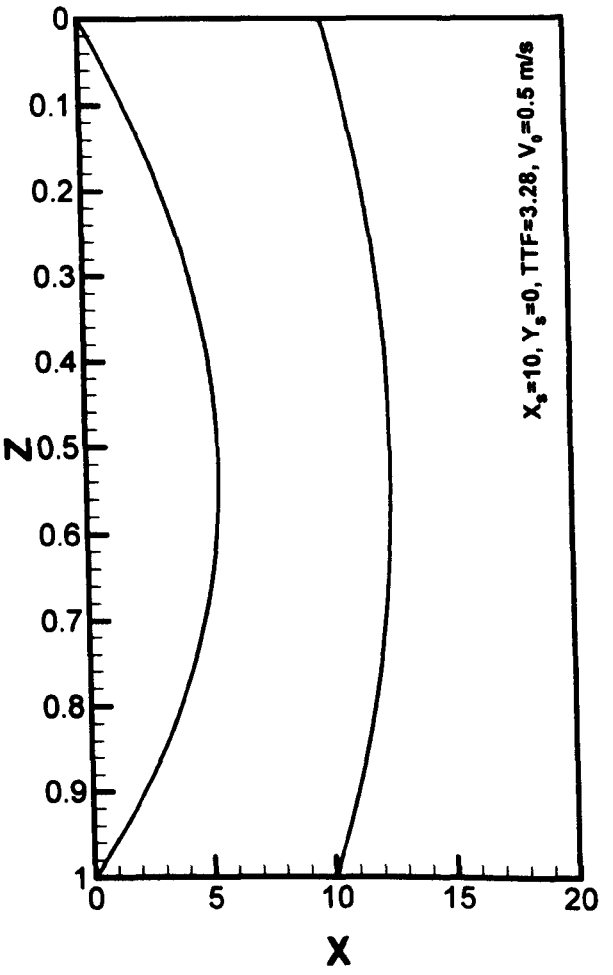

Figure 8.5(b)

Figure 8.5 12" Riser pair transit from initial design position to final equilibrium under current velocity of 0.5 m/s. (a) Transition of different parts of the riser. (b) Geometry of the equilibrium.

8.3.2.2 Staggered Arrangement

Figures 8.6 and 8.7 show the case when the riser pair is in a staggered arrangement. The streamwise direction separation is set as 10 diameters, with cross flow direction spacing of 2 and 2.5 diameters respectively. The flow velocity is 0.5 m/s. As shown in Chapter VII, the equilibrium of the riser pair is stable under such an ocean current condition. In this case also, the riser pair is initially located at their corresponding design position. Figures 8.6 and 8.7 show the whole transition course of the middle point of the riser. It is very similar to the tandem arrangement. Initially, the riser is pushed towards downstream quickly, as shown in the velocity figure, meanwhile, the riser is pulled towards the wake centreline.

Very swiftly, the velocity of the downstream riser dies out and it rests at its equilibrium. Under such a flow velocity, even for the case of transverse location of 2.5 diameters, there is only one equilibrium state. Therefore, Figure 8.7 is similar to Figure 8.6.

However, for the case of transverse spacing with 2.5 diameters, when the flow velocity is further increased, as shown in Figure 8.8 where flow velocity is 0.67 m/s, more than one equilibrium state can be reached depending on the initial state. The initial position 1 corresponds to the state of design position. Under such a condition, the upstream riser is also located at its corresponding design position initially, and it is seen that finally the downstream riser rests at final equilibrium position 1 (called as stable outer equilibrium in this Chapter). As indicated in the Figure 8.8(b), after an acceleration in stream wise direction and attraction towards wake centreline, the movement of the downstream riser dies out rapidly when near the equilibrium. The second initial arrangement is made as such that the upstream riser is close to its equilibrium whilst the downstream riser is close to its equilibrium in streamwise direction. However, transversely the downstream riser is located towards the wake centreline. Presumably the downstream riser has a symmetrical parabolic deflection with its centre point located at (*20*, *0.5*) and, as can be seen from figure 8.8(a), the downstream riser is attracted to the second equilibrium state, i.e. stable inner equilibrium.

Figure 8.9 shows the boundary between which the different initial conditions leads to different equilibrium states. The upstream riser is assumed to have the same initial state near its equilibrium with the streamwise displacement of its midpoint of 10 diameters. The initial position of the downstream riser varies from 15 diameters to 22 diameters in streamwise location, and from wake centreline to the 5 diameters in the transverse location. It is shown in the figure that there is a boundary, when the initial position is above the boundary, where the downstream riser will ultimately rests on the outer equilibrium.

Alternatively, when the initial position is located underneath the boundary, the downstream riser will approach and rest on the inner equilibrium. When the initial location of the downstream riser is on the boundary, it leads to an unstable equilibrium, which is located between the two stable equilibrium states.

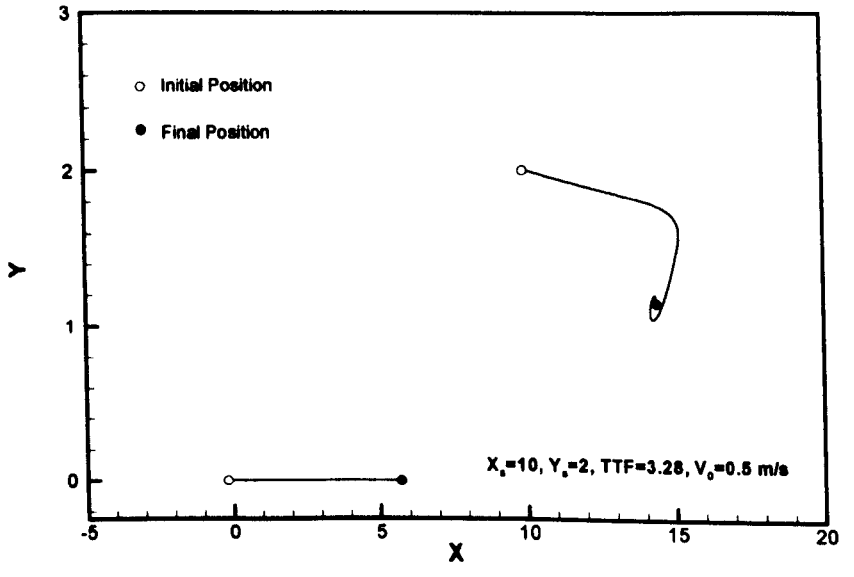

Figure 8.6(a)

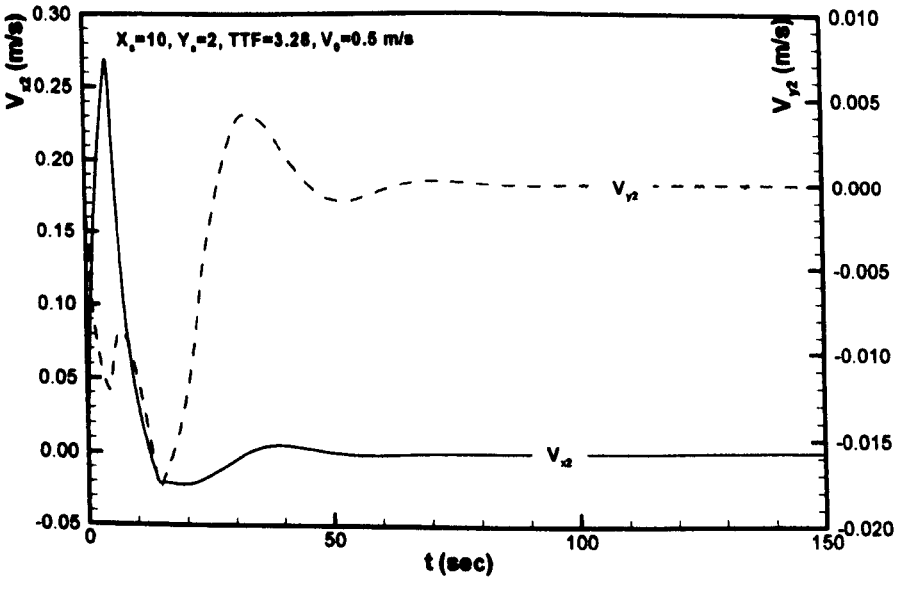

Figure 8.6(b)

Figure 8.6 Transition from design position to equilibrium for arrangement of (10, 2) under current of V_0=0.5 *m/s*. (a)Trajectory of upstream and downstream riser middle point, (b) Velocity history of the downstream riser middle point.

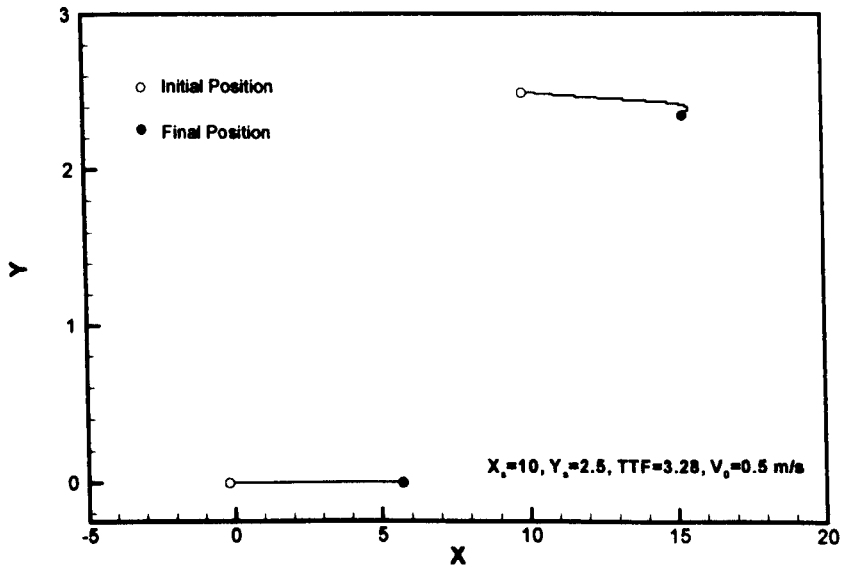

Figure 8.7(a)

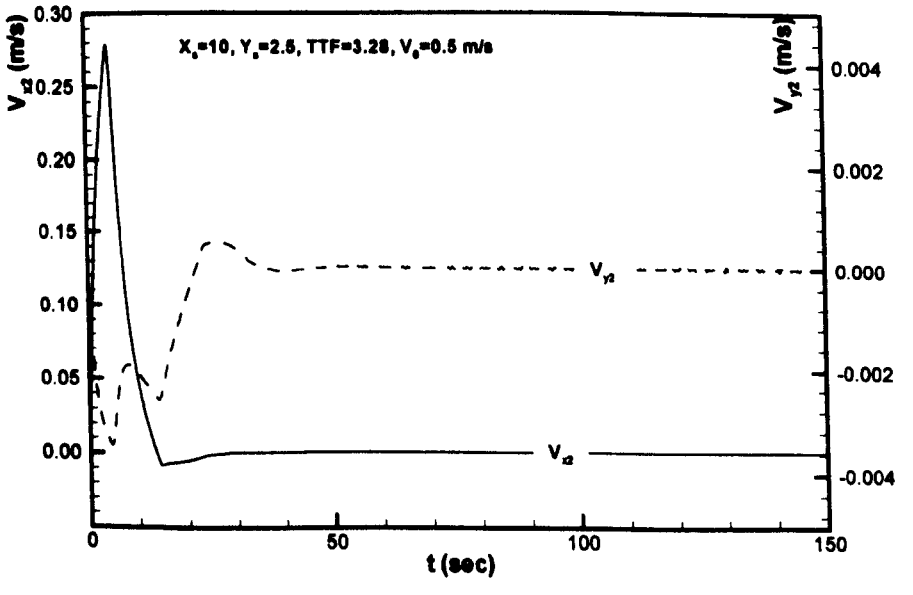

Figure 8.7(b)

Figure 8.7 Transition from design position to its equilibrium for arrangement of (10, 2.5) under current of V_0=0.5 *m/s*. (a)Trajectory of upstream and downstream riser middle point, (b) Velocity history of the downstream riser middle point.

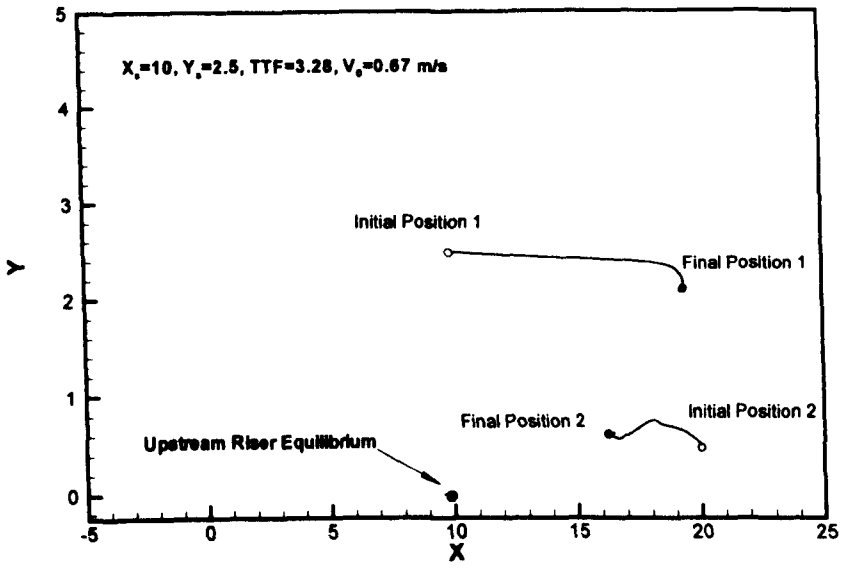

Figure 8.8(a)

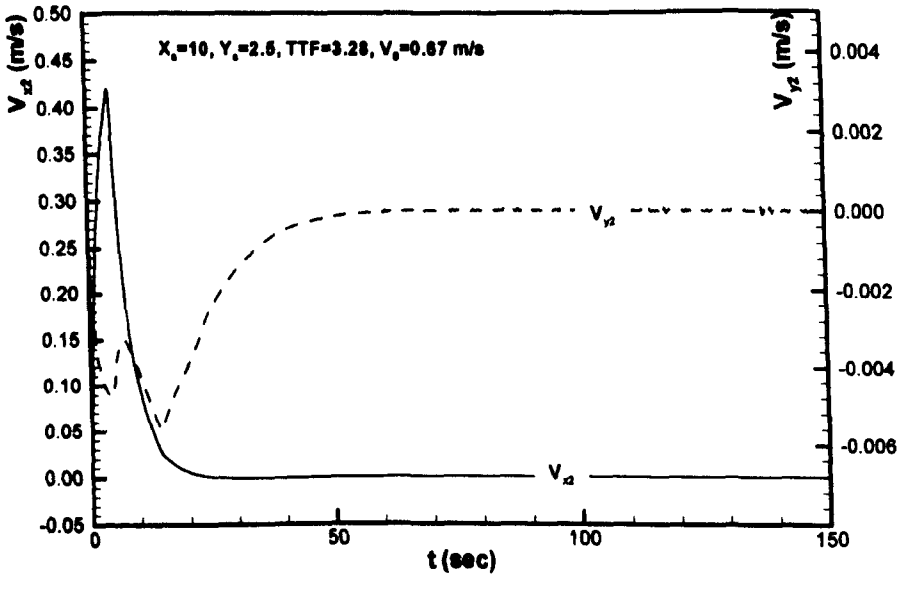

Figure 8.8(b)

Figure 8.8 Transition to different equilibrium from different initial position. (a) Transition of the riser middle point to equilibrium for different initial condition, (b) The velocity history of the downstream riser middle point when transition occurred from the design position.

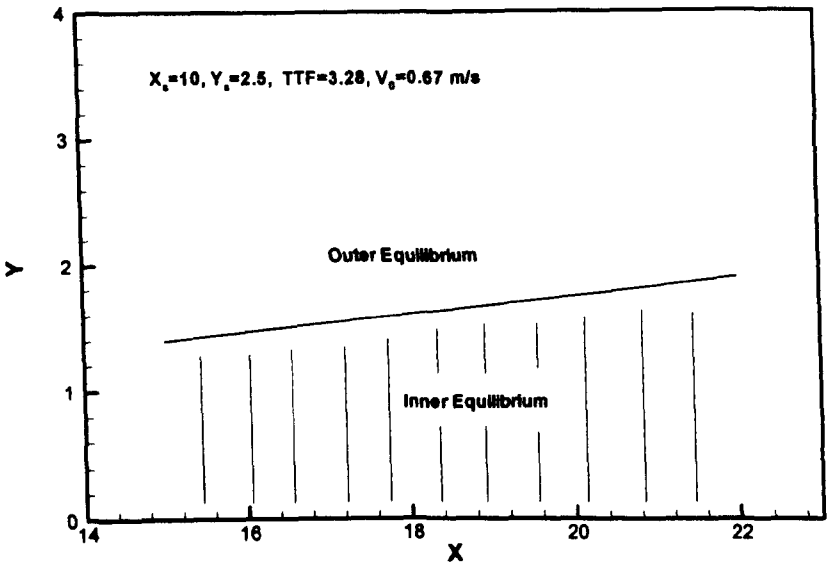

Figure 8.9 Attraction domain for two equilibrium, with X_S=10, Y_S=2.5, TTF=3.28, V_0=0.67 *m/s*, the upstream riser is initially located near its equilibrium.

8.3.3 Riser Pair in High Current (Post Loss of Stability)

8.3.3.1 Tandem Arrangement

The dynamic behaviour is examined when the current speed exceeds the critical state. Figure 8.10 shows the case when two risers are arranged in tandem with spacing of 10 diameters, and initially the two risers are located at their design positions. As shown in the figure, the downstream riser initially moves towards downstream. However, because there is no equilibrium state in the downstream, it moves back to the upstream and ultimately it collides with the upstream riser. Here, for simplicity, the effect of the upstream riser has been replaced by the effect of the wake force field. Therefore, the detail of the collision process has not been accounted for. Similarly to the scenario in the two-dimensional case, the downstream riser tends to be quickly pushed towards downstream after the collision. There is a process of slow recovery towards upstream and then a quick push back towards downstream. The time interval for a single process is about 26 Seconds in this particular case, which is in the same order of the first mode frequency. For such a case, the vortex shedding frequency is around 20 times higher than the first mode natural frequency. The

amplitude of the movement of the downstream riser is more than 10 diameters. Distinctively, the trajectory is different from the vortex-induced vibration. Figures 8.2(c) to (f) show the course of the movement at different time instants. As shown in the figures, when the middle position of the upstream riser is nearest to the downstream riser, the first contact will be most likely to occur near the middle position of the risers.

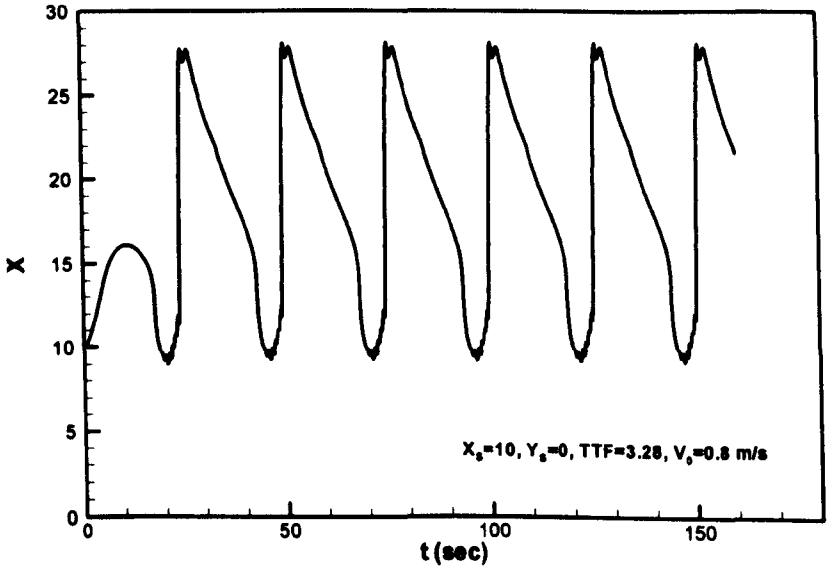

Figure 8.10(a)

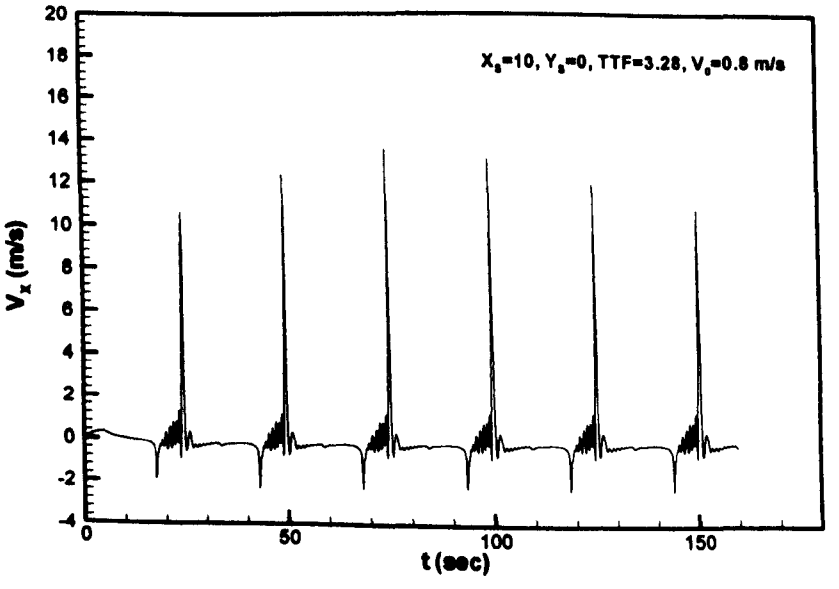

Figure 8.10(b)

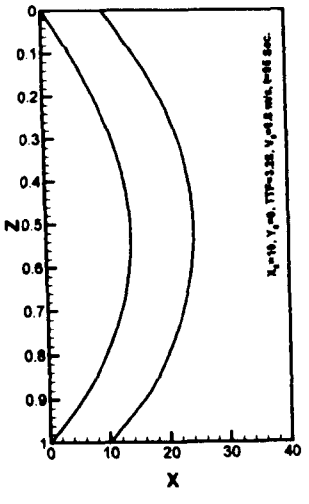

Figure 8.10(c)

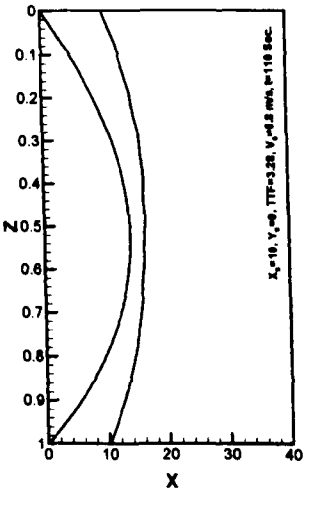

Figure 8.10(d)

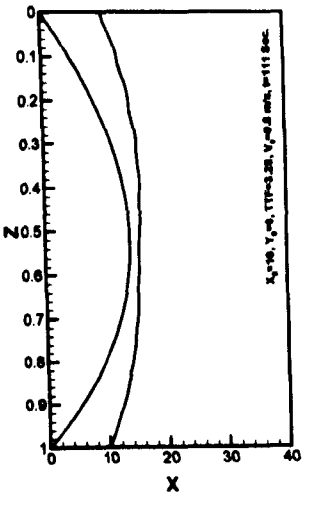

Figure 8.10(e)

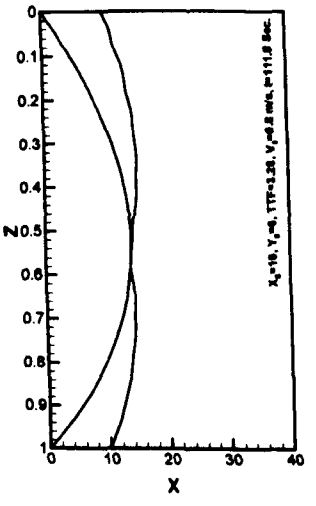

Figure 8.10(f)

Figure 8.10 The motion of the downstream riser after the flow velocity has exceeds the critical state, current speed: 0.8 m/s. (a) Streamwise direction displacement of the downstream riser middle point; (b) Streamwise direction velocity of the downstream riser middle point; (c) to (f) Variation of geometrical shape at different time instant. t=95, 110, 111 and 111.8 seconds respectively.

Further calculations are made to account for the effect of different design spacings, flow velocities and top tension factors on the movement amplitude, velocity and time intervals between successive collisions. The comparisons are shown in Tables 8.3 to 8.5. The movement range of the downstream riser is defined as the distance between the two extreme positions that the middle part of riser can reach. The maximum velocity of the downstream riser is defined as the peak velocity of the riser middle part moving towards upstream. In the comparison of different top tension factors and design spacing, the flow velocity is chose as such that it is close to and above the critical state. The calculation results show that when the flow velocity exceeds the critical state, the wandering around of the downstream riser will have the magnitude of more than 10 diameters, collisions between two risers will occur from time to time, and that the time interval between successive collisions is dependent on the flow velocity and design spacing. On the other hand, for the same design spacing, the motion amplitude of the downstream riser does not vary significantly with the flow speed, nor with the top tension factor. Such a result is not reflected in the two-dimensional simulation, and it is likely to be due to the unaccounted collision effect.

Table 8. 3 Comparison between different top tension factors (X_S=10, Y_S=0).

Top Tension Factor	1.20	1.64	3.28
Natural Period (*Sec*)	38.50	29.83	18.99
Critical velocity (*m/s*)	0.305	0.415	0.663
Flow Velocity (*m/s*)	0.35	0.42	0.70
Maximum Velocity Towards Upstream (*m/s*)	1.41	0.96	1.49
Motion Amplitude (xD)	18.0	18.2	18.2
Time Interval (*Sec.*)	59.2	88.7	36.4

Table 8. 4 Comparison between different designing spacing (TTF=3.28).

Design Spacing	10D	20D	30D
Critical velocity (*m/s*)	0.663	1.107	1.473
Flow Velocity (*m/s*)	0.70	1.12	1.55
Maximum Velocity Towards Upstream (*m/s*)	1.49	1.36	2.72
Motion Amplitude (×D)	18.2	16.7	10.0
Time Interval (*Sec.*)	36.4	101.5	45.1

Table 8. 5 Comparison between different flow speed (X_S=10, Y_S=0, TTF=3.28).

Flow Velocity (*m/s*)	0.70	0.75	0.80
Maximum Velocity Towards Upstream (*m/s*)	1.49	1.48	2.31
Motion Amplitude (×D)	18.2	18.2	18.4
Time Interval (*Sec.*)	36.4	28.5	25.5

The maximum motion velocity of the downstream riser towards upstream increases with the flow velocity. In order to make a comparison with the vortex-induced vibration, the maximum velocity of the VIV motion is estimated as follows:

Consider the case of flow velocity of 0.7 m/s, the corresponding vortex shedding frequency is 0.47 Hz should the Strouhaul number be taken as 0.2. If "lock in" occurs and, assuming the maximum motion amplitude to be 1 diameter, the correspond motion velocity is about 0.88 m/s.

According to the results presented in the tables, the motion caused by the wake-induced oscillation is clearly more significant than the vortex-induced vibration. Additionally, the

collision related to vortex-induced vibration occurs locally, while the wake-induced motion caused collision is often with all parts of the riser moving together, as shown in Figure 8.10, and hence, with much more energy participated in. Therefore, the wake-induced motion plays a very significant role in the collision.

8.3.3.2 Staggered Arrangement

Figures 8.11 to 8.14 show the cases when the two risers are in a staggered arrangement, with X_s=*10, 20* and Y_s=*1*, 2.5 respectively. The current velocity is close to and above the corresponding critical flow velocity for each individual case. The motion trajectories (Figure 8.11, 8.12, 8.13 and 8.14(c)) show that the characteristics of all the presented cases are similar. The motions are always in a clockwise direction, with the main acceleration course occurring when two risers are in inline positions. Such a motion shows that within the whole cycle of the movement, the streamwise fluid drag force tend to input energy to the riser's motion, as the drag force tends to be larger when the riser is located at outer part of the wake. This energy absorption of the downstream riser's motion is balanced by the energy dissipation caused by the fluid damping effect. The biggest acceleration occurred for two risers immediately before the collision, as seen from Figure 8.14(d). The process of the push back by current is much quicker than the recovery. The amplitude of the movement is generally larger than 10 diameters. Tables 8.6 to 8.8 show the effects of top tension factor, initial spacing, and flow velocity on the motion amplitude and velocity.

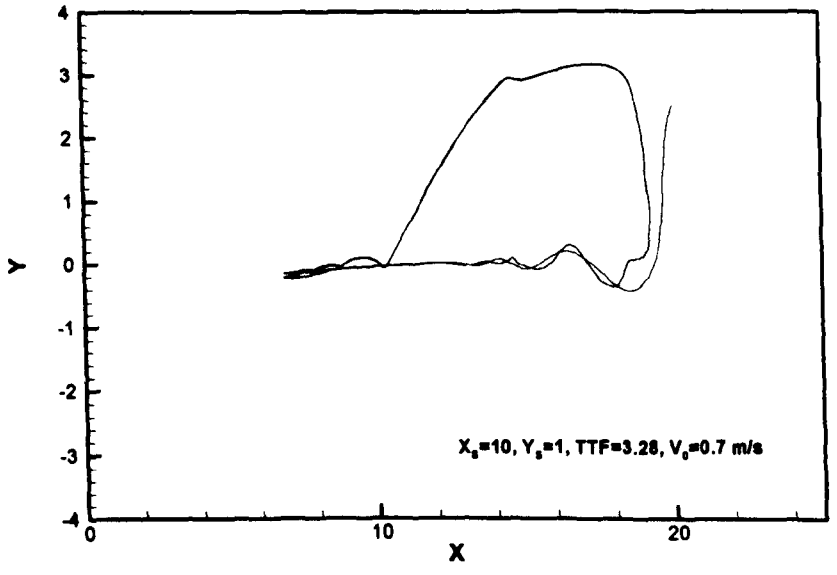

Figure 8. 11 Trajectory of downstream riser movement.

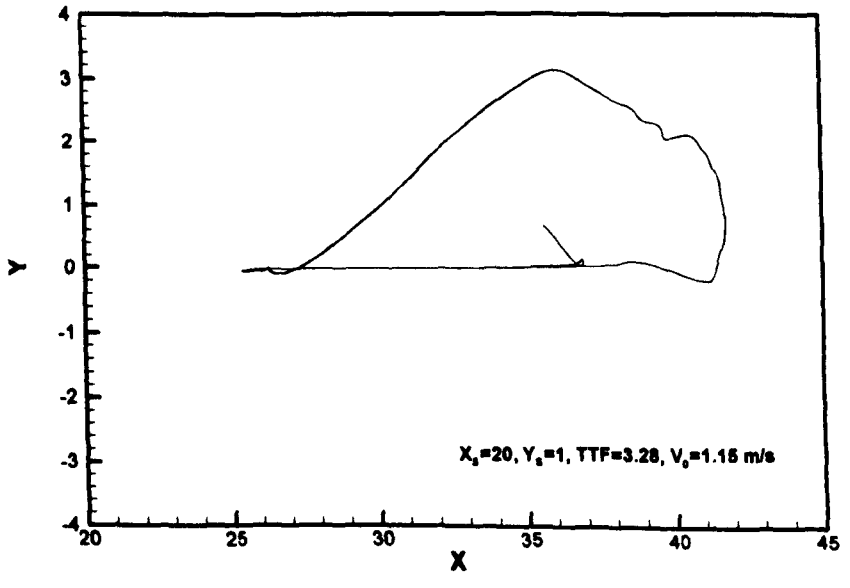

Figure 8. 12 Trajectory of downstream riser movement.

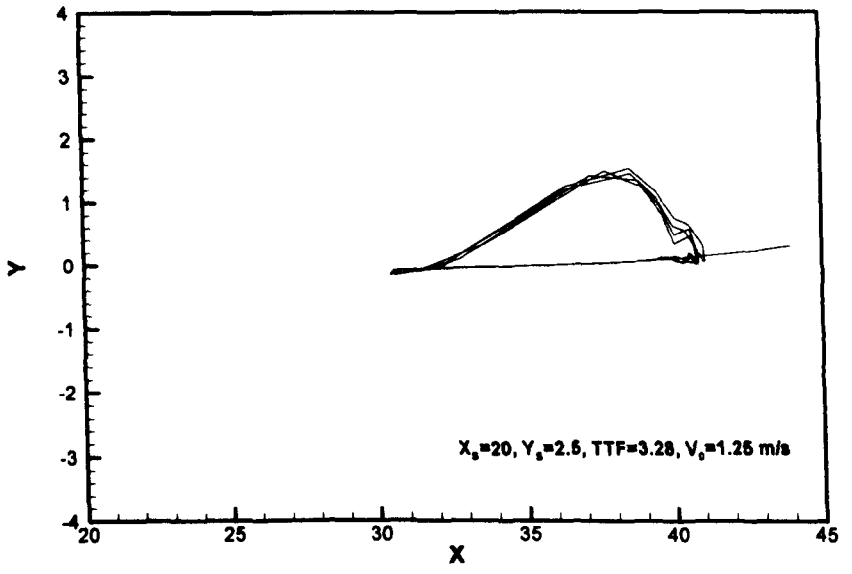

Figure 8.13 Trajectory of downstream riser movement.

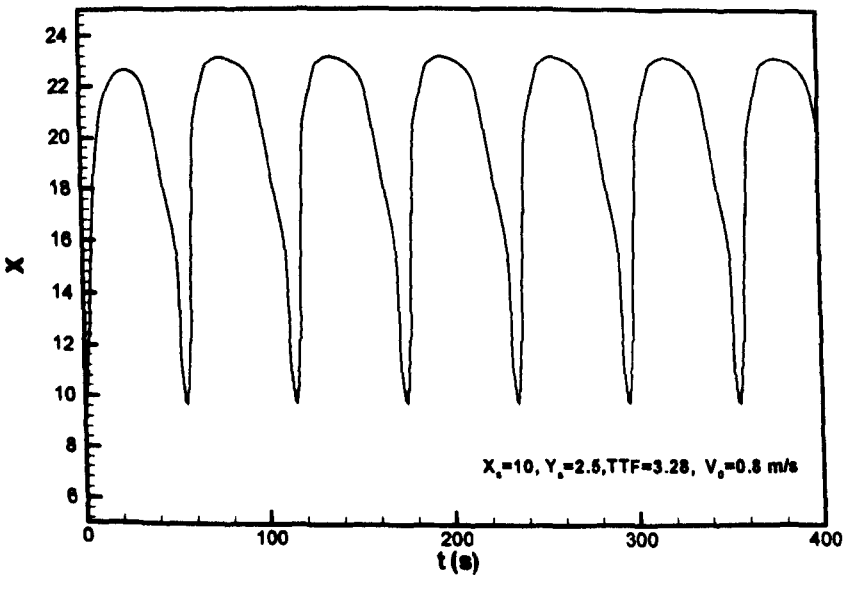

Figure 8.14(a)

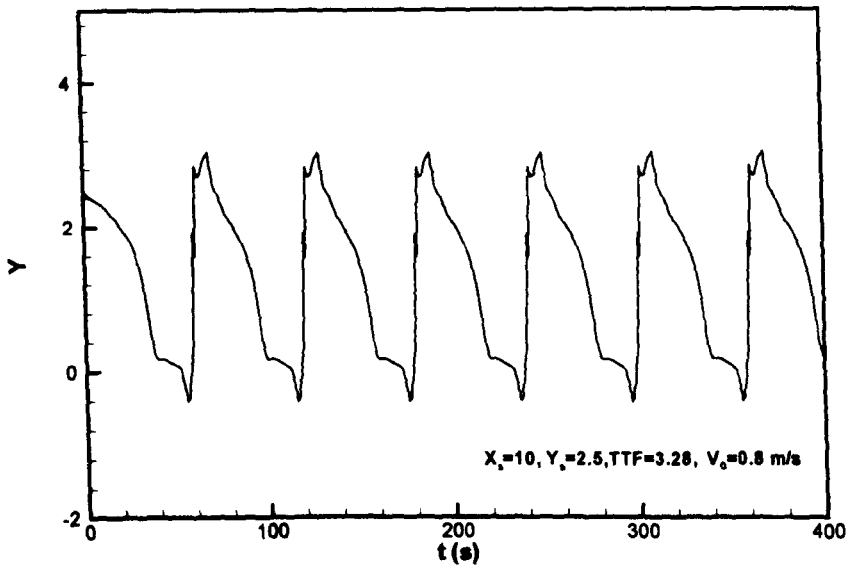

Figure 8.14(b)

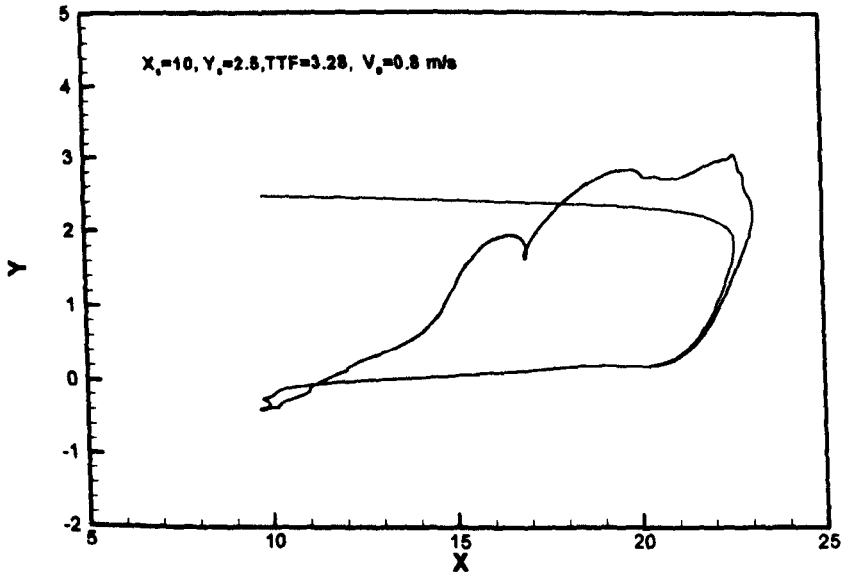

Figure 8.14(c)

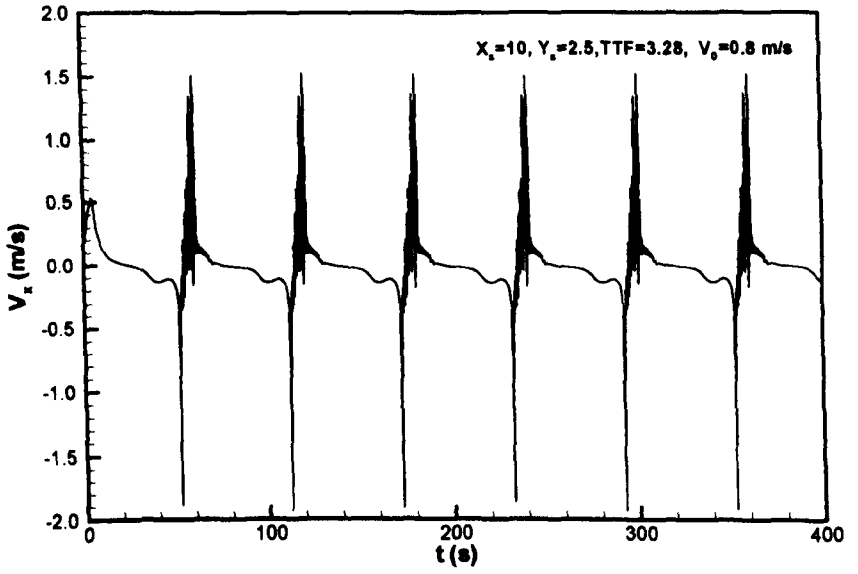

Figure 8.14(d)

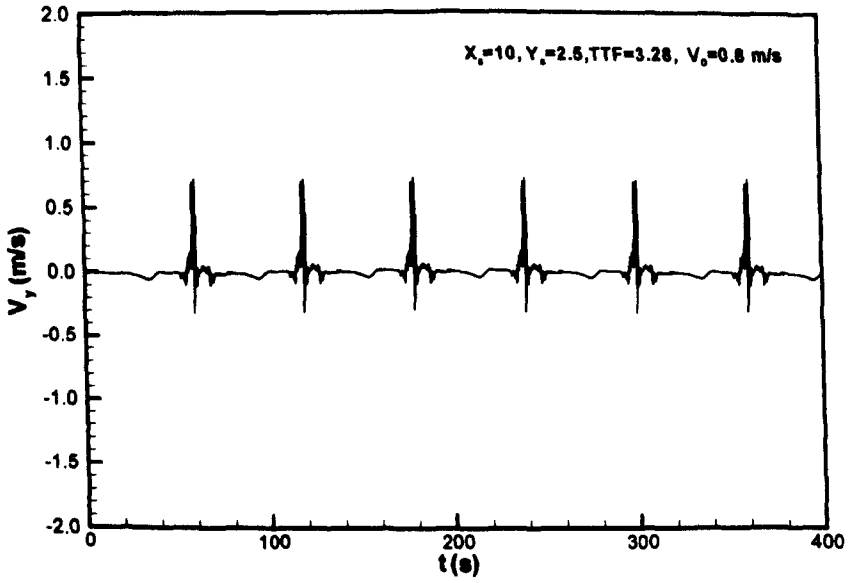

Figure 8.14(e)

Figure 8.14 Dynamics of a riser pair with top tension of 7.416×106 (N) under the 0.8 (m/s) current. All parameters in the figures are for the riser middle point position; (a) streamwise displacement (b) transverse direction displacement (c) trajectory of the middle point, (d),(e) streamwise and transverse direction velocity.

Table 8. 6 Comparison between different top tension factors for $X_S=10$, $Y_S=1$.

Top Tension Factor	1.20	1.64	3.28
Flow Velocity (*m/s*)	0.35	0.42	0.70
Maximum Velocity Towards Upstream (*m/s*)	1.37	1.50	1.45
Motion Amplitude (×D)	12.7	13.3	12.2
Time Interval (*Sec.*)	60.9	58.7	36.2

Table 8. 7 Comparison between different design spacing for the same top tension, *TTF=3.28*, $Y_S=1$.

Design Spacing (×D)	10	20	30
Flow Velocity (*m/s*)	0.70	1.15	1.55
Maximum Velocity Towards Upstream (*m/s*)	1.45	2.23	1.06
Motion Amplitude (×D)	12.2	16.1	9.9
Time Interval (*Sec.*)	36.2	61.2	62.5

Table 8. 8 Comparison between different flow speed *TTF=3.28*, $X_S=10$, $Y_S=1$.

Flow Velocity (*m/s*)	0.70	0.75	0.80
Maximum Velocity Towards Upstream (*m/s*)	1.45	1.83	1.97
Motion Amplitude (×D)	12.2	12.0	11.9
Time Interval (*Sec.*)	36.2	27.5	23.9

It is seen that, as with the cases of tandem arrangement, the movement amplitude is insensitive to the flow velocity once the critical flow velocity has been exceeded. This also applies to the relationship between movement amplitude and the top tension factor.

However, the amplitude varies significantly with the design spacing. The time interval between two successive collisions changes considerably with the flow velocity, and the motion speed before the collision is considerably high when compared to the vortex-induced motions. Such results are the same as the tandem arrangement.

8.4 Summaries

As a result of the analysis conducted in this chapter, following conclusions can be drawn.

1. With only time-averaged force considered, when the flow velocity is lower than the critical flow velocity, the downstream risers tend to approach their equilibrium quickly should there be any disturbance. When there is more than more equilibrium then, depending on the initial state of the riser, it can approach to different equilibrium state.

2. When the flow velocity exceeds the critical state corresponding to the specific arrangement and top tension, the downstream riser will start to wander around. This kind of movement is a low frequency, large amplitude motion, which can ultimately bring the two risers to collide with each other intermittently.

3. The frequency of the collision (the inverse of the time interval between two successive collisions) is dependent on flow velocity, which generally is in the same order of magnitude as the first mode frequency. Relative to the vortex-induced vibration, such a movement is very low in frequency.

4. The amplitude of the movement is dependent on the design spacing and insensitive to the top tension factor and flow speed.

5. Because the motion mainly occurs in the streamwise direction, the collision caused by such wake-induced motion mainly occurs in the direction of flow. It is significantly

more important in the contribution towards the collision than the vortex-induced vibration regarding its synchronised motion and high movement speed.

6. The minor discrepancy to the two-dimensional simulation may be attributed to the unaccounted collision course during the movement of the two risers. The detailed explanation calls for a proper collision model to be incorporated into the analysis.

Chapter IX

DISCUSSION

9.1 General Remarks

As set out in the beginning of this thesis, this investigation focuses on finding the mechanism of the interaction between two risers and providing effective tools to identify the critical state of the interaction. It also aims to provide information about the dynamic behaviour when risers lose their equilibrium. This thesis started with the force prediction for the downstream cylinder located in the wake, which forms the basis for the subsequent analysis. This was followed by stability analysis, continuation study and dynamics simulation, with the investigations further extended into the three-dimensional. These ultimately addressed the real scenarios for riser design and operation. Various calculation examples have been presented throughout the thesis.

9.2 Contributions of the Thesis

The following are the main contributions of this thesis to the body of knowledge:

9.2.1 Time-Averaged Force Prediction

The application of free streamline theory to account for the fluid forces exerted on the wake located downstream cylinder gives a new insight into the mechanism of the fluid forces on the downstream cylinder, which is more intuitive and acceptable than the

previous arguments. Although the importance of such efforts will be lessened with the further enhancing of CFD power in the near future, it still will be very helpful in the construction of a dynamics model and understanding the dynamics related phenomena. In addition, it will be beneficial to the understanding of CFD results.

9.2.2 Mechanism of Riser Collision

The present investigation is the very first one endeavoured solely on the investigation of the stability of the TLP/Spar riser interaction and identification of the critical state by continuation analysis. The study disclosed the collision mechanism of two risers, a phenomenon which has been recognized in recent years but never be appropriately addressed.

In parallel with this investigation, there is work conducted in industry such as that by Marintek and MCS. Both of them set out to identify the critical state of riser interaction. The former used a shooting method to seek the equilibrium state and the latter used the available commercial "Flexcom" software package. Neither method can explain accurately the mechanism of the collision, nor can they identify the critical state accurately and unproblematically. Both can easily mislead users to the conclusion that the two risers are brought into contact gradually, because of the progressive closing of the two risers with the increase of the current velocity. Furthermore, their explanations can distort the contribution of collision energy, should it be investigated. In this sense, the present investigation clarifies the mechanism of riser collision and provides effective tools to identify the critical state.

9.2.3 Dynamics Simulation

The dynamics simulation conducted in this thesis portrays the wake-induced dynamic behaviour of the cylinders, both in two-dimensional and three-dimensional space. The analysis provides an approximate energy description for the risers immediately before the

collision, which clearly shows that it is at least in the same order of magnitude as the vortex-induced vibration. In the past, nearly all the work on collision investigation was based on the vortex-induced vibration, the results of this investigation reinforces the importance which the wake-induced oscillation has in participating in the riser collision.

9.2.4 Riser Statics

The statics analysis revealed the non-negligible effects of the wake on the interaction in a very concrete and quantitative way. The parametrical investigation shows the importance of the wake effects in different perspectives. In addition, the difficulties of the laboratory simulation of very large scale marine riser interactions were addressed. The contribution of such an analysis lies in the provision of a quantitative knowledge to the riser engineers rather than theoretical one.

9.2.5 Comparison Between Different Cylinder Interactions

The present investigation, in two-dimensional space, is the most comprehensive and fundamental research into the interaction between two cylinders ever conducted. It not only covers a much wider area of wake field than has been tried before elsewhere, but also addresses the issue on the mass parameter, which is a topic that has been neglected in the past research. The investigation identified the peculiarities of marine riser interaction. Such a study is beneficial to marine riser engineers as well as researchers in other engineering disciplines.

9.2.6 Multiple Equilibrium States

The first identification of multiple equilibrium states can be significant to the further understanding of multiple riser interactions. Although the importance of multiple equilibrium states or possible disturbances caused by unsteady flow or vortex-induced vibration have not been elaborated upon in this thesis, further investigation could result in an exciting chapter on riser dynamics.

9.3 Applications of the Research

9.3.1 Riser Design

This investigation provides important guidelines on how to avoid riser collision, based on the prediction of the critical states provided in the continuation analysis. Hence, riser designers can identify the necessary top tension and design spacing, under specified design ocean current. Further negotiations can then be made within the integrated system design, based on such predictions, during the riser designing process.

9.3.2 Riser Operation

This thesis shows how to predict the possibility of riser collision under specified ocean currents. Therefore, should severe weather occur, the riser operator can know beforehand whether the riser operation should continue or be suspended.

9.3.3 Damage evaluation

The dynamics simulation provides important information on the possible damage that can occur should collision between risers happen. Based on such data, it can not only guide the riser operators to take sensible measure under severe weather, but also, it provides a valuable reference to aid in identifying the cause of the damage should any such damage emerge.

9.4 Recommendations for Further Studies

As the offshore industry seems determined to move towards deep and ultra deep water, the riser interaction issue demands that even more questions be answered. Based on the present investigation, the following areas would be of interest and important to the further understanding of riser interaction,

1. The role of vortex-induced vibration to the timer-averaged force induced collision, both on the critical state identification and the contribution to the collision. The vortex-induced vibration constitutes a significant disturbance to the riser

equilibrium. Particularly as identified in the continuation investigation, there can be multiple equilibrium states coexisting under certain riser arrangements and flow conditions. The interaction between vortex-induced vibration and the timer-averaged force effect, and also the interaction between multiple equilibrium states can be important and interesting to the investigation of the dynamics of the risers.

2. The dynamic simulation on the riser collision. The collision between two risers depends on many factors, such as wall surface characteristics, the material of the two risers, and the contacting point during the collision and many others. The detailed investigation using an appropriate model can ultimately identify more accurately the damage to the riser and the dynamic behaviour of the riser after collision.

3. The extension from two risers to multiple riser interaction. The ultimate objective of the investigation into riser interaction is to understand the mechanism of riser cluster interaction, such as for TLP and Spar risers. Based upon the present investigation, further investigations could be started into three-riser interaction, with one located in the wake formed by the other two risers. By using same methodology as in this thesis, investigations can be made into understanding the effects of the additional risers, and ultimately lead to the understanding of the multiple riser interaction.

4. Due to the deepwater challenges identified in the first chapter, the interaction between the risers and the whole system is also a key issue in deepwater development. An understanding of the effects of the whole system dynamics on the inter-riser interaction (the interaction studied in this thesis) is important to the further understanding of the inter-riser interaction mechanism.

Chapter X

CONCLUSIONS

Based on the investigations described in this thesis, the following conclusions can be drawn:

- The application of the free streamline theory to account for fluid forces exerted on the wake-located downstream cylinder is successful. When lacking the necessary fluid force information, it is an effective tool to provide the data necessary for the investigation of the dynamics of the two cylinders interaction.

- The present investigation in two dimensional space is the most comprehensive and fundamental research on the interaction between two cylinders conducted so far, which not only covers a much wider area of the wake field that has not been tried before elsewhere, but also addresses the issue on the mass parameter which is a topic has been neglected in the past research. Combining the stability analysis and continuation investigation, the study disclosed the mechanism of the cause of the two cylinder potential collision, a phenomenon which has been recognised in recent years and has never been appropriately addressed. The present continuation is the very first exercise in accurately identifying the critical state of the two cylinder collision. The

dynamic simulation explains the phenomenon of the two cylinder interaction in time domain, which is helpful to the understanding of the experimental observations and for the further estimation of the possible damage incurred should collision occur.

- The three dimensional investigation is an extension of the two dimensional study. However, from the perspective of quantitative study, it is essential part of the investigation of the two risers interaction. Starting from the statics investigation, the examination of the interaction effects reveals the non-negligible effects of the wake on the interaction. The parametrical investigation shows the importance of the wake effect in different ways. The difficulties of the laboratory simulation of the very large scale marine riser interaction were also addressed. The continuation investigation cross-confirms the two dimensional investigation results, and, more practically, the investigation provided some general data regarding the critical state to avoid the riser collision. It is hoped that this can work as a design guideline for riser clearance. The dynamics simulation in three-dimensional space clarified the dynamic behaviour of the two risers interaction, and presents some valuable information on the riser collision investigation.

NOMENCLATURE

Without specific explanation, the symbols used in this thesis are referred to as follows:

a: Mass parameter $\left(=\frac{\rho D^2}{2m}\right)$;

A, A_0, A_i: Cylinder cross section area, the whole area and the inner area

b: Wake velocity ratio $\left(=\frac{U}{V_0}\right)$,

or half wake width, where the wake velocity deficit is half of the magnitude on wake centreline at same streamwise location.

C_D, C_L: Drag and lift coefficients for downstream cylinder respectively $\left(=\frac{F_{D,L}}{\frac{1}{2}\rho V_o^2 D}\right)$;

$\overline{C}_D, \overline{C}_L$: Drag and lift coefficient referenced by the wake velocity $\left(=\frac{F_{D,L}}{\frac{1}{2}\rho U^2 D}\right)$;

C_{D0}, C_{L0}: Drag and lift coefficients for downstream cylinder respectively at equilibrium position;

C_p, C_{pc}: Pressure coefficients based on free stream flow velocity and wake flow velocity respectively

D: Diameter of cylinder;

E: Young's modulus;

F_x, F_y : Fluid force in x, y direction respectively;

g : Gravity acceleration speed;

H_w : Flow tension factor.

I : Cross section area momentum;

$\vec{k}$: Unit vector along cylinder axis pointing towards readers

k_T : Stiffness of tensioner system

$K(q_m, q_n)$: Induced velocity at q_m by vortex located at q_n with unit strength

K_x, K_y : Spring stiffness in x, y direction respectively

l : Length of the cylinder;

$l_0, l_{Z0}, \Delta l_Z$: Unstrained length, vertical distance between top connector and bottom connector and the deviation of the vertical distance with the existence of dynamic movement.

m : Mass, including mass of cylinder per unit length and fluid added mass $(= m_S + m_a)$;

m_S : Structure mass of the cylinder in air

m_a : Fluid added mass of the cylinder

$\vec{n}$: Local normal unit vector of the surface on cylinder or wake boundary

P, P_0, P_i, P_a : Pressure, static pressure outside the cylinder, inner pressure insider the cylinder, and pressure on the surface of water respectively

q_j, q_m : Locations of elements on cylinder surface and wake boundary

r : The ratio between the lift coefficient and drag coefficient $\left(= \frac{C_L}{C_D}\right)$

$\vec{R}(q_m, q_n)$: vector from q_m to q_n

R_k: stiffness ratio between y direction and x direction in two dimensional case $= \left(\frac{K_y}{K_x}\right)^{\frac{1}{2}}$

s: Co-ordinate along the cylinder length

S: cylinder centre to centre spacing

T: Tension within cylinder;

T_e: Effective tension within riser

(u_i, v_i): Induced flow velocity at location of (x_i, y_i)

u: Wake velocity deficit

(u_j, v_j): local flow velocity at j-th element

U: Wake flow velocity;

U_0: Wake flow velocity deficit on the wake centreline

U_r: Resultant velocity $\left(= \sqrt{(U - \dot{x})^2 + \dot{y}^2}\right)$

U_R: Reduced velocity $\left(= \frac{V_o}{\omega_x D}\right)$

U_∞: inflow velocity to the cylinder (used in the free stream line theory illustration)

V_0: Free incoming flow velocity;

(x_i, y_i): Co-ordinate of i-th element on wake boundary

(x_0, y_0): Co-ordinate of the flow separation point

x_v, x_m: distance between the virtual source and real cylinder in the wake consideration, modified streamwise location of the downstream cylinder

(x, y): Co-ordinate of the downstream cylinder

(X, Y): Non-dimensionalised co-ordinates of the downstream cylinder;

Z : Vertical co-ordinate for a three dimensional case

α: Azimuth angle on the cylinder;

β : The deviation angle of flow velocity induced by the movement of the cylinder

ρ : Density of fluid

τ : Nondimensionalised time variable $(= \omega_x t)$;

θ : Spring coupling angle.

$\Gamma(q_n)$: Vortex strength at position q_n

ξ : Structure damping coefficient;

ω_x, ω_y : Natural circular frequency in x and y direction respectively

Δl : Element length on wake boundary

$(\Delta x_j, \Delta y_j)$: Correction of the position of wake boundary due to the modification of induced flow velocity

$(\dot{x}), (\ddot{x})$: Upper dot and upper dot dot represent first and second order derivatives with respect to time t or τ respectively.

subsript:

1, 2 :upstream and downstream cylinder

REFERENCES

Ahlbrandt, T. S., Charpentier, R. R., Klett, T.R., Schmokerl, J. W., and Schenk, C. J. (2000) Analysis of Assessment Results, Chapter AR in U.S. Geological Survey Digital Data Series 60.

Akima, H. (1970) A new method of interpolation and smooth curve fitting based on local procedures. *Journal of the ACM*, **17**:589-602.

Akin, J. E. (1982) Application and Implementation of Finite Element Methods. London: Academic Press.

American Bureau of Shipping (2001) Guide for Building and Classing Subsea Pipeline Systems and Risers. Houston, USA.

American Petroleum Institute (1992) Bulletin on Comparison of Marine Drilling Riser Analyses, API Bulletin 16J, First Edition.

American Petroleum Institute (1998) Design of Risers for Floating Production Systems (FPSs) and Tension-Leg Platforms (TLPs). 1st Ed. Boston: API; ISBN: 19912731.

Arie, M.; Kiya, M.; Moriya, M., and Mori, H. (1983) Pressure Fluctuations on the Surface of Two Circular Cylinders in Tandem Arrangement. Journal of Fluids Engineering. 105:161-167.

Bearmean, P. W. (1968) The Flow About A Circular Cylinder In The Critical Reynolds Number Regime, Nat. Phys. Lab. Aero. Rep. No. 1257

Bearman, P. W., Fackrell, J. E. (1975) Calculation of Two Dimensional and Axisymmetric Bluff-Body Potential Flow, *Journal of Fluid Mechanics*, **72**, Part 2, 229-241

Bearman, P. W., Morel, T. (1983) Effect Of Free Stream Turbulence On The Flow Around Bluff Bodies, *Progress Aerospace Science*, **20**, 97-123.

Bernitsas, M. M. (1982) Problems in Marine Riser Design. Marine Technology. **19**(1):73-82.

Bernitsas M. M., Kokarakis J. E. (1988) Importance of Nonlinearities in Static Riser Analysis. *Applied Ocean Research*, **10**(1):2-9

Best, M. S., Cook, N. J. (1967) The Forces On A Circular Cylinder In A Shear Flow. University of Bristol, Aeronautical Engineering Department, Report 103.

Biermann, D. and Hernstein, W. H. Jr. (1933) The Interference Between Struts in Various Combinations. NACA Rep. 468.

Bisplinghoff, R. L.; Ashley, H., and Halfman, R. L. (1955) Aeroelasticity. Addison-Wesley.

Blevins, R. D. (1990) Flow-Induced Vibration. New York: Van Nostrand Reinhold; ISBN: 0-442-20651-8

Bokaian A. and Geoola, F. (1984) Proximity-Induced Galloping Of Two Interfering Circular Cylinders. *Journal of Fluid Mechanics*, **146**:417-49

Bokaian, A. and Geoola, F. (1984) Wake-Induced Galloping of Two Interfering Circular Cylinders. *Journal of Fluid Mechanics*, **146**:383-415.

Bokaian, A. (1989) Galloping Of A Circular Cylinder In The Wake Of Another. *Journal of Sound and Vibration*, **128**(1):71-85.

Bokaian, A. (1992) Vortex-Excited Instability Prediction Of Marine Risers and Tethers. Proceedings of the 2nd International Offshore and Polar Engineering Conference; San Francisco, CA, USA. pp264-275. ISBN: 1-880653-02-8.

BP Amoco. (20002) Statistical Review of World Energy.

Brika, D. and Laneville, A. (1999) The flow interaction between a stationary cylinder and a downstream flexible cylinder. Journal of Fluid and Structures. 13:579-606.

Bryndum, M. B. and Andersen, H. (1999) Norwegian Deepwater Programme 2D Model Testing of Risers. Danish Hydraulic Institute Report.

Burke B. G. (1973) Analysis of Marine Riser for Deep Water. Offshore Technology Conference. OTC1771, pp449-464.

Cheers, F. (1950) A Note on Galloping Conductors. National Research Council of Canada Report MT-14.

Chen, S. S. (1986) A review of flow-induced vibration of two circular cylinders in crossflow. Journal of Pressure Vessel Technology. 108(Nov.):382-393.

Cook, L. (1999) Deep water – A Global Perspective, AAPG Conference Paper, Birmingham, England, Sep. 13.

Cooper, K. R. (1973) Wind Tunnel and Theoretical Investigations into the Aerodynamic Stability of Smooth and Stranded Twin Bundled Power Conductors. NRC Laboratory Technical Report LA-117.

Dalton, C. and Helfinstine, R. A. (1971) Potential Flow Past a Group of Circular Cylinders. *Journal of Basic Engineering*, Transaction of ASME. Dec:636-642.

de Boor, C. (1978) A Practical Guide to Splines, Springer-Verlag, New York.

DeCamp, D. (2000) Meeting the Challenge: Advancing Seismic Technology in Frontier Exploration and Development. Offshore Technology Conference; Houston, USA. 223-227.

Dove, P. G., Weisinger, D.; Abbassian, F., and Hooker, J. (2000) The Development and Testing of Polyester Moorings for Ultradeep Drilling Operations. Offshroe Technology Conference; Houston, USA. pp825-836.

Drennen III, W. T. (2000) Yesterday's Frontier is Today's Challenge: Deepwater Exploration and Development. Offshore Technology Conference; Houston, USA. pp429-430.

Duggal, A. S., Niedzwecki, J. M. (1993) an Experimental Study of Tendon/Riser Pairs in Waves, Offshore Technology Conference, OTC7239, pp323-333.

Fisher W. and Ludvig M. (1966) Design of Floating Vessel Drilling Riser. *Journal of Petroleum Technology*, 272-80

Furnes, G. K. (2000) On Marine Riser Responses in Time- and Depth-Dependent Flows. *Journal of Fluids and Structures*, **14**, 257-273

Gardner T. N. and Kotch, M. A. (1976) Dynamic Analysis of Riser and Caissons by Finite Element Method. Offshore Technology Conference. OTC2651, pp405-421.

Garside, R.; Snell, R. O. and Cook, H. (2001) Deepwater Technology and Deepwater Developments. Proceedings of the 11th International Offshore and Polar Engineering Conference; Stavanger, Norway, pp1-5.

Gordon, J. E. (1978) *Structures or Why Things Don't Fall Down.* Plenum, New York.

Gosse, C. G. and Barksdale, G. L. (1969) The Marine Riser - a Procedure for Analysis. Offshore Technology Conference. OTC1080, pp109-116.

Halse, K. H. (2000) Norwegian deepwater program: Improved Predictions of Vortex-Induced Vibrations. Offshore Technology Conference, OTC11996

Hannus, H., Engebretsen, K., Borresen, R., and Schamaun, P. (2000) Achieving a Step Change in Ultra-Deepwater TLP Capital Costs With the Innovative Step-Diameter Tendon System. Offshore Technology Conference, Houston, USA. pp801-808.

Hardy, C. and Dyke, P. Van. (1995) Field Observation on Wind-Induced Conductor Motions. Journal of Fluids and Structures. **9**:43-60.

Hartlen, R. T. and Currie, I. G. (1970) Lift-Oscillator Model of Vortex-Induced Vibration. Journal of the Engineering Mechanics Division, ASCE. 5, 577-591.

Hemon, P. (1999) An Improvement of the Time Delayed Quasi-steady Model for the Oscillations of Circular Cylinders in Cross-Flow. Journal of Fluids and Structures. **13**:291-307.

Heurtier, J. M., Buhan, P., Fontaine, L. C., Biolley, F. and Berhault, C. (2001) Coupled Dynamic Response of Moored FPSO with Risers. The Proceedings Of The 11th International Offshore and Polar Engineering Conference, Stavanger, Norway, pp319-327.

Hori, E. (1959) Experiments on Flow ~Around a Pair of Parallel Circular Clinders. Proc. 9th Japan National Congress for Appl. Mech.Tokyo; 231-234.

Huagui, Li. (1994) Society of Petroleum Engineers of AIME, (Paper) SPE.

Huang, S. (1992) Analysis and Control of Marine Cable Systems, Ph.D Thesis, University of Strathclyde

Hull, T. E., Enright, W. H. and Jackson K. R. (1976) *User's guide for DVERK, A subroutine for solving non-stiff ODEs*, Department of Computer Science Technical Report 100, University of Toronto.

Hunt, J. C. R. and Richards, D. J. W. (1969) Overhead Line Oscillations and the Effect of Aerodynamic Dampers. Proceedings of the Institute of Electrical Engineers (London); 116, 1869-1874.

Huse, E. (1992) Current Force On Individual Elements of Riser Arrays. Proceedings of the 2nd International Offshore and Polar engineering Conference; San Francisco, USA. pp256-263 .

Huse, E. (1993) Interaction In Deep-Sea Riser Arrays. Offshore Technology Conference. OTC7237, pp313-322.

Huse, E. (1996) Experimental Investigation of Deep Sea Interaction. Offshore Technology Conference. 2, pp367-372.

Huse, E. and Kleiven, G. (2000) Impulse And Energy In Deepsea Riser Collisions Owing To Wake Interference. Offshore Technology Conference, OTC11993.

Irvine, H. M. (1981) *Cable Structures.* MIT, USA

Jendrzejczyk, J. A. & Chen S. S. & Wambsganss M. W. (1979) Dynamic Response of a Pair of Circular Tubes Subjected to Liquid Cross Flow. Journal of Sound and Vibration. 67:263-273.

Kaasen, K. E., Lie, H. Solaas, F. and Vandiver, J. K. (2000) Norwegian Deepwater Program: Analysis of Vortex-Induced Vibrations of Marine Risers Based on Full-Scale Measurements, OTC 11997, Houston.

King, R. A (1977) Reivew of Vortex Shedding Research and its Application. 1977; 4, 141-171.

King, R. & Johns D. J. (1976) Wake Interaction Experiments with Two Flexible Circular Cylinders in Flowing Water. Journal of Sound and Vibration. 45(2):259-283.

Krolikowski, L. P., Gay, T. A. (1980) An Improved Linearization Technique for Frequency Domain Riser Analysis, OTC 3777. 1980 Offshore Technology Conference, Texas, USA.

Kubicek, M. and Marek, M. (1983). Computational Methods in Bifurcation Theory and Dissipative Structures, Springer-Verlag, New York.

Larsen, C. M., Vikestad, K. and Vandiver, J. K. (1996) One Multi-frequency Vortex Induced Vibrations of Long Marine Risers. Proceedings of the 1996 MTS/IEEE Oceans Conference [Part 1 of 3]. Oceans Conference Record(IEEE).

Lever, J. H. and Weaver D. S. (1986) On the Stability Behaviour of Heat Exchanger Tube Bundles. Part 1 Modified Theoretical Model. *Journal of Sound and Vibration.* **107**,375-410.

Lewis, R. I. (1991) Vortex Element Methods for Fluid Dynamic Analysis of Engineering Systems. Cambridge Engine Technology Series, Cambridge University Press, Cambridge.

Li, Y. and Morrison, D. G. (2000) The 'Colliding Participating Mass': A Novel Technique To Quantify Riser Collisions. Proceedings of ETCE/OMAE2000 Joint Conference Energy for the New Millennium, New Orleans.

Maekawa, T. (1964) Study On Wind Pressure Against ACSR Double Conductor. *Electrical Engineering in Japan*, **84**.

Magne, K., Nygdrd, M. K., Botros, F. R. and Hannus, H. (2001) Evaluation of Effect of Contact Between Top Tensioned Risers in Deep and Ultra Deep Waters, Proceedings of the 11th International Offshore and Polar Engineering Conference, Stavanger, Norway, June 17-22

Mair, W. A. and Maull, D. J. (1971) Aerodynamic Behaviour Of Bodies In The Wakes Of Other Bodies. *Philosophical Transactions of the Royal Society*, A. **269**.

Minami, K., Kurban, A. P. A., Khalil, C. N. and Kuchpil, C. (1999) Ensuring Flow and Production in Deepwater Environment. Offshore Technology Conference; Houston, USA. pp671-679.

Mitchell, A. R. (1980) The Finite Difference Method in Partial Differential Equations. Chichester:Wiley.

Modi, V. J., Calisal, S. M., Atadan, A. S. and Guo, Y. (1994) Proceedings of the International Offshore and Polar Engineering Conference. **2**, pp 224-230.

Moe, G. and Amtsen, Ø. (2001) An Analytic Model for Static Analysis of Catenary Risers. The Proceedings of The 11th International Offshore and Polar Engineering Conference; Stavanger, Norway. pp248-254.

More, J., Garbow, B. and Hillstrom, K. (1980). Rep. No. Argonne National Labs Report ANL-80-74, Argonne, Illinois.

Morgan, G. W. (1975) Applied Mechanics of Marine Riser Systems. *Petroleum Engineering.* 10-7

Morison, J. R.; O'Brien, M. P.; Johnson, J. W., and Schaaf, S. A. (1950) The Force Exerted by Surface Waves on Piles. Petrol. Trans., AIME. 189:149-154.

Moriya, M. and Sakamoto, H. (1985) Fluctuating Fluid Forces Acting on a Sownstream Circular Cylinder in a Staggered Arrangement. Trans. JSME. 51(467):2098-2114.

Niedzwecki, J. M., Thoresen, G. and Remeseth S. (1994) Riser Response to Vertical Current Profiles and Regular Waves. Faltinsen *et al.* Hydroelasticity in Marine Technology. 39-54.

O'Brien, P. J. and McNamara, J. F. (1989) *Engineering Structures* **11**(4), 223-33

Odell, P. R. (1999) A Guide to Oil Reserves and Resources [Web Page]. Accessed 2001 Jul. Available at: *http://www.greenpeace.org/~climate/arctic99/reports/ odell317.html.*

Ohya, Y., Okajima, A., and Hayashi, M. (1989) Wake interference and vortex shedding. *Encyclopedia of Fluid Mechanics.* pp. 169-224.

Ormberg, H., Stansberg, C. T., Yttervik, R. and Kleiven, G. (1999) Integrated Vessel Motion And Mooring Analysis Applied In Hybrid Model Testing. Proceedings of the International Offshore and Polar Engineering Conference. **1**, 339-346.

Overvik, T.; Moe, G., and Hjort-Hansen. (1983) Flow Induced Motions of Multiple Risers. *Journal of Energy Resources Technology*, **105**, 83-89.

Paidoussis, M. P., Price, S. J. and Mark, B. (1988) Current Induced Oscillation and Instabilities of a Multi-Tube Flexible Risers. *Journal of Fluids and Structures*, **2**, 503-513

Pantazopoulos, M. S. (1994) Vortex Induced Vibration Parameters: Critical Review. Proceedings of the International Conference on Offshore Mechanics and Arctic Engineering, pp199-255.

Parkinson, G. V. and Jandali, T. (1970) A Wake Source Model For Bluff Body Potential Flow, *Journal of Fluid Mechanics*, **40**, 577-594

Parkinson, G. V. (1971) Wind-Induced Instability of Structures. Philosophical Transactions of the Royal Society of London. A269:395-409.

Parkinson, G. V. (1989) Phenomena and Modelling of Flow-Induced Vibrations of Bluff Bodies. Prog. Aerospace Science. 26:169-224.

Patrikalakis, N. M. and Yoon, D. Y. (1990) Dynamics Of Disconnected Risers Under Rigid And Compliant Hang-Off. *Journal of Offshore Mechanics and Arctic Engineering* **112**(2),106-14

Price, S. J. (1975) Wake Induced Flutter of Power Transmission Conductors. *Journal of Sound and Vibration*, **38**, 125-147

Price, S. J. (1976) The Origin and Nature of the Lift Force on the Leeward of Two Bluff Bodies. *Aeronautical Quarterly*, **27**, 154-168

Price, S. J. and Paidoussis, M. P. (1984) The Aerodynamic Force Acting on Groups of Two and Three Circular Cylinders When Subject to a Cross-Flow. Journal of Wind Engineering and Industrial Aerodynamics. 17:329-347.

Price, S. J., Paidoussis, M. P., Mark, B. and Mureithi, W. N. (1989) Current-Induced Oscillations And Instabilities Of A Multi-Tube Flexible Riser: Water Tunnel Experiments. Proceedings of the International Offshore Mechanics and Arctic Engineering Symposium, **I**, pp447-454

Price, S. J. and Paidoussis, M. P. (1989). The Flow Induced Response of a Single Flexible Cylinder in an In-line Array of Rigid Cylinders. *Journal of Fluids and Structures*, **3**:61-82

Price, S. J. and Abdallah, R. (1990) On the Efficiency of Mechanical Damping and Frequency Detuning In Alleviating Wake-Induced Flutter Of Overhead Power Conductors. *Journal of Fluids and Structures*, **4**(4), 1-34.

Price, S. J., Paidoussis, M. P. and Al-Jabir, A. M. (1993) Current-Induced Fluidelastic Instability Of A Multi-Tube Flexible Riser: Theoretical Results And Comparison With Experiments. *Journal of Offshore Mechanics and Arctic Engineering*, Transactions of the ASME, **115**(4), 206-212

Price, S. J. (1995) A Review of Theoretical Models For Fluidelastic Instability of Cylinder Arrays In Cross-Flow. *Journal of Fluids and Structures*, **9**, 463-518.

Rajabi, F. (1989) Interference Problems Associated with Risers in Floating Production Systems, Phase I - Summary Report, Brown and Root Development Inc., Houston Texas, September.

Rawlins, C. B. (1974) Discussion On 'On The Use Of Damped And Undamped Quasi-Static Aerodynamic Models In The Study Of Wake-Induced Flutter IEEE Power Engineering Society Summer Meeting , Anaheim, California

Roberts, B. W. Low frequency, Aeroelastic vibraiopns in a cascade of circular cylinders. I.Mech.E. Mechanical Engineering Science Monograph. 1966(4).

Robinson, R. W. and Hamilton, J. (1992). A Criterion for Assessing Wind Induced Crossflow Vortex Vibrations in Wind Sensitive Structures. London: HMSO; OTH 92 379.

Roshko, A. (1954) A new hodograph for free streamline theory. N.A.C.A. Tech. Note, No. 3168

Sagatun, S. et al. (1999) Riser Collision – Assessment Of Impact Energy. OMAE, St John's, Canada.

Sarpkaya, T. (1979) Vortex-Induced Oscillations - A Selective Review. *Journal of Applied Mechanics*, **46**, 241-258.

Sarpkaya, T. and Isaacson, M. (1981) Mechanics of Wave Forces on Offshore Structures. New York: Von Nostrand Reinhold Co., ISBN: 0-442-25402-4.

Sattamini, S. R. and Ferranti, A. J. (1993) Computational Analysis Of Deep Water Risers During Installation And Hang-off. Proceedings of the Third International Offshore and Polar Engineering Conference.

Savkar, S. D. (1970) Wake-Induced Oscillation in Transmission Line Bundles. IEEE Summer Power Meeting And EHV Conference, Los Angeles, California, July.

Schlichting, H. (1968) Boundary Layer Theory. New York: McGraw Hill Book Company.

Seydel, R. (1994). From Equilibrium To Chaos—Practical Bifurcation and Stability Analysis. Elsevier Science Publishing Co.

Simpson, A. (1971) On the Flutter of a Smooth Circular Cylinder in a Wake. *Aeronautical Quarterly*, Feb., 25-41.

Simpson, A. (1971) Wake Induced Flutter of Circular Cylinders: Mechanical Aspects, *Aeronautical Quarterly*, May, 101-118

Simpson, A. (1979) Fluid Dynamic Stability Aspects of Cables. Shaw, T. L. Mechanics of Wave Induced forces on Cylinders. Pitmas Advanced Publishing Program.

Simiu, E. and Scanlan, R. H. (1986) Wind Effects on Structures. New York: Wiley & Sons.

Snell, R. and Banon, H. (2000) Deepwater Concepts Selection, Understanding the Risk of Innovation. Proceedings of the Deep Offshore Technology Conference, New Orleans.

Sockel, H. and Kronke, I. (1987) Wind Tunnel Model Tests On A Group Of Power Station Chimneys. Poster 1, Int. Conf. Flow Induced Vibrations, Bowness-on-Windmere, UK, May. pp563-573.

Sparkman, G. W. and Smith, T. (1998) Deepwater Drilling - Identifying the Technical Challenges. Offshore Technology Conference; Houston, USA, pp301-306.

Teigen, P., Loseth, S. and Skomedal, N. G. (1990) Dynamic Analysis Of Flexible Risers. A Comparison With A Random Vortex Method And The Morison's Equation. Proceedings of the International Offshore Mechanics and Arctic Engineering Symposium. **1**, B, 379-384.

Ting, D. S-K, Wang, D. J., Price, S. J. and Paidoussis, M. P. (1998) An Experimental Study on Fluidelastic Forces for Two Staggered Circular Cylinders in Cross-Flow. *Journal of Fluids and Structures*, **12**, 259-294.

Triantafyllou, M. S., Gopalkrishnan, R. and Grosenbaugh, M.A. (1994) Vortex-Induced Vibrations in a Sheared Flow: A New Predictive Method. Faltinsen *et al.* Hydroelasticity in Marine Technology. 31-37. Balkema, Rotterdam.

Tsui, Y. T. (1977) One Wake-Induced Flutter of a Circular Cylinder in the Wake of Another. *Journal of Applied Mechanics*, 194-200.

Tsui, Y. T. (1986) On Wake-Induced Vibration of a Conductor In the Wake of Another Via a 3-D Finite Element Method. *Journal of Sound and Vibration*, **107**(1), 39-58

Vandiver, J. K. (1998) Research Challenges in the Vortex-Induced Vibration Prediction of Marine Risers. Offshore Technology Conference; Texas, Houston, USA. OTC8698.

Vlahopoulos, N. and Bernitsas, M. M. (1991) Three-Dimensional Nonlinear Dynamics Of Nonintegral Riser Bundle. *Journal Of Ship Research*, **35**(1), 40-57.

Watters, A.J., Smith, I. C. and Garrett, D. L. (1998) Lifetime Dynamics Of A Deep Water Riser Design. *Applied Ocean Research* **20**(1), 69-81

Wiencke, M. (2000) Demo 2000: Qualifying Deepwater E&P Technology by Pilot Demonstration. Proceedings of the Deep Offshore Technology Conference.

Willden, R. H. J., Graham, J. M. R. and Giannakidis, G. (2001) Vortex-Induced Vibration of Single and Multiple Risers in a Sheared Current. The Proceedings of the 11th International Offshore and Polar Engineering Conference, Stavanger, Norway. pp406-411.

Williamson, C. H. K. (1996) Vortex Dynamics In The Cylinder Wake, *Annual Review of Fluid Mechanics*, 477-539

Wu, W., Huang, S. and Barltrop, N. (1999) Lift and Drag Forces on a Cylinder in the Wake of an Upstream Cylinder, OMAE, St John's, Canada

Wu, W., Huang, S. and Barltrop, N. (2000) Stability Analysis Of A Cylinder In The Wake Of An Upstream One STAB'2000, Australia.

Wu, W., Huang, S. and Barltrop, N. (2001) Multiple Stable/Unstable Equilibria of a Cylinder in the Wake of an Upstream Cylinder. 20th International Conference on Offshore Mechanics and Arctic Engineering , Rio de Janeiro. OFT-1170. Also appeared in Journal of Offshore Mechanics and Arctic Engineering, Vol. 125, May 2003, 103-107.

Wu, W., Huang, S. and Barltrop, N. (2001) Stationary and Hopf Bifurcations of Equilibrium Positions of a Cylinder Situated in Near and Far Wake Fields of an

Upstream Cylinder. ISOPE'2001; Stavanger, Norway, OFT-128. Also appeared in Journal of Offshore and Polar Engineering, March, 2002. Vol. 12, No.1

Wu, W., Huang, S. and Barltrop, N. (2002) Current induced instability of two circular cylinders. Applied Ocean Research. Vol. 24, 287-297.

Wong, H.Y. (1985) Design Against Wind-Induced Vibration Of Multi-Flue Chimney Stacks. *Engng Struct.*, **7**, 2-9.

Zdravkovich, M. M. (1974) Flow Induced Vibrations of Two Cylinders in Tandem, and Their Suppression. *Proc. Intl. Symp. Flow Induced Structural Vibrations*; Jarlsruhe. Springer; 1974: pp631-639.

Zdravkovich, M. M. and Pridden, P. L. (1977) Interference Between Two Circular Cylinders: Series of Unexpected Discontinuities. *Journal of Industrial Aerodynamics.* 1(2):255-270.

Zdravkovich, M. M. (1977) Review of Flow Interference Between Two Circular Cylinders in Various Arrangements. *Journal of Fluids Engineering*, Transactions of the American Society of Mechanical Engineers, **99**, 618-633

Zdravkovich, M. M. (1987) The Effects of the Interference Between Circular Cylinders In Cross Flow. Journal of Fluids and Structures. 1:239-261.

Zdravkovich, M. M. (1997) Flow Around Circular Cylinders. Oxford University Press.

Appendix A

BIFURCATION STRUCTURE AT LOSING STABILITY

A Continuation Analysis Based on the System in Parallel With Chapter III

A.1 General Remarks

A systematic continuation investigation has been presented in Chapter IV regarding the variation of equilibrium positions with the flow velocity and their corresponding stability for a prescribed initial arrangement. However, the specification of the system provided therein is different from that in Chapter III. In order to give a parallel explanation for the bifurcation structure in the analysis made in Chapter III, an alternative specification of the dynamic system is presented in this appendix.

If the co-ordinate system is originated at the centre of upstream cylinder, and assuming the downstream cylinder is always in an equilibrium position under any prescribed flow velocity, then the dynamic system for the downstream cylinder can be written in the following standard form,

$$\dot{\tilde{x}} = \tilde{f}(\tilde{x}) \tag{A.1}$$

$$\tilde{f}(\tilde{x}) = \begin{Bmatrix} x_2 \\ aU_R^2\sqrt{\left(1-\frac{x_2}{bU_R}\right)^2+\left(\frac{x_4}{bU_R}\right)^2}\left[\left(1-\frac{x_2}{bU_R}\right)C_D+\frac{x_4}{bU_R}C_L\right]-2\xi_x x_2 - x_1 - aU_R^2 C_{D0} \\ x_4 \\ aU_R^2\sqrt{\left(1-\frac{x_2}{bU_R}\right)^2+\left(\frac{x_4}{bU_R}\right)^2}\left[\left(1-\frac{x_2}{bU_R}\right)C_L-\frac{x_4}{bU_R}C_D\right]-2R_k R_\xi \xi_x x_4 - R_k^2 x_3 - aU_R^2 C_{L0} \end{Bmatrix} \quad \text{(A.2)}$$

With $\tilde{x} = \begin{Bmatrix} x_1 \\ x_2 \\ x_3 \\ x_4 \end{Bmatrix}$

Where x_1, x_3 denote the streamwise and transverse displacements of the cylinder from the equilibrium position $(X_0,\ Y_0)$, i.e.

$$\begin{cases} x_1 = X - X_0 \\ x_3 = Y - Y_0 \end{cases} \quad \text{(A.3)}$$

and C_{D0}, C_{L0} are fluid drag and lift coefficients at equilibrium position $(X_0,\ Y_0)$. The definitions of other parameters are the same as in Chapter III. The Jacobian matrix of system (A.2) is

$$J_{i,j} = \frac{\partial \tilde{f}_i}{\partial x_j} \qquad (i,j = 1,2,3,4) \quad \text{(A.4)}$$

Which is the matrix for stability analysis and it is exactly the same as the one utilised in Chapter III.

Let cylinder mass parameter be set as *0.2*, stiffness ratio set as *1.01* and supposing there is no spring coupling, the streamwise position varies from *5* to *15* and transverse position

varies from *0* to *2*. The whole wake field is investigated systematically. The results are presented according to wake centreline, inner wake position and outer wake position respectively as follows:

A.2 Wake Centreline

Figure (A.1) to (A.4) are continuation results for the equilibrium positions of *(5,0), (8,0), (12,0), (15,0)*. It is seen that for all four cases, there is a bifurcation point, which is called the "critical state". When flow velocity is under the critical value, the prescribed position is always stable. However, there is an unstable equilibrium position accompanying the prescribed one located somewhere upstream. When the critical velocity is reached, a transcritical stationary bifurcation occurs, with an exchange of stability. The prescribed position begins to lose stability, whilst the stability is gained at the other branch, which is located somewhere downstream. If the eigenvalue characteristics of corresponding equilibria in one dimensional space are checked, then the stable position is found to be a stable node and the unstable position is a saddle point as depicted on Figures (A.2). Figure (A.5) and (A.6) show the variation of eigenvalues with the different flow velocities (The flow velocity is not shown in the figure here). It is seen that with the increase of flow velocity, for the branch from A_0 to T to B_0, one pair of the eigenvalues landed on the real axis before losing stability, with one moving toward the positive real axis and the other towards the negative direction. At critical state of T, the eigenvalue reaches the origin. If there is a further increase of flow velocity, the eigenvalue transverses the imaginary axis and lands on the right half of the eigenvalue plane. The other branch of A_1 to T to B_1, on the other hand, does the same, but in the reverse order.

Compared with the analysis made in Chapter *III*, the variation of eigenvalues along A_0 to T to B_0 conforms to the critical state of stationary bifurcation. Meanwhile, the results show a downstream stable equilibrium position that has a corresponding unstable equilibrium

position located upstream when near the critical state. At critical state, the two positions converge with each other, which is the result shown in Chapter *IV*.

A.3 Inner Wake Position

Figures A.7 to Figure A.16 show the continuation for the equilibrium position at transverse location of $Y_0=1$ while X_0 varies from *5* to *15*. It is clear that there are two turning points and one transcritical bifurcation point in the results. The path of A_0 to T_0 to B_0 is the stability variation route that was investigated in Chapter *III*, and the state of transcritical bifurcation T_0 is the critical state, which was defined in Chapter *III*. Checking the eigenvalues variation depicted in Figure A.9, clearly T_0 is a stationary bifurcation point. Meanwhile, there are other three equilibrium positions when the flow velocity is close to the critical state T_0, among which two are unstable. Referring to Figure A.10, both two turning points correspond to the stationary bifurcation.

Checking the results against the analysis made in Chapter *IV*, the transcritical bifurcation point T_0 corresponds to the state of Q in Chapter *IV*. This implies that the loss of stability investigated in Chapter *III* does not necessarily cause the two cylinders to collide with each other, because there are other equilibrium positions at which the cylinder can be stable. The two turning points T_1 and T_2 correspond to the two turning points *D(S)* and *M(D)* in Chapter *IV*.

A.4 Outer Wake Position

Figures A.17 to A.22 show the cases when the equilibrium positions are located at $Y_0=2$. They show that characteristics of the bifurcation are the same as the cases for $Y_0=1$. Generally there are two turning points and one transcritical bifurcation point. The minor difference is that two turning points are all located somewhere further in than the prescribed equilibrium position. At a large flow velocity, the stable equilibrium position is

located well outside of the wake. Such a solution is caused by the parameters of the dynamic system. Because the prescribed position is presumably the equilibrium position, which may include those cases where the downstream cylinder is initially located outsider the wake, the unstable position here can be considered to be accidentally entrapped into the equilibrium position in the wake. The results also exhibit a much smaller region of flow velocity when there are four equilibrium positions. This suggest that the region for multiple equilibria is getting smaller at outer wake, conforming to the result of Chapter *IV*.

Figures A.23 and A.24 are two special cases for demonstrating eigenvalue variation for a small mass parameter $a=2\times10^{-1}$ at $X_0=5$. For two different stiffness ratios, $R_k=1.5$ and 2.0, to choose such a high R_k is purely for the convenience of illustrating how the eigenvalue varies with the flow velocity. It is seen that with the increase of flow velocity, Hopf bifurcation can be regained at a certain velocity, and ultimately, the cylinder will lose stability via stationary bifurcation. Nevertheless, when the stiffness ratio is high, the stability after Hopf bifurcation may not be able to be regained.

A.5 Remarks

The analysis presented in this appendix is fully consistent with the conclusion drawn in Chapter III and Chapter IV. It also provides an alternative insight into the structure of possible bifurcation which the system can show. This appendix also shows the imperfection of the traditional stability analysis described in Chapter III, for example the difficulty in explaining behaviour after loss of stability. The bifurcation structure for the case investigated in this appendix for $a=0.2$ confirms that it is mainly a stationary bifurcation.

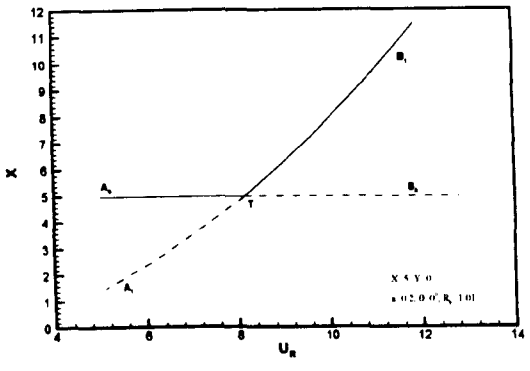

Figure A.1 Continuation for Equilibrium Position *(5,0).*

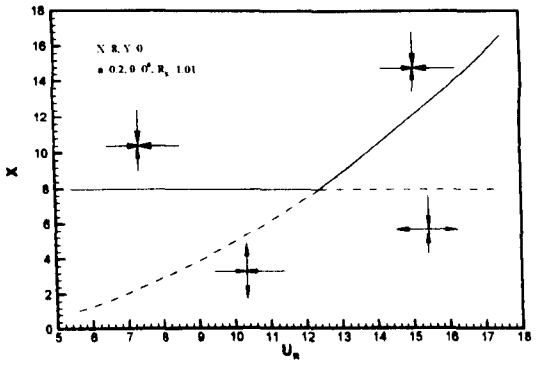

Figure A.2 Continuation for Equilibrium Position *(8,0), stable node Vs Saddle .*

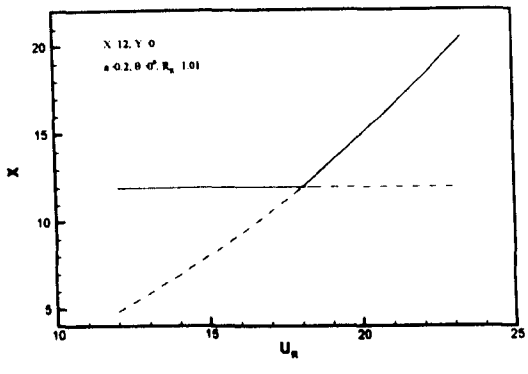

Figure A.3 Continuation for Equilibrium Position *(12,0).*

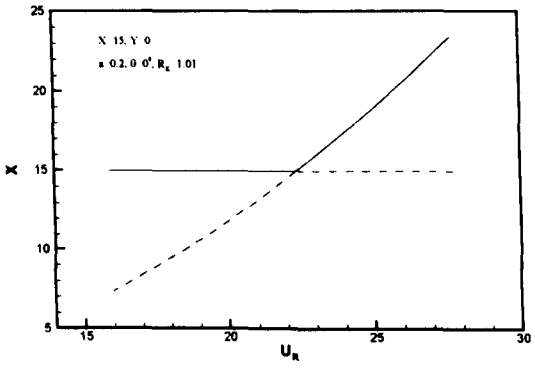

Figure A.4 Continuation for Equilibrium Position *(15,0).*

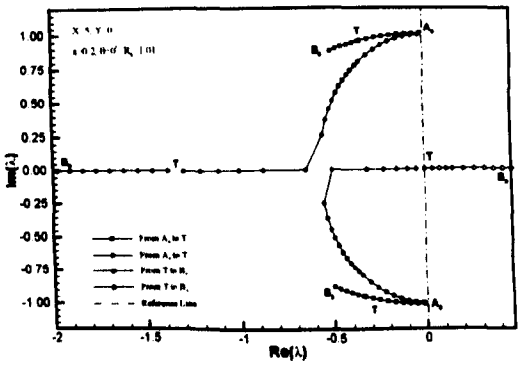

Figure A.5 Eigenvalues Variation for Position *(5,0)* for Branch A_0 to B_0.

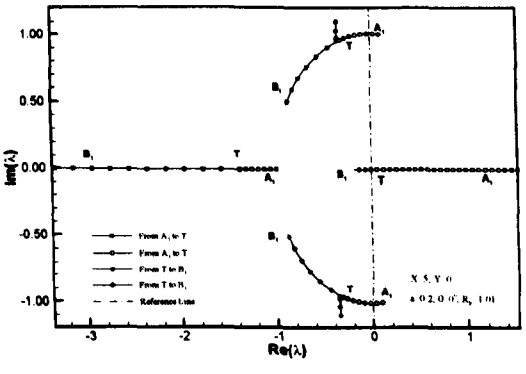

Figure A.6 Eigenvalues Variation for Position *(5,0)* for Branch A_1 to B_1.

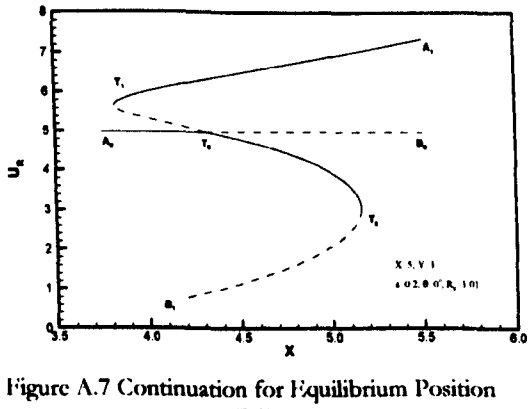

Figure A.7 Continuation for Equilibrium Position *(5,1).*

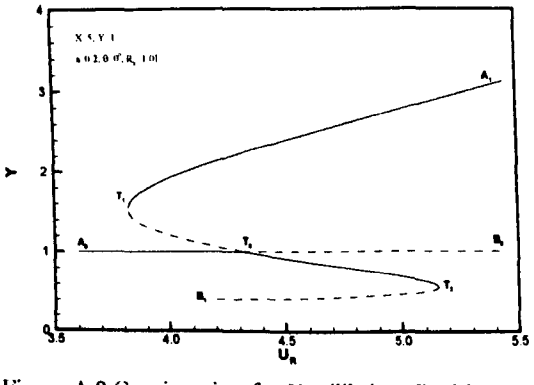

Figure A.8 Continuation for Equilibrium Position *(5,1).*

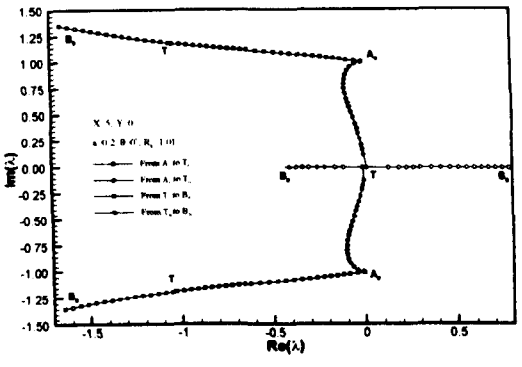

Figure A.9 Eigenvalues Variation for Position *(5,1)* for Branch A_0 to B_0.

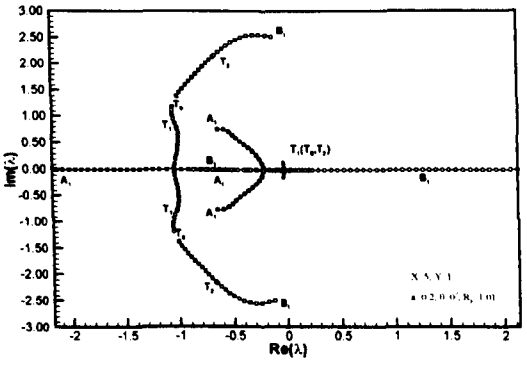

Figure A.10 Eigenvalues Variation for Position *(5,1)* for Branch A_1 to B_1.

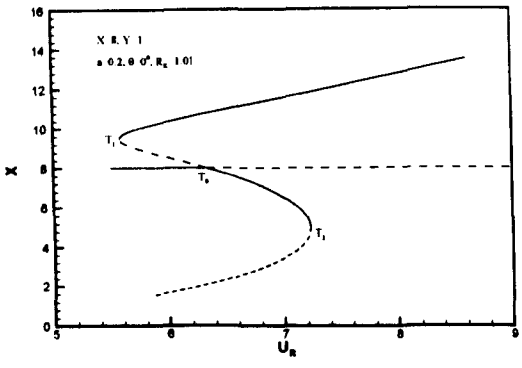

Figure A.11 Continuation for Equilibrium Position of *(8,1)*.

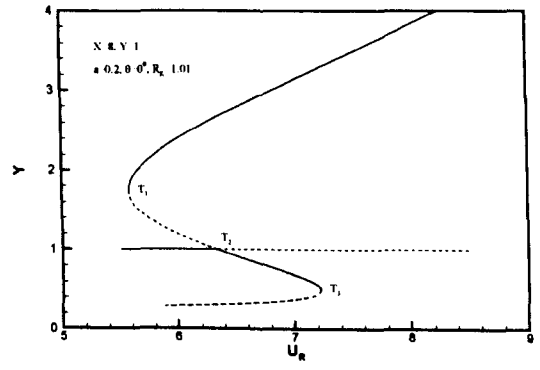

Figure A.12 Continuation for Equilibrium Position of *(8,1)*.

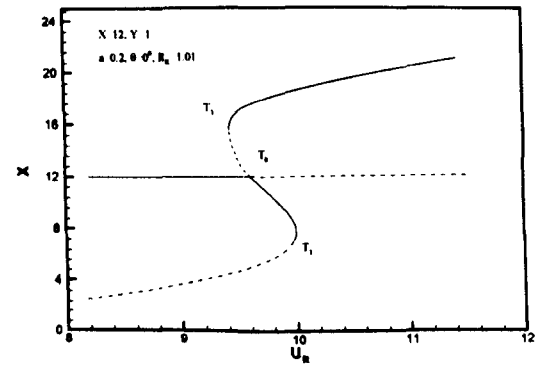

Figure A.13 Continuation for Equilibrium Position *(12,1)*.

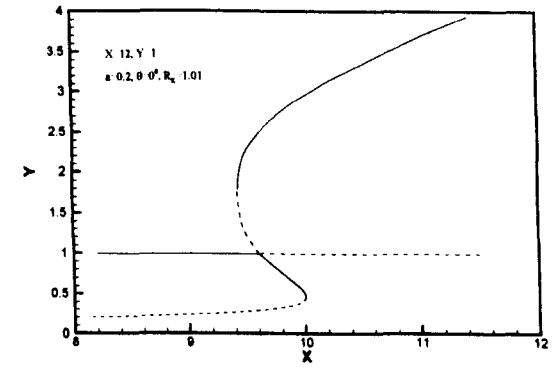

Figure A.14 Continuation for Equilibrium Position *(12,1)*.

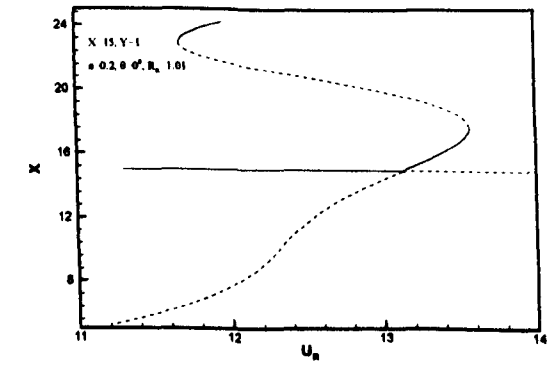

Figure A.15 Continuation for Equilibrium Position *(15,1)*.

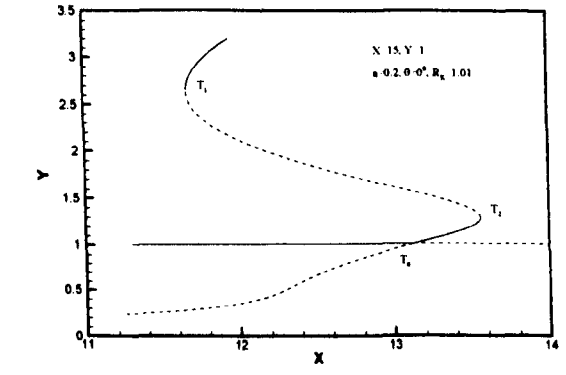

Figure A.16 Continuation for Equilibrium Position *(15,1)*.

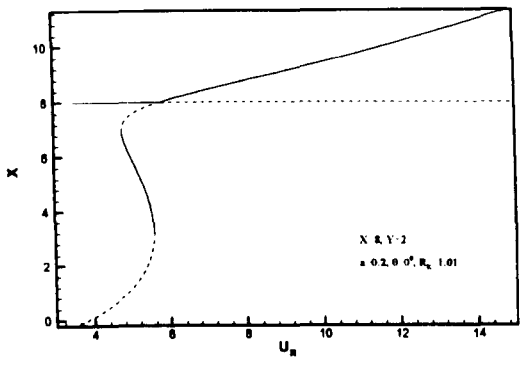

Figure A.17 Continuation for Equilibrium Position *(8,2)*.

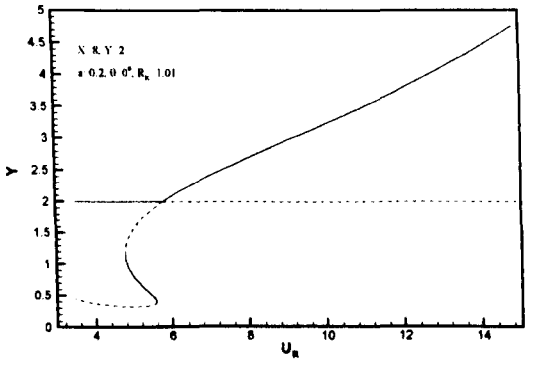

Figure A.18 Continuation for Equilibrium Position *(8,2)*.

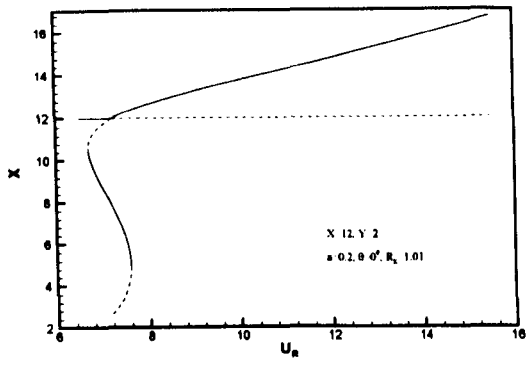

Figure A.19 Continuation for Equilibrium Position *(12,2)*.

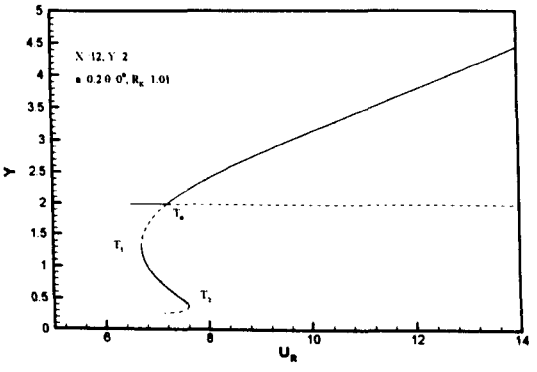

Figure A.20 Continuation for Equilibrium Position *(12,2)*.

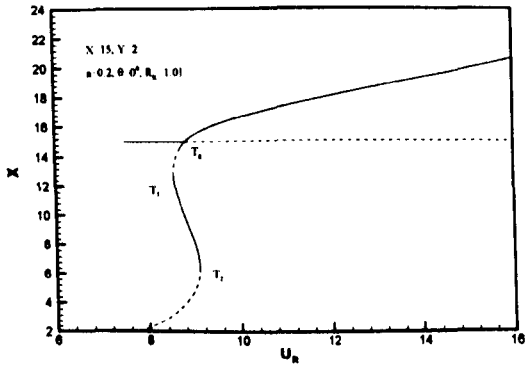

Figure A.21 Continuation for Equilibrium Position *(15,2)*.

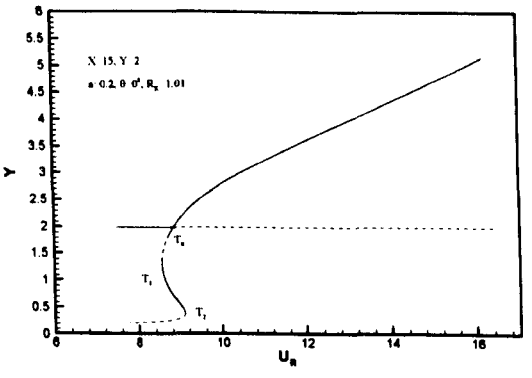

Figure A.22 Continuation for Equilibrium Position *(15,2)*.

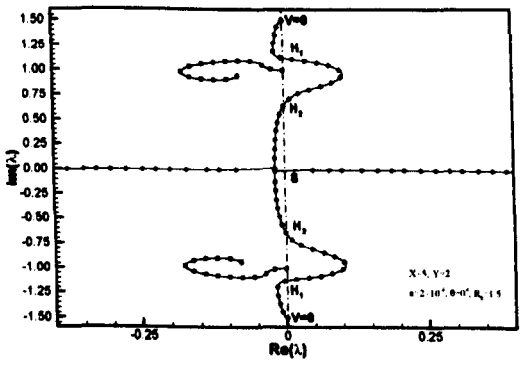

Figure A.23 Eigenvalues Variation for Position *(5,2)*.

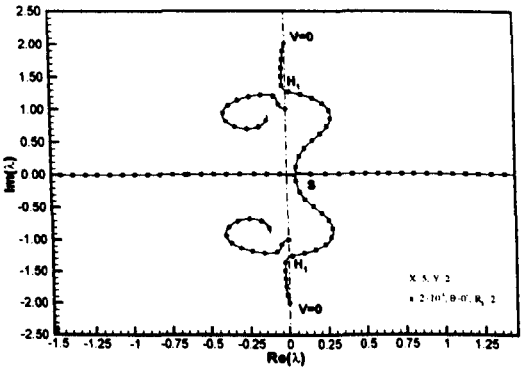

Figure A.24 Eigenvalues Variation for Position *(5,2)*.

Appendix B

FLUID ADDED MASS COEFFICIENT AND INTERACTION FORCE WHEN ONE CYLINDER IS NEAR TO ANOTHER AND WITH DIFFERENT MOVING VELOCITY

Potential flow interaction

B.1 General Remarks

According to that potential flow theory, when one cylinder is moving at constant velocity in a reservoir of otherwise stationary fluid, there is no force acting on the cylinder (d'Alembert Paradox, the net force on a single body without circulation in a steady ideal flow is zero). When the cylinder is accelerating in such fluid, however, one force (which is proportional to the acceleration of the cylinder) is applied by the flow. Such a force is defined as the fluid added mass force, which acts to oppose the cylinder's acceleration.

In general, added mass can be associated with both translation and rotation of the body. The added mass force on a rigid three-dimensional body accelerating from still in a reservoir of stationary fluid is the sum of added mass forces associated with all six possible rigid body accelerations (Blevins, 1990),

$$F_j = -\sum_{i=1}^{6} m_{ij} \frac{du_i}{dt} \tag{B.1}$$

Here, m_{ij} is the fluid added mass term, u_i denote three translation and three rotation velocity. For the case of one circular cylinder in two-dimensional flow, then the only nonzero terms in (B.1) are

$m_{11} = m_{22} = \rho\pi a^2$.

Here, a is the radius of the cylinder and ρ is the fluid density.

However, when there are other objects in the flow, especially when they are close to each other, the fluid added mass will be position dependent because the nearby objects will affect the disturbed flow.

In two-dimensional flow, assuming there are two cylinders located nearby and they are labelled as 1 and 2 respectively, the fixed to earth co-ordinate system is used to identify the moving direction by x and y. The definition of the interaction force and the fluid added mass force, caused by acceleration of the two cylinders, can be defined as:

$$\begin{bmatrix} F_{1x} \\ F_{1y} \\ F_{2x} \\ F_{2y} \end{bmatrix} = -\begin{bmatrix} m_{11xx} & m_{11xy} & m_{12xx} & m_{12xy} \\ m_{11yx} & m_{11yy} & m_{12yx} & m_{12yy} \\ m_{21xx} & m_{21xy} & m_{22xx} & m_{22xy} \\ m_{21yx} & m_{21yy} & m_{22yx} & m_{22yy} \end{bmatrix} \times \begin{bmatrix} \frac{du_{1x}}{dt} \\ \frac{du_{1y}}{dt} \\ \frac{du_{2x}}{dt} \\ \frac{du_{2y}}{dt} \end{bmatrix} \tag{B.2}$$

Here, $u_{1x}, u_{1y}, u_{2x}, u_{2y}$ represent the x and y direction velocities of cylinder 1 and 2 respectively. $m_{iixx}, m_{iixy}, m_{iiyx}, m_{iiyy}$ are added masses caused by cylinder's own acceleration, $m_{ijxx}, m_{ijxy}, m_{ijyx}, m_{ijyy}$ are interaction forces caused by the acceleration of the cylinder nearby. The determination of these terms has to be found by solving the fluid flow.

In this appendix, numerical computation is carried out to explain the variation of fluid added mass of the cylinder in the presence of another cylinder nearby. The computation is based on the potential flow theory with the complex potential method(Dalton and Helfinstine 1971). The investigated individual cylinder is moving at different speed.

B.2 Solitary Cylinder

For the convenience of explanation, it is better to start with the case of a solitary cylinder. If a solitary cylinder with radius a is moving in an unbounded stationary fluid with velocity U at an angle of α between moving direction and x axis (ref. Figure B.1), then the complex potential can be described as

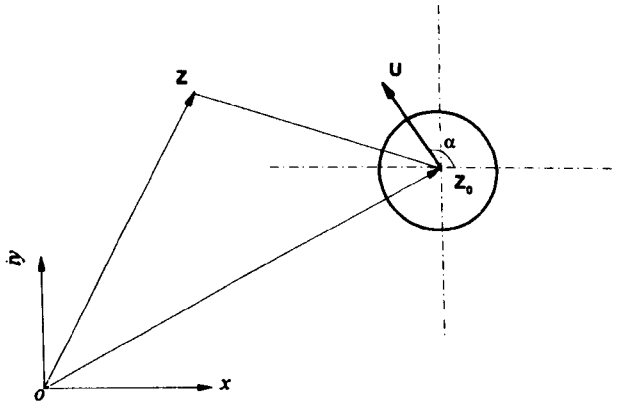

Figure B.1 Schematic diagram for treatment of solitary cylinder.

$$w = -\frac{Ua^2 e^{i\alpha}}{Z - Z_0} \tag{B.3}$$

Here w is the complex potential,

$$w = \phi + i\psi \tag{B.4}$$

ϕ is the velocity potential function and ψ is the stream function

Z is the complex variable with

$$Z = x + iy \tag{B.5}$$

the co-ordinate system is earth-fixed, and

$$Z_0 = x_0 + iy_0 \tag{B.6}$$

is the instantaneous position of the cylinder which varies with time.

Expression (B.3) denotes the flow field at any given position Z, disturbed by the motion of the cylinder at position Z_0. The effect of the disturbance is equivalent to a doublet.

The flow velocity in the flow field can be represented as

$$V(Z) = \frac{dW(Z)}{dZ} = u(Z) - iv(Z) \tag{B.7}$$

Where u and v are the x and y direction components of the flow velocity in Cartesian co-ordinate system.

In order to find the fluid forces acting on the moving cylinder, the Bernoulli equation is utilised, which is

$$\frac{\partial \phi}{\partial t} + \frac{(p - p_0)}{\rho} + \frac{V^2 - U^2}{2} = g(t) \tag{B.8}$$

Here p is the pressure in the flow field, if fluid forces on the cylinder is of concern, the pressure is then taken at the surface of cylinder. p_0 is the pressure in undisturbed fluid, $g(t)$ is an arbitrary function of time (assumed to be zero in this case).

The fluid force acting on the cylinder per unit length can be obtained by integrating pressure around the cylinder as follows,

$$F = \oint_{c_0} (p - p_0) ds = -\rho \oint_{c_0} \frac{\partial \phi}{\partial t} ds - \frac{\rho}{2} \oint_{c_0} (V^2 - U_0^2) ds \tag{B.9}$$

Where $ds = (Z - Z_0)d\theta$, and c_0 represents the circumference of the cylinder. By substituting expressions (B.7), (B.8) into (B.9), the fluid force can be written in the following way

$$F = -\rho\pi a^2 \frac{dU}{dt} \tag{B.10}$$

Such a force is the fluid added mass force, and if the definition of (B.1) is applied, the added mass is equal to the amount of fluid expelled by the cylinder ($\rho\pi a^2$). It represents the mass of fluid entrained by the cylinder when the cylinder is accelerating. This is also called virtual mass or hydrodynamic mass.

B.3 Two Cylinders

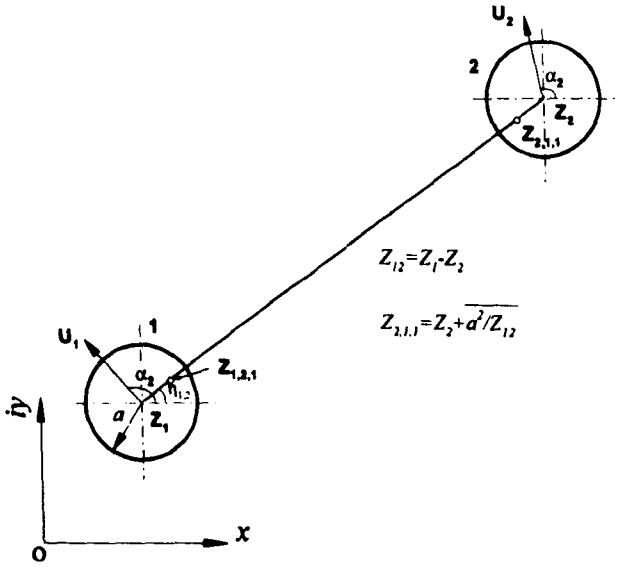

Figure B.2 Schematic diagram of two cylinder interaction for added mass evaluation.

When one cylinder is moving in the stationary fluid, with another cylinder nearby, or when two cylinders move in a stationary fluid at their own velocity, the methodology is similar. However, because of the interaction between two cylinders, extra expressions are needed to account for such an interaction.

As shown in Figure B.2, two cylinders are labelled as 1 and 2 respectively. They are located at position Z_1 and Z_2 in complex co-ordinate system. The moving velocities for two cylinders are U_1 and U_2, with angles of α_1 and α_2 between x axis and the direction of movement respectively. Without considering interaction, the disturbances caused by two individual cylinders' movement can be represented by

$$w_j = -\frac{U_j a^2 e^{i\alpha_j}}{Z - Z_j} \qquad (j=1, 2) \tag{B.11}$$

However, the total flow velocity disturbed by the two cylinders can not satisfy the impenetrable condition on the cylinders, which is the essential boundary condition for flow field, i.e.

$$\left(V - U_j\right)\cdot \vec{n}_j = 0 \qquad (j=1, 2) \tag{B.12}$$

Here, $\vec{n}_j$ is the unit normal vector of cylinder j. If the boundary conditions for two cylinders are treated separately, and only cylinder 2 is considered, because cylinder 1 is equivalent to a doublet, by arranging a mirror doublet within cylinder 2, the boundary condition on cylinder 2 can be automatically satisfied. The mirror doublet is denoted by number index of (2,1,1), which means at position of cylinder 2 caused by source doublet within cylinder 1, and it is the first mirror doublet, then the complex potential can be expressed as:

$$w_{2,1,1} = -\beta_{2,1,1} U_1 a^2 \frac{e^{i\alpha_{2,1,1}}}{Z - Z_{2,1,1}} \tag{B.13}$$

Where

$$\beta_{2,1,1} = \frac{a^2}{|Z_1 - Z_2|^2}$$

$$Z_{2,1,1} = Z_2 + \frac{a^2}{(\bar{Z}_1 - \bar{Z}_2)} \tag{B.14}$$

$$\alpha_{2,1,1} = \pi + 2\eta_{12} - \alpha_1 \tag{B.15}$$

However, the aforementioned 3 doublet can not satisfy the boundary condition for cylinder 1. In order to satisfy the boundary condition for cylinder 1, mirror doublets have to be arranged within cylinder 1 for the two doublets located at cylinder 2. They are numbered as (2,1,1) and (2,1,2), which are the images of Z_1 and (1,2,1) respectively. Their complex velocity is

$$w_{1,2,1} = -\beta_{1,2,1} U_2 a^2 \frac{e^{i\alpha_{1,2,1}}}{Z - Z_{1,2,1}} \tag{B.16}$$

$$\beta_{1,2,1} = \frac{a^2}{|Z_2 - Z_1|^2} \tag{B.17}$$

$$Z_{1,2,1} = Z_1 + \frac{a^2}{(\bar{Z}_2 - \bar{Z}_1)} \tag{B.18}$$

$$\alpha_{1,2,1} = \pi + 2\eta_{21} - \alpha_2 \tag{B.19}$$

$$w_{1,2,2} = -\beta_{1,2,2} U_1 a^2 \frac{e^{i\alpha_{1,2,2}}}{Z - Z_{1,2,2}}$$

$$\beta_{1,2,2} = \frac{a^2}{|Z_{2,1,1} - Z_1|^2} \beta_{2,1,1} \tag{B.20}$$

$$Z_{1,2,2} = Z_1 + \frac{a^2}{(\bar{Z}_{2,1,1} - \bar{Z}_1)} \tag{B.21}$$

$$\alpha_{1,2,2} = \pi + 2\eta_{21} - \alpha_{2,1,1} \tag{B.22}$$

The above additional two mirror doublets violated the boundary condition for cylinder 2 again, so further mirror doublets are needed. Such a process will continue infinitely. The general complex potential of the mirror doublet can be written as:

$$w_{i,j,k} = -\beta_{i,j,k} a^2 \frac{e^{i\alpha_{i,j,k}}}{Z - Z_{i,j,k}} \times \begin{cases} U_j & (k = 1,3,5...2n+1) \\ U_i & (k = 2,4,6...2n) \end{cases} \tag{B.23}$$

$$\beta_{i,j,k} = \frac{a^2}{\left| Z_{j,i,k-1} - Z_i \right|^2} \beta_{j,i,k-1} \tag{B.24}$$

$$Z_{i,j,k} = Z_i + \frac{a^2}{\left(\overline{Z}_{j,i,k-1} - \overline{Z}_i \right)} \tag{B.25}$$

$$\alpha_{i,j,k} = \pi + 2\eta_{ji} - \alpha_{j,i,k-1} \tag{B.26}$$

Here, $i = 1, j = 2$ or $i = 2, j = 1$ with $k = 1,2,...$

However, it is seen that the strength of the mirror doublet is diminishing, as shown in equation (B.24), $\beta_{i,j,k} < \beta_{i,j,k-1}$, and the whole flow complex potential is a summation of the complex potential caused by all these singularities which will converge. The final flow complex potential can be expressed as:

$$w = w_1 + w_2 + \sum_{k=1}^{\infty} w_{1,2,k} + \sum_{k=1}^{\infty} w_{2,1,k} \tag{B.27}$$

The flow velocity is,

$$u - iv = \frac{dW}{dZ}$$

$$= U_2 a^2 \left[\frac{e^{i\alpha_2}}{(Z - Z_2)^2} + \sum_{k=1,3,5\ldots}^{\infty} \beta_{1,2,k} \frac{e^{i\alpha_{1,2,k}}}{(Z - Z_{1,2,k})^2} + \sum_{k=2,4,6\ldots}^{\infty} \beta_{2,1,k} \frac{e^{i\alpha_{2,1,k}}}{(Z - Z_{2,1,k})^2} \right] \quad \text{(B.28)}$$

$$+ U_1 a^2 \left[\frac{e^{i\alpha_1}}{(Z - Z_1)^2} + \sum_{k=1,3,5\ldots}^{\infty} \beta_{2,1,k} \frac{e^{i\alpha_{2,1,k}}}{(Z - Z_{2,1,k})^2} + \sum_{k=2,4,6\ldots}^{\infty} \beta_{1,2,k} \frac{e^{i\alpha_{1,2,k}}}{(Z - Z_{1,2,k})^2} \right]$$

The Bernoulli equation (B.9) is used to determination of fluid force.

$$F_j = \oint_{c_j} (p - p_0) ds = -\rho \oint_{c_j} \frac{\partial \phi}{\partial t} ds - \frac{\rho}{2} \oint_{c_j} (V^2 - U_0^2) ds \quad \text{(B.29)}$$

Here c_j is the circumference of the j-th cylinder. It can be seen that, when two cylinders move at different velocities, the fluid forces can not be expressed as a linear summation of two dynamic head, because of the coupling between two velocity in the dynamic head. Such a component represents the potential flow interaction force when two cylinders are moving at constant velocity. On the other hand, the force is a linear function of the two cylinders acceleration. As fluid added mass is the main interest here, assuming the two cylinders started from still, by applying the definition of (B.2), all the coefficients can then be obtained.

B.4 Computation Results and Discussion

When two cylinders are arranged in tandem layout, Figures B.3 to B.6 show the different added mass terms. It is seen when the two cylinders are separated by more than two diameters, all the added mass coefficients approach to the case for solitary cylinder, i.e. the interaction effect diminishes. When the two cylinders are close to each other, e.g. less than 1.5 diameters, the interaction increases dramatically with the further decrease in the spacing. Such an effect applies both to the interaction term like m_{ijxx}, m_{ijyy} $(i \neq j)$ and the added

mass term as m_{iixx}, m_{iiyy}. As the result of flow symmetrical characteristics, the term of m_{ijxy} and m_{ijyx} are null.

Figures B.7 and B.8 show the interaction force terms when the two cylinders are arranged in a staggered layout. The data shown in the figures are the fluid force acting on the cylinder 1 caused by the acceleration of cylinder 2 in x direction. It is seen that when the spacing between two cylinders is larger than 2 diameters, the effect of the interaction is small. The interaction force is pronounced only when the spacing between two cylinders is very small. The interaction term is largest when η=45^0.

Based on the above calculation results, it can be concluded that the interaction effect due to the fluid force, caused by the acceleration of the two cylinders, is not prominent when the two cylinders are separated with more than 2 diameters. Only when the spacing is very small, can the effect then be significant. If the time domain simulation for the two cylinders interaction is considered, when the two cylinders are very close to each other, the collision will be likely to occur, and the collision effect will be much more significant than the fluid added mass force terms. The above analysis justified the insignificance of the interaction effect due to the added mass force terms in the dynamics simulation.

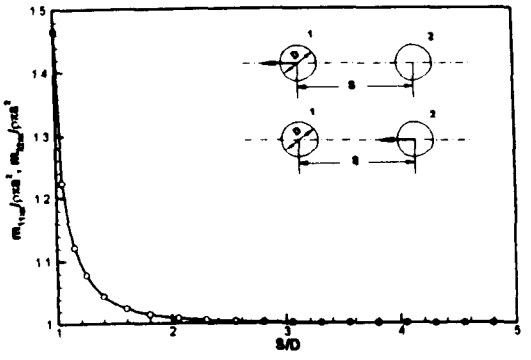

Figure B.3 Fluid added mass coefficient.

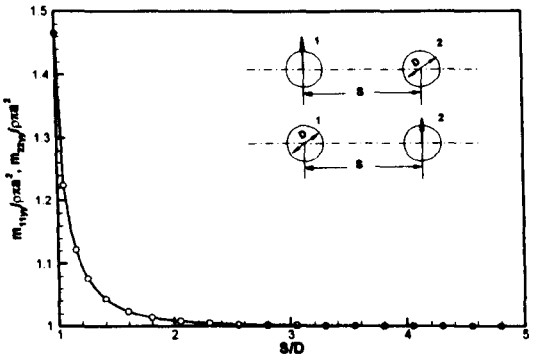

Figure B.4 Fluid added mass coefficient.

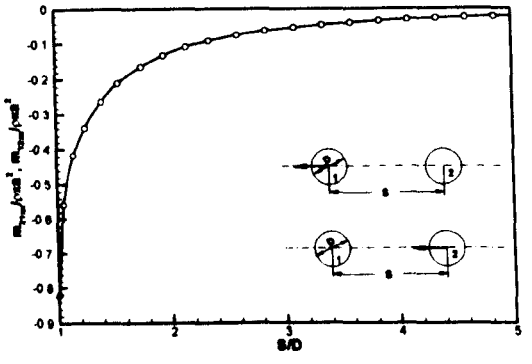

Figure B.5 Interaction force coefficient.

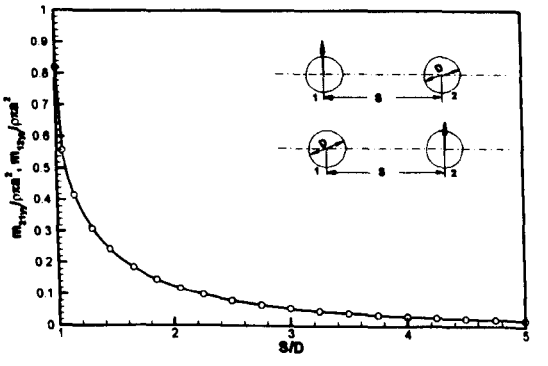

Figure B.6 Interaction force coefficient.

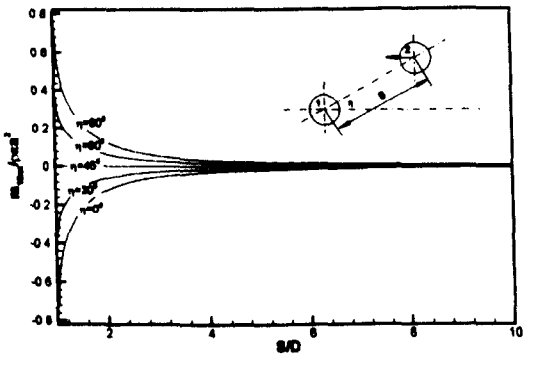

Figure B.7 The interaction force on cylinder 1 caused by the acceleration of cylinder 2.

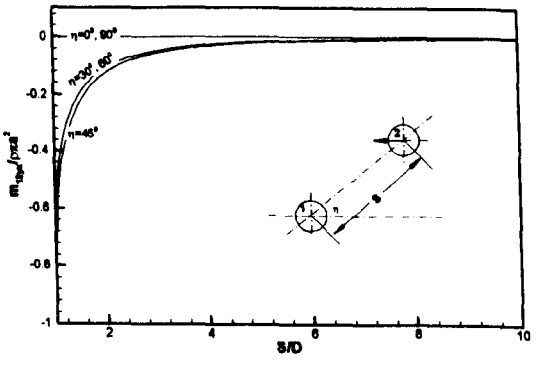

Figure B.8 The interaction force on cylinder 1 caused by the acceleration of cylinder 2.

B.5 References

Blevins, R. D. Flow-Induced Vibration. New York; 1990

Dalton, C. and Helfinstine, R. A. Potential Flow Past a Group of Circular Cylinders. Journal of Basic Engineering, Transaction of ASME. 1971 Dec: 636-642.